UNIVERSIDADE DE SÃO PAULO
INSTITUTO DE GEOCIENCIAS

Main mafic and accessory mineralogy in granites and greisens from selected occurrences in the A-type Graciosa Province, S-SE-Brazil, and petrological implications

ASTRID SIACHOQUE VELANDIA

Tese apresentada ao Programa Geociências (Mineralogia e Petrologia) para a obtenção do título de Doutor(a) em Ciências

Área de concentração: Petrologia Ígnea e Metamórfica

Orientador: Prof. Dr. Silvio Roberto Farias Vlach

São Paulo
2020

Serviço de Biblioteca e Documentação do IGc/USP

Ficha catalográfica gerada automaticamente com dados fornecidos pelo(a) autor(a) via programa desenvolvido pela Seção Técnica de Informática do ICMC/USP

Bibliotecários responsáveis pela estrutura de catalogação da publicação:

Sonia Regina Yole Guerra - CRB-8/4208 | Anderson de Santana - CRB-8/6658

Siachoque Velandia, Astrid Main mafic and accessory mineralogy in granites and greisens from selected occurrences in the A-type Graciosa Province, S-SE-Brazil, and petrological implications/ Astrid Siachoque Velandia; orientador Silvio Roberto Farias Vlach. - São Paulo, 2020.
160 p.

Tese (Doutorado - Programa de Pós-Graduação em Mineralogia e Petrologia) -- Instituto de Geociências, Universidade de São Paulo, 2020.

1. Granites and greisens. 2. Mafic silicate minerals. 3. Accessory minerals. 4. EPMA and LAICPMS. 5. A-type Graciosa Province. I. Vlach, Silvio Roberto Farias, orient.

UNIVERSIDADE DE SÃO PAULO

INSTITUTO DE GEOCIÊNCIAS

Main mafic and accessory mineralogy in granites and greisens from selected occurrences in the A-type Graciosa Province, S-SE-Brazil, and petrological implications

ASTRID SIACHOQUE VELANDIA

Orientador: Prof. Dr. Silvio Roberto Farias Vlach

Tese de Doutorado

Nº 622

COMISSÃO JULGADORA

Dr. Silvio Roberto Farias Vlach

Dr. Fábio Ramos Dias de Andrade

Dr. Guilherme Augusto Rosa Gualda

Dr. Frederico Castro Jobim Vilalva

Dr. Nilson Francisquini Botelho

SÃO PAULO

2020

AKNOWLEDGEMENTS

First, I am deeply grateful to my supervisor, Prof. Dr. Silvio Roberto Farias Vlach, for the patience guidance, assistance and advice he has provide during this project. I am truly honored and blessed to have the opportunity to work and share my passion for the granites with him.

I thank FAPESP and CNPq for financing this work (processes 08/00562-0 and 2019/17343-4) and (proc. 307583/2008-2) respectively, and CAPES for the doctoral scholarship (Finance Code 001).

I am thankful to the Institute of Geosciences and the Department of Mineralogy and Geotectonics for laboratory facilitates (NAP Geoanalitica/IGc-USP). Special thanks go to Marcos Mansueto and Leandro S. Mores for their assistance in the EMPA analyses. Also, many thanks to Vinicius Martins for helping with the LA-ICPMS analyses.

I also thank my colleague Caio A. Santos by its collaboration of part of this thesis.

I especially thank Maria Isabel and Andres for their constant support and hugs, their help and advices to make this thesis, and especially their significant love to me. We have grown together, throughout every step of this journey, the last four and a half years would not so memorable without them. *I am be grateful for you guys in my life! I look forward to many more years of friendship and to keep you very close to me. Love you so much.*

My gratitudes are also for my friends Ana Maria, Anny, Carolina, Dorilia, Giovanna, Ginneth, Lina, Lizeth, Maria Paula, Melina, Mikaella, Natalia, Tatiana, Veronica, Viviana, Claudio, Cristian, Daniel, Jonathan, Juan Sebastian, Santiago, Pedro and Wesley, for their friendship and for making my experience in Brazil unforgettable.

I would like to thank all members of my soccer teams *LAAUSP* and *COBRAS* and of my music band *Stereo Roca* for sharing my passions: the great emotion of playing football and the exciting feeling of playing music.

Finally, I dedicated this work to my mother Betcy! For always being there for me, loving me, and sending me blessings during this experience. My father Ernesto and my brother Andres, whose have been supported me in their own way. You three are my motivation, thanks for your infinity love.

“Remamos
Sabiendo cual es el precio
Con los puños apretados
Sin pensar en detenernos

Remamos
Con la cara contra el viento
Con la valentía adelante
Con un pueblo entre los dedos

Remamos
Con un nudo aquí en el pecho
Soñando que al otro lado
Se avecina otro comienzo

¿Cómo callar?
¿Cómo dejar atrás lo que te pega?
Vengo a ofrecerme hoy

Remamos…”

Kany Garcia

ABSTRACT

A-type granites from the Graciosa Province in S-SE Brazil are broader grouped in two main petrographic associations: one alkaline including metaluminous and peralkaline alkali-feldspar granites and syenites, while the other aluminous is constituted by metaluminous to slightly peraluminous syeno- and monzo-granites. These granites are geochemically characterized by high iron and alkali contents and relative elevated abundances of LILEs, HFSEs, REEs and F. Moreover, they include a large variety of Fe- and HFSE-rich primary mafic silicate minerals as well as REE-rich magmatic and hydrothermal accessory minerals. This thesis studied main mafic silicates and accessory minerals in granites and greisens from the Mandira Granite Massif and the Desemborque and Papanduva Plutons in the province. Our results are grouped in four chapters and the main insights show that: 1) the Mandira Granite Massif contains magmatic calcic, sodic-calcic and sodic amphiboles and Al-rich annite as well as hydrothermal calcic and sodic amphiboles, annite, chlorite and stilpnomelane. The Mandira granites crystallized at 720-750°C and 130-170 MPa (plagioclase-hornblende geothermobarometer) under relatively low to moderate f_{O2} conditions while during the late to post-magmatic evolution, the redox conditions indicate high oxidizing conditions and hydrothermal temperatures 250-272°C (chlorite-thermometry). 2) The Mandira and Papanduva peralkaline granites include late-magmatic and hydrothermal astrophyllite with relatively LILEs- and LREE-rich, the late-magmatic is more enriched in Zr-Nb than the hydrothermal which is more enriched in Ti. The last one was formed as result of the replacement of primary sodic amphiboles (in Mandira) and clinopyroxenes (in Papanduva). Accordingly, astrophyllite compositions offer additional information of redox conditions as well as magmatic and hydrothermal environments in peralkaline granitic systems. 3) In syenogranites and greisens from the Desemborque pluton we found the occurrence of columbite crystals characterized by predominant enrichment of HFSEs and HREEs which were formed from early to late post-magmatic stages. 4) Accessory minerals in the Desemborque rocks are magmatic zircon (syenogranites) and post-magmatic zircon, monazite, xenotime and fluorite (greisen), while in the Mandira granites are magmatic and post-magmatic zircon and fluorite and post-magmatic fluorides (fluocerite and gagarinite). In both occurrences, the post-magmatic phosphates and the fluorides were formed by several hydrothermal alterations of zircons due to post-magmatic fluids. In general, all zircons experienced post-magmatic alterations leading to progressive increase of HFSEs and REEs from primary to hydrothermal altered zircon. This hydrothermal activity was dating in monazite crystals from the Desemborque pluton given ages of 584 ± 3 Ma using the CHIME method. Highlighting, this

thesis follows the magmatic, late magmatic and post-magmatic processes during the evolution of the Graciosa rocks which are registered in the mafic and accessory minerals studied here. In this sense the late to post-magmatic processes are associated with the circulation of hydrothermal HFSE- and F-rich fluids derived from the destabilization of magmatic minerals and subsequently promoted the significant enrichment of incompatible elements in the final evolutionary stages of the granitic systems.

Keywords: Granites and greisens, mafic silicate minerals, accessory minerals, late- to hydrothermal alteration processes, A-type Graciosa Province.

RESUMO

Os granitos tipo A da Província Graciosa no S-SE Brasil são agrupados em duas associações petrográficas principais: uma alcalina incluindo sienitos e álcali feldspato granitos metaluminosos e peralcalinos, enquanto a outra é aluminosa, a qual é constituída por sienogranitos e monzogranitos metaluminosos a ligeiramente peraluminosos. Esses granitos são geoquímicamente caracterizados por altos teores de ferro e álcalis e abundâncias relativamente elevadas de LILE, HFSE, REE e F, além disso, eles incluem uma grande variedade de minerais máficos primários ricos em Fe e HFSE, bem como minerais acessórios magmáticos e pos-magmáticos ricos em REE. Nesta tese, foram estudados os principais silicatos máficos e minerais acessórios em granitos e greisens do Maciço Granítico Mandira e dos plutons Desemborque e Papanduva dentro da província. Nossos resultados estão agrupados em quatro capítulos e as principais contribuições mostram que: 1) o Maciço Granitico Mandira contém anfibólios cálcicos, sódico-cálcicos e sódicos e annita rica em Al magmáticos, bem como anfibólios sódicos, annita, clorita e estilpnomelano pos-magmáticos. Os granitos de Mandira se cristalizaram a 720-750 °C e 130-170 MPa (geotermobarômetro de plagioclásio-hornblenda) sob condições relativamente baixas a moderadas de f_{O2}, enquanto durante a evolução tardi a pós-magmática, as condições redox indicam condições mais oxidantes e temperaturas hidrotermais na faixa de 250-272 ° C (termometria por clorita). 2) Nos granitos peralcalinos do Mandira e Papanduva, há astrofilita tardi a pos-magmatica, e ambas são relativamente ricas em LILE e LREE; no entanto, a tardi-magmática é mais enriquecida em Zr-Nb do que a pos-magmática, que é mais enriquecida Ti. Esta última foi formada como resultado da substituição de anfibólios sódicos primários (em Mandira) e clinopiroxênios (em Papanduva). Consequentemente, as composições de astrofilita oferecem informações adicionais sobre condições redox, bem como ambientes magmáticos e hidrotermais em sistemas graníticos peralcalinos. 3) Nos sienogranitos e greisens do plúton Desemborque incluem-se cristales de columbita caracterizados por enriquecimento predominante de HFSE e HREE, que são formados desde os estágios hidrotermais precoces até tardios. 4) Os minerais acessórios nas rochas do plúton Desemborque são zircão magmático (sienogranitos) e zircão, monazita, xenotima e fluorita hidrotermais (greisen), enquanto nos granitos de Mandira são zircão e fluorita magmáticos e fluorita e fluoretos pos-magmáticos (fluocerita e gagarinita). Em ambas ocorrências, os fosfatos e os fluoretos pos-magmáticos foram formados por várias alterações hidrotermais no zircão devido a fluidos pós-magmáticos. Em geral, todos os tipos de zircão sofreram alterações pós-magmáticas, levando a um aumento progressivo de HFSE e REE desde

o zircão alterado primário para o hidrotermal. Esta atividade hidrotermal foi datada pela ocorrência de monazita nas rochas do Desemborque com uma idade de 584 ± 3 Ma, usando o método CHIME. Destaca-se que esta tese descreveu os processos magmáticos, tarde-magmáticos e hidrotermais durante a evolução das rochas da Graciosa, que estão registrados nos minerais máficos e acessórios estudados aqui. Nesse sentido, os processos tardios a hidrotermais estão associados à circulação de fluidos pós-magmáticos ricos em HFSE e F, os quais são derivados da desestabilização de minerais magmáticos e subsequentemente promoveram um enriquecimento significativo dos elementos incompatíveis nos estágios evolutivos finais do sistema granítico.

Palavras-chave: Granitos e greisens, minerais silicáticos máficos, minerais acessórios, processos de alteração tarde a hidrotermal, Província Graciosa tipo A.

SUMMARY

1. PREAMBLE

1.1. Structure Of The Thesis

This doctoral thesis is composed of four chapters in the article format which are linked by the common Neoproterozoic post-collisional A-type Graciosa magmatism in the SE-Brazil. This thesis also includes a general introduction and materials and methods (below) and a general summary section (Chapter 6). Figures and tables are list separately in each chapter. Appendix A and B contain the chemical EPMA and LA-ICP-MS microanalyses from the selected minerals of this study.

Chapter 2 is a work about chemical evolution of mafic silicate minerals within the distinct metaluminous and peralkaline granitic facies in the Mandira Granite Massif. It also presents the estimation of P-T crystallization conditions.

Chapter 3 form a comparison between the textural and mineral chemistry of the two textural astrophyllite types in peralkaline granites from the Mandira Massif and Papanduva Pluton and comparing with others astrophyllite-bearing worldwide localities. This contribution involves the first calculations of astrophyllite/melt partition coefficients reported in the literature.

Chapter 4 includes the textural and chemically (major and trace-elements) characterization of columbite within granites and associated greisens in the Desemborque Pluton and the explication of its genesis and evolution during crystallization history. This work provides new trace-element data for columbite in greisens which are scarce in the literature.

Chapter 5 corresponds to a detail study of zircon and related accessory minerals such monazite, xenotime and fluorides from peralkaline and syenogranites and related greisens of the Mandira and Desemborque Plutons, respectively. This work highlights the textural and chemical variations of these accessory minerals which provide records on hydrothermal imprints over the selected samples, in order to constrain the late- to hydrothermal processes in the evolutionary history of the both studied plutons.

1.2. Introduction

A-type granites were firstly defined by Loiselle and Wones (1979) as alkaline, anorogenic and anhydrous rocks and then as ferroan granites by Frost et al. (2001). They are typically form in post-collisional or extensional to post-orogenic or anorogenic tectonic settings involving fractional crystallization of mantle-derived alkaline mafic magmas (Eby, 1990, 1992; Turner et al., 1992; Bonin, 2007), partial melting of crustal source (Collins et al., 1982; Whalen et al., 1987; Creaser et al., 1991; Patiño Douce, 1997; Shellnutt and Iizuka, 2011), or a mixtures of both (Poitrasson et al., 1995), and thus these granites are related to multiple petrogenetic processes, resulting in some contrasting mineralogical and geochemical characteristics of distinct of A-type granitic groups (e.g. Eby, 1992; Bonin, 2007; Dall'Agnol and de Oliveira, 2007; Gualda and Vlach, 2007b; Vilalva and Vlach, 2014; among others).

Mineralogically, A-type granites commonly include primary Fe-rich mafic silicate minerals such hedenbergite, aegirine-augite, hastingsite, ferro-ferri-hornblende, ferrorichterite, ferrowhinchite, arfvedsonite, riebeckite and/ or annite; and a variety of primary REE-rich accessory minerals such zircon, apatite, allanite, chevkinite and titanite, as well as exotic Zr-Ti-Nb-bearing minerals such astrophyllite, aenigmatite, and/or neptunite (see references therein). Geochemically, they are characterized by high alkalis, HFSE and HREE contents, FeO_T/MgO and Ga/Al ratios, as well as halogens (in particular F) contents (c.f. Wang et al., 2018). Accordingly, A-type granites have long attracted considerable scientific and commercial attention because they could achieve potentially economic concentrations of the REEs, Y, HFSE, Th, U, Nb, Ta, Sn and W (Schmitt et al., 2002; Dall'Agnol et al., 2012; Huang et al., 2018; Li et al., 2018; Siegel et al., 2018; Xie et al., 2018).

In Brazil, A-type granites are widely distributed from the Archean until the Neoproteriozoic in several provinces of the Amazon and the São Francisco Cratons, as well as in the Borborema Province, and the central Tocantins and Mantiqueira Provinces. The last one, represent an orogenic setting during the Brazilian Orogeny in the Ediacaran Period (Silva et al., 2005), which also include minor provinces such the Graciosa Province selected as the focus of this research.

The Graciosa Province, S-SE Brazil (Gualda and Vlach, 2007a) included numerous A-type syenitic and granitic plutons, as well as associated basic, intermediate and acid volcanics, gabbros, K-rich diorites and monzodiorites and hybrid rocks. The Graciosa A-type syenites and granites are grouped in two distinct primary alkaline and aluminous petrographic associations

(Gualda and Vlach, 2007b). The *alkaline association* consist of metaluminous alkali feldspar syenites to hypersolvus peralkaline alkali-feldspar granites formed under relatively reducing conditions, close to the fayalite-quartz-magnetite (FQM) buffer. In contrast, the *aluminous* association includes metaluminous to moderately peraluminous subsolvus biotite (±hornblende) syeno- and monzogranites formed under more oxidizing conditions; many rocks show rapakivi textures (Gualda and Vlach, 2007b; Vlach and Gualda, 2007).

Vilalva et al. (2019) argued that the Graciosa Province provides an ideal setting to investigate the petrogenesis, evolution, composition and geotectonic significance of A-type granites, once previous mineralogical studies indicated that they included several accessories and rare REE- and HFSE-rich minerals (Gualda and Vlach, 2007b, 2007a; Vlach and Gualda, 2007; Vilalva et al., 2013). However, mineralogical studies of accessory minerals are still poorly known in this province. Accessory minerals, record microtextural and geochemical features which provide significant clues of the magmatic-hydrothermal processes acting during evolution of A-type granitic rocks (Johan and Johan, 2005; Vlach and Gualda, 2007; Uher et al., 2009, 2014; Lisowiec et al., 2013; Breiter, 2016; Huang et al., 2018).

In this research we present a detailed petrographic textural and chemical data including EPMA and LA-ICP-MS in-situ microanalyses of mafic HFSE-rich silicate and REE-rich accessory minerals for representative A-type granites of both alkaline and aluminous associations within the Guaraú and Mandira Granite Massifs at the Graciosa Province. These massifs are relevant among the Graciosa rocks because they were affected by late- to post-magmatic fluids during their evolution resulting in the occurrence of hydrothermal albitized granites, pegmatites, greisens and adularia-bearing quartz-feldspar metassomatites (Oliveira et al., 1987; Oliveira, 1989; Garcia, 2015), and thus are key occurrences to evaluate late- to post-magmatic processes during evolution history of the studied Graciosa rocks, such as new insights into the hydrothermal imprints in A-type granites worldwide.

1.3. Objectives

- To examine in detail the main mafic silicate and accessory minerals, focusing in textures, microtextures and crystallization sequences of selected granites from both petrographic alkaline and aluminous associations.

- To characterize geochemical major and trace element compositions for the mentioned minerals using EPMA and LA-ICP-MS in-situ microanalyses in order to evaluate compositional variations and evolution of the studied rocks
- To calculated intensive crystallization parameters (T, P, volatile activities) using the chemical compositions measured in the main mafic silicates (amphiboles, biotite and astophyllite) to inferred emplacement and f_{O2} conditions for the studied granites.
- To calculate chemical Th-U-Pb_T ages in post-magmatic monazite using the CHIME method in order to constraint the timing of hydrothermal activity.

1.4. Materials and Methods

This study involved different petrography, whole-rock and mineral geochemistry analytical techniques. Samples for this study were collected by the supervisor of this project and other colleagues in previous fieldworks and also included several thins sections kindly provided by M.C.B. Oliveira.

1.4.1. Petrography

Thin sections were primarily examined using a *Zeiss Axioplan* microscope under transmitted and reflected lights, focus on mineralogy, textures/micro-structures features, and the mineral sequence of crystallization. Photographic record of the main rock and mineral features was obtained with an *AxioCam MRc* camera, attached to the *Zeiss* microscope at the Laboratory of Petrography-Institute of Geosciences/University of São Paulo.

1.4.2. Whole-Rock Geochemistry

X Ray Fluorescence (XRF) analysis was obtained for 6 selected samples, by using the PANalytical Axios MAX Advanced equipment. Major elements were melted, glass, disks, while trace elements (Ba, Ce, Co, Cr, Cu, Ga, La, Nb, Nd, Ni, Pb, Rb, Sc, Sr, Th, U, V, Y, Zn and Zr) were done over pressed powder disks, following the procedures described by Mori et al. (1999). A sub set of selected 3 samples were analyzed for trace elements by Inductively Couple Plasma Mass Spectrometry (ICP-MS), with the Perkin Elmer ELAN 6100DRC equipment, following the analytical routine developed by Navarro et al. (2008).The analyzed samples were prepared at the *Mineral Separation Laboratory* and in *the Sample Treatment Laboratory* (LTA), following the required quality standards (Sertek, 2010). After cleaning, the samples were crushed with a

hydraulic crusher. The selected samples were then powdered with a ring mill pulverizer with agate elements to obtain a ca. 200 μm mesh powder. A 7.5 aliquot of this powder was micronized with a MacCrone micronizer made up of agate elements for 30 min. After over dried at 100°C for 48 hours, 7 g were mixed with 1.4% of binder wax (C6H8O3N2) and pressed with a manual press. The melted glass discs were obtained by mixing 1 g of the sample with 9 g of LiBO2 (Lithium metaborate), which were melted at 1000°C for 20 minutes. Loss on ignition (LOI) values were estimated by weighting the dried samples before and after placing them into an oven at 900°C.

1.4.3. Mineral Geochemistry

Major and trace elements compositions as well as Th-U-Pb_T chemical ages were obtained using the following methods.

1.4.3.1. Electron Probe Micro Analyzer (EPMA)

Qualitative and quantitative work was carried out at Laboratory at the NAP GeoAnalitica-Institute of Geosciences/University of São Paulo using a JEOL JXA-FE-8530 equipment provided with field emission gun, five wavelengths dispersive (WD) and one energy dispersive (ED) spectrometers. Back-scattered electron (BSE) and cathodoluminescence (CL) imaging and, semiquantitative energy dispersive spectroscopic (EDS) microanalyses were carried out prior followed by quantitative (WDS) microanalysis. A total of 986 WDS microanalyses were obtained in the following minerals: feldspars (80), amphibole (208), astrophyllite (68), biotite (175), chlorite (35), stilpnomelane (40) columbite (45), fluorides (30), monazite (68), xenotime (31) and finally zircon (206). WDS analyses were performed with conventional analytical routines for amphiboles and phyllosilicates (e.g. Gualda and Vlach, 2007c), with 15 kV, 20nA and 5 μm for the accelerating voltage, beam current and diameter spot, respectively. Total counting times, equally distributed between peak and background, vary from 10 to 60s. In the case of accessory minerals, they were analyzed using rigorous and accurate routines, separating in different groups according to the their corresponding LREEs and HREEs constituents under voltage 20 kV, beam current 50 nA, beam diameter of 3 μm (zircon and columbite) and 15 kV, 12 nA and 4 μm (monazite, fluorides and xenotime), for details see chapters 4 and 5. Major and minor elements were determined using a variety of natural and synthetic standards from the Smithsonian Institution. Standardization and analytical protocol details (e.g., element set-up, counting times and detection limits) for the selected minerals are given in Table 1-1 to Table 1-5.

Table 1-1: Analytical setup used for WDS analyses of feldspars and amphiboles. D.L.= detection limit

			Feldspars			Amphibole		
Analyzer Cristal	Element	Spectral Line	Standard	Peak counting time (s)	D.L. (ppm)	Standard	Peak counting time (s)	D.L. (ppm)
TAP	Si	Kα	Anorthoclase	10	200	Hornblende	10	201
	Al	Kα	Anorthite	15	100	Hornblende	15	115
LIFL	Cr	Kα	-	-	-	Chromite	20	
	Fe	Kα	Fayalite	10	180	Fayalite	10	249
	Mn	Kα	Fayalite	40	90	Fayalite	40	105
	Zn	Kα	-	-	-	Willemite	5	517
PETJ	Cl	Kα	-	-	-	Sodalite	10	235
	K	Kα	Ortoclase	10	110	Ortoclase	10	138
	Ca	Kα	Wollastonite	5	140	Wollastonite	20	132
	Zr	Lα	-	-	-	Zircon	50	233
	Sr	Lα	Strontianite	40	190	-	-	-
	Nb	Lα	-	-	-	-	-	-
LIFL	Ti	Kα	Rutile	10	270	Rutile	5	300
	Ba	Lα	Benitoite	30	260	-	-	-
TAPH	F	Kα	-	-	-	Fluorapatite	10	484
	Na	Kα	Albite	5	190	Albite	10	118
	Mg	Kα	Diopside	10	100	Diopside	10	219

Table 1-2: Analytical setup used for WDS analyses of phyllosilicates. D.L.= detection limit

			Phyllosilicates					
			Astrophyllite		Biotite		Chlorite and Stilpnomelane	
Analyzer Cristal	Element	Standard	Peak counting time (s)	D.L. (ppm)	Peak counting time (s)	D.L. (ppm)	Peak counting time (s)	D.L. (ppm)
TAP	Si	Diopside	10	203	10	201	10	273
	Al	Anorthoclase	15	107	15	118	15	201
LIFL	Cr	-	-	-	-	-	-	-
	Fe	Fayalite	10	290	10	231	10	510
	Mn	Fayalite	20	159	20	150	20	252
	Zn	Willemite	5	541	5	514	30	339
PETJ	Cl	Sodalite	10	162	10	156	10	253
	K	Ortoclase	10	152	10	156	10	228
	Ca	Wollastonite	10	178	10	176	10	277
	Zr	Zircon	50	232	50	213	-	-
	Sr	-	-	-	-	-	-	-
	Nb	Ilmenite	40	268	-	-	-	-
LIFL	Ti	Rutile	10	393	10	327	10	462
	Ba	Benitoite	30	370	30	328	30	537
TAPH	F	Fluorapatite	10	524	10	504	10	804
	Na	Albite	10	119	10	108	10	157
	Mg	Diopside	10	110	10	109	10	186

Table 1-3: Analytical setup used for WDS analyses of fluorides. D.L.= detection limit

Analyzer Cristal	Element	Spectral Line	Standard	Gagarinite		Fluocerite	
				Peak counting time (s)	D.L. (ppm)	Peak counting time (s)	D.L. (ppm)
TAP	Na	Kα	Albite	5	908	5	352
	Y	Lα	YPO4	15	887	10	577
	Si	Kα	Wollastonite	10	218	10	173
LIFL	La	Lα	LaPO4	-	-	5	2565
	Ce	Lα	CePO4	30	722	5	2422
	Nd	Lβ	NdPO4	20	811	5	2568
	Pr	Lβ	PrPO4	30	1275	10	2947
	Sm	Lβ	SmPO4	20	828	10	2650
	Gd	Lβ	GdPO4	10	1144	10	2591
PETJ	Ca	Kα	CaF2	5	524	5	540
	Th	Mα	ThSiO4	30	1060	30	1253
	Sr	Lα	Strontianite	-	-	10	666
LIFL	Tb	Lα	TbPO4	20	1009	-	-
	Dy	Lβ	DyPO4	10	1841	-	-
	Er	Lα	ErPO4	10	1386	-	-
	Yb	Lα	YbPO4	10	1735	20	978
	Ho	Lβ	Sample-0079	20	4961	-	-
	Lu	Lβ	Synthetic-glass	10	5434	-	-
TAPH	F	Kα	CaF2	5	4175	5	5021
	Al	Kα	Anorthite	30	108	15	156

Table 1-4: Analytical setup used for WDS analyses of rare-earth phosphate minerals. D.L.= detection limit

Analyzer Cristal	Element	Standard	Monazite			Xenotime		
			Spectral Line	Peak counting time (s)	D.L. (ppm)	Spectral Line	Peak counting time (s)	D.L. (ppm)
TAP	Y	YPO4	Lα	15	114	Lα	15	273
	Si	Wollastonite	Kα	10	76	Kα	10	126
	Al	Anorthite	Kα	15	46	Kα	30	46
LIFL	Ca	Wollastonite	Kα	10	83	Kα	20	57
	La	LaPO4	Lα	10	368	-	-	-
	Ce	CePO4	Lα	10	353	Lα	30	161
	Nd	NdPO4	Lβ	10	517	Lα	20	177
	Pr	PrPO4	Lβ	10	544	Lβ	30	274
	Sm	SmPO4	Lβ	20	2148	Lα	20	174
	Gd	GdPO4	Lβ	20	1763	Lα	10	255
	Tb	TbPO4	-	-	-	Lα	20	291
	Fe	Fayalite	Kα	10	141	Kα	20	104
	Dy	DyPO4	Lβ	20	1977	Lα	10	438
	Er	ErPO4	-	-	-	Lα	10	299
	Yb	YbPO4	Lα	20		Lα	10	416
	Ho	Sample-0079	-	-	-	Lβ	20	966
	Lu	Synthetic-glass	-	-	-	Lβ	10	1129
PETJ	P	CePO4	Kα	10	157	Kα	10	221
	Th	ThSiO4	Mα	140	125	Mα	140	102
PETL	U	UO2	Mβ	200	42	Mβ	200	37
PETH	Pb	K-523	Mα	200	41	Mβ	200	50

Table 1-5: Analytical setup used for WDS analyses of Columbite–Tantalite and Zircon. D.L.= detection limit

Analyzer Cristal	Element	Spectral Line	Columbite–Tantalite			Zircon		
			Standard	Peak counting time (s)	D.L. (ppm)	Standard	Peak counting time (s)	D.L. (ppm)
TAP	F	Kα	Fluorapatite	5	2698	-	-	-
	Na	Kα	Albite	10	195	-	-	-
	Mg	Kα	Diopside	15	134	Basalt	20	120
	Al	Kα	Anorthite	15	131	Anorthite	20	114
LIFL	Fe	Kα	Ilmenite	10	252	Fayalite	15	152
	Mn	Kα	Ilmenite	10	219	Fayalite	15	128
	Ta	Lα	Ta	10	408	-	-	-
	Gd	Lβ	GdPO4	20	505	GdPO4	15	504
	Yb	Lα	YbPO4	20	283	-	-	-
	Dy	Lβ	-	-	-	DyPO4	15	517
	Er	Lα	-	-	-	ErPO4	15	277
	Yb	Lα	-	-	-	YbPO4	15	943
	Sm	Lβ	-	-	-	SmPO4	15	558
PETJ	Nb	Lα	Nb	10	1168	-	-	-
	Ca	Kα	Diopside	10	180	-	-	-
	Ti	Kα	Ilmenite	10	291	-	-	-
	Si	Kα	-	-	-	Zircon	10	464
	Zr	Lα	-	-	-	Zircon	10	1577
	Ca	Kα	-	-	-	Anothite	10	158
	Y	Lα	-	-	-	YPO4	25	273
PETL	Sr	Lα	Strontianite	20	263	-	-	-
	W	Mβ	W	20	775	-	-	-
	Y	Lα	YPO4	40	198	-	-	-
	Zr	Lα	Zircon	25	214	-	-	-
	Sb	Lβ	Sb	40	285	-	-	-
	V	Kβ	V	20	612	-	-	-
LIFL	Hf	Lα	-	-	-	Zircon	15	300
	Ti	Kα	-	-	-	Ilmenite	20	176
	La	Lα	-	-	-	LaPO4	15	389
	Ce	Lα	-	-	-	CePO4	15	344
	Nd	Lβ	-	-	-	NdPO4	15	511
	Ta	Lα	-	-	-	Ta	25	-
PETH	P	Kα	-	-	-	CePO4	20	141
	Si	Kα	Diopside	10	163	-	-	-
	Th	Mα	Rhyolitic glass	60	327	Rhyolitic glass	30	393
	U	Mβ	Rhyolitic glass	40	381	Rhyolitic glass	30	359
	Pb	Mβ	Pb	60	236	-	-	-
	Nb	Lα	-	-	-	Nb	25	167

Compositional maps: Quantitative WDS maps showing compositional variations in selected zircon crystals. The operation conditions follow a beam current of 50 nA, an acceleration voltage of 20 kV and a dwell time of 140 ms. All images were processed using the software Adobe Photoshop CS6.

Th-U-Pb_T dating: Monazite was analyzed with distinct operating conditions relative to the other accessory minerals in order to obtain chemical Th-U-Pb_T ages. Chemical analyses and dating followed the detailed procedures developed by the supervisor of this work (in Vlach, 2010), with operation conditions of 15 kV, 300 nA, and 4 μm for the accelerating voltage, beam

current and spot size, respectively. The instrumental setup and Th, U and Pb calibration were checked up with a natural monazite and xenotime reference materials from the Sao Paulo State (E-20 and E00-25 samples, respectively Vlach and Gualda (2000). The JED-2003 (v.1.12.1) software package was used to perform the calibration, overlap correction and elements quantification. Individual analyses were treatment using an Age-Mona Excel spreadsheet to calculate ages and respective deviations (Suzuki et al., 1994). The uncertainties are obtained by propagating counting errors (2σ, standard deviation). While, most of the individual monazite calculations show ages nearly concordant to the zircon U-Pb (LA-ICP-MS) age of 580 Ma of the corresponding rocks (Desemborque Pluton from the Graciosa Province, Vilalva et al., 2019). Thus, monazite chemical ages were computed by isochrons and weighted averaging using the IsoPlot software v.4.2 (Ludwig, 2003), drawing the fit through the origin. The complete monazite chemical U-Th-Pb_T ages refer to a 95% confidence level.

1.4.3.2. Laser Ablation Inductively Coupled Plasma Mass Spectrometry (LA-ICMPS)

In situ trace-element analyses were conducted in primary amphiboles, astrophyllite, columbite, monazite, xenotime and zircon, by the detailed optical, electronic and EDS analyses and BSE-images mention before. Trace element abundances were analyzed using a Thermo Fisher Scientific iCAP Q ICP-MS instrument coupled with a New Wave UP-213 laser ablation system at the Laboratory of the NAP GeoAnalitica-Institute of Geosciences/University of S*ão* Paulo. Analytical conditions for amphiboles and astrophyllite were a laser spot of 40 μm under a repetition frequency of 15Hz and energy fluence of 2.85 J/cm^2. For columbite, monazite, xenotime and zircon, the analytical conditions were a laser spot of 25 μm, 20 Hz of frequency with energy fluence of 1.97 J/cm^2. The analysis consisted in of a ~60 s background measurement followed by data acquisition for ~60 s and dwell time of 8 ms for each isotope of the reported element, followed by 30s of washout time. NIST-610 SRM glass was used as external standard in all minerals (Jochum et al., 2011). The reference material zircon ZR-91500 was used to monitor the analytical accuracy and reproducibility. Drift corrections, data reductions and conversions were carried out using the Glitter (v.4.4.4) program.

2. MAGMATIC AND HYDROTHERMAL MAFIC SILICATES IN THE A-TYPE MANDIRA GRANITE MASSIF, GRACIOSA PROVINCE, SE-BRAZIL: OCCURRENCE, COMPOSITIONAL VARIATIONS AND CRYSTALLIZATION CONDITIONS

Astrid Siachoque[a], Caio A. Santos[a], Silvio R.F. Vlach[a]
a. Institute of Geosciences -University of São Paulo, São Paulo-Brazil.

ABSTRACT

The Mandira Granite Massif, at the northeastern most part of the A-type Graciosa province (S-SE Brazil), is subdivided in three main units Mandira, Mandira 1 and Acaraú. The Mandira and Acaraú units are made of peralkaline alkali feldspar granites separated by alkaline-1 and alkaline-2 petrographic associations respectively, and the Mandira 1 unit is composed of metaluminous to slightly peraluminous syenogranites of aluminous affinity. Here we report chemical compositions and textural features of amphiboles, biotite, chlorite and stilpnomelane, trace REE partitions controls of amphiboles, and intensive crystallization parameters inferred among the three Mandira units. Our results show that amphiboles crystallized in both magmatic and late- to post-magmatic stages of crystallization and their compositions vary from Ca, Na-Ca to Na groups. Trace element and REE distribution exhibit significant abundances of LREEs, Nb and Ta for the Ca-rich amphiboles, while the Na-Ca and Na- amphiboles show strong preference of Li, HFSE, HREEs, Y, Th and U. Biotite in peralkaline granites crystallized as late to- post-magmatic phase (in most cases substituting amphiboles), whereas in the syenogranites biotite is predominant magmatic. Biotite in the Mandira Granite Massif is Fe-rich and a distinct Al-Fe rich biotite variety was found in the albitized granites. The estimated crystallization conditions suggest that the Mandira granites were emplaced at shallower crustal levels (~2.2 km) under 130-170 MPa and 723-750°C intervals, and relatively low fugacity conditions ($-1 \leq \Delta QFM \leq 0$). Crystallization of Na-rich amphiboles pointing to high oxidizing conditions, up to above the MH buffer and suggesting crystallization conditions far more oxidizing during late-magmatic evolution. Finally, extensive crystallization of chlorite in syenogranites and related greisens within the massif indicates hydrothermal temperatures between 239 and 283 °C for the post-magmatic stage of evolution.

Keywords: Granites, crystallization parameters, A-type Graciosa Province.

2.1. Introduction

Amphibole and biotite are common ferromagnesian minerals and valuable constituents of granitic rocks. The textural features and chemical compositions of these minerals usually provide significant information about intensive crystallization parameters and help tracking the evolution of the host granitic magma during its emplacement (see references therein). For example, many works have long study the amphibole occurrences in granites to determinate composition and differentiation of magma, by detailing their major- and trace element variations and/or via mineral-melt partition coefficients (*e.g*. Marks et al., 2004; Tiepolo et al., 2007; Papoutsa and Pe-piper, 2014; Vilalva et al., 2016; Siegel et al., 2017; Vasyukova and Williams-Jones, 2019). In the case of biotite of magmatic origin, many studies had determined that its structural and compositional variations reflect the nature, redox conditions, and tectonic environments of the hosting granite (Eugster and Wones, 1962; Wones and Eugster, 1965; Speer, 1984; Abdel-rahman and Abder-Rahman, 1994; Nachit et al., 2005) and thus biotite can be used as a petrogenetic indicator of different magmatic rocks (Colombo et al., 2010; Karimpour et al., 2011; Hossain and Tsunogae, 2014; Sarjoughian et al., 2015; Moshefi et al., 2018). Moreover, current studies have shown that chemical compositions of biotite are also valuable indicators to constrain halogens fugacity and thus the physicochemical conditions of fluids in granitic magmatic-hydrothermal systems (Ayati et al., 2008; Siahcheshm et al., 2012; Teiber et al., 2015; Zhang et al., 2016; Jin et al., 2018). On the other hand, the precipitation of hydrothermal minerals like chlorite is common in granitic systems since chlorite formation is usually related to the alteration of primary ferromagnesian minerals, particularly biotite, and thus its occurrence provide useful information about temperatures of hydrothermal fluids altering the granitic bodies (Caritat et al., 1993; Zimak, 1999; Inoue et al., 2010; Ciesielczuk, 2012; Wang et al., 2018a).

The Mandira Granite Massif (Oliveira, 1989) occurs into the geological setting of the A-type Graciosa Province, southern Brazil (Gualda and Vlach, 2007a) and includes coeval peralkaline alkali-feldspar granites and metaluminous syenogranites. These petrographic granitic facies were locally altered by late fluids resulting in the formation of hydrothermal albitized granites and greisens. Amphiboles and biotite are the main mafic minerals among all Mandira granitic facies that crystallized in distinct textural types, while chlorite represents the most important hydrothermal mineral only in the syenogranites and the associated greisens. In this sense, the objectives of this contribution are: (1) to detail the textural features of amphiboles, biotite and chlorite and their relationships with other minerals within the different

granitic facies; (2) to constrain the chemical evolution of amphibole and biotite textural groups; (3) to investigate the amphibole/melt REE partition coefficients for each Mandira amphibole-group; (4) to estimate intensive crystallization parameters such pressure, magmatic and hydrothermal temperatures, oxygen and halogen fugacity in suitable Mandira granites. The inferences obtained from this study will allow for better understanding the role of rock-forming mafic minerals during evolution of the Mandira Massif Granite at the A-type Graciosa Province.

2.2. The Mandira Granite Massif

The Mandira Granite Massif is one among several intrusions in the Graciosa Province of A-type granites and syenites (Gualda and Vlach, 2007a), emplaced by 580 Ma, during a post-collisional stage of the Brasiliano/Oan-African Orogeny in southern Brazil (Vlach et al., 2011; Vilalva et al., 2019; Figure 2-1A). The massif appears at the northeastern most part of the province, close to the Atlantic coastline. It is elongated along the N40°E direction, covering an exposure area about 50 Km^2, and intrude high-grade gneiss-migmatite rocks and low-grade mica schists of the Atuba and Turvo-Cajati complexes (Oliveira, 1989), respectively; most of its external contacts are covered by quaternary alluvial sediments (Figure 2-1B).

Oliveira (1989) presented the first studies on the massif, this author recognized the A-type nature of the granitic rocks, subdivided the massif according to three main units, named Mandira, Mandira 1 and Acaraú, and described some sparse associated occurrences of gabbroic/dioritic rocks at the NW region of the massif, some basic-intermediate dikes, and a variety of hydrothermal rocks (Figure 2-1B). The contacts among these rocks are inferred due to field difficulties. Given unit's distributions and our previous knowledge on similar occurrences in the province, we consider that they probably constitute distinct granite plutons or stocks. Furthermore, our descriptions adopt a somewhat different nomenclature, to conform the broader subdivision of the petrographic associations, as proposed by Gualda and Vlach (2007b, 2007a) for the whole province. The Mandira and Acaraú units are made up by peralkaline alkali feldspar granites from the alkaline association, while the Mandira 1 unit is constituted by metaluminous to slightly peraluminous biotite (± hornblende) granites from the aluminous association, as summarized in the following. Modal and geochemical data for representative samples from those studied units in this work are presented in Table 2-1 and Table 2-2, respectively.

2.2.1. Mandira unit

The Mandira Unit is predominant within the massif, cropping out over 30 km^2. It is made up by three distinct plutons, disposed along the NE direction (Figure 2-1B). From the petrographic standpoint, the dominant rock types are relatively homogeneous, grayish to reddish colored, *hypersolvus* alkali feldspar granites, with massive to slightly oriented structures, given mainly by imprinted solid-state deformation, and equi- to inequigranular, medium and coarse-grained textures. Herein, we group these rocks in an alkaline 1 petrographic association. The studied samples are made up by mesoperthitic alkali feldspar ($Or_{94-98}Ab_{2-5}$; 55-65 vol.%), quartz (30-45%) and sodic amphibole (5-7%), as the main mafic primary phase. Granophyric intergrowths between alkali-feldspar and quartz are observed in some samples. Astrophyllite, ilmenite and zircon are the main primary accessories, while albite (as interstitial aggregates and/or *swapped rims* over alkali feldspar crystals), biotite, fluorite, hematite, fluocerite, gagarinite, hematite, monazite and thorite are typical late- to post-magmatic phases.

Samples from this unit (see also Oliveira, 1989) are strongly ferroan, with Fe# [= $FeO^T/(FeO^T + MgO)$, wt.% oxide] close to the unit (0.99) and an Agpaitic (or Peralkalinity) Index [AI = $(Na_2O+K_2O)/Al_2O_3$, molar] around 1.05. Trace element compositions show relatively enriched of HFSE, HREE, actinides (Th and U) with significant contents of Zn (173 ppm), F (2913 ppm), Rb (238 ppm), Zr (553 ppm), Y (225 ppm) and REE totals of 410 ppm (Table 2-2).

2.2.2. Mandira 1 unit

This unit crops out as four distinct stocks distributed along the massif (Figure 2-1B), covering a total area of 12 km^2. Their structural relationships with the main Mandira Unit are not properly known; Oliveira (1989) suggested that they are somewhat younger, however this was not confirmed by recent high-resolution zircon U/Pb dating (unpublished data). The main rock types are grayish to slightly reddish biotite (± hornblende) syenogranites with predominant massive structures and textures varying from medium- to coarse-grained inequigranular to porphyritic, in this case with alkali feldspar megacrysts. Typical rapakivi textures appear in some samples. Granite porphyries, with alkali-feldspar mantled by plagioclase, quartz and plagioclase megacrysts in a fine-grained mesostasis, occur as crosscutting dikes in some areas. The main granites are composed of perthitic alkali feldspar ($Or_{58-97}Ab_{2.2-39}$; 48-55 vol.%), quartz (27-35%) and plagioclase ($Ab_{62-98}An_{0.5-14}$; 9-12%), containing biotite (4-6%) and calcic amphibole (3-5%) as the main mafic minerals. The primary accessories are apatite, allanite,

magnetite, ilmenite and zircon, whereas fluorite is post-magmatic. Chlorite, epidote, sericite and stilpnomelane are typical secondary phases after biotite and feldspars.

These rocks are metaluminous, with $0.98 \leq [Al_2O_3/(CaO+Na_2O+K_2O)$ or A/CNK$] \leq 1.0$, and ferroan ($0.92 \leq$ Fe# ≤ 0.97). Trace element compositions show high abundances of mainly F (2813 ppm), Rb (167 ppm), Sr (59 ppm), Zr (462 ppm), Ba (570 ppm) and REE_T (504 ppm) with preferential enrichment of LREE relative to HREE.

2.2.3. Acaraú Unit

It is a small occurrence (8 km^2) that appears at the southernmost area of the massif (Figure 2-1B), composed by grayish to greenish massive alkali feldspar granites, with inequigranular to porphyritic, medium- to coarse-grained textures. In the field, the darkest greenish varieties resemble to some extend charnokitic rocks (Oliveira, 1989). As compared with the peralkaline granites from the Mandira Unit, the most typical granites from this unit differ mainly by the occurrence of sodic-calcic primary amphiboles, and of chevkinite, apatite and titanite as primary accessories; sodic amphibole, biotite, allanite, fluorite, ilmenite, stilpnomelane and xenotime are typical late- to post-magmatic phases. Of note, two alkali-feldspar granite samples from the Oliveira's collection present solely a calcic amphibole and, thus, a more typical metaluminous character. These rocks are grouped together in an alkaline 2 petrographic association. They also present high Fe# values (1.0) and IA (up to 1.03) similar to the Mandira peralkaline granites (alkaline 1 association). The Acaraú peralkaline granites have larger abundances of F (4182 ppm), Zn (182 ppm) and REE_T (426 ppm) being enriched in most of LREEs relative to the Mandira peralkaline granites (Table 2-2).

2.2.4. Hydrothermal Altered Rocks

A variety of rocks formed during the hydrothermal alterations within the massif, are associated mainly with the northern stock from the Mandira 1 Unit (Figure 2-1B, see details in Oliveira, 1989). They include albitized granites, greisens and adularia-bearing quartz-feldspar metassomatites, with equi- to inequigranular or heterogranoblastic textures. Albitized granites contains albite and variable quartz and alkali feldspar contents, accompanied by biotite, hematite, fluocerite, sphalerite and zircon. Otherwise, greisens and metassomatites are composed mainly of quartz, chlorite and sericite; the accessory phases being chalcopyrite, sphalerite, pyrite, fluorite, galena, monazite, cassiterite, topaz, thorite, xenotime and zircon.

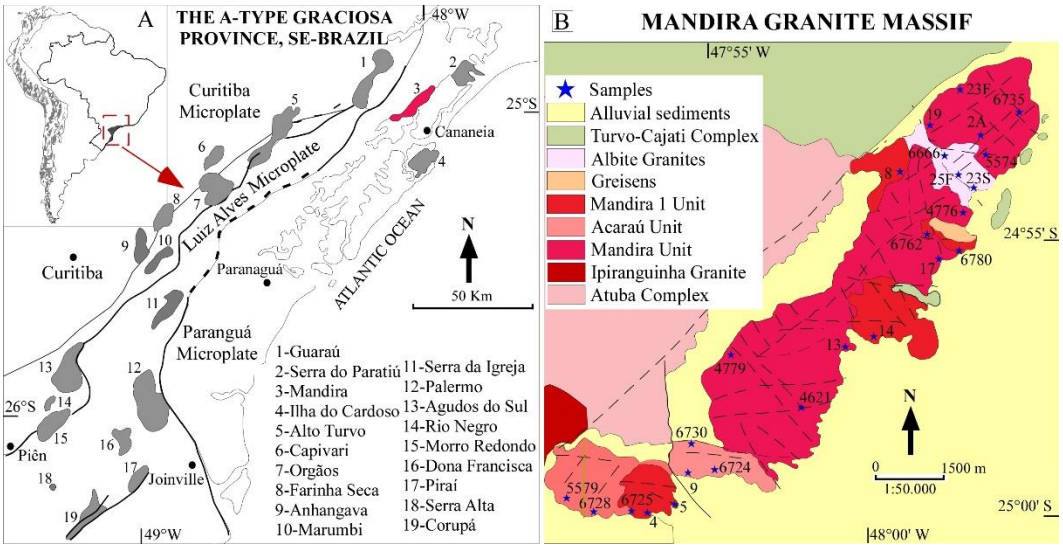

Figure 2-1. Location of the study area. A) Geological setting of the Neoproterozoic A-type Graciosa province in SE Brazil (from Vilalva et al., 2019). B) Detailed geological map of the Mandira Massif Granite (Oliveira, 1989)

2.3. Methods

The studied samples include some collected by us, and several small rock slabs kindly provided by M.C.B. Oliveira. The analytical work was done at the laboratories of the GeoAnalitica core facility, at the University of São Paulo. After conventional petrographic exams under the petrographic microscope over polished thin sections (30-60µm thick), 25 samples were selected for detailed quantitative mineral analysis (amphiboles, biotite, chlorite and stilpnomelane). These were performed with the electron probe micro analyzer (EPMA), and with the Inductively Coupled Plasma Mass Spectrometry equipment, coupled with Laser Ablation (LA-ICP-MS), in the case of amphiboles. Whole rock geochemical analyses were also obtained for the most fresh and representative samples of each granite unit.

2.3.1. EPMA analyses

Textural and mineral chemistry analyses were focused on the main mafic primary and hydrothermal mafic silicates through electron backscattered (BSE) imaging and quantitative spot analysis by wavelength dispersive spectrometry (WDS), using both conventional JEOL JXA-8600S and field emission JEOL JXA-FE-8530 microprobes. The analytical conditions for the WDS analysis were 15 kV, 20 nA, 5-10 µm for the column accelerating voltage and beam current and diameters, respectively. The total counting times, equally distributed for peak and background, vary from 10s (major and volatile elements) to 40s (minor elements). The used natural and synthetic standards come from the Smithsonian Institute and Geller^{TM} (Rose, 2011)

and were: Arenal hornblende (Si and Al in amphiboles), diopside (Si, Mg), fayalite (Fe, Mn), anorthoclase (Al), wollastonite (Ca), orthoclase (K), rutile (Ti), albite (Na), zircon (Zr), willenite (Zn), benitoite (Ba), sodalite (Cl) and fluorapatite (F). Matrix effects and conversions of the raw data were performed with the PROZA and PRZ/Armstrong software available with the 8600S and FE-8530 microprobes, respectively.

Amphiboles structural formulae were computed according to Leake et al. (1997) with the MinCal software, considering the maximum Fe^{3+} estimate obtained with the Schumacher's method (see Gualda and Vlach, 2005) and classified according the scheme of Hawthorne et al. (2012). The structural formulae for biotite was calculated on the basis of 11O, assuming all Fe as Fe^{2+} and its classification follows Rieder et al. (1998). Chlorite data was processed with the software WinCcac (Yavuz et al., 2015), considering 28O (Zang and Fyfe, 1995). This normalization allows a roughly estimate the Fe^{3+} and H_2O contents. Samples were classified according Guggenheim et al. (2007). Data for stilpnomelane were processed on the basis of 27O, normalizing the $Fe^{3+}/\Sigma Fe$ with the method of Malczewski and Popiel (2008) and its classification follows Hutton (1938).

2.3.2. LA-ICPMS analyses

Trace element analyses over amphiboles from 7 selected samples were performed both in spot and raster modes, totalizing 32 individual amphibole analyses. Elemental abundances were measured using a Thermo Scientific ICAP-Q spectrometer, coupled to a New Ware UP-213 LA system with a 213 nm Y(Nd)AlG laser. The NIST 610 glass was used as an external standard, and SiO_2 wt.% contents, measured with the EPMA, were used as internal standards. The ablations were done at 15-Hz pulse frequency with an energy fluence of ~2.14 J/cm^2 and a laser spot size of 80 μm (raster) or 55 μm (spot). The analysis consisted in of a ~60 s background measurement followed by data acquisition for ~60 s and dwell time of 8 ms for each isotope of the reported element, followed by 30 s of washout time. Raw data reduction were carried out using the Glitter software (Griffin, 2008).

2.3.3. Whole-rock geochemical analysis

Major and some trace elements were quantified by X Ray Fluorescence Spectrometry (XRF), using PANanalytical AXIOS MAX Advanced equipment, and following the method presented by Mori et al. (1999), while most trace elements were analyzed by ICP-MS, using the Perkin Elmer ELAN 6100DRC equipment, according to the method described in Navarro

et al. (2008). Normative compositions were computed considering Fe^{3+}/Fe_T = 0.5 with the *GCDkit* software (Janoušek et al., 2006).

2.4. Results

2.4.1. Mineral Textures

2.4.1.1. Amphiboles

Amphibole are the most abundant mafic phase in the whole Mandira Massif and occur in distinct magmatic and post-magmatic generations. The main textures of the peralkaline alkali feldspar granites, in which primary amphiboles are disposed interstitially to alkali-feldspar and quartz, point to an agpaitic crystallization sequence.

The amphiboles from the alkaline 1 association are homogeneously distributed as isolated crystals or as clusters of few crystals. Two main primary textural generations may be recognized: large euhedral prismatic crystals (up to 5 mm), present brownish-bluish pleochroic colors and are inclusion free (Figure 2-2A), while smaller euhedral to subhedral crystals (up to 2 mm) with dominant dark bluish colors sometimes present zircon inclusions Figure 2-2B). They often display subtle irregular zoning in BSE-images. A third, subordinate, generation appears as fine bluish acicular crystals or fibrous crystal aggregates closely associated with post-magmatic interstitial biotite crystals (Figure 2-2C).

In alkaline-2 association, amphibole appears homogeneously disperse as isolated or grouped crystals. Magmatic amphiboles form either euhedral large (4-6 mm) inclusions-free crystals with tabular habit and brownish-green pleochroism (Figure 2-2D), or euhedral and subhedral medium crystals (1-2 mm) showing large prismatic forms, dark blue pleochroism and inclusions of ilmenite and/or zircon (Figure 2-2E). Late- to post-magmatic amphiboles are interstitial between felsic minerals appearing either as fine-grained blue crystals with fibrous, acicular along margins of primary amphiboles (Figure 2-2F) or exhibit radiate textures in aggregates with biotite.

In the aluminous association, amphiboles are mainly magmatic phases. Mostly crystals occur as large euhedral tabular crystals (2-4 mm), with inclusions of magnetite along cleavages (Figure 2-2G). Some grains are partly replaced by biotite (Figure 2-2H). Distinct amphiboles appear as subhedral to anhedral medium-grained (1-2 mm) dark brown-green colored crystals.

They crystallize usually in poikilitic arrangement with quartz and magnetite inclusions, showing corroded limits and altered cores (Figure 2-2I).

2.4.1.2. Biotite

Biotite is the typical phyllosilicate in Mandira Massif and in general is associated with amphiboles in all crystallization stages. In the alkaline petrographic associations, biotite is mainly post-magmatic occurring in two textural types.

The alkaline 1 association present platy biotite with a brown to orange pleochroic scheme, which appears as subhedral and anhedral, individual or grouped small (2-4 mm) crystals with ilmenite, fluorite and zircon inclusions (Figure 2-3A), or forming crystal clusters, where it is partially replaced by riebeckite or hematite (Figure 2-3B). On the other hand, in the alkaline 2 association biotite is subhedral to anhedral (2-3 mm) with brownish-green pleochroism, depicts corroded margins, and contains inclusions of magnetite and zircon. The crystals occur in close relation with the sodic-calcic amphiboles, replacing them along rims (Figure 2-2C), or in aggregates with fluorite, ilmenite, magnetite and/or stilpnomelane.

Biotite is a typical primary phase solely in the syenogranites. It appears as euhedral do subhedral crystals (2-4 mm) with contrasted pale to dark green pleochroism (Figure 2-3D). Crystals may contain minute apatite, ilmenite, magnetite and zircon inclusions. In those samples where amphibole and biotite coexist, biotite replaces the calcic amphiboles and sometimes biotite aggregates form typical pseudomorphs after them, whereas when amphiboles absent (mainly in some samples from the central-northern stocks), biotite is interstitial to the felsic minerals, and appears partly to completely replaced by chlorite (Figure 2-2F).

The albitized granites by its turn present a distinct generation of biotite characterized by euhedral to subhedral fine-grained (up to 1 mm) crystals with a brownish-greenish pleochroism and platy or irregular forms (Figure 2-2E). Most crystals display a concentric zoning pattern with loss of pleochroism and core to rim increase of birefringence. They are commonly overgrown by fluorite or hematite.

2.4.1.3. Chlorite

Chlorite is the most common hydrothermal phyllosilicate in the syenogranites and associated greisens. In the syenogranites, chlorite occur as dark green pseudomorphs after

biotite (Figure 2-3F) or as interstitial grains associated with sericite, as a feldspar replacement product, while in the greisens, chloritization is the most extensive alteration type in these rocks, in which chlorite is in the form of pale-green fibrous platy intergrowths homogeneously distributed along the groundmass. This type of chlorite is usually coupled with sphalerite and chalcopyrite (Figure 2-3G).

2.4.1.4. Stilpnomelane

Stilpnomelane is an unusual post-magmatic phyllosilicate found in some granites of the both alkaline-2 and aluminous associations. In the alkaline-2 association, stilpnomelane occur either as isolated large irregular crystals (3-5 mm) with strongly dark-brown to green-pale pleochroism and displaying platy or radiated habit (Figure 2-3H), or as brownish acicular crystals replacing margins of primary sodic-calcic amphiboles (Figure 2-3I). Contrary, in the aluminous association stilpnomelane always form fine-grained fibrous brown crystals extensively distributed along discontinuities of primary feldspars.

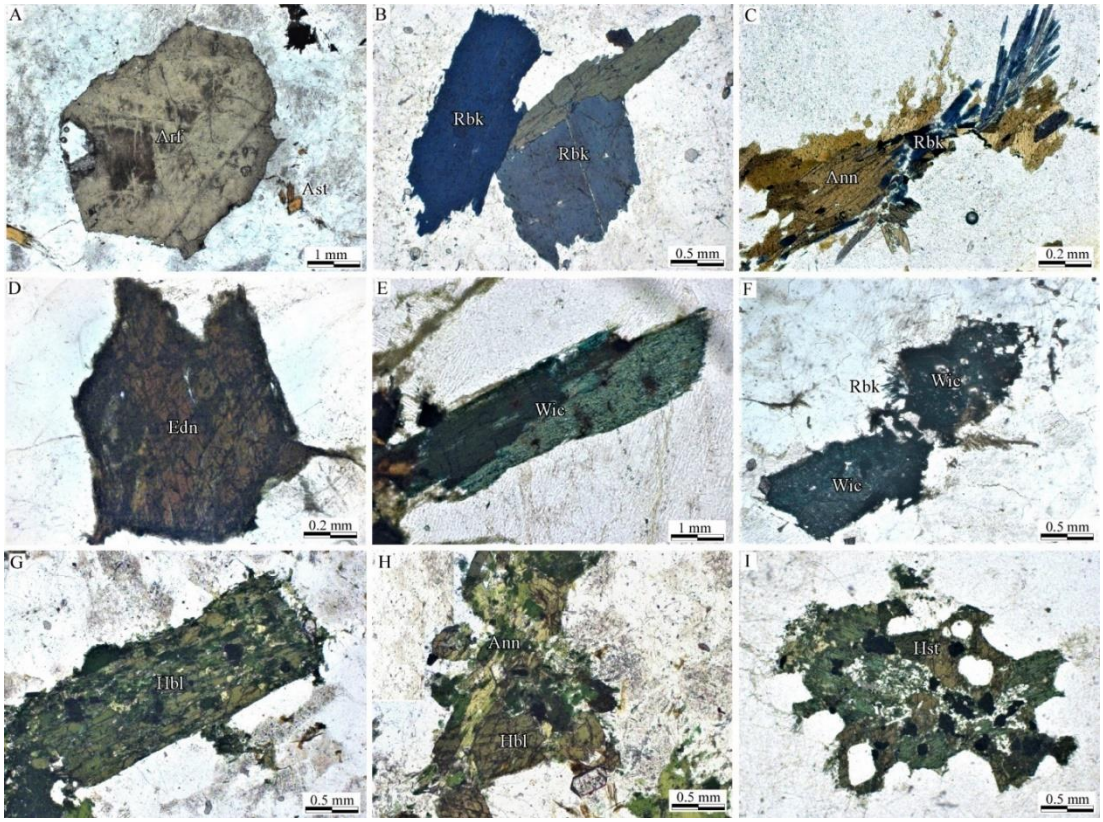

Figure 2-2: Microtextural features of amphiboles from the Mandira Massif Granite. All photomicrographs obtained under plane polarized light. A) Arfvedsonite (Arf) tabular megacrysts interstitial to alkali feldspar and quartz of the matrix (alkaline-1 association). B) Riebeckite (Rbk) large crystals with prismatic, tabular forms and corroded margins (alkaline-1 association). C) Post-magmatic riebeckite with fibrous habit intergrown with annite (Ann)

crystals (alkaline-1 association). D) Edenite (Edn) crystal with tabular form and subtle zoning (alkaline-2 association). E) Winchite large crystal showing strongly zoning pattern (alkaline-2 association). F) Winchite (Wic) crystals partially altered by riebeckite along margins (alkaline-2 association). G) Hornblende (Hbl) large crystal partially zoned and with magnetite inclusions (aluminous association). H) Hornblende partially replaced by annite overgrowths (Ann) along cleavage planes and fractures (aluminous association). I) Hastingsite (Hst) crystal with poikilitic texture showing magnetite inclusions and partially altered core (aluminous association).

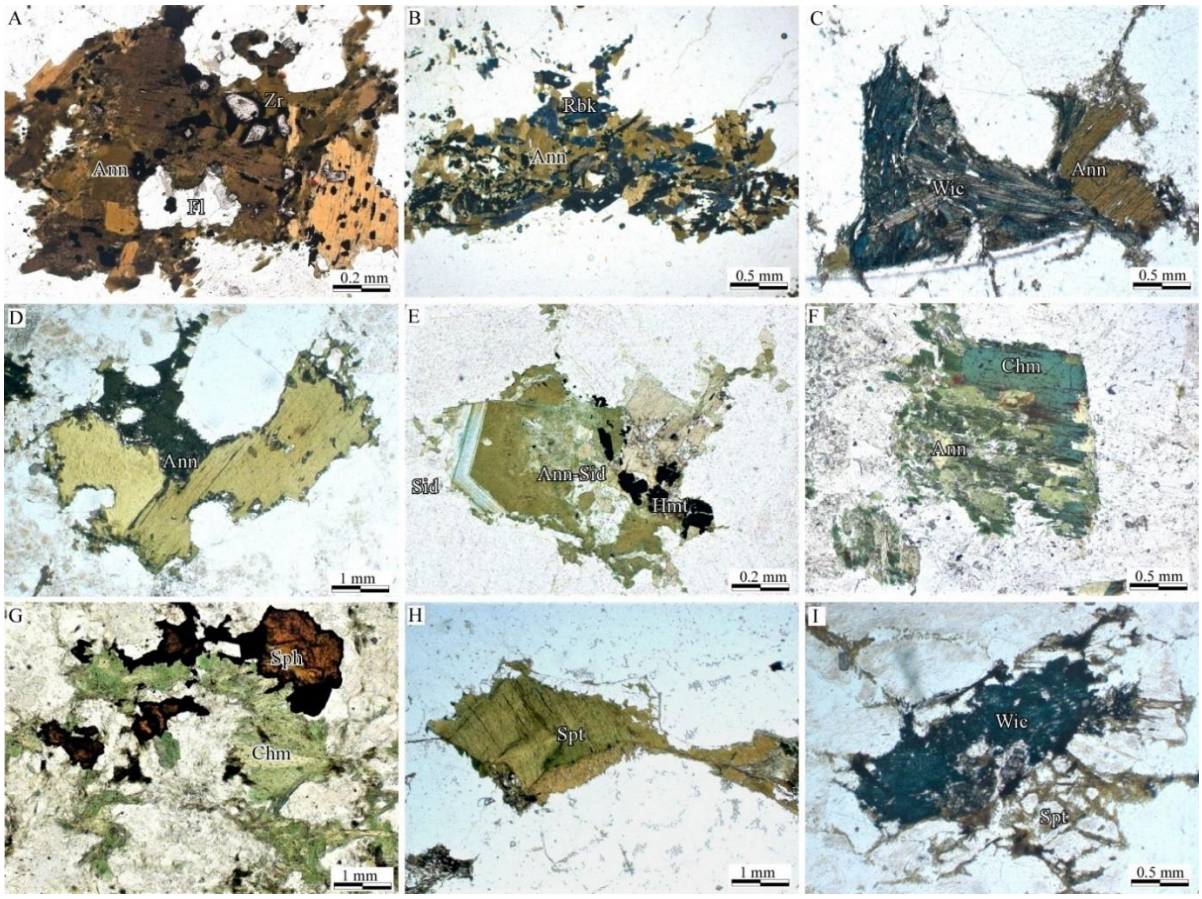

Figure 2-3: Microtextural features of phyllosilicates from the Mandira Massif Granite. All photomicrographs obtained under plane polarized light. A) Annite (Ann) interstitial crystals in aggregate including minute fluorite (Fl), and zircon (Zr) grains (alkaline-1 association). B) Typical assemblage of post-magmatic annite and riebeckite forming local aggregates random distributed in the groundmass (alkaline-1 association). C) Annite (Ann) intergrown around primary winchite (Wic) crystal (alkaline-2 association). D) Annite grouped crystals displaying platy habit and corroded margins (aluminous association). E) Annite-siderophyllite paragenetic association including fluorite (Fl) and hematite (Hem) grains (albitized granite). F) Pseudomorphic replacement of biotite by chlorite in syenogranite (aluminous association). G) Chlorite extensively intergrown with sphalerite in quartz-sericite greisen (aluminous association). H) Stilpnomelane irregular crystals displaying well-development of cleavage and partially corroded margins (alkaline-2 association). I) Stilpnomelane fine-grained fibrous crystals interstitial to feldspar and partially replacing winchite (Wic) crystals (alkaline-2 association).

2.5. Mineral Chemistry And Compositional Variations

Representative WDS chemical compositions and structural formulae for the studied minerals, as well as LA-ICP-MS data for amphiboles, are presented in Table 2-2 to Table 2-7 and discussed in the following; the complete data set is presented as supplementary materials.

2.5.1. Amphibole

2.5.1.1. Main compositional variations

The amphibole compositions from the Mandira Massif vary widely from calcic to sodic-calcic and sodic groups (Figure 2-4). The primary calcic varieties classify are ferro-edenite and ferro-hornblende (alkaline-2 association) and ferro-ferri-hornblende and hastingsite (aluminous association). Primary arfvedsonite and riebeckite are the main sodic amphiboles in the alkaline-1 association, while the sodic-calcic ferro-ferri-winchite is the main primary phase in the alkaline-2 association. Post-magmatic amphiboles correspond to ferro-actinolite in the Ca-amphibole bearing varieties of the alkaline-2 association and to riebeckite in all the peralkaline granites.

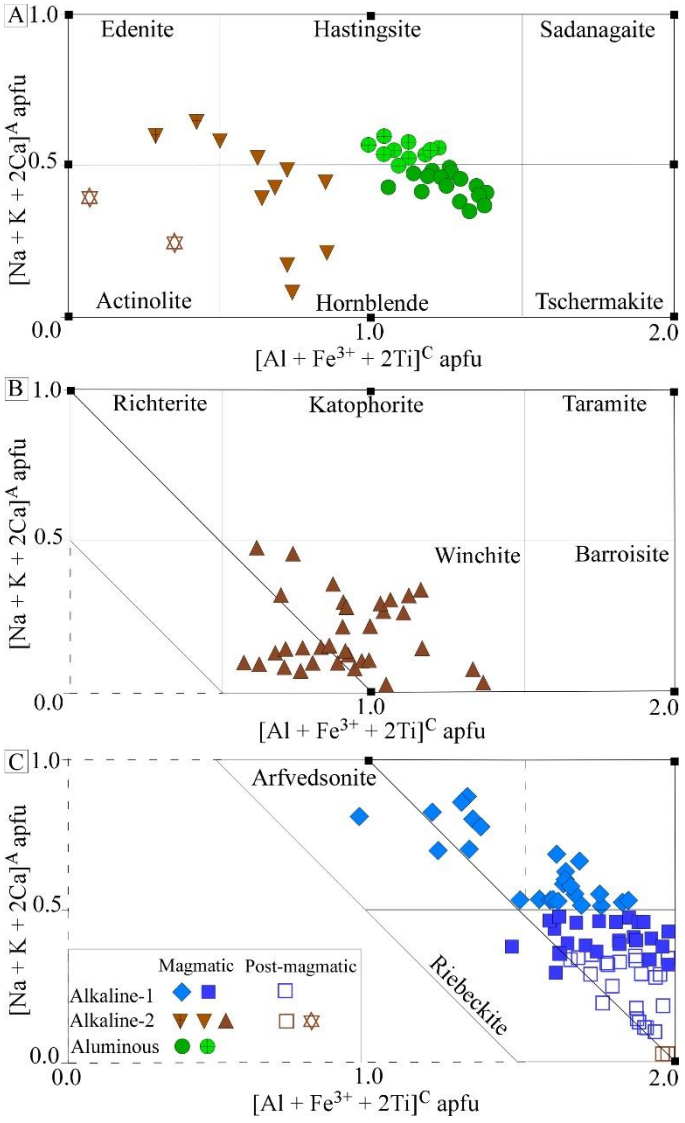

Figure 2-4: Classification diagrams (apfu) showing the amphibole groups: A) Ca-group, B) Na-Ca-group and C) Na-group and different types of amphiboles from the Mandira Massif Granite (after Hawthorne et al., 2012).

In most cases, the studied amphiboles show significant compositional variations (*cf.* Table 2-3, Table 2-4 and supplementary materials); the most typical are represented in the cationic diagrams depicted in Figure 2-5, which allow examine the main operating coupled cationic substitution schemes. Thus, comparing the primary calcic varieties from the alkaline-2 and aluminous associations, ferro-ferri-hornblende and hastingsite show the greatest Ca (up to 1.75 and 1.72), Al (up to 1.62 and 1.50), Ti (up to 0.22 and 0.23), F (up to 0.24 and 0.18) and Cl (up to 0.10 and 0.14) values in apfu, respectively, whereas the ferro-hornblende and ferro-edenite record intermediate to lower apfu values of Ca (up to 1.57 and 1.61), Al (up to 0.93 and 0.83), Ti (up to 0.12 and 0.17), F (up to 0.06 and 0.08) and Cl (up to 0.05 and 0.02), respectively (Table 2-4). Moreover, the Fe/Mg ratios are significantly higher in ferro-hornblende (18-101) and ferro-edenite (26-40) relative to the very low values of the ferro-ferri-hornblende (3-7) and hastingsite (3-12). Of note, the average amphibole *Fox* ratio [= $Fe^{3+}/(Fe^{3+}+Fe^{2+})$, cations] is rather higher 0.18 in the syenogranites as compared with the value of 0.08 for the alkaline-2 association (Table 2-4 and Figure 2-5A). The post-magmatic ferro-actinolite presents the lowest Ca (up to 1.52), Al (up to 0.23) and Ti (< 0.01) apfu values among all calcic varieties, however the F content are relative high (up to 0.10) and the Fe/Mg ratios are intermediate between the ferro-edenite and ferro-hornblende in the same samples from the alkaline-1 association.

The sodic-calcic ferro-ferri-winchite, dominant in the alkaline association 2, is distinguish by Ca (up to 1.49 apfu), Na (up to 1.37 apfu), Al (up to 0.8), Ti (up to 0.18) and with F and Cl reach 0.13 and 0.05 apfu values (Table 2-3). In comparison with primary calcic varieties of this association, the Fe/Mg and fox ratios largely varies between 13 to 129 and 0.09 to 0.26, respectively (Table 2-4 and Figure 2-5A). Moreover, in the zoned ferro-ferri-winchite crystals cores to rims compositions show enriched of Na (from 0.53 to 1.18 apfu), K (from 0.03 to 0.20 apfu), Al (from 0.11 to 0.80 apfu) and *Fox* ratios (from 0.09 to 0.26) as reflected by the cationic relationship between peralkaline [(Na+K)/Al] and *Fox* ratios with the Si+Na+K values (Figure 2-5A and Figure 2-5B).

Our EPMA analytical data for the sodic amphiboles present issues, as revealed by the systematic inappropriate cationic sums in the T- (> 8 apfu) and C-sites (≤ 5 apfu). These are relatively common features and are due mainly the presence of significant Li contents in such amphiboles (*e.g.* Hawthorne et al., 1994). In fact, our LA-ICP-MS results demonstrate Li contents in between ca. 1.500 and 2.500 ppm in arfvedsonite and riebeckite from the alkaline 1 association, in high contrast with the measured contents in the calcic (up to 40 ppm) and sodic calcic (up to 195 ppm) varieties (cf. Table 2-3). Our analytical results give average Li values of

0.30 and 0.26 apfu in the structural formulae of arfvedsonite and riebeckite, respectively (cf. Table 2-4). As there is a strong correlation between Li^{+} and Fe^{3+} for charge balance in the formulae (c.f. Hawthorne et al., 1994). our Li measurements allow a more accurate Fe^{3+} estimate and turns comparisons more reliable. Thus, arfvedsonite records the highest alkali contents (Na^{B} up to 1.99 and K up to 0.29 apfu), and moderately to high Fe^{2+} and Fe^{3+} (up to 4.19 and 1.69 apfu, respectively), while primary riebeckite shows lower Fe^{2+} values (up to 3.46 apfu), while Fe^{3+} is higher (up to 1.86 apfu). Some crystals show increase in both Na^{B} and Fe^{3+} from crystal cores to rims (see supplementary material). On the other hand, the post-magmatic riebeckite in the studied granites exhibits the highest Fe^{3+} (up to 2.29 apfu) values and, therefore, the highest fox ratios (up to 0.5) among all the sodic amphiboles.

The coupled cationic substitution schemes responsible for the main observed compositional variations of Mandira amphiboles are represented in Figure 2-5C and Figure 2-5D, may be summarized by the following reactions:

$$[Na + K]^{A} + [Fe^{2+}]^{C} \leftrightarrow [\square]^{A} + [Fe^{3+}]^{C} \qquad (2.1)$$

$$2[Ti + Zr]^{C} + [Mg + Fe^{2+} + Mn + Zn]^{C} + Al_{T} \leftrightarrow 3[Al + Fe^{3+}]^{C} + Si \qquad (2.2)$$

where the equation (2.1) represents the substitution of Fe^{2} by Fe^{3+} (*e.g.* Strong and Taylor, 1984) and the equation (2.2) accounts for substitutions occurring in the amphibole strcutral C-site (*e.g* Vilalva et al., 2016). Both reactions yield significant coefficients of determination ($0.88 \leq r^{2} \leq 0.92$). The behavior of the agpaitic or peralkalinity index [(Na+K)/Al] and the *fox* ratios *vs*. Si+Na+K trend (Figure 2-5A and Figure 2-5B), also describe significant chemical variations within the amphibole groups. Of importance, both the peralkaline and oxidation rates increase as the crystallization of the sodic-calcic and sodic amphiboles proceeds, resulting in the observed Na-Fe^{3+} increase towards crystal rims.

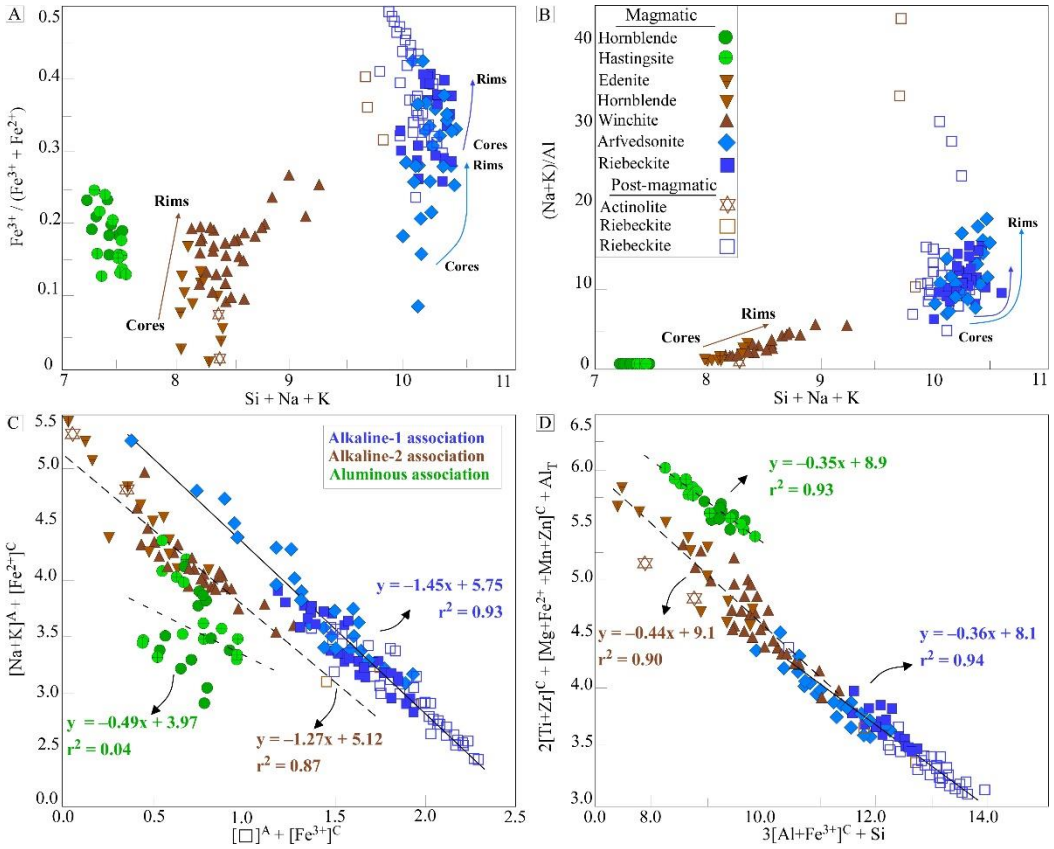

Figure 2-5: A-B) Compositional variations (apfu) of amphiboles from the Mandira granites. C-D) Coupled substitution plots showing the relationships between $[vacancy]^A + [Fe^{3+}]^C$ vs $[Na,K]^A + [Fe^{2+}]^C$ (after Strong and Taylor, 1984) and $3[Al, Fe^{3+}]^C + Si$ vs $2[Ti, Zr]^C + [Mg,Fe^{2+},Mn,Zn]^C + [Al]^T$ (after Vilalva et al. 2015).

2.5.1.2. Trace- and REE element compositions

Representative trace element analyses for the main amphibole types are listed in Table 2-3. Multielement and rare earth patterns are shown in Figure 2-6. Trace element patterns show corresponding strong negative Pb, Sr, Zr, Ti and V-Co anomalies, and slightly positive Rb and Nb anomalies for all amphibole-groups. Some differences are positive anomalies and significant abundances of Ta (up to 105 ppm) among calcic and sodic-calcic varieties from the alkaline-2 association, and of Li (up to 2533) in sodic amphiboles of the alkaline-1 association, whereas the calcic amphiboles in the aluminous association display negative and depleted values of Sn (up to 28 ppm).

REE patterns show contrasted behavior between the amphibole groups as well as within each group (Figure 2-6). In general, the total REE abundances increase from the sodic (up to 245 ppm) to the sodic-calcic (up to 524 ppm) and to the calcic varieties (up to 2665 ppm). The calcic-amphibole patterns in the aluminous and alkaline-2 associations are much contrasted: the first have much higher ΣREE (up to 7660 ppm or about one magnitude order) and the patterns

depicts a smooth LREE fractionation over the HREE ($6.3 \leq La_N/Yb/_N \leq 8.7$), as well fractionation in both the LREE and HREE sides, with $2.0 \leq La_N/Sm_N \leq 3.3$ and $1.3 \leq Gd_N/Lu_N \leq 2.4$ and Eu/Eu* ≅ 0.11. On the other hand, the second present a less fractionated pattern, and ΣREE up to 2064 ppm, with $0.4 \leq La_N/Yb/_N \leq 2.8$; the LREE side has a subtle concave shape, with $0.33 \leq La_N/Sm_N \leq 1.38$, while in the HREE side, with $0.9 \leq Gd_N/Lu_N \leq 2.1$, and subtle relative enrichment from Er to Lu is observed; the negative Eu anomaly is more pronounced with Eu/Eu* reaching 0.09.The sodic-calcic variety has much lower ΣREE (977 ppm or about two order of magnitude) than the calcic variety of the alkaline-2 association and LREE/HREE fractionation ($0.11 \leq La_N/Yb/_N \leq 4.6$), relative flatter LREE patterns $0.11 \leq La_N/Sm_N \leq 1.64$ and concave HREE pattern $0.5 \leq Gd_N/Lu_N \leq 1.4$ with discrete steep enrichment from Er to Lu; Eu anomalies ranges 0.04-0.17. Among the sodic amphiboles, afvedsonite and riebeckite record similar REE patterns, but riebeckite has higher ΣREE. REE profiles are relatively flat through the LREEs with a notice HREE enrichment ($0.07 \leq Gd_N/Yb_N \leq 0.34$) and slope up from Ho to Lu; Eu anomalies ranges 0.04-0.11.

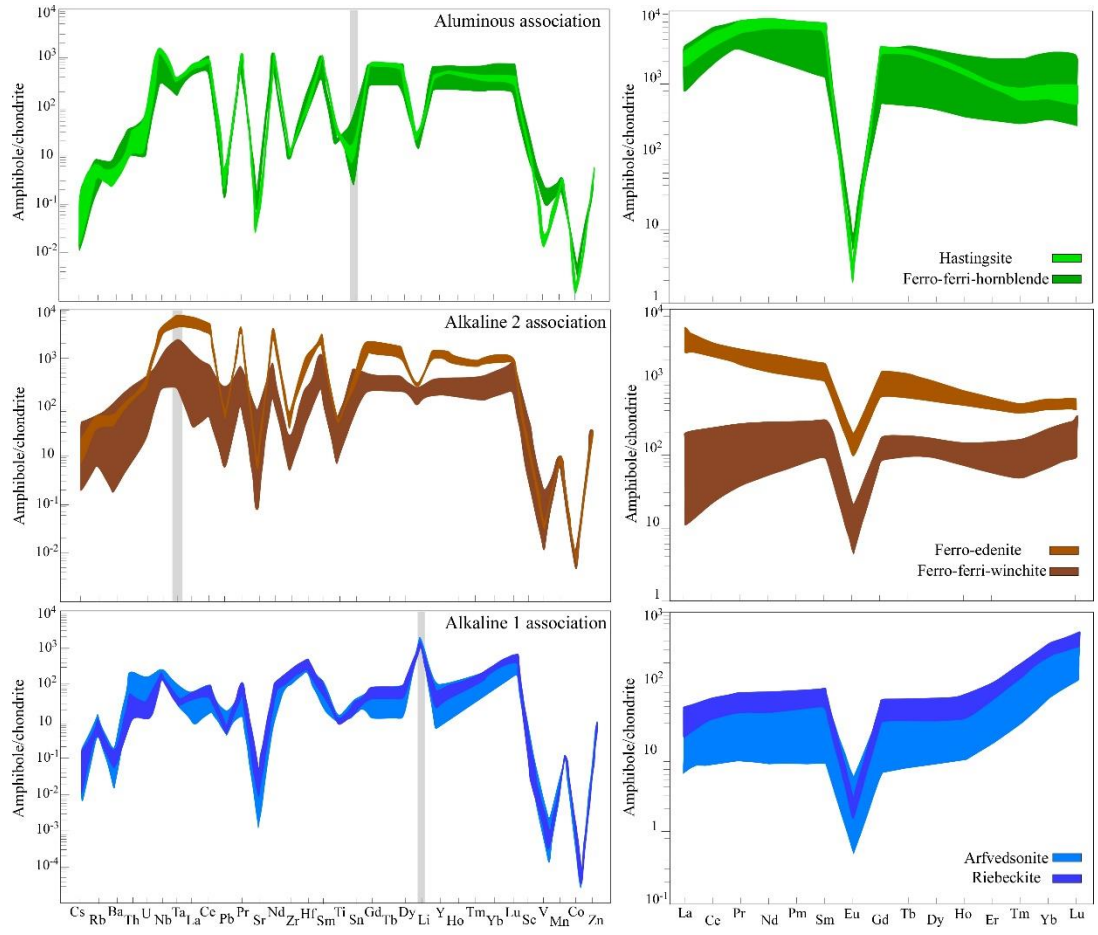

Figure 2-6: Chondrite-normalized trace element (left column) and REE patterns (right column) for amphiboles from the Mandira Massif Granite normalized to the chondrite values of McDonough and Sun (1995).

2.5.2. Biotite compositional variations

Representative biotite compositions are given in Table 2-5 and the Supplementary Materials. All biotite varieties from the Mandira Massif are iron-rich and classify as annite, however, ^{VI}Al and Fe# [Fe^{2+}/(Fe^{2+}+Mg)] show significant variability among these varieties (Figure 2-7). Primary annite in the aluminous association has ^{VI}Al and Fe# varies between 0.12 to 0.45 and 0.75 to 0.86 (apfu), respectively (Figure 2-7A); Mg, Ti, Zn reach values up to 0.62, 0.14 and 0.10 apfu and the volatiles up to 0.70 F and 0.48 Cl wt% (Table 2-5).

Late- to post-magmatic annites in peralkaline granites are relatively enriched in Fe and depleted in Al (Figure 2-7A). Annite in the alkaline-1 association has relatively higher values of both ^{VI}Al (up to 0.07 apfu) and the #Fe varies 0.98-0.99 (apfu), as well of Ti (up to 0.18), Mn (up to 0.13) and largely higher F up to 2.18 wt% contents (Figure 2-7C and Table 2-5). Annite in the alkaline-2 association record ^{VI}Al up to 0.76 and #Fe between 0.95 to 0.98, and Ti and Mn reaching 0.16 and 0.11 (apfu), respectively. Of note, Cl contents in the alkaline-2 annite are rather high up to 0.14 wt% whereas F is relatively depleted (up to 0.24 wt%) when compared to the alkaline-1 annite variety (Figure 2-7C).

Biotite in the albitized granites show contrasting compositions in comparison with the main Mandira units plotted between the annite-siderophyllite compositions (Figure 2-7A). This hydrothermal variety display systematic compositional variations between core to rim crystals reflected by the progressive increase of ^{VI}Al 0.35-0.51 (cores) to 0.38-1.14 (rims) as well of Ti 0.04 to 0.14 (cores to rims), but decrease of #Fe 0.98 (cores) to 0.93 (rims) and of Mn 0.07 to 0.02 (cores to rims). Interestingly, annite-siderophyllite crystals record the highest F contents from 2.21 (cores) to 3.24 (rims) among all biotite varieties (Figure 2-7C). Of note, the volatiles values within all biotite varieties are very similar with those measured in amphiboles from each Mandira facies as shown in Figure 2-7C, suggesting positive correlation between halogens distribution in amphiboles/biotites with magma compositions.

The most significant compositional variations in our biotite varieties, may be related to the siderophyllite exchange vector (Speer, 1984), given by the reaction:

$$(Fe^{2+} + Mg + Mn) \leftrightarrow Ti + {}^{VI}Al \qquad (2.3)$$

as shown in Figure 2-7D, which is mainly controlled by the siderophyllite exchange (Speer, 1984).

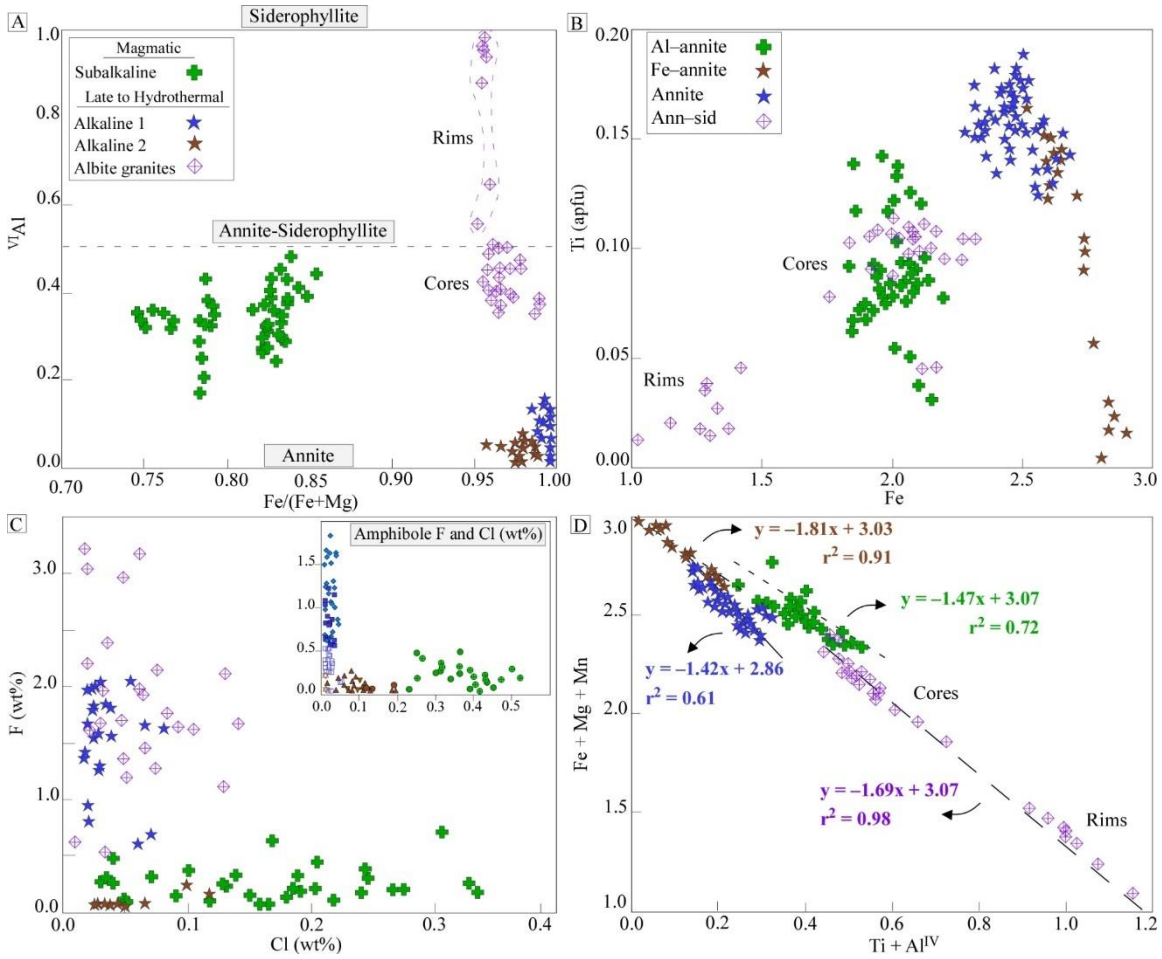

Figure 2-7: Compositional variations (apfu) of biotites from the Mandira Massif Granite. A) Classification ^{VI}Al vs Fe/(Fe+Mg) diagram, end members are after (Rieder et al., 1998). B) Binary plot of Ti vs. Fe. C) Chemical relationships of volatiles F and Cl contents (wt%) among biotites and amphibole-groups. D) Cationic substitution of Ti+^{VI}Al vs Fe+Mg+Mn according to Speer (1984).

2.5.3. Chlorite compositional variations

As expected, the analyzed chlorite varieties show relatively high Fe/Mg ratios and classify as chamosite (Figure 2-8A). The post-magmatic chlorite in the greisens records the highest Al_T contents (up to 5.93 apfu), as well as #Fe (up to 0.98), with Mg up to 0.21, ^{IV}Al up to 3.05 and ^{VI}Al up to 2.87, and Ti up to 0.02 (apfu), while in the aluminous syenogranites, these values are up to 5.45 Al^T, #Fe in between 0.85-0.87, ^{IV}Al and ^{VI}Al up to 2.91 and 2.58 respectively, and Ti up to 0.01 (Table 2-6). The estimated ^{VI}[Al+Fe^{3+}] are roughly constant and slightly higher in the chlorite from the greisens.

The main observed chemical variations should be described by the coupled substitution:

$$^{IV}Al + {}^{VI}Al \leftrightarrow Si + (Fe^{2+} + Mg) \qquad (2.4)$$

as suggested by Zane et al. (1998) and represented in Figure 2-8B, which form a compositional trend showing ^{IV}Al increase with evolution, as observed in the Al-rich chlorite crystals from the greisens.

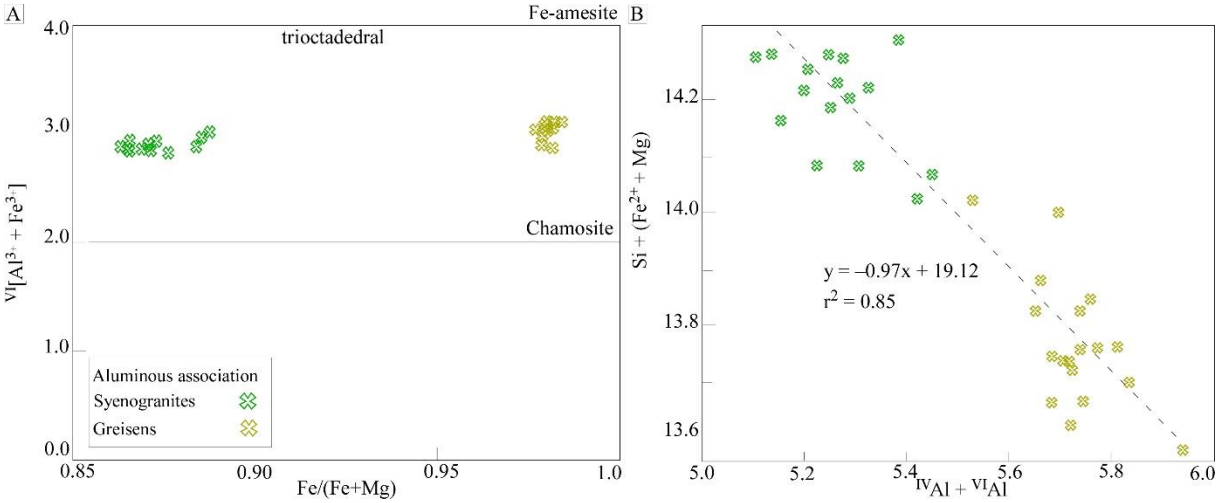

Figure 2-8_ Compositional variations (apfu) of chlorites from the Mandira Massif Granite. A) Classification VI [Al3++ Fe3+] vs Fe/(Fe+Mg) diagram (after Guggenheim et al. (2007). B) Cationic substitution of IVAl +VIAl vs Si + (Fe2+ + Mg) as suggested by Zane et al. (1998).

2.5.4. Stilpnomelane compositional variations

The post-magmatic stilpnomelane show high Fe compositions and according to the Fe^{3+}/Fe^{2+}partition all measured crystals were classify as ferristilpnomelane, however there are notice chemical differences between crystals from the alkaline-2 and aluminous association (Table 2-7). Stilpnomelane in the syenogranites record relatively high Al_T (up to 1.56 apfu), Mg (up to 0.64 apfu) and Mn (up to 0.31) contents whereas in the peralkaline granites Al, Mg and Mn values reach up to 1.26, 0.15 and 0.22 (apfu), respectively (Table 2-7); and thus, the Fe_T contest show a opposite behavior being higher in stilpnomelane from the alkaline-2 association (up to 5.69 apfu) than in the stilpnomelane from the syenogranites(up to 4.96 apfu). This is reflected in the relationship between the Al_T contents and the Fe/Mn ratios as shown in Figure 2-9A.

The main compositional variation of stilpnomelane among Mandira units may be described by the coupled substitution of the type:

$$^{IV}Al + {}^{VI}Al \leftrightarrow Si + (Fe + Mg + Mn) \quad (5)$$

as previously described by Eggleton (1972).

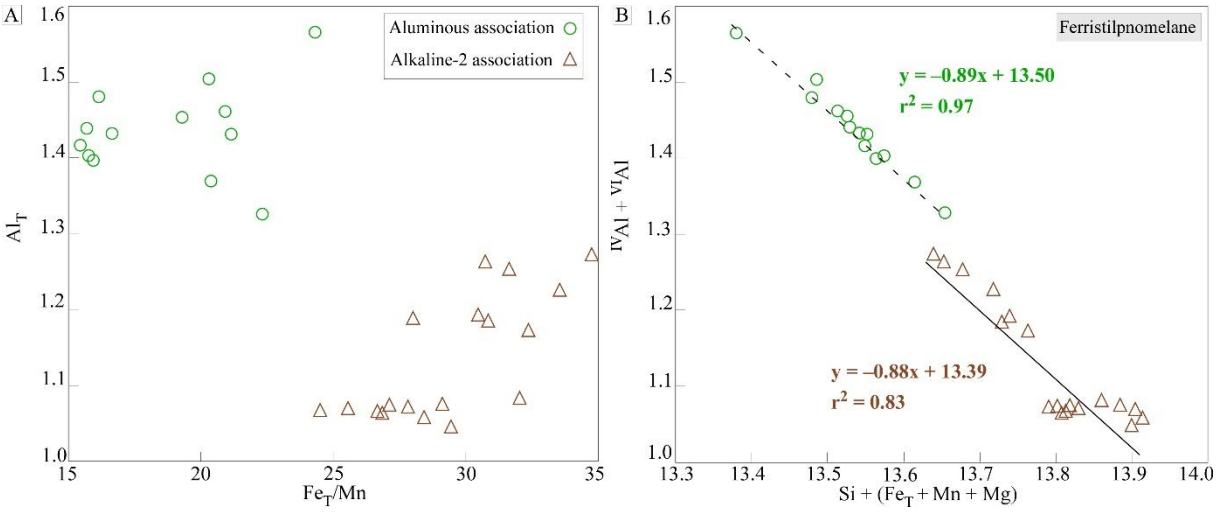

Figure 2-9: Compositional variations (apfu) of stilpnomelane from the Mandira Massif Granite. A) Binary plot of AlT vs Fe/Mn rarios. B) Cationic substitution of IVAl +VIAl vs Si + (Fe + Mn+ Mg) as suggested by Eggleton (1972).

2.6. Discussion

2.6.1. Estimates on crystallization conditions

2.6.1.1. Temperature and lithostatic pressure

Temperature and pressure estimates are in general more suitable for the syenogranites, due to compositional restrictions over the most common geothermobarometers (e.g. Holland and Blundy, 1994; Anderson and Smith, 1995; Molina et al. 2015). Our estimates are based on the concepts of zircon and apatite saturation in silica melts and related formalism as given by Watson and Harrison (1983), Harrison and Watson (1984) and Miller et al. (2003); as well as the amphibole-plagioclase thermobarometers of Holland and Blundy (1994) and Molina et al. (2015); in this latter case, only plagioclase with anorthite contents up to 10 mol.% were considered. To avoid analytical issues, we use solely our new whole-rock chemical data.

Zircon and apatite saturation temperatures give very similar values (T_{Zr} = 823°C and T_{Ap} = 816°C), which are interpreted as the best estimates to the close-to-liquidus temperatures for original aluminous melts. Close-to-solidus plagioclase-hornblende temperatures (Holland and Blundy, 1994) range in between 720 and 750°C, averaging 723 (±35) °C. These values, should be interpreted with caution, given the high Fe# (~0.81) values of our ferro-ferri hornblende and hastignsite, a fact that also prevent the use of the Al-in-hornblende geobarometers (cf. Anderson and Smith 1995).

Of note, Vilalva et al. (2019) obtained somewhat higher values for the alkali-feldspar granites from the alkaline-1 association, about 843 ±17°C, by using the Ti-in-zircon method of Ferry and Watson (2007), in agreement with the expected relatively low H_2O contents of the original melts that originated these rocks. In the case of peralkaline granites in general, qualitative estimates of the close-to-solidus temperature may be inferred obtained from their mineral mafic assemblages. Thus, given the presence of sodic-calcic and sodic-amphiboles, the maximum solidus temperatures are expected to be in between 655 and 750°C (Ernst, 1962, 1968; Scaillet and Macdonald, 2001).

Previous temperature estimates for the main hydrothermalism event in the massif presented by Oliveira (1989) based on the study of fluid inclusions in quartz from the associated greisens, which gave values in between 165 and 350°C. We try to apply the chlorite thermometry to add further data and to compared results. The available thermometers (Cathelineau and Nieva, 1985; Kranidiotis and MacLean, 1987; Cathelineau, 1988; Kavalieris et al., 1990; Hillier and Velde, 1991; Jowett, 1991; de Caritat et al., 1993; Zang and Fyfe, 1995; El-Sharkawy, 2000), give significant contrasted temperatures, however, the Al^{IV} geobarometers $TZF_{\text{-95AlIV}}$ and $TES_{\text{-00AlIV}}$ of Zang and Fyfe (1995) and El-Sharkawy (2000), respectively, yield comparable temperatures, in the ranges $TZF_{\text{-95AlIV}}$ = 266-279°C (syenogranites) and 263-283°C (greisens) and, $TES_{\text{-00AlIV}}$ = 244-256°C (syenogranites) and 239-255°C, (greisens). On the other hand, the calibrations considering a Fe/(Fe+Mg) correction over the Al^{VI} contents (*e.g.* Kranidiotis and Maclean, 1987; Jowett, 1991; Xie et al., 1997) resulted in significantly lower (down to 164) or higher (up to 661) values, incompatible with the fluid inclusions data. Thus, we consider the averages of $TZF_{\text{-95AlIV}}$ = 272°C and $TES_{\text{-00AlIV}}$ = 250°C (Figure 2-10A) as our best estimates.

The geobarometer of Molina et al. (2015), based on the Al-Si partitioning between plagioclase and amphibole from the syenogranites, gave pressures ranges 130-170 (±150) MPa, compatible with shallow emplacement levels. Despite the high uncertainty, this is currently our best estimated for the emplacement of these rocks at the Mandira Massif and, given the almost coeval nature of the intrusions, is extended for the whole massif. This is in agreement with the normative data for both alkaline and aluminous granite types, which plot, close to the 100-150 MPa cotetic lines in in the Qz-Ab-Or diagram (not shown), as well as with the observed textures (e.g. granophyric intergrowths between alkali-feldspar and quartz) and our previous inferences for the whole plutonism in the Graciosa Province, all of them pointing to relatively shallow (1-2 km) emplacement levels (c.f Gualda and Vlach, 2007a; Vilalva and Vlach, 2014).

2.6.1.2. Redox conditions

Quantitative estimates for the oxygen fugacity (f_{O2}) conditions during crystallization is hard task in rocks as those studied and, in most cases, solely qualitative information may be extracted (Figure 2-10C-B). Herein, we use both the Fe# numbers of calcic amphibole and biotite (Wones, 1981; Anderson and Smith, 1995; Anderson et al. 2008), and the *fox* ratios (*e.g.* Clowe et al., 1988; Papoutsa and Pe-piper, 2014; Vilalva et al., 2016) to provide some qualitative information. Of importance, the *fox* ratio is highly dependent of the adopted Fe^{3+}/Fe^{2+} partition scheme to compute the amphibole structural formulae and we chose to take the maximum ratios.

The syenogranites is the solely granites with the appropriated mineral assemblage controlling the Fe# values in amphibole and biotite. The high Fe# numbers of amphibole suggest crystallization at relatively low f_{O2} conditions (Figure 2-10B), while biotite Fe# values indicates conditions around $-1 \leq \Delta QFM \leq 0$, close the limits between the granite rocks from the ilmenite and the magnetite series (Figure 2-10C). On the other hand, the *fox* values for primary calcic and sodic-calcic amphiboles vary between 0.5 and 0.25 indicating low to moderate f_{O2} crystallization conditions, somewhat above the QFM buffer (Clowe et al., 1988) for both the aluminous and alkaline-2 granites. Of importance, the obtained estimates from the calcic amphiboles and biotites indicate that the aluminous rocks in the Mandira Massif were formed under relatively low $f_{O2,}$ as compared with other aluminous intrusions within the Graciosa Province ($0.08 \leq fox \leq 0.42$ and $0 \leq \Delta QFM \leq +3$, cf. Gualda and Vlach, 2007b, 2007c; Vilalva and Vlach, 2014).

In the case of the Li-bearing primary sodic amphiboles in the alkaline-1 association the *fox* values gradually increase from 0.20 to 0.40 pointing to high oxidizing conditions, up to above the MH buffer (*e.g.* Vilalva et al., 2016). This indicates crystallization conditions under conditions far more oxidizing than those inferred for the amphiboles from the alkaline-2 association and the syenogranites.

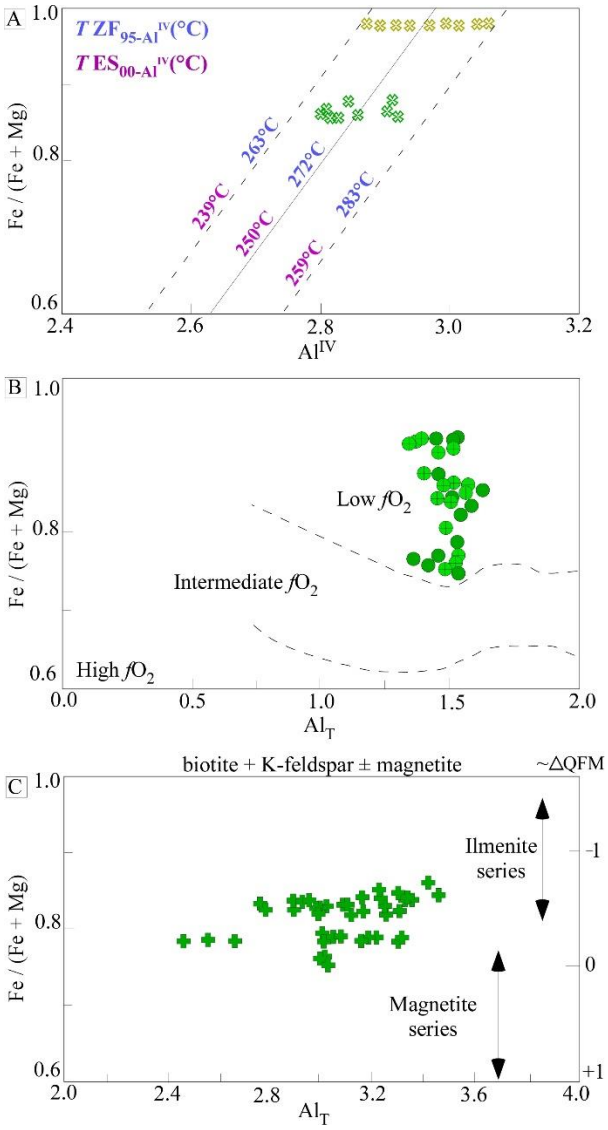

Figure 2-10: Diagrams with intensive crystallization parameters for Mandira granites. A) The corresponding AlIV chlorite geothermometers of (Zang and Fyfe, 1995) and (El-Sharkawy, 2000) for aluminous Mandira synogranites. Redox conditions estimates during the crystallization of Mandira granites in the AlT vs Fe/(Fe+Mg) plot (apfu) showing A) amphibole compositions with the approximate relative fO2 values according to Anderson and Smith (1995) and B) biotite compositions compared to the QFM buffer base on the calibration of Wones (1981) (PH2O = Ptotal), as suggested by (Anderson et al., 2008). Symbols as in Figure 2-4and Figure 2-6.

2.6.1.3. Volatile fugacities

The halogen contents of hydrous minerals are sensitive indicators to constrain physicochemical conditions of late-stage or post-magmatic fluids (Ayati et al., 2008; Siahcheshm et al., 2012; Idrus, 2018; Moshefi et al., 2018). The measured F and Cl contents in biotite are shown in Figure 2-11C and compared to those measured in amphiboles as mentioned in section 4.2. In order to discuss the behavior of halogens between magmatic and late- to hydrothermal annite types within the massif, we firstly show the correlation of the mole fraction of Mg (X_{Mg}) and and F (X_F) according to the principle of Fe-F avoidance of Munoz (1984) in

Figure 2-11A. The primary annites in the syenogranites present the highest values of the X_{Mg} (0.11-0.22) and X_F up to 0.033; hydrothermal annite-siderophyllite in albitized granites have intermediate X_{Mg} (0.01-0.03) and X_F up to 0.13 values between annites from syenogranites and peralkaline granites; finally late- to post-magmatic annite types in peralkaline granites show the lowest X_{Mg} and X_F values down to 0.03 and 0.06, respectively (see supplementary material). These results show that all annite types plot over the "Clusters" field in the X_{Mg} vs X_F diagram (Figure 2-11A), this behavior is generally ascribed to Fe- or F-rich biotite which indicates possible grouping of atoms (e.g. Fe-F, OH-OH) to minimize violations of the Fe-F avoidance (c.f Mason 1992).

The distribution of halogens in biotite depends also on the crystallization temperature (Munoz, 1992) and so, we may computed the halogen fugacity ratios as (f_{HF}/f_{HCl}) and (f_{H2O}/f_{HF}) for a given temperature. Considering our temperature estimates and that biotite is a relatively late phase in the magmatic crystallization, we chose for primary annite in the syenogranites a temperature of 750°C, whereas for the late- to post-magmatic annite-syderophyllite, we selected a temperature of 350°C. Our results vary in between $-4.3 \leq \log(f_{HF}/f_{HCl}) \leq -0.9$ and $4.3 \leq \log(f_{H2O}/f_{HF}) \leq 7.2$ and are depicted in Figure 2-11B. The calculated log fugacity ratios among all annite generations show progressive decrease of log (f_{HF}/f_{HCl}) ratios and increase of (f_{H2O}/f_{HF}) ratios with the transition between the magmatic to the late- and hydrothermal annite varieties, suggesting the strong dependence of temperatures to these parameters as well as the preference of F for the post-magmatic stages of crystallization. Accordingly, annite from the syenogranites record the highest log (f_{HF}/f_{HCl}) ratios up to -0.9 while these values in annite from peralkaline and albitized granites reach -2.1 and -2.9, respectively (*cf.* Supplementary Materials). Interestingly, annites from the alkaline-1 association have comparable log (f_{HF}/f_{HCl}) ratios to the present in annite-siderophyllite from the albitized granites in between -3.0 to -4.3 (Figure 2-11B).

Finally, additional evaluation of biotite-fluid equilibrium may be through the X_{Mg} vs. $\log(X_{F/XCL})$ diagram coupled to the fugacity halogen log (f_{HF}/f_{HCl}) ratios represented by the dashed lines as show in Figure 2-11C (e.g. Salazar-Naranjo and Vlach, 2018). In this diagram, we separated the different calculated log (f_{HF}/f_{HCl}) ratios at fixed 750°C (magmatic) and 350°C (hydrothermal) temperatures, as argue before. Magmatic annites in syenogranites show a relatively large dispersion between the -1 to almost -3 dashed lines, similarly, the late to hydrothermal annite-siderophyllites from the peralkaline (alkaline-1 association) and albiized granites are largely distributes between the -2 and -4 log (f_{HF}/f_{HCl}) lines, indicating that biotite-

fluid equilibrium is likely related to fluids of different compositions. In contrast, annites in the peralkaline granites from the alkaline-2 association plot over the log (f_{HF}/f_{HCl}) = -2, suggest an equal biotite-fluid equilibration.

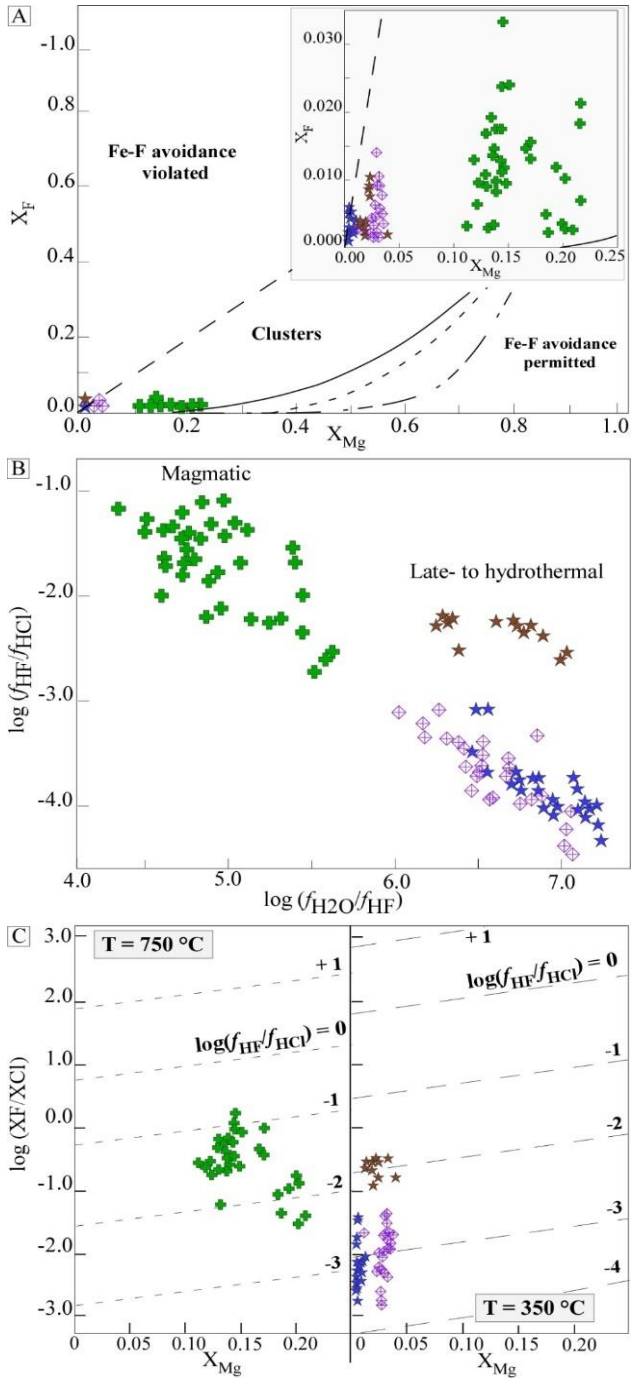

Figure 2-11:Volatile fugacities of biotite from Mandira Massif. A) Fe-F avoidance diagram showing the relationship between the Mg (XMg) and F (XF) mole fractions after Mason (1992). B) Fugacity ratios expressed as log(fHF/fHCl) vs. log(fH2O/fHF). C) Molar fraction of (Mg) vs. halogen mole fraction in hydroxyl sites. Equal ratio lines calculated following Munoz (1992), assuming biotite-fluid equilibrium at 750°C for primary annites and at 350°C for late- to post-magmatic annite-siderophyllite types (after Salazar-Naranjo and Vlach, 2018). Symbols as in Figure 2-6.

2.6.2. Evolution trends of amphiboles

Amphiboles are the most important ferromagnesian minerals in the Mandira granites and their compositional variations may become key indicators of the magmatic evolution in such silicic systems (e.g. Giret et al., 1980; Strong and Taylor, 1984; Mitchell, 1990; Larocque and Canil, 2010; Papoutsa and Pe-piper, 2014; Vilalva et al., 2015; Siegel et al., 2017). We examine such variations in the diagram Ca^{2+} + ^{IV}Al vs. (Si + Na + K) presented in Figure 12 and compared with the available data for other occurrences from the Graciosa Province. Three main groups are clearly seen in the diagram: a relatively homogeneous group of calcic amphiboles from the syenogranites; a compositionally expanded group with the calcic and sodic-calcic amphiboles from the alkaline association 2, which reinforces the previous established connection between the metaluminous Ca-amphibole bearing alkali-feldspar granites and the peralkaline varieties in this association; a relatively less expanded group with the sodic amphiboles from the main alkaline association 1 and the post-magmatic amphiboles from the alkaline association 2. Of note, there is a large compositional gap between the primary sodic-calcic amphiboles and the post-magmatic sodic riebeckite in the alkaline association 2, which is related to the late destabilization of ferro-ferri-winchite and replacement by riebeckite, in a contrasted Na-rich and more oxidizing environment (c.f. Giret et al., 1980). Similarly, Gualda and Vlach (2007c) reported a large compositional gap within alkaline plutons from the Serra da Graciosa among the province (Fig.12). In comparison with our data, this gap is related to compositional variations (cores to rims), such progressive increase in Na-Fe^{3+} toward the rims, between two amphiboles groups of calcic- to sodic and sodic-calcic to sodic compositions. Sodic amphiboles from the dominant alkaline association 1, vary from intermediate arfvedsonite/riebeckite compositions to an almost pure riebeckite end member, Again, the main factor responsible for this evolution is the progressive increase of Na and Fe^{3+} and consequent increasing peralkalinity and oxidizing conditions with evolution in these evolved melts and/or fluids, which leads to the substitution of arfvedsonite by riebeckite in the late- to post-magmatic crystallization stages, a trend in part comparable to those amphibole oxidation trends reported by Strong and Taylor (1984) and our typical post-magmatic riebeckite records the highest f_{O2} conditions.

Mandira amphiboles trends show some differences among the amphibole compositional trends previously reported within syenites and granites from the Graciosa Province. The homogeneous compositions of calcic-amphiboles in Mandira syenogranites reflect the shortest trend when compared to calcic-amphibole trends from the Orgãos/Capivari and Quiriri plutons

of aluminous behavior; despite the Mandira alkaline-2 trend show comparable trajectory (from calcic- to sodic-calcic and sodic compositions) with the alkaline-trend of the Farinha seca/Orgãos plutons, our alkaline-2 trend terminated is less differentiated reaching the pure end member riebeckite field; Mandira alkaline-1 trend partially overlap the trajectories from the Papanduva and Corupá peralkaline plutons, especially from the intermediated field of the arfvedsonite to riebeckite compositions. On the whole, the measured amphibole compositional variations reinforce the contrasted patterns of the alkaline association 1 and 2 of peralkaline alkali feldspar granites, as well as the syenogranites and the main unit grouping of Oliveira (1989). Furthermore, it is arguably suggested that the evolution of the peralkaline melts, particularly in the case of the association 2, was highly dependent on amphibole, while they exert a relatively less important role in the case of the syenogranites. In this context, the alkali-feldspar granites from the association 2 were formed from relatively more primitive and volatile-poor alkaline melts, as compared with those from the alkaline-1 association.

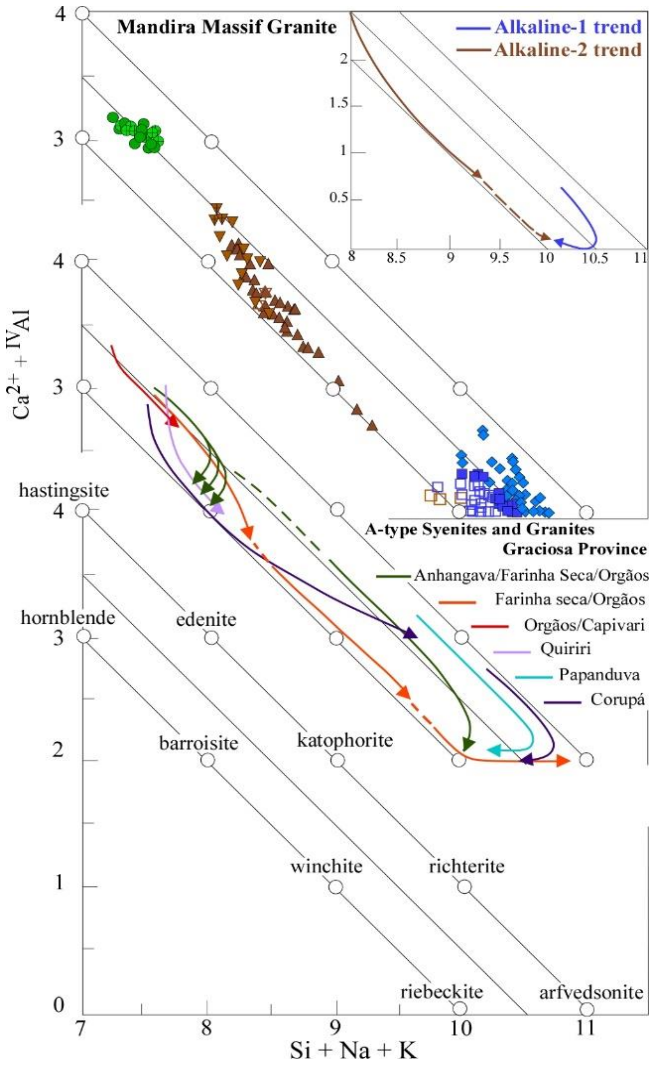

Figure 2-12: Cationic Si+Na+K vs. Ca+IVAl plot (apfu) for amphibole from the Mandira granites including other plutons from the Graciosa Province, as well as and compositional trends of amphibole reported in interesting localities worldwide. Symbols as in Figure 2-4.

2.6.3. REE partitioning

It is well known that trace elements and REEs incorporation in mineral structure is crystal-chemical controlled (Bottazzi et al., 1999; Hilyard et al., 2000; Tiepolo et al., 2000, 2007; Wood and Blundy, 2014; Shimizu et al., 2017). We apply the Lattice Strength Model (LSM; Blundy and Wood, 1994) to examine the REE partitions into the amphibole structure, starting from the computed amphibole-melt partition coefficients ($^{amph/L}D_{REE}$), as obtained with our amphibole and host whole-rock compositions. Previous alkali amphibole-melt partition studies demonstrated that REEs are incorporated in two crystallographic sites; the HREEs (Dy-Lu) and Sc occupy the 6-fold [M2] site, while the L-MREEs (La-Tb) concentrate in the larger 8-fold [M4] site (Bottazzi et al., 1999; Reguir et al., 2012; Vilalva et al., 2015; Vasyukova and Williams-Jones, 2019a). On the other hand, the REEs are incorporated in the single site the M4-site, substituting for Ca, in the case of the calcic amphiboles (Bottazzi et al., 1999; Hilyard et al., 2000). The obtained partition coefficients were fitted to the LSM using the software developed by Dalou et al. (2018); the best parameters are listed in Table 8 and represented in the Onuma-type diagrams in Fig. 13.

As expected, the partition coefficients are highest for ferro-ferri-hornblende and decrease progressively through ferro-ferri-winchite to riebeckite Figure 2-13; the fitted parabolic curves are somewhat distinct for alkali amphiboles, especially in the HREEs partition where the ferro-ferri-winchite show a large parabolic curve centered at a radius of 0.77 whereas the riebeckite curve is a little more close-fitted centered at 0.80. This could be explained by likely bimodal distribution of some of the MREE (Dy to Er) in both the M2 and M4 sites (c.f. Vasyukova and Williams-Jones, 2019). Moreover, distinct REE partitioning between Na-Ca and Na-rich alkali amphiboles may be related to the preference of REEs to charge-balance Na^{+} incorporation (Wood and Blundy, 1997). For example, Vilalva et al. (2015) show that higher Al contents in the melt also enhances REEs incorporation into the amphibole structure following the coupled substitution of $Si + Fe^{+3} + Na \leftrightarrow Al^{IV} + REE + Ca$. Our data correlate well with this equation, which gives a $r^2 = 0.97$ (not shown) supporting the high REE concentrations into the Al-Ca-richer ferro-ferri-winchite, whereas in riebeckite the

incorporation of the REEs could be probably limited by its relatively high contents of Na-Fe^{3+} (*e.g.* Siegel et al., 2017).

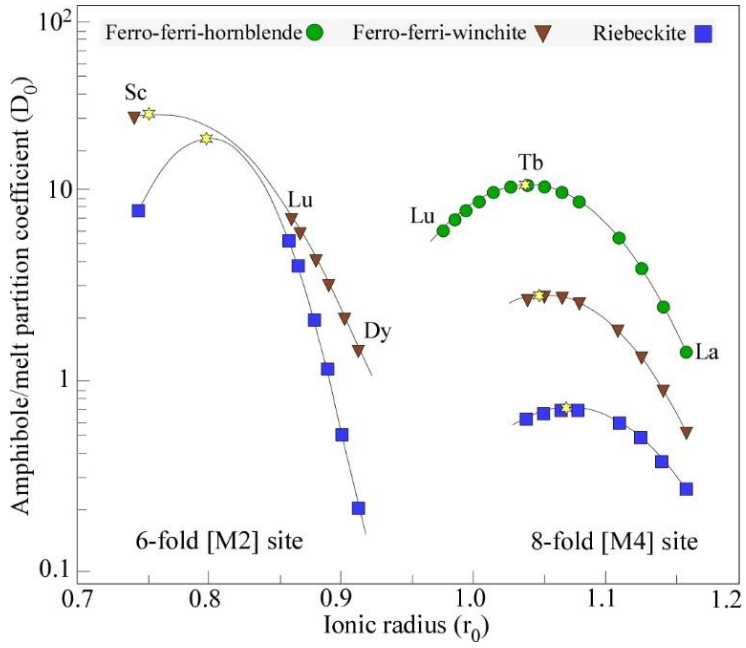

Figure 2-13: Amphibole-melt REE and Sc3+ partition coefficients calculated from representative amphiboles according to the Lattice Strain Model (LSM) which were calculated at P = 100 MPa and T = 700 °C, considering LREE and HREE partition into two different crystallographic sites except for hornblende. The yellow stars indicate the calculated radii for the two sites.

2.7. Final Remarks And Conclusions

The Mandira Massif Granite in the northern part of the Graciosa Province, southern Brazil include three granitic Mandira, Mandira 1 and Acaraú units. The studied samples from these units are peralkaline alkaline-feldspar granites grouped in two alkaline-1 and alkaline-2 associations (from Mandira and Acaraú units, respectively) and metaluminous to slightly peraluminous syenogranites of aluminous affinity (from the Mandira 1 unit). This contribution focused on the textural and chemical examination of amphibole-groups and phyllosilicates among representative samples of the mentioned units and provided significant information of magma composition, intensive crystallization parameters and mineralogical evolution of the massif. The most important inferences are listed as follows:

1) Amphiboles crystallized in both magmatic and late to post-magmatic stages of crystallization and have major compositions vary widely from calcic to sodic-calcic and sodic groups. The primary calcic varieties classify are ferro-edenite and ferro-

hornblende (alkali association 1) and ferro-ferri-hornblende and hastignsite (aluminous association). Primary arfvedsonite and riebeckite are the main amphiboles in the alkaline association 1 while the sodic-calcic ferro-ferri-winchite is the main primary phase in the alkaline association 2. Post-magmatic amphiboles correspond to ferro-actinolite in the Ca-amphibole bearing varieties of the alkaline association 2 and to riebeckite in all the peralkaline granites.

2) Trace element compositions of primary calcic, sodic-calcic and sodic amphiboles present relatively high abundances of LILE and HFSEs and significant high REE concentrations in the calcic varieties following by about 1 or 2 low concentrations in the sodic-calcic and sodic varieties. Moreover, REE partitions indicate strong preference of the LREEs for calcic amphiboles, contrary to the significant HREE-enrichment of sodic-calcic and sodic-amphiboles.

3) Biotite crystallized after amphibole in all Mandira units however it occurs as late- to post-magmatic phase in peralkaline granites while in the syenogranites biotite is a predominant primary phase. All biotite varieties from the Mandira Massif are iron-rich and classify as annite. A distinct variety was found in albitized granites within the massif and was classify as annite-siderophyllite of hydrothermal origin.

4) Calculated temperatures and lithostatic pressure for Mandira syenogranites indicated close-to-liquidus temperatures in between 816 and 823°C; close-to-solidus plagioclase-hornblende temperatures averaging 723 (±35) °C; and while chlorite-hydrothermal temperatures from these granites and related greisens point to values varies from 250°C and 272°C. The associated pressures of emplacement ranges 130-170 (±150) MPa, compatible with shallow (1-2 km) emplacement levels and were extended for the whole massif.

5) Estimation on redox conditions were made using the Fe# and *fox* ratios in primary amphiboles and biotite. In the case of syenogranites, the high Fe# numbers of calcic amphiboles suggest crystallization at relatively low f_{O2} conditions, while biotite Fe# values indicates conditions around $-1 \leq \Delta QFM \leq 0$, close the limits between the granite rocks from the ilmenite and the magnetite series. On the other hand, the *fox* values for primary calcic and sodic-sodic amphiboles suggest low to moderate f_{O2} crystallization conditions, somewhat above the QFM buffer for both the syenogranites and alkaline-1 granites. While for the Li-bearing primary sodic amphiboles in the alkaline-1

association the *fox* values gradually increase with magma evolution pointing to high oxidizing conditions, up to above the MH buffer and suggesting crystallization conditions far more oxidizing than those inferred for the amphiboles from the alkaline-2 association and the syenogranites.

6) Finally, calculated log (f_{H2O}/f_{HF}) halogen fugacity ratios among all annite generations show progressive decrease of log (f_{HF}/f_{HCl}) ratios and increase of (f_{H2O}/f_{HF}) ratios with the transition between the magmatic to the late- and hydrothermal annite varieties, suggesting the strong dependence of temperatures to these parameters as well as the preference of F for the post-magmatic stages of crystallization.

Acknowledgements

Staff do GeoAnalitica, FAPESP for financing this work (Proc. 2019/17343-4), (Proc. 08/00562-0) and (Proc. 2009/04321-0), and CAPES for the doctoral scholarship (Finance Code 001).

Table 2-1: Modal (point-counting, volume %) compositions of representative peralkaline and syenogranites from the Mandira Massif Granite

Unit	Mineral															
	Afs	Qz	Pl	Ab	Amp	Bt	Mag	Ilm	Zrn	Ap	Aln	Ast	Chv	Tnt	Fl	Sc. Min.
Mandira MAN-13	54	30	-	3	7	-	-	1	1	-	-	2	-	-	1	1
Mandira 1 MAN-5	41	31	10	2	3	6	2	-	1	0.5	1	-	-	-	0.5	2
Acaraú MAN-9	53	32	-	2	5	1	1	-	1	0.5	1	-	1	0.5	1	1

Mineral abbreviations of rock-forming minerals from Whitney and Evans 2010; Ast: Astrophyllite; Chv: Chevkinite; Sc. Min: Secondary Minerals

Table 2-2: Major (X-ray powder diffratometry) and trace element (ICP-MS) geochemical compositions of representative peralkaline and syenogranites from the Mandira Massif Granite

	X-ray fluorescense (XRF)		
Samples	MAN-13A	MAN-5	MAN-9A
Unit	Mandira	Mandira 1	Acaraú
SiO_2 (wt%)	77.33	76.31	75.92
TiO_2	0.12	0.15	0.11
Al_2O_3	10.93	11.62	11.81
Fe_2O_3	1.99	1.51	1.95
MnO	0.03	0.02	0.03
MgO	0.01	0.05	0.00
CaO	0.24	0.55	0.31
Na_2O	3.99	3.33	4.25
K_2O	4.49	5.11	4.64
P_2O_5	0.00	0.01	0.00
LOI	0.40	0.46	0.30
Total	99.53	99.12	99.32
Fe#	0.99	0.97	1.00
A/CNK	0.91	0.96	0.93
A.I	1.05	0.95	1.03
T(°C)sat(ap)	n.c	789.36	n.c
T(°C)sat(zr)	894	812	844
Q*	38.58	37.73	33.91
Mag*	1.43	0.28	0.21
Ilm*	0.23	1.10	1.25
Zn (ppm)	173	59	182
Ga	27	18	25
Cr	14	<13	21
F	2913	2813	4181

LOI: lost on ignition; Fe#: FeOt/(FeO+MgO); A.I Agpaitic Index; Q*, Mag*, Ilm*: normative quartz, magnetite, ilmenite; Tsat(zr) and Tsat(ap): zircon and apatite saturation temperatures nc: not calculated

	Inductively coupled plasma mass spectrometry (ICP-MS)		
Samples	MAN-13A	MAN-5	MAN-9A
Unit	Mandira	Mandira 1	Acaraú
Sc (ppm)	0.5	2.8	0.9
Rb	238	167	160
Sr	4.8	59.4	4.9
Y	225	66.9	74.5
Zr	553	462	358
Nb	56.2	35.6	37.7
Cs	3.7	3.0	2.6
Ba	0.6	570	46.0
La	45.3	116	90.8
Ce	111	222	177
Pr	17.2	23.8	20.5
Nd	81.8	85.8	77.5
Sm	27.3	14.6	14.8
Eu	0.4	1.0	0.5
Gd	35.0	11.7	12.8
Tb	6.0	1.8	2.1
Dy	36.3	10.4	11.7
Ho	7.8	2.2	2.5
Er	21.1	6.4	7.3
Tm	2.8	1.0	1.1
Yb	16.2	6.4	6.9
Lu	2.1	1.0	1.0
Hf	20.3	12.1	11.0
Pb	32.1	17.3	20.9
Th	18.9	18.4	12.8
U	4.0	3.1	2.1
REE	410	504	426

Table 2-3: Major and trace element compositions for amphiboles from the Mandira Massif Granite

Samples	**13A2**	**13A2**	**13A2**	**4777**	**4777**	**4777**	**5**	**5**	**5**	**6724**	**6724**	**6724**	**5579**	**5579**	**5579**
Point_ID	11	17	20	1	4	5	1	2	4	1	2	3	1	5	8
Group	Sodic						Calcic						Sodic-calcic		
Unit	Mandira (Alkaline 1)						Mandira 1 (Aluminous)						Acaraú (Alkaline 2)		
SiO_2 (wt%)	49.96	49.62	50.15	47.22	49.01	51.71	41.78	41.96	41.83	41.75	41.28	41.21	48.27	47.24	44.27
TiO_2	1.00	0.88	0.38	1.38	0.32	0.08	1.92	1.12	1.83	1.83	1.77	1.75	0.12	0.40	1.00
Al_2O_3	0.93	0.92	0.85	1.37	1.24	0.95	8.40	8.04	8.54	7.38	7.39	7.55	2.30	3.14	4.91
FeO^T	34.58	33.17	35.28	33.13	34.31	35.68	27.37	27.84	27.93	32.60	32.81	33.09	35.25	34.43	33.70
MnO	0.36	0.42	0.32	0.29	0.27	0.29	0.83	0.93	0.77	0.66	0.68	0.67	0.50	0.53	0.57
MgO	0.05	0.04	-	0.06	-	0.03	3.50	3.63	3.33	1.58	1.64	1.53	0.31	0.68	0.43
CaO	0.18	0.16	0.02	1.62	2.51	0.03	9.98	10.10	10.03	10.06	10.06	9.83	7.82	8.06	8.86
ZrO_2	-	0.27	-	-	-	-	-	0.01	0.13	-	-	-	-	0.03	-
ZnO	-	0.58	-	0.27	0.37	0.33	0.07	0.13	-	0.12	0.17	0.17	0.24	0.36	0.29
Na_2O	7.09	7.36	7.17	7.26	7.08	7.54	1.81	2.02	1.42	1.77	1.57	1.57	2.19	2.18	2.26
K_2O	1.18	1.19	1.15	0.93	0.89	1.22	1.12	0.94	1.07	1.22	1.20	1.17	0.42	0.85	0.94
F	1.15	0.99	0.93	1.49	2.25	0.54	0.25	-	0.06	-	-	0.17	0.01	0.03	0.12
Cl	0.01	0.01	0.02	-	0.04	-	0.36	0.22	0.39	0.42	0.35	0.47	0.08	0.11	0.19
Sum	96.96	96.036	96.61	95.453	98.799	98.86	97.417	96.958	97.33	99.389	98.9349	99.199	97.54	98.085	97.58
O=F=Cl	0.486	0.417	0.397	0.626	0.957	0.229	0.186	0.050	0.111	0.095	0.079	0.177	0.021	0.037	0.092
Total	96.47	95.62	96.208	94.827	97.842	98.631	97.231	96.909	97.219	99.294	98.8554	99.023	97.519	98.048	97.49
Li (ppm)	2166	1999	1569	2059	2429	2135	26.49	30.46	27.11	39.28	35.27	33.93	186.69	170.37	192.16
Be	12.98	16.83	23.68	43.45	15.4	21.05	11.99	8.99	17.14	30.07	20.02	12.78	42.65	51.48	140.58
Sc	1.08	1.05	1.89	7.91	1.272	1.11	91.96	65.91	53.79	45.16	55.60	49.47	25.95	124.74	21.96
V	0.38	0.30	0.54	1.263	0.256	0.107	59.14	89.03	69.21	11.01	15.45	7.52	2.00	22.09	3.49
Ga	9.55	11.18	11.89	12.52	12.46	12.61	37.33	34.71	41.36	58.51	51.80	51.47	18.46	34.36	46.91
Rb	14.70	15.04	13.37	14.03	26.88	10.91	12.66	5.18	9.24	15.04	9.62	11.69	17.25	20.36	11.86
Sr	0.23	0.73	3.25	0.508	0.1112	0.257	9.30	9.46	10.44	2.46	2.44	2.45	11.89	3.06	1.21
Y	10.85	41.20	70.60	54.07	19.55	101.36	663.03	472.78	685.27	696.78	671.72	687.58	125.23	229.78	331.57
Zr	1778	666.87	513.11	716.9	702.33	483.33	94.68	87.66	94.06	101.95	107.24	107.02	59.71	103.64	71.20
Sn	45.82	37.58	41.42	21.38	62.21	23.5	4.35	5.57	10.55	28.02	17.60	11.97	448.48	27.07	574.14
Ba	1.52	3.67	20.84	1.164	0.898	0.757	19.72	14.01	26.53	8.18	11.78	11.65	13.76	3.51	0.75
La	0.99	6.43	11.67	14.14	2.12	11.68	179.72	180.28	119.35	127.91	171.12	169.80	12.65	55.29	48.23
Ce	5.19	29.03	44.90	52.36	9.18	47.5	630.91	586.59	469.73	464.57	544.31	537.66	38.40	164.04	186.50
Pr	0.93	5.23	8.18	8.6	1.603	8.43	104.60	86.64	90.71	87.17	105.53	102.72	8.04	25.55	33.45
Nd	4.42	25.42	39.14	41.88	8.01	45.23	523.27	392.25	462.99	459.96	541.33	528.10	47.37	119.95	171.23
Sm	1.82	10.03	13.94	13.49	2.89	17.16	151.43	98.55	146.01	145.07	159.09	162.25	22.08	35.58	57.04
Eu	0.02	0.13	0.20	0.214	0.0527	0.283	1.79	1.80	1.97	1.05	1.45	1.42	0.42	0.40	1.02
Gd	1.61	8.51	11.39	11.04	2.49	16.19	137.35	86.16	133.40	136.29	139.45	150.72	24.16	33.32	48.26
Tb	0.42	1.59	2.10	2.057	0.525	3.000	24.44	15.45	23.30	24.30	25.11	26.24	4.78	7.17	8.82
Dy	3.26	10.47	14.43	12.59	4.000	19.87	146.47	94.85	136.36	142.43	147.69	156.68	28.61	51.25	54.05
Ho	0.95	2.58	3.71	3.72	1.244	4.86	28.12	19.03	27.54	26.67	27.73	29.01	5.03	10.67	10.21
Er	5.43	13.39	15.68	13.44	6.63	19.57	66.83	48.95	70.81	66.69	68.49	68.71	11.47	31.35	27.34
Tm	2.04	4.21	4.26	3.61	2.274	4.82	8.58	6.96	9.70	9.64	9.21	8.87	1.49	5.25	5.03
Yb	29.84	55.28	51.27	39.49	31.85	55.86	54.33	45.96	66.48	66.43	62.31	57.82	13.91	47.83	49.92
Lu	7.16	12.68	11.02	9.00	7.75	11.67	6.77	6.18	8.80	10.23	9.35	8.94	3.45	9.66	10.21
Hf	56.22	26.75	26.06	28.52	31.53	19.36	6.17	5.85	7.48	7.54	9.35	8.85	7.49	9.44	11.26
Ta	0.06	0.54	0.56	0.975	0.361	0.412	2.43	2.61	3.20	4.58	4.93	4.64	3.44	3.09	24.54
Pb	9.55	12.22	13.27	13.24	17.7	20.68	4.28	3.79	8.24	7.29	16.17	6.67	7.49	10.82	26.70
Nb	12.66	39.05	48.46	62.65	31.41	38.73	148.97	124.37	151.31	318.33	364.05	335.91	57.79	275.55	293.41
Th	0.04	0.09	0.72	1.914	1.617	0.971	0.53	0.31	1.00	0.44	0.37	0.43	0.68	3.12	0.28
U	0.03	0.03	0.24	0.557	0.617	0.406	0.14	0.08	0.18	0.25	2.10	0.13	0.56	0.35	0.03
REE+Y	74.936	226.18	302.49	279.7	100.17	367.48	2727.6	2142.4	2452.4	2465.2	2683.89	2696.5	347.09	827.09	1042.9

EMPA major oxides (in wt. %) and LA-ICPMS trace element compositions (in ppm); -: below detection limit

Table 2-4: Structural formula for amphiboles from the Mandira Massif Granite

Samples	**4777**	**13A2**	**5574**	**5**	**5**	**5**	**6728**	**6728**	**5579**	**9A**
Crystal	c1	11	c5	c2	c3	c8	c1	c5	c1	
Point_ID	1-c	11-c	5-c	1-c	6-c	10-i	1-c	5-r2	1-c	
Mineral	Arfvedsonite	Riebeckite	Riebeckite	Ferro-Hornblende	Ferro-ferri-Hornblende	Hastingsite	Ferro-Edenite	Ferro-Actinolite	Ferro-ferri-Winchite	Riebeckite
Unit	Mandira (Alkaline 1)			Mandira 1 (Aluminous)			Acaraú (Alkaline 2)			
Structural formula based on 23O										
Si (apfu)	7.736	7.829	7.785	6.6202	6.661	6.708	7.195	7.774	7.674	8.066
^{IV}Al	0.264	0.171	0.215	1.3798	1.339	1.292	0.805	0.226	0.326	0.000
T-site	**8.000**	**8.000**	**8.000**	**8.0000**	**8.000**	**8.000**	**8.000**	**8.000**	**8.000**	**8.066**
^{VI}Al	0.000	0.000	0.281	0.1896	0.135	0.238	0.036	0.000	0.105	0.052
Ti	0.170	0.118	0.018	0.2291	0.112	0.192	0.120	0.000	0.014	0.000
Fe^{3+}	0.970	1.769	1.552	0.5663	0.742	0.436	0.398	0.359	0.794	1.539
Zr	0.000	0.000	0.002	0.0001	0.002	0.004	0.000	0.000	0.000	0.002
Zn	0.033	0.000	0.049	0.0082	0.014	0.008	0.024	0.039	0.028	0.029
Mg	0.015	0.012	0.008	0.8279	0.557	1.121	0.244	0.093	0.073	0.032
Li	0.204	0.289	nc	0.0054	0.000	0.003	0.000	nc	0.026	nc
Fe^{2+}	3.569	2.763	3.030	3.0606	3.313	2.937	4.178	4.509	3.892	3.346
Mn^{2+}	0.040	0.048	0.060	0.1118	0.126	0.059	0.000	0.000	0.067	0.000
C-site	**5.000**	**5.000**	**5.000**	**5.000**	**5.000**	**5.000**	**5.000**	**5.000**	**5.000**	**5.000**
Fe^{2+}	0.000	0.000	0.000	0.0000	0.000	0.000	0.115	0.101	0.000	0.027
Mn^{2+}	0.000	0.000	0.000	0.0000	0.000	0.000	0.087	0.082	0.000	0.035
Li	0.088	0.005	nc	0.000	0.000	0.000	0.000	nc	0.000	nc
Ca	0.285	0.030	0.011	1.6948	1.752	1.706	1.533	1.450	1.332	0.130
Na	1.627	1.965	1.989	0.3052	0.248	0.294	0.24	0.367	0.668	1.741
B-site	**2.000**	**2.000**	**2.000**	**2.000**	**2.000**	**2.000**	**2.000**	**2.000**	**2.000**	**1.934**
Na	0.679	0.189	0.144	0.2498	0.255	0.310	0.45	0.156	0.007	0.000
K	0.194	0.236	0.188	0.2254	0.229	0.211	0.186	0.079	0.085	0.013
A-site	**0.873**	**0.425**	**0.332**	**0.475**	**0.484**	**0.521**	**0.636**	**0.235**	**0.092**	**0.013**
Cations	15.873	15.425	15.332	15.475	15.406	15.521	15.637	15.235	15.092	15.013
F	0.770	0.570	0.380	0.1239	0.131	0.158	0.085	0.107	0.004	0.020
Cl	0.000	0.002	0.003	0.0976	0.0827	0.096	0.027	0.002	0.021	0.000
FC (Max)	8SiAl	8SiAl	13eCNK	13eCNK	13eCNK	13excCNK	8SiAl	8SiAl	13eCNK	15eCK
Fe#	0.997	0.997	0.998	0.814	0.879	0.751	0.951	0.982	0.985	0.994
^{A}[Na+K+2Ca]	0.873	0.425	0.332	0.475	0.484	0.521	0.567	0.235	0.092	0.013
^{C}[Al+Fe^{3+}+2Ti]	1.310	2.004	1.870	1.214	1.100	1.058	0.601	0.359	0.928	1.956
[Ca^{2+}+^{IV}Al]	0.100	0.201	0.226	3.075	3.183	2.997	2.362	1.676	1.658	0.175
[Si+Na+K]	10.460	10.219	10.106	7.401	7.222	7.524	8.036	8.376	8.434	9.683
[Na+K]/Al	18.023	13.976	4.679	0.497	0.435	0.533	1.043	2.660	1.763	33.593
Fe^{3+}/(Fe^{3+}+Fe^{2+})	0.332	0.390	0.339	0.156	0.234	0.129	0.078	0.072	0.170	0.403

Structural formulae (in apfu) for amphiboles from the Mandira Massif. Point_ID: spot identification; c: core; r: rim; i: intermediate zone

Table 2-5: Major compositions and structural formula for biotite from the Mandira Massif Granite

Sample	**5574**	**6735**	**2A**	**5**	**14A**	**6780**	**9A**	**5579**	**6728**	**25F**	**6666B**	**6666B**
Crystal	c1	c2	c1	c1	c5	c1	c1	c2	c3	c2	c5	c7
Point_ID	1-r2	2-r1	2-c	1-c	1-c	1-c	1-i	2-c	3-c	2-c	5-r1	7-r1
Mineral	Fe-annite			Al-annite			Fe-annite			Annite-siderophyllite		
Unit	Mandira (Alkaline 1)			Mandira 1 (Aluminous)			Acaraú (Alkaline 2)			Albitized granites		
SiO_2 (wt%)	38.90	36.52	36.87	35.02	35.45	36.51	35.16	35.14	35.66	35.99	41.56	41.96
TiO_2	2.49	2.84	2.29	1.49	2.08	2.10	2.44	2.20	1.42	1.77	0.26	0.61
Al_2O_3	9.48	9.50	9.24	15.32	17.49	13.19	11.33	11.16	10.24	15.14	19.74	19.48
FeO^T	34.23	33.63	36.17	30.50	30.83	31.25	38.20	36.83	39.03	30.19	20.21	19.98
MnO	0.79	0.53	1.17	0.43	0.36	0.28	0.06	0.24	0.48	0.45	0.49	0.44
MgO	0.08	0.08	0.09	3.30	2.92	4.73	0.44	0.41	0.52	0.74	0.52	0.54
CaO	0.02	0.04	0.00	0.01	0.01	-	-	-	0.03	0.01	-	0.01
ZnO	0.02	0.68	0.00	0.09	0.06	-	0.38	0.01	0.44	0.30	-	-
BaO	0.60	-	0.03	0.13	0.07	-	-	0.31	-	-	0.15	0.18
Na_2O	0.03	0.06	0.04	0.01	0.06	0.02	-	0.03	0.01	0.04	0.05	0.05
K_2O	9.11	9.00	8.87	9.16	9.17	9.39	8.44	8.78	8.38	9.49	10.16	10.21
F	2.03	1.13	1.16	0.31	0.32	0.63	0.07	0.06	0.15	1.46	3.18	3.05
Cl	0.03	0.00	0.02	0.26	0.20	0.17	0.05	0.04	0.12	0.07	0.06	0.02
Sum	97.81	94.00	99.42	95.57	98.51	98.28	96.52	95.21	96.49	95.64	96.38	96.53
O=F=Cl	0.86	0.47	0.49	0.19	0.18	0.31	0.04	0.03	0.09	0.63	1.35	1.29
Total	98.53	94.36	98.93	96.15	99.08	98.10	97.03	95.68	97.04	95.75	97.38	97.71
Structural formula based on 11O												
Si (apfu)	3.192	3.111	3.097	2.829	2.758	2.891	2.923	2.955	2.992	2.944	3.194	3.208
^{IV}Al	0.808	0.889	0.903	1.171	1.242	1.109	1.077	1.045	1.008	1.056	0.806	0.792
T-site	**4.000**	**4.000**	**4.000**	**4.000**	**4.000**	**4.000**	**4.000**	**4.000**	**4.000**	**4.000**	**4.000**	**4.000**
^{VI}Al	0.110	0.064	0.012	0.288	0.362	0.122	0.033	0.062	0.005	0.404	0.982	0.964
Ti	0.154	0.182	0.145	0.091	0.122	0.125	0.152	0.139	0.090	0.109	0.015	0.035
Fe	2.349	2.396	2.541	2.061	2.006	2.069	2.655	2.591	2.739	2.066	1.299	1.278
Mn	0.055	0.038	0.083	0.030	0.024	0.019	0.004	0.017	0.034	0.031	0.032	0.029
Mg	0.010	0.011	0.011	0.398	0.339	0.558	0.054	0.051	0.066	0.090	0.059	0.061
Zn	0.036	0.042	0.031	0.005	0.004	0.000	0.023	0.019	0.027	0.018	0.008	0.010
M-site	**2.714**	**2.733**	**2.823**	**2.873**	**2.856**	**2.893**	**2.922**	**2.879**	**2.960**	**2.718**	**2.395**	**2.376**
Ca	0.002	0.004	0.000	0.001	0.001	0.000	0.000	0.000	0.005	0.001	0.000	0.001
Ba	0.000	0.000	0.007	0.004	0.002	0.000	0.000	0.001	0.005	0.000	0.000	0.000
Na	0.005	0.010	0.950	0.002	0.009	0.003	0.000	0.008	1.777	0.007	0.007	0.008
K	0.954	0.978	0.000	0.944	0.910	0.948	1.777	1.870	0.000	0.990	0.996	0.996
I-site	**0.961**	**0.992**	**0.956**	**0.951**	**0.922**	**0.952**	**1.777**	**1.879**	**1.786**	**0.998**	**1.004**	**1.005**
Cations	7.675	7.725	7.779	7.823	7.777	7.844	7.817	7.825	7.862	7.715	7.399	7.381
OH*	1.469	1.696	1.690	1.887	1.896	1.818	1.975	1.979	1.943	1.612	1.219	1.260
F	0.527	0.304	0.308	0.078	0.079	0.159	0.018	0.015	0.040	0.379	0.773	0.738
Cl	0.004	0.000	0.002	0.035	0.026	0.023	0.007	0.006	0.017	0.009	0.008	0.002
Fe#	0.996	0.996	0.996	0.838	0.855	0.787	0.980	0.981	0.977	0.958	0.957	0.954
$\log(X_F/X_{OH})$	-2.545	-2.850	-2.898	-1.732	-1.865	-1.891	-2.454	-2.546	-2.739	-2.7609	-2.1837	-2.740
$\log(X_{Cl}/X_{OH})$	-0.445	-0.632	-0.739	-1.382	-1.383	-1.060	-2.050	-2.117	-1.980	-0.4008	-0.1979	-0.233
$\log(f_{H2O}/f_{HF})$	6.786	7.089	7.139	4.628	4.740	4.846	6.721	6.811	6.298	7.0403	6.4614	7.019
$\log(f_{H2O}/f_{HCl})$	2.968	3.155	3.262	3.112	3.123	2.760	4.559	4.628	4.186	2.9041	2.7021	2.736
$\log(f_{HF}/f_{HCl})$	-3.818	-3.934	-3.878	-1.516	-1.616	-2.086	-2.162	-2.184	-2.113	-4.1363	-3.7594	-4.284

Point_ID: spot identification; c: core; r: rim; i: intermediate zone; -: below detection limit

Table 2-6: Major compositions and structural formula for chlorite from the Mandira Massif Granite

Samples	14							6769					
Crystal		c1		c2		c3			c2			c3	
Point_ID	1-c	1-r1	1-r2	2-c	3-r1	3-c	3-r2	2-r1	2-c	2-r2	3-r1	3-r2	3-r3
Mineral	Chamosite							Chamosite					
Unit	Mandira 1 (Aluminous) - Syenogranite							Mandira 1 (Aluminous) - Greisen					
SiO_2 (wt%.)	22.11	22.24	22.47	22.75	22.71	22.46	22.46	21.71	21.37	21.88	21.69	21.49	21.80
TiO_2	0.01	0.11	0.06	0.01	0.04	0.10	0.04	0.12	0.08	0.03	0.06	0.01	0.10
Al_2O_3	19.99	20.20	19.73	19.96	18.92	18.86	19.54	21.05	20.72	20.68	20.49	20.33	19.92
FeO	42.53	42.51	42.17	41.53	42.92	42.67	42.87	44.86	44.66	44.57	44.48	44.51	44.99
MnO	0.85	0.74	0.66	0.73	0.73	0.74	0.68	1.39	1.48	1.39	1.51	1.47	1.36
MgO	3.31	3.36	3.84	3.88	3.91	3.65	3.43	0.59	0.52	0.58	0.58	0.57	0.54
CaO	0.03	0.03	0.08	0.05	0.05	0.07	0.04	0.05	0.00	0.00	0.00	0.02	0.02
ZnO	0.09	0.07	0.07	0.04	0.05	0.07	0.09	0.06	0.13	0.04	0.11	0.12	0.11
BaO	-	-	-	-	-	-	0.02	-	0.02	-	0.02	-	-
Na_2O	0.03	0.00	0.03	0.03	0.01	0.00	0.00	0.00	0.00	0.00	0.00	0.00	0.02
K_2O	0.01	0.02	0.03	0.04	0.00	0.03	0.03	0.03	0.00	0.18	0.04	0.00	0.07
F	-	-	-	0.05	0.01	-	-	-	0.04	0.01	0.02	0.01	0.01
Cl	0.02	0.01	0.00	0.01	0.02	0.00	0.00	0.01	0.00	0.00	0.00	0.02	0.03
Sum	88.97	89.29	89.14	89.06	89.37	88.64	89.21	89.87	89.03	89.36	89.00	88.55	88.95
O=F	0.00	0.00	0.00	0.02	0.00	0.00	0.00	0.00	0.02	0.00	0.01	0.00	0.00
O=Cl	0.00	0.00	0.00	0.00	0.00	0.00	0.00	0.00	0.00	0.00	0.00	0.01	0.01
Total	99.47	99.79	99.64	99.54	99.86	99.14	99.71	100.37	99.51	99.86	99.49	99.04	99.44
Structural formula based on 14O													
Si (apfu)	2.542	2.546	2.572	2.602	2.598	2.595	2.578	2.518	2.505	2.555	2.543	2.532	2.565
^{IV}Al	1.458	1.454	1.428	1.398	1.402	1.405	1.422	1.482	1.496	1.445	1.457	1.468	1.436
T-site	**4.000**	**4.000**	**4.000**	**4.000**	**4.000**	**4.000**	**4.000**	**4.000**	**4.000**	**4.000**	**4.000**	**4.000**	**4.000**
^{VI}Al	1.252	1.271	1.233	1.292	1.148	1.162	1.221	1.395	1.367	1.402	1.373	1.356	1.326
Ti	0.001	0.009	0.005	0.000	0.003	0.008	0.004	0.010	0.007	0.003	0.005	0.001	0.009
Mn^{3+}	0.000	0.000	0.000	0.000	0.000	0.000	0.000	0.000	0.000	0.000	0.000	0.000	0.000
Fe^{3+} *	0.189	0.154	0.154	0.081	0.234	0.205	0.178	0.049	0.113	0.010	0.066	0.105	0.074
Fe^{2+}	3.901	3.915	3.882	3.891	3.872	3.917	3.937	4.302	4.264	4.343	4.295	4.282	4.353
Mn^{2+}	0.083	0.072	0.064	0.070	0.071	0.073	0.066	0.137	0.147	0.138	0.150	0.147	0.136
Zn	0.007	0.006	0.006	0.003	0.005	0.006	0.008	0.005	0.012	0.003	0.009	0.011	0.010
Mg	0.567	0.573	0.655	0.662	0.667	0.629	0.587	0.103	0.091	0.102	0.102	0.099	0.094
M-Site	**6.000**	**6.000**	**6.000**	**6.000**	**6.000**	**6.000**	**6.000**	**6.000**	**6.000**	**6.000**	**6.000**	**6.000**	**6.000**
Ca	0.004	0.004	0.010	0.006	0.006	0.008	0.005	0.006	0.000	0.000	0.000	0.002	0.002
Ba	0.000	0.000	0.000	0.000	0.000	0.000	0.001	0.000	0.001	0.000	0.001	0.000	0.000
Na	0.006	0.001	0.006	0.007	0.002	0.000	0.001	0.001	0.001	0.000	0.000	0.000	0.004
K	0.001	0.003	0.005	0.006	0.000	0.004	0.004	0.004	0.000	0.026	0.005	0.000	0.010
A-site	**0.011**	**0.008**	**0.020**	**0.018**	**0.008**	**0.013**	**0.011**	**0.011**	**0.002**	**0.027**	**0.007**	**0.003**	**0.017**
OH*	7.996	7.999	8.000	7.981	7.993	8.000	8.000	7.997	7.985	7.997	7.993	7.991	7.991
F	0.000	0.000	0.000	0.018	0.004	0.000	0.000	0.002	0.015	0.002	0.008	0.004	0.004
Cl	0.004	0.001	0.000	0.001	0.003	0.000	0.000	0.002	0.000	0.001	0.000	0.005	0.005
Fe#	0.878	0.877	0.860	0.857	0.860	0.868	0.875	0.977	0.980	0.977	0.977	0.978	0.979
$3(Mg+Fe^{2+})$	13.405	13.466	13.612	13.657	13.617	13.637	13.572	13.212	13.067	13.334	13.190	13.144	13.340
$2Al^{VI} + \Delta$	2.5032	2.5414	2.4662	2.5846	2.2966	2.3248	2.4414	2.790	2.733	2.804	2.747	2.712	2.652
$Si+(Mg+Fe^{2+})$	7.0107	7.0343	7.1092	7.1541	7.1366	7.1401	7.1016	6.922	6.860	7.000	6.939	6.914	7.011
T_{CN85}-Al^{IV}(°C)	323	322	317	310	311	312	315	328	331	320	323	325	318
T_{ZF95}-Al^{IV}(°C)	277	276	272	266	267	267	270	273	275	265	268	270	263

Point_ID: spot identification; c: core; r: rim; i: intermediate zone; -: below detection limit; *: estimated by using the stoichiometric H_2O and Fe_2O_3 (wt%.) contents

Table 2-7: Major compositions and structural formula for stilpnomelane chlorite from the Mandira Massif Granite

Samples	**5579**			**6662**			**6730**			**MAN-4**						
Crystal	c3			c6b			c1			c3				c9		
Point_ID	3-r2	3-c		6b-r1	6b-c		1-r1	1-c	1-r2	3-c	3b-c	3b-r1		9-c	9-c2	9-c3
Mineral	Ferri-stilpnomelane									Ferri-stilpnomelane						
Unit	Acaraú (Alkaline-1 association)									Mandira 1 (Aluminous)						
SiO_2 (wt%.)	43.58	42.94		43.94	43.92		43.92	43.51	43.52	43.03	42.89	43.13		45.40	43.68	44.75
TiO_2	0.00	0.13		0.04	0.05		0.06	0.05	0.01	0.02	0.03	0.00		0.00	0.01	0.00
Al_2O_3	4.97	4.91		5.67	5.89		4.87	5.01	4.89	6.85	6.66	7.00		6.26	6.86	6.46
FeO	37.02	36.03		35.42	35.07		36.69	37.08	36.52	32.79	32.57	32.12		31.70	32.66	32.05
MnO	1.36	1.39		1.04	0.99		1.23	1.26	1.27	1.55	1.52	1.56		1.40	1.67	1.55
MgO	0.34	0.37		0.30	0.34		0.49	0.56	0.54	1.93	1.95	1.80		1.92	1.87	1.92
ZnO	0.97	0.91		0.40	0.60		0.36	0.27	0.21	0.17	0.08	0.08		0.15	0.15	0.14
CaO	0.05	0.15		0.07	0.13		0.08	0.08	0.07	0.17	0.12	0.16		0.11	0.13	0.08
BaO	0.14	0.18		0.00	0.07		0.06	0.09	0.09	0.13	0.14	0.17		0.13	0.14	0.06
Na_2O	0.17	0.13		0.25	0.23		0.40	0.38	0.37	0.27	0.10	0.38		0.09	0.18	0.24
K_2O	1.44	1.62		2.01	2.01		1.40	1.50	1.35	2.46	3.25	2.68		2.81	2.70	2.50
F	0.02	0.00		0.06	0.00		0.00	0.02	0.02	0.00	0.04	0.00		0.05	0.00	0.05
Cl	0.00	0.00		0.00	0.01		0.01	0.00	0.00	0.00	0.04	0.01		0.01	0.01	0.02
Sum	90.06	88.76	#	89.19	89.31	#	89.58	89.82	88.86	89.38	89.39	89.08	#	90.02	90.06	89.82
H2O*	8.22	8.06		7.64	7.66		7.82	7.90	7.79	7.83	7.63	7.65		7.57	7.83	7.70
O=F,Cl	-0.02	0.00		-0.03	0.00		0.00	-0.01	-0.01	0.00	-0.03	0.00		-0.02	0.00	-0.02
Total	100.4	98.8		99.1	99.2		99.7	100.1	99.0	99.3	99.1	98.8		99.6	100.0	99.5
Structural formula based on 14O																
Si (apfu)	7.898	7.917		8.048	8.032		7.992	7.904	7.974	7.790	7.821	7.860		8.161	7.856	8.044
^{IV}Al	1.062	1.067		0.952	0.968		1.008	1.073	1.026	1.210	1.179	1.140		0.839	1.144	0.956
T-site	**8.959**	**8.984**		**9.000**	**9.000**		**9.000**	**8.977**	**9.000**	**9.000**	**9.000**	**9.000**		**9.000**	**9.000**	**9.000**
^{VI}Al	0.000	0.000		0.272	0.301		0.036	0.000	0.030	0.251	0.253	0.363		0.487	0.310	0.413
Ti	0.000	0.018		0.005	0.007		0.008	0.007	0.002	0.003	0.004	0.000		0.000	0.002	0.000
Fe^{3+} *	2.413	2.389		2.333	2.306		2.401	2.422	2.406	2.135	2.136	2.105		2.049	2.112	2.072
Fe^{2+}	3.198	3.167		3.093	3.057		3.183	3.211	3.190	2.830	2.831	2.790		2.716	2.800	2.746
Mn	0.209	0.217		0.162	0.154		0.190	0.193	0.197	0.238	0.235	0.241		0.213	0.254	0.236
Zn	0.129	0.124		0.054	0.082		0.049	0.037	0.028	0.023	0.011	0.011		0.020	0.021	0.019
Mg	0.092	0.101		0.082	0.093		0.134	0.152	0.146	0.521	0.530	0.489		0.515	0.501	0.515
Ca	0.009	0.029		0.013	0.025		0.015	0.016	0.014	0.033	0.024	0.030		0.021	0.024	0.016
Ba	0.010	0.013		0.000	0.005		0.004	0.007	0.006	0.009	0.010	0.012		0.009	0.010	0.004
Na	0.061	0.046		0.088	0.081		0.141	0.134	0.132	0.095	0.035	0.134		0.032	0.062	0.082
K	0.333	0.381		0.470	0.469		0.325	0.348	0.316	0.568	0.756	0.623		0.644	0.619	0.573
A-site	**6.454**	**6.485**	**#**	**6.571**	**6.579**	**#**	**6.486**	**6.527**	**6.469**	**6.706**	**6.825**	**6.799**	**#**	**6.706**	**6.715**	**6.676**
Cations	15.413	15.468		15.571	15.579		15.486	15.504	15.469	15.706	15.825	15.799		15.706	15.715	15.676
OH*	3.501	3.383		2.959	2.983		3.265	3.357	3.300	3.375	3.192	3.142		2.871	3.279	3.068
F	0.011	0.002		0.035	0.000		0.000	0.010	0.012	0.000	0.023	0.000		0.026	0.000	0.027
Cl	0.000	0.000		0.000	0.003		0.003	0.000	0.000	0.000	0.012	0.002		0.004	0.003	0.005
Fe#	0.984	0.982		0.985	0.983		0.977	0.974	0.975	0.905	0.904	0.909		0.903	0.907	0.904
Fe/Mn	26.88	25.59		33.53	34.81		29.39	29.13	28.40	20.89	21.16	20.33		22.36	19.31	20.42

Point_ID: spot identification; c: core; r: rim; i: intermediate zone; -: below detection limit; *: estimated by using the stoichiometric H_2O and Fe_2O_3 (wt%.) contents; Fe3+/ΣFe % used** Malczewski and Popiel (2008).

Table 2-8: Amphibole-melt REE partition coefficients for the different calcic, sodic-calcic and sodic groups from the Mandira Massif.

REE	Hornblende	Winchite	Riebeckite
D_{La}	1.261	0.441	0.210
D_{Ce}	2.272	0.750	0.302
D_{Pr}	3.708	1.156	0.401
D_{Nd}	5.496	1.615	0.491
D_{Sm}	8.778	2.314	0.583
D_{Eu}	9.860	2.476	0.585
D_{Gd}	10.529	2.517	0.563
D_{Tb}	10.700	2.433	0.521
D_{Dy}	10.362	1.259	0.166
D_{Ho}	9.648	1.940	0.424
D_{Er}	8.731	2.881	0.969
D_{Tm}	7.754	4.003	1.880
D_{Yb}	6.815	5.718	3.723
D_{Lu}	5.972	6.909	5.251
D_{Sc}		25.565	7.648
Calculated parameters			
D_0 M2	10.708	25.863	20.922
E (kbar)	3092	3065	9389
r_0 (A)	1.042	0.755	0.800
T (°C)	750	700	700
D_0 M4		2.519	0.5876
E (kbar)		3023	2485
r_0 (A)		1.0553	1.0715
T (°C)		700	700

3. ASTROPHYLLITE IN PERALKALINE GRANITES FROM THE A-TYPE GRACIOSA PROVINCE, S-SE-BRAZIL: TEXTURAL, COMPOSITIONAL VARIATIONS AND IMPLICATIONS

Astrid Siachoque[a] and Silvio R.F. Vlach[a]
b. Institute of Geosciences -University of São Paulo, São Paulo-Brazil.

ABSTRACT

Astrophyllite is a common "agpaitic" accessory mineral in highly evolved peralkaline granites from the Mandira and Papanduva plutons at the A-type Graciosa Province (SE-Brazil). Textural relations point to the existence of three distinct late-magmatic and post-magmatic generation of astrophyllite in these plutons, namely Ast-1 and Ast-2a and Ast-2b. Ast-1 crystals are late-magmatic and have higher Zr and Nb contents. The Ast-2a and Ast-2b crystallized during post-magmatic stages and have the highest Ti abundances. Trace-element compositions are marked by relative enrichment in LILE, HFSE, LREE and transition metals relative to the corresponding bulk rock. Ast-2b crystals from the Papanduva Pluton have the most contrasting compositions marked by lower HFSE and REE abundances. The observed chemical contrast intra- and inter-plutons are mainly related to the degree of peralkalinity, and to previous and concomitant crystallization of Na-, HFSE- and REE-bearing mafic and accessory minerals. In fact, astrophyllite-melt partition defines a strong compability of HFSE and REE in Na-richer astrophyllite crystals from the Mandira Pluton. These observations, along with chemical signatures of Mandira and Papanduva granites, suggest that the late-magmatic astrophyllite group (Ast-1) crystallized from the original peralkaline melt at reduced fO_2 conditions in Mandira Pluton but at distinct oxidizing conditions in Papanduva Pluton. Conversely, the precipitation of the subsequent post-magmatic astrophyllite groups (Ast-2a and 2b) occurred via disequilibrium process and substitution reactions of early sodic amphiboles and clinopyroxenes triggered by the circulation of hydrothermal K^+ and Ti^{4+}-rich fluids under relative reduced environments.

Keywords: Mineral chemistry, astrophyllite-melt partitioning, peralkaline granites, Graciosa Province

3.1. Introduction

Peralkaline rocks are generally enriched in large ion lithophile elements (LILE), halogens (mainly F), rare earth elements (REEs), and high field strength elements (HFSE) such as Zr, Hf, Nb, Ta and U (*e.g.*, Sørensen, 1997; Marks and Markl, 2017). Such enrichment may result in the crystallization of a plethora of otherwise rare minerals, including complex Zr-Ti silicates, with variable amounts of volatiles, Na, K, Ca, and Fe. Of importance, the presence of these minerals defines the so-called agpaitic rocks, as opposed to miaskitic rocks where zircon and ilmenite are the main sinks for HFSE (*e.g.*, Khomyakov, 1995; Sørensen, 1997; Marks and Markl, 2017). Although originally the terms "agpaitic and miaskitic" has been restricted to SiO2-undersatured felsic rocks, as the for the Strange Lake, Pilanesber Complex and Papanduva plutons, to mention a few, which its use for such SiO2-oversaturated rocks (Vilalva et al., 2016; Andersen et al., 2017; Siegel et al., 2017).

Among the agpaitic minerals, astrophyllite [$K_2NaFe_7Ti_2(Si_4O_{12})_2O_2(OH)_4F$] is one important HFSE-bearing accessory minerals in peralkaline systems. Most occurrences are described in nepheline syenites (Macdonald, 1973; Piilonen et al., 2003b; Andersen et al., 2014), peralkaline granites (Abdel-Fattah and Abdel-Rahman, 1992; Birkett et al., 1996; Marks et al., 2003; Siegel et al., 2018), and related pegmatites (Macdonald and Saunders, 1973; Layne et al., 1982; Macdonald et al., 2007); it is less abundant in rhyolitic volcanic rocks (Žáček et al., 2016). In these systems, astrophyllite occur either as a primary, in general late-magmatic, or as post-magmatic phase, with significant compositional variability, which monitor and estimate extensive and intensive parameters (e.g., fluid compositions, T, fO_2, aH_2O) acting during its crystallization (Abdel-Fattah and Abdel-Rahman, 1992; Piilonen et al., 2003b, 2004).

Astrophyllite is the main mineral of the astrophyllite supergroup (Sokolova et al., 2017). Its crystal-chemical properties have been broadly discuss by Belov (1963, 1976); Peng and Ma (1963); Piilonen et al. (2003a, 2003b); Sokolova and Cámara (2008); Cámara et al. (2010); Sokolova (2012), among others. Sokolova et al. (2017) have recently reviewed the classification for the astrophyllite supergroup minerals, with the general formula $A_{2p}B_rC_7D_2(T_4O_{12})_2IX^O{}_{D2}X^O{}_{A4}X^P{}_{Dn}W_{A2}$, where C = $^{[6]}Fe^{2+}$, Mn, Fe^{3+}, Na, Mg or Zn; D = $^{[6,5]}$Ti, Nb, Zr, Fe^{3+}; T = Si, Al; $A_{2p}B_rIW_{A2}$ (**I** block) where p = 1,2; r = 1,2; A = K, Cs, Ba, H_2O, □; I represents the composition of the central part of the I block, excluding peripheral layers of the form $A_{2p}B_rW_{A2}$; $X^O{}_D$ = O; $X^O{}_A$ = OH, F; $X^P{}_{Dn}$ = F, O, OH, H_2O, □, where n = 0, 1, 2 for $(X^P{}_D)_n$; W_A = H_2O, □; and space group $P1^-$. The supergroup encompasses thirteen minerals divided

into three groups based on crystal-chemical criteria, namely astrophyllite, kupletskite and devitoite groups. In the astrophyllite group, HOH blocks connect via D–X^{P}_{D}–D bridges, and Fe^{2+} is dominant at C_7 site. Besides astrophyllite, the group includes the minerals niobophyllite, zircophyllite, tarbagataite, nalivkinite and bulgakite (Sokolova, 2012; Sokolova et al., 2017).

As part of a larger project aiming to characterize the main and accessory mineralogy of the Graciosa Province of A-type granites and syenites, S-SE Brazil (Gualda and Vlach, 2007b, 2007e, 2007a; Vlach and Gualda, 2007; Vlach, 2012; Vilalva et al., 2013; Vilalva and Vlach, 2014), we present in this contribution textural and geochemical elemental data (EPMA, LA-ICPMS), for distinct late- and post-magmatic astrophyllite generations in the main peralkaline granites from the Mandira Massif (Mandira unit) and the Papanduva Pluton in the province. Based of textural and mineral chemical data, we provide some insights into the crystallization conditions of the late and post-magmatic environments and discuss the main replacement reactions from alkali-rich mafic and accessory minerals in these plutons, as well as the role of hydrothermal fluids in the mobilization and concentration of rare metals and their precipitation as post-magmatic accessory phases.

3.2. Geological Background

The Mandira Massif and Papanduva Plutons belong to the Graciosa Province of A-type granites and syenites in south-southern Brazil (Figure 3-1A), formed at ~580 Ma in a post-collisional extensional regime related to the geodynamic evolution of the south-southeastern part of the Gondwana supercontinent (Gualda and Vlach, 2007a; Vlach et al., 2011; Vilalva et al., 2019). The province includes metaluminous to moderately peraluminous (aluminous petrographic association), as well as metaluminous to peralkaline syenitic and granitic rocks (alkaline petrographic association), intrusive into the Archean and Paleo- to Neoproterozoic rocks of the Luis Alves Microplate, and Curitiba Microplates, and Paranaguá Terrain (Siga Júnior et al. (1993); Gualda and Vlach (2007a); Basei et al. (2009); Passarelli et al. (2018). The main geological, petrographic and geochemical features of these plutons are presented in Kaul and Cordani (2000); Gualda and Vlach (2007a, 2007b); Vlach and Gualda (2007); Vilalva et al. (2019) and references therein. Based on chemical and isotopic evidences, Vilalva et al. (2019) argue that the Graciosa magmatism was formed through partial melting of a metasomatized lithospheric mantle, followed by variable degrees of crustal contamination at depth.

The Mandira and Papanduva plutons encompass of the more evolved, astrophyllite-bearing peralkaline granites of the Graciosa Province. Bellow, we summarized their main petrographic, mineralogical and geochemical features. Further details are found in Oliveira, (1989) and Vilalva and Vlach (2014), respectively

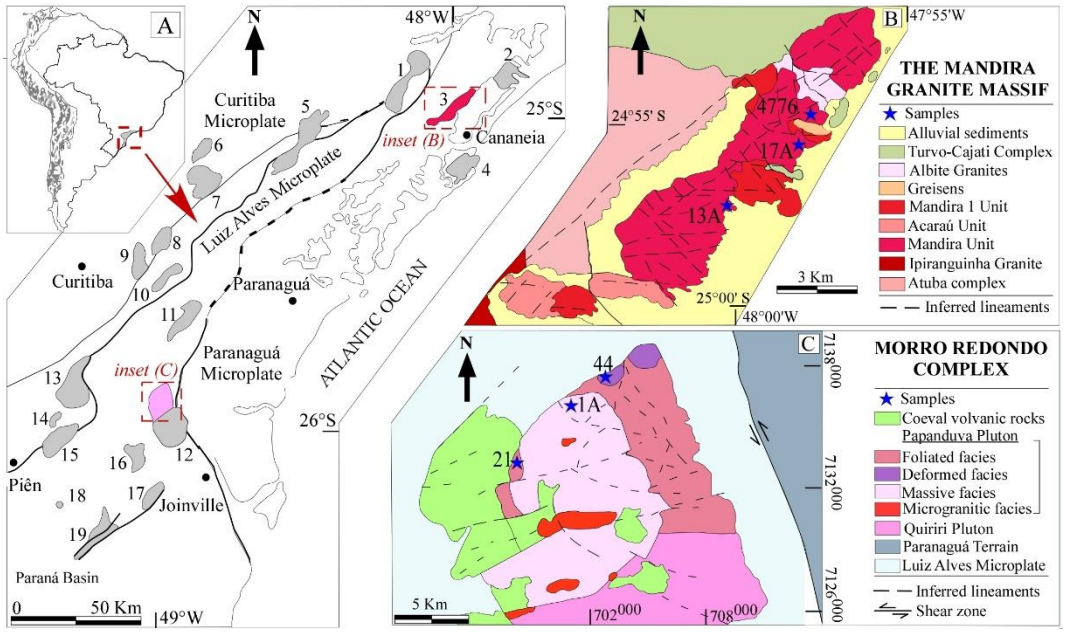

Figure 3-1: Geological location of the study area (southern Brazil). (A) Distribution of the A-type granitic and syenitic plutons that form the A-type Graciosa Province. (B) Detailed geological map of the Mandira Massif and (C) of the Papanduva Pluton, showing the locations of astrophyllite-bearing samples.

3.2.1. The Mandira Massif

The Mandira Massif included three main units, named Mandira, Mandira 1 and Acaraú, and associated hydrothermal rocks and greisens (Figure 3-1B; Oliveira, 1989; Siachoque et al. submitted). The Mandira and Acaraú units are made of metaluminous to peralkaline alkali-feldspar granites, while the Mandira 1 is constituted by biotite syenogranites, intrusions. Astrophyllite appears solely in the Mandira Unit (Figure 3-1). Of note, high-resolution zircon U/Pb data gave 567 ± 6 Ma, somewhat younger than most dated occurrences in the province (Vilalva et al., 2019). These *hypersolvus g*ranites present grayish to reddish colors a dominant massive structure, with some local orientation given by late solid-state deformation; the main textures are hypidiomorphic, inequigranular to porphyritic (with alkali feldspar megacrysts), and medium- to coarse-grained. Mandira granites present an agpaitic crystallization order, in which the primary amphiboles start their crystallization when

significant amount of alkaline feldspar and quartz were formed yet. Figure 3-2 depicts the inferred crystallization order for the main and accessory minerals.

The studied peralkaline alkali-feldspar granites are ferroan, with Fe# [FeO^T / (FeO^T + MgO), wt%] numbers (≥ 0.99) and alkali contents (8.48 ≤ $Na_2O + K_2O$ ≤ 8.89); and an agpaitic (or peralkalinity) index, AI=($Na_2O + K_2O$)/Al_2O_3 in a molecular basis, in between 1.031 and 1.053.

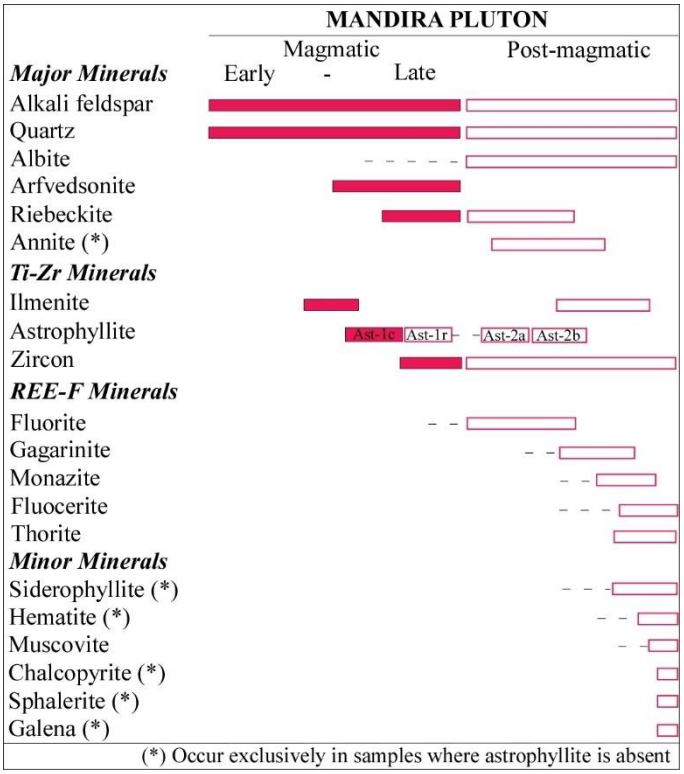

Figure 3-2: Crystallization sequence observed in the studied samples from the Mandira Pluton showing the mineral assemblages at early, late and post-magmatic stages.

3.2.2. The Papanduva Pluton (PAP)

The Papanduva Pluton is a relatively small intrusion cropping out in the northern portion of the Morro Redondo Complex, which also includes metaluminous biotite (± calcic amphibole) syeno- and monzogranites, as well as contemporaneous, mainly silicic, volcanics (Figure 3-1C). It is made up by leucocratic hypersolvus alkali-feldspar granites with a variety of mineralogical and textural features, grouped into (i) massive, (ii) deformed, (iii) foliated and (iv) microgranitic petrographic facies (Vilalva and Vlach, 2014); zircon U/Pb data indicate a crystallization age about 580 ± 5 Ma (Vilalva et al., 2019). The massive varieties include arfvedsonite, riebeckite, aegirine and aegirine-augite as the main mafic minerals; chevkinite,

zircon, aenigmatite, astrophyllite and ilmenite are magmatic accessories, whereas allanite, fluorite and magnetite are post-magmatic minerals; while the deformed and, particularly the foliated facies are characterized by a HFSE-rich, typically agpaitic, rare accessory mineralogy that includes, besides astrophyllite, late to post-magmatic narsarsukite, elpidite, neptunite, britholite-(Ce), nacareniobsite-(Ce), turkestanite, bastnäsite-(Ce), among others (Vilalva et al., 2013; Vilalva and Vlach, 2014). The microgranite facies do not contain astrophyllite. The main mineral crystallization order inferred for a typical agpaitic variety is illustrated and compared with the corresponding peralkaline varieties from Mandira in Figure 3-3.

From the geochemical standpoint, these rocks present Fe# numbers over 0.96, ($8.7 \leq Na_2O + K_2O \leq 9.3$); and AI in between 1.042 and 1.282. Of note, these granites present the highest AI values of the whole province and the measured abundances for most HFSEs show well-defined positive correlations with the AI (Vilalva and Vlach, 2014).

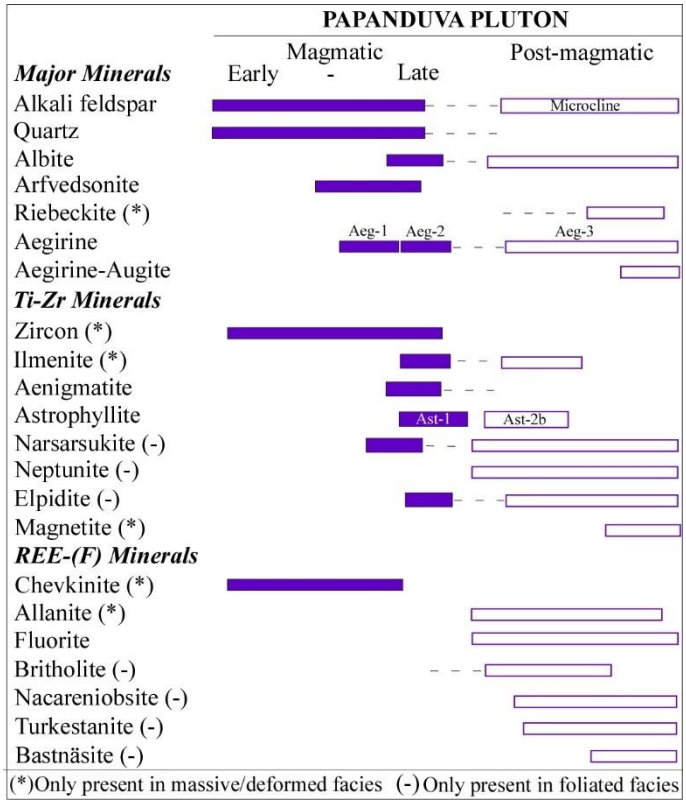

Figure 3-3: Crystallization sequence observed in the studied samples from the Papanduva Pluton showing the mineral assemblages at early, late and post-magmatic stages.

3.3. Sampling and Methods

We select six samples, three of each studied occurrence (see locations in Figure 3-1B and 3.1C), for detailed textural and chemical analysis. Textural studies and chemical analysis over

30-80 μm polished-thin sections where done with a conventional petrographic microscope, the Electron Probe Micro Analyzer (EPMA), and the Laser Ablation Inductively Coupled Mass Spectrometer (LA-ICP-MS) over. The laboratory work was performed in the NAP GeoAnalitica-USP core facility, at the Institute of Geosciences, University of São Paulo.

3.3.1. EPMA analyses

Back-scattered electron images in compositional mode (BSE-Compo) and quantitative WDS spot microanalyses were obtained in a JEOL JXA-FE-8530 microprobe, provided with a field emission gun and two large area (TAP and PET) analyzer crystals. The analytical conditions were: 15 kV for the column accelerating voltage and 20 nA and 5 μm for the beam current and diameter, respectively; total counting times, equally divided between peak and background, vary in between 10 and 40s. The used standard were: diopside for Si and Mg, fayalite for Fe and Mn, anorthoclase for Al, wollastonite for Ca, orthoclase for K, rutile for Ti, albite for Na, zircon for Zr, willemite for Zn, benitoite for Ba, ilmenite for Nb, sodalite for Cl and fluorapatite for F, most of them from the Smithsonian collection. Raw data correction for matrix effects and conversions to mass were computed with the PRZ/Armstrong software furnished by JEOL. The detection limits for all elements are below 0.01 wt.%. The astrophyllite mineral formulae were calculated following Sokolova et al. (2017).

3.3.2. LA-ICP-MS analyses

Trace element abundances were determined using a Thermo Fisher Scientific iCAP-Q ICP-MS instrument coupled to a New Ware UP-213 laser ablation system in a total of 34 individual spot microanalyses. These were performed using a laser spot of 40 μm under a repetition frequency of 15Hz and energy fluence of ~2.85 J/cm^2. The analysis consisted in of a ~60 s background measurement followed by data acquisition for ~60 s and dwell time of 8 ms for each isotope of the reported element, followed by 30 s of washout time. The NIST glass standard SRM 610 was used to correct signal drift during the analytical process, while the basalt glass standard BHVO-2G was employed as the main external standard. The SiO_2 wt% contents measured with the EPMA was our internal standard. Drift correction, data reduction and elemental abundance determinations were carried out using the Glitter software (Griffin, 2008).

3.4. Results

3.4.1. Main textural features

As above described and represented in Figure 3-2and Figure 3-3, the studied perlkaline granites are characterized by an agpaitic crystallization sequence. In this scenario, astrophyllite occurs in three distinct textural generations, namely (i) Ast-1, (ii) Ast-2a and (iii) Ast-2b. The Ast-2a crystals were only found in the Mandira Massif, whereas Ast-1 and Ast-2b are ubiquitous in both Mandira Massif and Papanduva Plutons.

(i) Ast-1 occurs as subhedral to euhedral, 1.5-2.5 mm long, platy to prismatic crystals with a strong pleochroism from deep orange to lemon-yellow. These are late-magmatic phases and appear as isolated crystals (Figure 3-4A) and/or in aggregates of a few 2-3 grains (Figure 3-4B), interstitial to quartz and feldspars. They are often associated with arfvedsonite, riebeckite or aegirine, with mostly lobate contacts, suggesting co-precipitation (Figure 3-4B-C). Nevertheless, some flakes of Ast-1 are found also as inclusions within riebeckite in the Mandira Massif.

(ii) Ast-2a appears as euhedral to subhedral, up to 1.0 mm long, platy crystals forming aggregates, interstitial to quartz and alkali feldspar (Figure 3-3D and Figure 3-3H), sometimes associated with riebeckite and ilmenite. These aggregates are also interpreted as representatives of the late- to post-magmatic crystallization.

(iii) Ast-2b crystallizes as post-magmatic, 0.1- 0.5 mm long, needle-shaped crystals that appear isolated or in radiating groups over riebeckite (Mandira Massif, Figure 3-3E and Figure 3-3I), and arfvedsonite, aegirine and narsarsukite (Papanduva Pluton; Figure 3-3F).

BSE images indicates significant compositional zoning in the Ast-1 crystals from the Mandira Massif (Figure 3-4G), while the other astrophyllite types are predominant homogeneous crystals (Figure 3-4H).

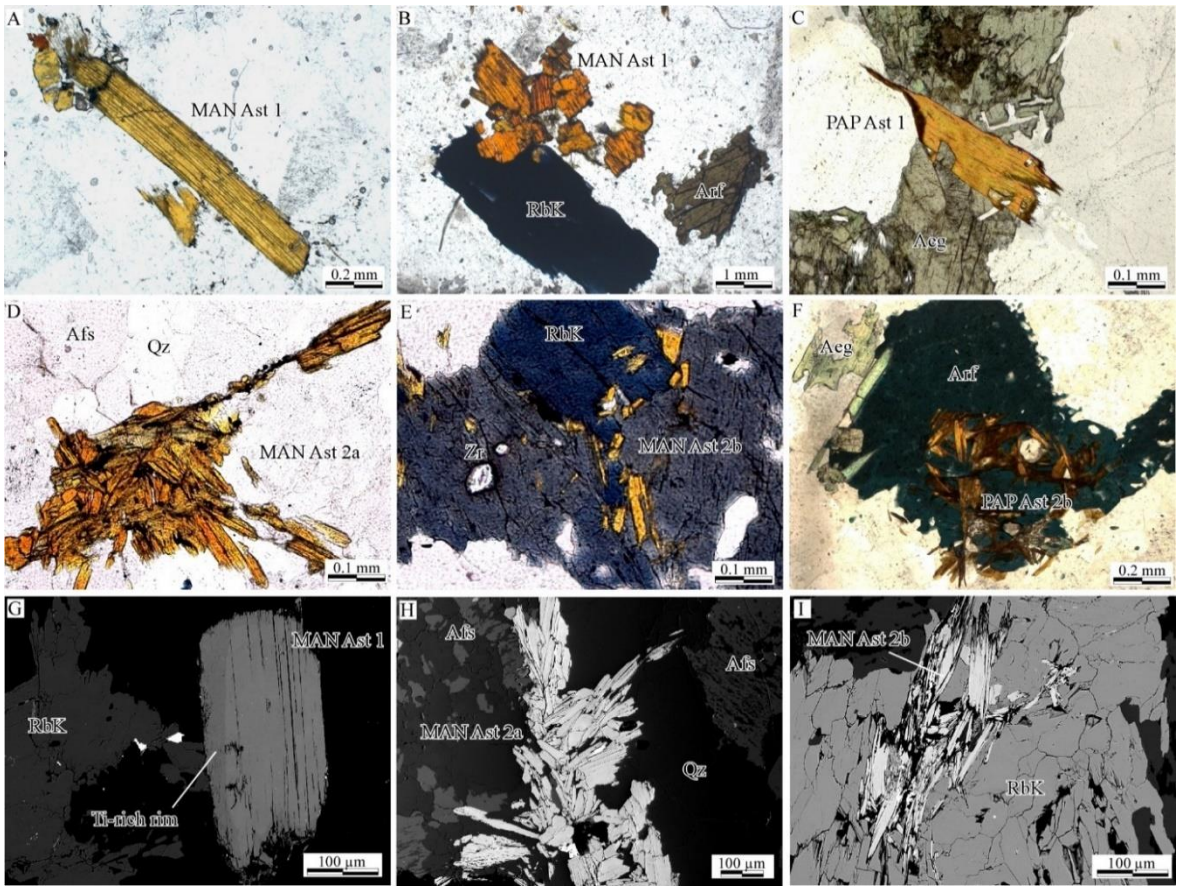

Figure 3-4: Optical transmitted light (A to F) and back-scattered electronic (G to I) photomicrographs showing the textural aspects of the astrophyllite generations. (A) Early large euhedral yellow astrophyllite in riebeckite alkali feldspar granite from the MAN pluton. (B) Magmatic astrophyllite crystals exhibit lamellar habit and deep-orange pleochroic scheme, closely associated with riebeckite in Mandira alkali feldspar granite. (C) Late-magmatic subhedral astrophyllite in co-precipitation texture with aegirine among quartz crystals in alkali feldspar granite from PAP pluton. (D) Post-magmatic tabular, grouped astrophyllite crystals interstitial to primary alkali feldspar and quartz in alkaline feldspar microgranite from MAN pluton. (E) Crystal of riebeckite with intergrowths of post-magmatic astrophyllite along fractures planes and rims in microgranite from the MAN pluton. (F) Arfvedsonite megacryst partially replaced by acicular astrophyllite and aegirine in deformed alkaline feldspar granite from the PAP pluton. (G) Euhedral magmatic zoned astrophyllite crystal in close relation with ribeckite from the MAN pluton. (H) Skeletal crystals of astrophyllite among alkali feldspar and quartz and (I) Acicular astrophyllite crystals replacing riebeckite along fractures in Mandira alkali feldspar granite. Mineral abbreviations: Aeg - aegirine; Arf - arfvedsonite; Asf - alkali feldspar; Rbk - riebeckite; Qz - quartz.

3.4.2. Compositional variations

Representative analyses for the recognized astrophyllite generations are given in Table 3-1 and Table 3-2. The complete data set is presented in the companion Supplementary Materials.

3.4.2.1. Major and minor elements

Astrophyllite compositional variations are mainly related to the relative proportions of Ti, Zr and Nb contents (Piilonen et al., 2003a, 2003b). The main chemical parameters that

allow distinguish astrophyllite from niobophyllite and zircophyllite. Figure 3-5A depict a Ti-Zr-Nb ternary plot representing our data; we also plot in Figure 3-5B typical average compositions of astrophyllite from worldwide SiO_2 over- and or under-saturated alkaline intrusions for comparison purposes.

The Ast-1 primary generation in Mandira records the highest Zr (up to 0.54 apfu) and Nb (up to 0.30 apfu) contents, with Ti ranging in between 1.26 and 1.49 apfu; Fe (up to 6.73 apfu) is strongly dominant over Mn (up to 0.34 apfu). The zoned crystals show increasing Ti (1.62-1.75 apfu) and decreasing Zr (up to 0.21 apfu) and Nb (up to 0.08) towards crystal rims. Compositions similar to the main Ast-1 crystals were reported in primary astrophyllite crystals from the Oslo Rift Valley, the Oktyabrsky Massif, and the Mongolian Altai (Andersen et al., 2013; Kryvdik and Sharygin, 2014; Žáček et al., 2016); while rim compositions approached those of secondary astrophyllite in the Strange Lake (Piilonen et al., 2003a). As compared with Mandira, the Ast-1 crystals from the Papanduva Pluton present higher Ti contents (up to 1.68 apfu), accompanied by somewhat lower Zr (up to 0.45 apfu) and Nb (up to 0.28 apfu) abundances. Of importance, they have significant higher Mn contents (up to 0.91 apfu) and, thus, lower Fe values (up to 6.18 apfu). These compositions are akin to either magmatic or hydrothermal/metasomatic astrophyllite from St. Peters Dome and Kûgnat Fjeld Complex (Macdonald and Saunders, 1973), the Mount Gharib Complex (Abdel-Fattah and Abdel-Rahman, 1992) and to those from Luskfjell, Norway, the Oslo Rift Valley and the Illimaussaq Complex (Piilonen et al., 2003a; Macdonald et al., 2007).

In the case of the Mandira Massif, the Ast-2a generation and the crystal rims of the zoned Ast-1a crystals share compositional similarities marked by intermediate Zr, Nb and Ti proportions in relation to our whole data set (Figure 3-5A), while the Ast-2b crystals have relatively high Ti (up to 1.80 apfu) and Nb and Zr contents in between 0.03 to 0.22, and 0.07 to 014 (apfu), respectively. Of note, the Ast-2a compositions overlap those of hydrothermal astrophyllite in the Kangerdlugssuaq Intrusion, Mount Saint Hilaire (Layne, 1982; Piilonen et al., 2003a).

The post-magmatic astrophyllite Ast-2b from both the Mandira Massif and the Papanduva Pluton have similar compositions defined by the highest Ti (up to 1.89 and 2.01 apfu, respectively) and the lowest Zr (up to 0.13 apfu) and Nb (up to 0.12 apfu) measured contents. Nevertheless, the concentrations of Al and the alkali elements do vary between Ast-2b in each occurrence. Thus, the Ast-2b generation is nearly Al-free, with higher alkalis contents (Na to 1.59 apfu and K up to 1.56 apfu), in Papanduva, while Al contents up to 0.26 apfu were measured in Mandira crystals. The Ti-Nb-Zr compositions of this generation is

comparable to the secondary astrophyllites described in the Kangerdlugssuaq Intrusion, the Khibina Massif and the Oslo Rift Valley (Piilonen et al., 2003a, 2003b; Andersen et al., 2013).

The main compositional variations observed in the studied astrophyllite generations are depicted in Figure 3-5, which reinforces the compositional contrasts between the primary and the post-magmatic crystals and within each focused occurrence. The main variations, as expected, involves Ti, Zr and Nb as depicted in the Nb+Zr *vs* Ti diagram Figure 3-5A; the primary and post-magmatic crystals show specific trends with contrasted slopes, with both the Ti contents and the negative slope being higher in Papanduva. Of importance, the external most rim compositions of the primary crystals from Mandira plotted in the midway of such trends, and the Ast-2b generation is richer in Ti than Ast-2a. Both magmatic and pos-magmatic Papanduva generations present significant higher Ti contents, as compared with the Mandira samples.

The diagram Al+Ca vs Si+Na+K (Figure 3-6B), although to a lesser extent, show similar contrasts and emphasizes the relatively highest and the lowest average Al+Ca values in the primary and post-magmatic astrophyllite from Papanduva, respectively, as compared with those equivalents from Mandira. Single site substitutions, as (Mn,Mg) ↔ Fe are represented in Figure 3-6C; this substitution was important solely in the primary Ast-1 generation in the Papanduva Pluton. There are some chemical contrast between astrophyllite generations in each pluton, especially in the Papanduva Pluton, in which we notice that the Ast-1 crystals show a good negative correlation to the substitution of Mn + Mg ↔ Fe (Figure 3-6C), while in the Ast-2b group this relation is absent. This can be related to important changes in f_{O2} conditions in the crystallization environments (see discussion section).

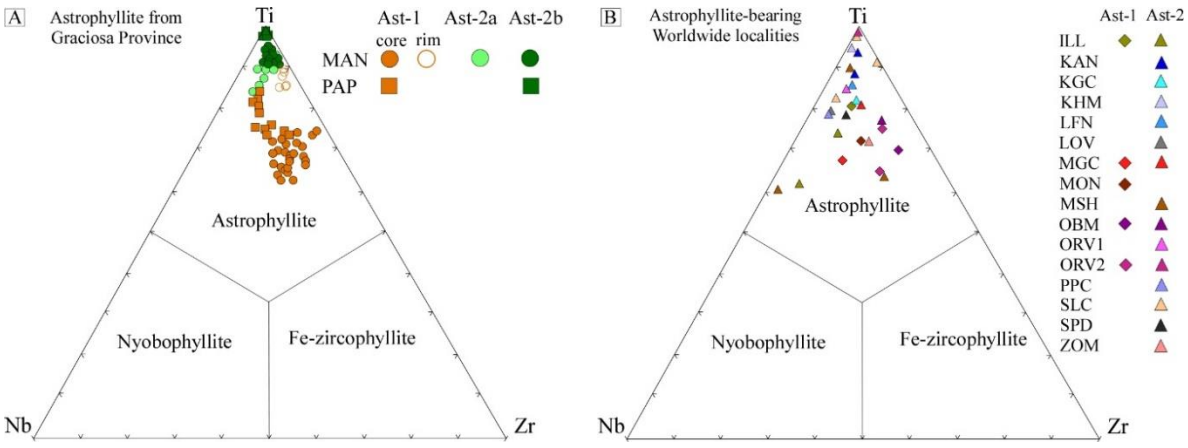

Figure 3-5: Nb-Zr-Ti ternary classification diagram showing (A) the measured astrophyllite compositions for both Mandira Massif (MAN) and Papanduva pluton (PAP) and (B) astrophyllite compositions for interesting localities worldwide. ILL: Illimaussaq Complex (Macdonald et al., 2007); KAN: Kangerdlugssuaq (Layne et al., 1982);

KGC: Kûngnat Fjeld Complex (Macdonald, 1973); KHB: Khibina Massif; LFN: Lusk fjell Norway; LOV: Lovozero Massif; MSH: Mount Saint Hilan; ORV1: PPC: Pies Peak Colorado; Oslo Rift Valley; ZOM: Zomba-Malosa (data from (Piilonen et al., 2003a); MGC: Mount Gharib Complex (Abdel-Fattah and Abdel-Rahman, 1992); MON: Mongolian Altai (Žáček et al., 2016); OBM: Oktyabrsk Massif (Kryvdik and Sharygin, 2014); ORV2: Oslo Rift Valley (Andersen et al., 2014); SLC: Strange Lake Complex (Birkett et al., 1996); SPD: St. Peters Dome (Macdonald and Saunders, 1973).

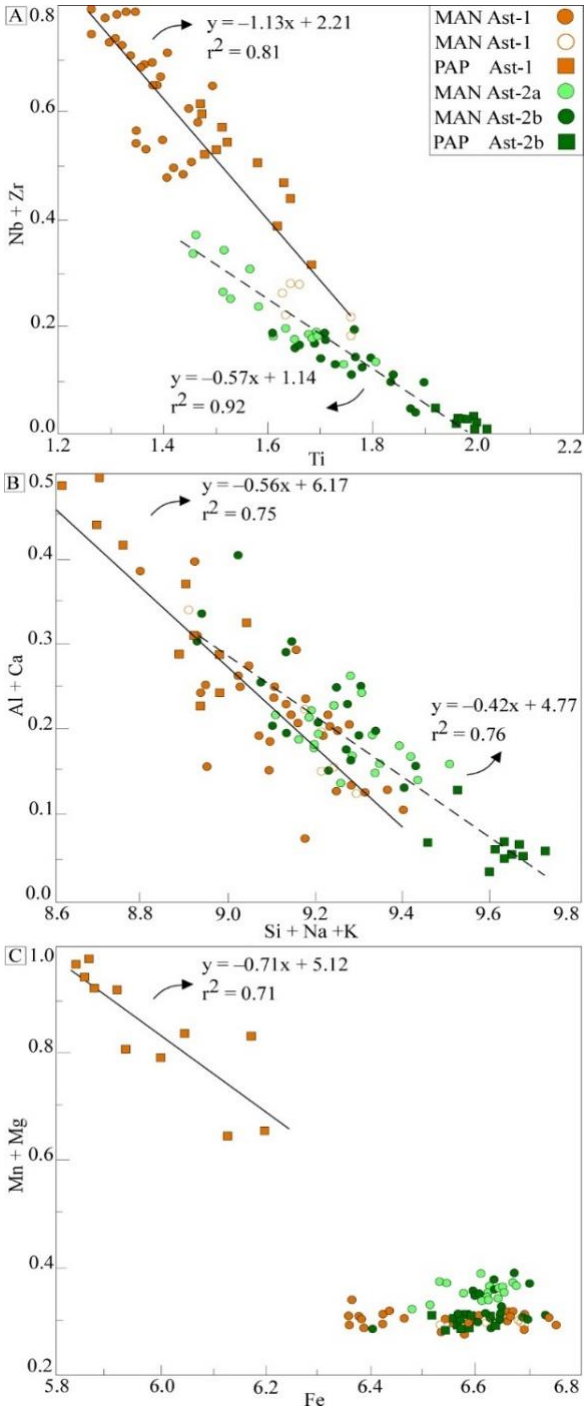

Figure 3-6: Binary plots showing compositional variations (apfu) related to (A) the Nb + Zr ↔ Ti substitution in the C-site; (B) the Mn+Mg ↔ Fe substitution in the D-site; and, (C) the Al+Ca against Si+ Na+K diagram.

3.4.3. REE and Trace elements compositions

Representative trace element and rare earth element (REE) astrophyllite patterns are shown in Figure 3-7. Overall, both mineral and whole-rock patterns are characterized by strong negative Ba, Ga, Pb, Sr and Sc and slight to moderate Pb anomalies. Astrophyllite is relatively enriched in most of the LILEs, HFSEs, transition metals and LREEs relative to the host-rock bulk composition, except for the post-magmatic Ast-2b crystals, with lower HFSE (mainly Zr and Hf) contents than the host-rock, as well as the lowest Th, U, Nb, Ta, Ga, Hf, Li, Y, REE, and Sc measured contents. The Mandira Ast-2b crystals also have low abundances of Th, Nb, Ta, and Sc, however its LREE contents are the highest observed (Figure 3-7A).

The REE patterns for all astrophyllite crystals register an overall trend of relative enrichment of the LREEs over the HREEs [$12.5 \leq (La_N/Yb_N) \leq 100$], and a well pronounced negative Eu anomaly, with $0.01 \leq Eu/Eu^* \leq 0.1$ (Figure 3-7B), when compared to the bulk host rocks. The patterns are concave upwards at the LREE side and regularly descendent at the HREE side. Comparing the Mandira and Papanduva patterns, the former has the highest LREE contents, even though the opposite scenario is registered in bulk rock compositions. In general, the observed patterns suggest that astrophyllite can be an important LREE sink in the Graciosa peralkaline granites.

The most contrasted REE pattern is observed for the Papanduva post-magmatic Ast-2b crystals, which have the lowest REE abundances (1- to 2-fold lower than the others), and a contrasted REE pattern at the HRRE side, which shows a convex shape, with $2.63 \leq Gd_N/Yb_N \leq 4.76$; the Eu anomaly is also less pronounced.

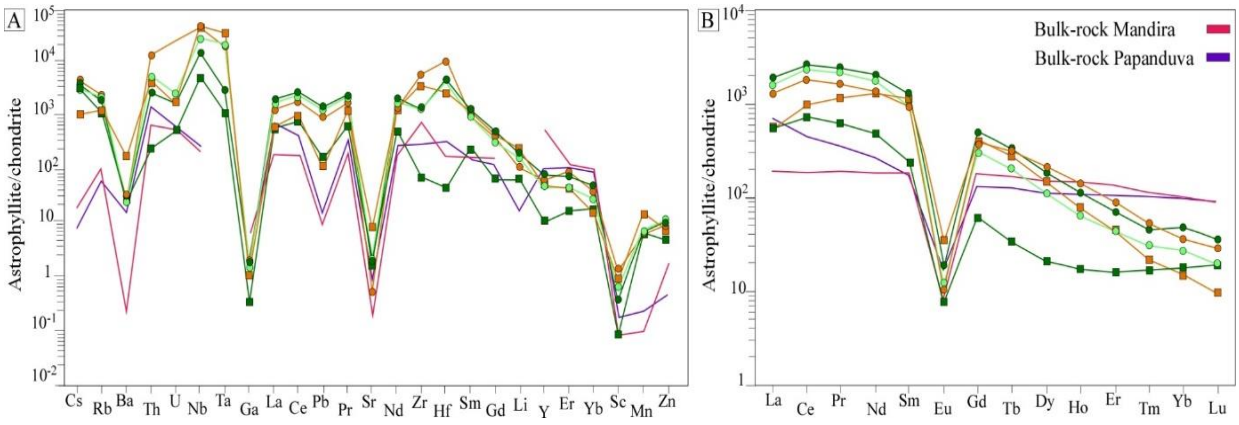

Figure 3-7: Median (A) REE and (B) trace element patterns for astrophyllite generations from MAN and PAP plutons with the corresponding bulk rocks. The data were normalized to the chondrite values of McDonough and Sun (1995). Symbols as in Figure 3.5.

3.4.4. Inter-site partition of the REEs, Ti, Zr and Hf

The behavior of the trace elements and REE in mafic and accessory minerals is governed by a combination of crystal chemical constraints and magmatic processes (Wood and Blundy, 1997; Bottazzi et al., 1999; Vilalva et al., 2015; Michely et al., 2017; Siegel et al., 2017; Vasyukova and Williams-Jones, 2019). The described relative enrichment in HFSEs in the studied astrophyllite reinforces the main roles of the trace element distribution, as well as the influence of the previous and/or concomitant crystallization of relatively REE-rich mafic and accessory phases, such arfvedsonite, riebeckite, fluorite and zircon (Mandira Massif) and ferrorichterite, chevkinite, zircon and (Na, K)-rich zirconosilicates (Papanduva Pluton). Accordingly, we attempt to modelling astrophyllite-melt partition coefficients for the distinct granites as a function of ionic radius, applying the Lattice Strain Model (LSM, Blundy and Wood, 1994, 2003). Thus a first approximation of the partition coefficients ($D^{ast/melt}$) for REE, Ti, Zr, and Hf were estimated for the late-magmatic Ast-1 crystals, using our whole-rock compositions (Table 3-3). The results define parabolic distributions in Onuma-type diagrams, which were adjusted with the software Double Fit (Dalou et al., 2018), by ordering the REE into the 6-fold coordinated [C] site, and Zr, Ti and Hf into the 5,6 [D] site (Figure 3-8). Calculations were conducted for a temperature of 550 ^{o}C, as estimate for the late-magmatic stages within the Graciosa peralkaline granites (cf. Vilalva et al., 2016). The relevant fitted LSM parameters are listed in (Table 3-3). The results show a decreasing HFSE and REE compatibility from the Mandira to the Papanduva occurrences. The fitted parabolic curves are roughly similar for the HFSE, with the inflexion at an ideal radius of ~0.65 Å. Curves are also similar for the HREE, but very distinct for the LREE. The LREE-rich Mandira sample defines a smooth parabolic curve centered at an ideal radius of 1.02 Å, whereas the Papanduva sample describes a large curve centered at a radius of 0.97 Å.Our data reveal that the Mandira sample is Na-richer and have higher Zr and Nb, and lower Ti contents than the Papanduva sample, as shown in Figure 3-5 to Figure 3-7; nevertheless, they show higher compatibility for the HFSE elements (Figure 3-8). These evidences point out to an important influence of the composition and structure of the melt in equilibrium, as well as the competition for the HFSE budget among astrophyllite and other early and/or contemporaneous minerals in the Papanduva Pluton, such as aenigmatite, ilmenite, and Ti-aegirine (Vilalva et al., 2016). Conversely, the lattice-strain modelling for the REEs suggests a major crystal chemical control on their partitioning, especially the preference of trivalent REEs to charge-balance Na^{+} incorporation by the coupled

substitution $Na^{+} + REE^{3+} \leftrightarrow 2Ca^{2+}$, which gives a $r^2 = 0.81$ (not shown) reflecting the highest REE concentrations into the Na-richest Mandira primary crystals.

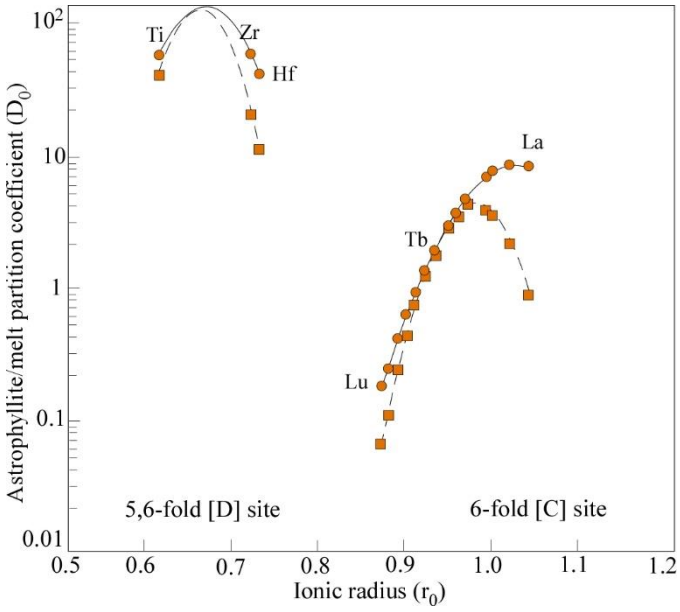

Figure 3-8: Astrophyllite-melt REE and HFSE partition coefficients calculated from representative magmatic astrophyllites according to the Lattice Strain Model (LSM) which were calculated at P = 100 MPa and T = 550 °C. Symbols as in Figure 3-5

3.5. Discussion

Although the original definition of agpaitic rocks was restricted to peralkaline syenitic rocks (e.g., Sørensen, 1997), the case has been changed so that peralkaline granitic rocks carrying HFSE-rich mineral assemblages are now included in the agpaitic rock group (Marks et al., 2011; Estrade et al., 2014). According, we discuss the formation of astrophyllite in the Mandira Massif and the Papanduva Pluton, following the typical agpaitic-like evolutionary model expanded for granitic systems characterized by late- to post-magmatic precipitation of HFSE-rich accessory minerals (e.g. Marks et al., 2011; Vasyukova and Williams-Jones, 2019). In these environments, the formation of contrasted rare mineralogical assemblages in quartz-bearing systems depends in part on the relative activities of the alkalis, as shown in the diagram illustrating qualitatively the effect of the relative chemical potential of Na_2O and K_2O species over the mineral assemblages in these rocks (Figure 3-9).

Despite the comparable fractionation trends for astrophyllite in both the studied occurrences from the Graciosa Province (c.f Figure 3-5A and Figure 3-8), the contrasted

mineral assemblages show that crystallization of astrophyllite and analogous Ti-Zr minerals define a distinct evolutionary path, particularly for the most agpaitic variety in the Papanduva Pluton, thus we discuss the formation of astrophyllite in separate as follows.

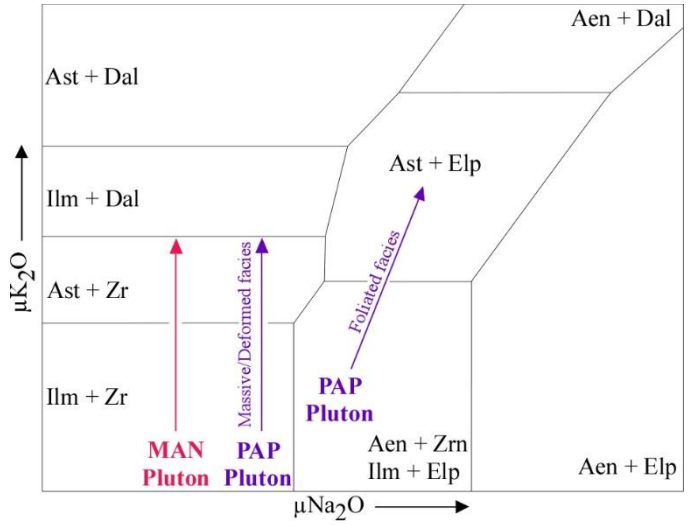

Figure 3-9: A diagram showing the qualitative K2O and Na2O activity for peralkaline systems proposed by Marks et al. (2011). Note the astrophyllite evolution trajectories for both MAN and PAP plutons.

3.5.1. Primary astrophyllite in the Mandira Massif

Textural relationships in the peralkaline granites from this massif pluton show that crystallization of astrophyllite initiates as a late-magmatic phase (c.f Figure 3-2). Nevertheless, the two textural astrophyllite types suggest separated stages of crystallization and thereby distinct formation processes. We believe that the origin of the Ast-1 generation is directly related to the peralkaline Mandira melt since crystals are interstitial to early felsic minerals and commonly appear associated with primary sodic amphiboles which are indicative of high f_{O2} conditions above the MH buffer (Siachoque et al. in chapter 2). In fact, chemical compositions suggest that the incorporation of the main constituents such Ti and Zr in the Ast-1 crystals is from the original melt, certainly related to the coeval crystallization of competing Ti-Zr accessory minerals such ilmenite and zircon. Once ilmenite crystallizes as an early phase, commonly included into sodic amphiboles, it incorporated most of the original Ti budget from the melt. The occurrence of zircon in Mandira granites is related mainly to the late- and post-magmatic stages, therefore, Ast-1 generation crystallizing before zircon and incorporated most part of the original Zr with significant Nb and already low Ti. Zoning in some of the Ast-1 crystals suggest disequilibrium processes as crystallization proceeds causing gradually decrease

of Zr-Nb contents with increasing of Ti towards crystal rims. This re-equilibration also facilitates the formation of the subsequent Ast-2a generation according to its Zr and Nb-poor and Ti-rich compositions but that we consider as a post-magmatic phase given its almost similar geochemical patterns when compared to the Ast-2b (e.g. Figure 3-11A). Moreover, the REE compositions of the Ast-1 group are indicative of the LREE compatibility in these crystals relative to the HREE which can be explained by the preference distribution of the latter elements into common arfvedsonite and riebeckite within Mandira granites (Siachoque et al. in chapter 2).

3.5.2. Primary astrophyllite in the Papanduva Pluton

Primary Ast-1 astrophyllite in this pluton precipitates also in the late magmatic stage. It occurs mainly in the less evolved massive petrographic facies, in which the alkali contents are slightly lower, and crystallized long with two textural generations of aegirine, one with relatively Ti- and Zr-rich cores, the other one with high Mn contents (Vilalva et al., 2016) and aenigmatite or Mn-rich ilmenite in samples lacking aenigmatite. The Ast-1 astrophyllite has also high abundances of Mn. Of note, our data reveal that the PAP Ast-1 crystals also have significant higher Mn concentrations than the MAN Ast-1 crystals (Table 3.1 and Figure 3-11C). Thus, it is inferred that it crystallized under slightly more oxidizing and Ti-richer environmental condition as compared with the equivalent primary Ast-1 crystals from Mandira, close to slightly higher than the QFM (Quartz-Fayalite-Magnetite) buffer (cf. Nicholls and Carmichael, 1969; Czamanske and Mihalik, 1972). Its chemical fingerprint was certainly influenced by the composition of the residual melt, in a scenario of intense competition with another mafic and accessory minerals for the HFSE and REE budgets. For instance, we deduce that, contrarily to the Mandira case, its lower Zr and HREE contents are related to early zircon crystallization and the lower LREE abundances to the preferential partition of these elements into chevkinite, a common accessory phase in the astrophyllite-bearing Papanduva granites. Furthermore, sodic-calcic and sodic amphiboles and aegirine are also important REE sinks within these rocks (Vilalva et al., 2016).

3.5.3. The replacement of sodic amphiboles and aegirine by astrophyllite

Most among the exotic HFSE- and REE-bearing minerals in peralkaline systems are of late magmatic and/or hydrothermal origin, indicating a major fluid role in the generation of such mineralogical complexity (*e.g.* Vasyukova and Williams-Jones, 2019). In fact, variable degrees of hydrothermal/metasomatic alterations are key features in many peralkaline rocks and manifested by typical post-magmatic/hydrothermal mineral assemblages developed through the destabilization of primary HFSE- and REE-rich minerals, in response of changing fluid properties, as well as temperature, pressure and f_{O2}.

The textural relationships observed in the studied samples show that the formation of the Ast-2b astrophyllite generation in both occurrences is certainly due to the partial replacement of primary Na-Fe bearing minerals such riebeckite (in Mandira), and arfvedsonite and/or aegirine (in Papanduva) at a post-solidus stage. These Na mafic silicates carry significant HFSE and/or REE contents (Vilalva et al., 2016; Siegel et al., 2017; Siachoque et al. in chapter 2). Therefore, we must consider both their chemical compositions and the nature of the hydrothermal fluids to explain the formation of post-magmatic astrophyllite. The chemical reactions are illustrated in each case through gain-loss diagrams depicted in (Figure 3-10). As shown, the substitutions of the sodic-rich mafic minerals by Ast-2a and Ast-2b astrophyllite results in significant gains of Rb, Cs, HFSE (except for Zr and Hf), LREEs and actinides, and loss of Ca, Na, Sc, Y-HREEs. This is in agreement with the findings of Abdel-Rahman (1992), which suggested that the substitution of sodic amphiboles by astrophyllite occur as a result of metasomatic reactions involving peralkaline residual fluids; according, the following reactions involving these phases may acted in our case:

$$3[Na_2(Fe_3^{+2}Fe_2^{+3})Si_8O_{22}(OH)_1F_1]_{Rbk} + [4K^+ + 5Ti^{4+} + 10H_2O]_{Fluid1} \leftrightarrow 2[K_2NaFe_7^{+2}Ti_2Si_8O_{26}(OH)_4F]_{Ast\text{-}2b} + [FeTiO_3]_{Ilm} + 8[SiO_2]_{Qz} + [4Na^+ + 16H^+ + F^-]_{Fluid2} \quad (1)$$

$$3[Na_3(Fe_4^{+2}Fe^{+3})Si_8O_{22}(OH)_{1.5}F_{0.5}]_{Arf} + [4K^+ + 4Ti^{4+} + 7.5H_2O]_{Fluid1} \leftrightarrow 2[K_2NaFe_7^{+2}Ti_2Si_8O_{26}(OH)_4F]_{Ast\text{-}2b} + [NaFe^{+3}Si_2O_6]_{Aeg\text{-}3} + 6[SiO_2]_{Qz} + [6Na^+ + 7H^+ + 0.5F^-]_{Fluid2} \quad (2)$$

$$8[NaFe^{+3}Si_2O_6]_{Aeg\text{-}1} + [4K^+ + 4Ti^{4+} + 2F^- + 12H_2O]_{Fluid1} \leftrightarrow 2[K_2NaFe_7^{+2}Ti_2Si_8O_{26}(OH)_4F]_{Ast\text{-}2b} + [6Na^+ + 8H^+]_{Fluid2} \quad (3)$$

All these reactions point to the K- and Ti-rich nature of the fluids altering the sodic primary phases. The released of K^+ into the fluid is probably due to the alkali metasomatism acting in both occurrences, leading to intense albitization, as reported by Oliveira (1989) and Vilalva and Vlach (2014) respectively, whereas the Ti^{4+} in solution may come from the destabilization of primary Fe-Ti minerals. Such alkali metasomatism is described, for instance, in the peralkaline Strange Lake granite, where the inferred temperatures have high salinity (25 wt.% NaCl). In the case of the Papanduva Pluton, the alkali metasomatism could be preceded by a cooling-induced oxidation stage, triggered by the substitution of arfvedsonite and Fe-richterite by aegirine (Vilalva et al., 2016) and contributing, at least in part, to the K^+ released to the fluid.

All the above reactions change the fluid compositions, releasing H^+, F^- and Na^+ and so leads to decreasing pH and increasing salinity. In the Mandira case, the substitution of riebeckite by astrophyllite (Eq. 1) should result in the co-precipitation of hydrothermal quartz and ilmenite, whereas the released of Na^+ and HF^-, along with Y-HREEs, may contributed to the formation of gagarinite-(Y), as evidenced through our textural relations (Figure 3-2). The coeval replacement of arfvedsonite and aegirine by astrophyllite in the Papanduva Pluton (Eqs. 2 and 3) did not favor the formation of ilmenite, as observed in Mandira and, certainly, this was due to the fact that crystallization conditions at this stage are within the 'no-oxide' field in the T-fO2 space, where aenigmatite is the stable phase instead of the Fe-Ti oxides (Nicholls and Carmichael, 1969; Vilalva et al., 2016). These two reactions release more Na^+ and increase its activity within the fluids, allowing the precipitation of post-magmatic aegirine and, to a certain extent, of Na-rich rare phases. In fact, the Papanduva granites have higher peralkalinity as compared with Mandira (Section 3.2 and Figure 3-10), and the most evolved among them (the foliated facies), with ubiquitous Ast-2b astrophyllite, carry a variety of REE- and HFSE-bearing accessory minerals, including elpidite and other (Na, K)-zirconosilicates instead of zircon (Vilalva and Vlach, 2014; Vilalva et al., 2016). The remaining HF^- are arguably related to the formation of bastnäsite-(Ce) at very late stages.

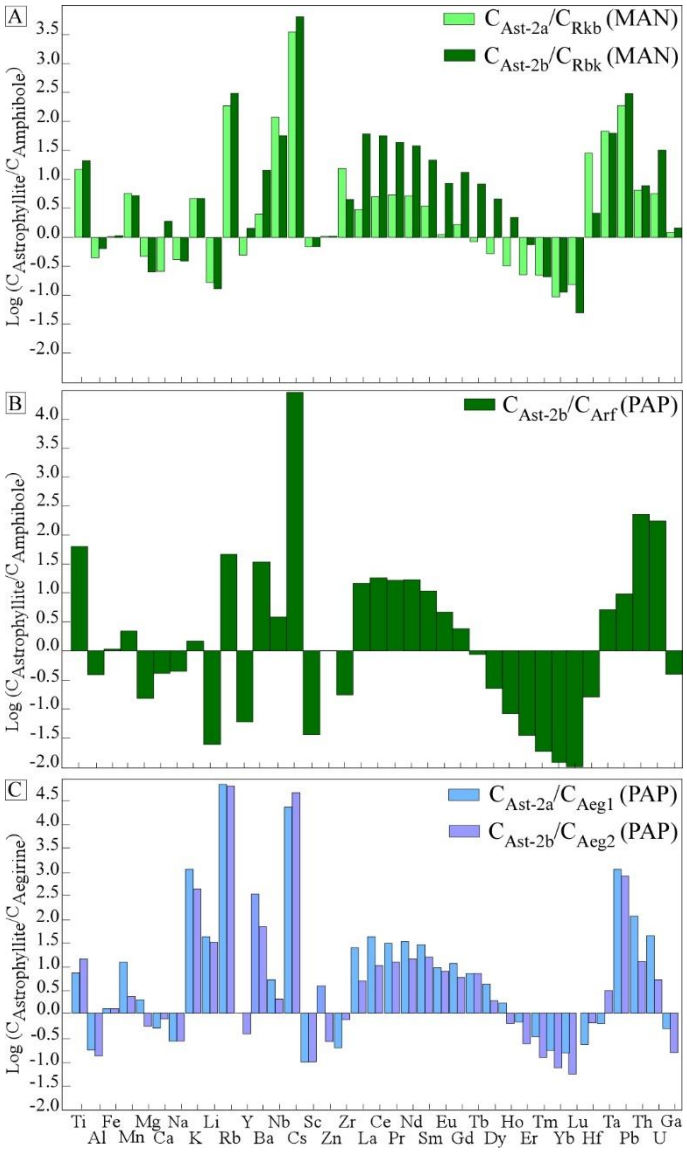

Figure 3-10: Gain-loss diagram between astrophyllite and sodic amphiboles and aegirine from the MAN and PAP plutons, respectively.

3.5.4. Zr-Ti and Fe-Mn relationships in astrophyllite as petrogenetic indicators

Correlations between astrophyllite compositions and crystallization environments, considering both the SiO_2-undersaturated and SiO_2-saturated systems were firstly evaluated by Piilonen et al. (2003b, 2004). Based on the available data, the authors suggested the cationic plot Nb-Zr *vs* Mn# [= Mn/(Mn+Fe), cations] as a potential discriminator between astrophyllite formed during (i) magmatic or post-magmatic and (ii) hydrothermal or metassomatic environments. We plot our and the available literature data in that diagram in Figure 3-11A, and the main emerging conclusion is that our textural and chemical data do not agree in full with such a proposal.

In fact, we observed that the Zr/(Zr+Ti) and the Mn# parameters (Figure 3-11B) work better to discriminate magmatic and post-magmatic environments of crystallization for astrophyllite, once most of the worldwide astrophyllite compositions correlate to our primary and secondary groups, and we suggest the use of the Zr/(Zr+Ti) parameter instead of Nb-Zr. In addition, variations of the Mn# values can be related to the oxidizing conditions, they allow qualitative f_{O2} estimates. In fact, astrophyllite from Papanduva, KAN, ILL, LFN, LOV, MSH, ORV (see Figure 3.5 legend for abbreviations) occurrences, usually coexisting with sodic pyroxenes, present Mn# values in between 0.1-0.5, which is indicative of relatively higher f_{O2} oxidizing conditions. On the contrary, astrophyllite with Mn# < 0.1 were formed at relatively Fe-rich environments, most of them resulting from the replacement of sodic amphiboles, as from the Mandira, MGC, PAP, SPD and STC occurrences, preferentially under relative reduced environments.

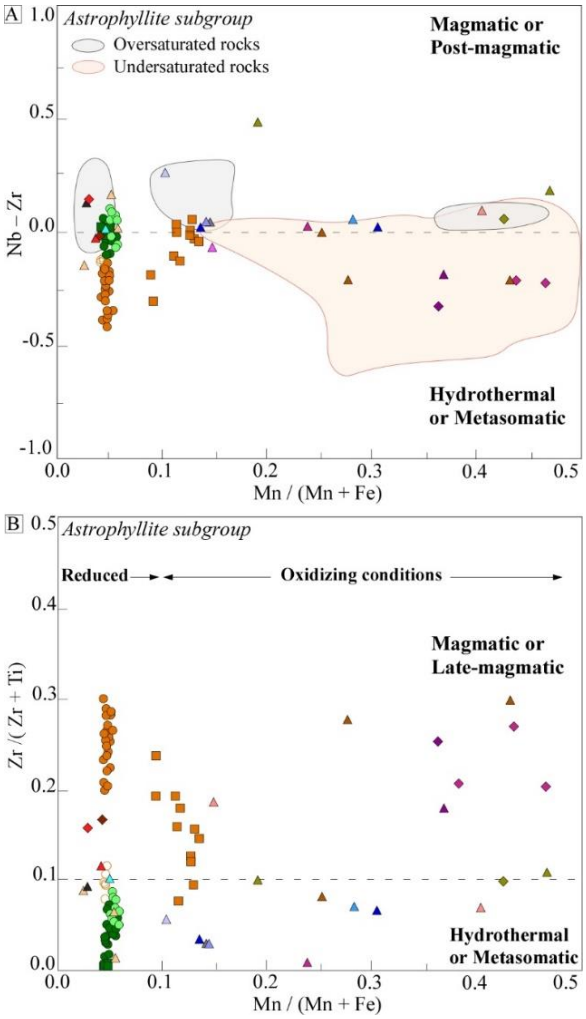

Figure 3-11: Discrimination plots for the astrophyllite subgroup minerals. A) Nb-Zr versus Mn/(Mn+Fe) diagram which display the distinct environments for astrophyllite formation. B) An updated of the Piilonen et al. (2004) discrimination plot showing the relation between Zr/(Zr+Ti) and Mn/(Mn+Fe), in which the conditions of formation for astrophyllite occurrences in A-type localities worldwide are best correlated

3.6. Conclusions

Textural and chemical data for late-magmatic and post-magmatic astrophyllite in agpaitic peralkaline granites from the Mandira Massif and Papanduva Pluton in the Graciosa Province of A-type granites and syenites (S-SE Brazil) allow drawn the following main conclusions:

1) Astrophyllite is a relatively common accessory mineral in the Mandira and Papanduva occurrences. Three main textural generations were discriminated, one late-magmatic (Ast-1) characterized by relatively higher Zr and Nb contents, two post-magmatic (Ast-2a and Ast-2b), both with higher Ti abundance.
2) Trace element compositions indicated, in general, a relative enrichment in LILEs, HFSEs and LREEs relative to the bulk host rocks, except for Ast-2b crystals in the Papanduva Pluton with distinctively lower HFSEs and REEs contents. The chemical contrasts among the astrophyllite inter- and intra-occurrences generations are related to the degree of peralkalinity and with the previous and/or concomitant crystallization of sodic-rich mafic minerals and HFSE- and REE-bearing accessory minerals.
3) Astrophyllite-melt partitioning defines a stronger compatibility of the HFSEs and REEs, particularly in the Na-richest astrophyllite crystals from the Mandira granites.
4) The precipitation of the post-magmatic Ast-2a and Ast-2b crystals is related to disequilibrium processes and substitution reactions involving early-precipitated sodic amphiboles and clinopyroxenes, and relatively K^{+}- and Ti^{4+}-rich hydrothermal fluids.
5) Chemical asttrophyllite parameters as Zr/(Zr+Ti) and Mn(Mn+Fe) can be used to trace magmatic-hydrothermal crystallization environments, as well as to qualitatively monitor their *redox* conditions.

Acknowledgements

Staff do GeoAnalitica, FAPESP for financing this work (Proc. 08/00562-0) and (Proc. 2019/17343-4), and CAPES for the doctoral scholarship (Finance Code 001).

Table 3-1: Major and trace element compositions for astrophyllite from the Mandira and Papanduva Plutons.

Samples	MAN-13A2				MAN-4776			MAN-13A2			MR-01A				MR-21	
Point_ID	10-c	13-c	14-c	14-r1	1-c	2-r1	3-r1	5-r	1-c	21-c	1-r	2-c	3-c	4-c	3-i	4-i
Group	MAN Ast-1				MAN Ast-2a			MAN Ast-2b			PAP Ast-1				PAP Ast-2b	
Facies	Riebeckite alkali-feldpar granite				Riebeckite alkali-feldpar granite						Massive				Foliated	
SiO_2 (wt%)	34.24	34.520	34.48	35.80	35.27	35.19	35.35	35.66	34.97	35.22	34.32	34.87	35.07	35.01	36.23	36.32
TiO_2	8.37	7.970	7.90	9.68	8.92	10.71	9.01	10.20	11.31	11.21	9.95	8.68	9.72	9.62	11.52	12.00
Al_2O_3	0.83	0.598	0.69	0.46	0.68	0.62	0.49	0.46	0.91	0.77	0.92	0.29	0.49	0.66	0.06	0.07
FeO^T	34.83	35.080	35.04	35.62	34.02	34.86	35.38	35.37	35.12	35.46	32.74	32.81	31.43	31.23	35.47	35.25
MnO	1.70	1.670	1.74	1.63	1.74	2.04	2.00	1.94	1.71	1.61	4.19	3.30	4.57	4.60	1.63	1.75
MgO	-	0.020	-	-	0.02	-	0.01	-	0.02	0.01	0.11	0.09	0.18	0.21	-	-
CaO	0.36	0.319	0.13	0.13	0.25	0.23	0.03	0.13	0.41	0.42	1.00	0.62	0.48	0.63	0.18	0.47
Na_2O	2.49	2.790	2.83	2.87	2.80	2.80	3.02	3.09	2.76	2.83	2.23	2.43	2.63	2.62	3.72	3.46
K_2O	5.33	5.290	5.44	5.03	5.31	5.35	5.40	5.15	5.24	4.92	5.27	5.42	5.49	5.60	5.35	5.26
ZnO	0.40	0.467	0.32	0.34	0.48	0.39	0.37	0.47	0.37	0.43	-	-	-	-	-	-
ZrO_2	4.02	3.510	3.52	1.60	0.91	0.86	1.18	0.74	0.53	0.22	1.28	4.16	2.14	1.53	0.10	0.09
Nb_2O_5	0.34	1.322	1.66	0.42	1.43	0.36	2.02	0.90	0.36	0.13	1.65	1.48	2.24	2.08	0.340	0.170
F	1.28	1.300	-	1.15	0.99	0.96	0.69	0.83	1.19	1.30	0.58	0.54	0.50	0.42	0.830	0.860
Sum	94.19	94.86	93.75	94.72	92.82	94.36	94.95	94.94	94.89	94.54	94.24	94.69	94.94	94.21	95.43	95.70
O=F	0.54	0.55	0.00	0.48	0.42	0.40	0.29	0.35	0.50	0.55	0.24	0.23	0.21	0.18	0.35	0.36
Total	93.65	94.31	93.75	94.24	92.40	93.95	94.66	94.59	94.39	93.99	94.00	94.46	94.73	94.03	95.08	95.34
Li (ppm)	131.38	145.85	147.16	183.29	245.43	198.56	253.71	289.10	136.10	260.68	371.83	206.17	190.14	359.56	84.06	70.48
Sc	10.43	7.36	8.13	4.17	3.50	3.75	3.82	2.81	7.24	1.42	5.23	8.90	8.10	3.45	0.523	0.572
Ti	49129	43646	47460	53250	63668	57281	59836	58179	47031	58952	52746	46964	45444	51315	57616	62155
Ga	19.18	17.40	16.49	8.38	18.29	16.00	13.57	14.88	12.19	16.37	7.39	6.98	7.78	10.95	3	2.76
Rb	5531.8	4426.3	4974.7	4289.6	5535.5	4736.1	4278.0	4277.7	4944.9	4456.8	2381.8	2751.3	2490.7	2522.4	2723.6	2628.4
Sr	5.66	3.22	1.76	1.54	12.93	15.40	19.66	17.95	3.60	4.97	34.57	30.94	115.69	29.43	16.73	13.13
Y	205.49	217.09	28.33	27.27	132.02	35.56	33.38	142.78	22.69	93.19	55.92	21.86	18.85	81.44	16.42	16.44
Zr	31073	24592	25640	12408	11122	11363	11392	7131	21538	3570	16027	27942	25462	10530	322	369
Nb	4051	9156	10738	2856	7361	5889	6459	4734	10153	2019	9137	8091	13148	11225	1777	1344
Cs	778.82	654.50	655.97	861.59	826.06	638.95	405.98	675.22	855.45	814.59	328.33	145.06	135.46	137.63	729.67	599.3
Ba	66.65	48.68	28.02	13.46	60.22	54.33	64.31	44.22	26.85	70.37	449.35	193.18	466.51	316.03	67.48	58.78
La	409.90	284.75	230.83	78.53	421.81	320.24	393.79	360.24	160.18	544.54	115.87	102.12	91.21	147.49	125.6	129.46
Ce	1300.8	1021.9	999.9	316.6	1444.3	1192.1	1543.5	1114.7	639.7	1981.5	543.67	437.03	415.93	633.02	434.6	435.16
Pr	142.42	144.08	150.23	42.70	215.81	160.74	206.14	149.71	88.57	278.55	96.57	78.33	77.63	113.86	58.96	53.95
Nd	561.0	592.2	634.5	159.2	919.7	628.9	809.1	659.4	359.2	1186.3	542.80	403.67	418.82	631.10	238.01	203.1
Sm	144.85	154.94	131.36	26.65	159.31	105.11	147.11	118.46	68.25	252.24	170.77	109.35	108.07	163.25	38.64	32.5
Eu	0.92	1.22	0.34	0.16	0.78	0.53	0.70	0.93	0.12	1.32	4.17	0.79	2.03	1.17	0.452	0.513
Gd	103.22	117.33	51.37	9.29	76.16	42.60	64.53	62.72	28.64	138.14	99.26	48.95	44.18	73.85	12.17	11.67
Tb	16.24	18.91	4.66	1.19	8.44	5.03	8.05	7.36	2.87	16.61	13.66	5.92	5.12	8.05	1.301	1.227
Dy	69.35	102.05	14.30	7.70	30.82	20.28	29.62	32.09	10.36	60.54	51.26	20.23	17.34	27.07	6.59	4.75
Ho	12.82	16.49	1.89	1.66	4.19	2.81	3.64	4.72	1.52	7.59	5.89	2.02	1.82	3.36	1.152	0.886
Er	25.14	28.05	4.21	3.92	8.49	6.57	6.11	10.97	4.19	12.00	7.53	2.72	2.58	7.21	3.33	2.48
Tm	1.98	2.72	0.55	0.81	0.74	0.92	0.58	1.34	0.53	0.97	0.30	0.16	0.20	0.78	0.523	0.529
Yb	10.32	11.48	4.34	5.18	4.81	6.35	2.71	9.28	3.31	6.67	0.98	0.85	1.02	2.79	3.7	2.9
Lu	1.28	1.23	0.65	0.42	0.49	0.78	0.29	1.15	0.48	0.65	0.11	0.11	0.14	0.23	0.498	0.517
Hf	1348.5	1228.1	1124.2	1048.3	699.9	796.2	755.0	829.0	1065.5	86.8	506.2	1002.0	1357.1	283.8	5.6	10.9
Ta	30.97	293.76	846.55	62.08	432.97	257.49	239.36	50.69	124.57	27.16	854.75	192.98	1562.1	432.20	28.96	15.44
Pb	2821.0	1499.7	1787.1	2117.9	3110.0	3136.8	3079.2	2788.9	1283.8	4007.2	223.6	176.3	199.5	224.5	354.6	376.1
Th	25.09	23.32	2.75	2.67	193.76	275.18	25.12	139.34	1.47	4.61	0.49	0.22	0.14	3.03	12.07	3.99
U	9.58	6.10	8.16	8.58	23.23	28.20	6.24	19.34	5.07	4.71	8.18	9.65	4.35	8.15	5.02	3.18

EMPA major oxides (in wt. %) and LA-ICPMS trace element compositions (in ppm); MAN: Mandira Pluton; PAP: Papanduva Pluton

Table 3-2: Structural formula for astrophyllite from the Mandira and Papanduva Plutons.

Samples	MAN-13A				MAN-4776				MAN-13A2		MR-01A				MR-21	
Point_ID	10-c	13-c	14-c	14-r1	1-c	2-r1	3-r1	5-r	20-c	21-c	1-r	2-c	3-c	4-c	3-i	4-i
Group	MAN Ast-1				MAN Ast-2a			2b	MAN Ast-2b		PAP Ast-1				PAP Ast-2b	
Facies	Riebeckite alkali-feldpar granite				Riebeckite alkali-feldpar granite						Massive				Foliated	
Structural formula based on 28.5O																
Si	7.815	7.849	7.825	8.020	8.011	7.877	7.896	7.929	7.795	7.849	7.719	7.801	7.787	7.866	8.024	8.007
Al	0.185	0.151	0.175	0.000	0.000	0.123	0.104	0.071	0.205	0.151	0.244	0.162	0.165	0.134	0.000	0.000
T-site	**8.000**	**8.000**	**8.000**	**8.020**	**8.011**	**8.000**	**8.000**	**8.000**	**8.000**	**8.000**	**7.963**	**7.963**	**7.952**	**8.000**	**8.024**	**8.007**
Ti	1.437	1.363	1.348	1.631	1.524	1.803	1.514	1.706	1.896	1.879	1.683	1.473	1.512	1.481	1.919	1.990
Nb	0.036	0.141	0.176	0.044	0.152	0.037	0.211	0.093	0.037	0.014	0.174	0.246	0.287	0.166	0.035	0.018
Zr	0.447	0.389	0.389	0.175	0.101	0.093	0.129	0.081	0.057	0.024	0.140	0.281	0.202	0.353	0.011	0.000
Sn	0.000	0.000	0.000	0.000	0.000	0.000	0.000	0.000	0.000	0.000	0.000	0.000	0.000	0.000	0.000	0.000
Mg	0.000	0.007	0.000	0.000	0.007	0.000	0.002	0.000	0.007	0.002	0.003	0.000	0.000	0.000	0.000	0.000
Al	0.037	0.009	0.009	0.121	0.182	0.040	0.025	0.048	0.003	0.053	0.000	0.000	0.000	0.000	0.016	0.000
D-site	**1.958**	**1.909**	**1.923**	**1.970**	**1.965**	**1.974**	**1.881**	**1.928**	**2.000**	**1.972**	**2.000**	**2.000**	**2.000**	**2.000**	**1.981**	**2.007**
Fe^{2+}	6.648	6.670	6.649	6.673	6.462	6.525	6.608	6.576	6.546	6.608	6.157	5.985	5.917	6.111	6.569	6.498
Mn	0.329	0.322	0.334	0.309	0.335	0.387	0.378	0.365	0.323	0.304	0.798	0.753	0.760	0.609	0.306	0.327
Mg	0.000	0.007	0.000	0.000	0.007	0.000	0.002	0.000	0.007	0.002	0.037	0.044	0.050	0.043	0.000	0.000
Zn	0.068	0.078	0.054	0.056	0.081	0.065	0.061	0.077	0.062	0.070	0.000	0.000	0.000	0.000	0.000	0.000
Zr	0.000	0.000	0.000	0.000	0.000	0.000	0.000	0.000	0.000	0.000	0.000	0.069	0.083	0.001	0.000	0.010
Li	0.000	0.000	0.000	0.000	0.072	0.024	0.000	0.000	0.063	0.016	0.008	0.060	0.055	0.104	0.000	0.000
Na	0.000	0.000	0.000	0.000	0.044	0.000	0.000	0.000	0.000	0.000	0.000	0.089	0.135	0.132	0.125	0.165
Ca	0.000	0.000	0.000	0.000	0.000	0.000	0.000	0.000	0.000	0.000	0.000	0.000	0.000	0.000	0.000	0.000
C-site	**7.045**	**7.076**	**7.038**	**7.038**	**7.000**	**7.000**	**7.049**	**7.019**	**7.000**	**7.000**	**7.000**	**7.000**	**7.000**	**7.000**	**7.000**	**7.000**
Ca	0.088	0.078	0.031	0.031	0.060	0.054	0.008	0.032	0.097	0.101	0.241	0.254	0.274	0.304	0.043	0.111
Na	0.912	0.922	0.969	0.969	0.940	0.946	0.992	0.968	0.903	0.899	0.759	0.746	0.726	0.696	0.957	0.889
Ba	0.000	0.000	0.000	0.000	0.000	0.000	0.000	0.000	0.000	0.000	0.000	0.000	0.000	0.000	0.000	0.000
B-site	**1.000**	**1.000**	**1.000**	**1.000**	**1.000**	**1.000**	**1.000**	**1.000**	**1.000**	**1.000**	**1.000**	**1.000**	**1.000**	**1.000**	**1.000**	**1.000**
K	1.552	1.534	1.575	1.437	1.539	1.528	1.539	1.461	1.490	1.399	1.512	1.468	1.501	1.444	1.512	1.479
Cs	0.008	0.007	0.000	0.000	0.008	0.006	0.004	0.007	0.016	0.008	0.003	0.001	0.001	0.001	0.000	0.000
Na	0.190	0.308	0.276	0.277	0.249	0.269	0.316	0.364	0.289	0.324	0.213	0.223	0.129	0.145	0.515	0.425
Ba	0.001	0.001	0.000	0.000	0.001	0.001	0.001	0.000	0.000	0.004	0.009	0.000	0.000	0.000	0.008	0.000
Li	0.039	0.043	0.043	0.053	0.000	0.034	0.073	0.083	0.032	0.060	0.101	0.000	0.000	0.000	0.000	0.000
Rb	0.089	0.071	0.079	0.068	0.088	0.075	0.067	0.067	0.075	0.070	0.038	0.044	0.039	0.040	0.000	0.000
Pb	0.031	0.017	0.020	0.023	0.035	0.034	0.034	0.030	0.005	0.044	0.002	0.002	0.002	0.002	0.000	0.000
A-site	**1.910**	**1.980**	**1.994**	**1.859**	**1.920**	**1.947**	**2.033**	**2.012**	**1.908**	**1.908**	**1.878**	**1.738**	**1.672**	**1.632**	**2.034**	**1.904**
Cations	19.913	19.965	19.955	19.888	19.896	19.920	19.964	19.959	19.908	19.880	19.841	19.701	19.624	19.632	20.03	19.919
F	0.924	0.935	0.000	0.815	0.710	0.678	0.487	0.585	0.839	0.916	0.413	0.328	0.218	0.268	0.581	0.600
Zr/(Zr+Ti)	0.237	0.222	0.224	0.097	0.062	0.049	0.078	0.045	0.029	0.013	0.077	0.192	0.158	0.193	0.006	0.005
Ti/(Ti+Nb)	0.763	0.778	0.776	0.903	0.938	0.951	0.922	0.955	0.971	0.987	0.923	0.808	0.842	0.807	0.994	0.995
Fe#	0.953	0.954	0.952	0.956	0.951	0.944	0.946	0.947	0.953	0.956	0.885	0.888	0.886	0.909	0.956	0.952
Mn#	0.047	0.046	0.048	0.044	0.049	0.056	0.054	0.053	0.047	0.044	0.115	0.112	0.114	0.091	0.044	0.048

Structural formulae for astrophyllite from the Mandira (MAN) and Papanduva Plutons (PAP). Point_ID: spot identification; c: core; r: rim; i: intermediate zone

Table 3-3: Astrophyllite-melt REE partition coefficients for the magmatic astrophyllite group from the Mandira and Papanduva Plutons.

	XRF	
Samples	MAN-13A	MR-01
Unit	Mandira	Papanduva
SiO_2 (wt%)	77.33	75.98
TiO_2	0.12	0.21
Al_2O_3	10.93	10.83
Fe_2O_3	1.99	2.91
MnO	0.03	0.06
MgO	0.01	0.01
CaO	0.24	0.26
Na_2O	3.99	4.34
K_2O	4.49	4.66
P_2O_5	0.00	0.01
LOI	0.40	0.44
Total	99.53	99.71
Fe#	0.99	1.00
A/CNK	0.91	0.86
A.I	1.05	1.12
T(°C)sat(zr)	894	n.c
Zn (ppm)	173	147
Ga	27	30
Zr	531	1217
F	2913	n.c

LOI: lost on ignition; Fe#: FeOt/(FeO+MgO); A/CNK: Alumina Saturation Index; A.I Agpaitic Index; n.c: not calculated; XRF: X-ray fluorescense; ICP-MS: Inductively coupled plasma mass spectrometr; LSM: Lattice Strain Model

	ICP-MS	
Samples	MAN-13A	MR-01
Unit	Mandira	Papanduva
Sc (ppm)	0.5	1.2
Rb	238	136
Sr	4.8	5.2
Y	225	168
Zr	553	
Nb	56.2	66
Cs	3.7	2
Ba	0.6	40
La	45.3	164
Ce	111	274
Pr	17.2	33
Nd	81.8	120
Sm	27.3	26
Eu	0.4	1
Gd	35.0	26
Tb	6.0	4
Dy	36.3	28
Ho	7.8	6
Er	21.1	17
Tm	2.8	2
Yb	16.2	16
Lu	2.1	2
Hf	20.3	34
Pb	32.1	50.1
Th	18.9	42.1
U	4.0	4.4

	LSM	
Sample	MAN-13A	MR-01
REE	Ast-1	Ast-1
D_{La}	0.311	0.334
D_{Ce}	0.367	0.295
D_{Pr}	0.395	0.272
D_{Nd}	0.416	0.268
D_{Sm}	0.453	0.294
D_{Eu}	0.538	0.552
D_{Gd}	0.494	0.358
D_{Tb}	0.569	0.391
D_{Dy}	0.626	0.421
D_{Ho}	0.596	0.226
D_{Er}	0.388	0.190
D_{Tm}	0.167	0.041
D_{Yb}	0.069	0.010
D_{Lu}	0.110	0.022
D_{Ti}	0.720	0.425
D_{Zr}	0.605	0.076
D_{Hf}	0.710	0.719
Calculated parameters		
D_0 D-site	9.324	4.472
E (kbar)	311.8	68.40
r_0 (A)	1.018	0.969
T (°C)	550	550
D_0 C-site	143.45	109.17
E (kbar)	798.8	1213.1
r_0 (A)	0.659	0.651
T (°C)	550	550

4. OCCURRENCE AND COMPOSITION OF COLUMBITE-(FE) IN THE REDUCED A-TYPE DESEMBORQUE PLUTON, GRACIOSA PROVINCE (S-SE BRAZIL)

Astrid Siachoque[a], Rodolfo P. Garcia[a], Silvio R.F. Vlach[a]
a. Institute of Geosciences -University of São Paulo, São Paulo-Brazil.

ABSTRACT

The main biotite granites in the Desemborque pluton, from the A-type Graciosa Province (S-SE Brazil), underwent post-magmatic alterations leading the formation of greisenized granites and greisens. Among hydrothermal rocks were found rare Nb-Ta-Sn oxide minerals such cassiterite and columbite and this study focusses the detailed textural and chemically characterization of the columbite occurrences. Our results show that columbite occurs in two distinct textural types between both syenogranites and greisens. The columbite-1 form small euhedral to subhedral, prismatic crystals with concentric or irregular zoning showing two substages of crystallization: i) an early-stage Nb-rich cores with #Ta = Ta/(Ta +Nb) ratios varies from 2.30 to 8.06 and #Mn= Mn/(Mn + Fe) ratios between 17.22 to 21.25 (in apfu), and ii) a later-stage Ta-rich rims with #Ta and #Mn ranges 11.46–26.81 and 14.35–22.30, respectively. Cationic correlations also show increase of Ti (0.017–0.110), W (0.01–0.09), and Zr (0.001–0.039) from cores to rims. The columbite-2 occur as minute anhedral patchily crystals coexisting with cassiterite, zircon and/or secondary REE-fluorides. Chemical compositions show low #Ta values 0.79–3.78 but high #Mn 20.64-38.42values relative to the columbite-1 crystals, and Ti, W, and Zr up to 0.089, 0.065, 0.006, respectively. Moreover, REE and trace elements distribution show significant abundances of HREE, U, Sn, W, Nb and Ta among columbite crystals with REEs total for columbite-1 type varies 906–1362 ppm from core to rim crystals, whereas the columbite-2 type has relative higher REEs up to 3996 ppm. These features allow us to infer that that formation of columbite-1 group was related either to post-magmatic alterations in syenogranites or greisen-crystallization hydrothermal processes at early-stage of hydrothermal activity, whereas the columbite-2 recrystallized from a REE-rich residual melt derived from fluid-induced alterations such the breakdown of pre-existing zircon, fluorite and possible columbite-1 crystals at distinct final-stage of hydrothermal evolution.

Keywords: Columbite-Fe, microtextures, mineral chemistry, granites and greisens, A-type Graciosa Province.

4.1. Introduction

Columbite is the main Nb-oxide included in the orthorhombic columbite-tantalite group minerals (CGM). End-members of this group are designated as columbite-(Fe), columbite-(Mn), tantalite-(Fe), and tantalite-(Mn) after Burke (2008), with the general formula AB_2O_6, where Fe^{2+} or Mn^{2+} occupies the *A*-site and Nb^{5+} or Ta^{5+} the *B*-site (Černý and Ercit, 1985, 1989; Ercit, 1994). The CGM minerals have a wide range of composition and structural variations which are mainly related to cationic order-disorder between *A* and *B*-sites (Černý and Ercit, 1985; Wenger et al., 1991; Cerny et al., 1992; Ercit et al., 1995; Černý et al., 1998), and reflect changes in the unit cell dimensions and, in the oxygen octahedra (Cerny and Turnock, 1971; Grice et al., 1976). In general, the structures of both ordered and disordered within members of CGM included minor substitutions of Ti, Sn, W, Zr, Hf, Sc, REEs and other elements (Melcher et al., 2015).

The occurrence of CGM minerals have attracted significant attention since they are hosted in several Ta-Nb-Sn metallogenetic provinces (Melcher et al., 2015, 2016) and references therein). Moreover, the columbite-tantalite pair form a certain U-Pb geochronometer to dating magmatic and hydrothermal events in Nb-Ta ore deposits (*e.g.* Romer and Smeds, 1994; Romer and Lehmann, 1995; Smith et al., 2004; Dewaele et al., 2011; Melcher et al., 2015; Che et al., 2019). CGM commonly occur in pegmatites, leucogranites, rare-metal granites and greisens (Belkasmi et al., 2002; Neiva et al., 2015; Zhu et al., 2015; Alfonso et al., 2018; Novák et al., 2018; Che et al., 2019), and also is often found in highly evolved rocks such peralkaline granites, nepheline syenites and carbonatites (Möller, 1989; Bastos Neto et al., 2009; René and Škoda, 2011; Huang et al., 2015). They are usually associated with other Nb-Ta-Sn oxides such cassiterite, ixiolite, pyrochlore, rutile, wodginite and wolframite (Minuzzi et al., 2006; Mackay and Simandl, 2015; Llorens González et al., 2016; Feng et al., 2019; René, 2019). In this sense, compositional variations of the CGM become important guides to constraint magmatic and post-magmatic evolution of rare-metal related systems (Breiter et al., 2007; Lichtervelde et al., 2007; Martins et al., 2011; Wise et al., 2012; Badanina et al., 2015; Ballouard et al., 2016b).

In Brazil, CGM are found in pegmatites from the Lourenço-Amapá Province (Melcher et al., 2015), Seridó Belt - Borborema Province (Beurlen et al., 2005; Baumgartner et al., 2006) and from São João do Rei and Araçuaí districts - Mina Gerais State (Francesconi, 1972 and Dias and Chaves, 2015, respectively). Abundant columbite was reported in the massive cryolite zone from the Pitinga Mine - Amazonas State (Minuzzi et al., 2006; Bastos Neto et al., 2009). However, no one mineral chemistry study of columbite in greisens is informed yet in Brazil.

This study aims to investigate the textural features and chemical evolution of columbite found in reduced (ilmenite-type) biotite granites and the associated greisens in the Desemborque pluton from the A-type Graciosa Province, SE-Brazil. We provide new constraints on trace element compositions of columbite in granites and greisens, then on the hydrothermal processes and characteristics of the rare Nb-Ta oxides in the studied rocks.

4.2. The Desemborque Pluton

The Desemborque Pluton in the Guaraú Massif (Oliveira et al., 1987) is one among the most interesting plutons from the Graciosa Province in S-SE Brazil (Figure 4-1A). This province of A-type granites and syenites (Gualda and Vlach, 2007a) are made up several plutons and related volcanic and subvolcanic rocks emplaced in shallow continental crust during a post-collisional extensional regime associated to the geodynamic evolution of the south-southeastern part of the Gondwana area at 580 Ma (Vlach et al., 2011; Vilalva et al., 2019). The intrusions are grouped in two main petrographic associations: one alkaline, include metaluminous and peralkaline alkali-feldspar granites and syenites, while the other, aluminous, is constituted by metaluminous to slightly peraluminous syeno- and monzo-granites (Gualda and Vlach, 2007b, 2007a).

The Desemborque Pluton (Figure 4-1B) is a small subcircular intrusion (ca. 50 km^2) in the northeastern province area and intrudes the Atuba and Turvo-Cajati low- and medium- to high-grade metasedimentary complexes, respectively (Faleiros, 2008). The pluton is relatively homogeneous and composed mainly of biotite syenogranites, alkali feldspar granites, granite porphyries and microgranites are scarce (Garcia, 2015). Local simple pegmatites and hydrothermal altered rocks, as albitized granites and greisens, the latter resulting from the alteration of the main granite biotite granites (Oliveira et al., 1987; Garcia, 2015) are also of local occurrence. Fresh hydrothermally altered rocks are hard to see given the extensive weathering, thus albite granite and greisen were sample in a unique site. Nevertheless, this site well demonstrates the contact relationships and the transitions from the biotite granite to the enclosed albite granite and greisen (Figure 4-2). In the following we focus our descriptions in these main rocks varieties.

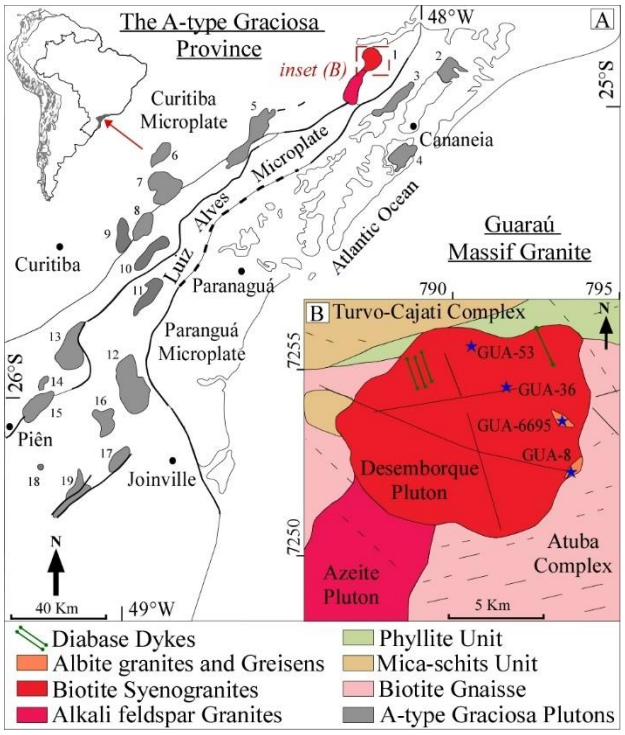

Figure 4-1: Location of the study area. A) Geological setting of the Neoproterozoic A-type Graciosa province in SE Brazil. The A-type granites and syenites of the Graciosa Province are: (1) Guaraú Massif; (2) Serra do Paratiú/Cordeiro; (3) Mandira Massif; (4) Ilha do Cardoso; (5) Alto Turvo; (6) Capivari; (7) Órgãos; (8) Farinha Seca; (9) Anhangava; (10) Marumbi; (11) Serra da Igreja; (12) Morro Redondo Complex; (13) Palermo; (14) Agudos do Sul; (15) Rio Negro; (16) Dona Francisca; (17) Piraí; (18) Serra Alta; (19) Corupá. B) Detailed geological map of Guaraú Massif Granite (Desemborque Pluton). The blue stars indicate the locations of columbite-bearing samples.

4.2.1. The biotite syenogranites

The biotite syenogranite display variably inequigranular medium- to coarse-grained and porphyritic textures (Figure 4-2C). They are composed of early perthite orthoclase-(Or_{58-71}), oligoclase-albite(Ab_{78-95}) and quartz (Figure 4-3). Biotite is a magmatic predominant mafic phase among these rocks and its compositions vary from annite to siderophyllite (Garcia, 2015). Zircon is the most abundant magmatic accessory mineral following by late-magmatic ilmenite and fluorite. Cassiterite, columbite, hematite, magnetite, monazite and xenotime are the post-magmatic accessories which are commonly included in aggregates of biotite. Secondary minerals are phengite, sericite, fluorides-(HREE) and thorite.

Geochemically, these rocks present average contents of 76.78 wt% SiO_2, 12.18 wt% Al_2O_3, 4.39 wt% K_2O, 4.06 wt% Na_2O and 1.07 wt% Fe_2O_3, thus present predominant metaluminous signature with A/CNK [molar = $Al_2O_3/(CaO + Na_2O + K_2O)$] index vary between 0.96-0.99, and show high Fe# numbers (~0.99) that contrast to other Graciosa granites within the aluminous association. Trace elements compositions show relatively high abundance

of Li (~129 ppm), and Rb (~ 421 ppm), REEs, Y and HFSEs, especially Zr and Nb, (up to 405, 315, 208, and 78 ppm, respectively), while Sn, Th and U concentrations are relatively low (~15, ~20, and ~6 ppm, respectively). Of note, F also show relevant concentrations (up to 5920 ppm). Zircon U-Pb geochronological data point to crystallization ages of 580 ± 8 Ma (Vilalva et al., 2019).

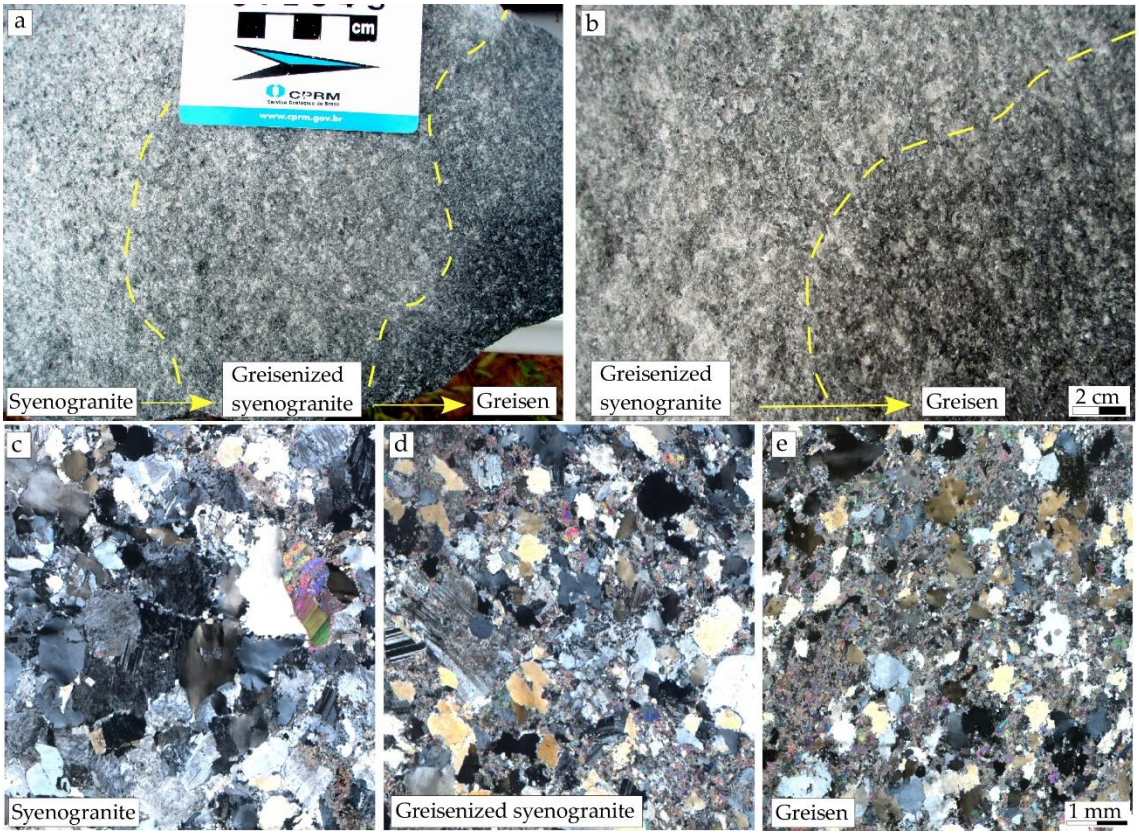

Figure 4-2: Textural aspects of granites and greisen from the Desemborque pluton. A) and B) Transitional contact between the syenogranite, greisenized granite and greisen and (B) between the greisenized granite and the greisen (sample GUA-08). Microtextures of C) syenogranite, D) greisenized granite and E) greisen. Photomicrographs taken in plane (on left) and cross-polarized (on right) light.

4.2.2. Greisenized Granite

The greisenized granite present equi-to inequigranular fine-grained texture (Figure 4-2D). It is composed mainly of albite-(Ab_{99}) and quartz, with minor orthoclase (perthite). Annite from the original hosted syenogranite is partial to completed replaced by zinnwaldite. Other minerals found in this rock are fluorite, ilmenite, hematite, phengite and sphalerite. Geochemically, the albite granite has intermediate compositions between the greisen and the hosted biotite syenogranite with relatively higher Fe_2O_3 (2.1 wt%) but lower Na_2O (2.96 wt%)

contents than the hosted granite. Among trace elements, the albite granite present significant contents of Rb (464 ppm), Y (164 ppm), Li (195 ppm), Sn (42 ppm), and F (6424 ppm).

4.2.3. Greisen

The studied sample is characterized by fine- to medium-grained heterogranoblastic textures (Figure 4-2E), and its mineral assemblage is characterized by quartz, zinnwaldite-(Li) and albite-(Ab_{99}) strongly replaced by sericite. Zircon, cassiterite, columbite, fluorite, monazite, thorite and xenotime are the accessory minerals. Galena, sphalerite and topaz are distinct accessories only found in these rocks. For comparison, geochemical compositions of these rocks present significant enrichment of Fe_2O_3 (5.27 wt%), Li (385 ppm), Rb (897 ppm), Sn (116 ppm), and F (9000 ppm) and discrete enriched of Nb (85 ppm), Th (35 ppm), relative to the hosted granites.

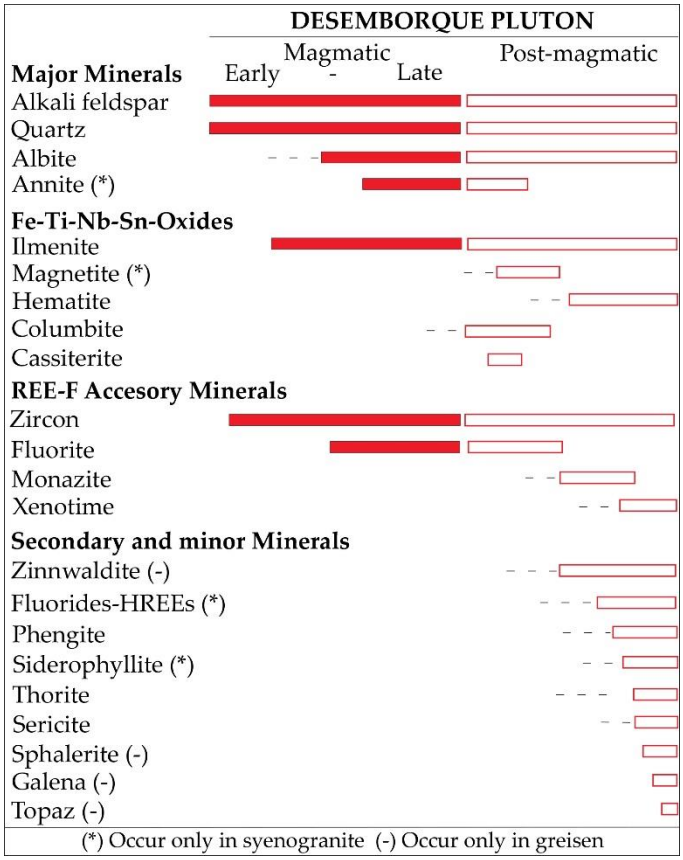

Figure 4-3: Crystallization sequence of the studied samples from the Desemborque Pluton showing the mineral assemblages at early, late and post-magmatic stages.

4.3. Analytical Methods

Columbite crystals were identified by combining optical electron microscopy (SEM) and semiquantative energy dispersive spectrometry (EDS) analyses. Back-scattered electron images (BSE) were obtained to study internal textures and compositional variations. After textural descriptions, the chemical compositions of columbite crystals were determined using a JEOL JXA-FE-8530 microprobe at the Laboratory of the NAP GeoAnalitica-Institute of Geosciences/University of São Paulo. A total of 42 analyses were conducted with an accelerating voltage of 20 kV, beam current of 15 nA, beam diameter of 3 μm and maximum total peak-counting times varying between 5 and 40 s. Standards used for analysis included: diopside for Si, Ca and Mg; ilmenite for Fe, Ti and Mn; anorthite for Al; albite for Na, zircon for Zr; fluorapatite for F; strontianite for Sr; yttrium-phosphate for Y; synthesized glasses for Gd and Th prepared by the Smithsonian Institute; and pure Pb, Sb, V, Ta, Nb, and W. The detection limit among all elements varies from 0.012 to 0.292 wt%. The columbite structural formulae was calculated based on 6 oxygens and 3 atoms per formula unit (apfu).

Trace elements of columbite crystals were analyzed using a Thermo Fisher Scientific iCAP Q ICP-MS instrument coupled with a New Ware UP-213 laser ablation system at the mentioned laboratory. Analytical conditions were a laser spot of 25 μm, 20 Hz of frequency with energy fluence of ~1.97 J/cm^2. Signal measurements and gas background on sample were 60 and 40 s, respectively. The instrument was calibrated with the NIST standard SRM 610 glass to correct signal drift during the analytical process and the basalt glass standard BCR-2G was used as external standard to calibrate major and trace elements. The detection limits, accuracy and precision of these analyses are reported in supplementary materials.

4.4. Columbite Occurrence

Petrographic observations reveal two textural types of columbite within the Desemborque rocks. The first type of columbite-1 appears most common in the greisen and rarely in the syenogranites. It occurs as minute (30-60 μm) crystals forming clusters at the groundmass. Crystals usually display subhedral, prismatic or surrounded forms and BSE-images shown variably zoned textures (Figure 4-4). Sometimes zoning shows a combination of homogeneous dark Nb-cores (Col-1a) and bright Ta-rims (Col-1b), also with locally patchy textures along rims Figure 4-4B). In other crystals, zoning is irregular with Nb-rich inner parts surrounded by

concentrically Ta-rich margins (Figure 4-4B), with lobate contacts between them. Moreover, Ta-rims show variable width or fine sizes and are partially dissolved, especially in greisens.

A distinct columbite-2 appears predominantly in syenogranites and less common in the greisen. This type occurs as irregular interstitial crystals with variable forms and sizes (up to 100 µm). They are commonly found in close relation with fluorite into biotite aggregates. Others minor accessory related with the coloumbite-2 crystals are cassiterite, ilmenite, zircon and fluocerite. Internal textures revealed altered domains and corroded margins partly replaced by secondary REE-fluorides (Figure 4-4C). Occasionally, these crystals overgrown the inner parts of cassiterite (Figure 4-4D).

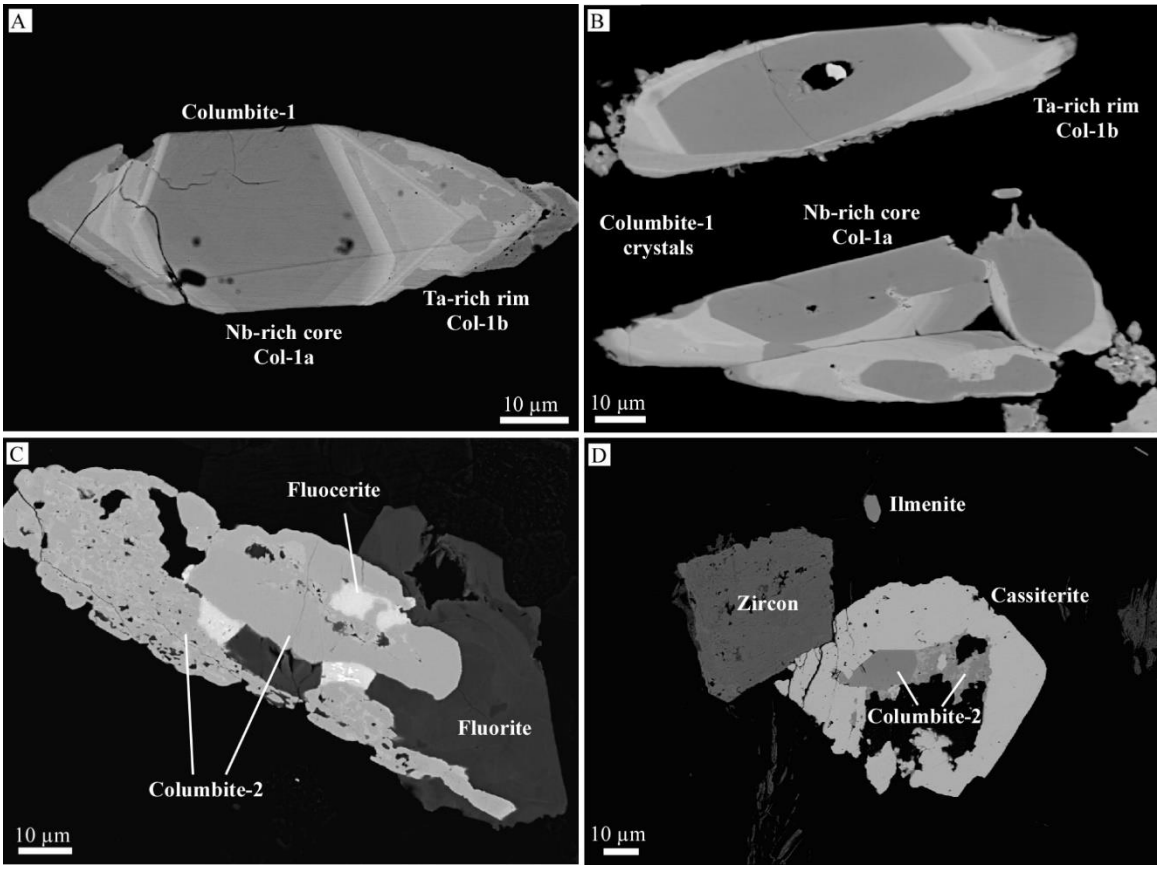

Figure 4-4: BSE images showing the textures and compositional variations in columbite crystals from Desemborque Pluton. (A) Euhedral columbite-1 crystal displaying heterogeneous zoning and irregular microcraks along rims; the darker domains are characterized by high Nb values whereas the brighter domains along rims are enriched in Ta (Sample GUA-50C). (B) Columbite-1 crystals with heterogenous zoning textures with Nb-rich inner domains surrounded by partially corroded Ta-rich margins (GUA-08). (C) Columbite-2 in co-precipitation texture with fluorite; note the reaction between fluorite and fluocerite partially replacing the columbite crystals along rims (Sample GUA-53). (D) Intergrown of secondary columbite-2 partially altering the inner part of cassiterite crystal (GUA-36).

4.5. Mineral Chemistry

4.5.1. Main compositions

Table 4-1 and Table 4-2 list the representative compositions and structural formula of columbite types from the Desemborque Pluton; the complete dataset is present in supplementary data. Columbite compositions are plot in the #Ta vs. #Mn diagram (Figure 4-5). All analyzed crystals are Fe-rich and classify as columbite-(Fe), however, core to rim profiles show systematic Nb-Ta compositional variations in mostly crystals, where rims are enriched in Ta and plot in the intermediate columbite-tantalite-(Fe) compositions (Figure 4-5A).

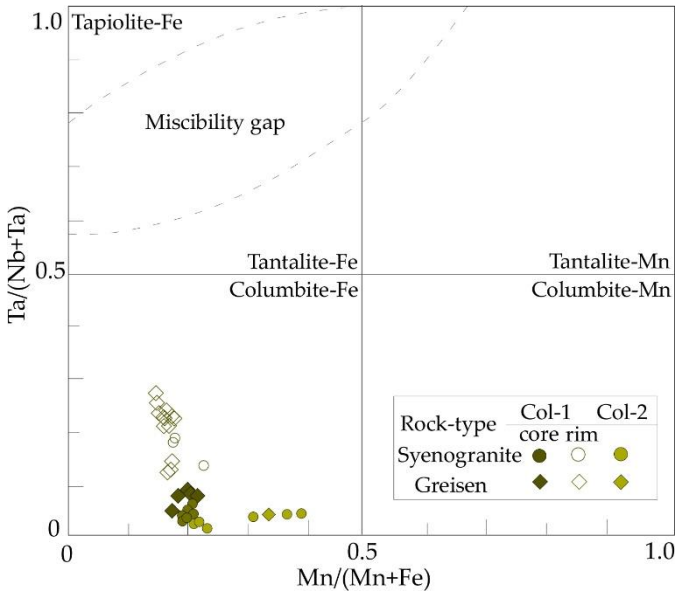

Figure 4-5: Columbite-Tantalite classification diagram for A) columbite generations (Col-1 and Col-2) from the Desemborque pluton after Ercit (1994).

Core to rim profiles show comparable compositions for the columbite-1 group between the syenogranite and the greisen. The columbite-1a (cores) type have similar Nb contents in the both granite and greisen (up to 1.86 apfu), but its Ta and W contents are relative minor in syenogranite (up to 0.15 and 0.06 apfu, respectively) than in the greisen (up to 0.10 and 0.09 apfu respectively). Contents of Fe are also similar and thus predominant (up to 0.84 apfu) over the Mn (up to 0.21 apfu) in both rock types. Contrary, the columbite-1b (rims) type reach Nb contents up to 1.60 apfu (granite) and 1.71 apfu (greisen) with a systematic increase of Ta up to 0.32 apfu (granite) and 0.48 apfu (greisen) and Fe (up to 0.87 apfu in both rocks). Mn is relative lesser in both rock types (up to 0.18 apfu), and W only in the greisen (up to 0.08 apfu)

when compared to the col-1a type. In contrast, crystals of the columbite-2 groups from the granite and greisen have distinct compositions without significant chemical variations. They show average contents in the granite and greisen of Nb = 1.84 and 1.77, Ta = 0.45 and 0.07, Fe = 0.72 and 0.67, Mn = 0.29 and 0.33, and W = 0.02 and 0.06 (in apfu), respectively.

Compositional variations between the two columbite types in the studied rocks are shown in Figure 4-6. These are associated with the cationic relations between Nb ↔ Ta; Mn ↔ Fe; $2(V,Nb,Ta,Sb)^{5+} \leftrightarrow (Si,Ti,Zr,Th,U)^{4+}+(W)^{6+}$; and W+Ti ↔ #Mn. All cationic substitutions give good coefficient correlation (r^2>0.97).

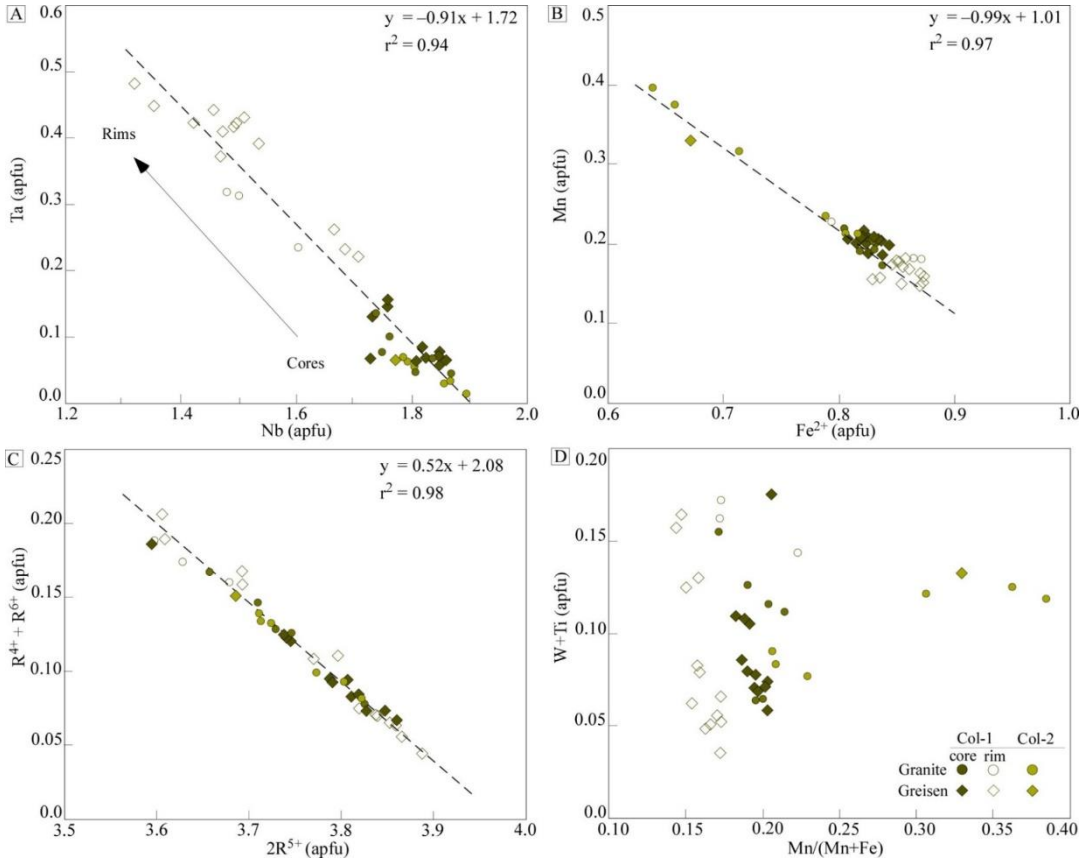

Figure 4-6: Cationic diagrams (in apfu) showing compositional variation in columbite (Col-1 and Col-2) types from Desemborque Pluton: A) Ta vs. Nb: B) Mn vs. Fe; C) R^{4+} + R^{6+} vs. $2R^{5+}$; D) W+Ti vs. Mn/(Mn+Fe).

4.5.2. Trace element compositions

Multi-element (columbite and host rock) and REEs (columbite) patterns are shown in Figure 4-7. Trace element patterns for columbite are like the bulk host rock with pronounced

negative anomalies for Sr, Eu, Pb and Sn related to the fractionation of early phases, to a certain extent (e.g. plagioclase and cassiterite), and positive for U and Hf, except for Y that show moderately negative anomaly for the both columbite types (Figure 4-7A). Differences between the columbite 1 and 2 types are marked in the abundances of the HFSEs and some elements since columbite-1 crystals, especially in the col-1b type (Ta-rich rim crystals), present higher Zr, Hf and W concentrations while crystals from the columbite-2 type have higher abundances of Y, Th, Pb, Sc and Ti (Figure 4-7A and Table 4-2). REE chondrite normalized patterns for both columbite-1 and 2 groups are relative enriched in HREE over the LREE [$0.001 < (La/Yb)_N < 0.042$], with presumably negative Eu anomalies varying from 0.04 to 0.28 (Figure 4-7A), when compared to the bulk host rock. However, columbite-1 crystals have REE abundances that are 1- to 2-fold lower than those for the columbite-2 and a distinct, steeply positive slope through the LREEs [$0.05 < (La/Sm)_N < 0.11$]. In contrast, REE patterns in columbite-2 crystals are relative flatter, though with some dispersion in the LREE region, which may be related to the altered domains in these crystals (Figure 4-4C-D) and consequently large associated uncertainties (supplementary data).

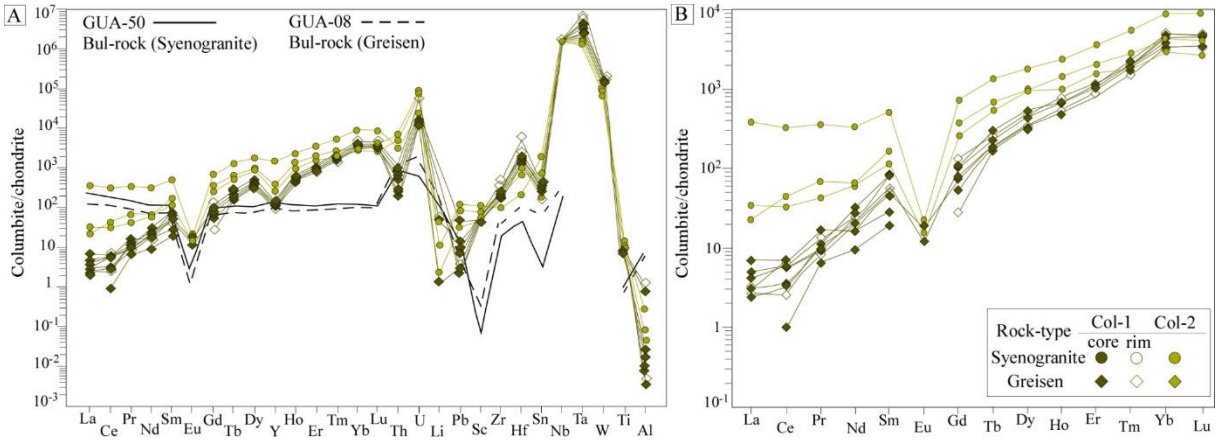

Figure 4-7: Chondrite normalized (A) trace element and (B) REE patterns for columbite generations from the Desemborque pluton with the corresponding bulk rock. The data were normalized to the chondrite values of (McDonough and Sun, 1995).

4.6. Discussion

4.6.1. Genesis of the columbite generations in the Desemborque Pluton

The explanation of the origin of columbite-group minerals is always a challenge given the complex textures, chemical evolution and relationships with other rare-metal minerals. A

detailed combined textural and chemical evaluation to study Nb-Ta oxide minerals is always necessary because they could form as primary phases, or as product of hydrothermal alterations (Ballouard et al., 2016b, 2016a). In granites, the formation of the Nb- and Ta-bearing minerals has been genetically associated with a combination of magmatic and hydrothermal environments (Belkasmi et al., 2002; Huang et al., 2002; Breiter et al., 2007; Zhu et al., 2015; Xie et al., 2016, 2018a; Alfonso et al., 2018). For example, the occurrence of disseminate columbite-(Fe) grains in the Podlesí granite (Czech Republic) was interpreted by Breiter et al. (2007) to be magmatic in origin where the main portion of the columbite precipitated from the melt. In the Songshugang granite (China), columbite-(Fe) was formed in two different magmatic and hydrothermal stages during rare-elemen mineralization (Zhu et al., 2015). In the Laiziling granite (China), crystallization of columbite-group minerals was developed during late-magmatic stages of evolution according to Xie et al. (2018). Finally, in the Penouta granite (Spain), formation columbite-tantalite minerals displaying oscillatory zoning and patchy textures were explained as result of the evolution of the melt during the magmatic-hydrothermal transition (Llorens González et al., 2016; Alfonso et al., 2018).

In this study, the occurrence of columbite-(Fe) found in both syenogranites and the greisen is associated with hydrothermal activity characterized by mineralogical replacement and fluid-induced alteration processes during late to post-magmatic stages of crystallization. During late- to post-magmatic transition, hydrothermal activity in the Desemborque pluton started with the intrusion on metasediments, in which the pluton is undoubtedly fractured along contacts promoting the circulation of aqueous-rich fluids. The interaction of later fluids with the Desemborque rocks can be pervasive resulting in mineralogical and chemical transformations among syenogranites. This is reflected in the partial to complete replacement of primary rock-forming minerals (feldspars and biotite) leading to exsolution of post-magmatic F-rich fluids. The circulation of such fluids promotes the progressively hydrothermal element-transport and significant changes on the original syenogranitic compositions and mineralogical assemblages, in the study case, to the formation of the albitized granites and greisens at the apical eastern part of the pluton (Figure 4-1). The main chemical changes are related to the enrichment of incompatible elements such Rb, Sn, Nb, Th, U, and especially of Li and F from the syenogranites to the greisenized granite and the greisen, coupled to the precipitation of abundant Li-rich micas, fluorite, cassiterite and columbite.

Numerous experiments have been concluded that in reduced Li- and F-rich aluminous magmas, Nb and Ta tend to remain in the melt and the degree of solubility of these both

elements commonly increase in low temperature evolutionary stages (Keppler, 1993; Linnen and Keppler, 1997; Linnen, 1998; Chevychelov et al., 2005; Linnen and Cuney, 2005; Zaraisky et al., 2010), and this explains why the Desemborque columbite minerals crystallized in late to post-magmatic stages of evolution. Moreover, the textural relationships of columbite generations with equivalent chemical compositions in both rocks support the late- to post-magmatic crystallization related to the hydrothermal element-mobilization processes mentioned before, during fluid-induced alterations on syenogranites and the greisen-crystallization processes.

Despite the similar features in both rocks and its hydrothermal origin, the notable textural and geochemical variations between columbite-1 and columbite-2 groups suggest different hydrothermal stages of formation. In the case of the columbite-1 type, zoning of columbite-1 crystals took placed in two-stages: i) an early-stage corresponding to the Nb-cores (Col-1a) and then ii) a later-stage marked by the Ta-domains surrounding the Nb-cores (Figure 4-4A-B). This pattern can be explained by the general tendency of Nb to crystallizes prior to Ta among the structure of the columbite mineral as previously suggested by Linnen and Keppler, 1997; Stepanov et al., 2014; and Ballouard et al. (2016b, 2016a). The systematic zoning of these crystals tracks a progressive differentiation trend by the increase of the Ta/Nb ratios from core to rims (Figure 4-6A and Figure 4-6B). Enrichment of other elements such W, Zr and Hf, W are also registered from core to rim profiles, whereas REE patterns are very similar between the both Nb-cores and Ta-rims crystals.

Columbite-2 type has a close relationship with cassiterite and secondary REE-fluorides, characterized particularly as patchy overgrowths or irregular grains penetrating margins (Figure 4-4C-D), which suggest replacement-crystallization processes by fluid-driven reactions at very final hydrothermal stage of evolution. In general, secondary textures in columbite-group minerals have been related with partial replacement of early columbite or with dissolution textures due to metasomatic processes (Abdalla et al., 1998; Huang et al., 2002; Zhu et al., 2015; Alfonso et al., 2018; Xie et al., 2018a). As mentioned before, the destabilization of primary minerals (e.g. biotite) or even the breakdown of pre-existing columbite-1 crystals may release some F-, HFSE and REE-rich fluids, which could reprecipitated to form the columbite-2 group. This is compatible with the chemical compositions among secondary columbite crystals such the relative enrichment of REE+Y and other minor trace elements U, Th, Pb and Ti (Figure 4-6 and Figure 4-7), when compared to the primitive columbite-1 type supporting the influenced of fluid-induced reactions in enrichment of these elements. Moreover, the

variable increase of Mn and consequent Mn/(Mn+Fe) ratios within crystals from the columbite-2 relative to those columbite-1 crystals, could be attribute to the hydrothermal element distribution among others Mn- and Fe-rich post-magmatic phases such ilmenite and/or hematite.

4.6.2. Comparision with other columbite-(Fe) occurrences from worldwide localitites

In Figure 4-8 we show the schematic quadrilateral #Ta vs. #Mn diagram with the compositional evolution trends of columbite-group minerals (CGM) from worldwide localities previously compilated by (René and Škoda, 2011), we also plotted recently data of CGM from others rare-metal granites (colored lines) in order to compare with our columbite-(Fe) generations. Compositions of the Desemborque columbite-1 type form an evolution trend with moderate degree of fractionation and consequent low Ta/Nb ratios (0.02 – 0.36). This trend is partially comparable to those from the Podlesí and Geyersberg Granites which are characterized by 1) increasing of the Ta/Nb ratios due to the fractionation of the Li-micas granites during evolution in the case of Podlesí Granite, and 2) due to the hydrothermal alterations processes (muscovitization, greisenization) acting in the high F-P_2O_5-Li-mica granitic rocks at Geyersberg. In the case of the Desemborque columbite-2 type, its compositions show a limit evolution trend characterized by the increase of the Mn/Fe ratios (0.260 – 0.623) and lack variation of the Ta/Nb ratios. This trend no has corresponding behavior with others columbite trends among the compiled data. We consider that this incompability could be referring either to variable increasing of the Mn/(Mn+Fe) ratios in CGM typically attribute to magmatic fractional crystallization in rare-metal enriched granites and granite pegmatites (c.f. Belkasmi et al., 2000; Linnen and Cuney, 2005), which is not the case of the columbite-2 type from this study, or due to the relative different Fe-Mn fractionation between minerals from the paragenetic assemblages of the listed granitic systems (e.g. Linnen and Cuney, 2005; René and Škoda, 2011).

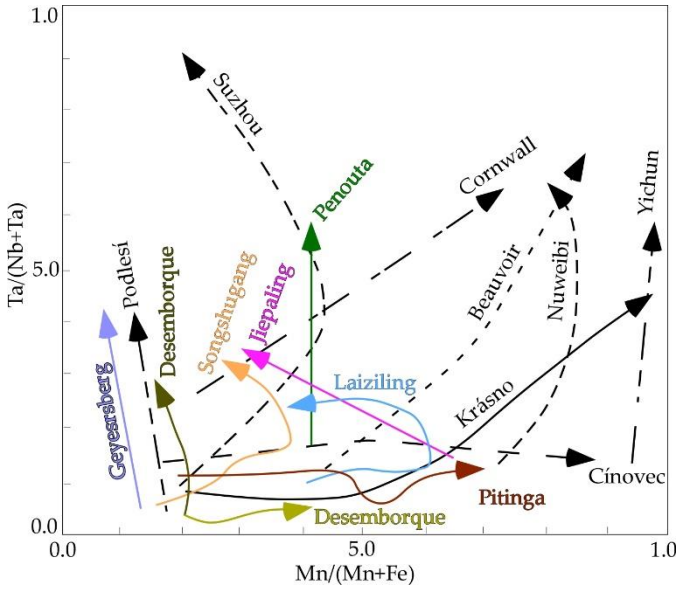

Figure 4-8: Compositional-trend compositions of columbite from F- and Li-rich rare-metal granitic systems worldwide after René and Škoda (2011). Desemborque, Brazil (this work); Geyersberg, Germany (René, 2019); Laiziling, South China (Xie et al., 2018a); Penouta, Spain (Llorens González et al., 2016); Z15: Songshugang, Northeastern China (Zhu et al., 2015); Krásno, Germany (René and Škoda, 2011), Podlesí, Czech Republic (Breiter et al., 2007); Yichun, China (Belkasmi et al., 2002); Cínovec, Czech Republic (Rub et al., 1998); Cornwall, England (Scott et al., 1998); Suzhou, China (Wang et al., 1997); Nuweibi, Egypt (Abdalla et al., 1998); Beauvoir, France (Wang, 1998).

Concentrations of additional REE and trace elements of CGM in granites and greisens are rarely reported in literature. Nevertheless, Melcher et al. (2015, 2016) offer a robust compilation on major and trace elements of CGM hosted in pegmatites from relevant Ta-Nb-Sn provinces worldwide. We used the median trace-element values of columbite-(Fe) types from the Melcher's dataset for comparison with our trace-element compositions (Figure 4-9). In general, we observed that the normalized REE patterns of CGM are always dominated by the HREEs over the LREEs; U, Zr, Hf and W show a systematic increase in all patterns while Eu, Pb, Sn, Ti, Li and Al are usually depleted. The behavior of elements such Y, Th and Sc are broadly variable among all columbite-(Fe) data set, which can be attributed to the melt compositions, co-precipitation of other phases and/or hydrothermal overprints. In the Desemborque pluton, the negative anomalies of Y and Th between the both columbite generations can be explained by the competition with early-crystallized hydrothermal xenotime. For the other worldwide localities, we require further examination on mineralogy and inter-element correlations between these columbite-(Fe) types and hosting rocks that is far beyond the scope of this work. Nevertheless, similarities among the columbite-(Fe) data set point to strong preference of this mineral to incorporate, besides the main Nb and Ta, HFSEs (mainly Zr and Hf), HREEs, U and W elements.

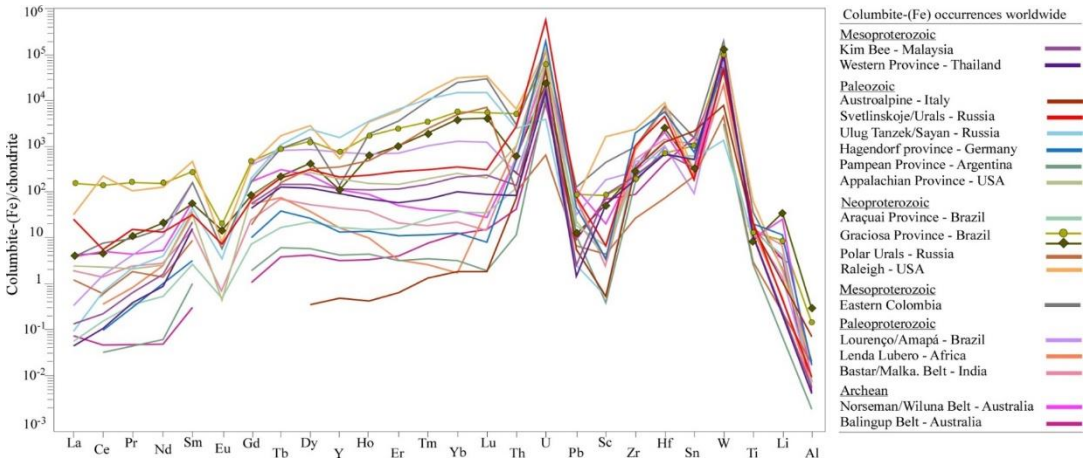

Figure 4-9: Median chondrite-normalized rare-earth and trace element patterns for columbite-(Fe) occurrences from studied granites and associated greisens of the A-type Graciosa Province and from pegmatites from worldwide province (data from Melcher et al., 2015, 2016).

Acknowledgements

Staff do GeoAnalitica, FAPESP for financing this work (Proc. 08/00562-0) and (Proc. 2019/17343-4), and CAPES for the doctoral scholarship of this corresponding author and and for the master scholarship of the third author (Finance Code 001).

4.7. Conclusions

The occurrence of columbite in the studied syenogranites and the greisen from the Desemborque pluton is associated to hydrothermal activity acting during evolution. Textural and geochemical characterization for this mineral revealed to columbite types formed in different hydrothermal stages of crystallization. The first columbite-1 type is characterized by isolated crystals with prograde zonation and thus two-substages: an early hydrothermal stage corresponding to Nb-rich crystal cores surrounding by Ta-rich rims in a later hydrothermal stage of crystallization. The second columbite-2 type form irregular patchy Mn-rich crystals in replacement textures with cassiterite and secondary REE-fluorides indicating a post-magmatic crystallization during fluid-induced hydrothermal alterations. REEs and trace-element compositions show a chemical evolution for this rare Nb-Ta oxide during the hydrothermal activity of the Desemborque pluton reflecting in the enrichment of REEs, Y, Th, U, Sn and Ti from the early-formed columbite 1 to the late-stage columbite-2 type.

Table 4-1: Representative EMPA compositions and structural formula of columbite in the Desemborque Pluton

Sample	**GUA-50C1**			**GUA-08**					**GUA-53**		
Type	Columbite-1			Columbite-1					Columbite-2		
Point_ID	1-c	1-r1	1-r2	7-c2	7-r1	7-r2	8-c	8-r1	3-r1	4b-r2	4b-c
Rock type	Syenogranite			Greisen					Syenogranite		
SiO_2	0.06	0.06	0.09	0.12	0.07	0.06	0.08	0.07	0.08	0.09	0.06
TiO_2	2.15	2.19	2.30	0.98	0.82	0.84	1.03	2.31	1.49	1.42	1.48
Al_2O_3	0.17	0.02	0.04	0.03	0.03	0.03	0.01	0.04	0.02	0.01	0.01
FeO	17.33	16.97	16.88	16.69	16.59	17.11	16.94	16.37	17.02	16.82	16.66
MnO	3.56	3.48	3.50	4.17	2.99	3.52	4.12	2.71	4.37	4.40	4.90
MgO	-	-	0.04	0.03	-	0.01	0.01	0.03	0.02	0.01	0.01
CaO	-	-	-	0.06	0.01	-	-	-	0.19	0.04	0.16
SrO	-	0.01	0.00	0.02	-	-	0.02	0.00	-	-	0.04
Sb_2O_5	0.04	-	-	-	-	0.01	0.02	0.01	-	-	-
V_2O_3	0.03	-	-	0.07	0.03	-	-	-	-	-	-
WO_3	4.11	3.90	4.18	1.76	1.41	1.80	1.38	2.85	1.72	1.51	0.92
ThO_2	-	0.02	0.04	0.01	0.02	0.03	0.01	0.03	-	-	0.02
UO_2	-	0.06	0.06	0.05	-	-	-	0.31	-	-	0.04
PbO	0.05	0.06	0.07	0.04	0.08	0.09	0.04	0.09	0.02	0.04	0.05
Na_2O	0.02	-	0.04	0.03	0.02	-	0.02	-	-	0.01	-
Gd_2O_3	0.03	-	0.04	-	0.01	0.02	0.02	0.06	0.09	0.00	0.00
Yb_2O_3	0.06	0.02	0.05	0.03	0.04	0.03	0.09	0.11	0.21	0.31	0.14
Y_2O_3	0.01	-	0.01	-	-	-	-	0.05	0.15	0.10	0.08
ZrO_2	0.27	0.21	0.30	0.16	0.11	0.05	0.12	1.27	0.21	0.16	0.09
Nb_2O_5	66.96	54.16	53.01	65.98	52.54	62.85	71.46	45.90	71.58	72.10	74.10
Ta_2O_5	4.96	18.76	19.15	9.05	24.61	14.41	4.06	27.96	1.93	2.21	0.98
F	0.06	0.05	-	-	-	-	-	0.04	0.35	0.00	0.02
Total	99.85	99.97	99.81	99.28	99.38	100.9	99.44	100.2	99.45	99.25	99.75
Structural formula based on 3 cations and 6 oxygens											
W (apfu)	0.062	0.062	0.066	0.027	0.023	0.028	0.021	0.047	0.026	0.022	0.013
Nb	1.749	1.501	1.480	1.758	1.496	1.686	1.859	1.319	1.856	1.867	1.896
Ta	0.078	0.313	0.319	0.145	0.421	0.233	0.064	0.483	0.030	0.034	0.015
Ti	0.093	0.101	0.106	0.043	0.039	0.038	0.045	0.110	0.064	0.061	0.063
Zr	0.008	0.006	0.009	0.004	0.003	0.002	0.003	0.039	0.006	0.005	0.003
Sb	0.001	0.000	0.000	0.000	0.000	0.000	0.000	0.000	0.000	0.000	0.000
V	0.001	0.000	0.000	0.003	0.001	0.000	0.000	0.000	0.000	0.000	0.000
Y	0.000	0.000	0.000	0.000	0.000	0.000	0.000	0.002	0.005	0.003	0.002
Gd	0.001	0.000	0.001	0.000	0.000	0.000	0.000	0.001	0.002	0.000	0.000
Yb	0.001	0.000	0.001	0.001	0.001	0.001	0.002	0.002	0.004	0.005	0.002
Th	0.000	0.000	0.001	0.000	0.000	0.000	0.000	0.000	0.000	0.000	0.000
U	0.000	0.001	0.001	0.001	0.000	0.000	0.000	0.004	0.000	0.000	0.000
Pb	0.001	0.001	0.001	0.001	0.001	0.001	0.001	0.002	0.000	0.001	0.001
Si	0.003	0.004	0.005	0.007	0.004	0.004	0.005	0.005	0.004	0.005	0.003
Al	0.011	0.001	0.003	0.002	0.002	0.002	0.001	0.003	0.001	0.001	0.001
Sum B	**2.009**	**1.991**	**1.993**	**1.992**	**1.993**	**1.995**	**2.002**	**2.021**	**1.999**	**2.014**	**2.003**
Fe	0.837	0.870	0.864	0.822	0.874	0.849	0.815	0.871	0.816	0.806	0.788
Mn	0.174	0.181	0.181	0.208	0.159	0.177	0.201	0.146	0.212	0.213	0.235
Mg	0.001	0.001	0.001	0.001	0.001	0.001	0.001	0.002	0.000	0.001	0.001
SumA	**1.012**	**1.052**	**1.047**	**1.031**	**1.035**	**1.027**	**1.017**	**1.018**	**1.029**	**1.020**	**1.024**
#Ta	0.172	0.172	0.174	0.202	0.154	0.172	0.198	0.144	0.206	0.209	0.230
#Mn	0.043	0.172	0.177	0.076	0.220	0.121	0.033	0.268	0.016	0.018	0.008

#Ta: Ta/(Ta+Nb); #Mn: Mn/(Mn + Fe); -: below detection limit

Table 4-2: LA-ICP-MS trace element compositions of columbite in the Desemborque Pluton

Sample	**GUA-08**								**GUA-53**		
Rock type	Greisen								Syenogranite		
Mineral	Columbite 1								Columbite 2		
Point_ID	2-r	2b-c	2c-c	3b-r	3c-c	3d-c	3e-c	3f-c	4-c	15-c	1-c
Li (ppm)	86.29	66.28	1.94	b.d.l	b.d.l	b.d.l	b.d.l	b.d.l	3.38	16.2	17.7
Mg	257	192.2	617	32.45	29.44	27.97	29.03	31.27	73.5	166	74.4
Al	9879	7272	271	36.47	125	30.07	186	64.0	363	2398	652
Sc	360	287.1	266	364	297	272	274	300	286	694	451
Ti	3860	3438	2793	2973	3320	3087	3279	4093	3959	6443	5845
Mn	29118	26874.3	27243	26130	24870	27722	27478	28676	32333	69562	53819
Fe	90102	94627	87775	105609	96765	87284	94899	101574	30418	23981	37170
Zn	151	182	190	266	230	217	250	137	270	259	146
Ga	9.99	10.43	1.53	0.82	1.23	1.25	0.94	1.00	5.81	2.6	0.92
Rb	254	258	2.65	b.d.l	6.22	b.d.l	b.d.l	0.83	2.78	13.2	9.05
Sr	5.15	0.82	4.39	0.42	0.39	0.33	0.49	1.87	110	1.96	1.00
Y	203	174	155	148	168	158	160	196	2421	397	593
Zr	1921	903	661	897	808	698	752	1134	788	388	872
Nb	419426	419426	419426	419426	419426	419426	419426	419426	419426	419426	419426
Sn	700	707	392	303	379	474	507	680	295	3340	1212
Cs	11.93	13.35	0.47	0.38	0.47	0.44	0.48	0.67	0.75	0.93	0.82
Ba	7.19	4.91	9.07	b.d.l	b.d.l	2.75	b.d.l	b.d.l	208	5.56	b.d.l
La	0.72	1.68	0.76	0.65	0.97	b.d.l	0.62	1.16	90.6	8.17	5.38
Ce	3.87	4.01	2.11	1.57	3.6	0.59	1.95	3.75	196	20.2	27.0
Pr	0.83	1.00	0.95	1.23	0.93	0.61	b.d.l	1.48	32.7	4.03	6.46
Nd	11.01	14.55	b.d.l	b.d.l	9.63	4.27	9.11	7.40	147	27.2	29.6
Sm	7.86	12.06	4.23	6.80	12.03	2.89	7.04	9.06	78.1	17.9	25.4
Eu	b.d.l	b.d.l	b.d.l	b.d.l	b.d.l	b.d.l	0.93	0.66	1.35	0.77	b.d.l
Gd	26.08	20.02	15.79	5.47	16.84	10.47	14.44	20.59	144	51.4	73.9
Tb	9.46	8.17	5.87	6.7	6.81	7.82	6.81	10.92	48.6	19.3	24.2
Dy	117	106	93.52	81.4	88.57	89.28	82.25	130.5	443	238	239
Ho	42.23	37.9	28.91	27.86	29.83	28.31	26.65	35.51	128	55.3	80.0
Er	184	179	147	132	155	137	140	168	581	251	332
Tm	51.51	58.1	47.31	38.66	42.67	40.88	40.6	50.88	134	46.4	68.2
Yb	796	690	618	519	517	542	522	683	1471	472	631
Lu	113	114	91.3	84.65	87.68	85.01	85.1	111	225	65.0	98.0
Hf	614	208	124	267.2	166	159	161	221	117	22.2	73.5
Ta	66381	33630	50238	110794	75792	36850	34611	26700	16924	20856	24531
W	17345	14596	8354	10463.3	10234	9302.1	10210	12360	6745	10663	10156
Pb	20.03	36.42	7.41	9.26	116	5.40	15.73	22.46	82.1	307	227
Th	30.25	16.71	8.83	11.38	20.06	5.84	6.07	31.3	90.5	149	194
U	409	167.3	94.6	122	168	88.62	89.22	153	175	492	606
Nb/Ta	6.06	14.36	9.55	3.50	5.93	11.66	12.44	16.19	25.21	19.85	17.00
Zr/Hf	3.15	5.14	5.53	3.79	5.20	4.52	4.83	5.16	6.64	17.35	12.81
U/Th	13.79	9.78	9.51	8.99	8.44	15.13	14.83	6.37	1.71	3.28	3.03
Sn/W	0.03	0.05	0.04	0.03	0.04	0.05	0.05	0.06	0.04	0.22	0.12
REEs	1547	1175	1207	727	968	965	948	1203	3997	1246	1573
LREEs	25.5	31.2	9.35	9.23	25.6	8.32	19.0	19.2	671	131	115
HREEs	1522	1143	1198	718	943	956	928	1183	3325	1115	1459

Trace element LA-ICP-MS compositions (ppm); c: core; r: rim zone; b.d.l.: below detection limit

5. ZIRCON AND RELATED ACCESSORY MINERALS: TEXTURAL AND COMPOSITIONAL CONSTRAINTS ON HYDROTHERMAL OVERPRINTS FROM GRANITES AND GREISENS FROM THE A-TYPE GRACIOSA PROVINCE, SE-BRAZIL.

Astrid Siachoque[a] and Silvio R.F. Vlach[a]
a. Institute of Geosciences -University of São Paulo, São Paulo-Brazil.

ABSTRACT

Granites and greisens in the A-type Graciosa Province (southern Brazil) experienced intensive late to post-magmatic alterations by the exsolution of HFSE- and F-rich fluids during magmatic to hydrothermal evolution. Most of these alterations are recorded in magmatic zircons and late crystallized/recrystallized metamictic and hydrothermal zircons, but also in paragenetic relations with secondary accessory minerals such monazite, xenotime, fluorite, fluocerite and gagarinite. This study presents a combination of textural/microstructural and chemical features from the mentioned accessory minerals in order to identify hydrothermal alterations processes in selected peralkaline and metaluminous granites as well as greisens from the Mandira Massif and the Desemborque Pluton. Zircon internal textures show the development of BSE-dark patchily, porous-spongy, resorption and/or fractures altered domains related to metamictization processes via fluid-induced alterations. Zircon major and trace element compositions across the altered domains exhibit depletion of Zr and Si with progressive enrichment of non-formula elements such Hf, REEs, Y, Nb, Ta, Th, U, Ti, P, Al, Fe and Ca from magmatic to metamictic and hydrothermal zircons indicating that hydrothermal fluids played an important role in element remobilization and concentration. These chemical features of zircons reflect differences of Zr/Hf, LREE/HREE and Th/U ratios during hydrothermal evolutionary events occurring in the both studied occurrences. In addition, the crystallization of secondary monazite, xenotime, fluocerite and gagarinite in granites is associated to replacement of pre-existing zircon and/or fluorite by dissolution-reprecipitation processes during hydrothermal alterations. Chemical U-Th-Pb dating of monazite crystals from the Desemborque Pluton yielded an Ediacaran age of 584 ± 3 Ma indicating the first documented evidence of the hydrothermal activity within the Graciosa rocks.

Keywords: zircon secondary microtextures, hydrothermal phosphates and fluorides, fluid-driven hydrothermal alterations, CHIME monazite ages.

5.1. Introduction

Zircon is one of the most studied accessory minerals given its importance for geochronology, petrogenesis of igneous rocks and evolution of Earth's crust and mantle (Hanchar and Hoskin, 2003; Hoskin and Schaltegger, 2003). Zircon is the most important accessory mineral carrier of REEs and HFSEs that can preserve the growth history of evolution in granites due to the strongly resistance to hydrothermal alterations (Corfu et al., 2003; Hoskin and Schaltegger, 2003). Morphology and chemistry of zircon are usually studied to determinate the degree of granite fractionation, nature and crystallization age of the parental granitic magma (Breiter et al., 2007, 2014a; Claiborne et al., 2010; Gagnevin et al., 2010), and to evaluate metallogenic affinity and mineral exploration processes in specialized granites (Wang et al., 2000; Nardi et al., 2013; Lamarão et al., 2014, 2018; Gardiner et al., 2017; Li et al., 2018b). However, igneous zircons can easily be altered by volatile-rich fluids in magmatic-hydrothermal systems, resulting in structural transformations (secondary textures) and chemical variations across the primary textures (Geisler et al., 2007; Lisowiec et al., 2013; Park et al., 2016; Kovaleva et al., 2017). Numerous works have largely investigated hydrothermal alterations on zircons throughout chemical compositions, particularly by the trace element compositions, which are potential indicators for known the nature and timing of fluid-driven alterations during magmatic to hydrothermal transition in granitic systems (Hoskin, 2005; Rayner et al., 2005; Schaltegger et al., 2005; Yang et al., 2014; Bell et al., 2016, 2019; Kim et al., 2018). There are others works involving textural and chemical relations between zircons and further REE-rich accessory minerals (e.g. monazite, xenotime, thorite) which may also provide significant constrains into hydrothermal activity in granites (Uher et al., 2009, 2014; Lisowiec et al., 2013; Breiter, 2016; Huang et al., 2018).

In southern Brazil, several A-type syenites and granites were emplaced in extensional, post-collisional regime during the final stages of the Brasiliano/Pan-American Orogeny in the Ediacaran Period and they display two primary peralkaline and aluminous petrographic associations. Mineralogical assemblages from rocks from the A-type Graciosa Province have been broadly studied in the last two decades by the second author and collaborators (Gualda and Vlach, 2005, 2007b, 2007e, 2007a; Vlach and Gualda, 2007; Vlach et al., 2011; Vlach, 2012; Vilalva and Vlach, 2014; Vilalva et al., 2016, 2019). However, detailed mineralogical investigations on REE-rich accessory minerals to investigate hydrothermal processes are still lacking. Among the Graciosa granites, we chose to examine samples from the Desemborque Pluton and Mandira Massif Granite, once their main petrographic granitic facies were affected

by late-stage fluids during evolution resulting in the formation of hydrothermal altered granites, pegmatites and greisens (Oliveira et al., 1987; Oliveira, 1989; Garcia, 2015), thus they represent key occurrences to investigate the hydrothermal records over granitic rocks at the Graciosa Province. Granites and the associated hydrothermal rocks from the (i) Desemborque and (ii) Mandira granites are characterized by complex magmatic and post-magmatic accessory mineral assemblages which includes: (i) ilmenite, zircon, fluorite, monazite, xenotime, thorite, cassiterite, columbite, magnetite, (REE+Y)-fluorides, hematite, sphalerite, galena and topaz, and (ii) ilmenite, zircon, astrophyllite, fluorite, fluocerite, gagarinite, monazite, hematite, thorite, chalcopyrite and galena. In order to contribute to the application of microtextural and chemical properties of accessory minerals to identify late- to post-magmatic hydrothermal alterations in peralkaline and aluminous granites from the Graciosa Province, we examine here the mineral chemistry and textural/microstructural records of zircons, monazite, xenotime, fluorite, fluocerite and gagarinite accessory minerals from the selected granitic occurrences.

5.2. Geological Background

The Graciosa Province includes widely A-type granitic and syenitic plutons and associated volcanics and gabbro-diorites rocks grouped in two alkaline and aluminous petrographic associations (Gualda and Vlach, 2005; Vlach and Gualda, 2007) intrusive into Archean and Paleo- to Neoproterozoic rocks of the Luis Alves and Curitiba Microplates, and Paranaguá Terrain (Figure 5-1; Siga Júnior et al., 1993; Gualda and Vlach, 2005; Basei et al., 2009; Passarelli et al., 2018). The province formed at ~580 Ma in an extensional, post-collisional regime related to the Brasialino/Pan-African Orogeny in the southern part of Brazil (Vlach et al., 2011). Recently chemical and isotopic evidences show that the Graciosa magmatism was formed through partial melting of a metasomatized lithospheric mantle, followed by variable degrees of crustal contamination at depth (Vilalva et al., 2019). In such context, this contribution concerns representative samples from the Desemborque Pluton and Mandira Massif which outcrops in the north-northern part of the province (Figure 5-1). The main petrographic features of these plutons are summarized here as follows.

5.2.1. The Desemborque Pluton

The Desemborque Pluton corresponds to the northern part of the Guaraú Massif Granite, that also includes the Azeite pluton both of them intruding metasediments from the Atuba and Turvo-Cajati complexes (Figure 5-1B, Oliveira et al., 1987). It consists of leucocratic meta- to slightly peraluminous biotite syenogranites and related albitized granites, greisens and pegmatites. The biotite syenogranitic present variably inequigranular, porphyritic and/or granophyric medium-grained textures, composed of alkali feldspar, quartz and plagioclase. Both feldspars commonly show massive sericite alteration. Biotite compositions vary from annite-(Fe), protholitionite-(Fe,Li), zinnwaldite-(Li) to syderophyllite-(Al) (Garcia, 2015). Zircon is the most abundant accessory mineral. Other late to post-magmatic accessories are ilmenite, fluorite, cassiterite, columbite, hematite, magnetite, monazite, phengite, REE-fluorides, thorite, and xenotime. The associated greisens show fine to medium-grained heterogranoblastic textures, and consist mainly of quartz, sericite and zinnwaldite-(Li). Mineral assemblages are similar than those of the hosted biotite granites but in these rock galena, sphalerite, topaz and hydrothermal zircon are distinct accessories.

5.2.2. The Mandira Massif Granite

The Mandira Massif Granite includes three main granitic units named Mandira, Mandira 1 and Acaraú units (Figure 5-1C). The Mandira unit was selected for this work and consists of leucocratic hypersolvus peralkaline granites and locally albitized granites having fine to medium-grained inequigranular, but locally granophyric textures. The granites are composed mainly of alkali-feldspar and quartz and minor albite. Arfvedsonite, riebeckite, astrophyllite, annite and siderophyllite are the mafic minerals. Accessory minerals are zircon, ilmenite, fluorite, fluocerite, gagarinite, hematite and thorite. Other accessories such chalcopyrite, galena, phengite and sphalerite are only found in the albitized rocks.

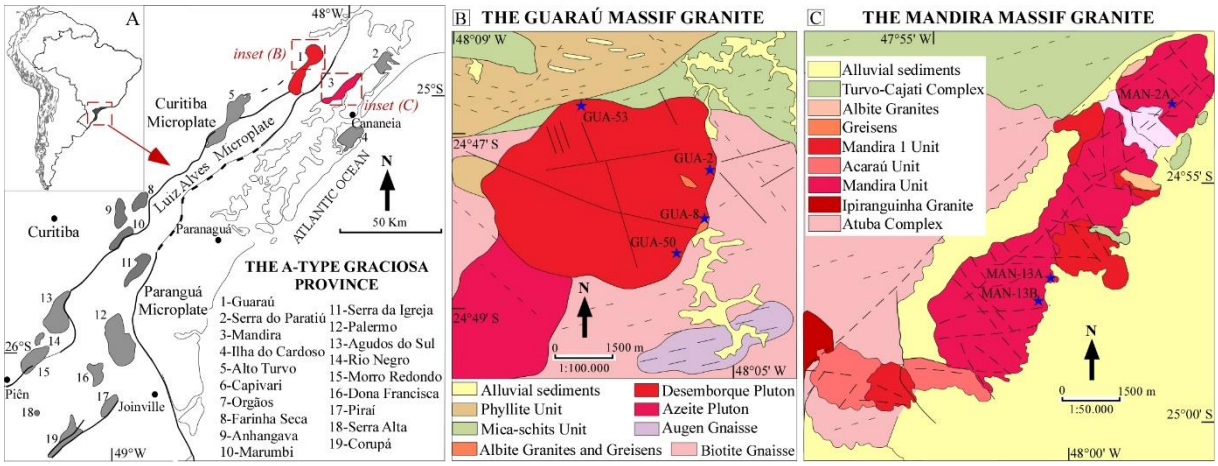

Figure 5-1: Location of the study area. A) Geological setting of the Neoproterozoic A-type Graciosa province in SE Brazil. B) Detailed geological map of Guaraú and C) Mandira Massifs. Blue stars correspond to the selected samples from this study.

5.3. Analytical Methods

5.3.1. EPMA analyses

Eight samples of granites and greisens from both Desemborque Pluton and Mandira Unite (Figure 5-1) were selected for the present study based on previous work for detailed textural and chemical analysis of zircon and related accessory minerals presented in this study. The analytical work involved extensive imaging and quantitative spot analyses with the Electron Probe Micro-Analyzer (EPMA) and the Inductively Coupled Plasma Mass Spectrometer provided with Laser Ablation sapling (LA-ICPMS) and was carried out at the GeoAnalitica Core Facility in the Institute of Geosciences at the University of São Paulo.

5.3.1.1. EPMA analyses

The EPMA work was carried out with the JEOL JXA-FE-8530 microprobe, provide with a field-emission gun, five wavelength (WD) and one energy disperse (ED) spectrometers one WD spectrometer has large TAPH and PETH analyzer crystals. Polished thin section (30-60 μm) were analyzed through extensive electron backscattered imaging (BEI) and qualitative energy dispersive spectrometry (EDS) under 15 kV, 20nA and 1 μm for the column accelerating voltage, and beam current diameter, respectively, for general mineral recognition and detailed analysis of the main textures and micro-structures of the focused minerals.

Semi-quantitative X ray imaging for selected zircon crystals was carried out by combining WDS and EDS signals under 20 kV, 50 nA, with a dwell time of 140 ms. BSE and CL images were obtained simultaneously. Quantitative WDS spot analyses were obtained under the same conditions, with a beam diameter of 3 μm and total integrated counting times from 10 to 60s, equally divided between peak and background measurements. U contents were corrected for the Th spectral overlap.

Monazite chemical analyzes and dating followed the analytical procedures and settings described by Vlach (2010). The analytical conditions were 15 kV, 300 nA and *ca*. 4 μm; Pb was measured with the PETH crystal. Similar conditions were set up for xenotime analysis, however the beam diameter was enlarged to *ca*. 6 μm given to minimize sample damage. WDS scans over K, S and As main spectral lines over typical monazite and xenotime crystals were done under the same analytical conditions; in all cases these elements were absent (below detection limits). Analyses were performed in the assisted mode, using the Age_Mona Excel spreadsheet (Vlach, 2010) to perform the needed interference corrections of Y and Th over Pb and Th over U and compute individual spot ages.

In both cases, our calibrations were checked against our internal reference monazite and xenotime age standards (TC-3, *ca*. 790 Ma monazite and Er-13A, *ca*. 590 Ma monazite and xenotime, *cf*. Vlach, 2010). Monazite isochronic and weighted average ages were calculated with the IsoPlot software v.4.2 (Ludwig, 2003), considering a 95% confidence level.

The main associated fluorides were analyzed under15 kV, 12 nA and a variable beam diameter 3 to 5 μm to minimize F loss. F contents in the LREE-bearing varieties were correct for Ce overlap.

In all WDS analyzes the PRZ-Armstrong software furnished by JEOL was used to perform matrix corrections and conversions of the raw data. Structural formulae were computed with the MinCal software (Gualda and Vlach, 2005). Measured spectral lines, standards used and attained detection limits in each case are summarized in the Supplementary Materials.

5.3.1.2. LA-ICPMS analysis

Trace element compositions owere measured with a Thermo Scientific ICAP-Q instrument, coupled to a New Ware UP-213 laser ablation system under a laser spot of 25 μm and repetition frequency of 20 Hz at energy of 1.97 J/cm^2. The analysis consisted in of a ~60 s background measurement followed by data acquisition for ~60 s and dwell time of 8 ms for

each isotope of the reported element, followed by 30s of washout time. The NIST SRM 610 glass was used as external standard, while the ZrO_2, CaO and Y_2O_3 wt% contents obtained by EMPA were the internal standards. The reference materials BCR-2G basaltic and zircon ZR-91500 were used to monitor the accuracy and reproducibility. Drift corrections, data reductions and conversions were carried out usgin the Glitter (v.4.4.4) program (Griffin, 2008). Analyzed elements, deviations and related analytical and statistical parameters are given as Supplementary Materials.

5.4. Results

5.4.1. Zircon main textures and microtextures

Zircon, with a variety of textures and microstructures, is a ubiquitous phase in all studied rocks and appears associated with contrasted mineral assemblages. Some typical zircon features in BSE images, from the studied rocks are highlighted in Figure 5-2. For the sake of simplicity and description purposes, we identified three main zircon types, all of them occurring in both the studied targets, namely (i) magmatic, (ii) magmatic with hydrothermal superimposed alteration and (iii) hydrothermal. Of course, this subdivision is somewhat arbitrary, and except for the most typical magmatic and hydrothermal zircon crystallized in the granites and greisens, respectively, their limits with the altered types are not so straightforward. As well, the qualitative interpretation of the BSE brightness patterns is more difficult, as it depends on both the composition and the microstructural late effects (*e.g.*, metamictization) and related chemical modifications (e.g. Nasdala et al., 2001, 2009, 2010; Corfu et al., 2003; Geisler et al., 2007).

In the biotite syenogranites from the Desemborque Pluton, magmatic zircons appears as small (30-80 μm), euhedral, bypiramidal crystals with well-developed oscillatory zoning with a few minute inclusions (mainly apatite) or is inclusion absent of; in most crystals, the BSE contrasted relatively bright and dark zones present variable thickness (Figure 5-2A). It occurs as either isolated crystals interstitial to early feldspars and quartz or enclosed in biotite crystals forming mafic interstitial aggregates. Late- to post-magmatic (relatively Hf-rich, cf. below) and post-magmatic xenotime overgrowths may be seen in some crystals. The altered zircon shows heterogeneous textures that were differentiated by the degree of alteration in two types. Less to moderate altered zircon type is characterized by BSE-dark irregular domains with

several microcracks and partially resorption zones and sometimes this type of zircon present Hf-rich overgrowths along margins with high BSE intensity (Figure 5-2B). Strong altered zircon type is defined by complicated textures with microcracks, irregularly spotted or dark patchily domains, and dissolved areas (Figure 5-2C); these textures are interpreted as resulted of metamictic processes involving zircon-fluid interaction (c.f. Nasdala et al., 2001; Corfu et al., 2003; Geisler et al., 2003). The hydrothermal zircon in greisens and sometimes in the syenogranites are represented by relatively large (up to 250 μm) crystals showing variably forms. Its texture is always highly spongy-porous and present fractures and partially corroded margins (Figure 5-2C). Hydrothermal zircons occur either as isolated or forming aggregates of 2-4 crystals embedded in zinnwaldite-(Li), partially replaced by thorite (Figure 5-2D) and/or intimate related with fluorite, monazite and xenotime (Figure 5-8E).

In the arfvedsonite/riebeckite peralkaline granites from the Mandira unit, primary zircons form small (30-80 μm) crystals characterized by two-stages of crystallization reflecting in the subhedral to euhedral magmatic cores with subtle oscillatory zoning following by recrystallization of late-stage irregular rims (Figure 5-2F). They are usually embedded in riebeckite aggregates. Microtextures revealed hydrothermal overprints indicating by radial microcraks in the inner parts and partially BSE-dark dissolved cores, and development of numerous porous (spongy-texture) in late-stage margins as well as corrosive margins and/or sharp terminations limits (Figure 5-2F-G). The hydrothermal zircon is characterized by large (up to 150 μm) irregular isolated crystals occurring interstitial between feldspars and quartz. Crystals are partially to strongly altered showing corroded margins, dissolved dark-domains, cavities and/or spongy textures (Figure 5-2H-I). Sometimes, they appear in close association with ilmenite and/or fluorite, in reaction textures with secondary fluocerite, gagarinite, thorite or hematite (Figure 5-2G and Figure 5-8I).

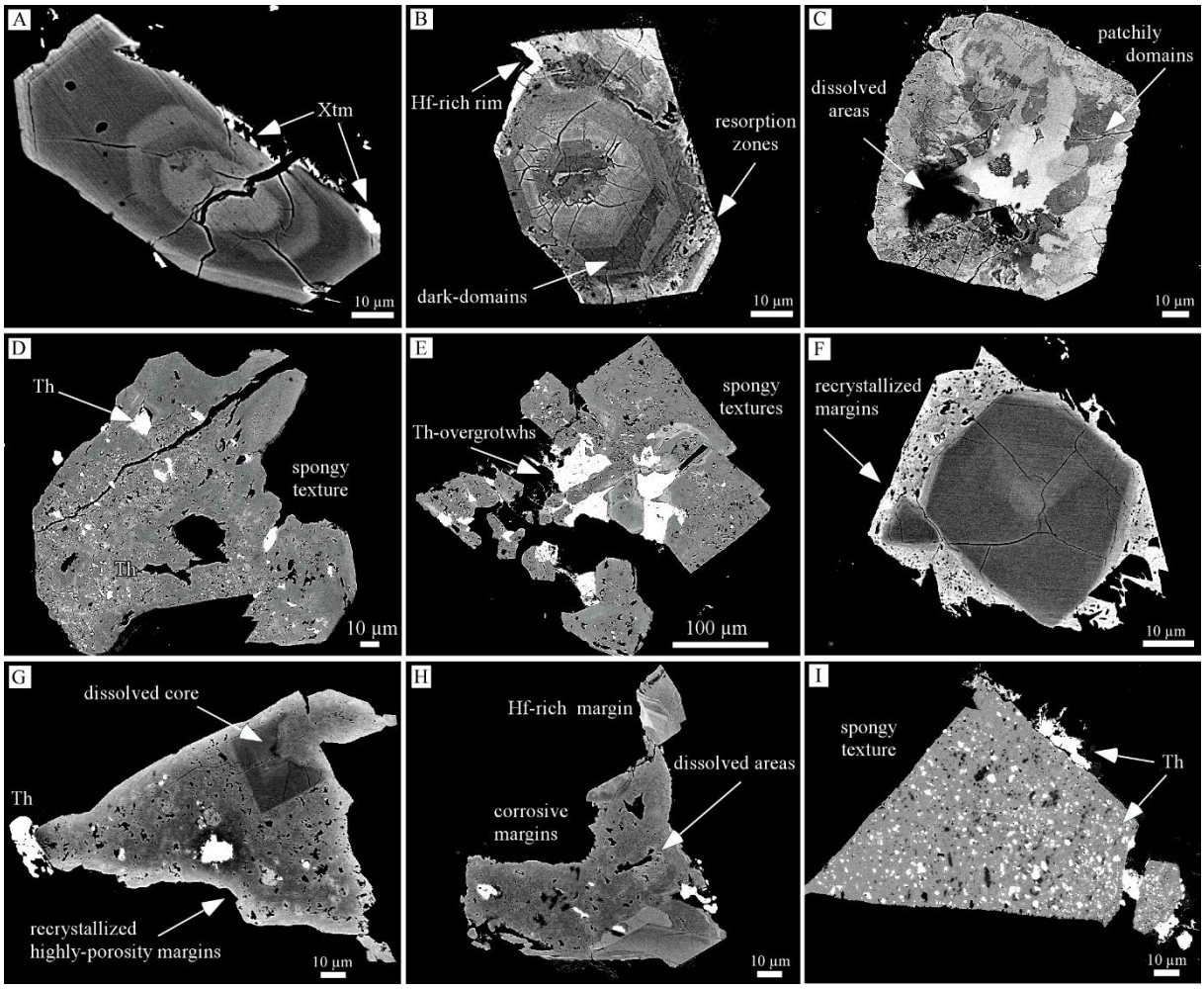

Figure 5-2: BSE images showing the microtextures and internal alterations in zircon crystals from the Desemborque (A-F) and Mandira Plutons (G-I). A) Magmatic zircon displaying prismatic habit and oscillatory zoning with altered BSE-dark domains microcracks (Sample GUA-50C2, syenogranite). B) Euhedral magmatic zircon showing oscillatory zoning with BSE-bright bands that were partially overprinted by secondary patchily and resorptions textures derived from metamictization (Sample GUA-50C1, syenogranite). C) Metamictic zircon with development of inward patchy domains and related microcracks, and locally dissolved zones (Sample GUA-2, syenogranite). D) Hydrothermal zircon partially fractured and with overprinted spongy texture with inclusions of thorite (Th) (Sample GUA-08, greisen). E) Cluster of irregular hydrothermal zircons with spongy textures and extensive intergrowths of thorite between zircon crystals (Sample GUA-8, greisen). F) Zircon showing two sub-stages of crystallization an early-formed magmatic core that was affected by self-irradiated processes and fractures and the next late-stage recrystallized zircon margins showing sharp terminations and highly-porosity texture (Sample MAN-13A, peralkaline granite). G) Zircon showing fractured BSE-dark core (self-irradiated) with late-stage recrystallized zircons showing corrosive margins and spongy-textures (Sample MAN-2A, peralkaline granite). H) Zircon exhibit irregular form, corrosive margins and dissolved areas (Sample MAN-13B, peralkaline granite). I) Hydrothermal spongy zircon with widespread precipitation of thorite either as inclusions or as intergrowths along margins (Sample MAN-13B, peralkaline granite).

5.5. Zircon Chemistry

Representative zircon chemical data are presented in Table 5-1 (WDS analyses and structural formulae) and Table 5-2 (LA-ICPMS analyses); the complete data set is given as Supplementary Material. Of note, most analyses of hydrothermally altered and/or hydrothermal

crystals or crystal zones, particularly from the Desemborque Pluton, record systematically low oxide totals (96-98 wt.%) even presenting reasonable structural formulae, a feature *most* typical of zircon affected by hydrothermal alteration (e.g. Nasdala et al., 2009).

5.5.1. Main compositions variations

Magmatic zircon types from the Desemborque and Mandira occurrences have contrasted HfO_2 contents, being in average higher in the former (1.44 wt.%) than in the latter (0.94 wt.%), while the hydrothermal types present the highest HfO_2 contents, up to 8.9 and 6.2 wt.%, and the altered types have intermediate contents, up to 1.83 and 1.34 wt. %, respectively. The Zr/Hf variations against Zr are represented in Figure 5-3, which show that magmatic, hydrothermally altered and hydrothermal zircon crystals present decreasing average ratios, with maxima at 107 and 134, 80 and 108, and 55 and 62 for the Desemborque and Mandira, respectively.

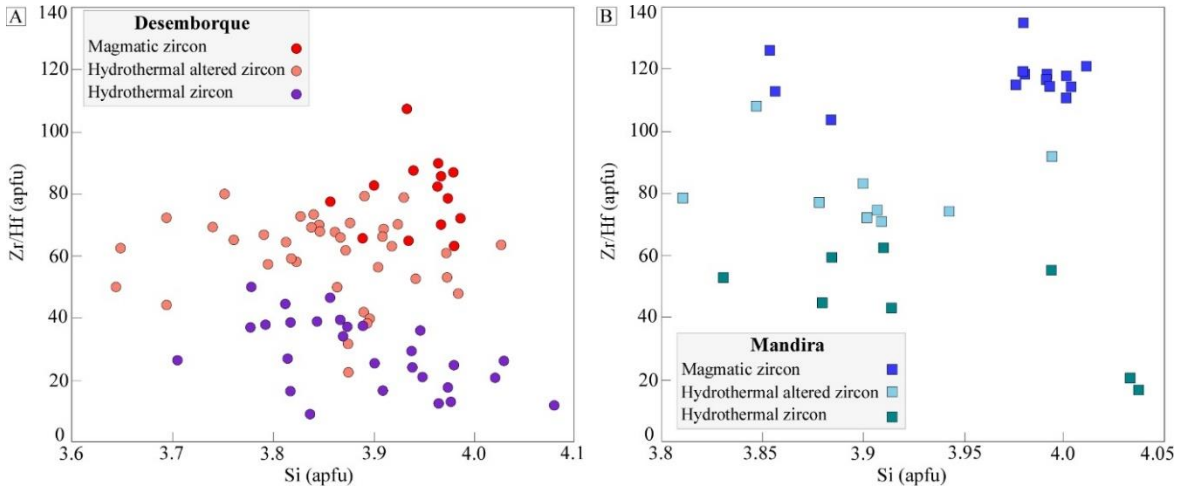

Figure 5-3: Variation cationic diagram of Zr/Hf ratios vs. Si for zircon groups from the A) Desemborque and B) Mandira.

Among the non-formula elements, the average contents of most, as CaO, ThO_2, Y_2O_3, U_2O_3, and P_2O_5, increase from the magmatic to the altered and from the latter to the hydrothermal types in both occurrences, accompanied by decreasing ZrO_2 and SiO_2 abundances (Table 5-1 and Supplementary Materials), with exception of Y_2O_3 in the hydrothermal zircon from the Desemborque Pluton, which lower contents as compared with the altered and magmatic types. Such compositional variations are depicted in Figure 5-4, which reinforces the

increasing Si/(Zr+Hf) ratios and REE+Y contents towards the hydrothermal zircon types in both targets, as well as the strong correlations between the HfO_2/Y_2O_3 and ZrO_2/Y_2O_3 ratios, with increasing HfO_2/Y_2O_3 values in the sequence magmatic, altered and hydrothermal zircon types from both occurrences.

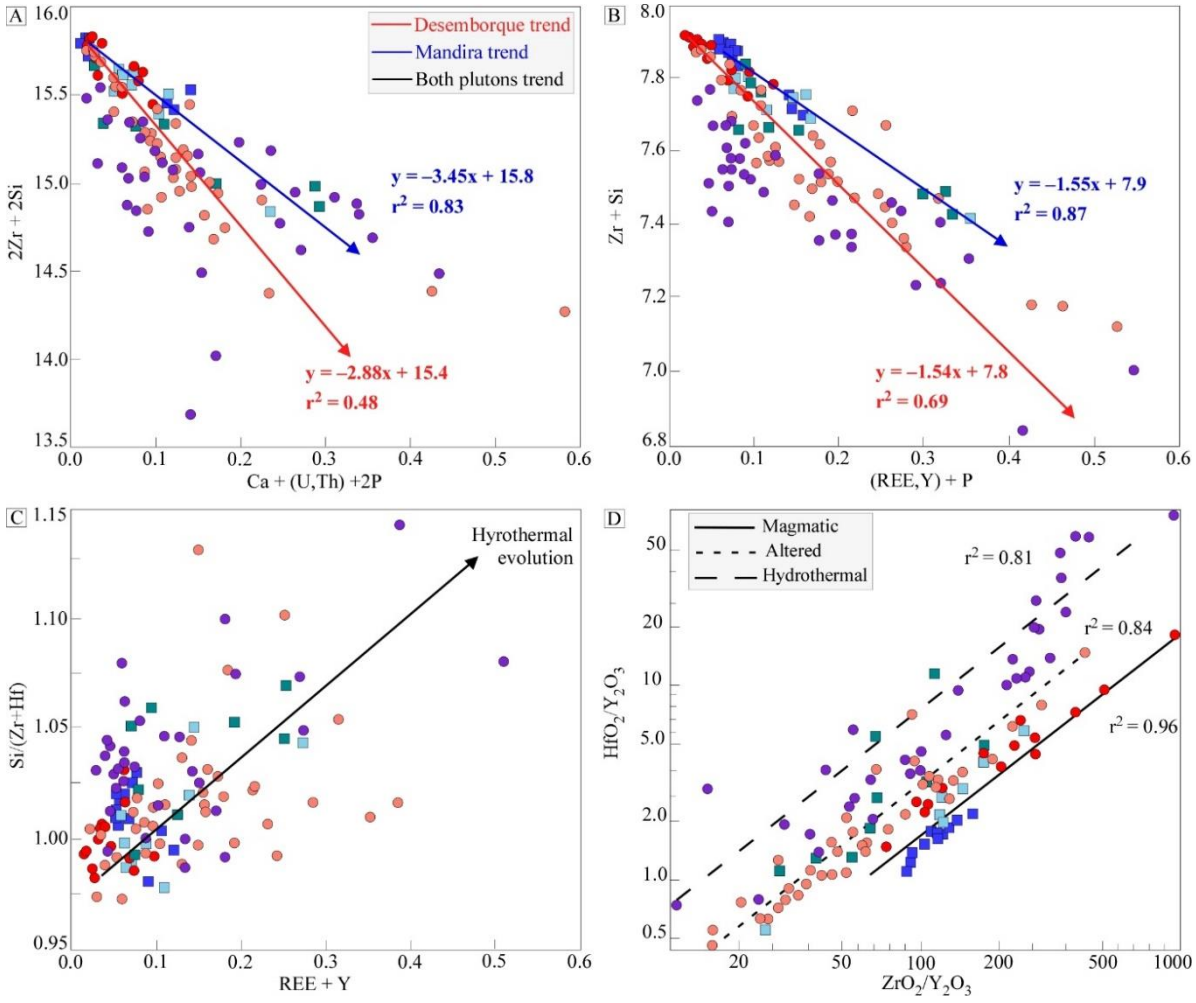

Figure 5-4: Chemical major compositions of magmatic, altered and hydrothermal zircons from the Desemborque and Mandira occurrences showing the cationic variations of A) brabantite component substitution; B) the xenotime + pretulite component substitution; C) Si/(Zr+Hf) vs. REE+Y diagram (in apfu); and D) HfO_2/Y_2O_3 vs. $ZrO_2/Y2O_3$ diagram (in wt%).

These compositional variations are also represented as semi-quantitative X ray maps for Hf, Y, Th, U, Y, P and Ca, in Figure 5-5 showing the internal compositional variation of two zircon crystals from the Desemborque and one from the Mandira, respectively. The first crystal represents a magmatic zircon with two chemical signs of alteration, defined by 1) strong dissolved margins with relatively high Y, P and U concentrations indicating the xenotime component substitution and then 2) a transitional enrichment of Hf in the outermost parts of

these margins. The second crystals. The second crystal is a hydrothermal zircon showing moderately to highly enrichment of Hf along internal domains as well as remarkably spongy texture including Th-rich inclusions and somewhat of U and Y concentrations. The third crystal also represent a hydrothermal zircon with moderately enriched of Hf-, Y- and mildly P, whereas Th and U are relatively depleted.

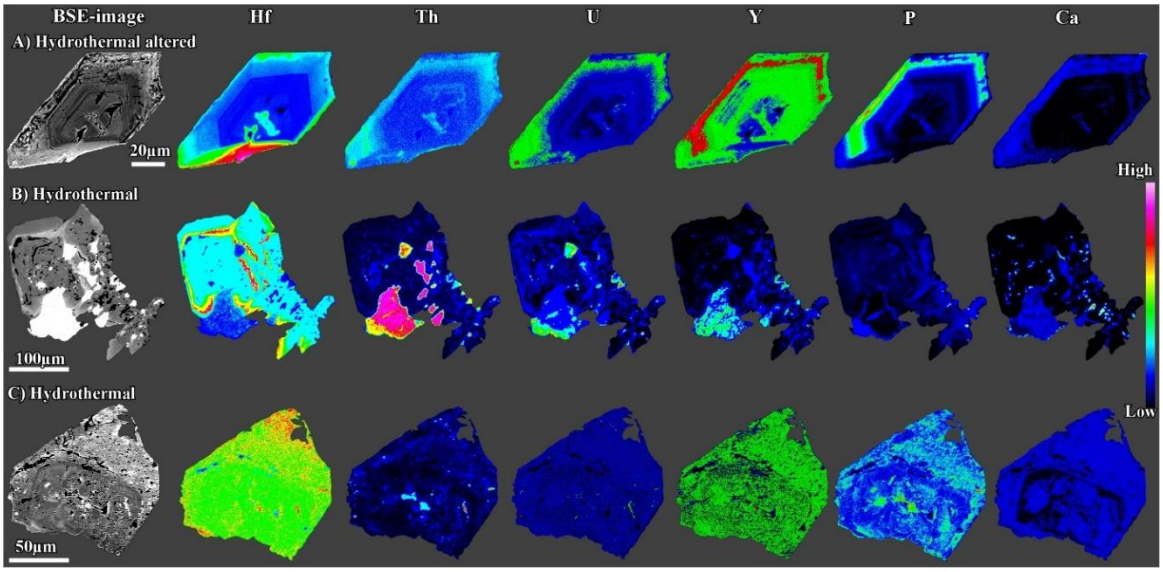

Figure 5-5: High-resolution X-ray elemental (Hf, Th, U, Y, P, Ca) maps for magmatic, altered and hydrothermal zircon crystals. A) Magmatic altered zircon. Note the two stages of alteration defined by strong altered/metamictic margins with enriched in Y, P and U and then a subsequent inward enrichment of Hf along outermost margins. B) Hydrothermal zircon with high distinctly concentrations of Hf along internal domains, in addition Th-, U-and Y are enriched as rounded overgrowths. Hydrothermal zircon with high concentrations of Hf and Y and moderate of P whereas Th, U and Ca are depleted.

Besides the single Hf ↔ Zr homovalent substitution, the mains described chemical variations may be related to coupled substitution reactions involving the brabantite and the xenotime and pretulite molecules (e.g. Romans et al., 1975; Breiter et al., 2006), as follows:

$$Ca^{2+} + (Th,U)^{4+} + 2P \leftrightarrow 2Zr^{4+} + 2Si^{4+} \quad (1)$$

$$(REE, Y)^{3+} + P^{5+} \leftrightarrow Zr^{4+} + Si^{4+} \quad (2)$$

as represented in Figure 5-4. Overall, the moderate to elevated contents of Hf, Th, U, P and Ca reflect some chemical changes among internal domains of zircons as expected when crystals are affected by late- to post-magmatic fluid-induced alterations (e.g. Breiter et al., 2006; Geisler et al., 2007; Lisowiec et al., 2013; Park et al., 2016; Kim et al., 2018).

5.5.2. Trace element patterns

Multi-element (zircon and host rock) and REEs (zircon) patterns are shown in Figure 5-6. Trace element patterns of magmatic zircons are characterized by equivalent patterns to their host-rocks with pronounced positive anomalies of Th, U and negative of Pb (Figure 5-6A-B), whereas the altered and hydrothermal zircons show a distinct but subtle negative anomaly of Y relative to their corresponding host-rocks. This could be related to the crystallization of coeval Y-rich phases during the post-magmatic evolution such xenotime in the Desemborque Pluton, and gagarinite in the Mandira unit (see below). In general, trace element abundances show a progressive relative enrichment in REEs, HFSEs, Th, U, Pb, Ti and P from magmatic through altered and hydrothermal zircons in the both studied occurrences, however zircon crystals in the Desemborque pluton are 1-fold higher in such elements in the average than the Mandira granites (cf. Table 5-2).

Magmatic zircons in the Desemborque have REEs abundances vary from 1809 to 4547 ppm, whereas in the Mandira the total REEs vary from 2622 to 3521 ppm. REEs patterns in both cases show a comparable steeply increase of the slope from LREEs to HREEs [$73 \leq Yb/Ce_N \leq 117$ and $56 \leq Yb/Ce_N \leq 139$], and positive Ce and strong negative Eu anomalies [Eu/Eu* up to 0.01] like those typical of normal igneous zircons (Hoskin and Schaltegger, 2003). Of note, the Ce anomaly in magmatic zircons from the Mandira granites are significant larger with Ce/Ce* up to 76 in comparison with the Desemborque magmatic zircons which have Ce/Ce* up to 3.9 (Figure 5-6C-D).

Altered zircons from the Desemborque pluton record the highest REEs abundances among all zircon groups vary from 11730 to 28077 ppm, while the Mandira altered zircons have REEs ranging 3642 to 9235 ppm. In general, REEs patterns of this textural group between the both occurrences are characterized by increasing patterns from LREE to HREE [$8 \leq (Yb/Ce)_N \leq 32$ and $63 \leq (Yb/Ce)_N \leq 202$], weak positive Ce (up to 3.86 and 2.57) and elevated negative Eu anomalies (up to 0.02 and 0.05). Of note, metamictic zircons from the Desemborque pluton show a distinct rather enriched in the LREE and MREE patterns suggesting distinctly hydrothermal fluid compositions.

Hydrothermal zircons from the Desemborque pluton have higher REEs abundances vary from 6521 to 23806 ppm than those from the Mandira granites 5108 to 15335 ppm. The HREE patterns in both plutons are very similar in some features such the steeply increasing of the HREEs [$22 \leq Yb/Ce_N \leq 222$ and $30 \leq Yb/Ce_N \leq 302$] and strong negative Eu (up to 0.07 and 0.06) anomalies (Figure 5-4A-B). However, the hydrothermal zircons from the Desemborque

pluton show contrasting LREEs behavior with relative flatter patterns [$2.0 \leq Sm/La_N \leq 6.9$] and thus small positive Ce anomalies [$0.9 \leq (Ce/Ce^*) \leq 1.5$]. These REEs patterns are akin to those most typical hydrothermally crystallized zircons (Hoskin, 2005).

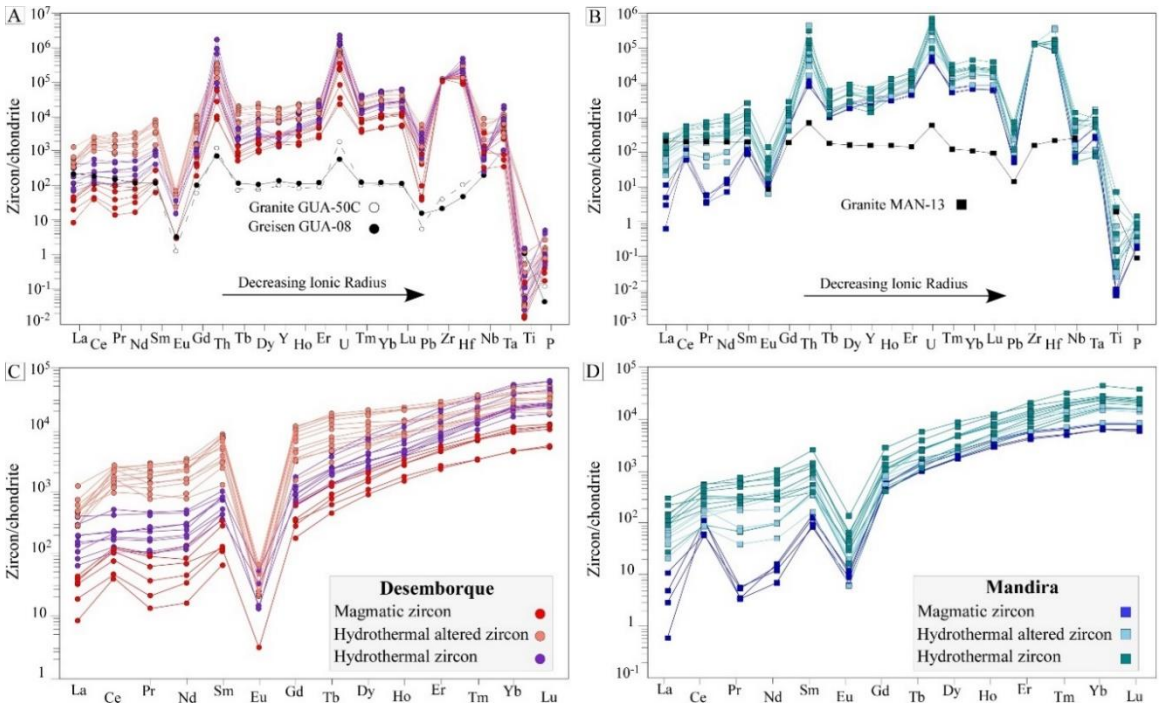

Figure 5-6: Chondrite-normalized trace elements and REE patterns for magmatic zircons, altered and hydrothermal zircons and host granites and greisen from the A-C) Desemborque and B-D) Mandira occurrences, respectively. Chondrite values are from McDonough and Sun (1995).

5.6. Hydrothermal phosphates

Monazite-(Ce) and xenotime are typical hydrothermal phases within both the syenogranites and greisens from the Desemborque Pluton; however, they do not appear in the Mandira samples, pointing to contrasting hydrothermal environment and evolution.

5.6.1. Monazite-(Ce)

From a descriptive point of view, two main monazite crystal types were recognized. The first type (Mz-1) forms small to moderate (up to 100 µm) prismatic or rounded crystals showing either heterogeneous or homogeneous textures on BSE-images. In syenogranites, they appear as rounded grouped crystals with subtle dissolved domains in contact with zircons. In greisens, Mz-1 occurs interstitial between zinnwaldite, sericite and quartz of the groundmass showing partially zoned domains, patchy textures with fractures and corroded margins (Figure

5-7A). The second type (Mz-2) appears as small (15-60 µm) irregular crystals in contact with either zircon or fluorite. In syenogranite, Mz-2 occurs in interstices of annite aggregates, closely associated with fluorite grains, in penetrating contacts around fluorite margins (Figure 5 7B), (Figure 5-7B). In greisens, Mz-2 occurs either as irregular crystals hosted in fluorite or as intergranular crystals replacing or filling cavities between zircon crystals (Figure 5-7C).

Representative chemical compositions for the identified monazite types are presented in Table 5-3 and the remaining data as Supplementary Materials. A total of 81 chemical ages from the both monazite-1 and monazite-2 groups were computed, which record variable contents of Th (0.82 – 8.66 wt%), U (0.001 – 0.156 wt%), Y (0.04 – 2.40 wt%) and Pb (0.024 – 0.223 wt%). In general, the Mz-1 type present relatively high average contents of La_2O_3 = 11.97 wt%, Ce_2O_3 = 32.44 wt%, P_2O_5 = 28.6 wt%, and ThO_2 = 4.99 wt%, while the Mz-2 type present slightly higher average contents of La_2O_3 = 13.61 wt% and P_2O_5 = 29.3 wt%, but lesser average contents of Ce_2O_3 = 32.23 wt% and ThO_2 = 1.85 wt% than the Mz-1 type. Accordingly, the correlation between Th and La/Ce ratios (in apfu) well separates the two textural monazite types as shown in Figure 5-8A.

There are significant differences among the minor and REEs compositions (EPMA) between the Mz-1 and Mzi-2 types. The total REE+Y abundances in Mz-1 varies from 500915 to 569709 ppm, whereas in Mz-2 these values range from 555592 to 575528 ppm (Table 5-3Figure 5-8). REE patterns from EMPA analyzes show LREE-enriched patterns and strongly fractionation along the HREEs with LREE/HREE ratios from 11 to 128, while those from the LA-ICP-MS exhibit $LREE_N/HREE_N$ ratios from 9 to 21 and negative Eu/Eu* = 0.01 (Figure 5-8B). The more fractionated pattern with rather extremely high REE abundances when compared to the other analyzed crystals is represented by one Mz-2 type crystal from the greisen that is embedded in fluorite and contain several inclusions of fluocerite. For comparison, REEs compositions for representative crystals from the Mz-1 types were analyzed by the LA-ICP-MS technique (see supplementary material). They show REE+Y abundances vary from 170539 to 7370345 ppm which are between the down and upper limits from the completed EMPA dataset Figure 5-8B.

Compositional variations for the monazite groups are related to coupled cationic substitutions indicating the presence of cheralite and huttonite components (c.f. Förster, 1998)

$$Th+U \leftrightarrow Ca+Si \quad (3)$$

$$(Th,U) + Si \leftrightarrow (REE,Y)+ P \quad (4)$$

given the good correlation between as show in Figure 5-8C-D.

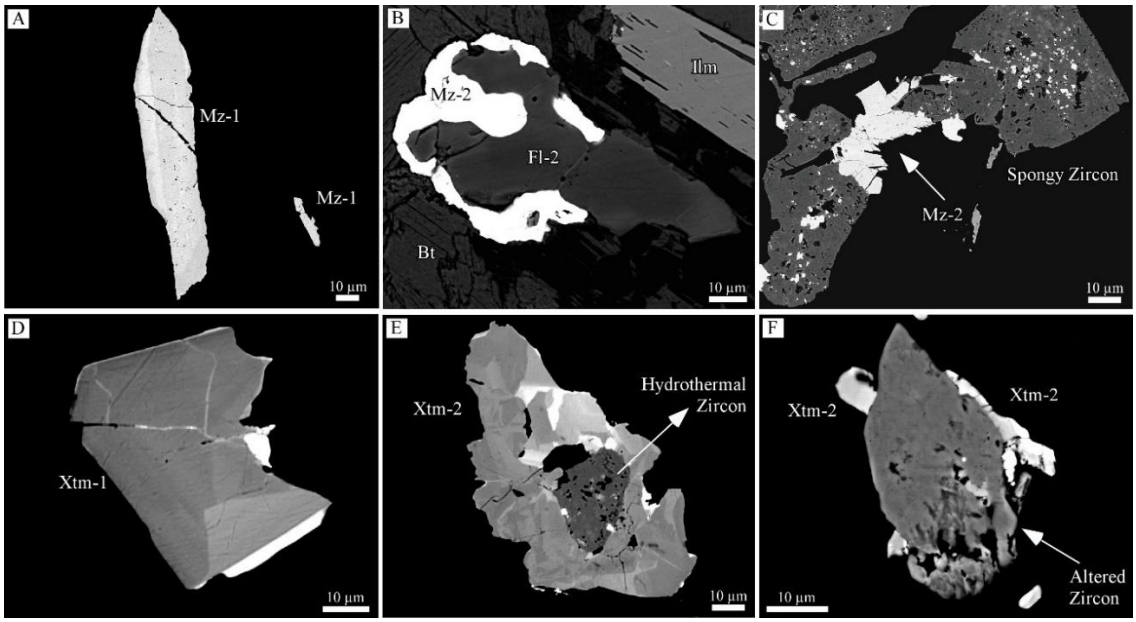

Figure 5-7: BSE images showing microstructures and textural relations of late to hydrothermal monazite and xenotime phosphates from the Desemborque Pluton. A) Euhedral subtle patchily monazite (Mz-1) crystals with fractures and corroded margins (Sample GUA-08, greisen). B) Secondary monazite (Mz-2) rimmed fluorite (Fl-2) which suggest reaction textures in association with biotite and ilmenite (Sample GUA-50C4, syenogranite). C) Secondary monazite (Mz-2) intergrown between spongy zircon crystals (Sample GUA-08, greisen). D) Subhedral xenotime (Xtm-1) with subtle zoning pattern and altered by microcraks (Sample GUA-08, greisen). E) Xenotime (Xtm-2) strongly zoned crystals including a hydrothermal zircon. F) Xenotime (Xtm-2) appearing as irregular overgrowths either towards rims or filling cavities in altered hydrothermal zircon (Sample GUA-08, greisen).

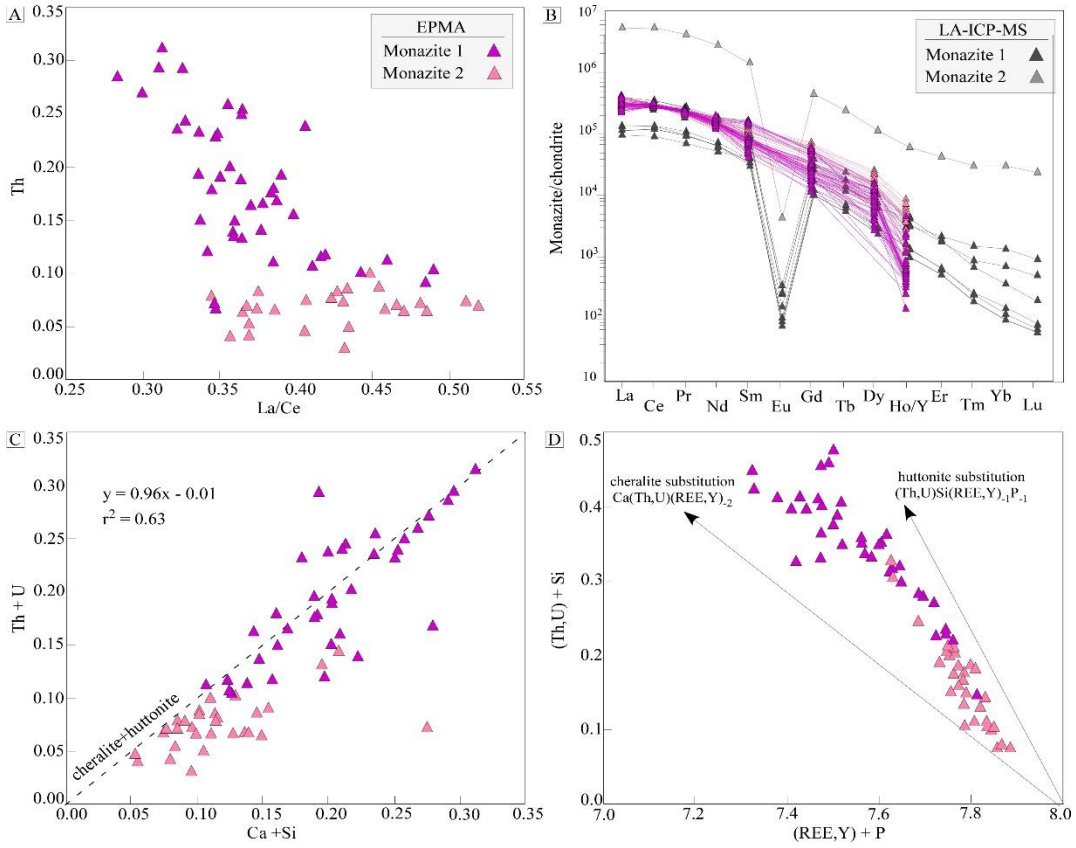

Figure 5-8: Compositional variations in hydrothermal monazite from the Desemborque pluton. A) Cationic relation between the La/Ce ratios and Th contents for both textural monazite groups. B) Chondrite-normalized REE patterns showing all analyzed crystals by EMPA and some representative crystals of the monazite 1 group analyzed by LA-ICP-MS from the greisen. Chondrite values are from McDonough and Sun, (1995). C-D) Cationic diagrams showing the relations of the cheralite and huttonite coupled substitutions in monazite (in apfu).

5.6.2. Xenotime

Xenotime occurs mainly in the greisens and rarely within syenogranites from the Desemborque pluton. Textural relations as observed in BSE images reveal also two main types. In greisens, early-formed xenotime (Xtm-1) forms small (up to 30 µm) subhedral isolated crystals displaying zoning patterns with BSE-bright and BSE-dark irregular domains, and corroded margins (Figure 5-7C). In both syenogranites and greisens, a distinct type of xenotime (Xtm-2) is found as alteration rims or overgrowths within zircon crystals appearing either as small irregular zoned crystals surrounding hydrothermal zircon (Figure 5-7E) or as thin epitaxial overgrowths at the contact of altered zircon (Figure 5-2A and Figure 5-8F). In some cases, they occur interstitial between fluorite crystals.

Representative chemical compositions for xenotime are listed in Table 5-3 and the remaining data in Supplementary Materials. Xenotime present moderate to high contents of Y_2O_3 = 23.1 – 45.9 wt%, P_2O_5 = 31.2 – 35.82 wt% and HREEs = 16.3 – 44.7 wt%. The totals REEs+Y ranging from 499696 to 578848 in ppm (measured by EMPA) and from 3652264 to 4879843 ppm (measured by LA-ICPMS). REE patterns from both measured crystals show a general steeply positive slope through the HREEs with $LREE_N/HREE_N$ ratios ranging 0.01– 0.05, and 0.02– 0.08 and strong negative Eu anomalies up to 0.005 (Figure 5-9A), respectively. The large dispersion between the LREE patterns may be related to the low measured concentrations of these elements among the xenotime crystals and thus some chemical uncertainties.

Figure 5-9B show the main compositional variation among zoned xenotime crystals that is related to the coupled cationic substitution of the type (c.f. Förster, 1998)

$$(REE+Y) + P \leftrightarrow (Th,U) + Si \qquad (5).$$

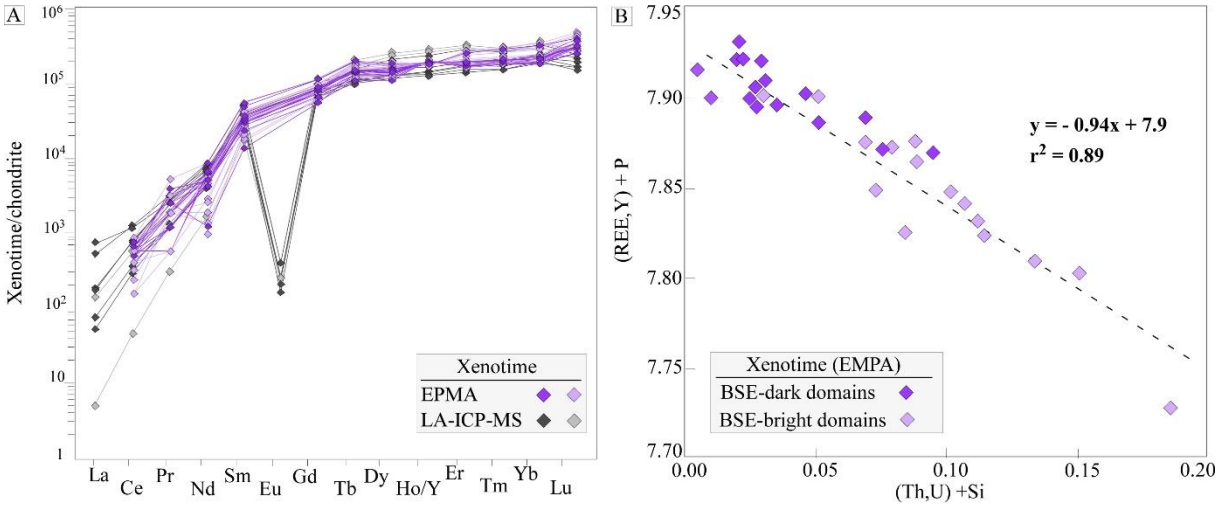

Figure 5-9: Compositional variations in hydrothermal xenotime from the Desemborque pluton. A) Chondrite-normalized REE patterns for all xenotime crystals measured by EMPA and for representative crystals measured by LA-ICP-MS. Chondrite values are from McDonough and Sun (1995). B) Coupled substitution (Th,U)+Si vs (REE,Y)+P (in apfu) for crystals from the xenotime-1 group.

5.7. Late- to hydrothermal fluorides

5.7.1. Fluorite

Fluorite is a late to post-magmatic mineral appearing in two textural types among all studied rocks from the both Desemborque and Mandira occurrences In the Desemborque syenogranites, late-magmatic fluorite (Fl-1) is characterized by isolated subhedral large tabular crystals (up to 400 µm) with slightly zoned displaying homogenous bright cores in BSE-images and patchily dark border domains. They are usually interstitial between felsic minerals and replaced either by secondary unidentified (REE+Y)-rich fluorides or columbite (Figure 5-10A). Post-magmatic fluorite (Fl-2) in syenogranites is found as irregular intergrowths filling cavities of biotite in reaction textures with Mz-2 type (Figure 5-7B). In greisens, a distinct hydrothermal fluorite (Fl-3) forms large irregular crystals with variably sizes (100-250 µm) occurring interstitial between quartz and zinnwaldite of the groundmass, sometimes in co-precipitation textures with zircon (Figure 5-10B). They tend to be partly resorbed and occurring in close association with secondary columbite, monazite or xenotime.

In the Mandira granites, late-magmatic fluorite (Fl-1) forms large irregular crystals (200-300 µm), showing numerous patchily domains, corroded margins and inclusions of secondary fluorides (Figure 5-10C). These crystals are interstitial and sometimes occur forming aggregates with riebeckite, arfvedsonite or astrophyllite. A distinct hydrothermal fluorite (Fl-

2) occurs as intergrowths in penetrating contacts with hydrothermal zircon and shows poikilitic core-textures containing several inclusions of fluocerite or gagarinite (Figure 5-10D).

Representative chemical compositions for fluorite from the Desemborque and Mandira occurrences are shown in Table 5-3Table 5-4 and in Figure 5-11. For comparison, fluorite in Mandira granites present relatively high F average contents (45.01 wt%) with Y and REEs averaging 2.20 wt% and 1.70 wt% respectively, whereas in the Desemborque pluton these values are 43.20 wt% F, .53 wt% Y and 3.52 wt% REEs.

5.7.2. Fluocerite-(Ce)

Fluocerite is hydrothermal accessory mineral found in the Mandira peralkaline granites and is firstly described in this work. It forms minute (15-30 μm) amorphous crystals with elongated or rounded forms usually occurring as inclusions in fluorite crystals (Figure 5-10C). Fluocerite is also found as intergrowths and closely associated with gagarinite along margins of either hydrothermal fluorite or zircon (Figure 5-10E-I). Chemical compositions show relative high contents of LREEs ranging 70.33 – 73.01 wt% with Ce as dominant element (32.41 – 39.20 wt%) and F contents in between 26.79 to 30.46 wt% (Table 5-4). Of note, fluocerite records the highest REEs abundances among the hydrothermal fluorides from the Mandira granites (c.f. Figure 5-11).

5.7.3. Gagarinite-(Y)

Gagarinite is a hydrothermal accessory mineral exclusively found in the peralkaline granites from the Mandira granites and also is firstly reported here. It appears as isolated or grouped small (10-70 μm) crystals usually included in fluorite (Figure 5-10C), or as secondary irregular intergrowths in reaction with fluocerite along hydrothermal zircon crystals (Figure 5-10E-I). Sometimes, gagarinite occurs filling cavities between quartz and riebeckite in textural reaction with post-magmatic astrophyllite (not shown). It is chemically characterized by relatively high REEs (16.21 – 22.86 wt%) and Y (11.85 – 12.67 wt%) contents and variable contents of Na in between 3.69 – 6.90 wt% (c.f. Table 5-4).

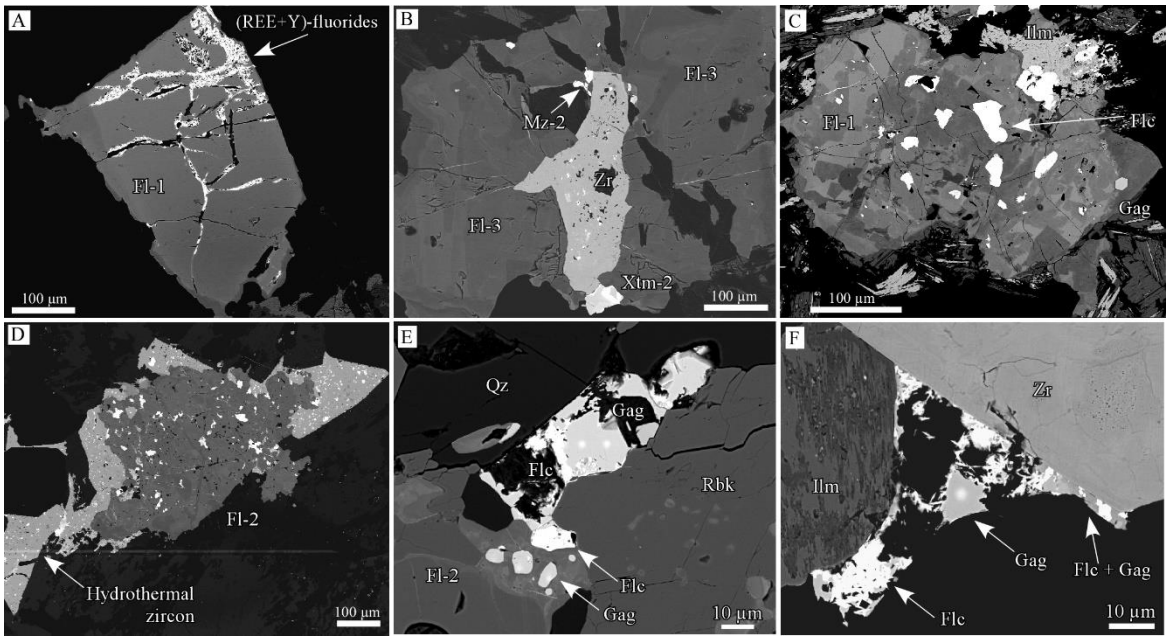

Figure 5-10. BSE images showing microstructures and textural relations of late to hydrothermal fluorite, fluocerite and gagarinite fluorides from the Desemborque and Mandira occurrences. A) Late-magmatic fluorite (Fl-1) partially replaced by secondary (REE+Y)-fluorides (Sample GUA-50C1, syenogranite). B) Hydrothermal fluorite (Fl-3) slightly zoned enclosing an irregular spongy zircon and minute overgrowths of secondary xenotime and monazite crystals (Sample GUA-08, greisen). C) Late-magmatic fluorite (Fl-1) showing patchily domains and inclusions of fluocerite and gagarinite (Sample MAN-2A, peralkaline granite). D) Hydrothermal fluorite (Fl-2) in co-precipitation texture and showing inward penetrating contacts with hydrothermal zircon (Sample MAN-2A, peralkaline granite). E) Reaction texture between hydrothermal fluorite (Fl-2) with riebeckite (Rbk). Of note, fluocerite (Flc) and gagarinite (Gag) irregular crystals intergrown between riebeckite and quartz after dissolution of fluorite (Sample MAN-13B, peralkaline granite). F) Interstitial gagarinite intergrown along margins of zircon and ilmenite. Notice the reaction between gagarinite (Gag) and fluocerite (Sample MAN-13A, peralkaline granite).

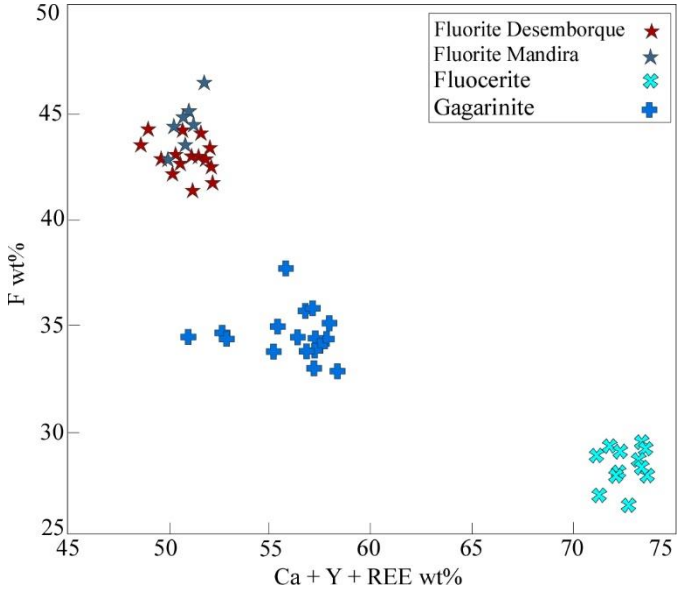

Figure 5-11: Chemical compositions of late to hydrothermal fluorite and secondary fluocerite and gagarinite from the Mandira granites.

5.8. U-Th-total Pb Monazite Dating by EPMA

Dating of hydrothermal events is a major issue related to the evolution of A-type magmas and our analytical EPMA procedure for monazite and xenotime analysis was directed to obtain simultaneous chemical and geochronological information through the Th-U-total Pb method. Our xenotime data however prove to be not appropriate for dating, due to their systematic low U, Th, and, thus, total Pb contents (c.f. Table 5-3 and Supplementary Materials) and consequent large age variations, with much high errors (up to a hundred million years).

On the other hand, monazite gave very significant results. Among the total of 81 obtained spot analyses from both Mz-1 and Mz-2 types, we discarded 15, which presents alternatively poor structural formulae, typical with significant (Si+P) excess on the P-site or with insignificant Th, U, and Pb contents resulting in relatively high age deviations ($2\sigma > 10\%$).

The comparison between the Th-Pb isochronic and the weighted average results show a similar age with corresponding errors as illustrated in Figure 5-12. All grouped Mz-1 and Mz-2 ages range from 555 to 615 Ma. Isochron ages obtained when grouped both hydrothermal Mz-1 and Mz-2 types are 586 ±8.2 (fit drawn to origin) and yield a MSWD = 0.34 and probability fit value of 1.0 (Figure 5-12A). The weighted average age of both types is 584 ±3.1 with a good MSWD = 0.71 and probability fit of 0.96 (Figure 5-12B), while average ages obtained from the Mz-1 and Mz-2 types are 583 ± 3 Ma (n = 36) and 587 ± 7 Ma (n = 30), respectively. The distinct ages between monazite types are directly linked to their notable variable compositions indicating that the Mz-2 type with the lower Th and Pb contents show the greatest ages error ($21 < 2\sigma < 68$) when compared to the Th-richer Mz-1 crystals ($13 < 2\sigma < 56$).

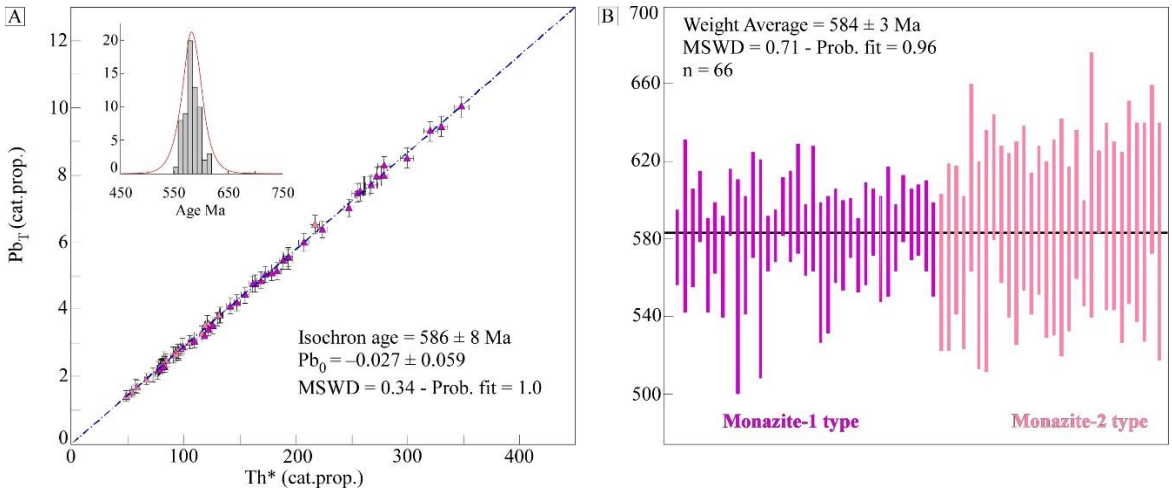

Figure 5-12: Chemical monazite dating showing A) the isochronic Th vs. Pb_T plot (in cationic proportions) forced through zero as proposed by Montel (1996) together with the age histogram with the best gaussian fit, and B) the weighted average age diagram for monazite groups from the Desemborque Pluton.

5.9. Discussion

5.9.1. Hydrothermal alteration processes registered by microtextures of zircons and related accessory minerals

In magmatic to hydrothermal evolution, some replacement mineral alterations were produced in the studied syenogranites and peralkaline granites such strong albitization and/or sericitization of early feldspars; replacement of primary annite by protholitionite to siderophyllite in the case of the Desemborque syenogranites (Garcia, 2015); replacement of riebeckite by astrophyllite in the Mandira peralkaline granites (Siachoque and Vlach-in chapter 3); and recrystallization of hydrothermal quartz. These metasomatic reactions between feldspars and primary silicate mafic minerals can produce the release of F-rich and/or HFSE-rich post-magmatic fluids (e.g. Salvi and Williams-jones, 2006; Ogunleye et al., 2006), which are interpreted as the driving force to hydrothermal alteration of zircons and subsequent precipitation of further REE-bearing hydrothermal accessory minerals. Vlach (2012) previously documented that post-magmatic HFSE- and F-enriched fluids is a common feature to the magmatic to hydrothermal evolution within the province and this was reinforced by Vilalva et al. (2019) to explain the hydrothermal alterations in zircon within granites from the Graciosa Province.

In this sense, the several alterations in zircon crystals from the both studied occurrences are interpreted as formed during multi-stage alterations by such late- to post-magmatic F-rich fluids that we defined as follows. The first-stage alteration is represented by fracturing and partially dissolved cores in magmatic zircon crystals (Figure 5-2A-B and F-G), while the second-stage alterations are more intensive resulting in the recrystallization of irregular patchily domains and replacement of the primary magmatic textures (cf. Figure 5-2C).These structural modifications are linked to chemical changes (or metamictization) supported by the moderate to significant depletion of Zr and Si, and high concentrations of non-formula elements such Hf, Y, Nb, Th, U, Pb, Al, Fe, and Ca along the altered domains (c.f. Figure 5-4) indicating re-equilibration of zircon by diffusion-reaction processes (c.f. Geisler et al., 2007). A third-stage alteration is pervasive leading the formation of highly porous-spongy textures and/or corrosive margins in later and hydrothermal zircons (Figure 5-2D-E, G-). The development of spongy-textures with several Th and U inclusions are broadly interpreted as resulted by coupled dissolution-reprecipitation processes (Putnis, 2002; Tomaschek, 2004; Geisler et al., 2007; Lisowiec et al., 2013; Park et al., 2016). In this case, the compositions of the altered internal

domains record significant enrichment in REEs, Hf, Y, Th, U and P (c.f. Figure 5-4). In some cases, both Desemborque and Mandira zircons show a distinctly four-stage fluid-induced alteration related to the final recrystallization of Hf-rich margins indicating highly fractionation of Hf in zircon during hydrothermal evolution (Figure 5-2B, H).

The post-magmatic formation of further REE-rich accessory minerals also reflecting hydrothermal alteration processes which are associated to destabilization of zircon and/or fluorite during late to hydrothermal evolution. In the Desemborque pluton, the precipitation of both secondary monazite and xenotime types along corrosive margins of zircon is undoubtedly released to fluid-interaction and subsequent destabilization of the hydrothermal zircon (Figure 5-7D, F). The replacement of zircon by monazite and xenotime can be explain by dissolution-reprecipitation processes, where zircon-fluid interaction removed most of the enriched LREE, HREE, Y, Th and Pb elements from hydrothermal zircons and reprecipitated in these minerals along the reaction margins. Moreover, the precipitation of secondary fluorides also reflects dissolution processes in this case of fluorite leading the element remobilization of F, REEs and Y along fractures and subsequent precipitation of secondary (REE+Y)-rich fluorides (cf. Figure 5-10A). In the Mandira granites, the destabilization of the Y-rich fluorite crystals may have involved hydrothermal mobilization of the REEs, i.e. decoupled of LREE and HREE, which then were fixed in the precipitation of fluocerite and gagarinite either as numerous inclusions or intergrowths within fluorite (Figure 5-10E-F). An alternative mechanism of formation for secondary fluorides is aimed to the third-stage alteration on zircon crystals (Figure 5-8I), indicating that the Interaction between zircon and such post-magmatic fluid may had released incompatible LREEs and some HREEs from dissolved zircon, which were closely incorporated in fluocerite-(Ce) and gagarinite-(Y) along zircon margins, respectively.

5.9.2. Tracking hydrothermal evolution trends of Desemborque and Mandira zircons with major and trace element compositional variations

Because zircon can occur during the entire crystallization process of melt differentiation in A-type granites (Breiter and Škoda, 2012; Breiter et al., 2014) its chemical compositions are crucial to tracing late- to post-magmatic hydrothermal events. For example, the variation of Zr/Hf ratio in zircon, i.e. Hf-enrichment, is generally associated to granitic magma differentiation (Linnen and Keppler, 2002; Hoskin and Schaltegger, 2003; Zaraisky et al., 2008; Claiborne et al., 2010; Breiter et al., 2014b), but also can be related to changes in melt

composition under the influence of low temperature volatile-rich (such H2O, Li, F or P) melt/fluids and/or to hydrothermal alterations (Rubin et al., 1989; Wang et al., 2010; Yin et al., 2012; Li et al., 2019). We use this parameter to restrict chemically the three zircon groups based on the microstructural interpretations and we observed a greater Hf fractionation across the hydrothermal evolutionary stages according to the decrease of atomic Zr/Hf ratios in zircon from magmatic (Zr/Hf > 60 and 100), to relatively hydrothermal altered (40-80 ≤ Zr/Hf ≤ 80-100) and hydrothermal (Zr/Hf < 40 and 60) zircon types (cf. Figure 5-3). The progressive enrichment of Hf from magmatic to hydrothermal zircon types in both occurrences is also accompanied by increase of REEs, Y, Nb, Th, U, Ti and P (cf. Figures 5.4 to 5.6). Increase of such incompatible non-formula elements in zircon have been largely attribute to interaction with post-magmatic F- and/or HFSE-rich fluids during granitic evolution (Nardi et al., 2012, 2013; Sheard et al., 2012; Yang et al., 2014; Vasyukova et al., 2016; Li et al., 2019), and this interpretation is compatible with the previous discussion of multiple fluid-induced alterations in the Desemborque and Mandira zircons.

An additional chemical distinction between magmatic and hydrothermal zircons may be made in the LREE discriminant diagrams proposed by Hoskin (2005), in which the Sm/La_N ratio and the abundances of La discriminate these two types of zircons in Figure 5-13A. However, in a recent work of Bell et al., (2016) the authors proposed use the LREE-I index (LREE-I = Dy/Nd + Dy/Sm, using concentrations rather than chondrite-normalized values) as an alternative quantitative correlation between the Sm/La_N ratio to recognized unaltered (magmatic) zircon of altered and/or contaminated by other phases (hydrothermal) zircon (Figure 5-13B). Thus, we compared these both diagrams to plot our zircon compositions and recently data of zircon from the both studied cases examined by Vilalva et al., (2019).

In the Hoskin's diagram, magmatic zircons from the Desemborque pluton ($1 \leq Sm/La_N \leq 10$) are closely plotted in the hydrothermal field, whereas those from the Mandira granites ($2 \leq Sm/La_N \leq 42$) plotted in area between magmatic and hydrothermal fields with an exception of one zircon ($Sm/La_N = 151$) that is included in the Hoskin's magmatic field. The hydrothermal altered and later hydrothermal zircon types from both occurrences ($2 \leq Sm/La_N \leq 19$) are mostly plotted inside or close to the hydrothermal field.

In the Bell's diagram, magmatic zircons (24 ≤ LREE-I ≤ 117) from the both cases fall within or near the unaltered magmatic zircon field with some zircons showing compositions of altered zircons (12 ≤ LREE-I ≤ 19). Hydrothermal altered zircons from the Desemborque pluton have compositions within the altered zircon field (5 ≤ LREE-I ≤ 11), while most of the altered

zircons from Mandira granites plotted inside the unaltered region (31≤ LREE-I ≤ 52) and two zircons plotted in the altered area (LREE-I = 8 and 9). Although hydrothermal zircons falling into an uncertain region between the two Bell's fields, they have low LREE-I values from 12 to 19 which are corresponding to those compositions of zircons dominated by alterations or contamination (LREE-I < 30) as proposed by Bell et al. 2016. Accordingly, we decide to use this index to correlate with some typical petrogenetic indicators in order to track the chemical evolution trends grouping the three zircon types.

Firstly, the Desemborque and Mandira zircons show direct correlation between Zr/Hf and LREE-I values, which become more negative with hydrothermal evolution (Figure 5-13C). As expected the Hf contents are increasingly found with lower LREE-I (Figure 5-13D), supporting that the moderate to extremely enrichment of Hf in Desemborque and Mandira zircons are reflect of fluid-driven alterations in zircon. Thus, we can conclude that the Hf-enrichment in zircons in this study is indicative of the progress of hydrothermal evolution rather than magmatic evolution.

Similarly, the relationship between Th/U show an inverse correlation with similar steeply trends for zircons in both occurrences during the hydrothermal evolution (Figure 5-13E). The $(Yb/Dy)_N$ also show an inverse relationship with high (Yb_N/Dy_N up to 10) vs low LREE-I values from magmatic to hydrothermal zircons in both plutons. Finally, we observed a distinct positive trend between $(Yb/Dy)_N$ and LREE-I from magmatic to altered zircons only in the Desemborque pluton very similar to the reported by Bell et al. 2019 in the Stone Mountain zircons that these authors interpreted as contamination by LREE-enriched secondary phases (Figure 5-13F). In this study, this distinct trend can be explained as result of different compositions and multiple fluid-induced alterations reflecting in the elevated LREE and MREE flat patterns of the hydrothermal altered zircon crystals.

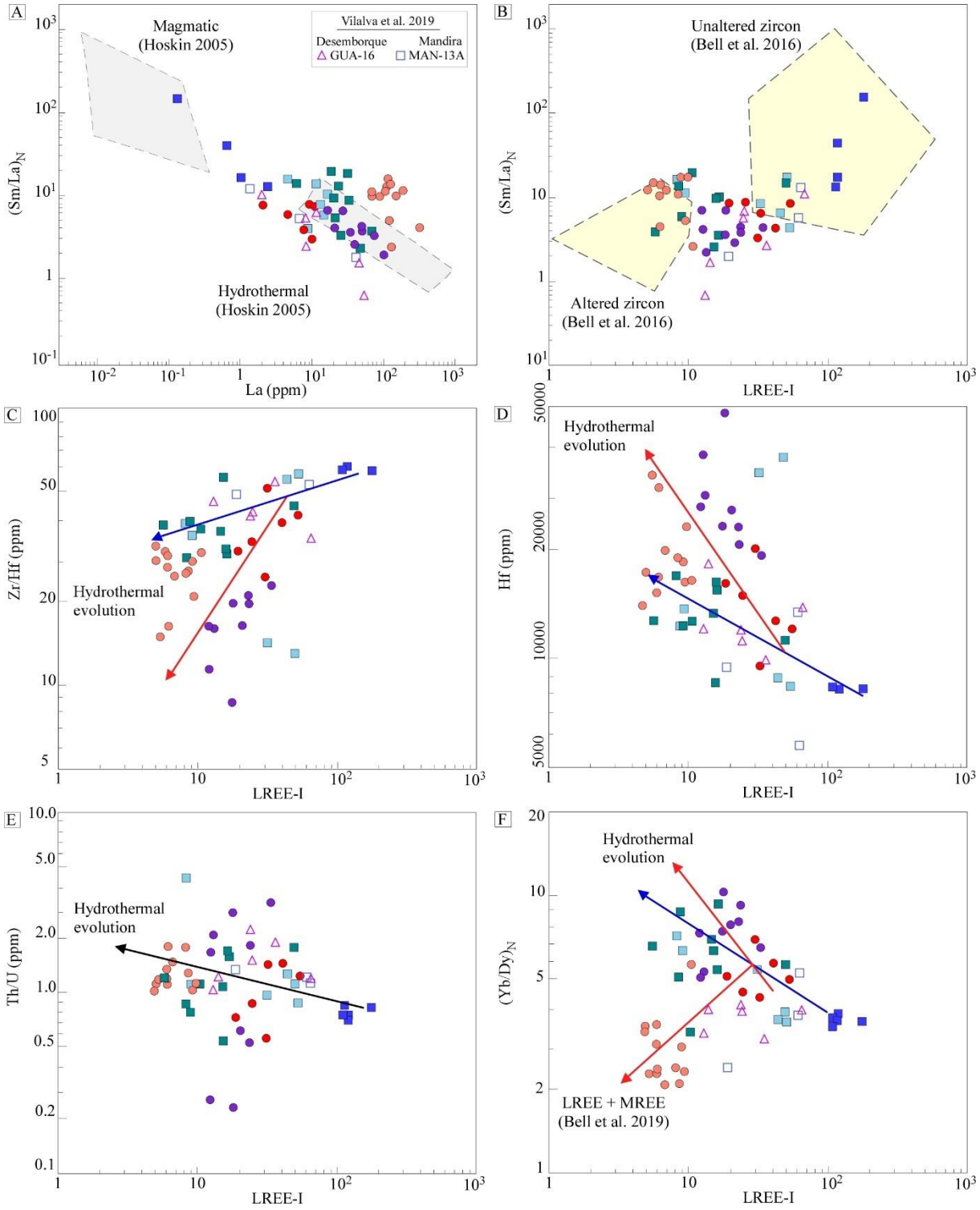

Figure 5-13. Binary plots with trace element compositional variations (in ppm). A) Sm/La_N vs La discrimination plot of magmatic and hydrothermal zircon from Hoskin, 2005. B) Sm/La_N vs LREE-I diagram showing the classification for unaltered magmatic zircon and altered hydrothermal zircon from Bell et al., 2016. Relationships between the LREE-I and various petrogenetic indicators of zircon evolution after Bell et al., 2019 of C) LREE-I vs. Zr/Hf. D) LREE-I vs. Hf. E) LREE-I vs. Th/U. F) LREE-I vs. $(Yb/Dy)_N$.

5.9.3. Timing of hydrothermal activity

The occurrence of monazite and xenotime among syenogranites and especially greisens from the Desemborque pluton are important signs of REE-bearing hydrothermal processes. These minerals are particularly well suited for dating by the EPMA chemical Th-U-Pb method. Application of this method in monazite crystals yield an Ediacaran age of 584 ± 3 Ma that is consistent with the reference crystallization age 580-583 (± 3-8) for the whole A-type magmatism in the Graciosa Province (Vlach et al., 2011; Vilalva et al., 2019), and thus monazite EPMA ages provide the first documented evidenced for the hydrothermal activity in the province. On the other hand, xenotime crystals are usually to small to allow multiple analyses, and in a few cases xenotime analyses strongly deviate from stochiometric compositions, especially the Pb contents which are unsuitable to use the chemical equation and lead to substantial analytical errors. Analyses in the larger xenotime crystals also caused difficulties to achieve chemical ages because of its compositional variations among crystals that we interpreted as fluid-induced re-equilibration processes according to the solid-solution between xenotime and thorite-coffinite (Figure 5-9A).

In the case of Mandira pluton, it is difficult to constraint the absolute chronological age of the hydrothermal activity because the lack of monazite/xenotime minerals on the Mandira peralkaline granites. However, recently U-Pb age determinations in zircons from the province reported by Vilalva et al. (2019) attract consideration given the contrasting crystallization age of 567 ± 6 Ma obtained for the Mandira pluton in comparison to the well restricted age of 580 Ma for the province. Because this isotopic age is derived from the same sample study here (MAN-13A), we can know suspect that zircons dated for these authors could have been likely affected by some of the multi-stage fluid-induced alterations observed here. In fact, the chemical comparison between the zircons studied by these authors with our data point to corresponding behavior with the metamict zircons (Figure 5-7). Although the determined 206Pb/238U age of 567 ± 6 reported by Vilalva and collaborators is a reasonably reliable average value (with > 80% concordance), the analytical spots in zircons exhibit systematic reverse age determinations such cores approximately younger than the rims, a common phenomenon ascribed to Pb loss of zircons by metamictization and hydrothermal fluid leaching (e.g. Hoskin, 2005; Kramers et al., 2009; Xu et al., 2012). In consequence, we suggest that the U-Pb (567 ± 6) ages may represent better the timing of the hydrothermal fluid-induced alterations within partially or fully metamictic domains observed within Mandira zircons rather than the magmatic crystallization age.

5.10. Conclusions

This contribution included the textural and chemical examination of accessory minerals in granites and greisens from the both Desemborque and Mandira occurrences at the Graciosa Province (S-SE Brazil) and shows the following conclusions:

In the case of the Desemborque Pluton

1) Magmatic zircon in syenogranites are strongly affected by late to post-magmatic fluids leading the internal structural and chemical transformations defined by metamictic textures and significant increase of Hf, REEs, Y, Nb, Ta, Th, U, Ti, P, Ca, Al and Fe along the altered zircon domains. In contrast, fluid-induced alterations in hydrothermal zircon from the greisens promotes in the development of spongy-textures characterized by high abundances of Hf, LREEs, Th and U.
2) During zircon/fluid interaction, REE were remobilized by the post-magmatic fluids promoting the precipitation of secondary monazite and xenotime especially at contact of the zircon margins.
3) The destabilization of fluorite crystals also favors the post-magmatic formation of (HREE+Y)-fluorides within the Desemborque syenogranites.
4) Hydrothermal monazite gave chemical average age of 584 ± 3 Ma (CHIME method) which is the first documented evidenced associated to hydrothermal activity in rocks from the Graciosa Province.

In the case of the Mandira granites

5) Magmatic, late-stage and hydrothermal zircon in peralkaline granites suffered post-magmatic alterations resulting in the partially dissolution of the magmatic cores and the formation of numerous porous (spongy textures) in the late-stage zircons. The structural transformations were linked to the progressive increase Hf, REEs, Nb, Ta, Th, U, Ti, and P, from primary to hydrothermal zircon.
6) The association of hydrothermal zircon with fluorite suggest that F-rich fluids would be involved in REE mobilization leading the formation of secondary fluocerite-(Ce) and gagarinite-(Y) fluorides, which are firstly described in this work.

Grouping both Desemborque and Mandira occurrences

7) Microstructures of zircons from the both Desemborque and Mandira occurrences revealed intensive late- to post-magmatic alterations during the late- to hydrothermal evolution ascribe to the circulation of post-magmatic F- and HFSE-rich fluids.
8) The structural transformations of zircons were grouped in at least four-stage of hydrothermal alterations which are related to the significant enrichments of especially Hf, REE, Y, Th and U from primary to hydrothermal altered zircons.
9) Despite the significant differences of compositions between Desemborque and Mandira zircons the chemical evolution trends of the distinct zircon types are equivalent for the both occurrences indicating that fluid-induced alterations were responsible for the progressive fractionation of Hf and the incompatible non-formula elements during evolution.

Acknowledgements

Staff do GeoAnalitica, FAPESP for financing this work (Proc. 08/00562-0) and (Proc. 2019/17343-4), and CAPES for the doctoral scholarship (Finance Code 001).

Table 5-1: Major compositions and structural formula for zircon types from the Desemborque and Mandira occurrences.

Pluton	**Desemborque Pluton**										**Mandira Granites**									
Facies	Biotite granite			Biotite granite			Greisen				Riebeckite alkali feldspar granite									
Sample	**GUA-50C2**			**GUA-02**			**GUA-08**				**MAN-13B**									
Point_ID	1b-c	1b-i	1b-i2	1-c	1-r1	1-r2	4-i	4-r1	4-r2	4-r3	1-c	1-r1	c1b	5-c	5-r1	8-r1	1-r3	7-r1	7-r2	8-r2
Type	Magmatic			Hydrothermal altered			Hydrothermal				Magmatic			Hydrothermal altered			Hydrothermal			
SiO_2 (wt%)	32.35	32.26	32.31	29.04	29.62	29.15	29.91	30.81	31.24	30.53	32.58	32.87	32.440	31.26	29.80	30.75	30.680	30.60	32.60	31.62
TiO_2	0.09	0.07	0.10	0.19	0.34	0.34	0.56	0.20	0.39	0.41	0.08	0.07	0.060	0.09	0.12	0.10	0.236	0.13	0.37	0.11
Al_2O_3	0.01	0.01	0.01	0.74	0.35	0.71	0.41	0.39	0.41	0.72	-	-	-	0.13	0.61	0.21	-	0.08	-	0.02
Fe_2O_3	0.15	0.23	0.46	1.74	1.69	2.21	0.79	0.72	0.71	1.42	0.09	0.14	0.073	0.74	1.19	0.86	0.914	1.02	0.09	0.49
MnO	-	0.01	0.01	0.45	0.47	0.45	0.44	0.40	0.37	0.69	-	-	-	0.15	0.26	0.21	0.061	0.16	0.00	0.08
MgO	-	-	-	0.01	0.02	0.02	-	-	-	-	-	-	-	-	0.04	0.03	-	-	-	0.02
CaO	-	-	-	0.30	0.39	0.30	0.11	0.13	0.13	0.15	-	-	-	0.11	0.16	0.15	0.043	0.09	-	0.03
ThO_2	-	-	0.03	0.76	0.57	0.73	0.28	0.11	0.16	0.20	-	0.04	-	0.57	0.94	0.23	1.840	0.74	0.37	0.15
UO_2	0.06	-	-	1.42	1.02	1.28	1.24	0.73	0.54	0.65	0.07	0.03	0.063	0.37	0.43	0.47	0.186	0.39	0.09	0.31
La_2O_3	-	-	-	0.09	0.05	0.12	-	-	-	-	-	-	-	-	-	-	-	-	-	-
Ce_2O_3	-	-	-	0.43	0.25	0.40	-	-	-	-	-	-	-	0.06	-	-	-	-	-	-
Nd_2O_3	-	-	0.08	0.14	-	0.12	-	-	-	-	-	-	-	-	-	-	-	-	-	-
Sm_2O_3	-	-	-	-	-	-	-	-	-	-	-	-	-	-	0.07	-	0.126	-	-	-
Gd_2O_3	-	-	-	0.14	0.10	0.13	-	-	-	-	0.06	-	-	0.13	0.34	0.10	0.227	0.14	-	-
Dy_2O_3	-	-	-	0.15	0.10	0.22	0.09	-	0.09	-	0.07	0.10	0.090	0.13	-	0.10	0.313	0.18	0.15	0.17
Er_2O_3	0.06	0.05	-	0.38	0.30	0.43	0.24	0.17	0.24	0.19	0.10	0.13	0.129	0.31	0.62	0.25	0.681	0.26	0.23	0.22
Yb_2O_3	0.20	0.11	0.08	1.44	1.46	1.89	0.87	0.63	1.25	0.58	0.30	0.32	0.220	0.94	1.27	0.87	1.980	0.76	0.36	0.88
Y_2O_3	0.29	0.13	0.17	1.93	1.26	1.80	0.16	0.26	0.21	0.16	0.53	0.75	0.573	1.12	2.29	0.52	0.861	0.96	0.92	0.36
ZrO_2	65.86	66.80	66.46	54.49	54.42	53.65	53.31	59.60	57.43	56.49	66.63	66.46	66.280	61.98	57.79	62.39	58.660	61.01	60.78	64.28
HfO_2	1.43	1.26	1.27	2.42	4.56	3.47	7.61	2.84	5.79	5.93	0.95	0.83	0.955	1.48	1.26	1.39	2.250	1.78	5.03	1.75
Nb_2O_5	-	-	-	0.11	0.09	0.21	0.04	-	-	0.04	-	-	0.019	-	-	-	0.048	0.03	-	0.02
Ta_2O_5	-	-	-	0.07	0.11	0.13	0.10	0.06	0.04	0.13	0.03	0.01	0.021	0.04	0.02	-	0.028	-	0.08	-
P_2O_5	0.05	0.07	0.05	0.26	0.15	0.21	0.04	0.09	0.07	0.07	0.05	0.03	0.028	0.27	0.76	0.23	1.002	0.27	0.26	0.21
Total	100.7	101.0	101.2	96.73	97.31	98.01	96.28	97.26	99.13	98.41	101.6	101.9	101.08	99.92	98.52	98.91	100.21	98.78	101.38	100.79
Structural formula based on 16 oxygens																				
Si (apfu)	3.974	3.965	3.940	3.893	3.949	3.814	3.965	3.947	3.974	3.909	3.979	3.980	4.003	3.909	3.810	3.878	3.879	3.884	4.033	3.910
Al	0.001	0.002	0.002	0.112	0.053	0.109	0.064	0.058	0.061	0.109	0.000	0.002	0.001	0.019	0.091	0.031	0.001	0.012	0.000	0.004
P	0.006	0.007	0.005	0.028	0.016	0.023	0.005	0.010	0.007	0.007	0.005	0.003	0.003	0.028	0.082	0.024	0.107	0.029	0.027	0.022
Si-site	**3.981**	**3.974**	**3.947**	**4.033**	**4.018**	**3.946**	**4.034**	**4.015**	**4.042**	**4.025**	**3.984**	**3.985**	**4.007**	**3.956**	**3.983**	**3.933**	**3.987**	**3.925**	**4.060**	**3.936**
Zr	3.921	3.944	3.947	3.443	3.422	3.423	3.446	3.723	3.562	3.527	3.921	3.913	3.898	3.780	3.603	3.837	3.604	3.776	3.627	3.876
Hf	0.050	0.044	0.045	0.090	0.168	0.130	0.288	0.104	0.210	0.217	0.033	0.029	0.034	0.053	0.046	0.050	0.081	0.064	0.179	0.062
Th	0.000	0.000	0.001	0.023	0.017	0.022	0.009	0.003	0.005	0.006	0.000	0.001	0.001	0.016	0.027	0.007	0.053	0.021	0.011	0.004
U	0.002	0.000	0.000	0.041	0.029	0.037	0.037	0.021	0.015	0.018	0.002	0.001	0.002	0.010	0.012	0.013	0.005	0.011	0.002	0.009
Y	0.019	0.009	0.011	0.133	0.086	0.125	0.011	0.017	0.014	0.011	0.034	0.042	0.038	0.075	0.156	0.035	0.058	0.065	0.061	0.024
La	0.000	0.000	0.000	0.005	0.002	0.006	0.000	0.000	0.000	0.001	0.000	0.000	0.001	0.000	0.000	0.000	0.000	0.001	0.000	0.001
Ce	0.000	0.000	0.000	0.020	0.012	0.019	0.000	0.001	0.000	0.000	0.000	0.002	0.001	0.003	0.002	0.001	0.000	0.002	0.000	0.000
Nd	0.001	0.001	0.003	0.007	0.000	0.006	0.000	0.001	0.001	0.000	0.000	0.001	0.000	0.000	0.002	0.002	0.003	0.002	0.000	0.000
Sm	0.000	0.000	0.002	0.001	0.001	0.003	0.001	0.000	0.000	0.000	0.000	0.000	0.001	0.002	0.003	0.001	0.006	0.002	0.000	0.000
Gd	0.001	0.000	0.000	0.006	0.004	0.006	0.002	0.002	0.001	0.001	0.003	0.001	0.000	0.005	0.014	0.004	0.009	0.006	0.002	0.002
Dy	0.001	0.000	0.002	0.006	0.004	0.009	0.004	0.001	0.004	0.000	0.003	0.004	0.004	0.005	0.019	0.004	0.013	0.007	0.006	0.007
Er	0.002	0.002	0.001	0.015	0.012	0.018	0.010	0.007	0.010	0.008	0.004	0.005	0.005	0.012	0.025	0.010	0.027	0.011	0.009	0.009
Yb	0.008	0.004	0.003	0.057	0.057	0.075	0.035	0.024	0.048	0.023	0.011	0.012	0.008	0.036	0.050	0.033	0.076	0.030	0.014	0.033
Ti	0.008	0.007	0.009	0.018	0.033	0.033	0.056	0.019	0.037	0.039	0.007	0.007	0.006	0.008	0.012	0.009	0.022	0.012	0.035	0.010
Fe^{3+}	0.014	0.022	0.043	0.170	0.164	0.218	0.078	0.069	0.068	0.137	0.008	0.013	0.007	0.070	0.114	0.082	0.087	0.097	0.009	0.045
Mn	0.001	0.001	0.001	0.050	0.052	0.049	0.050	0.043	0.040	0.075	0.000	0.001	0.000	0.016	0.028	0.022	0.007	0.018	0.000	0.008
Mg	0.003	0.000	0.001	0.003	0.003	0.003	0.001	0.002	0.000	0.000	0.001	0.003	0.000	0.003	0.008	0.005	0.001	0.003	0.000	0.004
Ca	0.001	0.001	0.000	0.042	0.053	0.042	0.016	0.018	0.018	0.021	0.002	0.001	0.002	0.015	0.023	0.020	0.006	0.012	0.000	0.003
Nb	0.000	0.000	0.000	0.007	0.005	0.012	0.002	0.001	0.000	0.003	0.000	0.000	0.001	0.000	0.000	0.000	0.003	0.002	0.000	0.001
Ta	0.001	0.000	0.001	0.002	0.004	0.004	0.004	0.002	0.001	0.005	0.001	0.000	0.001	0.001	0.001	0.000	0.001	0.000	0.003	0.000
A-site	**4.033**	**4.035**	**4.070**	**4.139**	**4.128**	**4.240**	**4.050**	**4.058**	**4.034**	**4.092**	**4.030**	**4.036**	**4.010**	**4.110**	**4.145**	**4.135**	**4.062**	**4.142**	**3.958**	**4.098**
Zr/Hf	78.42	89.64	87.71	38.26	20.37	26.33	11.97	35.80	16.96	16.25	118.82	134.93	114.65	71.32	78.33	76.74	44.49	59.00	20.26	62.52

EMPA major oxides (in wt. %) and LA-ICPMS trace element compositions (in ppm); -: below detection limit

Table 5-2: REEs and trace element compositions for zircon types from the Desemborque and Mandira occurrences.

Occurrence	**Desemborque Pluton**										**Mandira Granites**								
Facies	Biotite syenogranite			Biotite syenogranite			Greisen				Riebeckite alkali feldspar granite								
Sample	**GUA-50C**			**GUA-53**			**GUA-08**				**MAN-13B**								
Point_ID	2	8	1b	3	12	13	4-r	5	7a	9c	1a-r	1a-c	1b-c	1b-r1	7-r1	7-r2	8-r1	8-r2	5
Type	Magmatic			Hydrothermal altered			Hydrothermal				Magmatic			Hydrothermal altered			Hydrothermal		
P (ppm)	452	614	198.6	2693	1833	1094	585	1081	4102	2264	170	193	1105	493	788	1078	652	662	908
Sc	229	217	230.11	387	276	211	375	244	296	332	223	228	2032	216	208	186	207	208	200
Ti	62.81	6.36	16.43	469	110	12.32	8.92	97.54	90.49	20.19	4.16	2.86	3.95	290	13.22	119	55.53	168	2701
Mn	171	920	17.33	3879	2499	3017	4092	4624	7878	6423	b.d.l	b.d.l	b.d.l	433	189	548	741	1134	1387
Rb	34.01	72.29	36.46	25.03	30.45	4.79	6.64	556	53.62	15.29	2.41	0.99	1	10	1.92	2.39	13.15	6.71	11
Sr	5.76	13.34	4.38	93.53	99.82	51.16	93.49	58.05	86.11	92.7	0.94	0.66	0.68	29	6.48	17.97	27.06	52.03	64
Y	4554	4808	2355.6	25231	28757	12130	2000	3928	10482	5247	3989	5102	5645	7788	5795	5737	2728	5060	10181
Zr	481201	485125	492676	481201	481201	438485	421606	428195	446554	446554	492454	492454	492306	481201	462619	462619	469504	469504	458844
Nb	320	211.78	227.26	1433	1361	467	151	210	216	169	37.03	15.99	16.55	82	113	168	88.23	193	179
Mo	3.77	3.82	8.36	5.19	3.69	3.72	4.17	5.64	3.87	4.52	4.2	4.86	5.21	4	3.38	5.25	4.49	3.97	5
Sn	7.94	3.54	3.2	80.2	23.37	8.96	27.56	68.75	26.1	21.59	b.d.l	b.d.l	1.28	44	14.73	27.23	15.93	55.18	98
Ba	6.39	18.59	2.8	152	369	44.86	23.54	24.19	59.36	44.37	b.d.l	b.d.l	b.d.l	9	20.35	57.68	54.16	61	119
La	8.01	9.83	2.08	116	152	68.02	16.13	20.52	74.58	34.67	1.08	0.65	2.43	14	4.66	13.09	25.54	24.11	30
Ce	52.03	69.51	26.1	1047	1143	1501	69.03	83.88	339	120	64.98	33.5	34.61	106	51.57	98.81	134	267	316
Pr	3.62	6.18	1.28	170	197	130.1	10.68	10.04	45.6	17.12	0.499	0.47	0.31	7	6.1	15.28	24.47	50.84	65
Nd	21.66	35.03	7.79	1071	1150	786	64.18	58.18	240	97.04	5.12	6.3	6.94	44	41.74	78.82	124	352	453
Sm	20.79	19.46	10.5	1195	999	500	70.07	57.19	164	83.24	11.53	17.04	19.94	57	48.23	65.45	55.2	205	361
Eu	b.d.l	0.181	b.d.l	3.4	3.04	1.21	b.d.l	1.97	0.79	b.d.l	0.46	0.63	0.54	2	1.05	0.89	0.87	2.67	7
Gd	77.05	59.73	38.46	2102	1888	706	131.71	128	363	192	83.87	106	111	209	154	153.5	76.81	256	533
Tb	33.92	29.24	17.18	615	538	178	49.71	49.65	144	84.75	34.04	44.27	48.51	90	84.14	91.96	39.24	92.29	198
Dy	431	386	235.08	4847	4401	1506	595	667	1735	1045	409	525	575	1104	1108	1140	633	1086	2086
Ho	163	164	87.55	1231	1210	459.2	214	236	632	401	150	198	211	396	406	457	288	384	664
Er	744	781	396.96	4203	4293	1746.2	1169	1265	3379	2214	635	836	894	1603	1745	2108	1606	1879	2748
Tm	175	182	86.63	783	836	362	342	314	833	587	118	152	160	318	351	462	420	434	550
Yb	1604	1735	763.1	6614	6891	3309	3974	3491	8411	6298	970	1215	1264	2524	2746	4020	3799	3596	4361
Lu	295	297	136.21	1048	1049	478.5	666	666	1549	1152	139	184	193	376	370	530	521	488	565
Hf	12688	20047	12057	18736	19085	13861	48698	20622	23326	22855	8263	8256	8314	8824	36013	32805	16056	16738	12656
Ta	7.81	78.37	11.15	132	120	59.01	297	99.74	107	200	6.68	3.57	3.21	21	9.45	10.02	9.8	9.51	11
^{206}Pb	175	702	83.21	3012	4983	1168	3620	1007	2351	2792	127	97.41	102	202	339	637	634	678	660
^{207}Pb	23.67	90.87	9.43	2020	3994	623	266	116	180	172	8.96	6.25	7.06	33	69.3	252	179	206	223
^{208}Pb	31.78	132	13.38	2327.2	4500	741	1354	233	823	1054	14.21	11.15	10.17	43	106	281	250	312	275
Th	859	1746	294.72	10262	11107	4593	1907	2917	32417	24165	309	216	221	833	1213	2100	3958	2711	4468
U	595	3112	241.03	8143	6265	4381	8361	5503	11713	13184	371	297	293	661	1095	2168	2506	3134	4096
REEs	3629	3775	1809	28077	24751	11730	7371	7050	17910	12326	2622	3319	3521	6851	7117	9235	7747	9116	12937
LREEs	106	140	48	3522	3641	2985	230	230	863	352	83	58	64	229	152	271	363	900	1226
HREEs	3523	3634	1761	24551	21106	8744	7141	6818	17046	11974	2538	3260	3456	6620	6964	8963	7383	8214	11704
$(Sm/La)_N$	4.2	3.2	8.1	16.9	10.5	11.8	7.0	4.5	3.5	3.8	17.1	42.0	13.1	6.3	16.6	8.0	3.5	13.6	19.1
Ce/Ce*	2.3	2.2	3.9	1.6	1.6	3.9	1.3	1.4	1.4	1.2	21.4	14.6	9.6	2.6	2.3	1.7	1.3	1.8	1.7
Eu/Eu*	b.d.l	0.02	b.d.l	0.01	0.01	0.01	b.d.l	0.07	0.01	b.d.l	0.05	0.05	0.04	0.05	0.04	0.03	0.04	0.04	0.05

Trace element LA-ICP-MS compositions (ppm); b.d.l.: below detection limit

Table 5-3: Major compositions and structural formula for monazite and xenotime from the Desemborque pluton.

Occurrence	**Desemborque Pluton**														
Facies	Biotite granite			Greisen			Biotite granite			Greisen					
Sample	**GUA-50C1**			**GUA-08**			**GUA-50C**			**GUA-08**					
Point_ID	c1b	1e-c	1c-r1	11-c	11-r4	11-r5	2-c	5-c	5b-i	2-c	2-r4	10b-c2	6-i2	6-r1	6-i
Mineral	Monazite-1			Monazite-1			Monazite-2			Xenotime					
SiO_2 (wt%)	0.75	0.93	0.73	0.59	1.48	0.70	0.48	0.48	0.24	0.84	1.32	0.64	0.12	0.17	0.98
$Al2O_3$	0.02	0.01	0.02	0.06	0.02	0.02	0.04	0.24	0.04	-	0.18	-	-	-	-
CaO	0.07	0.08	0.16	1.21	0.09	0.21	0.33	0.23	0.18	0.01	0.01	0.06	-	0.02	0.01
FeO	0.47	0.21	0.12	0.05	0.16	0.06	0.35	0.89	0.41	0.20	0.33	0.03	0.12	0.26	0.12
La_2O_3	17.04	13.47	11.79	9.47	10.21	12.48	10.91	12.05	10.73	na	na	na	na	na	na
Ce_2O_3	34.88	32.51	30.52	30.86	29.39	33.84	30.25	31.58	30.16	0.06	0.04	-	0.06	0.08	0.02
Pr_2O_3	3.40	3.63	3.71	3.85	3.84	3.84	3.90	3.69	3.75	0.06	-	-	-	0.05	-
Nd_2O_3	9.82	12.19	13.46	12.49	14.14	11.52	14.31	12.07	13.36	0.38	0.33	0.08	0.35	0.38	0.20
Sm_2O_3	1.23	2.09	2.82	2.33	3.46	1.94	2.90	2.67	3.02	0.68	0.63	0.47	0.64	0.59	0.63
Gd_2O_3	0.52	1.14	1.50	0.61	1.51	0.91	1.67	1.70	2.05	2.26	2.00	2.11	1.92	1.80	2.30
Tb_2O_3	na	na	na	na	na	na	na	na	na	0.74	0.62	0.80	0.63	0.54	0.84
Dy_2O_3	0.33	0.46	0.57	-	0.61	0.35	0.55	0.54	1.03	4.67	3.99	5.95	4.23	3.77	5.78
Ho_2O_3	na	na	na	na	na	na	na	na	na	1.15	0.95	1.43	0.96	0.95	1.34
Er_2O_3	na	na	na	na	na	na	na	na	na	3.91	3.44	5.34	3.52	3.41	4.81
Yb_2O_3	-	-	-	-	-	-	-	-	-	4.15	3.93	5.91	4.62	4.36	5.70
Lu_2O_3	na	na	na	na	na	na	na	na	na	0.99	0.89	1.23	1.08	0.95	1.13
P_2O_5	28.97	28.44	28.53	28.60	27.39	28.57	29.16	29.03	29.01	33.65	36.19	33.60	35.31	35.82	33.41
ThO_2	2.85	3.16	3.08	8.04	6.26	4.47	1.74	1.78	1.15	0.32	0.20	38.75	0.16	0.16	1.21
UO_2	0.10	0.11	0.12	0.16	0.10	0.05	0.12	0.10	0.08	0.02	0.01	0.75	-	0.01	0.10
Y_2O_3	0.15	0.84	1.12	0.17	0.45	0.13	1.39	1.22	1.83	41.55	44.35	0.07	43.71	45.21	39.00
PbO	0.08	0.10	0.11	0.22	0.16	0.12	0.07	0.06	0.05	0.01	-	0.03	-	-	0.04
Total	100.9	99.35	98.31	99.27	99.25	99.44	98.13	98.29	97.05	95.65	99.46	97.23	97.47	98.52	97.65
Structural formula based on 16 oxygens															
Si (apfu)	0.119	0.148	0.115	0.110	0.239	0.112	0.076	0.076	0.053	0.079	0.078	0.087	0.017	0.022	0.066
P	3.880	3.848	3.877	3.878	3.767	3.876	3.916	3.933	3.937	3.927	3.957	3.937	3.990	4.002	3.930
P-site	**3.999**	**3.996**	**3.992**	**3.988**	**4.005**	**3.988**	**3.992**	**4.009**	**3.990**	**4.006**	**4.035**	**4.024**	**4.006**	**4.024**	**3.996**
Th	0.103	0.115	0.111	0.292	0.230	0.163	0.063	0.064	0.041	0.010	0.006	0.023	0.005	0.005	0.038
U	0.002	0.003	0.003	0.003	0.002	0.000	0.004	0.003	0.002	0.000	0.000	0.002	0.000	0.000	0.003
Al	0.004	0.002	0.004	0.012	0.004	0.003	0.007	0.044	0.007	0.000	0.029	0.000	0.000	0.000	0.000
Fe^{3+}	0.032	0.026	0.014	0.007	0.019	0.008	0.042	0.036	0.049	0.021	0.022	0.003	0.012	0.026	0.012
Y	0.013	0.071	0.094	0.015	0.038	0.011	0.117	0.102	0.153	3.111	3.158	2.898	3.168	3.189	2.931
La	0.977	0.791	0.708	0.599	0.607	0.738	0.654	0.712	0.650	na	na	na	na	na	na
Ce	1.991	1.895	1.833	1.832	1.735	1.985	1.785	1.835	1.812	0.003	0.002	0.000	0.003	0.004	0.001
Pr	0.196	0.211	0.215	0.224	0.226	0.224	0.225	0.212	0.214	0.003	0.001	0.000	0.001	0.002	0.001
Nd	0.555	0.693	0.747	0.723	0.814	0.659	0.808	0.691	0.748	0.019	0.015	0.004	0.017	0.018	0.010
Sm	0.067	0.115	0.154	0.128	0.192	0.107	0.158	0.146	0.163	0.033	0.029	0.022	0.030	0.027	0.030
Gd	0.027	0.060	0.079	0.032	0.081	0.048	0.088	0.089	0.107	0.104	0.092	0.096	0.089	0.081	0.105
Tb	na	na	na	na	na	na	na	na	na	0.034	0.027	0.036	0.028	0.023	0.038
Dy	0.017	0.023	0.029	0.008	0.031	0.018	0.028	0.027	0.052	0.209	0.174	0.263	0.186	0.165	0.256
Ho	na	na	na	na	na	na	na	na	na	0.051	0.040	0.062	0.041	0.040	0.059
Er	na	na	na	na	na	na	na	na	na	0.170	0.147	0.230	0.152	0.146	0.208
Tm	na	na	na	na	na	na	na	na	na	0.027	0.023	0.037	0.026	0.025	0.035
Yb	0.013	0.000	0.000	0.019	0.000	0.012	0.000	0.000	0.000	0.175	0.162	0.247	0.192	0.175	0.239
Lu	na	na	na	na	na	na	na	na	na	0.042	0.036	0.051	0.043	0.038	0.047
Ca	0.012	0.014	0.028	0.087	0.015	0.036	0.056	0.039	0.031	0.002	0.002	0.008	0.001	0.003	0.001
Pb	0.003	0.004	0.004	0.009	0.007	0.005	0.002	0.002	0.001	0.000	0.000	0.001	0.000	0.000	0.001
REE-site	**4.011**	**4.023**	**4.024**	**3.991**	**4.001**	**4.017**	**4.036**	**4.002**	**4.031**	**4.013**	**3.966**	**3.983**	**3.994**	**3.966**	**4.017**

EMPA major oxides (in wt. %); -: below detection limit; na: not analyzed

Table 5-4: Major compositions for fluorides from the Desemborque and Mandira plutons.

Occurrence	**Desemborque Pluton**						**Mandira Granites**								
Facies	Biotite syenogranite			Greisen			Riebeckite alkali feldspar granite								
Sample	**GUA-50C1**			**GUA-08**			**MAN-13A**			**MAN-13B**			**MAN-13B**		
Point_ID	3a-i	3a-r1	3a-r2	2a	3	3b	1	11c	11c-i	1d	2	8	1c	2c	2c-r1
Mineral	Fluorite			Fluorite			Fluorite			Fluocerite			Gagarinite		
Si (wt%)	0.00	0.03	0.00	0.05	0.03	0.06	0.02	0.04	0.05	0.07	0.05	0.03	0.19	0.07	0.07
Al	0.01	0.01	0.00	0.01	0.01	0.00	0.00	0.01	0.00	0.00	0.03	0.01	0.00	0.00	0.00
Ca	44.43	43.13	45.16	44.44	45.45	44.80	51.25	50.05	44.81	0.07	0.19	0.05	12.15	12.43	12.37
Na	0.16	0.15	0.19	0.18	0.18	0.25	0.02	0.13	0.97	0.11	0.07	0.08	5.80	4.53	4.55
Sr	na	na	na	na	na	na	na	na	na	0.06	0.00	0.00	na	na	na
Y	2.10	2.82	2.85	3.75	3.21	2.98	0.15	0.35	3.67	0.03	0.17	0.09	19.72	22.86	22.81
La	na	na	na	na	na	na	na	na	na	15.55	13.90	13.03	na	na	na
Ce	1.22	1.42	1.43	1.16	0.90	0.87	0.04	0.03	0.68	36.08	32.41	34.78	1.92	0.84	0.69
Nd	0.66	0.64	0.69	0.65	0.55	0.61	0.01	0.03	0.17	13.54	3.95	17.38	7.03	4.16	4.30
Pr	0.22	0.34	0.09	0.27	0.13	0.18	0.00	0.15	0.01	4.29	18.28	4.53	1.01	0.47	0.42
Sm	0.29	0.26	0.17	0.14	0.22	0.27	0.05	0.00	0.07	1.32	2.46	2.18	2.95	2.79	3.14
Gd	0.27	0.72	0.42	0.53	0.21	0.47	0.13	0.00	0.09	0.05	0.29	0.66	3.78	4.42	4.65
Th	0.00	0.14	0.20	0.10	0.04	0.02	0.00	0.00	0.00	0.60	1.21	0.13	0.00	0.09	0.03
Tb	0.13	0.07	0.01	0.00	0.07	0.11	0.00	0.00	0.09	na	na	na	0.63	0.60	0.65
Dy	0.43	0.54	0.54	0.30	0.28	0.51	0.00	0.07	0.46	0.14	0.20	0.00	3.98	4.67	5.08
Er	0.33	0.22	0.27	0.21	0.37	0.40	0.00	0.09	0.38	na	na	na	1.60	2.01	2.23
Yb	0.37	0.28	0.29	0.37	0.19	0.42	0.12	0.00	0.42	0.20	0.31	0.09	0.87	0.87	0.80
Ho	0.04	0.25	0.23	0.00	0.26	0.00	0.00	0.14	0.22	na	na	na	0.62	0.55	0.67
Lu	0.02	0.00	0.00	0.20	0.00	0.00	0.02	0.00	0.29	na	na	na	0.52	0.49	0.22
F	43.38	42.89	42.67	43.64	43.08	44.24	46.70	46.97	45.75	29.12	28.19	26.79	35.93	36.01	35.39
Total	94.05	93.90	95.22	96.01	95.17	96.19	98.50	98.05	98.14	101.21	101.71	99.82	98.71	97.87	98.06
REE	3.97	4.87	4.34	3.94	3.22	3.86	0.37	0.51	2.88	71.76	73.01	72.78	24.91	21.96	22.87
Y+REE	6.07	7.69	7.19	7.69	6.43	6.84	0.52	0.86	6.55	71.79	73.17	72.87	44.63	44.82	45.68

EMPA major elements (in wt. %); -: below detection limit; na: not analyzed

6. FINAL REMARKS

This thesis represents the application of both petrographic and geochemical analytical methods to detail texturally and quantitatively characterization of primary and secondary HFSE- and REE-rich mafic silicate and accessory minerals in A-type granitic rocks from the Graciosa Province, SE-Brazil. The studied rocks are peralkaline and syenogranites as well as albitized granites and greisens from the Mandira Granite Massif and the Desemborque and Papanduva Plutons.

The petrographic analysis included an initial step for description of textural/microstructures characteristics, paragenetic relationships and mineral crystallization sequences, following the detailed identification of zoning patterns, secondary internal alterations and replacement microtextures by back-scattered electron images (BSE) using an EPMA microprobe analyzer. The quantitative geochemical analyses involve major and minor as well as trace element compositions obtained with EMPA and LA-ICP-MS techniques: the results allowed the calculation of mineral formulae, normalization of trace and REE element distribution, and REE partition controls of mineral structure in the case of amphiboles and astrophyllite minerals. Additionally, whole-rock geochemical analysis for representative samples were obtained to determination of chemical characteristics of the studied granites.

The integration of all results supports the broader subdivision of both petrographic alkaline and aluminous associations within rocks of the Graciosa Province and offer new insights into the crystallization conditions, mineral formation and microstructural alterations during the late- to post-magmatic evolutionary processes related to hydrothermal alteration processes affected the studied rocks. The following conclusions can be drawn:

1) Amphiboles in the Mandira Massif crystallized in both magmatic and late to post-magmatic stages of crystallization. Compositions vary widely from calcic to sodic-calcic and sodic groups with relatively high abundances of LILE and HFSEs and significant high REE concentrations in the calcic varieties following by about 1 or 2 low concentrations in the sodic-calcic and sodic varieties.

2) Amphibole REE partitions indicate strong preference of the LREEs for calcic amphiboles, contrary to the significant HREE-enrichment of sodic-calcic and sodic-amphiboles.

3) Biotite in the Mandira Massif crystallized as late- to post-magmatic phase in peralkaline granites while in the syenogranites biotite is a predominant primary phase. All biotite varieties from the Mandira unit are iron-rich and classify as annite. A distinct variety was found in the albitized granites within the massif and was classify as annite-siderophyllite of hydrothermal origin.

4) Chlorite and stilpnomelane occur always as secondary minerals usually replacing primary minerals in the Mandira Massif. Chlorite is predominant in syenogranites and greisens while stilpnomelane is found in both peralkaline and syenogranites. Compositions of these mineral reflect the Al-rich and Fe-rich character of the hosting rocks, respectively.

5) Granites from the Mandira Massif crystallized at relatively low to moderate f_{O2} conditions (around $-1 \leq \Delta QFM \leq 0$), close the limits between the granite rocks from the ilmenite and the magnetite series, and these conditions gradually increase with magma evolution pointing to high oxidizing conditions, up to above the MH buffer and suggesting crystallization conditions far more oxidizing from syenogranites to evolved peralkaline granites. The associated temperatures and pressures of emplacement ranges 720-750 (±35) °C and 130-170 (±150) MPa respectively, compatible with shallow (1-2 km) emplacement levels and were extended for the whole massif. After emplacement, hydrothermal alterations affected these granites are related to post-magmatic fluids of low temperatures in part constrained by chlorite-thermometry which point to hydrothermal temperatures varies from 250°C and 272°C.

6) Astrophyllite is a typical accessory mineral in the Mandira and Papanduva occurrences from the province. Textural and chemical compositions revealed three main generations one late-magmatic (Ast-1) characterized by relatively higher Zr and Nb contents, two post-magmatic (Ast-2a and Ast-2b), both with higher Ti abundance. Trace element compositions indicated, in general, a relative enrichment in LILEs, HFSEs and LREEs relative to the bulk host rocks, except for Ast-2b crystals in the Papanduva Pluton with distinctively lower HFSEs and REEs contents.

7) Chemical asttrophyllite parameters as Zr/(Zr+Ti) and Mn(Mn+Fe) can be used to trace magmatic-hydrothermal crystallization environments, as well as to qualitatively monitor their *redox* conditions.

8) Astrophyllite REE partitions in late-magmatic generations defines a stronger compatibility of the HFSEs and REEs, particularly in the Na-richest astrophyllite crystals from the Mandira granites.

9) The precipitation of the post-magmatic Ast-2a and Ast-2b crystals is related to disequilibrium processes and substitution reactions involving early-precipitated sodic amphiboles and clinopyroxenes, and relatively K^{+}- and Ti^{4+}-rich hydrothermal fluids.

10) Columbite is a hydrothermal accessory mineral occurring in both syenogranites and greisens rocks from the Desemborque Pluton. Microtextures and chemical characteristics revealed to columbite generations formed in different hydrothermal stages of crystallization. The columbite-1 with two-substages: an early Nb-rich crystal cores surrounding by Ta-rich rims in a later hydrothermal stage of crystallization, while the interstitial patchy Mn-rich columbite-2 generation precipitate later in replacement textures with cassiterite and secondary REE-fluorides suggesting that its formation is related to fluid-induced hydrothermal alterations.

11) Columbite occurrences are characterized by a relatively enrichment of HREEs over the LREEs as well as systematic increase of U, Zr, Hf and W from primary to secondary generations.

12) Magmatic zircon in syenogranites from the Desemborque pluton are strongly affected by late to post-magmatic fluids leading the internal structural and chemical transformations defined by metamictic textures and significant increase of Hf, REEs, Y, Nb, Ta, Th, U, Ti, P, Ca, Al and Fe along the altered zircon domains. In contrast, fluid-induced alterations in hydrothermal zircon from the greisens promotes in the development of spongy-textures characterized by high abundances of Hf, LREEs, Th and U.

13) During zircon/fluid interaction, REE were remobilized by the post-magmatic fluids promoting the precipitation of secondary monazite and xenotime especially at contact of

the zircon margins in both syenogranites and greisens from the Desemborque Pluton. Similarly, the destabilization of fluorite crystals by fluid-induced alterations also favors the post-magmatic formation of (HREE+Y)-fluorides within the Desemborque syenogranites.

14) Hydrothermal monazite gave chemical average age of 584 ± 3 Ma (CHIME method) which is the first documented evidenced associated to hydrothermal activity in rocks from the Graciosa Province.

15) Magmatic, late-stage and hydrothermal zircon in peralkaline granites from the Mandira Massif suffered post-magmatic alterations resulting in the partially dissolution of the magmatic cores and the formation of numerous porous (spongy textures) in the late-stage zircons. The structural transformations were linked to the progressive increase Hf, REEs, Nb, Ta, Th, U, Ti, and P, from primary to hydrothermal zircon.

16) The association of hydrothermal zircon with fluorite among Mandira granites suggest that F-rich fluids would be involved in REE mobilization leading the formation of secondary fluocerite-(Ce) and gagarinite-(Y) fluorides, which are firstly described in this work.

17) Microstructures of zircons from the both Desemborque and Mandira occurrences revealed intensive late- to post-magmatic alterations during the late- to hydrothermal evolution ascribe to the circulation of post-magmatic F- and HFSE-rich fluids.

18) The structural transformations of zircons were grouped in at least four-stage of hydrothermal alterations which are related to the significant enrichments of especially Hf, REE, Y, Th and U from primary to hydrothermal altered zircons.

19) Despite the significant differences of compositions between Desemborque and Mandira zircons the chemical evolution trends of the distinct zircon types are equivalent for the both occurrences indicating that fluid-induced alterations were responsible for the progressive fractionation of Hf and the incompatible non-formula elements during evolution.

7. REFERENCES

Abdalla, H.M., Helba, H.., and Mohamed, F.., 1998, Chemistry of columbite-tantalite minerals in rare metal granitoids, Easterns Desert, Egypt: Mineralogical Magazine, v. 62, p. 821–836.

Abdel-Fattah, M., and Abdel-Rahman, 1992, Mineral chemistry and paragenesis of astrophyllite from Egypt:

Abdel-rahman, A.F.M., and Abder-Rahman, A.F.M., 1994, Nature of Biotites from Alkaline, Calc-alkaline, and Peraluminous Magmas: Journal of Petrology, v. 35, p. 525–541, doi:10.1093/petrology/35.2.525.

Alfonso, P. et al., 2018, Textural and mineral-chemistry constraints on columbite-group minerals in the Penouta deposit: evidence from magmatic and fluid-related processes: Mineralogical Magazine, v. 82, p. S199–S222, doi:10.1180/minmag.2017.081.107.

Andersen, T., Elburg, M., and Erambert, M., 2017, The miaskitic-to-agpaitic transition in peralkaline nepheline syenite (white foyaite) from the Pilanesberg Complex, South Africa: Chemical Geology, v. 455, p. 166–181, doi:10.1016/j.chemgeo.2016.08.020.

Andersen, T., Erambert, M., Larsen, A.O., and Selbekk, R.S., 2014, Petrology of nepheline syenite pegmatites in the Oslo Rift, Norway: Zr and Ti mineral assemblages in miaskitic and agpaitic pegmatites in the Larvik Plutonic Complex: Mineralogia, v. 44, p. 61–98, doi:10.2478/mipo-2013-0007.

Anderson, J.L., Barth, A.P., Wooden, J.L., and Mazdab, F., 2008, Thermometers and Thermobarometers in Granitic Systems: v. 69, p. 121–142, doi:10.2138/rmg.2008.69.4.

Anderson, J.L., and Smith, D.R., 1995, The effects of temperature and fO2 on the Al-in-hornblende barometer: American Mineralogist, v. 80, p. 549–559, doi:10.1016/0031-9201(95)03018-R.

Ayati, F., Yavuz, F., Noghreyan, M., Haroni, H.A., and Yavuz, R., 2008, Chemical characteristics and composition of hydrothermal biotite from the Dalli porphyry copper prospect, Arak, central province of Iran: Mineralogy and Petrology, v. 94, p. 107–122, doi:10.1007/s00710-008-0006-5.

Badanina, E. V., Sitnikova, M.A., Gordienko, V. V., Melcher, F., Gäbler, H.E., Lodziak, J., and Syritso, L.F., 2015, Mineral chemistry of columbite-tantalite from spodumene pegmatites of Kolmozero, Kola Peninsula (Russia): Ore Geology Reviews, v. 64, p. 720–735,

doi:10.1016/j.oregeorev.2014.05.009.

Ballouard, C., Branquet, Y., Tartèse, R., Poujol, M., Boulvais, P., and Vigneresse, J., 2016a, Nb-Ta fractionation in peraluminous granites: A marker of the magmatic-hydrothermal transition: REPLY: Geology, v. 44, p. e395–e395, doi:10.1130/G38169Y.1.

Ballouard, C., Poujol, M., Boulvais, P., Branquet, Y., Tartèse, R., and Vigneresse, J.L., 2016b, Nb-Ta fractionation in peraluminous granites: A marker of the magmatic-hydrothermal transition: Geology, v. 44, doi:10.1130/G37475.1.

Basei, M.A.S., Nutman, A., Siga, O., Passarelli, C.R., and Drukas, C.O., 2009, Chapter 7.2 The Evolution and Tectonic Setting of the Luis Alves Microplate of Southeastern Brazil: An Exotic Terrane during the Assembly of Western Gondwana: Developments in Precambrian Geology, v. 16, p. 273–291, doi:10.1016/S0166-2635(09)01620-X.

Bastos Neto, A.C., Pereira, V.P., Ronchi, L.H., De Lima, E.F., and Frantz, J.C., 2009, The world-class Sn, Nb, Ta, F (Y, REE, Li) Deposit and the massive cryolite associated with the albite-enriched facies of the madeira a-type granite, Pitinga Mining District, Amazonas State, Brazil: Canadian Mineralogist, v. 47, p. 1329–1357, doi:10.3749/canmin.47.6.1329.

Baumgartner, R., Romer, R.L., Moritz, R., Sallet, R., and Chiaradia, M., 2006, Columbite–Tantalite-Bearing Granitic Pegmatites from the Seridó Belt, Northeastern Brazil: Genetic constrains from U–Pb dating and Pb isotopes: The Canadian Mineralogist, v. 44, p. 69–86.

Belkasmi, M., Cuney, M., Pollard, P.J., and Bastoul, A., 2002, Chemistry of the Ta-Nb-Sn-W oxide minerals from the Yichun rare metal granite (SE China): genetic implications and comparison with Moroccan and French Hercynian examples: Mineralogical Magazine, v. 64, p. 507–523, doi:10.1180/002646100549391.

Belkasmi, M., Cuney, M., Pollard, P.J., and Bastoul, A., 2000, Chemistry of the Ta-Nb-Sn-W oxide minerals from the Yichun rare metal granite (SE China): genetic implications and comparison with Moroccan and French Hercynian examples: Mineralogical Magazine, v. 64, p. 507–523, doi:10.1180/002646100549391.

Bell, E.A., Boehnke, P., Barboni, M., and Harrison, T.M., 2019, Tracking chemical alteration in magmatic zircon using rare earth element abundances: Chemical Geology, v. 510, p. 56–71, doi:10.1016/j.chemgeo.2019.02.027.

Bell, E.A., Boehnke, P., and Harrison, T.M., 2016, Recovering the primary geochemistry of

Jack Hills zircons through quantitative estimates of chemical alteration: Geochimica et Cosmochimica Acta, v. 191, p. 187–202, doi:10.1016/j.gca.2016.07.016.

Belov, N. V, 1963, Essays on structural mineralogy. XIV. 97. Ba, Fe-titanosilicate-bafertisite. 98. Anion role of Ti and Zr. Titanates, zirconates, titanosilicates, zirconosilicates: Mineralogicheskii Sbornik L'vovskogo Geologicheskogo Obshchestva, v. 17, p. 22–29.

Belov, N. V, 1976, Essays on structural mineralogy: Nedra, Moscow, p. 8–9.

Beurlen, H., Soares, D.R., Thomas, R., Prado-Borges, L.E., and De Castro, C., 2005, Mineral chemistry of tantalate species new in the Borborema Pegmatitic Province, Northeast Brazil: Anais da Academia Brasileira de Ciencias, v. 77, p. 169–182.

Birkett, T.C., Trzcienski, W.E., and Stirling, J.A.R., 1996, Occurrence and compositions of some ti-bearing minerals in the Strange Lake intrusive complex, Quebec-Labrador boundary: Canadian Mineralogist, v. 34, p. 779–801.

Blundy, J., and Wood, B., 1994, Prediction of crystals-melt partition coefficients from elastic moduli: Letters to Nature, v. 372, p. 452–454.

Bonin, B., 2007, A-type granites and related rocks: Evolution of a concept, problems and prospects: Lithos, v. 97, p. 1–29, doi:10.1016/j.lithos.2006.12.007.

Bottazzi, P., Tiepolo, M., Vannucci, R., Zanetti, A., Brumm, R., Foley, S.F., and Oberti, R., 1999, Distinct site preferences for heavy and light REE in amphibole and the prediction of (Amph/L)D(REE): Contributions to Mineralogy and Petrology, v. 137, p. 36–45, doi:10.1007/s004100050580.

Breiter, K., 2016, Monazite and zircon as major carriers of Th, U, and Y in peraluminous granites: examples from the Bohemian Massif: Mineralogy and Petrology, v. 110, p. 767–785, doi:10.1007/s00710-016-0448-0.

Breiter, K., Förster, H.J., and Škoda, R., 2006, Extreme P-, Bi-, Nb-, Sc-, U- and F-rich zircon from fractionated perphosphorous granites: The peraluminous Podlesí granite system, Czech Republic: Lithos, v. 88, p. 15–34, doi:10.1016/j.lithos.2005.08.011.

Breiter, K., Lamarão, C.N., Borges, R.M.K., and Dall'Agnol, R., 2014a, Chemical characteristics of zircon from A-type granites and comparison to zircon of S-type granites: Lithos, v. 192–195, p. 208–225, doi:10.1016/j.lithos.2014.02.004.

Breiter, K., Lamarão, C.N., Borges, R.M.K., and Dall'Agnol, R., 2014b, Chemical

characteristics of zircon from A-type granites and comparison to zircon of S-type granites: Lithos, v. 192–195, p. 208–225, doi:10.1016/j.lithos.2014.02.004.

Breiter, K., and Škoda, R., 2012, Vertical zonality of fractionated granite plutons reflected in zircon chemistry: The Cínovec A-type versus the Beauvoir S-type suite: Geologica Carpathica, v. 63, p. 383–398, doi:10.2478/v10096-012-0030-6.

Breiter, K., Škoda, R., and Uher, P., 2007, Nb-Ta-Ti-W-Sn-oxide minerals as indicators of a peraluminous P- and F-rich granitic system evolution: Podlesí, Czech Republic: Mineralogy and Petrology, v. 91, p. 225–248, doi:10.1007/s00710-007-0197-1.

Burke, E.A.J., 2008, Tidying up mineral names: An IMA-CNMNC scheme for suffixes, hyphens and diacritical marks: Mineralogical Record, v. 39, p. 131–135.

Cámara, F., Sokolova, E., Abdu, Y., and Hawthorne, F.C., 2010, The crystal structures of niobophyllite, kupletskite-(cs) and Sn-rich astrophyllite: Revisions to the crystal chemistry of the astrophyllite-group minerals: Canadian Mineralogist, v. 48, p. 1–16, doi:10.3749/canmin.48.1.1.

Campos, B.C.S., Vilalva, F.C.J., Nascimento, M.A.L. do, and Galindo, A.C., 2016, Crystallization conditions of porphyritic high-K calc-alkaline granitoids in the extreme northeastern Borborema Province, NE Brazil, And geodynamic implications: Journal of South American Earth Sciences, v. 70, p. 224–236, doi:10.1016/j.jsames.2016.05.010.

Caritat, P., Hutcheon, I., and Walshe, J.L., 1993, Chlorite geothermometry: A review: Clays and Clay Minerals, v. 41, p. 219–239, doi:10.1346/CCMN.1993.0410210.

Caritat, P.D.E., Hutcheon, I.A.N., and Walshe, J.L., 1993, Chlorite geothermometry: a review: Clays and Clay Minerals, v. 41, p. 219–239.

Cathelineau, M., 1988, Cation site occupancy in chlorites and illites as a function of temperature: Clay Minerals, v. 23, p. 471–485, doi:10.1180/claymin.1988.023.4.13.

Cathelineau, M., and Nieva, D., 1985, A chlorite solid solution geothermometer the Los Azufres (Mexico) geothermal system: Contributions to Mineralogy and Petrology, v. 91, p. 235–244, doi:10.1007/BF00413350.

Černý, P., and Ercit, T.S., 1989, Mineralogy of Niobium and Tantalum: Crystal Chemical Relationships, Paragenetic Aspects and Their Economic Implications, *in* Möller, P., Černý, P., and Saupé, F. eds., Lanthanides, Tantalum and Niobium, Berlin, Heidelberg, Springer Berlin Heidelberg, p. 27–79.

Černý, P., and Ercit, T.S., 1985, Some recent advances in the mineralogy and geochemistry of Nb and Ta in rare-element granitic pegmatites: Bulletin de Minéralogie, v. 108, p. 499–532, doi:10.3406/bulmi.1985.7846.

Černý, P., Ercit, T.S., Wise, M.A., Chapman, R., and Buck, H.M., 1998, Compositional, structural and phase relationships in titanian ixiolite and titanian columbite - Tantalite: Canadian Mineralogist, v. 36, p. 547–561.

Cerny, P., Scott Ercit, T., and Wise, M.A., 1992, The Tantalite-Tapiolite Gap: Natural Assemblages Versus Experimental Data: Canadian Mineralogist, v. 30, p. 587–596.

Cerny, P., and Turnock, A.., 1971, Niobium-Tantalum minerals from granitic pegmatites at Greer Lake, Southeastern Manitoba: The Canadian Mineralogist, v. 10, p. 755–772.

Che, X.-D., Wang, R.-C., Wu, F.-Y., Zhu, Z.-Y., Zhang, W.-L., Hu, H., Xie, L., Lu, J.-J., and Zhang, D., 2019, Episodic Nb-Ta mineralisation in South China: Constraints from in situ LA-ICPM-MS columbite-tantalite U-Pb dating: Ore Geology Reviews, v. 105, p. 71.85, doi:.1037//0033-2909.I26.1.78.

Chevychelov, V.Y., Zaraisky, G.P., Borisovskii, S.E., and Borkov, D.A., 2005, Effect of melt composition and temperature on the partitioning of Ta, Nb, Mn, and F between granitic (alkaline) melt and fluorine-bearing aqueous fluid: Fractionation of Ta and Nb and conditions of ore formation in rare-metal granites: Petrology, v. 13, p. 305–321.

Ciesielczuk, J., 2012, Chlorite of hydrothermal origin in the Strzelin and Borów granites (Fore-Sudetic Block, Poland): Geological Quarterly, v. 56, p. 333–344, doi:10.7306/gq.1025.

Claiborne, L.L., Miller, C.F., and Wooden, J.L., 2010, Trace element composition of igneous zircon: A thermal and compositional record of the accumulation and evolution of a large silicic batholith, Spirit Mountain, Nevada: Contributions to Mineralogy and Petrology, v. 160, p. 511–531, doi:10.1007/s00410-010-0491-5.

Clowe, C.A., Popp, R.K., and Fritz, S.J., 1988, Experimental investigation of the effect of oxygen fugacity on ferric-ferrous ratios and unit-cell parameters of four natural clinoamphiboles: American Mineralogist, v. 73, p. 487, d:/TEMP/AmMin%5CnTOC1/AmMin%5CnTOC1(7735).pdf:pdf.

Collins, W.J., Beams, S.D., White, A.J.R., and Chappell, B.W., 1982, Nature and origin of A-type granites with particular reference to southeastern Australia: Contributions to Mineralogy and Petrology, v. 80, p. 189–200, doi:10.1007/BF00374895.

Colombo, F., Lira, R., and Dorais, M. j., 2010, Mineralogy and crystal chemistry of micas from the A-type el Portezuelo granite and related pegmatites, Catamarca (NW Argentina): Journal of geosciences, v. 55, p. 43–56, doi:10.3190/jgeosci.058.

Corfu, F., Hanchar, J.M., and Hoskin, P.W.O., 2003, Atlas of zircon textures, *in* Reviews in mineralogy and geochemistry, p. 469–500.

Creaser, R.A., Price, R.C., and Wormald, R.J., 1991, A-type granites revisited: assessment of a residual-source model: Geology, v. 19, p. 163–166, doi:10.1130/0091-7613(1991)019<0163:ATGRAO>2.3.CO.

Czamanske, G.K., and Mihalik, P., 1972, Oxidation During Magmatic Differentiation, Finnmarka Complex, Oslo Area, Norway: Part 1, The Opaque Oxides: Journal of Petrology, v. 13, p. 493–509, doi:10.1093/petrology/13.3.493.

Dall'Agnol, R., Frost, C.D., and Rämö, O.T., 2012, IGCP Project 510 "A-type Granites and Related Rocks through Time": Project vita, results, and contribution to granite research: Lithos, v. 151, p. 1–16, doi:10.1016/j.lithos.2012.08.003.

Dall'Agnol, R., and de Oliveira, D.C., 2007, Oxidized, magnetite-series, rapakivi-type granites of Carajás, Brazil: Implications for classification and petrogenesis of A-type granites: Lithos, v. 93, p. 215–233, doi:10.1016/j.lithos.2006.03.065.

Dalou, C., Boulon, J., T. Koga, K., Dalou, R., and Dennen, R.L., 2018, DOUBLE FIT: Optimization procedure applied to lattice strain model: Computers and Geosciences, v. 117, p. 49–56, doi:10.1016/j.cageo.2018.04.013.

Dewaele, S., Henjes-Kunst, F., Melcher, F., Sitnikova, M., Burgess, R., Gerdes, A., Fernandez, M.A., Clercq, F. De, Muchez, P., and Lehmann, B., 2011, Late Neoproterozoic overprinting of the cassiterite and columbite-tantalite bearing pegmatites of the Gatumba area, Rwanda (Central Africa): Journal of African Earth Sciences, v. 61, p. 10–26, doi:10.1016/j.jafrearsci.2011.04.004.

Dias, C.H., and Chaves, M.L. de S.C., 2015, Uncommon Nb-tantalate from the Cachoeira mine, Araçuaí pegmatite district (Minas Gerais): Rem: Revista Escola de Minas, v. 68, p. 401–408, doi:10.1590/0370-44672014680227.

Eby, G.N., 1992, Chemical subdivision of the A-type granitoids: Petrogenetic and tectonic implications: Geology, v. 20, p. 641, doi:10.1130/0091-7613(1992)020<0641:CSOTAT>2.3.CO;2.

Eby, G.N., 1990, The A-type granitoids: A review of their occurrence and chemical characteristics and speculations on their petrogenesis: Lithos, v. 26, p. 115–134, doi:10.1016/0024-4937(90)90043-Z.

Eggleton, R.A., 1972, The crystal structure of stilpnomelane. Part II. The full cell: Mineralogical Magazine, v. 38, p. 693–711, doi:10.1180/minmag.1972.038.298.06.

El-Sharkawy, M.F., 2000, Talc mineralization of ultramafic affinity in the Eastern Desert of Egypt: Mineralium Deposita, v. 35, p. 346–363, doi:10.1007/s001260050246.

Ercit, T.S., 1994, The geochemistry and crystal chemistry of columbite-group minerals from granitic pegmatites, southwestern Grenville Province, Canadian Shield: Canadian Mineralogist, v. 32, p. 421–438.

Ercit, T.S., Wise, M.A., and Cerny, P., 1995, Compositional and structural systematics of the columbite group: American Mineralogist, v. 80, p. 613–619, doi:10.2138/am-1995-5-619.

Ernst, W.., 1968, Amphiboles: Inc., Springer-Verlag New York, 233 p., doi:lO.l007/978-3-642-65474-9.

Ernst, W.G., 1962, Synthesis, Stability Relations, and Occurrence of Riebeckite and Riebeckite-Arfvedsonite Solid Solutions: The Journal of Geology, v. 70, p. 689–736, http://www.jstor.org/stable/30066372%5Cnhttp://www.jstor.org/stable/pdfplus/30066372.pdf?acceptTC=true.

Estrade, G., Salvi, S., Béziat, D., Rakotovao, S., and Rakotondrazafy, R., 2014, REE and HFSE mineralization in peralkaline granites of the Ambohimirahavavy alkaline complex, Ampasindava peninsula, Madagascar: Journal of African Earth Sciences, v. 94, p. 141–155, doi:10.1016/j.jafrearsci.2013.06.008.

Eugster, H.P., and Wones, D.R., 1962, Stability Relations of the Ferruginous Biotite, Annite: Journal of Petrology, v. 3, p. 82–125, doi:10.1093/petrology/3.1.82.

Faleiros, F.M., 2008, Evolução de terrenos tectono-metamórficos da serrania do ribeira e planalto alto turvo (sp, pr): Tese, p. 306, doi:10.1017/CBO9781107415324.004.

Feng, Y., Liang, T., Yang, X., Zhang, Z., and Wang, Y., 2019, Chemical Evolution of Nb-Ta Oxides and Cassiterite in Phosphorus-Rich Albite-Spodumene Pegmatites in the Kangxiwa–Dahongliutan Pegmatite Field, Western Kunlun Orogen, China: Minerals, v. 9, p. 166, doi:10.3390/min9030166.

Ferry, J.M., and Watson, E.B., 2007, New thermodynamic models and revised calibrations for the Ti-in-zircon and Zr-in-rutile thermometers: Contributions to Mineralogy and Petrology, v. 154, p. 429–437, doi:10.1007/s00410-007-0201-0.

Förster, H.J., 1998, The chemical composition of REE-Y-Th-U-rich accessory minerals in peraluminous granites of the Erzgebirge-Fichtelgebirge region, Germany, Part I: The monazite-(Ce)-brabantite solid solution series: American Mineralogist, v. 83, p. 259–272.

Francesconi, R., 1972, Pegmatitos da regiao de Sao Joao del rei - MG (Doctoral Thesis): Universidade de São Paulo, 110 p.

Frost, B.R., Barnes, C.G., Collins, W.J., Arculus, R.J., Ellis, D.J., and Frost, C.D., 2001, A geochemical classification for granitic rocks: Journal of Petrology, v. 42, p. 2033–2048, doi:10.1093/petrology/42.11.2033.

Gagnevin, D., Daly, J.S., and Kronz, A., 2010, Zircon texture and chemical composition as a guide to magmatic processes and mixing in a granitic environment and coeval volcanic system: Contributions to Mineralogy and Petrology, v. 159, p. 579–596, doi:10.1007/s00410-009-0443-0.

Garcia, R.P., 2015, Evolução magmática e hidrotermal de granitos de “tipo-A” reduzidos: o exemplo do Pluton Desemborque, Maciço Guaraú, SP. Master’s Dissertation.: Universty of São Paulo, 223 p., doi:10.11606/D.44.2015.tde-17062015-092009.

Gardiner, N.J., Hawkesworth, C.J., Robb, L.J., Whitehouse, M.J., Roberts, N.M.W., Kirkland, C.L., and Evans, N.J., 2017, Contrasting Granite Metallogeny through the Zircon Record: A Case Study from Myanmar: Scientific Reports, v. 7, p. 748, doi:10.1038/s41598-017-00832-2.

Geisler, T., Rashwan, A.A., Rahn, M.K.W., Poller, U., Zwingmann, H., Pidgeon, R.T., Schleicher, H., and Tomaschek, F., 2003, Low-temperature hydrothermal alteration of natural metamict zircons from the Eastern Desert, Egypt: Mineralogical Magazine, v. 67, p. 485–508, doi:10.1180/0026461036730112.

Geisler, T., Schaltegger, U., and Tomaschek, F., 2007, Re-equilibration of zircon in aqueous fluids and melts: Elements, v. 3, p. 43–50, doi:10.2113/gselements.3.1.43.

Giret, A., Bonin, B., and Leger, J.-M., 1980, Amphibole compositional trends in oversaturated and undersaturated alkaline plutoninc ring-complexes.: Canadian Mineralogist, v. 18, p. 481–495.

Grice, J.D., Ferguson, R.B., and Hawthorne, F.C., 1976, The crystal of structures of Tantalite, Ixiolite and Wodginite From Bernic Lake , Manitoba I. Tantalite and Ixiolite: Canadian Mineralogist, v. 14, p. 540–549.

Griffin, W.L., 2008, GLITTER: data reduction software for laser ablation ICP-MS: Laser Ablation ICP-MS in the Earth Sciences: Current practices and outstanding issues, p. 308–311.

Gualda, G.A.R., and Vlach, S.R.F., 2005, Stoichiometry-based estimates of ferric iron in calcic, sodic-calcic and sodic amphiboles: A comparison of various methods: Anais da Academia Brasileira de Ciencias, v. 77, p. 521–534, doi:10.1590/S0001-37652005000300012.

Gualda, G.A.R., and Vlach, S.R.F., 2007a, The Serra da Graciosa A-type granites and syenites, southern Brazil. Part 1: regional setting and geological characterization: Anais da Academia Brasileira de Ciências, v. 79, p. 405–430, doi:10.1590/S0001-37652007000300006.

Gualda, G.A.R., and Vlach, S.R.F., 2007b, The Serra da Graciosa A-type granites and syenites, southern Brazil. Part 1: Regional setting and geological characterization: Anais da Academia Brasileira de Ciencias, v. 79, p. 405–430, doi:10.1016/j.lithos.2006.06.002.

Gualda, G.A.R., and Vlach, S.R.F., 2007c, The Serra da Graciosa A-type Granites and Syenites, southern Brazil. Part 2: Petrographic and mineralogical evolution of the alkaline and aluminous associations: Lithos, v. 93, p. 310–327, doi:10.1016/j.lithos.2006.06.002.

Gualda, G. a R., and Vlach, S.R.F., 2007d, The Serra da Graciosa A-type Granites and Syenites, southern Brazil. Part 2: Petrographic and mineralogical evolution of the alkaline and aluminous associations: Lithos, v. 93, p. 310–327, doi:10.1016/j.lithos.2006.06.002.

Gualda, G. a R., and Vlach, S.R.F., 2007e, The Serra da Graciosa A-type Granites and Syenites, southern Brazil. Part 3: Magmatic evolution and post-magmatic breakdown of amphiboles of the alkaline association: Lithos, v. 93, p. 328–339, doi:10.1016/j.lithos.2006.03.070.

Guggenheim, S., Adams, J.M., Bain, D.C., Bergaya, F., Brigatti, M.F., Drits, V.A., Formoso, M.L.L., Galan, E., Kogure, T., and Stanjek, H., 2007, Summary of recommendations of nomenclature committees relevant to clay mineralogy: Report of the Association International pour l'Etude des Argiles (AIPEA) Nomenclature Committee for 2006 (Clays and Clay Minerals): Clays and Clay Minerals, v. 55, p. 646, doi:10.1346/CCMN.2007.0550611.

Hanchar, J.M., and Hoskin, P.W.O., 2003, Zircon, *in* Hanchar, J.M. ed., Reviews in Mineralogy and Geochemistry, Mineralogical society of America/geochemical society, p. 500, https://eleanor.lib.gla.ac.uk/record=b2313888~S6%0Ahttp://books.google.ru/books?id=c3gSAQAAIAAJ.

Harrison, T.M., and Watson, E.B., 1984, The behavior of apatite during crustal anatexis: Equilibrium and kinetic considerations: Geochimica et Cosmochimica Acta, v. 48, p. 1467–1477, doi:10.1016/0016-7037(84)90403-4.

Hawthorne, F.C., Oberti, R., Harlow, G.E., Maresch, W. V, Martin, R.F., Schumacher, J.C., and Welch, M.D., 2012, Nomenclature of the amphibole supergroup: American Mineralogist, v. 97, p. 2031–2048, doi:10.2138/am.2012.4276.

Hawthorne, F.C., Ungaretti, L., Oberti, R., Cannillo, E., and Smelik, E.A., 1994, The mechanism of [6]Li incorporation in amphiboles: American Mineralogist, v. 79, p. 443–451.

Hillier, S., and Velde, B., 1991, Octahedral occupancy and the chemical composition of diagenetic (low-temperature) chlorites: Clay Minerals, v. 26, p. 149–168, doi:10.1180/claymin.1991.026.2.01.

Hilyard, M., Nielsen, R.L., Beard, J.S., Patinõ-Douce, A., and Blencoe, J., 2000, Experimental determination of the partitioning behavior of rare earth and high field strength elements between pargasitic amphibole and natural silicate melts: Geochimica et Cosmochimica Acta, v. 64, p. 1103–1120, doi:10.1016/S0016-7037(99)00379-8.

Holland, T., and Blundy, J., 1994, Non-ideal interactions in calcic amphiboles and their bearing on amphibole-plagioclase thermometry: Contributions to Mineralogy and Petrology, v. 116, p. 433–447, doi:10.1007/BF00310910.

Hoskin, P.W.O., 2005, Trace-element composition of hydrothermal zircon and the alteration of Hadean zircon from the Jack Hills, Australia: Geochimica et Cosmochimica Acta, v. 69, p. 637–648, doi:10.1016/j.gca.2004.07.006.

Hoskin, P.W.O., and Schaltegger, U., 2003, The Composition of Zircon and Igneous and Metamorphic Petrogenesis: Reviews in Mineralogy and Geochemistry, v. 53, p. 27–62, doi:10.2113/0530027.

Hossain, I., and Tsunogae, T., 2014, Crystallization Conditions and Petrogenesis of the Paleoproterozoic Basement Rocks in Bangladesh : An Evaluation of Biotite and

Coexisting Amphibole Mineral Chemistry: v. 25, p. 87–97, doi:10.1007/s12583-014-0402-1.

Huang, X.L., Wang, R.C., Hu, H., Chen, X.M., and Liu, C.S., 2002, Vertical Variations in the Mineralogy of the Yichun Topaz Lepidolite Granite, Jiangxi Province, Southern China: The Canadian Mineralogist, v. 40, p. 1047–1068, doi:10.2113/gscanmin.40.4.1047.

Huang, F.-F., Wang, R.-C., Xie, L., Zhu, J.-C., Erdmann, S., Che, X.-D., and Zhang, R.-Q., 2015, Differentiated rare-element mineralization in an ongonite–topazite composite dike at the Xianghualing tin district, Southern China: An electron-microprobe study on the evolution from niobium–tantalum-oxides to cassiterite: Ore Geology Reviews, v. 65, p. 761–778, doi:10.1016/j.oregeorev.2014.08.008.

Huang, H., Wang, T., Zhang, Z., Li, C., and Qin, Q., 2018, Highly differentiated fluorine-rich, alkaline granitic magma linked to rare metal mineralization: A case study from the Boziguo'er rare metal granitic pluton in South Tianshan Terrane, Xinjiang, NW China: Ore Geology Reviews, v. 96, p. 146–163, doi:10.1016/j.oregeorev.2018.04.021.

Hutton, C.O., 1938, The stilpnomelane group of minerals: Mineralogical Magazine and Journal of the Mineralogical Society, v. 25, p. 172–206, doi:10.1180/minmag.1938.025.163.02.

Idrus, A., 2018, Halogen Chemistry of Hydrothermal Micas: a Possible Geochemical Tool in Vectoring to Ore for Porphyry Copper-Gold Deposit: Journal of Geoscience, Engineering, Environment, and Technology, v. 3, p. 30, doi:10.24273/jgeet.2018.3.01.1022.

Inoue, A., Kurokawa, K., and Hatta, T., 2010, Application of chlorite geothermometry to hydrothermal alteration in toyoha geothermal system, southwestern hokkaido, Japan: Resource Geology, v. 60, p. 52–70, doi:10.1111/j.1751-3928.2010.00114.x.

Janoušek, V., Farrow, C.M., and Erban, V., 2006, Interpretation of whole-rock geochemical data in igneous geochemistry: Introducing Geochemical Data Toolkit (GCDkit): Journal of Petrology, v. 47, p. 1255–1259, doi:10.1093/petrology/egl013.

Jin, C., Gao, X., Terry, W., and Zhao, T., 2018, Magmatic-hydrothermal evolution of the Donggou porphyry Mo deposit at the southern margin of the North China Craton : Evidence from chemistry of biotite: Ore Geology Reviews, v. 92, p. 84–96, doi:10.1016/j.oregeorev.2017.10.026.

Jochum, K.P. et al., 2011, Determination of reference values for NIST SRM 610-617 glasses following ISO guidelines: Geostandards and Geoanalytical Research, v. 35, p. 397–429,

doi:10.1111/j.1751-908X.2011.00120.x.

Johan, Z., and Johan, V., 2005, Accessory minerals of the Cínovec (Zinnwald) granite cupola, Czech Republic: indicators of petrogenetic evolution: Mineralogy and Petrology, v. 83, p. 113–150, doi:10.1007/s00710-004-0058-0.

Jowett, E.C., 1991, Fitting Iron and Mangesium into the Hydrothermal Chlorite Geothermometer, *in* Abstracts, P. of the P. with ed., GAC/MAC/SEG Joint Annual Meeting, Toronto, May 27-29, Geological Association of Canada – Mineralogical, p. A62, doi:.1037//0033-2909.I26.1.78.

Karimpour, M.H., Stern, C.R., and Mouradi, M., 2011, Chemical composition of biotite as a guide to petrogenesis of granitic rocks from Maherabad, Dehnow, Gheshlagh, Khajehmourad and Najmabad, Iran: Iranian journal of crystallography and mineralogy, v. 18, p. 89–100.

Kaul, P.F.T., and Cordani, U.G., 2000, Geochemistry of the Serra Do Mar Granitoid Magmatism and Tectonic Implications, Southern Brazil: Revista Brasileira de Geociências, v. 30, p. 115–119, doi:10.25249/0375-7536.2000301115119.

Kavalieris, I., Walshe, J.L., Halley, S., and Harrold, B.P., 1990, Dome-related gold mineralization in the Pani Volcanic Complex, north Sulawesi, Indonesia: a study of geologic relations, fluid inclusions, and chlorite compositions: Economic Geology, v. 85, p. 1208–1225, doi:10.2113/gsecongeo.85.6.1208.

Keppler, H., 1993, Influence of fluorine on the enrichment of high field strength trace elements in granitic rocks: Contributions to Mineralogy and Petrology, v. 114, p. 479–488, doi:10.1007/BF00321752.

Khomyakov, A.P., 1995, Mineralogy of hyperagpaitic alkaline rocks (O. S. Publications, Ed.): Oxford, Clarendon Press Oxford, 222 p.

Kim, E.J., Yang, S.J., No, S.G., Park, S.W., Lee, S.R., Kim, Y.D., and Jo, J., 2018, The characteristics of zircon as the evidence for post-magmatic remobilization of REE and HFSE in the northern Motzfeldt alkaline igneous complex, southern Greenland: Geosciences Journal, v. 22, p. 921–938, doi:10.1007/s12303-018-0003-6.

Kovaleva, E., Harlov, D., and Klötzli, U., 2017, Complicated secondary textures in zircon record evolution of the host granitic rocks: Studies from Western Tauern Window and Ötztal-Stubai Crystalline Complex (Eastern Alps, Western Austria): Lithos, v. 284–285,

p. 381–400, doi:10.1016/j.lithos.2017.04.018.

Kramers, J., Frei, R., Newville, M., Kober, B., and Villa, I., 2009, On the valency state of radiogenic lead in zircon and its consequences: Chemical Geology, v. 261, p. 4–11, doi:10.1016/j.chemgeo.2008.09.010.

Kranidiotis, P., and MacLean, W.H., 1987, Systematics of chlorite alteration at the Phelps Dodge massive sulfide deposit, Matagami, Quebec: Economic Geology, v. 82, p. 1898–1911, doi:10.2113/gsecongeo.82.7.1898.

Kryvdik, S.G., and Sharygin, V.V., 2014, Astrophyllite-group minerals from Azov region , Ukraine Astrophyllite-group minerals from Azov region , Ukraine, *in* p. 2–4, doi:10.13140/2.1.2904.0002.

Lamarão, C.N., Marques, G.T., de Oliveira, D.C., Costi, H.T., Borges, R.M.K., and Dall'Agnol, R., 2018, Morphology and composition of zircons in rare metal granites from Brazilian tin provinces: Journal of South American Earth Sciences, v. 84, p. 1–15, doi:10.1016/j.jsames.2018.03.003.

Lamarão, C.N., Dos Santos Silva, J., Borges, R.M.K., and Dall'Agnol, R., 2014, Morphological and compositional variations of zircon and their metallogenetic implications: The example of the Jamon, Serra dos Carajás and Velho Guilherme suites, Amazonian Craton: Brazilian Journal of Geology, v. 44, p. 105–120, doi:10.5327/Z2317-4889201400010009.

Larocque, J., and Canil, D., 2010, The role of amphibole in the evolution of arc magmas and crust: The case from the Jurassic Bonanza arc section, Vancouver Island, Canada: Contributions to Mineralogy and Petrology, v. 159, p. 475–492, doi:10.1007/s00410-009-0436-z.

Layne, G.D., 1982, Astrophyllite from Kangerdlugssuaq, East Greenland: Mineralogical Magazine, v. 45, p. 149–156, doi:10.1180/minmag.1982.045.337.17.

Layne, G.D., Rucklidge, J.C., and Kent Brooks, C., 1982, Astrophyllite from Kangerdlugssuaq, East Greenland: Mineralogical Magazine, v. 45, p. 149–156, doi:10.1180/minmag.1982.045.337.17.

Leake, B.E. et al., 1997, Nomenclature of amphiboles: Report of the subcommittee on amphiboles of the international mineralogical association, commission on new minerals and mineral names: Canadian Mineralogist, v. 35, p. 219–246.

Li, H., Palinkaš, L.A., Watanabe, K., and Xi, X.S., 2018a, Petrogenesis of Jurassic A-type

granites associated with Cu-Mo and W-Sn deposits in the central Nanling region, South China: Relation to mantle upwelling and intra-continental extension: Ore Geology Reviews, v. 92, p. 449–462, doi:10.1016/j.oregeorev.2017.11.029.

Li, H., Wu, J.H., Evans, N.J., Jiang, W.C., and Zhou, Z.K., 2018b, Zircon geochronology and geochemistry of the Xianghualing A-type granitic rocks: Insights into multi-stage Sn-polymetallic mineralization in South China: Lithos, v. 312–313, p. 1–20, doi:10.1016/j.lithos.2018.05.001.

Li, H., Zhou, Z.K., Evans, N.J., Kong, H., Wu, Q.H., and Xi, X.S., 2019, Fluid-zircon interaction during low-temperature hydrothermal processes: Implications for the genesis of the Banxi antimony deposit, South China: Ore Geology Reviews, v. 114, p. 103137, doi:10.1016/j.oregeorev.2019.103137.

Lichtervelde, M. V, Linnen, R.L., Salvi, S., and Didier, B., 2007, Textures and chemical evolutions in tantalum oxides: a discussion of magmatic versus metasomatic origins for Ta mineralization in the Tanco Lower Pegmatite, Manitoba, Canada: Economic Geology, v. 102, p. 257–276.

Linnen, R.L., 1998, The solubility of Nb-Ta-Zr-Hf-W in granitic melts with Li and Li + F: Constraints for mineralization in rare metal granites and pegmatites: Economic Geology, v. 93, p. 1013–1025, doi:10.2113/gsecongeo.93.7.1013.

Linnen, R.L., and Cuney, M., 2005, Granite-related rare-element deposits and experimental constraints on Ta-Nb-W-Sn-Zr-Hf mineralization, in Linnen RL and Samson IM, eds., rare-element geochemistry and mineral deposits., *in* Geological Association of Canada, GAC, Short Course,.

Linnen, R.L., and Keppler, H., 1997, Columbite solubility in granitic melts: Consequences for the enrichment and fractionation of Nb and Ta in the Earth's crust: Contributions to Mineralogy and Petrology, v. 128, p. 213–227, doi:10.1007/s004100050304.

Linnen, R.L., and Keppler, H., 2002, Melt composition control of Zr/Hf fractionation in magmatic processes: Geochimica et Cosmochimica Acta, v. 66, p. 3293–3301, doi:10.1016/S0016-7037(02)00924-9.

Lisowiec, K., Budzyń, B., Słaby, E., Renno, A.D., and Götze, J., 2013, Fluid-induced magmatic and post-magmatic zircon and monazite patterns in granitoid pluton and related rhyolitic bodies: Chemie der Erde, v. 73, p. 163–179, doi:10.1016/j.chemer.2012.07.005.

Llorens González, T., Moro Benito, M.C., Sanz Contreras, J.L., López Moro, F.J., García Polonio, F., and Fernández Fernández, A., 2016, Tin-tantalum-niobium mineralization in the Penouta deposit (NW Spain): Textural features and mineral chemistry to unravel the genesis and evolution of cassiterite and columbite group minerals in a peraluminous system: Ore Geology Reviews, v. 81, p. 79–95, doi:10.1016/j.oregeorev.2016.10.034.

Loiselle, M.C., and Wones, D.R., 1979, Characteristics and origin of anorogenic granites., *in* Geological Society of America Abstracts with Programs 11, p. 468.

Ludwig, K.R., 2003, Isoplot 3.00: a Geochronological Toolkit for Microsoft Excel, Berkeley. Geochronological Centre Special Publication, vol.4:

Macdonald, R., 1973, Chemical variation in minerals of the astrophyllite group: Mineralogical Magazine, v. 39, p. 97–111, doi:10.1180/minmag.1973.039.301.15.

Macdonald, R., Karup-Møller, S., and Rose-Hansen, J., 2007, Astrophyllite-group minerals from the Ilímaussaq complex, South Greenland (contribution to the mineralogy of Ilímaussaq no. 123): Mineralogical Magazine, v. 71, p. 1–16, doi:10.1180/minmag.2007.071.1.1.

Macdonald, R., and Saunders, M.J., 1973, Chemical variation in minerals of the astrophyllite group: Mineralogical Magazine, v. 39, p. 97–111, doi:10.1180/minmag.1973.039.301.15.

Mackay, D., and Simandl, G.J., 2015, Pyrochlore and columbite-tantalite as indicator minerals for specialty metal deposits: Geochemistry: Exploration, Environment, Analysis, v. 15, p. 167–178, doi:10.1144/geochem2014-289.

Marks, M., Halama, R., Wenzel, T., and Markl, G., 2004, Trace element variations in clinopyroxene and amphibole from alkaline to peralkaline syenites and granites: Implications for mineral-melt trace-element partitioning: Chemical Geology, v. 211, p. 185–215, doi:10.1016/j.chemgeo.2004.06.032.

Marks, M.A.W., Hettmann, K., Schilling, J., Frost, B.R., and Markl, G., 2011, The mineralogical diversity of alkaline igneous rocks: Critical factors for thetransition from miaskitic to agpaitic phase assemblages: Journal of Petrology, v. 52, p. 439–455, doi:10.1093/petrology/egq086.

Marks, M.A.W., and Markl, G., 2017a, A global review on agpaitic rocks: Earth-Science Reviews, v. 173, p. 229–258, doi:10.1016/j.earscirev.2017.06.002.

Marks, M.A.W., and Markl, G., 2017b, A global review on agpaitic rocks: Earth-Science

Reviews, v. 173, p. 229–258, doi:10.1016/j.earscirev.2017.06.002.

Marks, M., Vennemann, T., Siebel, W., and Markl, G., 2003, Quantification of Magmatic and Hydrothermal Processes in a Peralkaline Syenite–Alkali Granite Complex Based on Textures, Phase Equilibria, and Stable and Radiogenic Isotopes: Journal of Petrology, v. 44, p. 1247–1280, doi:10.1093/petrology/44.7.1247.

Martins, T., Lima, A., Simmons, W.B., Falster, A.U., and Noronha, F., 2011, Geochemical fractionation of Nb-Ta oxides in Li-bearing pegmatites from the Barroso-Alvão pegmatite field, northern Portugal: Canadian Mineralogist, v. 49, p. 777–791, doi:10.3749/canmin.49.3.777.

Mason, R.A., 1992, Models of order and iron-fluorine avoidance in biotite: The Canadian Mineralogist, v. 30, p. 343–354.

McDonough, W.F., and Sun, S., 1995a, The composition of the Earth: Chemical Geology, v. 120, p. 223–253.

McDonough, W.F., and Sun, S. s., 1995b, The composition of the Earth: Chemical Geology, v. 120, p. 223–253, doi:10.1016/0009-2541(94)00140-4.

Melcher, F., Graupner, T., Gäbler, H.E., Sitnikova, M., Henjes-Kunst, F., Oberthür, T., Gerdes, A., and Dewaele, S., 2015, Tantalum-(niobium-tin) mineralisation in African pegmatites and rare metal granites: Constraints from Ta-Nb oxide mineralogy, geochemistry and U-Pb geochronology: Ore Geology Reviews, v. 64, p. 667–719, doi:10.1016/j.oregeorev.2013.09.003.

Melcher, F., Graupner, T., Gäbler, H.-E., Sitnikova, M., Oberthür, T., Gerdes, A., Badanina, E., and Chudy, T., 2016, Mineralogical and chemical evolution of tantalum–(niobium–tin) mineralisation in pegmatites and granites. Part 2: Worldwide examples (excluding Africa) and an overview of global metallogenetic patterns: Ore Geology Reviews, doi:10.1016/j.oregeorev.2016.03.014.

Michely, L.T., Leitzke, F.P., Speelmanns, I.M., and Fonseca, R.O.C., 2017, Competing effects of crystal chemistry and silicate melt composition on trace element behavior in magmatic systems: insights from crystal/silicate melt partitioning of the REE, HFSE, Sn, In, Ga, Ba, Pt and Rh: Contributions to Mineralogy and Petrology, v. 172, doi:10.1007/s00410-017-1353-1.

Miller, C.F., McDowell, S.M., and Mapes, R.W., 2003, Hot and cold granites: Implications of

zircon saturation temperatures and preservation of inheritance: Geology, v. 31, p. 529–532, doi:10.1130/0091-7613(2003)031<0529:HACGIO>2.0.CO;2.

Minuzzi, O.R., Bastos Neto, A.C., Pereira, V.P., and Nunes, L., 2006, A Columbitização Do Pirocloro Do Albita Granito na Mina Pitinga (Am): Relações com a Mineralização de Criolita: Revista Brasileira de Geociências, v. 36, p. 124–137, doi:10.25249/0375-7536.200636s1124137.

Mitchell, R.H., 1990, A review of the compositional variation of amphiboles in alkaline plutonic complexes: LITHOS, v. 26, p. 135–156, doi:10.1016/0024-4937(90)90044-2.

Molina, J.F., Moreno, J.A., Castro, A., Rodríguez, C., and Fershtater, G.B., 2015, Calcic amphibole thermobarometry in metamorphic and igneous rocks: New calibrations based on plagioclase/amphibole Al-Si partitioning and amphibole/liquid Mg partitioning: Lithos, v. 232, p. 286–305, doi:10.1016/j.lithos.2015.06.027.

Möller, P., 1989, REE(Y), Nb, and Ta Enrichment in Pegmatites and Carbonatite-Alkalic Rock Complexes, *in* Möller, P., Černý, P., and Saupé, F. eds., Lanthanides, Tantalum and Niobium, Berlin, Heidelberg, Springer Berlin Heidelberg, p. 103–144.

Montel, J., 1996, Electron microprobe dating of monazite: Chemical Geology, v. 131, p. 37–53, doi:10.1016/0009-2541(96)00024-1.

Mori, P.E., Reeves, S., Correia, C.T., and Haukka, M., 1999, Development oof a fused glass disc XRF facility and comparison with the pressed powder pellet technique at Instituto de Geociencias, Sao Paulo University: Revista Brasileira de Geociencias, v. 29, p. 441–6, http://inis.iaea.org/Search/search.aspx?orig_q=RN:32037921%5Cnhttp://biblat.unam.mx/pt/revista/revista-brasileira-de-geociencias/articulo/development-oof-a-fused-glass-disc-xrf-facility-and-comparison-with-the-pressed-powder-pellet-technique-at-instituto-.

Moshefi, P., Hosseinzadeh, M.R., Moayyed, M., and Lentz, D.R., 2018, Comparative study of mineral chemistry of four biotite types as geochemical indicators of mineralized and barren intrusions in the Sungun Porphyry Cu-Mo deposit, northwestern Iran: Ore Geology Reviews, v. 97, p. 1–20, doi:10.1016/j.oregeorev.2018.05.003.

Munoz, J.L., 1992, Calculation of the HF and HCL fugacities from biotite compositions: Revised equations.

Munoz, J.L., 1984, F-OH and Cl-OH exchange in micas with applications to hydrothermal ore deposits: Reviews in Mineralogy, v. 11, p. 469–494.

Nachit, H., Ibhi, A., Abia, E.H., and Ben Ohoud, M., 2005, Discrimation entre biotites magmatiques primaires, biotites rééquilibrées et biotites néoformées: Comptes Rendus - Geoscience, v. 337, p. 1415–1420, doi:10.1016/j.crte.2005.09.002.

Nardi, L.V.S., Formoso, M.L.L., Jarvis, K., Oliveira, L., Bastos Neto, A.C., and Fontana, E., 2012, REE, Y, Nb, U, and Th contents and tetrad effect in zircon from a magmatic-hydrothermal F-rich system of Sn-rare metal-cryolite mineralized granites from the Pitinga Mine, Amazonia, Brazil: Journal of South American Earth Sciences, v. 33, p. 34–42, doi:10.1016/j.jsames.2011.07.004.

Nardi, L.V.S., Formoso, M.L.L., Müller, I.F., Fontana, E., Jarvis, K., and Lamarão, C., 2013, Zircon/rock partition coefficients of REEs, Y, Th, U, Nb, and Ta in granitic rocks: Uses for provenance and mineral exploration purposes: Chemical Geology, v. 335, p. 1–7, doi:10.1016/j.chemgeo.2012.10.043.

Nasdala, L., Hanchar, J.M., Rhede, D., Kennedy, A.K., and Váczi, T., 2010, Retention of uranium in complexly altered zircon: An example from Bancroft, Ontario: Chemical Geology, v. 269, p. 290–300, doi:10.1016/j.chemgeo.2009.10.004.

Nasdala, L., Kronz, A., Wirth, R., Váczi, T., Pérez-Soba, C., Willner, A., and Kennedy, A.K., 2009, The phenomenon of deficient electron microprobe totals in radiation-damaged and altered zircon: Geochimica et Cosmochimica Acta, v. 73, p. 1637–1650, doi:10.1016/j.gca.2008.12.010.

Nasdala, L., Wenzel, M., Vavra, G., Irmer, G., Wenzel, T., and Kober, B., 2001, Metamictisation of natural zircon: Accumulaton versus thermal annealing of radioactivity-induced damage: Contributions to Mineralogy and Petrology, v. 141, p. 125–144, doi:10.1007/s004100000235.

Navarro, M.S., Andrade, S., Ulbrich, H., Gomes, C.B., and Girardi, V.A.V., 2008, The direct determination of rare earth elements in basaltic and related rocks using ICP-MS: Testing the efficiency of microwave oven sample decomposition procedures: Geostandards and Geoanalytical Research, v. 32, p. 167–180, doi:10.1111/j.1751-908X.2008.00840.x.

Neiva, A.M.R., Gomes, C.L., and Silva, P.B., 2015, Two generations of zoned crystals of Columbite-group minerals from granitic aplite-pegmatite in the Gouveia area, central Portugal: European Journal of Mineralogy, v. 27, p. 771–782, doi:10.1127/ejm/2015/0027-2473.

Nicholls, J., and Carmichael, J.S.E., 1969, Peralkaline acid liquids: A petrological study: Contributions to Mineralogy and Petrology, v. 20, p. 268–294, doi:10.1007/BF00377480.

Novák, M., Chládek, Š., Uher, P., and Gadas, P., 2018, Complex magmatic and subsolidus compositional trends of columbite–tantalite in the beryl–columbite Šejby granitic pegmatite, Czech Republic: Role of crystal-structural constraints and associated minerals: Journal of Geosciences (Czech Republic), v. 63, p. 253–263, doi:10.3190/jgeosci.269.

Ogunleye, P.O., Garba, I., and Ike, E.C., 2006, Factors contributing to enrichment and crystallization of niobium in pyrochlore in the Kaffo albite arfvedsonite granite, Ririwai Complex, Younger Granites province of Nigeria: Journal of African Earth Sciences, v. 44, p. 372–382, doi:10.1016/j.jafrearsci.2005.12.006.

Oliveira, M.C.B., 1989, Petrografia do Maciço Granitico Mandira-SP. Master's Dissertation: University of Sao Paulo, 203 p.

Oliveira, M.C.B., Rodrigues, E. de P., Coutinho, J.M.V., Martins, F.A.G., Figuereido, M.C.H. de F., and Zaparolli, L.H., 1987, Petrologia de parte do Macizo granitico Guarau-SP., *in* I Simpósio Sul- Brasileiro Geologia. 1. Curitiba. SBG. Atas, 2, p. 571–594.

Papoutsa, A., and Pe-piper, G., 2014, Geochemical variation of amphiboles in A-type granites as an indicator of complex magmatic systems : Wentworth pluton, Nova Scotia, Canada: Chemical Geology, v. 384, p. 120–134, doi:10.1016/j.chemgeo.2014.07.001.

Park, C., Song, Y., Chung, D., Kang, I.-M., Khulganakhuu, C., and Yi, K., 2016, Recrystallization and hydrothermal growth of high U–Th zircon in the Weondong deposit, Korea: Record of post-magmatic alteration: Lithos, v. 260, p. 268–285, doi:10.1016/j.lithos.2016.05.026.

Passarelli, C.R., Basei, M.A.S., Siga, O., and Harara, O.M.M., 2018, The Luis Alves and Curitiba Terranes: Continental Fragments in the Adamastor Ocean, *in* Siegesmund, S., Basei, M.A.S., Oyhantçabal, P., and Oriolo, S. eds., Geology of Southwest Gondwana, Cham, Springer International Publishing, p. 189–215, doi:10.1007/978-3-319-68920-3_8.

Patiño Douce, A.E., 1997, Generation of metaluminous A-type granites by low-pressure melting of calc-alkaline granitoids: Geology, v. 25, p. 743, doi:10.1130/0091-7613(1997)025<0743:GOMATG>2.3.CO;2.

Peng, C.C., and Ma, C.S., 1963, Discovery of a new Si O ribbon crystal-structure analysis of astrophyllite: Scientia Sinica, v. 12, p. 272–276.

Piilonen, P.C., Lalonde, A.E., Mcdonald, M.A., Gault, A.R., and LaRsen, A.O., 2003a, Insights into astrophyllite-group minerals. I. Nomenclature, composition and development of a standardized general formula: The Canadian Mineralogist, v. 41, p. 1–26.

Piilonen, P.C., McDonald, A.M., and Lalonde, A.E., 2003b, Insights into astrophyllite-group minerals. II. Crystal chemistry: Canadian Mineralogist, v. 41, p. 27–54, doi:10.2113/gscanmin.41.1.27.

Piilonen, P.C., Rancourt, D.G., Evans, R.J., Lalonde, A. é E., McDonald, A.M., and Shabani, A.A.T., 2004, The relationships between crystal-chemical and hyperfine parameters in members of the astrophyllite-group: A combined57Fe Mossbauer spectroscopy and single-crystal X-ray diffraction study: European Journal of Mineralogy, v. 16, p. 989–1002, doi:10.1127/0935-1221/2004/0016-0989.

Poitrasson, F., Duthou, J.L., and Pin, C., 1995, The relationship between petrology and Nd isotopes as evidence for contrasting anorogenic granite genesis: Example of the corsican province (SE France): Journal of Petrology, v. 36, p. 1251–1274, doi:10.1093/petrology/36.5.1251.

Putnis, A., 2002, Mineral replacement reactions: from macroscopic observations to microscopic mechanisms: Mineralogical Magazine, v. 66, p. 689–708, doi:10.1180/0026461026650056.

Rayner, N., Stern, R.A., and Carr, S.D., 2005, Grain-scale variations in trace element composition of fluid-altered zircon, Acasta Gneiss Complex, northwestern Canada: Contributions to Mineralogy and Petrology, v. 148, p. 721–734, doi:10.1007/s00410-004-0633-8.

Reguir, E.P., Chakhmouradian, A.R., Pisiak, L., Halden, N.M., Yang, P., Xu, C., Kynický, J., and Couëslan, C.G., 2012, Trace-element composition and zoning in clinopyroxene- and amphibole-group minerals: Implications for element partitioning and evolution of carbonatites: Lithos, v. 128–131, p. 27–45, doi:10.1016/j.lithos.2011.10.003.

René, M., 2019, Nb-Ta-Ti oxides in topaz granites of the Geyer granite stock (Erzgebirge Mts., Germany): Minerals, v. 9, p. 14, doi:10.3390/iecms2018-05448.

René, M., and Škoda, R., 2011, Nb-Ta-Ti oxides fractionation in rare-metal granites: Krásno-Horní Slavkov ore district, Czech Republic: Mineralogy and Petrology, v. 103, p. 37–48, doi:10.1007/s00710-011-0152-z.

Rieder, M. et al., 1998, Nomenclature of Micas: Clays and Clay Minerals, v. 46, p. 586–595.

Romans, P.A., Brown, L.L., and White, J.C., 1975, An electron microprobe study of yttrium, rare earth, and phosphorus distribution in zoned and ordinary zircon: American Mineralogist, v. 60, p. 475–480.

Romer, R.L., and Lehmann, B., 1995, U-Pb columbite age of Neoproterozoic Ta-Nb mineralization in Burundi: Economic Geology, v. 90, p. 2303–2309, doi:10.2113/gsecongeo.90.8.2303.

Romer, R.L., and Smeds, S.A., 1994, Implications of UPb ages of columbite-tantalites from granitic pegmatites for the Palaeoproterozoic accretion of 1.90-1.85 Ga magmatic arcs to the Baltic Shield: Precambrian Research, v. 67, p. 141–158, doi:10.1016/0301-9268(94)90008-6.

Rose, T., 2011, The Status of the Smithsonian Microbeam Standards: Microscopy and Microanalysis, v. 17, p. 846–847, doi:10.1017/S1431927611005101.

Rub, A.K., Štemprok, M., and Rub, M.G., 1998, Tantalum mineralization in the apical part of the Cínovec (Zinnwald) granite stock: Mineralogy and Petrology, v. 63, p. 199–222, doi:10.1007/BF01164151.

Rubin, J.N., Henry, C.D., and Price, J.G., 1989, Hydrothermal zircons and zircon overgrowths, Sierra Blanca Peaks, Texas: American Mineralogist, v. 74, p. 865–869.

Salazar-Naranjo, A.F., and Vlach, S.R.F., 2018, On the crystallization conditions of the Neoproterozoic, high-K calc-alkaline, Bragança Paulista-type magmatism, southern Brasília Orogen, SE Brazil: Brazilian Journal of Geology, v. 48, p. 631–650, doi:10.1590/2317-4889201820180033.

Salvi, S., and Williams-jones, A.E., 2006, Alteration , HFSE mineralisation and hydrocarbon formation in peralkaline igneous systems : Insights from the Strange Lake Pluton , Canada: v. 91, p. 19–34, doi:10.1016/j.lithos.2006.03.040.

Sarjoughian, F., Kananian, A., Ahmadian, J., and Murata, M., 2015, Chemical composition of biotite from the Kuh-e Dom pluton, Central Iran: implication for granitoid magmatism and related Cu–Au mineralization: Arabian Journal of Geosciences, v. 8, p. 1521–1533, doi:10.1007/s12517-013-1242-5.

Scaillet, B., and Macdonald, R., 2001, Phase relations of peralkaline silicic magmas and petrogenetic implications.: Journal of Petrology, v. 42, p. 825–845,

doi:10.1093/petrology/42.4.825.

Schaltegger, U., Pettke, T., Audétat, A., Reusser, E., and Heinrich, C.A., 2005, Magmatic-to-hydrothermal crystallization in the W–Sn mineralized Mole Granite (NSW, Australia): Chemical Geology, v. 220, p. 215–235, doi:10.1016/j.chemgeo.2005.02.018.

Schmitt, A.K., Trumbull, R.B., Dulski, P., and Emmermann, R., 2002, Zr-Nb-REE Mineralization in Peralkaline Granites from the Amis Complex, Brandberg (Namibia): Evidence for Magmatic Pre-enrichment from Melt Inclusions: Economic Geology, v. 97, p. 399–413, doi:10.2113/gsecongeo.97.2.399.

Scott, P.W., Pascoe, R.D., and Hart, F.W., 1998, Columbite-tantalite, rutile and other accessory minerals from the St. Austell topaz granite, Cornwall: Proceedings of the USSHER Society, v. 9, p. 165–170.

Sertek, J.P., 2010, Estudo das contaminações Provenientes do processo de Cominuição de amostras geológicas: Universty of São Paulo, 186 p.

Sheard, E.R., Williams-Jones, A.E., Heiligmann, M., Pederson, C., and Trueman, D.L., 2012, Controls on the concentration of zirconium, niobium, and the rare earth elements in the Thor Lake rare metal deposit, Northwest Territories, Canada: Economic Geology, doi:10.2113/econgeo.107.1.81.

Shellnutt, J.G., and Iizuka, Y., 2011, Mineralogy from three peralkaline granitic plutons of the Late Permian Emeishan large igneous province (SW China): evidence for contrasting magmatic conditions of A-type granitoids: European Journal of Mineralogy, v. 23, p. 45–61, doi:10.1127/0935-1221/2010/0022-2073.

Shimizu, K., Liang, Y., Sun, C., Jackson, C.R.M., and Saal, A.E., 2017, Parameterized lattice strain models for REE partitioning between amphibole and silicate melt: American Mineralogist, v. 102, p. 2254–2267, doi:10.2138/am-2017-6110.

Siahcheshm, K., Calagari, A.A., Abedini, A., and Lentz, D.R., 2012, Halogen signatures of biotites from the Maher-Abad porphyry copper deposit, Iran: Characterization of volatiles in syn- to post-magmatic hydrothermal fluids: International Geology Review, v. 54, p. 1353–1368, doi:10.1080/00206814.2011.639487.

Siegel, K., Vasyukova, O. V., and Williams-Jones, A.E., 2018, Magmatic evolution and controls on rare metal-enrichment of the Strange Lake A-type peralkaline granitic pluton, Québec-Labrador: Lithos, v. 308–309, p. 34–52, doi:10.1016/j.lithos.2018.03.003.

Siegel, K., Williams-jones, A.E., and Hinsberg, V.J. Van, 2017a, The amphiboles of the REE-rich A-type peralkaline Strange Lake pluton – fi ngerprints of magma evolution: LITHOS, v. 288–289, p. 156–174, doi:10.1016/j.lithos.2017.07.012.

Siegel, K., Williams-Jones, A.E., and van Hinsberg, V.J., 2017b, The amphiboles of the REE-rich A-type peralkaline Strange Lake pluton – fingerprints of magma evolution: Lithos, v. 288–289, p. 156–174, doi:10.1016/j.lithos.2017.07.012.

Siegel, K., Williams-Jones, A.E., and van Hinsberg, V.J., 2017c, The amphiboles of the REE-rich A-type peralkaline Strange Lake pluton – fingerprints of magma evolution: Lithos, v. 288–289, p. 156–174, doi:10.1016/j.lithos.2017.07.012.

Siga Júnior, O., Basei, M., and Machiavelli, A., 1993, Evolução geotectônica da porção NE de Santa Catarina e SE do Paraná, com base em interpretações geocronológicas: Revista Brasileira de Geociências, v. 23, p. 215–222, http://www.rbg.sbgeo.org.br/index.php/rbg/article/viewFile/461/154.

Silva, L.C., McNaughton, N.J., Armstrong, R., Hartmann, L.A., and Fletcher, I.R., 2005, The neoproterozoic Mantiqueira Province and its African connections: A zircon-based U-Pb geochronologic subdivision for the Brasiliano/Pan-African systems of orogens: Precambrian Research, v. 136, p. 203–240, doi:10.1016/j.precamres.2004.10.004.

Smith, S.R., Foster, G.L., Romer, R.L., Tindle, A.G., Kelley, S.P., Noble, S.R., Horstwood, M., and Breaks, F.W., 2004, U-Pb columbite-tantalite chronology of rare-element pegmatites using TIMS and Laser Ablation-Multi Collector-ICP-MS: Contributions to Mineralogy and Petrology, v. 147, p. 549–564, doi:10.1007/s00410-003-0538-y.

Sokolova, E., 2012, Further developments in the structure topology of the astrophyllite-group minerals: Mineralogical Magazine, v. 76, p. 863–882, doi:10.1180/minmag.2012.076.4.04.

Sokolova, E., and Cámara, F., 2008, Re-investigation of the crystal structure of magnesium astrophyllite: European Journal of Mineralogy, v. 20, p. 253–260, doi:10.1127/0935-1221/2008/0020-1796.

Sokolova, E., Cámara, F., Hawthorne, F.C., and Ciriotti, M.E., 2017, The astrophyllite supergroup: nomenclature and classification: Mineralogical Magazine, v. 81, p. 143–153, doi:10.1180/minmag.2016.080.077.

Sørensen, H., 1997, The agpaitic rocks - an overview: Mineralogical Magazine, v. 61, p. 485–

498, doi:10.1180/minmag.1997.061.407.02.

Speer, J.., 1984, Micas in igneous rocks (S. W. (editor) Bailey, Ed.): Mineralogical Society of America, 299–356 p.

Stepanov, A., Mavrogenes, J.A., Meffre, S., and Davidson, P., 2014, The key role of mica during igneous concentration of tantalum: Contributions to Mineralogy and Petrology, v. 167, p. 1–8, doi:10.1007/s00410-014-1009-3.

Strong, D.F., and Taylor, R.P., 1984, Magmatic-subsolidus and oxidation trends in composition of amphiboles from silica-saturated peralkaline igneous rocks: TMPM Tschermaks Mineralogische und Petrographische Mitteilungen, v. 32, p. 211–222, doi:10.1007/BF01081613.

Suzuki, K., Adachi, M., and Kajizuka, I., 1994, Electron microprobe observations of Pb diffusion in metamorphosed detrital monazites: Earth and Planetary Science Letters, v. 128, p. 391–405, doi:10.1016/0012-821X(94)90158-9.

Teiber, H., Scharrer, M., Marks, M.A.W., Arzamastsev, A.A., Wenzel, T., and Markl, G., 2015, Equilibrium partitioning and subsequent re-distribution of halogens among apatite-biotite-amphibole assemblages from mantle-derived plutonic rocks: Complexities revealed: Lithos, v. 220–223, p. 221–237, doi:10.1016/j.lithos.2015.02.015.

Tiepolo, M., Oberti, R., Zanetti, A., Foley, S.F., Vannucci, R., and Foley, S.F., 2007, Trace-Element Partitioning Between Amphibole and Silicate Melt: Reviews in Mineralogy and Geochemistry, v. 67, p. 417–452, doi:10.2138/rmg.2007.67.11.

Tiepolo, M., Vannucci, R., Bottazzi, P., Oberti, R., Zanetti, A., and Foley, S., 2000, Partitioning of rare earth elements, Y, Th, U, and Pb between pargasite, kaersutite, and basanite to trachyte melts: Implications for percolated and veined mantle: Geochemistry, Geophysics, Geosystems, v. 1, doi:10.1029/2000GC000064.

Tomaschek, F., 2004, Zircon reequilibration by dissolution–reprecipitation: reaction textures from flux-grown solid solutions: Beihefte zum European Journal of Mineralogy, v. 12, p. 214.

Turner, S.P.P., Foden, J.D.D., and Morrison, R.S.S., 1992, Derivation of some A-type magmas by fractionation of basaltic magma: An example from the Padthaway Ridge, South Australia: Lithos, v. 28, p. 151–179, doi:10.1016/0024-4937(92)90029-X.

Uher, P., Kohút, M., Ondrejka, M., Konečný, P., and Siman, P., 2014, Monazite-(Ce) in

Hercynian granites and pegmatites of the Bratislava Massif, Western Carpathians: Compositional variations and Th-U-Pb electron-microprobe dating: Acta Geologica Slovaca, v. 6, p. 215–231.

Uher, P., Ondrejka, M., and Konečný, P., 2009, Magmatic and post-magmatic Y- REE -Th phosphate, silicate and Nb-Ta-Y- REE oxide minerals in A-type metagranite: an example from the Turčok massif, the Western Carpathians, Slovakia: Mineralogical Magazine, v. 73, p. 1009–1025, doi:10.1180/minmag.2009.073.6.1009.

Vasyukova, O. V., and Williams-Jones, A.E., 2019a, Closed system fluid-mineral-mediated trace element behaviour in peralkaline rare metal pegmatites: Evidence from Strange Lake: Chemical Geology, v. 505, p. 86–99, doi:10.1016/j.chemgeo.2018.12.023.

Vasyukova, O. V., and Williams-Jones, A.E., 2018, Direct measurement of metal concentrations in fluid inclusions, a tale of hydrothermal alteration and REE ore formation from Strange Lake, Canada: Chemical Geology, v. 483, p. 385–396, doi:10.1016/j.chemgeo.2018.03.003.

Vasyukova, O.V., and Williams-Jones, A.E., 2019b, Tracing the evolution of a fertile REE granite by modelling amphibole-melt partitioning, the Strange Lake story: Chemical Geology, v. 514, p. 79–89, doi:10.1016/j.chemgeo.2019.03.030.

Vasyukova, O. V., Williams-Jones, A.E., and Blamey, N.J.F., 2016, Fluid evolution in the Strange Lake granitic pluton, Canada: Implications for HFSE mobilisation: Chemical Geology, v. 444, p. 83–100, doi:10.1016/j.chemgeo.2016.10.009.

Vilalva, F.C.J., Simonetti, A., and Vlach, S.R.F., 2019, Insights on the origin of the Graciosa A-type granites and syenites (Southern Brazil) from zircon U-Pb geochronology, chemistry, and Hf and O isotope compositions: Lithos, v. 340–341, p. 20–33, doi:10.1016/j.lithos.2019.05.001.

Vilalva, F.C.J., and Vlach, S.R.F., 2014, Geology , petrography and geochemistry of the A-type granites from the Morro Redondo Complex (PR-SC), southern Brazil , Graciosa Province: v. 86, p. 85–116.

Vilalva, F.C.J.J., Vlach, S.R.F.F., and Simonetti, A., 2015, Chemical and O-isotope compositions of amphiboles and clinopyroxenes from A-type granites of the papanduva pluton, South Brazil: Insights into late- to post-magmatic evolution of peralkaline systems: Chemical Geology, v. 420, p. 186–199, doi:10.1016/j.chemgeo.2015.11.019.

Vilalva, F.C.J., Vlach, S.R.F., and Simonetti, A., 2016, Chemical and O-isotope compositions of amphiboles and clinopyroxenes from A-type granites of the Papanduva Pluton, South Brazil: Insights into late- to post-magmatic evolution of peralkaline systems: Chemical Geology, v. 420, p. 186–199, doi:10.1016/j.chemgeo.2015.11.019.

Vilalva, F.C.J., Vlach, S.R.F., and Simonetti, A., 2013, Nacareniobsite-(Ce) and Britholite-(Ce) in peralkaline granites from the Morr Redondo Complex, Graciosa Province, Southern Brazil: Occurrence and Compositional data: The Canadian Mineralogist, v. 51, p. 313–332, doi:10.3749/canmin.51.2.313.

Vlach, S.R.F., 2012, Micro-structural and compositional variations of hydrothermal epidote-group minerals from a peralkaline granite, Corupá Pluton, Graciosa Province, South Brazil, and their petrological implications: Anais da Academia Brasileira de Ciencias, v. 84, p. 407–425, doi:10.1590/S0001-37652012005000024.

Vlach, S.R.F., 2010, Th-U-PbT dating by electron probe microanalysis, part I. monazite: analytical procedures and data treatment: Geologia USP. Série Científica, v. 10, p. 61–85, doi:10.5327/Z1519-874X2010000100006.

Vlach, S.R.F., and Gualda, G. a R., 2007, Allanite and chevkinite in A-type granites and syenites of the Graciosa Province, southern Brazil: Lithos, v. 97, p. 98–121, doi:10.1016/j.lithos.2006.12.003.

Vlach, S.R.F., and Gualda, G.A.R., 2000, Microprobe monazite dating and the ages of some granitic and metamorphic rocks from southeastern Brazil: Revista Brasileira de Geociências, v. 30, p. 214–218.

Vlach, S.R.F., Siga, O., Harara, O.M.M., Gualda, G. a R., Basei, M. a S., and Vilalva, F.C.J., 2011, Crystallization ages of the A-type magmatism of the Graciosa Province (Southern Brazil): Constraints from zircon U-Pb (ID-TIMS) dating of coeval K-rich gabbro-dioritic rocks: Journal of South American Earth Sciences, v. 32, p. 407–415, doi:10.1016/j.jsames.2011.03.017.

Wang, R., 1998, Étude minéralogique et cristallochimique de cassitérite, niobo-tantalates et minéraux disséminés du granite de Beauvoir (Allier); implications métallogéniques.: Paul Sabatier, Toulouse.

Wang, Z., Chen, B., Yan, X., and Li, S., 2018a, Characteristics of hydrothermal chlorite from the Niujuan Ag-Au-Pb-Zn deposit in the north margin of NCC and implications for

exploration tools for ore deposits: Ore Geology Reviews, v. 101, p. 398–412, doi:10.1016/j.oregeorev.2018.08.003.

Wang, R.C., Fontan, F., Xu, S.J., Chen, X.M., and Monchoux, P., 1997, The association of columbite, tantalite and tapiolite in the Suzhou Granite, China: The Canadian Mineralogist, v. 35, p. 699–706.

Wang, X., Griffin, W.L., and Chen, J., 2010, Hf contents and Zr/Hf ratios in granitic zircons: Geochemical Journal, v. 44, p. 65–72, doi:10.2343/geochemj.1.0043.

Wang, L.X., Ma, C.Q., Zhang, C., Zhu, Y.X., and Marks, M.A.W., 2018b, Halogen geochemistry of I- and A-type granites from Jiuhuashan region (South China): Insights into the elevated fluorine in A-type granite: Chemical Geology, v. 478, p. 164–182, doi:10.1016/j.chemgeo.2017.09.033.

Wang, R.C., Zhao, G.T., Lu, J.J., Chen, X.M., Xu, S.J., and Wang, D.Z., 2000, Chemistry of Hf-rich zircons from the Laoshan I- and A-type granites, Eastern China: Mineralogical Magazine, v. 64, p. 867–877, doi:10.1180/002646100549850.

Watson, E.B., and Harrison, T.M., 1983, Zircon saturation revisited: temperature and composition effects in a variety of crustal magma types: Earth and Planetary Science Letters, v. 64, p. 295–304, doi:10.1016/0012-821X(83)90211-X.

Wenger, M., Armbruster, T., and Geiger, C.A., 1991, Cation distribution in partially ordered columbite from the Kings Mountain pegmatite, North Carolina: American Mineralogist, v. 76, p. 1897–1904.

Whalen, J.B., Currie, K.L., and Chappell, B.W., 1987, A-type granites: geochemical characteristics, discrimination and petrogenesis: Contributions to Mineralogy and Petrology, v. 95, p. 407–419, doi:10.1007/BF00402202.

Wise, M.A., Francis, C.A., and Černý, P., 2012, Compositional and structural variations in columbite-group minerals from granitic pegmatites of the Brunswick and Oxford fields, Maine: Differential trends in F-poor and F-rich environments: Canadian Mineralogist, v. 50, p. 1515–1530, doi:10.3749/canmin.50.6.1515.

Wones, D.R., 1981, Mafic Silicates as Indicators of Intensive Variables in Granitic Magmas: Mining Geology, v. 31, p. 191–212, doi:10.11456/shigenchishitsu1951.31.191.

Wones, D.R., and Eugster, H.P., 1965, Stability of biotite: Experiment, theory and application.: The american mineralogist, v. 50, p. 1228–1272.

Wood, B.J., and Blundy, J.D., 1997, A predictive model for rare earth element partitioning between clinopyroxene and anhydrous silicate melt: Contributions to Mineralogy and Petrology, v. 129, p. 166–181, doi:10.1007/s004100050330.

Wood, B., and Blundy, J.D., 2014, Trace Element Partitioning: The Influences of Ionic Radius, Cation Charge, Pressure, and Temperature, *in* Treatise on Geochemistry: Second Edition, Elsevier Ltd., v. 3, p. 327–353, doi:10.1016/B978-0-08-095975-7.00206-0.

Xie, X., Byerly, G.R., and Ferrell, R.E., 1997, IIb trioctahedral chlorite from the Barberton greenstone belt: Crystal structure and rock composition constraints with implications to geothermometry: Contributions to Mineralogy and Petrology, v. 126, p. 275–291, doi:10.1007/s004100050250.

Xie, L., Wang, R.C., Che, X.D., Huang, F.F., Erdmann, S., and Zhang, W.L., 2016, Tracking magmatic and hydrothermal Nb-Ta-W-Sn fractionation using mineral textures and composition: A case study from the late Cretaceous Jiepailing ore district in the Nanling Range in South China: Ore Geology Reviews, v. 78, p. 300–321, doi:10.1016/j.oregeorev.2016.04.003.

Xie, L., Wang, Z., Wang, R.-C., Zhu, J.C., Che, X., Gao, J., and Zhao, X., 2018a, Mineralogical constraints on the genesis of W-Nb-Ta mineralization in the Laiziling granite (Xianghualing distric, sout China): Ore Geology Reviews, v. 95, p. 695–712, doi:.1037//0033-2909.I26.1.78.

Xie, L., Wang, Z., Wang, R., Zhu, J., Che, X., Gao, J., and Zhao, X., 2018b, Mineralogical constraints on the genesis of W–Nb–Ta mineralization in the Laiziling granite (Xianghualing district, south China): Ore Geology Reviews, v. 95, p. 695–712, doi:10.1016/j.oregeorev.2018.03.021.

Xu, X.S., Zhang, M., Zhu, K.Y., Chen, X.M., and He, Z.Y., 2012, Reverse age zonation of zircon formed by metamictisation and hydrothermal fluid leaching: Lithos, v. 150, p. 256–267, doi:10.1016/j.lithos.2011.12.014.

Yang, W. Bin, Niu, H.C., Shan, Q., Sun, W.D., Zhang, H., Li, N.B., Jiang, Y.H., and Yu, X.Y., 2014, Geochemistry of magmatic and hydrothermal zircon from the highly evolved Baerzhe alkaline granite: Implications for Zr-REE-Nb mineralization: Mineralium Deposita, v. 49, p. 451–470, doi:10.1007/s00126-013-0504-1.

Yavuz, F., Kumral, M., Karakaya, N., Karakaya, M.T., and Yildirim, D.K., 2015, A Windows

program for chlorite calculation and classification: Computers and Geosciences, v. 81, p. 101–113, doi:10.1016/j.cageo.2015.04.011.

Yin, R., Wang, R.C., Zhang, A.C., Hu, H., Zhu, J.C., Rao, C., and Zhang, H., 2012, Extreme fractionation from zircon to hafnon in the Koktokay No. 1 granitic pegmatite, Altai, northwestern China: American Mineralogist, v. 98, p. 1714–1724, doi:10.2138/am.2013.4494.

Žáček, V., Buriánek, D., Pécskay, Z., and Škoda, R., 2016, Astrophyllite – alkali amphibole rhyolite , an evidence of early Permian A-type alkaline volcanism in the western Mongolian Altai: Journal of Geosciences (Czech Republic), v. 61, p. 93–103, doi:10.3190/jgeosci.205.

Zane, A., Sassi, R., and Guidotti, C. V., 1998, New data on metamorphic chlorite as a petrogenetic indicator mineral, with special regard to greenschist-facies rocks: Canadian Mineralogist, v. 36, p. 713–726.

Zang, W., and Fyfe, W.S., 1995, Chloritization of the hydrothermally altered bedrock at the Igarap?? Bahia gold deposit, Caraj??s, Brazil: Mineralium Deposita, v. 30, p. 30–38, doi:10.1007/BF00208874.

Zaraisky, G.P., Aksyuk, A.M., Devyatova, V.N., Udoratina, O. V., and Chevychelov, V.Y., 2008, Zr/Hf ratio as an indicator of fractionation of rare-metal granites by the example of the Kukulbei complex, eastern Transbaikalia: Petrology, v. 16, p. 710–736, doi:10.1134/s0869591108070047.

Zaraisky, G.P., Korzhinskaya, V., and Kotova, N., 2010, Experimental studies of Ta2O5 and columbite-tantalite solubility in fluoride solutions from 300 to 550°C and 50 to 100 MPa: Mineralogy and Petrology, v. 99, p. 287–300, doi:10.1007/s00710-010-0112-z.

Zhang, W., Lentz, D.R., Thorne, K.G., and Mcfarlane, C., 2016, Geochemical characteristics of biotite from felsic intrusive rocks around the Sisson Brook W – Mo – Cu deposit , west-central New Brunswick : An indicator of halogen and oxygen fugacity of magmatic systems: Ore Geology Reviews, v. 77, p. 82–96, doi:10.1016/j.oregeorev.2016.02.004.

Zhu, Z.Y., Wang, R.C., Che, X.D., Zhu, J.C., Wei, X.L., and Huang, X., 2015, Magmatic-hydrothermal rare-element mineralization in the Songshugang granite (northeastern Jiangxi, China): Insights from an electron-microprobe study of Nb-Ta-Zr minerals: Ore Geology Reviews, v. 65, p. 749–760, doi:10.1016/j.oregeorev.2014.07.021.

Zimak, J., 1999, Application of chlorite compositional geothermometres to hydrothermal veins in the variscan flysch sequences of the Nizky Jesenik upland, to alpine-type veins in te Sobotin region, and to the paragenesis with "'strigovite'" from Zulova Massif and Strezego: Acta Universitatis Palackianae Olomucenis, v. Geologica, p. 69–73.

APPENDIX A: ELECTRON MICROPROBE ANALYSIS AND STRUCTURAL FORMULAE OF MINERALS

Table 1: Sodic amphiboles in peralkaline alkali feldspar granites from the Mandira unit

Sample	**MAN-13A**													**MAN-13A2**		
Crystal	c9							c4						c11	c20	c21
Point_ID	1-c	2-c	3-i	4-ir	5-r	6-ir	7-r	8-c	9-i	10-i	11-r	12-r	8-r	11	20	21
SiO_2 (wt%)	50.07	50.29	50.22	50.60	50.06	50.46	50.66	49.62	49.74	49.52	49.77	49.98	50.86	49.96	50.15	51.19
TiO_2	0.57	0.57	0.52	0.45	0.11	0.74	0.71	0.88	0.59	0.82	0.90	0.09	0.62	1.00	0.38	0.10
Al_2O_3	1.28	1.28	1.13	0.98	1.45	1.00	0.86	0.92	1.22	0.96	0.91	1.21	0.84	0.93	0.85	1.21
FeO	35.50	34.57	35.58	35.00	34.94	34.36	33.91	33.17	33.23	33.12	33.14	33.59	34.07	34.58	35.28	35.60
MnO	0.35	0.29	0.32	0.33	0.36	0.42	0.32	0.42	0.26	0.37	0.33	0.29	0.38	0.36	0.32	0.34
MgO	0.02	0.03	0.03	0.02	0.03	0.02	0.05	0.04	0.03	0.03	0.02	0.02	0.04	0.05	0.00	0.03
CaO	0.22	0.41	0.19	0.72	0.01	0.14	0.06	0.16	0.08	0.08	0.13	0.01	0.10	0.18	0.02	0.00
ZrO_2	0.41	0.13	-	0.16	0.00	0.23	0.12	0.27	0.23	0.19	0.22	-	-	-	-	-
ZnO	0.39	0.41	0.37	0.47	0.50	0.49	0.33	0.58	0.49	0.40	0.38	0.36	-	-	-	-
Na_2O	7.16	7.21	7.04	6.92	7.23	7.38	7.28	7.36	7.14	7.08	7.21	7.36	7.00	7.09	7.17	7.06
K_2O	1.11	1.10	1.34	0.89	1.20	1.16	1.24	1.19	1.13	1.20	1.08	0.89	1.25	1.18	1.15	1.06
F	0.73	1.01	1.10	1.23	0.81	1.25	1.00	0.99	1.02	1.02	0.75	0.62	1.25	1.15	0.93	0.81
Cl	-	-	-	-	-	-	-	-	-	-	-	-	-	-	-	-
Li_2O*	0.40	0.42	0.36	0.36	0.36	0.41	0.41	0.43	0.46	0.36	0.41	0.36	0.47	0.47	0.34	0.36
O=F=Cl	0.31	0.43	0.46	0.52	0.34	0.53	0.42	0.42	0.43	0.43	0.32	0.26	0.53	0.49	0.40	0.34
Total	97.90	97.29	97.74	97.61	96.74	97.56	96.53	95.62	95.21	94.74	94.94	94.51	96.36	96.47	96.21	97.42
Parameters (in apfu)																
NF (Max)	8SiAl	13eCNK	13eCNK	13eCNK	13eCNK	13eCNK	13eCNK	13eCNK	13eCNK	13eCNK	13eCNK	13eCNK	13eCNK	8SiAl	13eCNK	13eCNK
Fe#	0.999	0.999	0.999	0.999	0.998	0.999	0.997	0.998	0.998	0.998	0.999	0.999	0.998	0.997	1.000	0.999
^{A}[Na+K+2Ca]	0.453	0.462	0.417	0.385	0.430	0.482	0.473	0.538	0.438	0.459	0.470	0.458	0.390	0.425	0.422	0.321
^{C}[Al+Fe^{3+}+2Ti]	1.885	1.879	1.978	1.821	1.977	1.855	1.809	1.782	1.923	1.797	1.804	1.803	1.927	2.004	1.893	2.001
Ca^{2+} + Al^{IV}	0.271	0.236	0.234	0.244	0.185	0.162	0.062	0.143	0.129	0.083	0.090	0.033	0.057	0.201	0.108	0.100
Si + Na + K	10.138	10.226	10.183	10.141	10.245	10.320	10.410	10.396	10.309	10.376	10.380	10.425	10.333	10.219	10.314	10.221
[Na+K]/Al	10.135	10.195	11.537	12.606	9.088	13.370	15.417	14.588	10.660	13.428	14.351	10.845	15.376	13.976	15.378	10.579
$Fe^{3+}/(Fe^{3+}+Fe^{2+})$	0.380	0.373	0.401	0.365	0.409	0.365	0.345	0.344	0.379	0.335	0.336	0.354	0.374	0.390	0.377	0.405

Point_ID: spot identification; c: core; r: rim; i: intermediate zone; - : below detection limit; *Li2O contents derived from the LA-ICP-MS analyses; na: not analyzed; NF(Max): Normalization factor according to the method of Schumacher (in Leake et al., 1997) for maximum Fe^{3+}; Fe# =[Fe_T/(Fe_T+Mg)]

Table 1. (*cont.*) Sodic amphiboles in peralkaline alkali feldspar granites from the Mandira unit

Sample	**MAN-13A**													**MAN-13A2**		
Crystal	c9							c4						c11	c20	c21
Point_ID	1-c	2-c	3-i	4-ir	5-r	6-ir	7-r	8-c	9-i	10-i	11-r	12-r	8-r	11	20	21
Structural formulae based on 23 oxygens																
Si (apfu)	7.766	7.832	7.798	7.875	7.817	7.861	7.948	7.885	7.885	7.931	7.932	7.968	7.959	7.829	7.896	7.900
Al^{IV}	0.234	0.168	0.202	0.125	0.183	0.139	0.052	0.115	0.115	0.069	0.068	0.032	0.041	0.171	0.104	0.100
Ti	0.000	0.000	0.000	0.000	0.000	0.000	0.000	0.000	0.000	0.000	0.000	0.000	0.000	0.000	0.000	0.000
T-site	**8.000**	**8.000**	**8.000**	**8.000**	**8.000**	**8.000**	**8.000**	**8.000**	**8.000**	**8.000**	**8.000**	**8.000**	**8.000**	**8.000**	**8.000**	**8.000**
Al^{VI}	0.000	0.067	0.004	0.055	0.084	0.045	0.108	0.057	0.112	0.113	0.102	0.195	0.114	0.000	0.053	0.120
Ti	0.066	0.067	0.060	0.052	0.013	0.087	0.084	0.105	0.071	0.099	0.108	0.011	0.072	0.118	0.045	0.011
Fe^{3+}	1.752	1.678	1.853	1.661	1.867	1.635	1.534	1.515	1.670	1.487	1.486	1.587	1.668	1.769	1.749	1.859
Zr	0.031	0.010	0.000	0.012	0.000	0.018	0.009	0.021	0.018	0.015	0.017	0.000	0.000	0.000	0.000	0.000
Zn	0.045	0.047	0.043	0.054	0.058	0.057	0.038	0.068	0.058	0.048	0.045	0.042	0.000	0.000	0.000	0.000
Mg	0.005	0.006	0.006	0.004	0.008	0.005	0.012	0.009	0.007	0.007	0.004	0.004	0.010	0.012	0.000	0.006
Li	0.203	0.261	0.225	0.225	0.226	0.256	0.258	0.275	0.295	0.232	0.262	0.231	0.293	0.289	0.214	0.223
Fe^{2+}	2.853	2.825	2.766	2.894	2.696	2.841	2.915	2.894	2.735	2.950	2.931	2.893	2.791	2.763	2.896	2.735
Mn	0.046	0.038	0.043	0.043	0.048	0.056	0.043	0.056	0.035	0.050	0.045	0.039	0.051	0.048	0.042	0.044
C-site	**5.000**	**5.000**	**5.000**	**5.000**	**5.000**	**5.000**	**5.000**	**5.000**	**5.000**	**5.000**	**5.000**	**5.000**	**5.000**	**5.000**	**5.000**	**5.000**
Li	0.044	0.000	0.000	0.000	0.000	0.000	0.000	0.000	0.000	0.000	0.000	0.000	0.000	0.005	0.000	0.000
Mn	0.000	0.000	0.000	0.000	0.000	0.000	0.000	0.000	0.000	0.000	0.000	0.000	0.000	0.000	0.000	0.000
Fe^{2+}	0.000	0.000	0.000	0.000	0.000	0.000	0.000	0.000	0.000	0.000	0.000	0.000	0.000	0.000	0.000	0.000
Ca	0.037	0.068	0.032	0.119	0.002	0.023	0.010	0.028	0.013	0.014	0.022	0.001	0.017	0.030	0.003	0.000
Na	1.919	1.932	1.968	1.881	1.998	1.977	1.990	1.972	1.987	1.986	1.978	1.999	1.983	1.965	1.997	2.000
B-site	**2.000**	**2.000**	**2.000**	**2.000**	**2.000**	**2.000**	**2.000**	**2.000**	**2.000**	**2.000**	**2.000**	**2.000**	**2.000**	**2.000**	**2.000**	**2.000**
Na	0.234	0.244	0.151	0.209	0.191	0.251	0.225	0.296	0.208	0.213	0.250	0.276	0.140	0.189	0.192	0.112
K	0.220	0.219	0.266	0.177	0.239	0.231	0.247	0.242	0.229	0.245	0.220	0.182	0.250	0.236	0.230	0.209
A-site	**0.453**	**0.462**	**0.417**	**0.385**	**0.430**	**0.482**	**0.473**	**0.538**	**0.438**	**0.459**	**0.470**	**0.458**	**0.390**	**0.425**	**0.422**	**0.321**
F	0.359	0.498	0.538	0.607	0.401	0.618	0.494	0.496	0.511	0.518	0.377	0.312	0.619	0.570	0.464	0.396
Cl	0.000	0.000	0.000	0.004	0.000	0.002	0.002	0.003	0.000	0.001	0.001	0.000	0.004	0.002	0.005	0.001
Cations	15.453	15.462	15.417	15.385	15.430	15.482	15.473	15.538	15.438	15.459	15.470	15.458	15.390	15.425	15.422	15.321

Table 2: Sodic amphiboles in peralkaline alkali feldspar granites from the Mandira unit

Sample	**MAN-13B**										**MAN-17A**					
Crystal	c1						c2				c5					
Point_ID	1-c	2-c	3-ri	4-r	5-ci	6-r	1-c	2-i	3-r	4-r	1-r	2-r	3-r	4-r	5-i	6-ci
SiO_2 (wt%)	50.43	50.10	49.25	51.08	49.20	51.36	50.97	51.04	50.62	50.89	50.67	51.88	51.21	51.18	50.32	50.27
TiO_2	0.41	0.37	0.48	0.01	0.77	0.00	0.07	0.02	0.02	0.06	0.11	0.00	0.03	0.14	0.78	0.84
Al_2O_3	1.24	1.06	1.38	0.82	1.25	0.79	1.25	1.28	0.97	1.01	1.06	0.43	0.38	0.53	0.92	0.94
FeO	35.21	35.37	34.99	35.13	35.56	36.37	36.12	36.37	35.55	36.33	34.16	36.35	36.19	35.35	33.17	34.20
MnO	0.47	0.39	0.36	0.43	0.42	0.27	0.42	0.46	0.35	0.37	0.28	0.21	0.32	0.35	0.37	0.48
MgO	0.00	0.04	0.04	0.01	0.03	0.01	0.01	0.01	0.02	0.01	0.04	0.02	0.03	0.03	0.05	0.07
CaO	0.78	1.14	0.71	0.01	0.97	0.02	0.01	0.03	0.00	0.02	0.02	0.03	0.00	0.00	0.17	0.26
ZrO_2	0.07	0.07	0.05	0.03	0.02	-	0.03	-	-	-	-	-	-	0.42	0.21	0.16
ZnO	0.39	0.40	0.27	0.35	0.36	0.37	0.40	0.32	0.28	0.24	0.43	0.30	0.43	0.42	0.55	0.45
Na_2O	6.61	6.69	6.72	6.89	6.52	6.89	6.91	6.86	6.69	6.62	7.14	7.15	6.91	7.01	7.26	7.25
K_2O	0.72	0.64	0.72	0.26	0.76	0.23	0.49	0.46	0.43	0.43	0.58	0.24	0.17	0.91	1.23	1.18
F	0.93	0.91	0.69	0.31	1.10	0.23	0.43	0.39	0.37	0.21	1.05	0.44	0.60	0.92	1.29	1.60
Cl	-	-	-	-	-	-	-	-	-	-	0.04	-	-	-	-	-
Li_2O*				0.36		0.36			0.36		0.36	0.36	0.36	0.36	0.41	0.41
O=F=Cl	0.39	0.38	0.29	0.13	0.46	0.10	0.18	0.17	0.15	0.09	0.45	0.18	0.25	0.39	0.54	0.68
Total	96.89	96.79	95.39	95.56	96.50	96.80	96.94	97.09	95.51	96.08	95.49	97.22	96.36	97.23	96.19	97.45
Parameters (in apfu)																
NF (Max)	13eCNK	13eCNK	13eCNK	13eCNK	13eCNK	13eCNK	13eCNK	13eCNK	13eCNK	13eCNK·C	13eCNK	13eCNK	8SiAl	13eCNK	13eCNK	13eCNK
Fe#	1.000	0.998	0.998	0.999	0.998	1.000	0.999	1.000	0.999	1.000	0.998	0.999	0.999	0.999	0.997	0.997
^{A}[Na+K+2Ca]	0.298	0.380	0.357	0.130	0.335	0.097	0.188	0.164	0.107	0.098	0.296	0.179	0.119	0.288	0.498	0.474
^{C}[Al+Fe^{3+}+2Ti]	1.600	1.465	1.618	2.140	1.664	2.234	1.860	1.895	2.236	1.928	1.955	2.071	2.163	1.929	1.748	1.859
Ca^{2+} + Al^{IV}	0.174	0.244	0.228	0.053	0.333	0.117	0.056	0.071	0.118	0.032	0.031	0.039	0.069	0.057	0.077	0.186
Si + Na + K	10.124	10.137	10.129	10.077	10.001	9.980	10.132	10.094	9.988	10.066	10.265	10.141	10.039	10.231	10.422	10.289
[Na+K]/Al	9.370	11.071	8.541	14.128	9.285	14.688	9.521	9.217	11.830	11.264	11.628	27.977	30.385	23.742	14.465	14.005
$Fe^{3+}/(Fe^{3+}+Fe^{2+})$	0.283	0.262	0.287	0.446	0.299	0.472	0.354	0.364	0.469	0.369	0.392	0.434	0.460	0.405	0.329	0.365

Point_ID: spot identification; c: core; r: rim; i: intermediate zone; - : below detection limit; *Li2O contents derived from the LA-ICP-MS analyses; na: not analyzed; NF(Max): Normalization factor according to the method of Schumacher (in Leake et al., 1997) for maximum Fe^{3+}; Fe# =[Fe_T/(Fe_T+Mg)]

Table 2. (*cont.*) Sodic amphiboles in peralkaline alkali feldspar granites from the Mandira unit

Sample	**MAN-13B**										**MAN-17A**					
Crystal	c1						c2				c5					
Point_ID	1-c	2-c	3-ri	4-r	5-ci	6-r	1-c	2-i	3-r	4-r	1-r	2-r	3-r	4-r	5-i	6-ci
Structural formulae based on 23 oxygens																
Si (apfu)	7.958	7.950	7.895	7.949	7.832	7.886	7.946	7.935	7.882	7.971	7.972	7.966	7.931	7.943	7.952	7.857
Al^{IV}	0.042	0.050	0.105	0.051	0.168	0.114	0.054	0.065	0.118	0.029	0.028	0.034	0.069	0.057	0.048	0.143
Ti	0.000	0.000	0.000	0.000	0.000	0.000	0.000	0.000	0.000	0.000	0.000	0.000	0.000	0.000	0.000	0.000
T-site	**8.000**	**8.000**	**8.000**	**8.000**	**8.000**	**8.000**	**8.000**	**8.000**	**8.000**	**8.000**	**8.000**	**8.000**	**8.000**	**8.000**	**8.000**	**8.000**
Al^{VI}	0.189	0.148	0.156	0.099	0.066	0.029	0.176	0.169	0.060	0.157	0.169	0.044	0.000	0.039	0.122	0.031
Ti	0.049	0.044	0.058	0.001	0.092	0.000	0.008	0.003	0.003	0.007	0.013	0.000	0.003	0.016	0.092	0.099
Fe^{3+}	1.313	1.229	1.345	2.038	1.414	2.206	1.668	1.721	2.170	1.758	1.761	2.027	2.157	1.857	1.442	1.630
Zr	0.006	0.005	0.004	0.002	0.002	0.000	0.002	0.000	0.000	0.000	0.001	0.000	0.000	0.032	0.016	0.012
Zn	0.046	0.046	0.032	0.041	0.042	0.042	0.046	0.037	0.032	0.027	0.050	0.034	0.049	0.048	0.064	0.052
Mg	0.001	0.009	0.010	0.003	0.007	0.002	0.003	0.002	0.004	0.002	0.008	0.004	0.006	0.006	0.011	0.015
Li	0.000	0.000	0.000	0.225	0.000	0.222	0.000	0.000	0.225	0.000	0.228	0.222	0.213	0.224	0.260	0.257
Fe^{2+}	3.333	3.466	3.345	2.535	3.321	2.465	3.042	3.008	2.459	3.001	2.733	2.640	2.530	2.731	2.942	2.840
Mn	0.063	0.052	0.049	0.056	0.056	0.035	0.056	0.060	0.046	0.049	0.038	0.028	0.042	0.046	0.050	0.064
C-site	**5.000**	**5.000**	**5.000**	**5.000**	**5.000**	**5.000**	**5.000**	**5.000**	**5.000**	**5.000**	**5.000**	**5.000**	**5.000**	**5.000**	**5.000**	**5.000**
Li	0.000	0.000	0.000	0.000	0.000	0.000	0.000	0.000	0.000	0.000	0.000	0.000	0.011	0.000	0.000	0.000
Mn	0.000	0.000	0.000	0.000	0.000	0.000	0.000	0.000	0.000	0.000	0.000	0.000	0.000	0.000	0.000	0.000
Fe^{2+}	0.000	0.000	0.000	0.000	0.000	0.000	0.000	0.000	0.000	0.000	0.000	0.000	0.000	0.000	0.000	0.000
Ca	0.132	0.194	0.122	0.002	0.166	0.003	0.002	0.005	0.000	0.003	0.003	0.005	0.000	0.000	0.028	0.043
Na	1.868	1.806	1.878	1.998	1.834	1.997	1.998	1.995	2.000	1.997	1.997	1.995	1.989	2.000	1.972	1.957
B-site	**2.000**	**2.000**	**2.000**	**2.000**	**2.000**	**2.000**	**2.000**	**2.000**	**2.000**	**2.000**	**2.000**	**2.000**	**2.000**	**2.000**	**2.000**	**2.000**
Na	0.153	0.252	0.210	0.079	0.180	0.053	0.090	0.073	0.021	0.012	0.179	0.133	0.087	0.108	0.251	0.238
K	0.145	0.129	0.147	0.051	0.155	0.044	0.098	0.092	0.086	0.086	0.117	0.046	0.033	0.180	0.247	0.236
A-site	**0.298**	**0.380**	**0.357**	**0.130**	**0.335**	**0.097**	**0.188**	**0.164**	**0.107**	**0.098**	**0.296**	**0.179**	**0.119**	**0.288**	**0.498**	**0.474**
F	0.464	0.454	0.348	0.153	0.554	0.112	0.211	0.194	0.180	0.105	0.523	0.212	0.294	0.450	0.643	0.793
Cl	0.000	0.004	0.002	0.002	0.002	0.000	0.000	0.004	0.001	0.000	0.011	0.000	0.000	0.002	0.003	0.003
Cations	15.298	15.380	15.357	15.130	15.335	15.097	15.188	15.164	15.107	15.098	15.296	15.179	15.119	15.288	15.498	15.474

Table 3: Sodic amphiboles in peralkaline alkali feldspar granites from the Mandira unit

Sample	**MAN-17A**					**MAN-19**										
Crystal						c1		c2			c3			c5		c6
Point_ID	7-ci	8-ci	9-ci	10-ci	11-ci	1-c	1-r	2-r	2-c	2-r2	3-r1	3-c	3-r2	5-c	5-r	6-c
SiO_2 (wt%)	50.39	48.15	49.69	49.20	49.94	50.59	50.65	50.71	50.70	50.96	50.61	51.01	50.49	50.29	51.42	50.51
TiO_2	0.66	1.02	0.65	1.22	0.33	0.37	0.48	0.37	0.30	0.22	0.34	0.30	0.32	0.33	0.05	0.13
Al_2O_3	1.00	1.13	1.04	1.12	0.91	1.47	1.36	1.32	1.20	1.45	1.22	1.29	1.40	1.39	1.13	1.50
FeO	34.99	34.41	33.42	35.02	35.10	35.53	35.72	35.67	36.20	36.16	35.54	35.32	35.20	36.18	36.15	35.83
MnO	0.35	0.43	0.37	0.49	0.38	0.52	0.47	0.65	0.65	0.54	0.57	0.60	0.70	0.46	0.46	0.47
MgO	0.06	0.04	0.05	0.04	0.04	0.03	0.03	0.04	0.06	0.03	0.07	0.06	0.06	0.04	0.02	0.01
CaO	0.14	1.55	0.97	0.89	0.22	0.04	0.04	0.16	0.19	0.04	0.09	0.10	0.10	0.10	0.01	0.05
ZrO_2	0.30	0.14	0.29	0.02	0.20	-	0.06	-	0.04	0.08	-	-	0.03	0.02	-	0.02
ZnO	0.53	0.43	0.34	0.37	0.41	0.44	0.49	0.44	0.33	0.57	0.45	0.33	0.35	0.40	0.43	0.36
Na_2O	6.97	7.03	7.12	6.79	7.17	6.88	6.71	7.13	6.96	6.88	6.72	6.93	7.03	6.91	6.88	6.81
K_2O	1.30	0.88	0.94	0.84	0.91	1.10	0.98	0.95	1.08	0.78	1.11	1.17	1.23	0.95	0.52	0.76
F	1.07	1.85	1.24	1.04	0.86	0.63	0.46	0.64	0.59	0.46	0.51	0.60	0.73	0.57	0.47	0.37
Cl	-	|	-	-	-	0.02	0.02	0.03	0.02	-	-	-	-	0.03	0.02	-
Li_2O*	0.36	0.41	0.41	0.36	0.36	0.36	0.36	0.36	0.36	0.36	0.36	0.36	0.36	0.36	0.36	0.36
O=F=Cl	0.45	0.79	0.52	0.44	0.36	0.27	0.20	0.28	0.25	0.20	0.22	0.25	0.31	0.25	0.20	0.16
Total	97.67	96.69	96.03	96.96	96.47	97.73	97.63	98.20	98.43	98.35	97.39	97.83	97.68	97.78	97.71	97.03
Parameters (in apfu)																
NF (Max)	13eCNK	8SiAl	13eCNK	8SiAl	13eCNK	13eCNK	13eCNK	8SiAl	13eCNK	13eCNK	13eCNK	13eCNK	13eCNK	8SiAl	13eCNK	13eCNK
Fe#	0.997	0.998	0.997	0.998	0.998	0.998	0.998	0.998	0.997	0.998	0.996	0.997	0.997	0.998	0.999	0.99947
^{A}[Na+K+2Ca]	0.379	0.824	0.550	0.535	0.402	0.273	0.193	0.333	0.358	0.186	0.240	0.312	0.363	0.305	0.137	0.18899
^{C}[Al+Fe^{3+}+2Ti]	1.950	1.196	1.603	1.617	1.920	2.166	2.245	2.085	2.003	2.267	2.173	2.052	2.044	2.112	2.238	2.24989
Ca^{2+} + Al^{IV}	0.197	0.484	0.268	0.361	0.201	0.232	0.240	0.249	0.250	0.258	0.219	0.177	0.222	0.269	0.156	0.23608
Si + Na + K	10.182	10.169	10.282	10.043	10.202	10.041	9.953	10.084	10.066	9.929	10.021	10.135	10.141	9.998	9.980	9.95291
[Na+K]/Al	12.860	11.066	12.249	10.775	14.017	8.489	8.921	9.632	10.491	8.366	10.034	9.816	9.239	8.920	10.468	7.99266
$Fe^{3+}/(Fe^{3+}+Fe^{2+})$	0.393	0.204	0.305	0.286	0.399	0.446	0.463	0.433	0.416	0.480	0.454	0.421	0.423	0.437	0.472	0.47147

Point_ID: spot identification; c: core; r: rim; i: intermediate zone; - : below detection limit; *Li2O contents derived from the LA-ICP-MS analyses; na: not analyzed; NF(Max): Normalization factor according to the method of Schumacher (in Leake et al., 1997) for maximum Fe^{3+}; Fe# =[Fe_T/(Fe_T+Mg)]

Table 3. (*cont.*) Sodic amphiboles in peralkaline alkali feldspar granites from the Mandira unit

Sample	**MAN-17A**					**MAN-19**										
Crystal						c1		c2			c3			c5		c6
Point_ID	7-ci	8-ci	9-ci	10-ci	11-ci	1-c	1-r	2-r	2-c	2-r2	3-r1	3-c	3-r2	5-c	5-r	6-c
Structural formulae based on 23 oxygens																
Si (apfu)	7.826	7.785	7.898	7.791	7.837	7.775	7.767	7.777	7.782	7.749	7.795	7.840	7.795	7.748	7.845	7.772
Al^{IV}	0.174	0.215	0.102	0.209	0.163	0.225	0.233	0.223	0.218	0.251	0.205	0.160	0.205	0.252	0.155	0.228
Ti	0.000	0.000	0.000	0.000	0.000	0.000	0.000	0.000	0.000	0.000	0.000	0.000	0.000	0.000	0.000	0.000
T-site	**8.000**	**8.000**	**8.000**	**8.000**	**8.000**	**8.000**	**8.000**	**8.000**	**8.000**	**8.000**	**8.000**	**8.000**	**8.000**	**8.000**	**8.000**	**8.000**
Al^{VI}	0.010	0.000	0.093	0.000	0.006	0.042	0.012	0.017	0.000	0.009	0.017	0.074	0.049	0.000	0.049	0.045
Ti	0.077	0.124	0.078	0.146	0.039	0.043	0.056	0.043	0.034	0.026	0.039	0.035	0.037	0.038	0.005	0.015
Fe^{3+}	1.786	0.948	1.354	1.326	1.836	2.039	2.121	1.983	1.934	2.206	2.078	1.909	1.922	2.036	2.178	2.174
Zr	0.023	0.011	0.022	0.002	0.015	0.001	0.004	0.000	0.003	0.006	0.000	0.001	0.002	0.002	0.000	0.001
Zn	0.061	0.051	0.040	0.043	0.047	0.050	0.056	0.049	0.037	0.064	0.051	0.038	0.040	0.045	0.048	0.041
Mg	0.013	0.009	0.013	0.008	0.009	0.008	0.008	0.010	0.014	0.008	0.017	0.013	0.013	0.008	0.005	0.002
Li	0.225	0.095	0.261	0.098	0.227	0.222	0.222	0.222	0.180	0.220	0.223	0.222	0.223	0.185	0.221	0.223
Fe^{2+}	2.759	3.703	3.089	3.311	2.770	2.528	2.460	2.592	2.713	2.392	2.500	2.631	2.623	2.626	2.434	2.437
Mn	0.047	0.058	0.050	0.066	0.051	0.068	0.061	0.085	0.085	0.070	0.075	0.078	0.091	0.060	0.060	0.061
C-site	**5.000**	**5.000**	**5.000**	**5.000**	**5.000**	**5.000**	**5.000**	**5.000**	**5.000**	**5.000**	**5.000**	**5.000**	**5.000**	**5.000**	**5.000**	**5.000**
Li	0.000	0.171	0.000	0.131	0.000	0.000	0.000	0.000	0.042	0.000	0.000	0.000	0.000	0.038	0.000	0.000
Mn	0.000	0.000	0.000	0.000	0.000	0.000	0.000	0.000	0.000	0.000	0.000	0.000	0.000	0.000	0.000	0.000
Fe^{2+}	0.000	0.000	0.000	0.000	0.000	0.000	0.000	0.000	0.000	0.000	0.000	0.000	0.000	0.000	0.000	0.000
Ca	0.023	0.268	0.166	0.152	0.038	0.007	0.007	0.027	0.032	0.006	0.015	0.017	0.017	0.017	0.001	0.009
Na	1.977	1.561	1.834	1.717	1.962	1.993	1.993	1.973	1.926	1.994	1.985	1.983	1.983	1.945	1.999	1.991
B-site	**2.000**	**2.000**	**2.000**	**2.000**	**2.000**	**2.000**	**2.000**	**2.000**	**2.000**	**2.000**	**2.000**	**2.000**	**2.000**	**2.000**	**2.000**	**2.000**
Na	0.122	0.642	0.360	0.366	0.220	0.057	0.002	0.147	0.145	0.035	0.021	0.082	0.121	0.118	0.036	0.040
K	0.257	0.182	0.190	0.169	0.183	0.216	0.191	0.186	0.212	0.152	0.218	0.230	0.242	0.187	0.101	0.149
A-site	**0.379**	**0.824**	**0.550**	**0.535**	**0.402**	**0.273**	**0.193**	**0.333**	**0.358**	**0.186**	**0.240**	**0.312**	**0.363**	**0.305**	**0.137**	**0.189**
F	0.526	0.948	0.622	0.520	0.425	0.307	0.222	0.310	0.286	0.223	0.248	0.290	0.357	0.276	0.224	0.182
Cl	0.001	0.006	0.002	0.002	0.001	0.004	0.005	0.008	0.005	0.000	0.004	0.000	0.000	0.008	0.004	0.000
Cations	15.379	15.824	15.550	15.535	15.402	15.273	15.193	15.333	15.358	15.186	15.240	15.312	15.363	15.305	15.137	15.189

Table 4: Sodic amphiboles in peralkaline alkali feldspar granites from the Mandira unit

Sample	**MAN-4621**			**MAN-4776**								**MAN-4777**				
Crystal	c1			c1		c2		c3	c6	c5		c6				
Point_ID	1-r1	1-c	1-r2	1-r1	1-r2	2-c	2-r	3-c	6-c	5-r1	5-r2	6-r2	6-i2	6-c	6-i1	6-r1
SiO_2 (wt%)	50.37	51.03	51.02	50.89	49.70	50.41	51.31	50.96	51.02	48.88	51.11	49.71	49.26	49.35	50.40	49.88
TiO_2	0.56	0.01	0.33	0.91	0.66	0.64	0.65	0.68	0.49	0.37	0.81	0.75	0.27	0.33	0.13	0.50
Al_2O_3	1.31	1.44	1.32	1.06	1.10	1.35	0.99	1.23	1.08	1.14	1.06	1.25	1.47	1.97	0.99	1.55
FeO	35.04	36.02	36.06	34.40	34.50	34.58	35.03	34.50	34.83	34.04	34.68	33.79	35.20	34.41	34.62	33.11
MnO	0.58	0.55	0.56	0.35	0.36	0.38	0.35	0.34	0.37	0.35	0.34	0.28	0.25	0.21	0.28	0.28
MgO	0.06	0.05	0.07	0.04	0.01	0.03	0.03	0.01	0.01	0.02	0.01	0.03	0.01	0.06	0.02	0.03
CaO	0.07	0.04	0.07	0.25	1.11	0.98	0.09	0.37	0.15	1.05	0.32	1.48	1.02	0.66	0.85	0.68
ZrO_2	0.34	0.08	0.04	0.09	0.08	-	0.08	0.06	0.06	0.05	0.05	na	na	na	na	na
ZnO	0.28	0.40	0.38	0.36	0.36	0.36	0.35	0.35	0.36	0.49	0.51	0.37	0.41	0.42	0.29	0.37
Na_2O	6.79	6.98	6.97	6.94	7.04	7.05	6.92	7.04	6.97	6.84	7.02	7.25	7.30	7.29	7.19	7.22
K_2O	1.10	0.89	0.99	1.30	1.12	0.97	1.18	1.18	1.01	0.98	1.00	0.87	0.99	1.05	0.83	1.15
F	0.65	0.40	0.64	0.80	1.06	1.03	0.64	0.84	0.79	1.32	0.67	1.09	0.82	0.87	0.98	0.55
Cl	-	0.02	-	-	-	-	-	0.02	0.02	0.03	-	0.02	0.04	0.04	-	0.02
Li_2O*	0.36	0.36	0.36	0.36	0.41	0.42	0.42	0.34	0.33	0.41	0.36	0.55	0.55	0.55	0.55	0.55
O=F=Cl	0.27	0.18	0.27	0.34	0.45	0.43	0.27	0.36	0.34	0.56	0.28	0.46	0.36	0.38	0.41	0.24
Total	97.23	98.10	98.54	97.41	97.06	97.75	97.77	97.57	97.15	95.42	97.66	96.97	97.23	96.82	96.71	95.64
Parameters (in apfu)																
NF (Max)	13eCNK	13eCNK	13eCNK	13eCNK	13eCNK	13eCNK	13eCNK	13eCNK	13eCNK	13eCNK	13eCNK	13eCNK	13eCNK	13eCNK	13eCNK	13eCNK
Fe#	0.997	0.998	0.997	0.998	0.999	0.998	0.999	0.999	0.999	0.999	0.999	0.999	1.000	0.997	0.999	0.999
^{A}[Na+K+2Ca]	0.265	0.245	0.262	0.389	0.558	0.476	0.307	0.416	0.323	0.500	0.353	0.632	0.668	0.521	0.480	0.551
^{C}[Al+Fe^{3+}+2Ti]	2.104	2.169	2.166	1.876	1.683	1.793	2.039	1.809	1.924	1.763	1.912	1.653	1.698	2.022	1.854	1.821
Ca^{2+} + Al^{IV}	0.220	0.218	0.235	0.138	0.366	0.333	0.129	0.149	0.103	0.367	0.154	0.440	0.443	0.423	0.275	0.256
Si + Na + K	10.046	10.027	10.027	10.251	10.191	10.143	10.178	10.267	10.220	10.133	10.199	10.192	10.148	10.098	10.206	10.294
[Na+K]/Al	9.433	8.617	9.533	12.063	11.609	9.398	12.726	10.431	11.682	10.822	11.878	10.285	8.919	6.682	12.830	8.485
$Fe^{3+}/(Fe^{3+}+Fe^{2+})$	0.428	0.461	0.452	0.350	0.331	0.349	0.405	0.337	0.374	0.362	0.364	0.323	0.354	0.423	0.392	0.357

Point_ID: spot identification; c: core; r: rim; i: intermediate zone; - : below detection limit; *Li2O contents derived from the LA-ICP-MS analyses; na: not analyzed; NF(Max): Normalization factor according to the method of Schumacher (in Leake et al., 1997) for maximum Fe^{3+}; Fe# =[Fe_T/(Fe_T+Mg)]

Table 4. (*cont.*) Sodic amphiboles in peralkaline alkali feldspar granites from the Mandira unit

Sample	**MAN-4621**			**MAN-4776**								**MAN-4777**				
Crystal	c1			c1		c2		c3	c6	c5		c6				
Point_ID	1-r1	1-c	1-r2	1-r1	1-r2	2-c	2-r	3-c	6-c	5-r1	5-r2	6-r2	6-i2	6-c	6-i1	6-r1
Structural formulae based on 23O																
Si (apfu)	7.792	7.788	7.776	7.904	7.820	7.829	7.886	7.913	7.922	7.813	7.899	7.810	7.729	7.688	7.867	7.859
Al^{IV}	0.208	0.212	0.224	0.096	0.180	0.171	0.114	0.087	0.078	0.187	0.101	0.190	0.271	0.312	0.133	0.141
Ti	0.000	0.000	0.000	0.000	0.000	0.000	0.000	0.000	0.000	0.000	0.000	0.000	0.000	0.000	0.000	0.000
T-site	**8.000**	**8.000**	**8.000**	**8.000**	**8.000**	**8.000**	**8.000**	**8.000**	**8.000**	**8.000**	**8.000**	**8.000**	**8.000**	**8.000**	**8.000**	**8.000**
Al^{VI}	0.031	0.048	0.012	0.099	0.024	0.075	0.066	0.139	0.119	0.027	0.092	0.041	0.000	0.048	0.049	0.146
Ti	0.065	0.002	0.038	0.107	0.079	0.075	0.075	0.079	0.058	0.045	0.094	0.089	0.032	0.038	0.016	0.059
Fe^{3+}	1.942	2.118	2.079	1.564	1.501	1.568	1.822	1.512	1.690	1.646	1.632	1.435	1.634	1.897	1.773	1.557
Zr	0.025	0.006	0.003	0.007	0.006	0.000	0.006	0.005	0.005	0.004	0.003	0.000	0.000	0.000	0.000	0.000
Zn	0.031	0.045	0.043	0.041	0.041	0.042	0.040	0.041	0.041	0.058	0.058	0.043	0.047	0.048	0.034	0.043
Mg	0.014	0.010	0.016	0.009	0.003	0.007	0.007	0.002	0.002	0.005	0.003	0.006	0.002	0.013	0.004	0.006
Li	0.224	0.221	0.220	0.225	0.259	0.261	0.258	0.210	0.204	0.263	0.223	0.345	0.268	0.342	0.342	0.346
Fe^{2+}	2.591	2.480	2.517	2.904	3.039	2.923	2.680	2.969	2.833	2.904	2.850	3.004	2.984	2.586	2.746	2.806
Mn	0.075	0.070	0.073	0.046	0.048	0.050	0.046	0.045	0.049	0.048	0.044	0.038	0.033	0.028	0.036	0.037
C-site	**5.000**	**5.000**	**5.000**	**5.000**	**5.000**	**5.000**	**5.000**	**5.000**	**5.000**	**5.000**	**5.000**	**5.000**	**5.000**	**5.000**	**5.000**	**5.000**
Li	0.000	0.000	0.000	0.000	0.000	0.000	0.000	0.000	0.000	0.000	0.000	0.000	0.077	0.000	0.000	0.000
Mn	0.000	0.000	0.000	0.000	0.000	0.000	0.000	0.000	0.000	0.000	0.000	0.000	0.000	0.000	0.000	0.000
Fe^{2+}	0.000	0.000	0.000	0.000	0.000	0.000	0.000	0.000	0.000	0.000	0.000	0.000	0.000	0.000	0.000	0.000
Ca	0.012	0.007	0.011	0.042	0.186	0.162	0.014	0.062	0.025	0.180	0.053	0.250	0.172	0.111	0.142	0.115
Na	1.988	1.993	1.989	1.958	1.814	1.838	1.986	1.938	1.975	1.820	1.947	1.750	1.751	1.889	1.858	1.885
B-site	**2.000**	**2.000**	**2.000**	**2.000**	**2.000**	**2.000**	**2.000**	**2.000**	**2.000**	**2.000**	**2.000**	**2.000**	**2.000**	**2.000**	**2.000**	**2.000**
Na	0.048	0.072	0.070	0.131	0.334	0.285	0.076	0.182	0.123	0.299	0.156	0.458	0.469	0.313	0.316	0.319
K	0.217	0.173	0.192	0.258	0.224	0.191	0.231	0.234	0.200	0.201	0.197	0.173	0.199	0.208	0.165	0.232
A-site	**0.265**	**0.245**	**0.262**	**0.389**	**0.558**	**0.476**	**0.307**	**0.416**	**0.323**	**0.500**	**0.353**	**0.632**	**0.668**	**0.521**	**0.480**	**0.551**
F	0.318	0.195	0.308	0.394	0.527	0.506	0.309	0.414	0.390	0.667	0.327	0.540	0.409	0.431	0.483	0.274
Cl	0.000	0.006	0.003	0.000	0.002	0.000	0.000	0.005	0.005	0.008	0.004	0.006	0.011	0.011	0.002	0.005
Cations	15.265	15.245	15.262	15.389	15.558	15.476	15.307	15.416	15.323	15.500	15.353	15.632	15.668	15.521	15.480	15.551

Table 5: Sodic amphiboles in peralkaline alkali feldspar granites from the Mandira unit

Sample	**MAN-4777**															
Crystal	c5		c4				c3				c2		c1			
Point_ID	5-r	5-c	4-r2	4-i2	4-i1	4-c	3-i2	3-r1	3-i1	3-c	2-r1	2-c	1-r2	1-i2	1-c	1-r3
SiO_2 (wt%)	50.51	51.71	49.41	49.40	50.72	49.01	50.83	47.48	49.48	51.74	50.75	51.62	49.84	45.87	47.22	48.87
TiO_2	0.75	0.08	1.60	0.36	0.25	0.32	0.50	0.82	0.41	0.18	0.77	0.26	0.89	2.37	1.38	0.47
Al_2O_3	1.09	0.95	1.23	1.71	1.09	1.24	1.04	1.48	1.22	0.81	1.06	0.95	0.75	1.82	1.37	1.30
FeO	33.89	35.68	34.60	35.25	35.43	34.31	34.42	33.22	35.50	37.69	34.68	38.40	33.52	32.84	33.13	33.81
MnO	0.23	0.29	0.25	0.24	0.27	0.27	0.23	0.29	0.25	0.26	0.27	0.23	0.26	0.31	0.29	0.18
MgO	0.01	0.03	0.05	0.02	0.02	0.00	0.05	0.00	0.04	0.04	0.01	0.05	0.01	0.02	0.06	0.01
CaO	0.19	0.03	1.52	0.13	1.57	2.51	0.85	0.31	1.60	0.12	0.96	1.08	0.17	1.96	1.62	0.69
ZrO_2	na	na	na	na	na	na	na	na	na	na	na	na	na	na	na	na
ZnO	0.35	0.33	0.38	0.33	0.30	0.37	0.31	0.37	0.40	0.33	0.30	0.33	0.36	0.24	0.27	0.38
Na_2O	7.17	7.54	7.20	7.52	7.20	7.08	7.49	7.15	7.45	7.37	7.11	7.17	7.32	7.10	7.26	7.13
K_2O	1.29	1.22	0.95	1.20	0.89	0.89	1.04	1.06	1.07	1.15	1.13	0.92	1.35	0.90	0.93	0.92
F	0.68	0.54	1.53	0.73	1.51	2.25	1.18	1.68	1.24	0.64	0.70	1.25	1.79	1.05	1.49	1.65
Cl	-	-	0.02	0.03	-	0.04	0.02	-	0.03	-	-	-	-	0.03	-	0.02
Li_2O*	0.46	0.46	0.52	0.52	0.52	0.52	0.48	0.48	0.48	0.48	0.42	0.42	0.44	0.44	0.44	0.44
O=F=Cl	0.29	0.23	0.65	0.31	0.64	0.96	0.50	0.71	0.53	0.27	0.29	0.53	0.75	0.45	0.63	0.70
Total	96.33	98.63	98.61	97.13	99.12	97.84	97.93	93.65	98.64	100.55	97.86	102.14	95.96	94.52	94.83	95.18
Parameters (in apfu)																
NF (Max)	13eCNK	13eCNK	8SiAl	13eCNK	13eCNK	13eCNK	13eCNK	13eCNK	8SiAl	8SiAl	13eCNK	8SiAl	13eCNK	8SiAl	8SiAl	13eCNK
Fe#	0.999	0.999	0.997	0.999	0.999	1.000	0.998	1.000	0.998	0.998	1.000	0.998	0.999	0.999	0.997	0.999
^{A}[Na+K+2Ca]	0.467	0.476	0.803	0.560	0.584	0.781	0.606	0.539	0.856	0.592	0.521	0.698	0.560	1.084	0.873	0.517
^{C}[Al+Fe^{3+}+2Ti]	1.880	1.902	1.338	2.029	1.668	1.356	1.651	1.992	1.299	1.646	1.704	1.317	1.765	0.973	1.310	1.833
Ca^{2+} + Al^{IV}	0.122	0.106	0.484	0.335	0.446	0.655	0.241	0.338	0.496	0.163	0.281	0.345	0.100	0.707	0.548	0.301
Si + Na + K	10.345	10.370	10.159	10.195	10.138	10.126	10.365	10.187	10.256	10.250	10.239	10.118	10.460	10.127	10.237	10.216
[Na+K]/Al	12.091	14.432	10.500	8.017	11.740	10.210	12.896	8.697	10.978	16.621	12.129	13.494	18.023	6.941	9.489	9.765
$Fe^{3+}/(Fe^{3+}+Fe^{2+})$	0.359	0.398	0.211	0.424	0.351	0.281	0.323	0.397	0.258	0.335	0.322	0.258	0.332	0.083	0.214	0.366

Point_ID: spot identification; c: core; r: rim; i: intermediate zone; - : below detection limit; *Li2O contents derived from the LA-ICP-MS analyses; na: not analyzed; NF(Max): Normalization factor according to the method of Schumacher (in Leake et al., 1997) for maximum Fe^{3+}; Fe# =[Fe_T/(Fe_T+Mg)]

Table 5. (*cont.*) Sodic amphiboles in peralkaline alkali feldspar granites from the Mandira unit

Sample	**MAN-4777**															
Crystal	c5		c4				c3				c2		c1			
Point_ID	5-r	5-c	4-r2	4-i2	4-i1	4-c	3-i2	3-r1	3-i1	3-c	2-r1	2-c	1-r2	1-i2	1-c	1-r3
Structural formulae based on 23 oxygens																
Si (apfu)	7.910	7.899	7.773	7.687	7.813	7.770	7.901	7.716	7.774	7.856	7.878	7.831	7.929	7.642	7.736	7.817
Al^{IV}	0.090	0.101	0.227	0.313	0.187	0.230	0.099	0.284	0.226	0.144	0.122	0.169	0.071	0.358	0.264	0.183
Ti	0.000	0.000	0.000	0.000	0.000	0.000	0.000	0.000	0.000	0.000	0.000	0.000	0.000	0.000	0.000	0.000
T-site	**8.000**	**8.000**	**8.000**	**8.000**	**8.000**	**8.000**	**8.000**	**8.000**	**8.000**	**8.000**	**8.000**	**8.000**	**8.000**	**8.000**	**8.000**	**8.000**
Al^{VI}	0.111	0.070	0.000	0.000	0.011	0.001	0.092	0.000	0.000	0.000	0.073	0.000	0.070	0.000	0.000	0.063
Ti	0.088	0.009	0.189	0.042	0.029	0.038	0.058	0.101	0.048	0.021	0.090	0.030	0.107	0.297	0.170	0.057
Fe^{3+}	1.593	1.813	0.960	1.945	1.600	1.279	1.444	1.791	1.203	1.605	1.451	1.257	1.481	0.378	0.970	1.657
Zr	0.000	0.000	0.000	0.000	0.000	0.000	0.000	0.000	0.000	0.000	0.000	0.000	0.000	0.000	0.000	0.000
Zn	0.040	0.037	0.044	0.037	0.034	0.043	0.036	0.045	0.047	0.037	0.034	0.037	0.043	0.030	0.033	0.045
Mg	0.003	0.006	0.011	0.005	0.003	0.000	0.010	0.000	0.009	0.010	0.002	0.012	0.002	0.005	0.015	0.003
Li	0.290	0.282	0.171	0.297	0.324	0.333	0.300	0.300	0.198	0.114	0.263	0.021	0.284	0.048	0.204	0.285
Fe^{2+}	2.846	2.744	3.592	2.642	2.964	3.270	3.030	2.724	3.462	3.180	3.052	3.615	2.979	4.197	3.569	2.866
Mn	0.030	0.037	0.033	0.031	0.035	0.036	0.030	0.040	0.033	0.033	0.036	0.029	0.035	0.044	0.040	0.025
C-site	**5.000**	**5.000**	**5.000**	**5.000**	**5.000**	**5.000**	**5.000**	**5.000**	**5.000**	**5.000**	**5.000**	**5.000**	**5.000**	**5.000**	**5.000**	**5.000**
Li	0.000	0.000	0.160	0.030	0.000	0.000	0.000	0.013	0.105	0.179	0.000	0.236	0.000	0.249	0.088	0.000
Mn	0.000	0.000	0.000	0.000	0.000	0.000	0.000	0.000	0.000	0.000	0.000	0.000	0.000	0.000	0.000	0.000
Fe^{2+}	0.000	0.000	0.000	0.000	0.000	0.000	0.000	0.000	0.000	0.000	0.000	0.000	0.000	0.000	0.000	0.000
Ca	0.032	0.005	0.256	0.022	0.259	0.426	0.142	0.054	0.269	0.019	0.160	0.175	0.029	0.349	0.285	0.118
Na	1.968	1.995	1.583	1.948	1.741	1.574	1.858	1.933	1.626	1.802	1.840	1.589	1.971	1.402	1.627	1.882
B-site	**2.000**	**2.000**	**2.000**	**2.000**	**2.000**	**2.000**	**2.000**	**2.000**	**2.000**	**2.000**	**2.000**	**2.000**	**2.000**	**2.000**	**2.000**	**2.000**
Na	0.209	0.238	0.613	0.321	0.409	0.602	0.400	0.319	0.642	0.369	0.298	0.521	0.287	0.892	0.679	0.328
K	0.257	0.239	0.190	0.239	0.175	0.180	0.206	0.220	0.214	0.224	0.223	0.178	0.274	0.192	0.194	0.189
A-site	**0.467**	**0.476**	**0.803**	**0.560**	**0.584**	**0.781**	**0.606**	**0.539**	**0.856**	**0.592**	**0.521**	**0.698**	**0.560**	**1.084**	**0.873**	**0.517**
F	0.338	0.263	0.762	0.360	0.736	1.128	0.578	0.865	0.615	0.307	0.341	0.601	0.902	0.554	0.770	0.833
Cl	0.001	0.000	0.006	0.007	0.001	0.011	0.004	0.003	0.009	0.001	0.001	0.000	0.000	0.008	0.000	0.005
Cations	15.467	15.476	15.803	15.560	15.584	15.781	15.606	15.539	15.856	15.592	15.521	15.698	15.560	16.084	15.873	15.517

Table 6: Sodic amphiboles in peralkaline alkali feldspar granites from the Mandira unit

Sample	**MAN-4777**		**MAN-4779**												
Crystal			c4		c3			c2			c1				
Point_ID	1-i1	1-r1	4-r1	4-c	3-r2	3-r1	3-c	2-r2	2-c	2-r1	1-i2	1-r2	1-r1	1-i1	1-c
SiO_2 (wt%)	48.80	49.99	49.83	49.66	49.64	48.32	49.46	49.48	49.33	49.50	48.30	49.84	47.28	47.79	47.73
TiO_2	0.40	0.09	0.01	0.06	0.05	1.42	0.15	0.07	0.04	0.95	1.02	0.08	0.44	1.14	1.27
Al_2O_3	1.42	0.94	1.22	1.25	1.34	1.33	1.34	1.29	0.88	1.01	1.58	1.26	1.53	2.05	1.56
FeO	34.50	33.95	35.08	37.30	34.46	35.80	35.36	36.20	37.22	35.80	35.27	35.74	34.58	35.37	36.82
MnO	0.25	0.21	0.33	0.33	0.34	0.41	0.39	0.37	0.32	0.30	0.42	0.39	0.39	0.47	0.45
MgO	0.04	0.05	0.00	0.01	0.04	0.02	0.03	0.02	0.01	0.03	0.03	0.05	0.02	0.05	0.00
CaO	1.31	0.03	0.02	0.00	0.00	0.05	0.00	0.00	0.01	0.17	0.33	0.01	2.50	0.43	1.05
ZrO_2	na	na	na	na	na	na	na	na	na	na	na	na	na	na	na
ZnO	0.26	0.24	0.26	0.30	0.22	0.18	0.26	0.27	0.28	0.23	0.34	0.29	0.17	0.24	0.26
Na_2O	7.34	7.40	6.93	7.25	7.02	6.72	7.17	7.11	6.79	6.78	7.09	7.01	6.80	6.97	6.80
K_2O	1.02	0.99	0.67	0.70	0.72	0.73	0.71	0.72	0.31	1.09	1.00	0.79	0.94	0.95	0.83
F	1.66	1.30	0.54	0.15	0.53	0.25	0.39	0.54	0.01	0.54	0.58	0.63	1.62	0.87	0.83
Cl	0.02	0.03	-	-	-	0.02	-	-	0.02	-	0.03	-	0.04	-	0.02
Li_2O*	0.44	0.44	na	na	na	na	na	na	na	na	na	na	na	na	na
O=F=Cl	0.71	0.55	0.23	0.06	0.23	0.11	0.16	0.23	0.01	0.23	0.25	0.26	0.69	0.37	0.35
Total	96.76	95.08	94.66	96.95	94.15	95.14	95.08	95.84	95.21	96.17	95.74	95.81	95.61	95.96	97.27
Parameters (in apfu)															
NF (Max)	13eCNK	13eCNK	13eCNK	8SiAl	13eCNK	13eCNK	13eCNK	8SiAl	8SiAl	13eCNK	13eCNK	13eCNK	13eCNK	13eCNK	8SiAl
Fe#	0.998	0.997	1.000	0.999	0.998	0.999	0.999	0.999	0.999	0.998	0.998	0.998	0.999	0.998	1.000
^{A}[Na+K+2Ca]	0.690	0.487	0.293	0.344	0.342	0.301	0.367	0.336	0.181	0.337	0.464	0.318	0.813	0.428	0.697
^{C}[Al+Fe^{3+}+2Ti]	1.621	1.844	1.715	1.869	1.643	1.887	1.722	1.807	1.957	1.768	1.735	1.768	0.948	1.856	1.202
Ca^{2+} + Al^{IV}	0.475	0.058	0.013	0.213	0.000	0.261	0.089	0.143	0.167	0.164	0.313	0.090	0.643	0.430	0.478
Si + Na + K	10.215	10.429	10.280	10.131	10.349	9.986	10.278	10.193	9.989	10.173	10.151	10.229	10.170	9.997	10.003
[Na+K]/Al	9.267	14.044	9.922	10.121	9.179	8.876	9.379	9.674	13.022	12.264	8.077	9.818	7.981	6.108	7.745
$Fe^{3+}/(Fe^{3+}+Fe^{2+})$	0.330	0.376	0.318	0.375	0.296	0.322	0.322	0.352	0.394	0.313	0.306	0.337	0.156	0.328	0.180

Point_ID: spot identification; c: core; r: rim; i: intermediate zone; - : below detection limit; *Li2O contents derived from the LA-ICP-MS analyses; na: not analyzed; NF(Max): Normalization factor according to the method of Schumacher (in Leake et al., 1997) for maximum Fe^{3+}; Fe# =[Fe_T/(Fe_T+Mg)]

Table 6. (*cont.*) Sodic amphiboles in peralkaline alkali feldspar granites from the Mandira unit

Sample	**MAN-4777**		**MAN-4779**												
Crystal			c4		c3			c2			c1				
Point_ID	1-i1	1-r1	4-r1	4-c	3-r2	3-r1	3-c	2-r2	2-c	2-r1	1-i2	1-r2	1-r1	1-i1	1-c
Structural formulae based on 23 oxygens															
Si (apfu)	7.749	7.947	7.989	7.787	8.008	7.748	7.911	7.857	7.835	7.865	7.744	7.912	7.798	7.643	7.703
Al^{IV}	0.251	0.053	0.011	0.213	0.000	0.252	0.089	0.143	0.165	0.135	0.256	0.088	0.202	0.357	0.297
Ti	0.000	0.000	0.000	0.000	0.000	0.000	0.000	0.000	0.000	0.000	0.000	0.000	0.000	0.000	0.000
T-site	**8.000**	**8.000**	**8.000**	**8.000**	**8.008**	**8.000**	**8.000**	**8.000**	**8.000**	**8.000**	**8.000**	**8.000**	**8.000**	**8.000**	**8.000**
Al^{VI}	0.015	0.124	0.220	0.019	0.255	0.000	0.163	0.098	0.000	0.054	0.042	0.148	0.095	0.029	0.000
Ti	0.048	0.011	0.001	0.007	0.006	0.171	0.018	0.008	0.004	0.113	0.123	0.009	0.055	0.138	0.154
Fe^{3+}	1.511	1.698	1.493	1.836	1.376	1.545	1.523	1.693	1.949	1.488	1.447	1.601	0.743	1.552	0.895
Zr	0.000	0.000	0.000	0.000	0.000	0.000	0.000	0.000	0.000	0.000	0.000	0.000	0.000	0.000	0.000
Zn	0.031	0.028	0.031	0.035	0.027	0.021	0.030	0.032	0.032	0.027	0.040	0.034	0.021	0.028	0.031
Mg	0.009	0.012	0.000	0.003	0.008	0.006	0.006	0.004	0.003	0.008	0.008	0.011	0.004	0.012	0.000
Li	0.283	0.283	0.000	0.000	0.000	0.000	0.000	0.000	0.000	0.000	0.000	0.000	0.000	0.000	0.000
Fe^{2+}	3.071	2.816	3.210	3.056	3.273	3.255	3.206	3.115	2.995	3.270	3.283	3.144	4.028	3.178	3.920
Mn	0.033	0.028	0.045	0.044	0.047	0.002	0.053	0.050	0.017	0.040	0.057	0.052	0.054	0.064	0.000
C-site	**5.000**	**5.000**	**5.000**	**5.000**	**4.992**	**5.000**	**5.000**	**5.000**	**5.000**	**5.000**	**5.000**	**5.000**	**5.000**	**5.000**	**5.000**
Li	0.000	0.000	0.000	0.000	0.000	0.000	0.000	0.000	0.000	0.000	0.000	0.000	0.000	0.000	0.000
Mn	0.000	0.000	0.000	0.000	0.000	0.055	0.000	0.000	0.026	0.000	0.000	0.000	0.000	0.000	0.061
Fe^{2+}	0.000	0.000	0.000	0.000	0.000	0.000	0.000	0.000	0.000	0.000	0.000	0.000	0.000	0.000	0.155
Ca	0.224	0.005	0.003	0.000	0.000	0.009	0.000	0.000	0.001	0.029	0.057	0.002	0.441	0.073	0.181
Na	1.776	1.995	1.997	2.000	2.000	1.936	2.000	2.000	1.973	1.971	1.943	1.998	1.559	1.927	1.603
B-site	**2.000**	**2.000**	**2.000**	**2.000**	**2.000**	**2.000**	**2.000**	**2.000**	**2.000**	**2.000**	**2.000**	**2.000**	**2.000**	**2.000**	**2.000**
Na	0.483	0.286	0.157	0.205	0.194	0.152	0.223	0.189	0.118	0.116	0.260	0.159	0.616	0.234	0.526
K	0.207	0.200	0.137	0.139	0.148	0.150	0.144	0.147	0.064	0.221	0.204	0.159	0.197	0.194	0.171
A-site	**0.690**	**0.487**	**0.293**	**0.344**	**0.342**	**0.301**	**0.367**	**0.336**	**0.181**	**0.337**	**0.464**	**0.318**	**0.813**	**0.428**	**0.697**
F	0.832	0.654	0.272	0.076	0.270	0.129	0.196	0.270	0.007	0.270	0.293	0.315	0.842	0.442	0.422
Cl	0.009	0.000	0.000	0.000	0.004	0.006	0.000	0.000	0.005	0.001	0.008	0.000	0.011	0.001	0.006
Cations	15.690	15.487	15.293	15.344	15.342	15.301	15.367	15.336	15.181	15.337	15.464	15.318	15.813	15.428	15.697

Table 7: Sodic amphiboles in peralkaline alkali feldspar granites from the Mandira unit

Sample	**MAN-5574**								**MAN-6735**						
Crystal	c1	c2	c4	c7		c8	c5	c6	c6				c4		
Point_ID	1-c	2-c	4-c	7-r	7-c	8-c	5-c	6-c	6-r2	6-i2	6-r1	6-i1	4-r2	4-r1	4-c
SiO_2 (wt%)	50.70	50.19	51.54	51.71	51.68	51.43	49.38	49.79	49.67	49.80	50.39	50.20	51.53	49.86	51.51
TiO_2	0.03	0.30	0.08	0.03	0.75	0.06	0.15	0.00	0.16	0.41	0.29	0.58	0.05	0.06	0.02
Al_2O_3	1.61	1.55	0.76	0.89	1.20	1.11	2.67	1.14	1.27	1.17	1.17	1.18	1.57	1.66	0.92
FeO	35.29	35.12	36.59	36.42	35.60	36.41	34.76	35.82	37.26	36.15	35.78	35.00	36.16	37.26	36.56
MnO	0.48	0.48	0.36	0.33	0.40	0.31	0.45	0.41	0.30	0.39	0.36	0.46	0.30	0.29	0.23
MgO	0.03	0.03	0.02	0.02	0.00	0.00	0.03	0.05	0.06	0.06	0.06	0.08	0.03	0.04	0.04
CaO	0.00	0.07	0.00	0.00	0.02	0.00	0.06	0.01	0.01	0.18	0.18	0.16	0.04	0.02	0.01
ZrO_2	0.02	0.05	0.02	0.04	0.02	-	0.02	0.04		na	na	na	na	na	na
ZnO	0.39	0.28	0.38	0.30	0.39	0.19	0.42	0.35	0.40	0.46	0.45	0.44	0.38	0.38	0.38
Na_2O	7.30	7.08	6.80	6.96	6.97	6.90	6.98	6.76	7.13	7.18	7.19	7.44	6.91	6.44	6.84
K_2O	0.95	1.12	0.19	0.25	0.11	0.33	0.93	0.41	1.00	1.17	1.10	1.13	0.90	0.35	0.37
F	0.89	0.67	0.34	0.33	0.27	0.41	0.76	0.28	0.49	0.26	0.82	0.83	0.30	0.14	0.34
Cl	-	-	-	-	-	-	-	-	-	0.02	0.02	0.02	-	0.05	0.02
Li_2O*	na	na	0.36	0.36	na	na	na	0.36	na	na	na	na	na	na	na
O=F=Cl	0.37	0.28	0.14	0.14	0.11	0.18	0.32	0.12	0.21	0.11	0.35	0.35	0.12	0.07	0.15
Total	97.31	96.66	97.28	97.51	97.30	96.98	96.32	95.31	97.55	97.14	97.46	97.16	98.03	96.47	97.08
Parameters (in apfu)															
NF (Max)	13eCNK	13eCNK	13eCNK	13eCNK	13eCNK	13eCNK	13eCNK	13eCNK	13eCNK	13eCNK	13eCNK	13eCNK	13eCNK	13eCNK	13eCNK
Fe#	0.998	0.999	0.999	0.999	1.000	1.000	0.998	0.998	0.997	0.997	0.997	0.996	0.999	0.998	0.998
^{A}[Na+K+2Ca]	0.409	0.406	0.049	0.106	0.114	0.144	0.332	0.158	0.364	0.460	0.445	0.538	0.252	0.070	0.133
^{C}[Al+Fe^{3+}+2Ti]	1.635	1.645	2.301	2.221	1.889	1.861	1.870	2.245	1.862	1.661	1.598	1.489	1.788	2.096	1.866
Ca^{2+} + Al^{IV}	0.048	0.083	0.132	0.113	0.011	0.006	0.226	0.212	0.230	0.180	0.104	0.081	0.054	0.221	0.002
Si + Na + K	10.361	10.323	9.917	9.993	10.102	10.139	10.106	9.923	10.133	10.280	10.340	10.457	10.198	9.800	10.131
[Na+K]/Al	8.101	8.321	14.962	13.171	9.673	10.576	4.679	10.172	10.124	11.166	11.117	11.419	7.874	6.610	12.697
$Fe^{3+}/(Fe^{3+}+Fe^{2+})$	0.298	0.292	0.488	0.466	0.327	0.349	0.339	0.479	0.373	0.314	0.294	0.256	0.330	0.410	0.357

Point_ID: spot identification; c: core; r: rim; i: intermediate zone; - : below detection limit; *Li2O contents derived from the LA-ICP-MS analyses; na: not analyzed; NF(Max): Normalization factor according to the method of Schumacher (in Leake et al., 1997) for maximum Fe^{3+}; Fe# =[Fe_T/(Fe_T+Mg)]

Table 7. (*cont.*) Sodic amphiboles in peralkaline alkali feldspar granites from the Mandira unit

Sample	**5574**								**6735**						
Crystal	c1	c2	c4	c7		c8	c5	c6	c6				c4		
Point_ID	1-c	2-c	4-c	7-r	7-c	8-c	5-c	6-c	6-r2	6-i2	6-r1	6-i1	4-r2	4-r1	4-c
Structural formulae based on 23 oxygens															
Si (apfu)	7.952	7.929	7.868	7.887	7.991	7.994	7.785	7.790	7.772	7.849	7.927	7.946	7.953	7.782	8.000
Al^{IV}	0.048	0.071	0.132	0.113	0.009	0.006	0.215	0.210	0.228	0.151	0.073	0.054	0.047	0.218	0.000
Ti	0.000	0.000	0.000	0.000	0.000	0.000	0.000	0.000	0.000	0.000	0.000	0.000	0.000	0.000	0.000
T-site	**8.000**	**8.000**	**8.000**	**8.000**	**8.000**	**8.000**	**8.000**	**8.000**	**8.000**	**8.000**	**8.000**	**8.000**	**8.000**	**8.000**	**8.000**
Al^{VI}	0.249	0.217	0.005	0.047	0.210	0.197	0.281	0.000	0.005	0.067	0.144	0.166	0.238	0.087	0.167
Ti	0.004	0.036	0.009	0.004	0.087	0.007	0.018	0.000	0.019	0.049	0.035	0.069	0.006	0.007	0.002
Fe^{3+}	1.378	1.357	2.278	2.167	1.505	1.650	1.552	2.245	1.819	1.496	1.384	1.186	1.539	1.995	1.694
Zr	0.002	0.004	0.001	0.003	0.002	0.000	0.002	0.003	0.000	0.000	0.000	0.000	0.000	0.000	0.000
Zn	0.045	0.033	0.042	0.034	0.045	0.022	0.049	0.040	0.046	0.053	0.052	0.051	0.043	0.044	0.043
Mg	0.008	0.007	0.004	0.004	0.000	0.000	0.008	0.012	0.014	0.014	0.014	0.019	0.006	0.008	0.008
Li	0.000	0.000	0.221	0.221	0.000	0.000	0.000	0.203	0.000	0.000	0.000	0.000	0.000	0.000	0.000
Fe^{2+}	3.250	3.283	2.393	2.479	3.099	3.083	3.030	2.442	3.057	3.269	3.323	3.448	3.128	2.858	3.055
Mn	0.064	0.064	0.046	0.042	0.053	0.040	0.060	0.055	0.040	0.052	0.048	0.061	0.039	0.000	0.030
C-site	**5.000**	**5.000**	**5.000**	**5.000**	**5.000**	**5.000**	**5.000**	**5.000**	**5.000**	**5.000**	**5.000**	**5.000**	**5.000**	**5.000**	**5.000**
Li	0.000	0.000	0.000	0.000	0.000	0.000	0.000	0.023	0.000	0.000	0.000	0.000	0.000	0.000	0.000
Mn	0.000	0.000	0.000	0.000	0.000	0.000	0.000	0.000	0.000	0.000	0.000	0.000	0.000	0.038	0.000
Fe^{2+}	0.000	0.000	0.000	0.000	0.000	0.000	0.000	0.000	0.000	0.000	0.000	0.000	0.000	0.011	0.000
Ca	0.000	0.012	0.000	0.000	0.003	0.000	0.011	0.002	0.002	0.030	0.031	0.027	0.007	0.003	0.002
Na	2.000	1.988	2.000	2.000	1.997	2.000	1.989	1.974	1.998	1.970	1.969	1.973	1.993	1.948	1.998
B-site	**2.000**	**2.000**	**2.000**	**2.000**	**2.000**	**2.000**	**2.000**	**2.000**	**2.000**	**2.000**	**2.000**	**2.000**	**2.000**	**2.000**	**2.000**
Na	0.220	0.181	0.012	0.058	0.092	0.079	0.144	0.076	0.164	0.224	0.224	0.311	0.075	0.000	0.060
K	0.189	0.226	0.036	0.048	0.021	0.065	0.188	0.082	0.200	0.236	0.220	0.227	0.177	0.070	0.073
A-site	**0.409**	**0.406**	**0.049**	**0.106**	**0.114**	**0.144**	**0.332**	**0.158**	**0.364**	**0.460**	**0.445**	**0.538**	**0.252**	**0.070**	**0.133**
F	0.440	0.334	0.163	0.157	0.132	0.203	0.380	0.139	0.244	0.129	0.407	0.416	0.144	0.068	0.167
Cl	0.000	0.003	0.000	0.006	0.000	0.003	0.003	0.000	0.000	0.005	0.006	0.004	0.000	0.013	0.006
Cations	15.409	15.406	15.049	15.106	15.114	15.144	15.332	15.158	15.364	15.460	15.445	15.538	15.252	15.070	15.133

Table 8: Sodic amphiboles in peralkaline alkali feldspar granites from the Mandira unit

Sample	**MAN-6735**														
Crystal	c3		c2						c1						
Point_ID	3-r	3-c	2-i2	2-r2	2-c	2-ci1	2-i1	2-r1	1-r2	1-r3	1-c	1-i3	1-i2	1-i1	1-r1
SiO_2 (wt%)	50.53	50.37	49.40	50.02	50.09	49.79	49.73	49.49	50.58	49.41	49.60	49.99	49.18	50.80	53.13
TiO_2	0.08	0.10	1.43	0.64	0.73	0.74	1.04	0.90	0.14	0.41	0.42	0.48	0.32	0.32	2.36
Al_2O_3	1.25	1.33	1.11	1.45	0.85	0.87	0.86	0.77	1.35	1.31	1.76	1.18	1.29	1.07	1.24
FeO	35.03	35.60	34.88	35.52	33.96	34.93	35.43	35.60	35.49	35.25	35.18	35.35	33.71	35.12	33.79
MnO	0.26	0.30	0.32	0.33	0.34	0.34	0.30	0.40	0.33	0.40	0.39	0.35	0.37	0.37	0.26
MgO	0.05	0.05	0.07	0.05	0.08	0.07	0.05	0.06	0.05	0.04	0.06	0.06	0.08	0.06	0.03
CaO	0.00	0.02	0.09	0.06	0.09	0.10	0.04	0.04	0.01	0.12	0.15	0.10	0.11	0.11	0.00
ZrO_2	na	na	na	na	na	na	na	na	na	na	na	na	na	na	na
ZnO	0.39	0.32	0.34	0.35	0.46	0.39	0.40	0.44	0.38	0.37	0.34	0.44	0.42	0.42	0.40
Na_2O	7.32	7.10	7.30	6.92	7.27	7.22	6.99	7.42	7.38	7.39	7.32	7.12	7.31	7.31	6.33
K_2O	0.94	0.93	1.11	1.28	1.43	1.33	1.14	1.15	1.04	1.18	1.23	1.22	1.29	1.18	1.02
F	1.06	0.38	0.30	0.38	0.83	1.02	0.68	0.82	0.88	0.63	0.67	0.54	0.68	1.17	0.85
Cl	-	0.03	-	-	-	0.03	-	-	0.03	-	-	-	0.02	0.03	-
Li_2O*	0.36	na	na	na	0.41	na	na	na	na	na	na	na	0.41	0.36	0.36
O=F=Cl	0.45	0.17	0.13	0.16	0.35	0.44	0.29	0.35	0.37	0.27	0.28	0.23	0.29	0.50	0.36
Total	96.81	96.36	96.24	96.86	96.19	96.38	96.38	96.75	97.29	96.24	96.83	96.62	94.89	97.82	99.42
Parameters (in apfu)															
NF (Max)	13eCNK	13eCNK	13eCNK	13eCNK	13eCNK	13eCNK	13eCNK	13eCNK	13eCNK	13eCNK	13eCNK	13eCNK	13eCNK	13eCNK	15excK
Fe#	0.998	0.998	0.996	0.997	0.996	0.996	0.997	0.997	0.997	0.998	0.997	0.997	0.996	0.997	0.999
^{A}[Na+K+2Ca]	0.398	0.364	0.495	0.381	0.526	0.528	0.393	0.534	0.464	0.546	0.521	0.453	0.542	0.449	0.198
^{C}[Al+Fe^{3+}+2Ti]	1.949	1.680	1.619	1.731	1.820	1.489	1.694	1.574	1.573	1.544	1.597	1.606	1.858	1.881	1.764
Ca^{2+} + Al^{IV}	0.122	0.051	0.144	0.131	0.115	0.051	0.101	0.122	0.041	0.130	0.169	0.094	0.175	0.140	0.000
Si + Na + K	10.276	10.313	10.351	10.250	10.411	10.477	10.292	10.412	10.423	10.416	10.352	10.359	10.368	10.309	10.117
[Na+K]/Al	10.423	9.563	11.858	8.817	15.895	15.359	14.842	17.384	9.837	10.286	7.592	11.051	10.416	12.422	9.278
$Fe^{3+}/(Fe^{3+}+Fe^{2+})$	0.399	0.310	0.257	0.306	0.355	0.253	0.293	0.280	0.284	0.278	0.282	0.288	0.377	0.380	0.234

Point_ID: spot identification; c: core; r: rim; i: intermediate zone; - : below detection limit; *Li2O contents derived from the LA-ICP-MS analyses; na: not analyzed; NF(Max): Normalization factor according to the method of Schumacher (in Leake et al., 1997) for maximum Fe^{3+}; Fe# =[Fe_T/(Fe_T+Mg)]

Table 8. (*cont.*) Sodic amphiboles in peralkaline alkali feldspar granites from the Mandira unit

Sample	**MAN-6735**														
Crystal	c3		c2						c1						
Point_ID	3-r	3-c	2-i2	2-r2	2-c	2-ci1	2-i1	2-r1	1-r2	1-r3	1-c	1-i3	1-i2	1-i1	1-r1
Structural formulae based on 23 oxygens															
Si (apfu)	7.878	7.952	7.871	7.878	7.900	7.966	7.906	7.885	7.961	7.890	7.856	7.924	7.844	7.877	8.059
Al^{IV}	0.122	0.048	0.129	0.122	0.100	0.034	0.094	0.115	0.039	0.110	0.144	0.076	0.156	0.123	0.000
Ti	0.000	0.000	0.000	0.000	0.000	0.000	0.000	0.000	0.000	0.000	0.000	0.000	0.000	0.000	0.000
T-site	**8.000**	**8.000**	**8.000**	**8.000**	**8.000**	**8.000**	**8.000**	**8.000**	**8.000**	**8.000**	**8.000**	**8.000**	**8.000**	**8.000**	**8.059**
Al^{VI}	0.108	0.199	0.080	0.147	0.058	0.130	0.067	0.031	0.212	0.135	0.185	0.144	0.086	0.073	0.222
Ti	0.009	0.011	0.172	0.076	0.086	0.089	0.125	0.108	0.016	0.049	0.050	0.057	0.038	0.038	0.269
Fe^{3+}	1.823	1.459	1.196	1.431	1.590	1.182	1.378	1.328	1.328	1.309	1.312	1.348	1.695	1.732	1.004
Zr	0.000	0.000	0.000	0.000	0.000	0.000	0.000	0.000	0.000	0.000	0.000	0.000	0.000	0.000	0.000
Zn	0.045	0.038	0.040	0.041	0.054	0.046	0.047	0.052	0.045	0.044	0.040	0.051	0.050	0.048	0.044
Mg	0.010	0.011	0.018	0.012	0.018	0.017	0.012	0.013	0.012	0.009	0.013	0.014	0.018	0.013	0.006
Li	0.225	0.000	0.000	0.000	0.259	0.000	0.000	0.000	0.000	0.000	0.000	0.000	0.262	0.224	0.139
Fe^{2+}	2.745	3.242	3.452	3.248	2.890	3.492	3.332	3.415	3.344	3.398	3.348	3.338	2.801	2.823	3.282
Mn	0.035	0.040	0.043	0.044	0.046	0.045	0.040	0.053	0.043	0.055	0.053	0.047	0.049	0.048	0.034
C-site	**5.000**	**5.000**	**5.000**	**5.000**	**5.000**	**5.000**	**5.000**	**5.000**	**5.000**	**5.000**	**5.000**	**5.000**	**5.000**	**5.000**	**5.000**
Li	0.000	0.000	0.000	0.000	0.000	0.000	0.000	0.000	0.000	0.000	0.000	0.000	0.000	0.000	0.081
Mn	0.000	0.000	0.000	0.000	0.000	0.000	0.000	0.000	0.000	0.000	0.000	0.000	0.000	0.000	0.000
Fe^{2+}	0.000	0.000	0.000	0.000	0.000	0.000	0.000	0.000	0.000	0.000	0.000	0.000	0.000	0.000	0.000
Ca	0.000	0.003	0.015	0.010	0.014	0.017	0.007	0.007	0.002	0.020	0.025	0.017	0.018	0.017	0.000
Na	2.000	1.997	1.985	1.990	1.986	1.983	1.993	1.993	1.998	1.980	1.975	1.983	1.982	1.983	1.860
B-site	**2.000**	**2.000**	**2.000**	**2.000**	**2.000**	**2.000**	**2.000**	**2.000**	**2.000**	**2.000**	**2.000**	**2.000**	**2.000**	**2.000**	**1.941**
Na	0.212	0.176	0.270	0.123	0.238	0.256	0.162	0.300	0.255	0.307	0.272	0.206	0.280	0.216	0.000
K	0.186	0.188	0.225	0.258	0.288	0.272	0.231	0.234	0.209	0.240	0.249	0.247	0.262	0.233	0.198
A-site	**0.398**	**0.364**	**0.495**	**0.381**	**0.526**	**0.528**	**0.393**	**0.534**	**0.464**	**0.546**	**0.521**	**0.453**	**0.542**	**0.449**	**0.198**
F	0.524	0.192	0.152	0.190	0.415	0.517	0.341	0.415	0.436	0.317	0.337	0.270	0.343	0.572	0.409
Cl	0.002	0.007	0.001	0.004	0.003	0.009	0.001	0.002	0.007	0.003	0.000	0.003	0.006	0.008	0.002
Cations	15.398	15.364	15.495	15.381	15.526	15.528	15.393	15.534	15.464	15.546	15.521	15.453	15.542	15.449	15.198

Table 9: Calcic amphiboles in metaluminous syenogranites from the Mandira unit

Sample	**MAN-5**															
Crystal	c2		c3				c4		c5		c6			c9	c8	
Point_ID	1	2	3	4	5	6	7	8	1	2	6-r1	6-c	6-r2	9-c	10-i	11-c
SiO_2 (wt%)	41.78	41.42	41.96	41.26	40.65	41.90	41.83	41.00	41.39	41.70	42.01	41.30	41.40	41.96	42.91	43.01
TiO_2	1.92	1.34	1.12	1.38	1.29	0.94	1.83	1.05	1.19	1.20	1.54	1.05	1.14	1.70	1.64	1.30
Al_2O_3	8.40	8.77	8.04	8.12	8.30	7.87	8.54	8.39	7.78	7.69	8.08	8.01	8.00	8.05	8.30	8.03
FeO	27.37	29.84	27.84	29.27	28.87	30.50	27.93	29.46	30.36	29.57	29.01	30.39	30.30	25.26	25.80	26.47
MnO	0.83	0.72	0.93	0.80	0.87	0.94	0.77	0.81	0.94	0.94	0.77	0.91	0.83	0.50	0.45	0.61
MgO	3.50	2.85	3.63	3.00	2.88	2.35	3.33	2.69	2.70	3.15	3.23	2.58	2.66	4.85	4.81	4.74
CaO	9.98	10.08	10.10	10.11	9.70	10.29	10.03	9.78	9.82	10.03	9.73	10.10	10.10	9.86	10.18	10.00
ZrO_2	-	0.04	-	-	-	0.02	0.13	-	-	-	-	-	0.07	-	0.05	0.03
ZnO	0.07	0.07	0.13	0.03	0.07	0.12	0.00	0.19	0.10	0.03	0.07	0.05	0.05	0.07	0.07	0.17
Na_2O	1.81	1.54	2.02	1.56	2.05	1.63	1.42	1.53	1.70	1.42	1.94	1.86	1.56	1.98	2.00	1.95
K_2O	1.12	1.19	0.94	1.11	1.10	1.13	1.07	1.13	1.23	1.13	1.14	1.32	1.25	1.05	1.06	1.02
F	0.25	0.26	-	-	0.42	-	-	0.18	0.22	0.20	0.29	0.28	0.28	0.36	0.32	0.50
Cl	0.36	0.31	-	-	-	0.34	0.39	0.25	0.43	0.40	0.50	0.50	0.39	0.31	0.36	0.36
Li_2O*	0.01	na	0.01	na	na	na	0.01	na	na	na	na	na	na	0.01	0.00	0.01
O=F=Cl	0.19	0.18	0.05	0.07	0.24	0.14	0.11	0.13	0.19	0.17	0.23	0.23	0.21	0.22	0.22	0.29
Total	97.23	98.26	96.91	96.84	96.21	98.03	97.22	96.34	97.67	97.29	98.09	98.12	97.82	95.76	97.75	97.91
Parameters (in apfu)																
NF (Max)	13eCNK	13eCNK	13eCNK	13eCNK	13eCNK	13eCNK	13eCNK	13eCNK	13eCNK	13eCNK	13eCNK	13eCNK	13eCNK	13eCNK	13eCNK	13eCNK
Fe#	0.814	0.855	0.811	0.845	0.849	0.879	0.825	0.860	0.863	0.840	0.834	0.869	0.865	0.745	0.751	0.758
^{A}[Na+K+2Ca]	0.475	0.406	0.527	0.435	0.543	0.484	0.345	0.386	0.447	0.371	0.465	0.567	0.455	0.508	0.521	0.465
^{C}[Al+Fe^{3+}+2Ti]	1.214	1.375	1.097	1.259	1.226	1.100	1.337	1.366	1.297	1.305	1.269	1.130	1.232	1.126	1.058	1.152
Ca^{2+} + Al^{IV}	3.075	3.183	3.057	3.148	3.121	3.091	3.091	3.110	3.090	3.087	3.021	3.144	3.138	2.998	2.997	2.962
Si + Na + K	7.401	7.222	7.470	7.287	7.422	7.393	7.253	7.276	7.357	7.284	7.444	7.422	7.317	7.510	7.524	7.503
[Na+K]/Al	0.497	0.435	0.539	0.463	0.549	0.497	0.408	0.447	0.531	0.463	0.548	0.560	0.490	0.545	0.533	0.538
$Fe^{3+}/(Fe^{3+}+Fe^{2+})$	0.156	0.234	0.180	0.210	0.200	0.183	0.192	0.244	0.240	0.245	0.204	0.196	0.218	0.155	0.129	0.192

Point_ID: spot identification; c: core; r: rim; i: intermediate zone; - : below detection limit; *Li2O contents derived from the LA-ICP-MS analyses; na: not analyzed; NF(Max): Normalization factor according to the method of Schumacher (in Leake et al., 1997) for maximum Fe^{3+}; Fe# =[Fe_T/(Fe_T+Mg)]

Table 9. (*cont.*) Calcic amphiboles in metaluminous syenogranites from the Mandira 1 unit

Sample	**MAN-5**															
Crystal	c2		c3				c4		c5		c6			c9	c8	
Point_ID	1	2	3	4	5	6	7	8	1	2	6-r1	6-c	6-r2	9-c	10-i	11-c
Structural formulae based on 23 oxygens																
Si (apfu)	6.620	6.515	6.660	6.580	6.555	6.661	6.605	6.568	6.583	6.618	6.622	6.580	6.582	6.685	6.708	6.709
Al^{IV}	1.380	1.485	1.340	1.420	1.445	1.339	1.395	1.432	1.417	1.382	1.378	1.420	1.418	1.315	1.292	1.291
Ti	0.000	0.000	0.000	0.000	0.000	0.000	0.000	0.000	0.000	0.000	0.000	0.000	0.000	0.000	0.000	0.000
T-site	**8.000**	**8.000**	**8.000**	**8.000**	**8.000**	**8.000**	**8.000**	**8.000**	**8.000**	**8.000**	**8.000**	**8.000**	**8.000**	**8.000**	**8.000**	**8.000**
Al^{VI}	0.190	0.140	0.164	0.106	0.132	0.135	0.194	0.152	0.041	0.057	0.123	0.084	0.081	0.197	0.238	0.185
Ti	0.229	0.159	0.134	0.166	0.157	0.112	0.217	0.126	0.142	0.143	0.183	0.126	0.136	0.204	0.192	0.152
Fe^{3+}	0.566	0.917	0.665	0.821	0.780	0.742	0.709	0.962	0.971	0.962	0.781	0.795	0.878	0.520	0.436	0.663
Zr	0.000	0.003	0.001	0.000	0.000	0.002	0.010	0.001	0.000	0.000	0.001	0.000	0.005	0.000	0.004	0.003
Zn	0.008	0.008	0.015	0.003	0.008	0.014	0.000	0.022	0.012	0.004	0.008	0.006	0.006	0.009	0.008	0.020
Mg	0.828	0.668	0.860	0.714	0.691	0.557	0.784	0.643	0.640	0.745	0.759	0.613	0.630	1.152	1.121	1.101
Li	0.005	0.000	0.004	0.000	0.000	0.000	0.004	0.000	0.000	0.000	0.000	0.000	0.000	0.004	0.003	0.003
Fe^{2+}	3.061	3.008	3.030	3.083	3.113	3.313	2.979	2.984	3.067	2.963	3.043	3.254	3.151	2.845	2.937	2.791
Mn	0.112	0.096	0.125	0.107	0.119	0.126	0.102	0.110	0.126	0.126	0.103	0.123	0.112	0.067	0.059	0.080
C-site	**5.000**	**5.000**	**5.000**	**5.000**	**5.000**	**5.000**	**5.000**	**5.000**	**5.000**	**5.000**	**5.000**	**5.000**	**5.000**	**5.000**	**5.000**	**5.000**
Li	0.000	0.000	0.000	0.000	0.000	0.000	0.000	0.000	0.000	0.000	0.000	0.000	0.000	0.000	0.000	0.000
Mn	0.000	0.000	0.000	0.000	0.000	0.000	0.000	0.000	0.000	0.000	0.000	0.000	0.000	0.000	0.000	0.000
Fe^{2+}	0.000	0.000	0.000	0.000	0.000	0.000	0.000	0.000	0.000	0.000	0.000	0.000	0.000	0.000	0.000	0.000
Ca	1.695	1.698	1.717	1.727	1.676	1.752	1.696	1.678	1.673	1.705	1.643	1.724	1.720	1.683	1.706	1.671
Na	0.305	0.302	0.283	0.273	0.324	0.248	0.304	0.322	0.327	0.295	0.357	0.276	0.280	0.317	0.294	0.329
B-site	**2.000**	**2.000**	**2.000**	**2.000**	**2.000**	**2.000**	**2.000**	**2.000**	**2.000**	**2.000**	**2.000**	**2.000**	**2.000**	**2.000**	**2.000**	**2.000**
Na	0.250	0.168	0.337	0.209	0.317	0.255	0.129	0.155	0.197	0.142	0.236	0.298	0.201	0.295	0.310	0.262
K	0.225	0.238	0.190	0.226	0.226	0.229	0.215	0.231	0.250	0.229	0.229	0.268	0.254	0.213	0.211	0.203
A-site	**0.475**	**0.406**	**0.527**	**0.435**	**0.543**	**0.484**	**0.345**	**0.386**	**0.447**	**0.371**	**0.465**	**0.567**	**0.455**	**0.508**	**0.521**	**0.465**
F	0.124	0.131	0.000	0.022	0.213	0.078	0.028	0.091	0.111	0.100	0.145	0.141	0.141	0.182	0.158	0.245
Cl	0.098	0.083	0.059	0.062	0.072	0.091	0.105	0.068	0.116	0.108	0.134	0.135	0.105	0.084	0.096	0.096
Cations	15.475	15.406	15.527	15.435	15.543	15.484	15.345	15.386	15.447	15.371	15.465	15.567	15.455	15.508	15.521	15.465

Table 10: Calcic amphiboles in metaluminous syenogranites from the Mandira unit

Sample	**MAN-5**					**MAN-6724**				**MAN-6725**				
Crystal				c9		c2			c1	c1		c2	c3	c4
Point_ID	12-c	13-c	14-ci	15-i	16-r	2-i	2-r	2-c	1-c	1-c	1-r	2-c	3-c	4-c
SiO_2 (wt%)	42.50	41.98	42.56	43.30	42.90	41.75	41.28	41.21	41.21	41.73	41.58	41.48	42.15	41.87
TiO_2	1.87	1.76	1.82	1.15	1.09	1.83	1.77	1.75	1.75	1.59	1.92	1.80	1.55	1.94
Al_2O_3	8.32	8.21	8.29	7.47	7.80	7.38	7.39	7.55	7.55	8.11	8.12	8.10	7.82	7.89
FeO	26.08	26.20	25.88	26.49	26.48	32.60	32.81	33.09	33.09	31.61	31.56	31.15	32.05	31.24
MnO	0.55	0.57	0.53	0.77	0.71	0.66	0.68	0.67	0.67	0.82	0.86	0.83	0.86	0.81
MgO	4.60	4.15	5.00	4.79	5.09	1.58	1.64	1.53	1.53	1.56	1.45	1.66	1.50	1.73
CaO	10.17	9.76	9.71	10.31	10.22	10.06	10.06	9.83	9.83	9.65	9.59	9.73	9.56	9.78
ZrO_2	0.02	-	-	0.06	0.05	na	na	na	na	na	na	na	na	na
ZnO	0.08	0.08	0.05	0.11	0.12	0.12	0.17	0.17	0.17	0.22	0.12	0.15	0.14	0.10
Na_2O	2.04	1.90	1.69	1.66	1.71	1.77	1.57	1.57	1.57	1.95	1.78	2.04	1.92	2.04
K_2O	1.05	1.02	1.10	0.93	0.97	1.22	1.20	1.17	1.17	1.27	1.24	1.24	1.33	1.17
F	0.32	0.20	0.48	0.27	0.25	-	-	-	-	-	-	-	-	-
Cl	0.32	0.34	0.25	0.31	0.30	0.42	0.35	0.47	0.47	0.44	0.45	0.52	0.44	0.43
Li_2O*	na	na	na	0.01	na	0.01	0.01	0.01	0.01	na	na	na	na	na
O=F=Cl	0.20	0.16	0.26	0.19	0.17	0.10	0.08	0.18	0.18	0.15	0.13	0.20	0.15	0.16
Total	97.71	96.00	97.11	97.47	97.53	99.29	98.86	99.02	99.02	98.93	98.61	98.69	99.29	98.99
Parameters (in apfu)														
NF (Max)	13eCNK	13eCNK	13eCNK	13eCNK	13eCNK	8SiAl	8SiAl	8SiAl	8SiAl	13eCNK	13eCNK	13eCNK	13eCNK	13eCNK
Fe#	0.761	0.780	0.744	0.756	0.745	0.920	0.918	0.924	0.924	0.919	0.924	0.913	0.923	0.910
^{A}[Na+K+2Ca]	0.539	0.459	0.353	0.418	0.417	0.525	0.572	0.516	0.516	0.492	0.428	0.539	0.471	0.522
^{C}[Al+Fe^{3+}+2Ti]	1.086	1.188	1.381	1.072	1.179	1.125	0.985	1.118	1.118	1.265	1.348	1.204	1.263	1.189
Ca^{2+} + Al^{IV}	3.045	2.980	2.981	2.953	3.017	3.088	3.118	3.103	3.103	3.030	3.035	3.059	2.966	3.029
Si + Na + K	7.494	7.479	7.372	7.465	7.400	7.412	7.338	7.304	7.304	7.462	7.393	7.480	7.505	7.493
[Na+K]/Al	0.541	0.514	0.478	0.500	0.496	0.573	0.525	0.510	0.510	0.565	0.526	0.580	0.588	0.586
$Fe^{3+}/(Fe^{3+}+Fe^{2+})$	0.130	0.155	0.233	0.186	0.232	0.159	0.127	0.158	0.158	0.183	0.186	0.158	0.187	0.151

Point_ID: spot identification; c: core; r: rim; i: intermediate zone; - : below detection limit; *Li2O contents derived from the LA-ICP-MS analyses; na: not analyzed; NF(Max): Normalization factor according to the method of Schumacher (in Leake et al., 1997) for maximum Fe^{3+}; Fe#

Table 10. (*cont.*) Calcic amphiboles in metaluminous syenogranites from the Mandira 1 unit

Sample	**MAN-5**					**MAN-6724**				**MAN-6725**				
Crystal				c9		c2			c1	c1		c2	c3	c4
Point_ID	12-c	13-c	14-ci	15-i	16-r	2-i	2-r	2-c	1-c	1-c	1-r	2-c	3-c	4-c
Structural formula based on 23O														
Si (apfu)	6.663	6.686	6.643	6.776	6.690	6.621	6.607	6.579	6.645	6.607	6.594	6.599	6.650	6.631
Al^{IV}	1.337	1.314	1.357	1.224	1.310	1.379	1.393	1.421	1.355	1.393	1.406	1.401	1.350	1.369
Ti	0.000	0.000	0.000	0.000	0.000	0.000	0.000	0.000	0.000	0.000	0.000	0.000	0.000	0.000
T-site	**8.000**	**8.000**	**8.000**	**8.000**	**8.000**	**8.000**	**8.000**	**8.000**	**8.000**	**8.000**	**8.000**	**8.000**	**8.000**	**8.000**
Al^{VI}	0.200	0.228	0.167	0.154	0.123	0.000	0.000	0.000	0.063	0.120	0.112	0.118	0.104	0.103
Ti	0.220	0.210	0.214	0.136	0.128	0.218	0.213	0.211	0.215	0.190	0.229	0.215	0.184	0.231
Fe^{3+}	0.445	0.539	0.786	0.646	0.800	0.688	0.558	0.697	0.559	0.765	0.778	0.655	0.791	0.623
Zr	0.002	0.001	0.000	0.004	0.004	0.000	0.000	0.000	0.000	0.000	0.000	0.000	0.000	0.000
Zn	0.009	0.009	0.006	0.013	0.014	0.014	0.020	0.020	0.023	0.026	0.015	0.018	0.017	0.011
Mg	1.076	0.985	1.164	1.117	1.184	0.375	0.392	0.364	0.539	0.369	0.343	0.393	0.352	0.408
Li	0.000	0.000	0.000	0.005	0.000	0.000	0.000	0.000	0.004	0.000	0.000	0.000	0.000	0.000
Fe^{2+}	2.975	2.951	2.592	2.821	2.654	3.637	3.816	3.708	3.511	3.420	3.408	3.489	3.438	3.514
Mn	0.073	0.077	0.071	0.102	0.094	0.069	0.000	0.000	0.088	0.110	0.115	0.112	0.115	0.109
C-site	**5.000**	**5.000**	**5.000**	**5.000**	**5.000**	**5.000**	**5.000**	**5.000**	**5.000**	**5.000**	**5.000**	**5.000**	**5.000**	**5.000**
Li	0.000	0.000	0.000	0.000	0.000	0.005	0.005	0.005	0.000	0.000	0.000	0.000	0.000	0.000
Mn	0.000	0.000	0.000	0.000	0.000	0.019	0.093	0.091	0.000	0.000	0.000	0.000	0.000	0.000
Fe^{2+}	0.000	0.000	0.000	0.000	0.000	0.000	0.018	0.014	0.000	0.000	0.000	0.000	0.000	0.000
Ca	1.708	1.666	1.624	1.729	1.707	1.710	1.725	1.682	1.720	1.637	1.629	1.658	1.616	1.659
Na	0.292	0.334	0.376	0.271	0.293	0.266	0.160	0.209	0.280	0.363	0.371	0.342	0.384	0.341
B-site	**2.000**	**2.000**	**2.000**	**2.000**	**2.000**	**2.000**	**2.000**	**2.000**	**2.000**	**2.000**	**2.000**	**2.000**	**2.000**	**2.000**
Na	0.329	0.252	0.134	0.232	0.224	0.277	0.327	0.277	0.340	0.235	0.177	0.288	0.203	0.286
K	0.210	0.207	0.219	0.186	0.194	0.248	0.245	0.239	0.249	0.256	0.251	0.252	0.268	0.236
A-site	**0.539**	**0.459**	**0.353**	**0.418**	**0.417**	**0.525**	**0.572**	**0.516**	**0.588**	**0.492**	**0.428**	**0.539**	**0.471**	**0.522**
F	0.157	0.098	0.237	0.136	0.125	0.002	0.000	0.084	0.056	0.061	0.034	0.094	0.063	0.079
Cl	0.084	0.092	0.066	0.083	0.079	0.112	0.095	0.128	0.110	0.117	0.121	0.141	0.117	0.116
Cations	15.539	15.459	15.353	15.418	15.417	15.525	15.572	15.516	15.588	15.492	15.428	15.539	15.471	15.522

Table 11: Sodic-calcic, calcic and sodic amphiboles in peralkaline from the Acaraú unit

Sample	**MAN-09**												**MAN-579**			
Crystal	c5		c2				c3		c1			c5a	c1	c2	c3	
Point_ID	1-c	1-r	2-c	2-i	6-i	7-i	8-ci	9	10-i	11-i	12-i	13	1-c	2-c	3-r1	3c
SiO_2 (wt%)	51.28	50.69	48.07	47.91	45.95	45.32	46.45	48.68	47.82	49.03	49.00	52.93	48.27	46.34	47.64	48.45
TiO_2	0.00	0.00	0.16	0.08	1.32	0.65	0.88	0.07	0.13	0.22	0.06	0.01	0.12	0.22	0.38	0.45
Al_2O_3	0.28	0.22	1.42	1.32	2.63	2.49	2.73	1.30	1.61	1.32	1.31	0.94	2.30	3.46	2.51	2.11
FeO	37.35	37.36	35.71	35.16	34.12	35.73	34.68	35.44	35.52	36.35	35.86	35.77	35.25	35.58	35.20	34.70
MnO	0.26	0.25	0.55	0.53	0.61	0.59	0.62	0.54	0.54	0.45	0.51	0.25	0.50	0.60	0.48	0.57
MgO	0.13	0.13	0.42	0.41	0.40	0.37	0.35	0.37	0.38	0.34	0.39	0.17	0.31	0.20	0.32	0.55
CaO	0.77	1.01	7.02	6.91	6.70	6.47	6.65	6.67	5.75	4.80	6.53	0.73	7.82	8.78	8.26	8.57
ZrO_2	0.02	-	0.03	-	0.04	0.08	-	-	0.05	0.13	0.06	-	-	0.04	0.03	-
ZnO	0.25	0.19	0.22	0.23	0.26	0.17	0.30	0.34	0.21	0.26	0.19	0.08	0.24	0.10	0.29	0.30
Na_2O	5.71	5.68	2.52	2.64	2.76	2.96	2.97	2.81	3.38	3.87	2.97	5.70	2.19	1.88	2.01	1.84
K_2O	0.07	0.04	0.46	0.47	0.92	0.65	0.90	0.41	0.46	0.29	0.37	0.06	0.42	0.59	0.56	0.54
F	-	-	0.12	0.07	0.14	-	0.09	0.12	0.18	-	0.17	-	0.01	0.09	0.08	0.02
Cl	-	-	-	-	0.08	0.09	-	-	-	-	-	-	0.08	0.19	0.10	0.03
Li_2O*	0.336	0.336	na	na	na	na	na	na	na	na	na	0.3355	0.04	0.04	0.05	0.05
O=F=Cl	0.02	0.00	0.05	0.03	0.08	0.02	0.05	0.05	0.09	0.01	0.08	0.02	0.02	0.08	0.06	0.01
Total	96.49	95.91	96.65	95.70	95.85	95.56	96.63	96.71	96.00	97.09	97.38	97.01	97.52	98.02	97.85	98.16
Parameters (in apfu)																
NF (Max)	15eNK	8SiAl	8SiAl	13eCNK	8SiAl	8SiAl	13eCNK	13eCNK	13eCNK	8SiAl	13eCNK	15eNK	13eCNK	13eCNK	13eCNK	13eCNK
Fe#	0.994	0.994	0.980	0.980	0.979	0.982	0.982	0.982	0.981	0.984	0.981	0.992	0.985	0.990	0.984	0.972
^{A}[Na+K+2Ca]	0.013	0.008	0.116	0.127	0.267	0.476	0.262	0.101	0.142	0.073	0.101	0.012	0.092	0.205	0.145	0.130
^{C}[Al+Fe^{3+}+2Ti]	1.592	1.695	0.912	0.903	1.029	0.611	1.096	0.958	1.158	1.325	0.987	1.220	0.928	0.913	0.882	0.763
Ca^{2+} + Al^{IV}	0.175	0.211	1.477	1.430	1.677	1.635	1.657	1.348	1.290	1.060	1.320	0.120	1.658	2.101	1.821	1.775
Si + Na + K	9.683	9.695	8.611	8.697	8.557	8.603	8.605	8.753	8.852	9.000	8.781	9.837	8.434	8.104	8.324	8.355
[Na+K]/Al	33.593	43.086	3.276	3.679	2.101	2.238	2.147	3.886	3.763	5.065	4.032	9.997	1.763	1.080	1.561	1.712
$Fe^{3+}/(Fe^{3+}+Fe^{2+})$	0.403	0.361	0.182	0.181	0.152	0.091	0.187	0.189	0.234	0.265	0.196	0.317	0.170	0.170	0.156	0.126

Point_ID: spot identification; c: core; r: rim; i: intermediate zone; - : below detection limit; *Li2O contents derived from the LA-ICP-MS analyses; na: not analyzed; NF(Max): Normalization factor according to the method of Schumacher (in Leake et al., 1997) for maximum Fe^{3+}; Fe# =[Fe_T/(Fe_T+Mg)]

Table 11. (*cont.*) Sodic-calcic, calcic and sodic amphiboles in peralkaline granites from the Acaraú unit

Sample	**MAN-09**												**MAN-579**			
Crystal	c5		c2				c3		c1			c5a	c1	c2	c3	
Point_ID	1-c	1-r	2-c	2-i	6-i	7-i	8-ci	9	10-i	11-i	12-i	13	1-c	2-c	3-r1	3c
Structural formulae based on 23 oxygens																
Si (apfu)	7.954	7.960	7.731	7.770	7.494	7.513	7.491	7.797	7.701	7.754	7.792	8.130	7.674	7.401	7.588	7.680
Al^{IV}	0.046	0.040	0.269	0.230	0.506	0.487	0.509	0.203	0.299	0.246	0.208	0.000	0.326	0.599	0.412	0.320
Ti	0.000	0.000	0.000	0.000	0.000	0.000	0.000	0.000	0.000	0.000	0.000	0.000	0.000	0.000	0.000	0.000
T-site	**8.000**	**8.000**	**8.000**	**8.000**	**8.000**	**8.000**	**8.000**	**8.000**	**8.000**	**8.000**	**8.000**	**8.130**	**8.000**	**8.000**	**8.000**	**8.000**
Al^{VI}	0.005	0.000	0.000	0.022	0.000	0.000	0.010	0.043	0.007	0.000	0.037	0.171	0.105	0.052	0.060	0.075
Ti	0.000	0.000	0.020	0.009	0.162	0.081	0.106	0.008	0.016	0.026	0.008	0.001	0.014	0.026	0.045	0.054
Fe^{3+}	1.950	1.770	0.873	0.863	0.705	0.449	0.873	0.898	1.119	1.273	0.934	1.458	0.794	0.808	0.732	0.581
Zr	0.002	0.000	0.002	0.000	0.003	0.007	0.001	0.000	0.004	0.010	0.005	0.000	0.000	0.003	0.002	0.000
Zn	0.029	0.022	0.026	0.028	0.031	0.021	0.036	0.041	0.026	0.031	0.022	0.009	0.028	0.011	0.034	0.035
Mg	0.031	0.031	0.100	0.099	0.098	0.092	0.085	0.089	0.091	0.079	0.091	0.039	0.073	0.047	0.075	0.130
Li	0.054	0.009	0.000	0.000	0.000	0.000	0.000	0.000	0.000	0.000	0.000	0.153	0.026	0.027	0.030	0.030
Fe^{2+}	2.893	3.136	3.931	3.906	3.948	4.351	3.805	3.848	3.665	3.534	3.834	3.136	3.892	3.944	3.957	4.019
Mn	0.035	0.033	0.048	0.073	0.052	0.000	0.084	0.073	0.073	0.047	0.069	0.032	0.067	0.081	0.065	0.077
C-site	**5.000**	**5.000**	**5.000**	**5.000**	**5.000**	**5.000**	**5.000**	**5.000**	**5.000**	**5.000**	**5.000**	**5.000**	**5.000**	**5.000**	**5.000**	**5.000**
Li	0.155	0.203	0.000	0.000	0.000	0.000	0.000	0.000	0.000	0.000	0.000	0.054	0.000	0.000	0.000	0.000
Mn	0.000	0.000	0.027	0.000	0.032	0.083	0.000	0.000	0.000	0.014	0.000	0.000	0.000	0.000	0.000	0.000
Fe^{2+}	0.000	0.000	0.000	0.000	0.000	0.155	0.000	0.000	0.000	0.000	0.000	0.000	0.000	0.000	0.000	0.000
Ca	0.128	0.171	1.209	1.200	1.171	1.149	1.149	1.145	0.992	0.814	1.112	0.120	1.332	1.502	1.410	1.455
Na	1.717	1.627	0.764	0.800	0.796	0.613	0.851	0.855	1.008	1.173	0.888	1.696	0.668	0.498	0.590	0.545
B-site	**2.000**	**2.000**	**2.000**	**2.000**	**2.000**	**2.000**	**2.000**	**2.000**	**2.000**	**2.000**	**2.000**	**1.870**	**2.000**	**2.000**	**2.000**	**2.000**
Na	0.000	0.101	0.022	0.029	0.075	0.339	0.078	0.017	0.047	0.014	0.026	0.000	0.007	0.084	0.030	0.021
K	0.013	0.008	0.094	0.098	0.192	0.137	0.185	0.083	0.096	0.059	0.075	0.011	0.085	0.121	0.115	0.109
A-site	**0.013**	**0.109**	**0.116**	**0.127**	**0.267**	**0.476**	**0.262**	**0.101**	**0.142**	**0.073**	**0.101**	**0.011**	**0.092**	**0.205**	**0.145**	**0.130**
F	0.019	0.000	0.059	0.034	0.072	0.003	0.044	0.061	0.092	0.000	0.088	0.022	0.004	0.044	0.038	0.008
Cl	0.000	0.004	0.002	0.000	0.022	0.026	0.015	0.004	0.012	0.009	0.011	0.002	0.021	0.051	0.028	0.009
Cations	15.013	15.109	15.116	15.127	15.267	15.476	15.262	15.101	15.142	15.073	15.101	15.011	15.092	15.205	15.145	15.130

Table 12: Sodic-calcic, calcic and sodic amphiboles in peralkaline from the Acaraú unit

Sample	**MAN-579**															**6728**
Crystal			c4	c4				c5	c6	c8			c9		c10	c5
Point_ID	3-i	3-r2	4-r1	4-i2	4-c	4-i1	4-r2	5-c	6-c	8-r1	8-c	8-r2	9-c	9-r	10-r	5-r2
SiO_2 (wt%)	45.79	45.61	47.91	48.89	50.26	47.55	47.58	47.24	46.16	46.10	44.27	45.71	47.54	48.28	49.49	49.19
TiO_2	0.67	0.79	0.15	0.05	0.03	0.42	0.27	0.40	0.72	0.34	1.00	1.06	0.05	0.10	0.05	0.00
Al_2O_3	4.21	4.26	2.25	2.15	1.45	2.51	2.67	3.14	3.93	3.95	4.91	4.21	2.63	2.04	1.41	1.22
FeO	34.85	33.67	35.36	35.62	35.67	35.30	35.38	34.43	32.75	34.97	33.70	33.71	36.17	35.95	35.73	37.60
MnO	0.48	0.52	0.65	0.48	0.35	0.60	0.59	0.53	0.56	0.46	0.57	0.62	0.59	0.60	0.51	0.61
MgO	0.41	1.15	0.21	0.33	0.25	0.24	0.17	0.68	1.42	0.37	0.43	0.71	0.16	0.19	0.29	0.40
CaO	7.97	8.22	8.80	7.41	3.79	8.87	8.71	8.06	8.38	7.82	8.86	7.45	8.54	8.44	7.66	8.56
ZrO_2	-	0.10	-	0.04	-	-	0.03	0.03	0.02	0.02	-	-	-	-	-	
ZnO	0.34	0.08	0.22	0.24	0.27	0.25	0.21	0.36	0.16	0.27	0.29	0.27	0.27	0.26	0.23	0.34
Na_2O	2.41	2.26	1.56	2.44	4.31	1.76	1.78	2.18	2.16	2.47	2.26	2.79	1.95	1.88	2.21	1.71
K_2O	0.97	0.98	0.35	0.42	0.15	0.50	0.51	0.85	0.96	0.90	0.94	0.87	0.46	0.39	0.35	0.39
F	-	0.12	-	-	-	0.06	0.08	-	0.06	-	0.12	0.19	-	-	-	0.21
Cl	0.09	0.11	0.12	0.09	-	0.12	0.11	0.11	0.11	0.13	0.19	0.09	0.18	0.19	-	
Li_2O*	0.05	0.05	0.02	0.00	0.02	0.02	0.00	0.04	0.05	0.04	0.04	0.04	0.04	0.04	0.04	na
O=F=Cl	0.04	0.08	0.03	0.03	0.01	0.05	0.06	0.04	0.05	0.03	0.09	0.10	0.05	0.06	0.02	0.09
Total	98.24	97.83	97.58	98.15	96.61	98.15	98.03	98.05	97.39	97.81	97.49	97.63	98.56	98.34	98.03	100.14
Parameters (in apfu)																
NF (Max)	13eCNK	13eCNK	15eNK	13eCNK	15eNK	13eCNK	13eCNK	13eCNK	13eCNK	13eCNK	13eCNK	13eCNK	13eCNK	13eCNK	15eNK	8SiAl
Fe#	0.980	0.943	0.989	0.984	0.988	0.988	0.991	0.966	0.928	0.981	0.978	0.964	0.992	0.990	0.986	0.982
^{A}[Na+K+2Ca]	0.294	0.293	0.072	0.085	0.031	0.161	0.144	0.212	0.292	0.281	0.434	0.310	0.143	0.091	0.072	0.235
^{C}[Al+Fe^{3+}+2Ti]	1.107	1.077	0.759	0.942	1.380	0.751	0.772	0.941	0.954	1.061	0.911	1.163	0.898	0.846	0.799	0.359
Ca^{2+} + Al^{IV}	2.084	2.153	1.846	1.536	0.721	1.930	1.896	1.875	2.079	1.988	2.384	1.990	1.916	1.778	1.464	1.676
Si + Na + K	8.211	8.140	8.217	8.548	9.267	8.231	8.249	8.337	8.213	8.292	8.050	8.320	8.227	8.313	8.584	8.376
[Na+K]/Al	1.191	1.121	1.309	2.079	5.012	1.367	1.304	1.435	1.169	1.275	0.964	1.315	1.411	1.723	2.857	2.660
$Fe^{3+}/(Fe^{3+}+Fe^{2+})$	0.191	0.189	0.135	0.173	0.252	0.126	0.129	0.167	0.159	0.191	0.128	0.187	0.180	0.165	0.146	0.072

Point_ID: spot identification; c: core; r: rim; i: intermediate zone; - : below detection limit; *Li2O contents derived from the LA-ICP-MS analyses; na: not analyzed; NF(Max): Normalization factor according to the method of Schumacher (in Leake et al., 1997) for maximum Fe^{3+}; Fe# =[Fe_T/(Fe_T+Mg)]

Table 12. (*cont.*) Sodic-calcic, calcic and sodic amphiboles in peralkaline granites from the Acaraú unit

Sample	**MAN-579**															**6728**
Crystal			c4	c4				c5	c6	c8			c9		c10	c5
Point_ID	3-i	3-r2	4-r1	4-i2	4-c	4-i1	4-r2	5-c	6-c	8-r1	8-c	8-r2	9-c	9-r	10-r	5-r2
Structural formulae based on 23 oxygens																
Si (apfu)	7.272	7.246	7.662	7.717	7.919	7.586	7.594	7.495	7.351	7.347	7.149	7.281	7.534	7.656	7.835	7.774
Al^{IV}	0.728	0.754	0.338	0.283	0.081	0.414	0.406	0.505	0.649	0.653	0.851	0.719	0.466	0.344	0.165	0.226
Ti	0.000	0.000	0.000	0.000	0.000	0.000	0.000	0.000	0.000	0.000	0.000	0.000	0.000	0.000	0.000	0.000
T-site	**8.000**	**8.000**	**8.000**	**8.000**	**8.000**	**8.000**	**8.000**	**8.000**	**8.000**	**8.000**	**8.000**	**8.000**	**8.000**	**8.000**	**8.000**	**8.000**
Al^{VI}	0.060	0.044	0.086	0.117	0.188	0.058	0.096	0.082	0.089	0.088	0.084	0.071	0.025	0.037	0.097	0.000
Ti	0.080	0.094	0.018	0.005	0.004	0.051	0.033	0.048	0.086	0.041	0.122	0.127	0.006	0.012	0.006	0.000
Fe^{3+}	0.886	0.844	0.639	0.814	1.184	0.593	0.610	0.763	0.693	0.890	0.584	0.838	0.861	0.786	0.690	0.359
Zr	0.000	0.008	0.001	0.003	0.000	0.000	0.002	0.003	0.002	0.002	0.000	0.001	0.001	0.000	0.000	0.000
Zn	0.039	0.010	0.027	0.028	0.031	0.030	0.024	0.042	0.019	0.031	0.034	0.032	0.031	0.031	0.027	0.039
Mg	0.097	0.272	0.051	0.077	0.059	0.058	0.041	0.162	0.338	0.088	0.104	0.170	0.037	0.046	0.067	0.093
Li	0.030	0.030	0.002	0.003	0.000	0.014	0.003	0.023	0.030	0.027	0.027	0.026	0.027	0.027	0.004	0.000
Fe^{2+}	3.743	3.629	4.090	3.888	3.516	4.117	4.112	3.806	3.669	3.770	3.967	3.653	3.933	3.982	4.041	4.509
Mn	0.065	0.069	0.087	0.065	0.017	0.081	0.079	0.071	0.075	0.062	0.078	0.083	0.079	0.080	0.068	0.000
C-site	**5.000**	**5.000**	**5.000**	**5.000**	**5.000**	**5.000**	**5.000**	**5.000**	**5.000**	**5.000**	**5.000**	**5.000**	**5.000**	**5.000**	**5.000**	**5.000**
Li	0.000	0.000	0.009	0.000	0.014	0.000	0.000	0.000	0.000	0.000	0.000	0.000	0.000	0.000	0.023	0.000
Mn	0.000	0.000	0.000	0.000	0.030	0.000	0.000	0.000	0.000	0.000	0.000	0.000	0.000	0.000	0.000	0.082
Fe^{2+}	0.000	0.000	0.000	0.000	0.000	0.000	0.000	0.000	0.000	0.000	0.000	0.000	0.000	0.000	0.000	0.101
Ca	1.356	1.399	1.508	1.253	0.640	1.516	1.489	1.370	1.430	1.335	1.533	1.271	1.450	1.434	1.299	1.450
Na	0.644	0.601	0.484	0.747	1.317	0.484	0.511	0.630	0.570	0.665	0.467	0.729	0.550	0.566	0.678	0.367
B-site	**2.000**	**2.000**	**2.000**	**2.000**	**2.000**	**2.000**	**2.000**	**2.000**	**2.000**	**2.000**	**2.000**	**2.000**	**2.000**	**2.000**	**2.000**	**2.000**
Na	0.098	0.095	0.000	0.000	0.000	0.060	0.040	0.041	0.097	0.098	0.240	0.133	0.049	0.012	0.000	0.156
K	0.196	0.198	0.072	0.085	0.031	0.101	0.104	0.172	0.195	0.183	0.194	0.178	0.094	0.079	0.072	0.079
A-site	**0.294**	**0.293**	**0.072**	**0.085**	**0.031**	**0.161**	**0.144**	**0.212**	**0.292**	**0.281**	**0.434**	**0.310**	**0.143**	**0.091**	**0.072**	**0.235**
F	0.025	0.062	0.003	0.007	0.000	0.033	0.040	0.015	0.032	0.006	0.060	0.097	0.010	0.014	0.005	0.107
Cl	0.023	0.030	0.032	0.024	0.016	0.032	0.029	0.029	0.031	0.034	0.052	0.024	0.049	0.052	0.018	0.002
Cations	15.294	15.293	15.072	15.085	15.031	15.161	15.144	15.212	15.292	15.281	15.434	15.310	15.143	15.091	15.072	15.235

Table 13: Sodic-calcic, calcic and sodic amphiboles in peralkaline from the Acaraú unit

Sample	**MAN-6728**														**6730**
Crystal	c5		c4		c3				c2					c1	c4
Point_ID	5-c	5-r2	4-c	4-i2	3-r3	3-i2	3-i1	3-c	2-r2	2-i2	2-c	2-i1	2-r1	1-c	4-r
SiO_2 (wt%)	49.46	49.12	45.81	45.70	44.60	44.35	44.85	44.60	43.71	46.20	45.40	43.72	48.11	44.08	51.51
TiO_2	0.03	0.07	0.78	1.13	1.28	1.53	1.27	1.41	0.95	0.60	0.38	1.27	0.06	0.97	0.03
Al_2O_3	1.31	1.31	3.86	3.15	3.76	4.23	3.09	3.32	4.37	3.02	3.16	4.34	1.24	4.37	0.63
FeO	36.30	36.37	35.08	36.12	32.75	33.37	33.61	33.94	33.47	34.13	35.05	34.66	37.06	34.36	36.18
MnO	0.67	0.61	0.55	0.54	0.54	0.60	0.54	0.59	0.50	0.49	0.52	0.61	0.67	0.63	0.51
MgO	0.42	0.38	1.07	0.56	0.81	0.76	0.50	0.73	0.36	0.51	0.51	0.49	0.44	1.00	0.42
CaO	8.21	8.41	8.85	8.25	8.34	7.52	7.88	7.87	8.86	8.59	8.69	9.22	8.80	8.76	5.05
ZrO_2	na	na	na	na	na	na	na	na	na	na	na	na	na	na	0.02
ZnO	0.33	0.32	0.31	0.29	0.29	0.30	0.21	0.32	0.27	0.27	0.27	0.30	0.36	0.20	0.14
Na_2O	1.89	1.95	1.98	2.29	2.25	2.68	2.62	2.62	2.31	2.03	2.05	2.18	1.67	2.18	3.70
K_2O	0.42	0.45	0.90	0.88	0.84	0.84	0.97	0.94	0.87	0.90	0.89	0.90	0.46	0.89	0.13
F	-	-	-	-	-	-	0.21	0.06	0.07	0.26	-	-	-	0.16	-
Cl	-	-	0.10	0.07	0.07	0.07	-	0.07	0.13	0.08	0.10	0.09	-	0.10	-
Li_2O*	0.04	0.04												0.04	0.04
O=F=Cl	0.00	0.01	0.02	0.01	0.02	0.02	0.10	0.04	0.06	0.13	0.02	0.04	0.00	0.09	0.00
Total	99.08	99.02	99.26	98.96	95.51	96.22	95.71	96.43	95.82	96.94	96.96	97.80	98.85	97.67	98.36
Parameters (in apfu)															
NF (Max)	15eNK	8SiAl	8SiAl	8SiAl	13eCNK	8SiAl	8SiAl	8SiAl	13eCNK	13eCNK	8SiAl	8SiAl	8SiAl	8SiAl	15eNK
Fe#	0.980	0.982	0.948	0.973	0.958	0.961	0.974	0.963	0.981	0.974	0.975	0.976	0.979	0.951	0.965
^{A}[Na+K+2Ca]	0.085	0.153	0.414	0.601	0.356	0.336	0.455	0.582	0.490	0.317	0.392	0.644	0.388	0.567	0.092
^{C}[Al+Fe^{3+}+2Ti]	0.745	0.651	0.685	0.299	0.864	1.153	0.733	0.518	0.725	0.694	0.652	0.434	0.077	0.601	0.622
Ca^{2+} + Al^{IV}	1.610	1.667	2.229	2.032	2.150	2.114	1.994	2.036	2.349	1.996	2.122	2.455	1.757	2.362	1.640
Si + Na + K	8.433	8.442	8.068	8.298	8.205	8.210	8.442	8.391	8.142	8.321	8.225	8.044	8.382	8.036	8.436
[Na+K]/Al	2.720	2.813	1.095	1.495	1.224	1.259	1.735	1.606	1.086	1.430	1.371	1.053	2.627	1.043	2.688
$Fe^{3+}/(Fe^{3+}+Fe^{2+})$	0.151	0.132	0.107	0.005	0.113	0.173	0.090	0.036	0.091	0.102	0.117	0.026	0.013	0.078	0.115

Point_ID: spot identification; c: core; r: rim; i: intermediate zone; - : below detection limit; *Li2O contents derived from the LA-ICP-MS analyses; na: not analyzed; NF(Max): Normalization factor according to the method of Schumacher (in Leake et al., 1997) for maximum Fe^{3+}; Fe# =[Fe_T/(Fe_T+Mg)]

Table 13. (*cont.*) Sodic-calcic, calcic and sodic amphiboles in peralkaline granites from the Acaraú unit

Sample	**MAN-6728**														**6730**
Crystal	c5		c4		c3				c2					c1	c4
Point_ID	5-c	5-r2	4-c	4-i2	3-r3	3-i2	3-i1	3-c	2-r2	2-i2	2-c	2-i1	2-r1	1-c	4-r
Structural formulae based on 23 oxygens															
Si (apfu)	7.772	7.756	7.278	7.398	7.315	7.192	7.399	7.354	7.218	7.497	7.394	7.162	7.765	7.163	7.814
Al^{IV}	0.228	0.244	0.722	0.602	0.685	0.808	0.601	0.646	0.782	0.503	0.606	0.838	0.235	0.837	0.186
Ti	0.000	0.000	0.000	0.000	0.000	0.000	0.000	0.000	0.000	0.000	0.000	0.000	0.000	0.000	0.000
T-site	**8.000**	**8.000**	**8.000**	**8.000**	**8.000**	**8.000**	**8.000**	**8.000**	**8.000**	**8.000**	**8.000**	**8.000**	**8.000**	**8.000**	**8.000**
Al^{VI}	0.015	0.000	0.000	0.000	0.043	0.000	0.000	0.000	0.068	0.073	0.000	0.000	0.000	0.000	0.045
Ti	0.004	0.008	0.093	0.138	0.158	0.186	0.158	0.175	0.118	0.073	0.046	0.156	0.007	0.119	0.020
Fe^{3+}	0.723	0.635	0.498	0.024	0.506	0.781	0.417	0.168	0.421	0.474	0.560	0.122	0.063	0.363	0.538
Zr	0.000	0.000	0.000	0.000	0.000	0.000	0.000	0.000	0.000	0.000	0.000	0.000	0.000	0.000	0.001
Zn	0.038	0.037	0.036	0.034	0.036	0.036	0.025	0.039	0.033	0.033	0.032	0.037	0.043	0.024	0.021
Mg	0.099	0.088	0.253	0.135	0.197	0.183	0.123	0.179	0.089	0.123	0.123	0.118	0.105	0.243	0.171
Li	0.000	0.000	0.000	0.000	0.000	0.000	0.000	0.000	0.000	0.000	0.000	0.000	0.000	0.000	0.000
Fe^{2+}	4.048	4.168	4.119	4.669	3.986	3.745	4.220	4.439	4.201	4.157	4.215	4.567	4.782	4.250	4.137
Mn	0.073	0.064	0.000	0.000	0.075	0.070	0.056	0.000	0.070	0.067	0.025	0.000	0.000	0.000	0.068
C-site	**5.000**	**5.000**	**5.000**	**5.000**	**5.000**	**5.000**	**5.000**	**5.000**	**5.000**	**5.000**	**5.000**	**5.000**	**5.000**	**5.000**	**5.000**
Li	0.026	0.026	0.000	0.000	0.000	0.000	0.000	0.000	0.000	0.000	0.000	0.000	0.000	0.026	0.000
Mn	0.016	0.018	0.074	0.074	0.000	0.013	0.020	0.082	0.000	0.000	0.046	0.085	0.091	0.086	0.016
Fe^{2+}	0.000	0.000	0.043	0.197	0.000	0.000	0.000	0.072	0.000	0.000	0.000	0.059	0.157	0.056	0.000
Ca	1.382	1.423	1.507	1.430	1.465	1.306	1.393	1.391	1.567	1.492	1.516	1.617	1.522	1.526	1.454
Na	0.576	0.533	0.376	0.299	0.535	0.681	0.587	0.455	0.433	0.508	0.438	0.239	0.230	0.306	0.530
B-site	**2.000**	**2.000**	**2.000**	**2.000**	**2.000**	**2.000**	**2.000**	**2.000**	**2.000**	**2.000**	**2.000**	**2.000**	**2.000**	**2.000**	**2.000**
Na	0.000	0.063	0.232	0.418	0.181	0.162	0.252	0.384	0.306	0.131	0.208	0.455	0.292	0.381	0.000
K	0.000	0.000	0.000	0.000	0.000	0.000	0.000	0.000	0.000	0.000	0.000	0.000	0.000	0.000	0.000
A-site	**0.085**	**0.153**	**0.414**	**0.601**	**0.356**	**0.336**	**0.455**	**0.582**	**0.490**	**0.317**	**0.392**	**0.644**	**0.388**	**0.567**	**0.092**
F	0.000	0.006	0.000	0.000	0.000	0.000	0.107	0.032	0.034	0.135	0.000	0.024	0.000	0.084	0.027
Cl	0.000	0.000	0.028	0.018	0.019	0.018	0.016	0.019	0.037	0.021	0.028	0.026	0.000	0.027	0.005
Cations	15.085	15.153	15.414	15.601	15.356	15.336	15.455	15.582	15.490	15.317	15.392	15.644	15.388	15.567	15.092

Table 14: Astrophyllite in peralkaline alkali feldspar granites from the Mandira unit

Sample	**MAN-5S**								**MAN-13A**		
Crystal	c1			c4		c3			c2		
Point_ID	1-c	2-i	3-r	1-ci	2-r	8-c	9-r	10-ri	1-c1	2- i1	3-r1
SiO_2 (wt%)	34.83	35.48	35.64	34.90	35.99	35.80	36.09	35.51	33.53	34.17	34.18
TiO_2	8.10	7.56	7.81	7.95	10.67	8.17	9.89	7.90	7.84	8.15	8.44
Al_2O_3	0.83	0.65	0.54	0.76	0.94	0.55	0.55	0.80	1.00	1.14	0.68
FeO	35.46	35.13	35.65	35.40	36.45	35.96	36.07	35.43	33.15	34.68	34.29
MnO	1.67	1.56	1.73	1.66	1.71	1.69	1.68	1.70	1.46	1.63	1.59
MgO	0.01	0.01	0.00	0.01	0.01	0.00	0.02	0.02	0.00	0.00	0.02
CaO	0.14	0.07	0.05	0.19	0.42	0.06	0.22	0.29	2.99	0.38	0.06
ZrO_2	4.29	5.01	4.37	5.02	1.72	4.95	1.82	4.52	4.26	4.22	3.25
ZnO	0.38	0.36	0.39	0.41	0.37	0.29	0.37	0.36	0.33	0.35	0.43
BaO	-	0.12	-	-	-	-	-	-	0.09	-	0.12
Na_2O	2.78	2.82	2.97	2.88	2.66	2.62	2.98	2.90	2.68	2.70	3.20
K_2O	5.25	5.39	5.20	5.27	5.21	5.16	5.20	5.39	5.17	5.33	5.26
Nb_2O_5	2.12	2.44	2.54	2.37	0.32	1.48	0.82	2.45	1.76	1.78	2.29
Cl	-	-	-	0.01	-	0.01	-	-	-	-	-
F	0.83	0.52	0.87	0.98	0.94	0.78	0.72	0.70	2.04	0.95	1.08
O=Cl=F	0.35	0.22	0.37	0.41	0.39	0.33	0.30	0.30	0.86	0.40	0.45
Total	96.34	96.90	97.36	97.37	97.00	97.18	96.12	97.65	95.45	95.07	94.43
Structural formulae based on 28.5 oxygens											
Si (apfu)	7.783	7.870	7.873	7.743	7.872	7.907	7.968	7.816	7.634	7.737	7.790
Al	0.219	0.000	0.000	0.000	0.000	0.000	0.000	0.000	0.000	0.000	0.000
Sum T	**8.003**	**7.870**	**7.873**	**7.743**	**7.872**	**7.907**	**7.968**	**7.816**	**7.634**	**7.737**	**7.790**
Ti	1.362	1.261	1.297	1.327	1.756	1.357	1.643	1.307	1.343	1.388	1.447
Zr	0.468	0.541	0.470	0.543	0.183	0.533	0.196	0.485	0.472	0.466	0.361
Nb	0.222	0.253	0.262	0.246	0.032	0.153	0.084	0.252	0.187	0.188	0.244
Sum D	**2.051**	**2.055**	**2.029**	**2.116**	**1.971**	**2.043**	**1.923**	**2.044**	**2.003**	**2.042**	**2.052**
Fe^{2+}	6.625	6.516	6.587	6.570	6.668	6.642	6.659	6.522	6.313	6.567	6.536
Mn	0.315	0.293	0.323	0.311	0.317	0.317	0.314	0.316	0.281	0.313	0.306
Mg	0.005	0.004	0.001	0.003	0.002	0.000	0.006	0.006	0.001	0.000	0.005
Zn	0.062	0.059	0.063	0.066	0.059	0.047	0.061	0.058	0.055	0.058	0.073
Na	0.000	0.127	0.026	0.050	0.000	0.000	0.000	0.098	0.350	0.063	0.079
Sum C	**7.007**	**7.000**	**7.000**	**7.000**	**7.046**	**7.006**	**7.039**	**7.000**	**7.000**	**7.000**	**7.000**
Ca	0.033	0.016	0.011	0.044	0.099	0.014	0.053	0.068	0.730	0.092	0.015
Ba	0.000	0.011	0.000	0.000	0.000	0.000	0.000	0.000	0.008	0.000	0.011
Na	0.967	0.984	0.989	0.956	0.901	0.986	0.947	0.932	0.270	0.908	0.985
Sum B	**1.000**	**1.000**	**1.000**	**1.000**	**1.000**	**1.000**	**1.000**	**1.000**	**1.000**	**1.000**	**1.000**
Na	0.238	0.101	0.255	0.234	0.227	0.135	0.326	0.205	0.563	0.216	0.351
K	1.497	1.525	1.464	1.491	1.452	1.455	1.464	1.514	1.503	1.540	1.530
Sum A	**1.734**	**1.637**	**1.720**	**1.724**	**1.679**	**1.590**	**1.790**	**1.719**	**2.074**	**1.756**	**1.892**
Cations	19.796	19.732	19.763	19.783	19.810	19.690	19.864	19.786	19.979	19.838	19.918
Cl	0.000	0.000	0.000	0.002	0.000	0.002	0.000	0.001	0.000	0.000	0.000
F	0.589	0.361	0.607	0.689	0.648	0.543	0.501	0.490	1.471	0.683	0.777

Point_ID: spot identification; c: core; r: rim; i: intermediate zone; - : below detection limit

Table 15: Astrophyllite in peralkaline alkali feldspar granites from the Mandira unit

Sample	**MAN-13A**											
Crystal			c2a									
Point_ID	4-esc2	5-c2	6-r	7-i	8-c	9-ci	10-i	11-i	12-i	13-i	14-ri	15-r
SiO_2 (wt%)	35.52	34.09	34.61	34.15	34.40	33.63	34.46	34.53	34.91	34.84	35.08	34.21
TiO_2	8.79	8.18	8.12	7.84	7.52	7.49	7.34	7.69	8.75	7.73	8.05	8.13
Al_2O_3	0.47	1.22	0.66	0.77	0.77	0.69	0.79	0.75	0.41	0.37	0.42	0.65
FeO	35.36	36.02	33.35	33.62	33.43	32.91	33.73	33.67	33.44	32.99	33.32	33.16
MnO	1.57	1.62	1.64	1.62	1.66	1.67	1.67	1.72	1.63	1.64	1.80	1.57
MgO	-	0.01	0.01	-	0.02	-	-	0.01	-	0.03	0.02	0.01
CaO	0.02	0.26	0.12	0.09	0.37	0.06	0.09	0.06	0.08	0.02	0.07	0.07
ZrO_2	3.53	4.48	3.98	4.39	4.23	4.58	3.97	4.02	4.52	4.79	4.50	4.14
ZnO	0.29	0.37	0.38	0.33	0.38	0.28	0.38	0.26	0.40	0.37	0.42	0.28
BaO	-	-	-	0.01	0.07	0.05	0.07	-	-	0.02	0.08	0.02
Na_2O	3.20	2.68	3.02	2.99	2.88	2.94	2.93	2.98	3.00	3.03	3.12	2.95
K_2O	5.42	5.53	5.24	5.29	5.37	5.31	5.14	5.28	5.18	5.14	5.04	5.24
Nb_2O_5	1.94	1.96	2.10	2.80	2.87	2.43	2.83	2.62	1.41	1.57	1.41	2.30
Cl	-	-	-	0.01	-	-	0.01	0.01	-	-	-	-
F	0.77	0.75	1.06	0.95	0.97	0.98	0.96	1.29	0.98	1.17	1.11	1.21
O=Cl=F	0.32	0.32	0.45	0.40	0.41	0.41	0.40	0.54	0.41	0.49	0.47	0.51
Total	96.55	96.87	93.84	94.44	94.52	92.61	93.97	94.32	94.28	93.20	93.99	93.42
Structural formulae based on 28.5 oxygens												
Si (apfu)	7.877	7.620	7.897	7.779	7.828	7.823	7.876	7.868	7.915	8.007	7.990	7.857
Al	0.000	0.000	0.000	0.000	0.000	0.000	0.000	0.000	0.000	0.000	0.000	0.000
T-site	**7.877**	**7.620**	**7.897**	**7.779**	**7.828**	**7.823**	**7.876**	**7.868**	**7.915**	**8.007**	**7.990**	**7.857**
Ti	1.467	1.376	1.394	1.344	1.287	1.311	1.262	1.318	1.492	1.336	1.379	1.405
Zr	0.381	0.488	0.443	0.487	0.469	0.519	0.443	0.446	0.499	0.537	0.500	0.464
Nb	0.202	0.205	0.224	0.298	0.305	0.264	0.303	0.279	0.149	0.169	0.150	0.247
D-site	**2.050**	**2.069**	**2.061**	**2.129**	**2.062**	**2.094**	**2.008**	**2.044**	**2.141**	**2.042**	**2.029**	**2.116**
Fe^{2+}	6.559	6.733	6.364	6.405	6.361	6.402	6.447	6.417	6.341	6.341	6.347	6.369
Mn	0.294	0.306	0.316	0.313	0.320	0.330	0.323	0.332	0.313	0.319	0.347	0.304
Mg	0.000	0.004	0.003	0.001	0.006	0.000	0.000	0.002	0.000	0.009	0.008	0.002
Zn	0.047	0.061	0.064	0.055	0.064	0.048	0.064	0.043	0.067	0.063	0.070	0.048
Na	0.100	0.000	0.252	0.226	0.249	0.221	0.167	0.205	0.279	0.268	0.228	0.276
C-site	**7.000**	**7.104**	**7.000**	**7.000**	**7.000**	**7.000**	**7.000**	**7.000**	**7.000**	**7.000**	**7.000**	**7.000**
Ca	0.004	0.063	0.029	0.023	0.089	0.016	0.023	0.016	0.019	0.005	0.018	0.017
Ba	0.000	0.000	0.000	0.001	0.006	0.005	0.007	0.000	0.000	0.002	0.007	0.002
Na	0.996	0.937	0.971	0.977	0.911	0.984	0.977	0.984	0.981	0.995	0.982	0.983
B-site	**1.000**	**1.000**	**1.000**	**1.000**	**1.000**	**1.000**	**1.000**	**1.000**	**1.000**	**1.000**	**1.000**	**1.000**
Na	0.281	0.225	0.114	0.116	0.110	0.120	0.156	0.126	0.059	0.086	0.169	0.056
K	1.534	1.578	1.524	1.539	1.559	1.574	1.499	1.534	1.499	1.506	1.463	1.536
A-site	**1.815**	**1.803**	**1.637**	**1.655**	**1.675**	**1.699**	**1.661**	**1.660**	**1.558**	**1.594**	**1.639**	**1.593**
Cations	19.865	19.918	19.772	19.769	19.770	19.806	19.757	19.773	19.723	19.744	19.771	19.741
Cl	0.000	0.001	0.000	0.003	0.000	0.000	0.003	0.003	0.000	0.000	0.000	0.000
F	0.537	0.529	0.764	0.684	0.697	0.724	0.692	0.926	0.704	0.849	0.801	0.881

Point_ID: spot identification; c: core; r: rim; i: intermediate zone; - : below detection limit

Table 16: Astrophyllite in peralkaline alkali feldspar granites from the Mandira unit

Sample	**MAN-4476**											
Crystal	c1		c2					c3			c4	
Point_ID	1-r1	1-c	2-r1	2-c1	2-c2	2-r2	2-r3	3-r1	3-r2	3-r3	4-r1	4-c
SiO_2 (wt%)	35.05	35.27	35.19	35.20	34.90	35.34	35.05	35.35	35.42	35.29	35.56	35.57
TiO_2	9.20	8.92	10.71	10.27	9.90	9.79	9.60	9.01	8.60	8.63	9.31	10.07
Al_2O_3	0.74	0.68	0.62	0.55	0.56	0.60	0.51	0.49	0.54	0.64	0.56	0.73
FeO	34.38	34.02	34.86	34.47	35.24	35.37	35.15	35.38	35.13	35.20	35.10	35.14
MnO	1.81	1.74	2.04	2.01	1.99	2.00	2.03	2.00	1.91	1.87	1.90	1.87
MgO	-	0.02	-	0.02	0.01	-	-	0.01	0.01	-	0.01	-
CaO	0.08	0.25	0.23	0.20	0.17	0.25	0.17	0.03	0.03	0.06	0.13	0.29
ZrO_2	0.91	0.91	0.86	0.86	1.12	1.02	1.12	1.18	1.16	1.29	1.07	0.92
ZnO	0.33	0.48	0.39	0.40	0.38	0.41	0.37	0.37	0.36	0.39	0.38	0.27
BaO	-	-	-	-	-	0.04	-	-	-	-	-	-
Na_2O	2.73	2.80	2.80	2.86	2.92	2.80	2.80	3.02	2.98	2.82	2.84	2.77
K_2O	5.45	5.31	5.35	5.18	5.22	5.41	5.30	5.40	5.39	5.40	5.46	5.50
Nb_2O_5	1.96	1.43	0.36	0.31	0.58	0.60	0.66	2.02	1.97	2.18	1.12	0.76
Cl	-	0.02	-	0.01	-	0.01	0.03	-	0.02	-	-	0.03
F	0.78	0.99	0.96	0.80	0.95	0.80	0.78	0.69	0.72	0.63	0.90	0.89
O=Cl=F	0.33	0.42	0.40	0.34	0.40	0.34	0.33	0.29	0.31	0.26	0.38	0.38
Total	93.08	92.42	93.95	92.80	93.54	94.12	93.25	94.66	93.92	94.12	93.97	94.42
Structural formulae based on 28.5 oxygens												
Si (apfu)	7.981	8.081	7.936	8.015	7.941	7.980	7.992	7.957	8.025	7.980	8.036	7.980
Al	0.000	0.000	0.000	0.000	0.000	0.000	0.000	0.000	0.000	0.000	0.000	0.000
T-site	**7.981**	**8.081**	**7.936**	**8.015**	**7.941**	**7.980**	**7.992**	**7.957**	**8.025**	**7.980**	**8.036**	**7.980**
Ti	1.576	1.537	1.817	1.759	1.695	1.663	1.647	1.526	1.466	1.468	1.583	1.699
Zr	0.101	0.101	0.094	0.096	0.125	0.113	0.125	0.130	0.128	0.142	0.118	0.101
Nb	0.209	0.153	0.038	0.033	0.062	0.064	0.070	0.213	0.209	0.231	0.118	0.080
D-site	**1.885**	**1.792**	**1.949**	**1.888**	**1.881**	**1.839**	**1.842**	**1.868**	**1.802**	**1.840**	**1.819**	**1.880**
Fe^{2+}	6.547	6.518	6.575	6.564	6.706	6.680	6.703	6.660	6.657	6.656	6.634	6.593
Mn	0.349	0.338	0.390	0.388	0.383	0.382	0.392	0.381	0.367	0.358	0.364	0.355
Mg	0.000	0.007	0.000	0.005	0.002	0.000	0.000	0.002	0.002	0.000	0.005	0.000
Zn	0.055	0.081	0.065	0.068	0.064	0.069	0.063	0.061	0.060	0.064	0.064	0.044
Na	0.048	0.056	0.000	0.000	0.000	0.000	0.000	0.000	0.000	0.000	0.000	0.007
C-site	**7.000**	**7.000**	**7.030**	**7.024**	**7.156**	**7.131**	**7.158**	**7.105**	**7.085**	**7.079**	**7.066**	**7.000**
Ca	0.019	0.061	0.055	0.049	0.041	0.061	0.043	0.008	0.007	0.015	0.032	0.069
Ba	0.000	0.000	0.000	0.000	0.000	0.003	0.000	0.000	0.000	0.000	0.000	0.000
Na	0.981	0.939	0.945	0.951	0.959	0.939	0.957	0.992	0.993	0.985	0.968	0.931
B-site	**1.000**	**1.000**	**1.000**	**1.000**	**1.000**	**1.000**	**1.000**	**1.000**	**1.000**	**1.000**	**1.000**	**1.000**
Na	0.176	0.248	0.279	0.311	0.329	0.287	0.280	0.326	0.316	0.251	0.277	0.267
K	1.583	1.552	1.539	1.505	1.515	1.558	1.542	1.551	1.558	1.558	1.574	1.574
A-site	**1.759**	**1.800**	**1.818**	**1.816**	**1.844**	**1.849**	**1.822**	**1.877**	**1.874**	**1.808**	**1.851**	**1.841**
Cations	19.824	19.857	19.896	19.890	19.973	19.960	19.952	19.937	19.930	19.877	19.921	19.893
Cl	0.001	0.008	0.000	0.004	0.000	0.005	0.012	0.000	0.007	0.000	0.000	0.010
F	0.562	0.716	0.683	0.574	0.682	0.573	0.561	0.490	0.518	0.448	0.643	0.632

Point_ID: spot identification; c: core; r: rim; i: intermediate zone; - : below detection limit

Table 17: Astrophyllite in peralkaline alkali feldspar granites from the Mandira unit

Sample	**MAN-4476**									
Crystal	c4		c5			c6			c7	c8
Point_ID	4-c2	4-c3	5-r1	5-r2	5-r3	6-r1	6-c	6-r2	7-c	8-c
SiO_2 (wt%)	35.63	35.75	35.66	35.35	35.69	35.77	35.24	35.33	35.95	35.66
TiO_2	9.97	9.95	10.20	10.57	9.83	9.45	9.66	10.13	8.92	9.44
Al_2O_3	0.51	0.48	0.46	0.59	0.46	0.43	0.59	0.46	0.51	0.51
FeO	34.78	35.23	35.37	35.21	35.10	35.19	35.14	34.87	34.98	34.86
MnO	1.93	1.88	1.94	1.92	1.93	2.07	2.00	1.94	2.10	1.93
MgO	-	-	-	0.01	0.02	0.03	-	0.01	0.01	-
CaO	0.23	0.17	0.13	0.20	0.19	0.07	0.16	0.14	0.02	0.10
ZrO_2	1.02	1.02	0.74	0.74	0.71	0.91	0.74	0.65	0.95	0.82
ZnO	0.42	0.31	0.47	0.42	0.37	0.33	0.37	0.47	0.43	0.46
BaO	-	-	-	-	-	0.06	-	-	-	0.01
Na_2O	2.86	3.04	3.09	2.84	2.98	3.03	2.97	3.11	2.92	3.06
K_2O	5.29	5.29	5.15	5.15	5.16	5.01	5.12	5.18	5.26	5.29
Nb_2O_5	0.71	0.61	0.90	0.38	0.83	0.79	0.73	0.54	1.50	0.87
Cl	0.01	0.04	-	0.01	0.01	0.01	0.01	0.03	-	-
F	0.70	1.02	0.83	0.81	0.77	0.81	0.82	0.91	0.71	0.87
O=Cl=F	0.30	0.44	0.35	0.34	0.33	0.34	0.35	0.39	0.30	0.37
Total	93.77	94.35	94.59	93.86	93.71	93.62	93.21	93.37	93.95	93.51
Structural formula based on 20 cations and 28.5 oxygens										
Si (apfu)	8.033	8.034	7.987	7.967	8.053	8.088	8.014	8.016	8.101	8.077
Al	0.000	0.000	0.000	0.000	0.000	0.000	0.000	0.000	0.000	0.000
T-site	**8.033**	**8.034**	**7.987**	**7.967**	**8.053**	**8.088**	**8.014**	**8.016**	**8.101**	**8.077**
Ti	1.691	1.682	1.719	1.792	1.668	1.607	1.653	1.729	1.512	1.608
Zr	0.112	0.111	0.081	0.081	0.078	0.101	0.082	0.071	0.104	0.090
Nb	0.075	0.065	0.094	0.040	0.088	0.084	0.078	0.057	0.158	0.092
D-site	**1.877**	**1.858**	**1.894**	**1.913**	**1.834**	**1.792**	**1.813**	**1.858**	**1.774**	**1.791**
Fe^{2+}	6.557	6.621	6.625	6.636	6.624	6.655	6.683	6.617	6.592	6.604
Mn	0.368	0.358	0.368	0.366	0.369	0.396	0.385	0.373	0.401	0.370
Mg	0.000	0.000	0.000	0.003	0.005	0.009	0.001	0.003	0.002	0.001
Zn	0.071	0.052	0.078	0.069	0.061	0.055	0.063	0.078	0.072	0.077
Na	0.003	0.000	0.000	0.000	0.000	0.000	0.000	0.000	0.000	0.000
C-site	**7.000**	**7.031**	**7.071**	**7.075**	**7.059**	**7.115**	**7.133**	**7.071**	**7.067**	**7.052**
Ca	0.056	0.041	0.032	0.048	0.046	0.017	0.039	0.035	0.005	0.023
Ba	0.000	0.000	0.000	0.000	0.000	0.005	0.000	0.000	0.000	0.001
Na	0.944	0.959	0.968	0.952	0.954	0.983	0.961	0.965	0.995	0.977
B-site	**1.000**	**1.000**	**1.000**	**1.000**	**1.000**	**1.000**	**1.000**	**1.000**	**1.000**	**1.000**
Na	0.303	0.366	0.374	0.289	0.349	0.345	0.348	0.403	0.281	0.367
K	1.521	1.517	1.471	1.481	1.485	1.445	1.485	1.499	1.512	1.529
A-site	**1.824**	**1.882**	**1.846**	**1.770**	**1.835**	**1.795**	**1.834**	**1.903**	**1.793**	**1.897**
Cations	19.870	19.932	19.918	19.882	19.902	19.907	19.952	19.970	19.871	19.953
Cl	0.005	0.014	0.000	0.004	0.003	0.005	0.004	0.010	0.000	0.000
F	0.500	0.725	0.589	0.577	0.553	0.576	0.587	0.653	0.502	0.623

Point_ID: spot identification; c: core; r: rim; i: intermediate zone; - : below detection limit

Table 18: Astrophyllite in peralkaline alkali feldspar granites from the Papanduva Pluton

Sample	**MR-01**										
Crystal	1				4		4'		3		
Point_ID	1-b	2-b	3-n	4-n	1-n	2-n	1-b	2-i	3-n	4-n	5
SiO_2 (wt%)	34.32	34.57	34.95	35.26	35.24	34.87	35.09	34.99	35.07	35.01	35.17
TiO_2	9.95	8.68	9.02	9.07	8.82	8.68	9.37	9.73	9.72	9.62	8.88
Al_2O_3	0.92	0.61	0.63	0.43	0.73	0.29	0.50	0.57	0.49	0.66	0.56
FeO	32.74	31.72	31.76	32.33	32.74	32.81	31.17	31.46	31.43	31.23	30.99
MnO	4.19	3.94	4.03	4.21	3.22	3.30	4.79	4.54	4.57	4.60	4.61
MgO	0.11	0.13	0.15	0.13	0.13	0.09	0.19	0.17	0.18	0.21	0.26
CaO	1.00	1.05	1.15	0.82	1.27	0.62	0.65	0.57	0.48	0.63	0.92
ZrO_2	1.28	3.18	2.62	3.06	3.25	4.16	2.47	2.05	2.14	1.53	2.53
ZnO	-	-	-	-	-	-	-	-	-	-	-
BaO	0.10	-	-	-	-	-	0.09	0.19	0.07	0.13	0.07
Na_2O	2.23	2.42	2.29	2.61	2.25	2.43	2.47	2.58	2.63	2.62	2.19
K_2O	5.27	5.10	5.28	5.18	5.07	5.42	5.19	5.38	5.49	5.60	5.55
Nb_2O_5	1.65	2.33	2.75	2.02	1.59	1.48	2.23	2.04	2.24	2.08	2.40
Cl	-	-	-	-	-	-	-	-	-	-	-
F	0.58	0.46	0.31	0.28	0.38	0.54	0.90	0.59	0.50	0.42	0.74
O=Cl=F	0.24	0.19	0.13	0.12	0.16	0.23	0.38	0.25	0.21	0.18	0.31
Total	94.91	94.69	95.69	95.28	95.28	95.30	94.73	94.61	95.54	95.21	94.56
Structural formulae based on 28.5 oxygens											
Si (apfu)	7.719	7.801	7.787	7.865	7.866	7.857	7.874	7.850	7.815	7.829	7.902
Al	0.244	0.162	0.165	0.113	0.134	0.077	0.126	0.150	0.129	0.171	0.098
Sum T	**7.963**	**7.963**	**7.952**	**7.978**	**8.000**	**7.934**	**8.000**	**8.000**	**7.944**	**8.000**	**8.000**
Ti	1.683	1.473	1.512	1.522	1.481	1.471	1.581	1.642	1.629	1.618	1.501
Zr	0.140	0.281	0.202	0.268	0.353	0.373	0.185	0.144	0.137	0.164	0.247
Nb	0.174	0.246	0.287	0.211	0.166	0.156	0.234	0.214	0.234	0.218	0.252
Sum D	**2.000**	**2.000**	**2.000**	**2.000**	**2.000**	**2.000**	**2.000**	**2.000**	**2.000**	**2.000**	**2.000**
Fe^{2+}	6.157	5.985	5.917	6.030	6.111	6.182	5.848	5.902	5.857	5.840	5.822
Mn	0.798	0.753	0.760	0.795	0.609	0.630	0.910	0.863	0.863	0.871	0.877
Mg	0.037	0.044	0.050	0.043	0.043	0.030	0.064	0.057	0.060	0.070	0.087
Zn	0.000	0.000	0.000	0.000	0.000	0.000	0.000	0.000	0.000	0.000	0.000
Na	0.000	0.089	0.135	0.067	0.132	0.000	0.092	0.098	0.015	0.134	0.183
Sum C	**7.000**	**7.000**	**7.000**	**7.000**	**7.000**	**7.000**	**7.000**	**7.000**	**7.000**	**7.000**	**7.000**
Ca	0.241	0.254	0.274	0.196	0.304	0.150	0.156	0.137	0.115	0.151	0.221
Ba	0.000	0.000	0.000	0.000	0.000	0.000	0.000	0.000	0.000	0.000	0.006
Na	0.759	0.746	0.726	0.804	0.696	0.850	0.844	0.863	0.885	0.849	0.771
Sum B	**1.000**	**1.000**	**1.000**	**1.000**	**1.000**	**1.000**	**1.000**	**1.000**	**1.000**	**1.000**	**0.992**
Na	0.213	0.223	0.129	0.258	0.145	0.211	0.138	0.161	0.236	0.153	0.000
K	1.512	1.468	1.501	1.474	1.444	1.558	1.486	1.540	1.561	1.597	1.591
Sum A	**1.878**	**1.738**	**1.672**	**1.732**	**1.632**	**1.836**	**1.632**	**1.717**	**1.846**	**1.817**	**1.591**
Cations	19.841	19.701	19.624	19.710	19.632	19.770	19.632	19.717	19.790	19.817	19.583
Cl	0.000	0.000	0.000	0.000	0.000	0.000	0.000	0.000	0.000	0.000	0.000
F	0.413	0.328	0.218	0.198	0.268	0.385	0.639	0.419	0.352	0.297	0.526

Point_ID: spot identification; c: core; r: rim; i: intermediate zone; - : below detection limit

Table 19: Astrophyllite in peralkaline alkali feldspar granites from the Papanduva Pluton

Sample	**MR-21**									
Crystal	1					3				
Point_ID	1-n	2-n	3-i	4-i	5-i	1-n	2-n	3-b	4-i	5-i
SiO_2 (wt%)	35.95	36.07	36.23	36.32	35.81	36.16	36.05	35.78	35.84	35.62
TiO_2	11.85	11.75	11.52	12.00	11.88	12.14	12.05	11.73	11.66	11.81
Al_2O_3		0.07	0.06	0.07	0.04	0.06	0.04		0.04	0.03
FeO	35.27	35.20	35.47	35.25	35.05	35.55	35.08	35.09	35.40	34.96
MnO	1.70	1.65	1.63	1.75	1.59	1.67	1.56	1.70	1.63	1.71
MgO						0.03	0.02	0.02		
CaO	0.14	0.20	0.18	0.47	0.17	0.22	0.24	0.22	0.21	0.17
ZrO_2			0.100	0.090			0.070			
ZnO	-	-	-	-	-	-	-	-	-	-
BaO			0.090							0.090
Na_2O	3.430	3.660	3.720	3.460	3.580	3.420	3.490	3.590	3.420	3.470
K_2O	5.530	5.230	5.350	5.260	5.380	5.310	5.400	5.280	5.410	5.380
Nb_2O_5		0.230	0.340	0.170	0.150			0.240	0.170	0.060
Cl	-	-	-	-	-	-	-	-	-	-
F	0.550	1.070	0.830	0.860	0.520	0.720	1.110	0.740	0.590	0.900
O=Cl=F	0.23	0.45	0.35	0.36	0.22	0.30	0.47	0.31	0.25	0.38
Total	95.56	94.68	95.17	95.34	93.95	96.35	94.64	94.08	94.12	93.82
Structural formulae based on 28.5 oxygens										
Si (apfu)	7.983	8.023	8.024	8.007	8.006	7.958	8.018	8.005	8.014	8.005
Al	0.000	0.000	0.000	0.000	0.000	0.016	0.000	0.000	0.000	0.000
Sum T	**7.983**	**8.023**	**8.024**	**8.007**	**8.006**	**7.974**	**8.018**	**8.005**	**8.014**	**8.005**
Ti	1.979	1.966	1.919	1.990	1.998	2.010	2.016	1.974	1.961	1.996
Zr	0.000	0.000	0.011	0.000	0.000	0.000	0.000	0.000	0.000	0.000
Nb	0.000	0.024	0.035	0.018	0.016	0.000	0.000	0.025	0.018	0.006
Sum D	**1.979**	**2.000**	**1.981**	**2.007**	**2.013**	**2.010**	**2.016**	**2.000**	**1.989**	**2.002**
Fe^{2+}	6.549	6.547	6.569	6.498	6.553	6.542	6.524	6.565	6.619	6.569
Mn	0.320	0.311	0.306	0.327	0.301	0.311	0.294	0.322	0.309	0.325
Mg	0.000	0.000	0.000	0.000	0.000	0.010	0.007	0.007	0.000	0.000
Zn	0.000	0.000	0.000	0.000	0.000	0.000	0.000	0.000	0.000	0.000
Na	0.070	0.143	0.125	0.165	0.146	0.076	0.167	0.106	0.073	0.105
Sum C	**7.000**	**7.000**	**7.000**	**7.000**	**7.000**	**7.000**	**7.000**	**7.000**	**7.000**	**7.000**
Ca	0.033	0.048	0.043	0.111	0.041	0.052	0.057	0.053	0.050	0.041
Ba	0.000	0.000	0.000	0.000	0.000	0.000	0.000	0.000	0.000	0.000
Na	0.967	0.952	0.957	0.889	0.959	0.948	0.943	0.947	0.950	0.959
Sum B	**1.000**	**1.000**	**1.000**	**1.000**	**1.000**	**1.000**	**1.000**	**1.000**	**1.000**	**1.000**
Na	0.440	0.483	0.515	0.425	0.446	0.435	0.395	0.504	0.460	0.448
K	1.566	1.484	1.512	1.479	1.534	1.491	1.532	1.507	1.543	1.542
Sum A	**2.135**	**1.967**	**2.034**	**1.904**	**1.980**	**2.053**	**1.927**	**2.011**	**2.003**	**1.998**
Cations	20.097	19.990	20.039	19.919	20.000	20.036	19.961	20.016	20.006	20.005
Cl	0.000	0.000	0.000	0.000	0.000	0.000	0.000	0.000	0.000	0.000
F	0.386	0.753	0.581	0.600	0.368	0.501	0.781	0.524	0.417	0.640

Point_ID: spot identification; c: core; r: rim; i: intermediate zone; - : below detection limit

Table 20: Biotite in peralkaline alkali feldspar granites from the Mandira unit

Sample	**MAN-2A**						**MAN-5S**	**MAN-8E**				
Crystal	c1		c2		c3		c2	c1	c2		c3	
Point_ID	1-r	1-c	2-r	2-c	3-r	3-c	1-ci	1-c	2-r	2-c	3-r	3-c
SiO_2 (wt%)	36.87	36.70	34.81	34.68	36.40	37.96	37.50	34.28	33.67	33.26	35.03	34.66
TiO_2	2.29	2.45	2.41	2.24	2.23	2.17	2.61	2.64	2.68	2.64	2.76	2.81
Al_2O_3	9.24	9.27	10.57	10.72	9.10	8.52	10.19	13.20	13.43	13.43	12.79	12.95
FeO	36.17	36.56	37.69	37.97	37.38	36.48	35.27	35.15	35.96	35.69	35.46	36.10
MnO	1.17	1.09	0.89	0.81	1.04	1.26	0.59	0.34	0.39	0.44	0.46	0.39
MgO	0.09	0.10	0.09	0.08	0.09	0.07	0.24	0.15	0.13	0.11	0.16	0.15
CaO	-	0.03	0.01	0.05	0.02	-	0.06	-	-	-	-	-
ZnO	0.50	0.51	0.46	0.41	0.50	0.53	0.93	0.24	0.26	0.24	0.15	0.17
BaO	-	-	-	0.10	-	-	0.02	0.08	0.10	-	0.01	0.09
V_2O_5	0.03	-	-	-	0.12	-	0.03	-	-	0.12	-	-
Na_2O	0.04	0.02	0.13	0.15	0.03	0.03	0.04	0.04	0.04	0.05	0.02	0.01
K_2O	8.87	8.62	8.73	8.79	8.87	8.30	8.38	9.14	8.90	8.93	9.17	9.29
F	1.16	1.07	1.29	1.26	1.24	1.17	1.90	0.82	0.60	0.70	0.95	0.81
Cl	-	-	-	-	-	-	-	-	0.06	0.07	-	-
O=F=Cl	0.49	0.45	0.55	0.54	0.53	0.50	0.80	0.35	0.27	0.31	0.40	0.34
Total	96.94	96.91	96.95	97.11	97.36	97.32	98.17	95.99	95.94	95.38	97.03	97.45
Structural formulae based on 11 oxygens												
Si (apfu)	3.097	3.080	2.937	2.925	3.066	3.172	3.091	2.860	2.813	2.802	2.895	2.860
Al	0.903	0.917	1.051	1.066	0.904	0.828	0.909	1.140	1.187	1.198	1.105	1.140
T-site	**4.000**	**3.998**	**3.988**	**3.992**	**3.970**	**4.000**	**4.000**	**4.000**	**4.000**	**4.000**	**4.000**	**4.000**
Al^{VI}	0.012	0.000	0.000	0.000	0.000	0.011	0.081	0.158	0.136	0.136	0.141	0.120
Ti	0.145	0.155	0.153	0.142	0.141	0.136	0.162	0.166	0.168	0.168	0.171	0.175
Fe	2.541	2.567	2.659	2.679	2.633	2.549	2.431	2.453	2.513	2.515	2.451	2.492
Mn	0.083	0.077	0.064	0.058	0.074	0.089	0.041	0.024	0.028	0.032	0.032	0.027
Mg	0.011	0.013	0.011	0.010	0.011	0.009	0.030	0.018	0.016	0.014	0.020	0.018
Zn	0.031	0.031	0.028	0.026	0.031	0.032	0.057	0.014	0.016	0.015	0.009	0.011
M-site	**2.823**	**2.843**	**2.915**	**2.915**	**2.891**	**2.827**	**2.802**	**2.833**	**2.877**	**2.879**	**2.825**	**2.842**
Ca	0.000	0.003	0.001	0.004	0.002	0.000	0.006	0.000	0.000	0.000	0.000	0.000
Ba	0.000	0.000	0.000	0.003	0.000	0.000	0.001	0.003	0.003	0.000	0.000	0.003
Na	0.007	0.003	0.021	0.025	0.005	0.005	0.007	0.006	0.006	0.008	0.003	0.002
K	0.950	0.923	0.939	0.946	0.953	0.885	0.881	0.973	0.948	0.960	0.967	0.978
I-site	**0.956**	**0.929**	**0.961**	**0.978**	**0.959**	**0.890**	**0.895**	**0.981**	**0.958**	**0.968**	**0.971**	**0.983**
Cations	**7.779**	**7.769**	**7.864**	**7.885**	**7.820**	**7.717**	**7.697**	**7.814**	**7.834**	**7.847**	**7.796**	**7.825**
OH*	1.690	1.715	1.651	1.659	1.667	1.689	1.504	1.781	1.832	1.803	1.749	1.787
F	0.308	0.283	0.345	0.337	0.331	0.310	0.495	0.216	0.159	0.186	0.249	0.212
Cl	0.002	0.002	0.004	0.004	0.002	0.001	0.001	0.003	0.009	0.010	0.003	0.000
Fe#	0.996	0.995	0.996	0.996	0.996	0.996	0.988	0.993	0.994	0.995	0.992	0.993

Point_ID: spot identification; c: core; r: rim; i: intermediate zone; - : below detection limit

Table 21: Biotite in peralkaline alkali feldspar granites from the Mandira unit

Sample	**MAN-13B**									**MAN-19**			
Crystal	c4				c1					c1		c2	
Point_ID	4-c	4-r	3-xt	4-ct	1-c	2-i	3-r	4-xt	5,xt	1-c	1-r	2-c	2-r
SiO_2 (wt%)	36.25	35.99	36.51	35.93	36.23	35.99	36.71	35.47	36.01	36.68	37.00	36.51	36.36
TiO_2	2.18	2.46	2.06	2.45	1.96	2.01	2.24	2.80	2.77	3.02	2.77	2.86	2.82
Al_2O_3	10.55	10.58	10.58	10.77	10.19	10.29	10.94	10.65	10.64	10.22	10.32	10.41	10.08
FeO	37.40	35.40	37.73	36.45	36.31	36.02	35.23	34.97	34.87	36.24	34.97	35.53	36.04
MnO	0.70	0.68	0.71	0.62	0.74	0.71	0.66	0.71	0.61	0.71	0.66	0.66	0.70
MgO	0.03	0.03	0.04	0.03	0.03	0.02	0.04	0.04	0.05	0.08	0.05	0.04	0.04
CaO	-	0.02	-	0.01	-	0.01	-	0.03	0.01	0.02	0.01	-	0.03
ZnO	0.30	0.26	0.24	0.34	0.50	0.48	0.47	0.52	0.46	-	-	-	0.02
BaO	0.05	0.02	0.00	0.02	-	0.02	0.02	0.06	0.00	0.45	0.59	0.57	0.65
V_2O_5	0.03	-	0.04	-	-	0.02	-	-	0.14	-	0.02	0.02	0.06
Na_2O	-	-	0.02	-	0.01	-	0.03	0.07	0.04	0.05	0.02	0.01	-
K_2O	9.06	8.88	8.85	8.83	8.53	8.81	8.48	8.61	8.57	8.89	9.02	8.90	8.80
F	1.66	1.47	1.90	1.56	2.01	1.97	1.54	1.93	1.56	1.50	1.09	1.54	1.41
Cl	0.02	-	-	0.02	-	0.02	-	-	-	-	-	-	-
O=F=Cl	0.70	0.62	0.80	0.66	0.84	0.83	0.65	0.81	0.66	0.63	0.46	0.65	0.59
Total	98.35	95.92	98.78	97.09	96.48	96.30	96.66	95.66	95.81	98.18	97.09	97.31	97.26
Structural formulae based on 11 oxygens													
Si (apfu)	3.012	3.034	3.022	3.005	3.059	3.046	3.059	3.004	3.033	3.032	3.071	3.038	3.036
Al	0.988	0.966	0.978	0.995	0.941	0.954	0.941	0.996	0.967	0.968	0.929	0.962	0.964
T-site	**4.000**	**4.000**	**4.000**	**4.000**	**4.000**	**4.000**	**4.000**	**4.000**	**4.000**	**4.000**	**4.000**	**4.000**	**4.000**
Al^{VI}	0.046	0.085	0.054	0.066	0.073	0.073	0.133	0.067	0.090	0.028	0.081	0.059	0.029
Ti	0.136	0.156	0.129	0.154	0.124	0.128	0.140	0.179	0.175	0.188	0.173	0.179	0.177
Fe	2.599	2.496	2.612	2.549	2.564	2.550	2.455	2.476	2.457	2.505	2.428	2.473	2.517
Mn	0.049	0.049	0.050	0.044	0.053	0.051	0.047	0.051	0.043	0.049	0.046	0.047	0.049
Mg	0.004	0.004	0.005	0.003	0.004	0.002	0.005	0.006	0.006	0.010	0.006	0.006	0.005
Zn	0.019	0.016	0.015	0.021	0.031	0.030	0.029	0.032	0.028	0.028	0.036	0.035	0.040
M-site	**2.853**	**2.806**	**2.865**	**2.837**	**2.849**	**2.834**	**2.810**	**2.810**	**2.799**	**2.808**	**2.770**	**2.798**	**2.817**
Ca	0.000	0.002	0.000	0.001	0.000	0.001	0.000	0.003	0.001	0.002	0.001	0.000	0.002
Ba	0.002	0.001	0.000	0.001	0.000	0.001	0.001	0.002	0.000	0.000	0.001	0.001	0.002
Na	0.000	0.000	0.004	0.000	0.001	0.001	0.005	0.012	0.007	0.008	0.004	0.001	0.000
K	0.960	0.955	0.934	0.942	0.919	0.952	0.901	0.930	0.921	0.937	0.955	0.945	0.937
I-site	**0.962**	**0.957**	**0.938**	**0.944**	**0.920**	**0.954**	**0.907**	**0.947**	**0.928**	**0.947**	**0.960**	**0.947**	**0.942**
Cations	**7.815**	**7.762**	**7.802**	**7.781**	**7.769**	**7.788**	**7.717**	**7.757**	**7.727**	**7.755**	**7.730**	**7.745**	**7.759**
OH*	1.561	1.605	1.501	1.585	1.464	1.470	1.593	1.482	1.584	1.607	1.714	1.595	1.627
F	0.437	0.393	0.498	0.412	0.536	0.527	0.406	0.517	0.415	0.392	0.286	0.405	0.372
Cl	0.003	0.002	0.001	0.003	0.000	0.003	0.000	0.001	0.001	0.001	0.000	0.000	0.000
Fe#	0.999	0.998	0.998	0.999	0.999	0.999	0.998	0.998	0.998	0.996	0.998	0.998	0.998

Point_ID: spot identification; c: core; r: rim; i: intermediate zone; - : below detection limit

Table 22: Biotite in peralkaline alkali feldspar granites from the Mandira unit

Sample	**MAN-23F**											
Crystal	c1					c2			c3			
Point_ID	1-ci	2-i	3-r	4-i	5-xt	6-ci	7-i	8-xt	9-c	10-i	11-r	12-xt
SiO_2 (wt%)	38.54	37.29	37.45	38.71	38.08	37.22	37.33	37.31	37.63	37.76	37.93	37.07
TiO_2	2.71	2.58	2.65	2.48	2.61	2.45	2.68	2.36	2.52	2.45	2.46	2.16
Al_2O_3	10.74	10.72	11.09	10.48	10.89	10.60	10.80	10.73	10.29	10.51	10.37	10.70
FeO	34.42	34.94	34.95	34.61	34.95	34.10	35.80	36.01	33.85	33.82	33.06	34.80
MnO	1.01	1.04	1.06	1.06	1.00	1.41	1.25	1.36	1.82	1.98	1.68	1.68
MgO	0.10	0.10	0.10	0.11	0.10	0.21	0.20	0.18	0.19	0.22	0.26	0.20
CaO	0.02	0.02	0.02	0.04	-	0.02	0.00	0.01	-	-	-	0.01
ZnO	0.94	0.93	1.00	0.78	0.97	0.79	0.83	0.88	0.80	0.80	0.61	0.60
BaO	0.07	-	-	-	-	0.02	-	-	-	-	-	0.03
V_2O_5	-	-	0.13	0.12	0.10	0.08	-	0.10	0.02	-	-	-
Na_2O	0.05	0.04	0.03	0.03	0.03	0.04	0.02	0.04	0.02	-	0.03	0.02
K_2O	8.79	8.90	8.87	9.08	8.96	9.13	9.07	9.00	9.06	8.99	9.02	8.91
F	1.90	1.78	1.65	2.00	1.88	1.56	1.55	1.86	1.99	1.80	2.04	1.79
Cl	-	0.02	-	0.02	-	0.04	0.02	-	0.02	0.04	0.06	-
O=F=Cl	0.80	0.75	0.70	0.85	0.79	0.67	0.66	0.78	0.84	0.77	0.87	0.76
Total	99.98	98.73	99.32	100.10	100.02	98.03	100.02	100.09	98.56	98.85	97.96	98.28
Structural formulae based on 11 oxygens												
Si (apfu)	3.109	3.059	3.047	3.128	3.080	3.070	3.030	3.037	3.094	3.091	3.123	3.059
Al	0.891	0.941	0.953	0.872	0.920	0.930	0.970	0.963	0.906	0.909	0.877	0.941
Sum T	**4.000**	**4.000**	**4.000**	**4.000**	**4.000**	**4.000**	**4.000**	**4.000**	**4.000**	**4.000**	**4.000**	**4.000**
Al^{VI}	0.131	0.096	0.110	0.126	0.118	0.100	0.064	0.067	0.092	0.104	0.129	0.100
Ti	0.165	0.159	0.162	0.151	0.158	0.152	0.164	0.144	0.156	0.151	0.153	0.134
Fe	2.322	2.397	2.379	2.339	2.364	2.352	2.431	2.452	2.328	2.315	2.277	2.401
Mn	0.069	0.072	0.073	0.073	0.068	0.098	0.086	0.094	0.127	0.137	0.117	0.118
Mg	0.012	0.012	0.012	0.013	0.012	0.026	0.024	0.021	0.023	0.026	0.032	0.025
Zn	0.056	0.056	0.060	0.046	0.058	0.048	0.050	0.053	0.048	0.049	0.037	0.037
Sum M	**2.755**	**2.793**	**2.796**	**2.748**	**2.778**	**2.777**	**2.818**	**2.832**	**2.774**	**2.782**	**2.745**	**2.814**
Ca	0.002	0.002	0.002	0.003	0.000	0.002	0.000	0.001	0.000	0.000	0.000	0.001
Ba	0.002	0.000	0.000	0.000	0.000	0.001	0.000	0.000	0.000	0.000	0.000	0.001
Na	0.008	0.007	0.004	0.005	0.005	0.007	0.003	0.007	0.003	0.000	0.005	0.004
K	0.905	0.931	0.920	0.936	0.925	0.960	0.939	0.935	0.951	0.939	0.947	0.937
Sum I	**0.917**	**0.940**	**0.926**	**0.945**	**0.929**	**0.969**	**0.942**	**0.942**	**0.954**	**0.939**	**0.953**	**0.943**
Cations	**7.672**	**7.732**	**7.722**	**7.693**	**7.707**	**7.746**	**7.760**	**7.774**	**7.728**	**7.721**	**7.698**	**7.757**
OH*	1.512	1.535	1.575	1.485	1.518	1.587	1.599	1.521	1.479	1.528	1.461	1.530
F	0.486	0.462	0.425	0.512	0.482	0.408	0.398	0.479	0.518	0.467	0.532	0.468
Cl	0.001	0.003	0.000	0.003	0.000	0.005	0.003	0.000	0.003	0.005	0.008	0.002
Fe#	0.995	0.995	0.995	0.994	0.995	0.989	0.990	0.991	0.990	0.989	0.986	0.990

Point_ID: spot identification; c: core; r: rim; i: intermediate zone; - : below detection limit

Table 23: Biotite in peralkaline alkali feldspar granites from the Mandira unit

Sample	**MAN-4621**						**MAN-5574**					
Crystal	c1		c3	c2		c4	c1			c2		
Point_ID	1-r1	1-r2	3-c	2-r	2-c	4-c	1-r1	1-c	1-r2	2-r1	2-c	2-r2
SiO_2 (wt%)	36.64	37.34	37.66	37.29	37.20	37.45	37.87	39.12	38.90	37.48	37.52	37.33
TiO_2	2.53	2.47	2.40	2.47	2.47	2.51	2.81	2.30	2.49	2.71	2.61	2.57
Al_2O_3	10.25	10.05	10.04	10.02	10.34	10.13	9.65	9.30	9.48	9.65	9.71	9.84
FeO	37.48	35.66	35.12	35.70	36.53	35.69	35.55	34.40	34.23	35.57	35.34	35.73
MnO	0.82	0.91	0.95	0.98	0.91	0.94	0.81	0.85	0.79	0.80	0.80	0.78
MgO	0.05	0.09	0.05	0.07	0.05	0.05	0.07	0.09	0.08	0.07	0.09	0.09
CaO	0.03	0.01	-	-	0.05	0.01	0.02	0.04	0.02	0.01	0.01	0.01
ZnO	-	0.00	-	-	-	-	-	-	0.02	0.04	-	0.01
BaO	0.77	0.58	0.56	0.68	0.55	0.66	0.70	0.68	0.60	0.52	0.54	0.54
V_2O_5	-	-	0.01	0.05	-	0.04	-	-	-	-	0.03	-
Na_2O	0.04	0.03	0.03	0.09	0.05	0.05	0.06	0.07	0.03	0.07	0.08	0.04
K_2O	8.91	9.01	8.88	9.07	8.64	9.16	9.02	9.08	9.11	8.87	9.01	9.01
F	1.39	1.59	1.75	1.67	1.47	1.55	1.59	2.12	2.03	1.66	1.63	1.38
Cl	-	-	-	-	-	0.04	0.03	-	0.03	0.07	0.08	0.02
O=F=Cl	0.59	0.67	0.74	0.70	0.62	0.66	0.68	0.90	0.86	0.71	0.71	0.58
Total	99.25	98.20	97.93	98.50	98.74	98.77	98.78	98.81	98.53	97.98	97.93	97.89
Structural formulae based on 11 oxygens												
Si (apfu)	3.016	3.086	3.114	3.080	3.058	3.081	3.111	3.207	3.192	3.106	3.109	3.092
Al	0.984	0.914	0.886	0.920	0.942	0.919	0.889	0.793	0.808	0.894	0.891	0.908
T-site	**4.000**	**4.000**	**4.000**	**4.000**	**4.000**	**4.000**	**4.000**	**4.000**	**4.000**	**4.000**	**4.000**	**4.000**
Al^{VI}	0.011	0.065	0.092	0.055	0.060	0.064	0.046	0.106	0.110	0.048	0.058	0.053
Ti	0.157	0.154	0.149	0.153	0.153	0.155	0.174	0.142	0.154	0.169	0.163	0.160
Fe	2.580	2.465	2.429	2.466	2.511	2.456	2.443	2.359	2.349	2.465	2.449	2.475
Mn	0.057	0.064	0.066	0.068	0.063	0.065	0.056	0.059	0.055	0.056	0.056	0.055
Mg	0.006	0.011	0.006	0.009	0.006	0.006	0.008	0.011	0.010	0.009	0.011	0.011
Zn	0.047	0.035	0.034	0.042	0.034	0.040	0.042	0.041	0.036	0.032	0.033	0.033
M-site	**2.857**	**2.793**	**2.777**	**2.793**	**2.827**	**2.786**	**2.769**	**2.718**	**2.714**	**2.779**	**2.770**	**2.787**
Ca	0.002	0.001	0.000	0.000	0.004	0.001	0.002	0.004	0.002	0.001	0.001	0.001
Ba	0.000	0.000	0.000	0.001	0.000	0.001	0.000	0.000	0.000	0.000	0.001	0.000
Na	0.006	0.005	0.005	0.014	0.009	0.008	0.010	0.011	0.005	0.011	0.012	0.007
K	0.936	0.950	0.937	0.955	0.906	0.961	0.945	0.950	0.954	0.938	0.952	0.952
I-site	**0.944**	**0.955**	**0.941**	**0.971**	**0.919**	**0.971**	**0.957**	**0.964**	**0.961**	**0.949**	**0.967**	**0.960**
Cations	**7.801**	**7.748**	**7.718**	**7.764**	**7.746**	**7.757**	**7.725**	**7.682**	**7.675**	**7.728**	**7.736**	**7.746**
OH*	1.638	1.584	1.542	1.564	1.616	1.591	1.583	1.449	1.469	1.556	1.561	1.636
F	0.362	0.416	0.458	0.436	0.382	0.403	0.413	0.550	0.527	0.435	0.427	0.362
Cl	0.000	0.000	0.000	0.000	0.002	0.005	0.004	0.002	0.004	0.009	0.012	0.002
Fe#	0.998	0.996	0.997	0.996	0.998	0.998	0.997	0.996	0.996	0.996	0.996	0.996

Point_ID: spot identification; c: core; r: rim; i: intermediate zone; - : below detection limit

Table 24: Biotite in peralkaline alkali feldspar granites from the Mandira unit

Sample	**MAN-5574**						**MAN-6735**				
Crystal	c3		c4				c1	c2		c3	
Point_ID	3-r	3-c	4-r3	4-r1	4-c	4-r2	1-r2	2-c	2-r1	3-r1	3-r2
SiO_2 (wt%)	38.98	37.37	37.89	37.51	38.53	37.35	37.12	36.63	36.52	37.02	37.51
TiO_2	2.54	2.59	2.75	2.59	2.81	2.67	2.76	2.78	2.84	2.91	2.67
Al_2O_3	9.46	9.68	9.77	9.64	9.57	9.97	9.30	9.29	9.50	9.61	9.97
FeO	34.26	35.27	35.01	35.49	33.44	35.28	35.96	35.34	33.63	35.63	35.73
MnO	0.82	0.72	0.79	0.85	0.77	0.78	0.65	0.55	0.53	0.57	0.40
MgO	0.11	0.10	0.08	0.06	0.10	0.04	0.11	0.06	0.08	0.09	0.08
CaO	0.01	-	0.02	0.04	0.03	0.02	-	0.01	0.04	0.01	0.05
ZnO	-	0.03	-	-	-	-	0.76	0.74	0.68	0.70	0.55
BaO	0.51	0.59	0.44	0.64	0.51	0.58	-	0.18	-	-	0.05
V_2O_5	0.03	0.00	0.01	0.06	0.00	0.00					
Na_2O	0.03	0.07	0.12	0.10	0.05	0.09	0.02	0.06	0.06	0.04	0.02
K_2O	8.91	9.10	8.85	9.04	8.76	8.88	9.17	9.02	9.00	9.21	8.67
F	1.86	1.49	1.93	1.73	1.82	1.63	2.02	1.42	1.13	2.18	1.08
Cl	0.03	-	-	-	0.02	-	-	0.02	-	-	-
O=F=Cl	0.79	0.63	0.81	0.73	0.77	0.69	0.85	0.60	0.47	0.92	0.46
Total	98.37	97.53	98.16	98.20	97.12	97.74	98.08	96.37	94.36	98.05	97.49
Structural formulae based on 11 oxygens											
Si (apfu)	3.197	3.107	3.125	3.106	3.186	3.094	3.092	3.089	3.111	3.079	3.102
Al	0.803	0.893	0.875	0.894	0.814	0.906	0.908	0.911	0.889	0.921	0.898
T-site	**4.000**	**4.000**	**4.000**	**4.000**	**4.000**	**4.000**	**4.000**	**4.000**	**4.000**	**4.000**	**4.000**
Al^{VI}	0.111	0.055	0.075	0.047	0.119	0.068	0.005	0.013	0.064	0.021	0.073
Ti	0.157	0.162	0.171	0.161	0.175	0.166	0.173	0.177	0.182	0.182	0.166
Fe	2.350	2.452	2.415	2.458	2.313	2.445	2.505	2.493	2.396	2.478	2.471
Mn	0.057	0.051	0.055	0.060	0.054	0.054	0.046	0.039	0.038	0.040	0.028
Mg	0.014	0.013	0.010	0.008	0.012	0.005	0.014	0.008	0.011	0.012	0.010
Zn	0.031	0.036	0.027	0.039	0.031	0.035	0.047	0.046	0.042	0.043	0.034
M-site	**2.719**	**2.769**	**2.752**	**2.772**	**2.704**	**2.774**	**2.790**	**2.776**	**2.733**	**2.776**	**2.782**
Ca	0.001	0.000	0.002	0.003	0.003	0.002	0.000	0.001	0.004	0.001	0.004
Ba	0.001	0.000	0.000	0.002	0.000	0.000	0.000	0.006	0.000	0.000	0.002
Na	0.005	0.011	0.019	0.016	0.008	0.015	0.003	0.010	0.010	0.006	0.003
K	0.932	0.965	0.931	0.955	0.924	0.938	0.974	0.970	0.978	0.978	0.914
I-site	**0.938**	**0.976**	**0.952**	**0.976**	**0.934**	**0.955**	**0.977**	**0.987**	**0.992**	**0.984**	**0.923**
Cations	**7.658**	**7.745**	**7.705**	**7.748**	**7.638**	**7.729**	**7.767**	**7.763**	**7.725**	**7.760**	**7.705**
OH*	1.513	1.606	1.496	1.547	1.521	1.573	1.468	1.620	1.696	1.426	1.717
F	0.482	0.392	0.503	0.453	0.476	0.427	0.532	0.378	0.304	0.574	0.283
Cl	0.005	0.002	0.001	0.000	0.003	0.000	0.000	0.002	0.000	0.000	0.000
Fe#	0.994	0.995	0.996	0.997	0.995	0.998	0.995	0.997	0.996	0.995	0.996

Point_ID: spot identification; c: core; r: rim; i: intermediate zone; - : below detection limit

Table 25: Biotite in metaluminous syenogranites from the Mandira 1 unit

Sample	**MAN-4**				**MAN-5**									
Crystal	c1		c2		c1						c2		c3	
Point_ID	1-r	1-c	2-r	2-c	1-c	2-ci	3-i	4-r1	4-r2	5-r	6-c	8-r	9-c	10-c
SiO_2 (wt%)	34.67	34.92	35.15	34.69	35.02	34.99	35.23	34.47	34.53	34.40	35.46	34.98	33.96	32.70
TiO_2	1.54	2.16	1.49	1.97	1.49	1.60	1.53	1.37	1.37	1.44	1.41	1.42	1.46	1.27
Al_2O_3	15.13	14.43	14.49	14.35	15.32	15.52	15.66	15.54	15.57	15.78	16.61	15.84	16.97	17.41
FeO	30.50	29.57	30.80	31.03	30.50	31.74	31.42	30.91	31.00	30.70	30.91	30.63	31.16	32.23
MnO	0.37	0.45	0.34	0.42	0.43	0.35	0.38	0.40	0.40	0.39	0.33	0.38	0.41	0.32
MgO	3.53	3.36	3.58	3.41	3.30	3.34	3.38	3.51	3.52	3.44	3.41	3.47	3.22	3.40
CaO	0.03	0.01	0.07	0.03	0.01	0.01	-	0.03	0.03	0.06	0.03	0.03	0.08	0.05
ZnO	0.09	0.08	0.16	0.10	0.09	0.02	0.07	-	-	0.11	-	0.06	0.04	0.07
BaO	-	0.02	0.04	0.02	0.13	0.03	0.08	0.02	0.02	0.01	-	-	0.06	0.10
V_2O_5	0.33	-	-	0.03	0.10	-	-	0.14	0.14	-	-	0.13	-	0.02
Na_2O	0.05	0.33	0.06	0.08	0.01	0.04	0.04	0.01	0.01	0.05	-	0.02	0.06	0.02
K_2O	9.42	9.45	9.37	9.40	9.16	9.12	9.17	8.75	8.77	8.88	9.44	8.97	8.47	7.50
F	-	-	-	-	-	-	-	-	-	-	-	-	0.26	-
Cl	0.14	0.48	0.35	0.34	0.26	0.21	0.25	0.17	0.17	0.19	0.12	0.16	0.04	0.05
O=F=Cl	0.13	0.20	0.15	0.18	0.19	0.23	0.22	0.06	0.06	0.10	0.07	0.06	0.12	0.03
Total	96.10	95.46	96.10	96.12	96.15	97.37	97.59	95.51	95.72	95.66	97.93	96.28	96.28	95.37
Structural formula based on 11 oxygens														
Si (apfu)	2.811	2.842	2.847	2.821	2.829	2.798	2.807	2.798	2.797	2.785	2.793	2.808	2.728	2.658
Al	1.189	1.158	1.153	1.179	1.171	1.202	1.193	1.202	1.203	1.215	1.207	1.192	1.272	1.342
T-site	**4.000**	**4.000**	**4.000**	**4.000**	**4.000**	**4.000**	**4.000**	**4.000**	**4.000**	**4.000**	**4.000**	**4.000**	**4.000**	**4.000**
Al^{VI}	0.258	0.227	0.231	0.196	0.288	0.261	0.278	0.284	0.283	0.291	0.335	0.307	0.335	0.326
Ti	0.094	0.132	0.091	0.120	0.091	0.096	0.092	0.084	0.084	0.088	0.083	0.086	0.088	0.077
Fe	2.069	2.013	2.087	2.110	2.061	2.123	2.094	2.098	2.100	2.079	2.036	2.056	2.094	2.191
Mn	0.026	0.031	0.023	0.029	0.030	0.024	0.026	0.028	0.028	0.027	0.022	0.026	0.028	0.022
Mg	0.426	0.407	0.432	0.413	0.398	0.399	0.401	0.425	0.425	0.415	0.400	0.416	0.386	0.412
Zn	0.005	0.005	0.010	0.006	0.005	0.001	0.004	0.000	0.000	0.006	0.000	0.004	0.002	0.004
M-site	**2.877**	**2.815**	**2.874**	**2.874**	**2.873**	**2.904**	**2.894**	**2.919**	**2.919**	**2.906**	**2.876**	**2.894**	**2.933**	**3.033**
Ca	0.002	0.001	0.006	0.002	0.001	0.001	0.000	0.003	0.003	0.005	0.002	0.003	0.007	0.004
Ba	0.000	0.001	0.001	0.001	0.004	0.001	0.003	0.001	0.001	0.000	0.000	0.000	0.002	0.003
Na	0.008	0.052	0.010	0.013	0.002	0.006	0.006	0.001	0.001	0.007	0.000	0.003	0.009	0.003
K	0.975	0.981	0.968	0.975	0.944	0.930	0.932	0.906	0.906	0.917	0.948	0.918	0.868	0.778
I-site	**0.986**	**1.034**	**0.985**	**0.991**	**0.951**	**0.938**	**0.941**	**0.910**	**0.911**	**0.930**	**0.951**	**0.924**	**0.886**	**0.788**
Cations	**7.863**	**7.850**	**7.859**	**7.865**	**7.823**	**7.842**	**7.835**	**7.829**	**7.830**	**7.836**	**7.827**	**7.817**	**7.819**	**7.821**
OH*	1.922	1.878	1.907	1.890	1.887	1.865	1.866	1.964	1.964	1.941	1.961	1.962	1.929	1.980
F	0.059	0.055	0.045	0.063	0.078	0.107	0.100	0.012	0.012	0.033	0.023	0.016	0.066	0.013
Cl	0.019	0.067	0.048	0.047	0.035	0.029	0.034	0.023	0.023	0.026	0.016	0.022	0.005	0.007
Fe#	0.829	0.832	0.828	0.836	0.838	0.842	0.839	0.832	0.832	0.834	0.836	0.832	0.844	0.842

Point_ID: spot identification; c: core; r: rim; i: intermediate zone; - : below detection limit

Table 26: Biotite in metaluminous syenogranites from the Mandira 1 unit

Sample	**MAN-5**										**MAN-14A**			
Crystal	c4		c5			c7			c9		c5			
Point_ID	11-c	12-r	13-ci	14-ri	15-xt	16-i	17-c	18-c	19-i	20-c	1-c	1-ci	1-ir	1-r2
SiO_2 (wt%)	34.67	34.17	36.64	36.16	35.49	36.62	35.04	34.03	34.62	35.17	35.45	35.05	35.19	34.51
TiO_2	1.31	1.42	1.13	1.06	1.25	1.22	1.12	1.23	1.09	1.20	2.08	1.99	1.73	1.55
Al_2O_3	15.64	16.21	15.56	16.14	16.63	15.53	15.75	15.76	15.84	16.07	17.49	17.81	16.92	16.58
FeO	30.64	31.69	28.16	28.20	28.92	28.70	28.15	29.32	27.74	29.08	30.83	30.41	30.51	30.24
MnO	0.52	0.42	0.43	0.52	0.51	0.47	0.47	0.51	0.54	0.41	0.36	0.30	0.39	0.39
MgO	3.46	3.47	5.31	5.36	5.02	5.34	4.87	4.45	5.00	4.91	2.92	2.97	3.14	3.10
CaO	0.07	0.03	-	-	0.08	0.07	0.05	0.88	0.02	0.02	0.01	0.01	-	-
ZnO	0.13	0.17	0.05	-	0.02	0.07	0.05	0.06	0.06	0.10	0.06	0.06	0.09	0.06
BaO	0.00	0.12	0.04	-	0.03	0.08	0.04	0.14	0.06	0.09	0.07	0.07	0.13	0.16
V_2O_5	-	0.14	0.13	-	-	-	0.19	0.13	0.35	0.25	-	-	-	-
Na_2O	0.04	0.03	0.02	0.06	0.03	0.03	-	0.03	0.03	0.07	0.06	0.02	0.03	0.04
K_2O	8.87	8.37	9.34	9.55	9.07	9.06	9.10	9.05	8.92	9.23	9.17	9.34	9.21	9.14
F	0.31	-	0.70	0.37	0.49	0.20	0.45	0.26	0.32	-	0.32	-	-	-
Cl	0.26	0.09	0.32	0.10	0.04	0.28	0.15	0.03	0.03	0.05	0.20	0.09	0.25	0.16
O=F=Cl	0.19	0.02	0.37	0.18	0.21	0.14	0.22	0.12	0.14	0.06	0.18	0.08	0.13	0.09
Total	95.93	96.49	97.57	97.44	97.47	97.62	95.33	95.92	94.61	96.84	99.08	98.43	97.86	96.19
Structural formulae based on 11 oxygens														
Si (apfu)	2.803	2.749	2.872	2.829	2.783	2.860	2.819	2.748	2.804	2.791	2.758	2.739	2.775	2.773
Al	1.197	1.251	1.128	1.171	1.217	1.140	1.181	1.252	1.196	1.209	1.242	1.261	1.225	1.227
T-site	**4.000**	**4.000**	**4.000**	**4.000**	**4.000**	**4.000**	**4.000**	**4.000**	**4.000**	**4.000**	**4.000**	**4.000**	**4.000**	**4.000**
Al^{VI}	0.293	0.286	0.309	0.317	0.320	0.289	0.313	0.248	0.317	0.294	0.362	0.379	0.349	0.344
Ti	0.080	0.086	0.067	0.062	0.074	0.072	0.068	0.075	0.067	0.072	0.122	0.117	0.103	0.093
Fe	2.071	2.132	1.846	1.845	1.897	1.874	1.894	1.980	1.879	1.930	2.006	1.987	2.013	2.032
Mn	0.036	0.029	0.029	0.035	0.034	0.031	0.032	0.035	0.037	0.028	0.024	0.020	0.026	0.027
Mg	0.417	0.416	0.620	0.625	0.587	0.621	0.584	0.536	0.604	0.581	0.339	0.346	0.369	0.371
Zn	0.008	0.010	0.003	0.000	0.001	0.004	0.003	0.004	0.004	0.006	0.004	0.004	0.006	0.003
M-site	**2.905**	**2.959**	**2.873**	**2.884**	**2.912**	**2.892**	**2.894**	**2.878**	**2.906**	**2.909**	**2.856**	**2.853**	**2.865**	**2.871**
Ca	0.006	0.003	0.000	0.000	0.007	0.006	0.005	0.076	0.002	0.002	0.001	0.001	0.000	0.000
Ba	0.000	0.004	0.001	0.000	0.001	0.002	0.001	0.005	0.002	0.003	0.002	0.002	0.004	0.005
Na	0.006	0.004	0.004	0.009	0.004	0.005	0.000	0.004	0.005	0.010	0.009	0.003	0.005	0.006
K	0.915	0.859	0.933	0.953	0.907	0.902	0.934	0.932	0.922	0.934	0.910	0.931	0.926	0.937
I-site	**0.927**	**0.869**	**0.938**	**0.961**	**0.919**	**0.915**	**0.940**	**1.017**	**0.930**	**0.949**	**0.922**	**0.938**	**0.935**	**0.948**
Cations	**7.832**	**7.828**	**7.811**	**7.845**	**7.830**	**7.807**	**7.834**	**7.895**	**7.836**	**7.858**	**7.777**	**7.791**	**7.801**	**7.820**
OH*	1.885	1.988	1.785	1.894	1.874	1.915	1.866	1.929	1.914	1.964	1.896	1.953	1.925	1.944
F	0.080	0.000	0.173	0.092	0.121	0.048	0.114	0.067	0.082	0.029	0.079	0.035	0.041	0.035
Cl	0.035	0.012	0.042	0.014	0.005	0.037	0.020	0.004	0.005	0.007	0.026	0.012	0.033	0.021
Fe#	0.832	0.837	0.749	0.747	0.764	0.751	0.764	0.787	0.757	0.769	0.855	0.852	0.845	0.846

Point_ID: spot identification; c: core; r: rim; i: intermediate zone; - : below detection limit

Table 27: Biotite in metaluminous syenogranites from the Mandira 1 unit

Sample	**MAN-14A**								**MAN-14B**			**MAN-6780**		
Crystal	c2		c3			c4			c2	c3	c4	c1		
Point_ID	2-ci	2-xt	3-c	3-i	3-r2	4-c	4-i	4-r	2-c	3-c	4-c	1-c	1-r	1-r
SiO_2 (wt%)	35.22	33.68	35.07	35.01	34.89	34.73	35.29	34.89	35.95	36.05	36.04	36.51	36.58	36.14
TiO_2	1.30	1.24	1.39	1.48	1.32	2.26	1.51	1.93	1.33	1.52	1.73	2.10	2.40	2.29
Al_2O_3	18.79	17.92	17.76	17.21	17.88	15.56	16.60	16.03	16.43	16.08	15.38	13.19	14.36	13.60
FeO	30.22	30.46	29.44	29.25	30.44	27.09	27.30	27.61	29.43	29.46	30.39	31.25	29.83	30.24
MnO	0.36	0.40	0.45	0.34	0.40	0.44	0.40	0.36	0.36	0.39	0.38	0.28	0.29	0.35
MgO	3.05	2.69	3.14	3.25	3.12	3.86	4.04	4.02	3.30	3.30	3.22	4.73	4.48	4.50
CaO	0.11	0.02	0.02	0.02	0.21	-	-	0.08	0.01	0.08	0.05	-	-	0.01
ZnO	0.07	-	0.07	0.09	0.08	0.10	-	0.13	0.01	-	-	-	-	-
BaO	0.09	0.14	0.05	0.06	-	0.07	-	0.04	0.09	0.10	0.09	-	-	-
V_2O_5	0.01	0.03	0.03	-	-	0.07	-	-	0.04	0.15	0.04	-	-	-
Na_2O	0.09	0.02	0.05	0.03	0.02	0.04	0.04	0.06	0.04	0.07	0.06	0.02	0.03	0.03
K_2O	8.75	9.08	9.17	9.09	9.23	8.79	8.89	8.87	9.12	9.20	9.14	9.39	9.19	9.34
F	0.32	-	0.25	-	-	0.20	0.22	-	-	-	0.21	0.63	0.32	0.69
Cl	0.14	0.04	0.13	0.20	0.06	0.21	0.19	0.23	0.16	0.14	0.29	0.17	0.07	0.16
O=F=Cl	0.17	0.04	0.14	0.12	0.03	0.13	0.14	0.09	0.05	0.07	0.15	0.31	0.15	0.33
Total	98.59	96.01	97.11	96.30	97.88	93.46	94.52	94.40	96.46	96.77	97.07	98.10	97.53	97.16
Structural formula based on 11 oxygens														
Si (apfu)	2.736	2.711	2.769	2.787	2.741	2.832	2.831	2.815	2.851	2.858	2.865	2.891	2.876	2.879
Al	1.264	1.289	1.231	1.213	1.259	1.168	1.169	1.185	1.149	1.142	1.135	1.109	1.124	1.121
T-site	**4.000**	**4.000**	**4.000**	**4.000**	**4.000**	**4.000**	**4.000**	**4.000**	**4.000**	**4.000**	**4.000**	**4.000**	**4.000**	**4.000**
Al^{VI}	0.456	0.412	0.422	0.401	0.396	0.328	0.401	0.340	0.387	0.360	0.306	0.122	0.206	0.157
Ti	0.076	0.075	0.082	0.088	0.078	0.138	0.091	0.117	0.079	0.091	0.103	0.125	0.142	0.137
Fe	1.963	2.051	1.944	1.947	2.000	1.847	1.831	1.863	1.952	1.953	2.020	2.069	1.961	2.015
Mn	0.024	0.027	0.030	0.023	0.027	0.030	0.027	0.025	0.024	0.026	0.026	0.019	0.019	0.024
Mg	0.353	0.323	0.370	0.386	0.366	0.469	0.484	0.483	0.390	0.390	0.382	0.558	0.525	0.534
Zn	0.004	0.000	0.004	0.005	0.005	0.006	0.000	0.008	0.000	0.000	0.000	0.000	0.000	0.000
M-site	**2.876**	**2.889**	**2.853**	**2.851**	**2.871**	**2.819**	**2.835**	**2.836**	**2.833**	**2.820**	**2.837**	**2.893**	**2.854**	**2.867**
Ca	0.009	0.002	0.002	0.001	0.017	0.000	0.000	0.007	0.001	0.007	0.004	0.000	0.000	0.001
Ba	0.003	0.004	0.002	0.002	0.000	0.002	0.000	0.001	0.003	0.003	0.003	0.000	0.000	0.000
Na	0.014	0.004	0.008	0.005	0.004	0.007	0.006	0.009	0.007	0.011	0.010	0.003	0.005	0.005
K	0.867	0.933	0.924	0.923	0.924	0.914	0.909	0.914	0.923	0.930	0.927	0.948	0.921	0.949
I-site	**0.893**	**0.942**	**0.935**	**0.931**	**0.946**	**0.924**	**0.916**	**0.930**	**0.933**	**0.951**	**0.943**	**0.952**	**0.926**	**0.954**
Cations	**7.769**	**7.831**	**7.788**	**7.781**	**7.817**	**7.742**	**7.751**	**7.766**	**7.766**	**7.771**	**7.780**	**7.844**	**7.780**	**7.822**
OH*	1.902	1.977	1.920	1.926	1.982	1.920	1.919	1.944	1.972	1.958	1.909	1.818	1.911	1.805
F	0.080	0.017	0.062	0.047	0.010	0.051	0.055	0.025	0.007	0.022	0.052	0.159	0.079	0.173
Cl	0.019	0.006	0.018	0.027	0.009	0.029	0.026	0.031	0.021	0.019	0.038	0.023	0.010	0.022
Fe#	0.847	0.864	0.840	0.835	0.845	0.798	0.791	0.794	0.833	0.834	0.841	0.787	0.789	0.790

Point_ID: spot identification; c: core; r: rim; i: intermediate zone; - : below detection limit

Table 28: Biotite in metaluminous syenogranites from the Mandira 1 unit

Sample	**MAN-6725**							**MAN-6762**						
Crystal	c1	c2		c5	c6	c7	c8	c1	c2		c5	c6	c7	c8
Point_ID	1-c	2-c	2-i	5-c	6-c	7-c	8-c	1-c	2-c	2-i	5-c	6-c	7-c	8-c
SiO_2 (wt%)	35.53	35.37	34.57	34.44	34.73	33.19	34.52	35.53	35.37	34.57	34.44	34.73	33.19	34.52
TiO_2	1.22	1.56	1.39	0.61	0.85	0.50	0.91	1.22	1.56	1.39	0.61	0.85	0.50	0.91
Al_2O_3	16.47	16.09	16.04	16.65	16.49	16.51	16.87	16.47	16.09	16.04	16.65	16.49	16.51	16.87
FeO	29.31	29.12	29.55	31.29	31.01	31.55	30.26	29.31	29.12	29.55	31.29	31.01	31.55	30.26
MnO	0.48	0.47	0.43	0.47	0.44	0.53	0.47	0.48	0.47	0.43	0.47	0.44	0.53	0.47
MgO	4.30	4.42	4.29	3.66	3.76	4.75	4.47	4.30	4.42	4.29	3.66	3.76	4.75	4.47
CaO	0.04	-	0.11	0.03	0.06	0.02	0.08	0.04	-	0.11	0.03	0.06	0.02	0.08
ZnO	-	0.03	-	-	-	-	-	-	0.03	-	-	-	-	-
BaO	0.12	0.04	0.07	0.12	0.08	-	0.01	0.12	0.04	0.07	0.12	0.08	-	0.01
V_2O_5	0.05	0.01	0.07	0.00	0.18	0.03	0.03	0.05	0.01	0.07	-	0.18	0.03	0.03
Na_2O	0.10	0.05	0.24	0.07	0.08	0.08	0.08	0.10	0.05	0.24	0.07	0.08	0.08	0.08
K_2O	9.21	9.46	8.78	8.99	9.11	7.24	8.46	9.21	9.46	8.78	8.99	9.11	7.24	8.46
F	0.36	0.49	0.47	0.34	0.40	0.29	0.40	0.36	0.49	0.47	0.34	0.40	0.29	0.40
Cl	-	-	-	0.01	0.01	0.01	-	-	-	-	0.01	0.01	0.01	-
O=F=Cl	0.15	0.21	0.20	0.14	0.17	0.13	0.17	0.15	0.21	0.20	0.14	0.17	0.13	0.17
Total	97.17	97.04	95.95	96.72	97.20	94.70	96.53	97.08	96.99	95.71	96.65	97.12	94.62	96.45
Structural formulae based on 11 oxygens														
Si (apfu)	2.804	2.799	2.775	2.762	2.773	2.705	2.748	2.804	2.799	2.775	2.762	2.773	2.705	2.748
Al	1.196	1.201	1.225	1.238	1.227	1.295	1.252	1.196	1.201	1.225	1.238	1.227	1.295	1.252
T-site	**4.000**	**4.000**	**4.000**	**4.000**	**4.000**	**4.000**	**4.000**	**4.000**	**4.000**	**4.000**	**4.000**	**4.000**	**4.000**	**4.000**
Al^{VI}	0.336	0.300	0.293	0.336	0.324	0.292	0.331	0.336	0.300	0.293	0.336	0.324	0.292	0.331
Ti	0.072	0.093	0.084	0.037	0.051	0.030	0.054	0.072	0.093	0.084	0.037	0.051	0.030	0.054
Fe	1.934	1.927	1.984	2.099	2.070	2.151	2.015	1.934	1.927	1.984	2.099	2.070	2.151	2.015
Mn	0.032	0.031	0.029	0.032	0.030	0.036	0.032	0.032	0.031	0.029	0.032	0.030	0.036	0.032
Mg	0.506	0.521	0.513	0.438	0.447	0.577	0.531	0.506	0.521	0.513	0.438	0.447	0.577	0.531
Zn	0.000	0.002	0.000	0.000	0.000	0.000	0.000	0.000	0.002	0.000	0.000	0.000	0.000	0.000
M-site	**2.880**	**2.875**	**2.903**	**2.942**	**2.923**	**3.087**	**2.963**	**2.880**	**2.875**	**2.903**	**2.942**	**2.923**	**3.087**	**2.963**
Ca	0.003	0.000	0.009	0.003	0.005	0.002	0.007	0.003	0.000	0.009	0.003	0.005	0.002	0.007
Ba	0.004	0.001	0.002	0.004	0.002	0.000	0.000	0.004	0.001	0.002	0.004	0.002	0.000	0.000
Na	0.015	0.008	0.037	0.011	0.012	0.012	0.013	0.015	0.008	0.037	0.011	0.012	0.012	0.013
K	0.927	0.955	0.899	0.920	0.928	0.753	0.859	0.927	0.955	0.899	0.920	0.928	0.753	0.859
I-site	**0.949**	**0.964**	**0.948**	**0.937**	**0.947**	**0.767**	**0.879**	**0.949**	**0.964**	**0.948**	**0.937**	**0.947**	**0.767**	**0.879**
Cations	**7.829**	**7.839**	**7.850**	**7.879**	**7.870**	**7.853**	**7.842**	**7.829**	**7.839**	**7.850**	**7.879**	**7.870**	**7.853**	**7.842**
OH*	1.911	1.877	1.880	1.913	1.896	1.923	1.899	1.911	1.877	1.880	1.913	1.896	1.923	1.899
F	0.089	0.123	0.120	0.086	0.102	0.076	0.101	0.089	0.123	0.120	0.086	0.102	0.076	0.101
Cl	0.000	0.000	0.000	0.001	0.001	0.001	0.000	0.000	0.000	0.000	0.001	0.001	0.001	0.000
Fe#	0.793	0.787	0.794	0.827	0.822	0.788	0.792	0.793	0.787	0.794	0.827	0.822	0.788	0.792

Point_ID: spot identification; c: core; r: rim; i: intermediate zone; - : below detection limit

Table 29: Biotite in peralkaline alkali feldspar granites from the Acaraú unit

Sample	**MAN-9A**								**MAN-5579**		**MAN-6730**	
Crystal	c1			c4			c5		c2	c3	c1	c1
Point_ID	1-i	2-i	13-c	4-ci	5-i	6-r	8	9	2-c	3-c	1-c	1-c
SiO_2 (wt%)	35.16	35.58	35.67	35.26	35.62	35.54	36.05	36.02	35.14	35.46	36.06	36.97
TiO_2	2.44	2.40	2.30	2.30	2.41	2.13	1.67	1.57	2.20	1.94	2.62	0.07
Al_2O_3	11.33	11.14	11.20	10.91	11.03	10.83	10.26	10.52	11.16	11.07	10.89	9.52
FeO	38.20	37.52	37.95	37.73	37.13	37.56	39.12	39.21	36.83	37.00	36.25	39.90
MnO	0.06	0.33	0.42	0.54	0.38	0.41	0.59	0.52	0.24	0.28	0.26	0.64
MgO	0.44	0.43	0.44	0.31	0.33	0.28	0.24	0.28	0.41	0.43	0.90	0.78
CaO	-	0.02	0.05	-	0.02	-	-	-	-	0.03	0.02	0.01
ZnO	0.38	0.33	0.33	0.29	0.27	0.31	0.36	0.32	0.01	-	0.11	0.22
BaO	-	0.10	0.12	0.04	0.07	-	-	-	0.31	0.31	0.03	-
V_2O_5	-	0.05	-	0.01	0.13	-	0.09	0.02	0.01	-		
Na_2O	-	-	0.01	-	0.02	0.01	-	-	0.03	0.03	0.01	0.03
K_2O	8.44	8.17	8.28	8.28	8.42	7.98	7.74	7.87	8.78	8.43	8.48	7.47
F	-	-	-	-	-	-	-	-	-	-	-	-
Cl	0.05	0.04	-	0.05	0.04	0.04	0.04	0.04	0.04	-	-	0.07
O=F=Cl	0.04	0.02	0.03	0.04	0.02	0.01	0.02	0.04	0.03	0.04	0.03	0.05
Total	97.03	96.73	97.48	96.30	96.50	95.71	96.93	97.16	95.68	95.64	96.46	96.78
Structural formulae based on 11 oxygens												
Si (apfu)	2.923	2.959	2.951	2.955	2.971	2.986	3.015	3.004	2.955	2.980	2.988	3.106
Al	1.077	1.041	1.049	1.045	1.029	1.014	0.985	0.996	1.045	1.020	1.012	0.894
T-site	**4.000**	**4.000**	**4.000**	**4.000**	**4.000**	**4.000**	**4.000**	**4.000**	**4.000**	**4.000**	**4.000**	**4.000**
Al^{VI}	0.033	0.051	0.043	0.032	0.056	0.058	0.026	0.038	0.062	0.076	0.052	0.049
Ti	0.152	0.150	0.143	0.145	0.151	0.134	0.105	0.099	0.139	0.123	0.163	0.004
Fe	2.655	2.609	2.625	2.644	2.590	2.639	2.736	2.735	2.591	2.600	2.512	2.804
Mn	0.004	0.023	0.029	0.038	0.027	0.029	0.042	0.037	0.017	0.020	0.018	0.046
Mg	0.054	0.053	0.054	0.039	0.041	0.035	0.030	0.035	0.051	0.054	0.112	0.098
Zn	0.023	0.021	0.020	0.018	0.017	0.019	0.022	0.020	0.019	0.019	0.006	0.014
M-site	**2.922**	**2.907**	**2.914**	**2.917**	**2.882**	**2.915**	**2.961**	**2.962**	**2.879**	**2.893**	**2.864**	**3.015**
Ca	0.000	0.003	0.009	0.001	0.003	0.000	0.000	0.000	0.000	0.005	0.004	0.001
Ba	0.000	0.006	0.007	0.003	0.004	0.000	0.000	0.000	0.001	0.000	0.002	0.000
Na	0.000	0.000	0.003	0.001	0.005	0.005	0.001	0.000	0.008	0.010	0.004	0.009
K	1.777	1.716	1.731	1.757	1.772	1.693	1.632	1.655	1.870	1.791	1.772	1.576
I-site	**1.777**	**1.726**	**1.750**	**1.761**	**1.785**	**1.698**	**1.632**	**1.655**	**1.879**	**1.806**	**1.782**	**1.586**
Cations	**7.817**	**7.778**	**7.798**	**7.805**	**7.785**	**7.772**	**7.788**	**7.799**	**7.825**	**7.804**	**7.766**	**7.821**
OH*	1.975	1.988	1.980	1.976	1.990	1.994	1.989	1.976	1.979	1.976	1.981	1.970
F	0.018	0.006	0.016	0.017	0.005	0.000	0.005	0.018	0.015	0.021	0.015	0.021
Cl	0.007	0.006	0.005	0.007	0.005	0.006	0.006	0.006	0.006	0.004	0.004	0.009
Fe#	0.980	0.980	0.980	0.985	0.984	0.987	0.989	0.987	0.981	0.980		

Point_ID: spot identification; c: core; r: rim; i: intermediate zone; - : below detection limit

Table 30: Biotite in albite granites from the Mandira Massif

Sample	**MAN-23S**							**MAN-25F**							
Crystal	c1	c3	c4			c5		c1		c2		c3		c4	
Point_ID	1-c	3-c	4-r1	4-r2	4-r3	5-c	5-r	1-c	1-c	2-r	2-c	3-r	3-ci	4-r	4-c
SiO_2 (wt%)	33.92	33.32	45.34	46.17	47.09	33.90	45.81	37.25	36.11	37.11	36.09	36.37	35.49	35.48	36.00
TiO_2	1.70	1.52	0.35	0.12	0.21	1.71	0.25	1.82	1.78	1.75	1.87	1.70	1.80	0.74	0.73
Al_2O_3	16.62	16.88	29.75	30.02	30.69	16.52	28.86	16.41	15.32	16.05	15.86	15.54	15.30	15.95	15.81
FeO	33.23	32.94	8.51	7.84	7.81	33.98	9.20	29.17	30.61	28.48	29.38	29.73	30.99	31.60	30.84
MnO	1.12	1.12	0.25	0.20	0.19	0.81	0.17	0.46	0.53	0.58	0.57	0.41	0.43	0.47	0.48
MgO	0.19	0.21	0.08	0.13	0.15	0.25	0.11	0.50	0.51	0.57	0.57	0.48	0.48	0.40	0.39
CaO	0.02	0.02	0.03	0.01	0.02	0.04	0.01	-	0.01	-	-	0.01	0.01	0.01	0.01
ZnO	0.04	0.02	0.02	0.04	-	-	0.00	0.28	0.29	0.24	0.29	0.26	0.20	0.24	0.25
BaO	0.00	0.10	-	0.05	0.01	-	0.08	0.10	0.03	-	-	-	0.02	-	-
V_2O_5	0.00	-	0.03	0.01	0.05	-	0.01	-	-	-	-	0.02	-	0.17	0.11
Na_2O	0.04	0.05	0.14	0.12	0.12	0.06	0.10	0.05	0.07	0.05	0.06	0.02	0.04	0.05	0.03
K_2O	9.06	9.04	10.77	10.96	10.65	9.02	10.79	9.75	9.80	9.91	9.72	9.66	9.72	9.65	9.76
F	0.63	0.52	0.51	0.57	0.50	0.54	0.63	1.98	1.99	2.41	2.21	2.19	2.07	2.07	2.01
Cl	0.01	-	0.02	-	-	0.03	0.02	0.03	0.06	0.06	0.02	-	-	-	-
O=F=Cl	0.27	0.22	0.22	0.24	0.21	0.23	0.27	0.84	0.85	1.03	0.94	0.92	0.87	0.87	0.85
Total	96.45	95.53	95.74	96.19	97.43	96.76	95.97	98.04	97.04	97.25	96.47	96.30	96.26	96.37	96.22
Structural formulae based on 11 oxygens															
Si (apfu)	2.771	2.746	3.151	3.181	3.185	2.764	3.188	2.963	2.935	2.981	2.932	2.961	2.911	2.911	2.949
Al	1.229	1.254	0.849	0.819	0.815	1.236	0.812	1.037	1.065	1.019	1.068	1.039	1.089	1.089	1.051
T-site	**4.000**	**4.000**	**4.000**	**4.000**	**4.000**	**4.000**	**4.000**	**4.000**	**4.000**	**4.000**	**4.000**	**4.000**	**4.000**	**4.000**	**4.000**
Al^{VI}	0.372	0.385	1.588	1.619	1.632	0.352	1.555	0.502	0.402	0.501	0.450	0.453	0.389	0.453	0.475
Ti	0.104	0.094	0.018	0.006	0.011	0.105	0.013	0.109	0.109	0.105	0.114	0.104	0.111	0.046	0.045
Fe	2.270	2.270	0.495	0.452	0.442	2.317	0.535	1.941	2.080	1.913	1.996	2.025	2.126	2.168	2.113
Mn	0.077	0.078	0.015	0.012	0.011	0.056	0.010	0.031	0.036	0.040	0.039	0.028	0.030	0.033	0.033
Mg	0.024	0.026	0.008	0.013	0.015	0.031	0.011	0.060	0.062	0.068	0.069	0.058	0.058	0.049	0.048
Zn	0.000	0.006	0.000	0.003	0.001	0.000	0.004	0.016	0.018	0.014	0.017	0.016	0.012	0.014	0.015
M-site	**2.847**	**2.860**	**2.123**	**2.104**	**2.111**	**2.860**	**2.129**	**2.658**	**2.708**	**2.642**	**2.686**	**2.684**	**2.726**	**2.763**	**2.730**
Ca	0.002	0.002	0.002	0.001	0.001	0.003	0.000	0.000	0.001	0.000	0.000	0.001	0.001	0.001	0.001
Ba	0.000	0.000	0.001	0.000	0.001	0.000	0.000	0.003	0.001	0.000	0.000	0.000	0.001	0.000	0.000
Na	0.006	0.008	0.018	0.016	0.016	0.009	0.014	0.008	0.011	0.007	0.009	0.003	0.007	0.007	0.005
K	0.944	0.950	0.955	0.963	0.919	0.938	0.958	0.989	1.016	1.015	1.007	1.003	1.016	1.010	1.019
I-site	**0.952**	**0.960**	**0.976**	**0.980**	**0.937**	**0.951**	**0.972**	**1.000**	**1.029**	**1.022**	**1.016**	**1.008**	**1.024**	**1.018**	**1.025**
Cations	**7.799**	**7.820**	**7.099**	**7.084**	**7.048**	**7.811**	**7.101**	**7.657**	**7.736**	**7.665**	**7.702**	**7.692**	**7.751**	**7.781**	**7.755**
OH*	1.836	1.864	1.885	1.874	1.894	1.856	1.860	1.498	1.480	1.378	1.429	1.434	1.462	1.464	1.479
F	0.163	0.136	0.112	0.124	0.106	0.139	0.138	0.497	0.512	0.613	0.568	0.565	0.537	0.536	0.521
Cl	0.001	0.000	0.003	0.002	0.000	0.005	0.002	0.004	0.008	0.009	0.002	0.001	0.001	0.000	0.000
Fe#	0.990	0.989	0.984	0.972	0.968	0.987	0.980	0.970	0.971	0.966	0.967	0.972	0.973	0.978	0.978

Point_ID: spot identification; c: core; r: rim; i: intermediate zone; - : below detection limit

Table 31: Biotite in albite granites from the Mandira Massif

Sample	**MAN-6666A**									**MAN-6666B**				
Crystal	c1					c2			c3	c1				c3
Point_ID	1-r1	1-i	1-c	1-i2	1-r2	2-r1	2-c	2-r2	3-c	1-r	1-c	1-i	1-r2	3-r1
SiO_2 (wt%)	36.56	37.89	35.76	36.53	36.38	35.98	35.99	35.37	37.27	41.65	37.11	36.52	38.96	44.34
TiO_2	1.67	1.70	1.48	2.30	1.74	1.67	1.77	1.71	1.51	0.30	1.44	1.62	1.33	0.22
Al_2O_3	15.77	16.13	15.28	15.17	15.21	15.15	15.14	14.74	15.94	19.67	15.91	15.92	17.64	20.56
FeO	32.30	27.39	29.94	28.50	29.07	29.34	30.19	30.08	28.55	21.50	29.84	31.45	26.98	15.97
MnO	0.51	0.39	0.44	0.51	0.39	0.42	0.45	0.40	0.32	0.55	0.56	0.51	0.50	0.34
MgO	0.74	0.79	0.77	0.75	0.71	0.77	0.74	0.69	0.64	0.54	0.72	0.65	0.64	0.62
CaO	0.03	0.06	0.02	0.01	0.01	0.06	0.01	0.08	0.01	-	0.01	0.01	0.01	-
ZnO	0.34	0.26	0.32	0.33	0.31	0.38	0.30	0.37	0.37	-	0.01	-	-	-
BaO	0.01	-	0.06	-	-	0.09	-	0.01	0.25	0.21	0.28	0.29	0.20	0.15
V_2O_5	-									0.02	0.02	-	-	-
Na_2O	0.03	0.04	0.04	0.06	0.04	0.02	0.04	0.08	0.03	0.05	0.07	0.04	0.06	0.11
K_2O	9.46	9.20	9.35	9.56	9.43	9.68	9.49	9.48	9.71	10.00	8.99	8.74	9.67	10.36
F	1.75	1.27	1.20	1.63	1.11	1.37	1.46	1.67	2.10	3.11	2.16	1.93	2.39	3.24
Cl	0.09	0.08	0.05	0.11	0.13	0.05	0.07	0.15	-	0.05	0.08	0.07	0.04	-
O=F=Cl	0.76	0.55	0.52	0.71	0.50	0.59	0.63	0.73	0.88	1.32	0.93	0.83	1.01	1.36
Total	99.39	95.92	94.86	95.63	94.89	95.11	95.75	94.64	96.92	98.72	97.33	97.82	99.01	97.69
Structural formulae based on 11 oxygens														
Si (apfu)	2.906	3.033	2.944	2.974	2.980	2.957	2.944	2.939	2.999	3.173	2.979	2.929	3.030	3.324
Al	1.094	0.967	1.056	1.026	1.020	1.043	1.056	1.061	1.001	0.827	1.021	1.071	0.970	0.676
T-site	**4.000**	**4.000**	**4.000**	**4.000**	**4.000**	**4.000**	**4.000**	**4.000**	**4.000**	**4.000**	**4.000**	**4.000**	**4.000**	**4.000**
Al^{VI}	0.383	0.555	0.428	0.429	0.450	0.424	0.404	0.383	0.511	0.940	0.484	0.433	0.647	1.140
Ti	0.100	0.102	0.092	0.141	0.107	0.103	0.109	0.107	0.091	0.017	0.087	0.098	0.078	0.012
Fe	2.147	1.834	2.062	1.940	1.992	2.017	2.066	2.090	1.921	1.370	2.003	2.109	1.755	1.001
Mn	0.034	0.026	0.030	0.035	0.027	0.029	0.031	0.028	0.022	0.036	0.038	0.035	0.033	0.021
Mg	0.087	0.094	0.094	0.091	0.086	0.094	0.090	0.085	0.077	0.062	0.086	0.078	0.074	0.069
Zn	0.020	0.016	0.019	0.020	0.019	0.023	0.018	0.023	0.022	0.012	0.017	0.017	0.012	0.008
M-site	**2.771**	**2.626**	**2.725**	**2.656**	**2.681**	**2.690**	**2.718**	**2.716**	**2.645**	**2.436**	**2.714**	**2.770**	**2.598**	**2.252**
Ca	0.002	0.005	0.002	0.001	0.001	0.005	0.001	0.007	0.001	0.000	0.001	0.001	0.001	0.000
Ba	0.000	0.000	0.002	0.000	0.000	0.003	0.000	0.000	0.008	0.001	0.001	0.000	0.000	0.000
Na	0.004	0.005	0.006	0.009	0.007	0.003	0.007	0.013	0.005	0.008	0.011	0.007	0.009	0.016
K	0.959	0.940	0.982	0.993	0.986	1.014	0.990	1.005	0.996	0.972	0.920	0.894	0.959	0.991
I-site	**0.966**	**0.950**	**0.991**	**1.003**	**0.993**	**1.025**	**0.998**	**1.025**	**1.010**	**0.980**	**0.933**	**0.902**	**0.969**	**1.007**
Cations	**7.737**	**7.577**	**7.716**	**7.659**	**7.674**	**7.715**	**7.715**	**7.741**	**7.655**	**7.416**	**7.647**	**7.672**	**7.568**	**7.259**
OH*	1.548	1.667	1.680	1.565	1.693	1.638	1.612	1.542	1.467	1.244	1.441	1.502	1.407	1.232
F	0.441	0.323	0.313	0.420	0.288	0.355	0.379	0.438	0.533	0.749	0.548	0.489	0.588	0.768
Cl	0.011	0.010	0.007	0.015	0.018	0.007	0.009	0.021	0.000	0.006	0.010	0.009	0.005	0.000
Fe#	0.961	0.951	0.956	0.955	0.959	0.955	0.958	0.961	0.961	0.957	0.959	0.964	0.960	0.936

Point_ID: spot identification; c: core; r: rim; i: intermediate zone; - : below detection limit

Table 32: Biotite in albite granites from the Mandira Massif

Sample	**MAN-6666B**												
Crystal					c5				c7				
Point_ID	3-c	3-i2	3-r3	3-i1	5-r1	5-r2	5-r3	5-c	7-r1	7-r2	7-r3	7-c1	7-c2
SiO_2 (wt%)	36.34	36.62	36.78	36.75	41.56	42.10	41.89	36.49	41.96	43.92	42.75	35.81	36.53
TiO_2	1.77	1.30	1.62	1.78	0.26	0.31	0.46	1.70	0.61	0.36	0.68	1.56	1.62
Al_2O_3	15.19	15.91	15.91	15.35	19.74	20.05	19.90	15.01	19.48	20.09	19.55	14.83	14.96
FeO	32.22	30.91	30.79	30.77	20.21	19.79	20.90	30.47	19.98	18.39	20.36	32.15	30.90
MnO	0.51	0.43	0.48	0.46	0.49	0.44	0.41	0.55	0.44	0.53	0.45	0.54	0.52
MgO	0.62	0.62	0.63	0.73	0.52	0.51	0.55	0.65	0.54	0.54	0.54	0.66	0.61
CaO	0.06	0.07	0.02	0.05	-	0.02	0.01	-	0.01	0.01	0.02	0.01	-
ZnO	-	-	0.03	-	-	0.00	-	0.03	-	-	-	-	-
BaO	0.25	0.40	0.19	0.23	0.15	0.27	0.18	0.27	0.18	0.17	0.18	0.22	0.27
V_2O_5	0.04	0.03	0.18	-	0.02	0.00	-	-	0.00	0.01	-	0.04	0.06
Na_2O	0.03	0.05	0.04	0.03	0.05	0.09	0.10	0.09	0.05	0.08	0.07	0.08	0.03
K_2O	9.02	9.02	8.80	9.44	10.16	9.90	9.78	9.50	10.21	10.12	10.09	9.32	9.16
F	1.65	1.51	1.68	1.61	3.18	2.97	2.96	2.13	3.05	3.23	2.79	1.85	1.71
Cl	0.09	-	0.03	0.02	0.06	0.05	-	0.13	0.02	0.02	-	0.20	0.05
O=F=Cl	0.72	0.64	0.71	0.68	1.35	1.26	1.25	0.93	1.29	1.36	1.18	0.82	0.73
Total	97.92	97.16	97.43	97.51	97.38	97.75	98.35	96.98	97.71	99.15	99.01	97.13	96.59
Structural formulae based on 11 oxygens													
Si (apfu)	2.927	2.948	2.951	2.955	3.194	3.207	3.183	2.966	3.208	3.282	3.222	2.924	2.971
Al	1.073	1.052	1.049	1.045	0.806	0.793	0.817	1.034	0.792	0.718	0.778	1.076	1.029
T-site	**4.000**	**4.000**	**4.000**	**4.000**	**4.000**	**4.000**	**4.000**	**4.000**	**4.000**	**4.000**	**4.000**	**4.000**	**4.000**
Al^{VI}	0.370	0.458	0.455	0.410	0.982	1.007	0.965	0.404	0.964	1.051	0.959	0.351	0.406
Ti	0.107	0.079	0.097	0.108	0.015	0.018	0.027	0.104	0.035	0.020	0.038	0.096	0.099
Fe	2.171	2.081	2.066	2.069	1.299	1.261	1.328	2.071	1.278	1.149	1.283	2.196	2.102
Mn	0.035	0.029	0.033	0.032	0.032	0.029	0.027	0.038	0.029	0.033	0.029	0.037	0.036
Mg	0.075	0.074	0.076	0.087	0.059	0.058	0.062	0.079	0.061	0.061	0.061	0.080	0.074
Zn	0.015	0.023	0.011	0.014	0.008	0.015	0.010	0.016	0.010	0.009	0.010	0.013	0.016
M-site	**2.772**	**2.744**	**2.738**	**2.719**	**2.395**	**2.387**	**2.418**	**2.712**	**2.376**	**2.324**	**2.380**	**2.773**	**2.733**
Ca	0.005	0.006	0.002	0.005	0.000	0.002	0.001	0.000	0.001	0.001	0.001	0.001	0.000
Ba	0.001	0.001	0.006	0.000	0.000	0.000	0.000	0.000	0.000	0.000	0.000	0.001	0.002
Na	0.005	0.009	0.007	0.004	0.007	0.013	0.015	0.014	0.008	0.012	0.011	0.012	0.004
K	0.927	0.926	0.901	0.968	0.996	0.962	0.948	0.985	0.996	0.964	0.970	0.971	0.950
I-site	**0.938**	**0.942**	**0.915**	**0.977**	**1.004**	**0.977**	**0.963**	**0.998**	**1.005**	**0.978**	**0.982**	**0.985**	**0.957**
Cations	**7.710**	**7.686**	**7.653**	**7.696**	**7.399**	**7.363**	**7.381**	**7.710**	**7.381**	**7.301**	**7.362**	**7.758**	**7.690**
OH*	1.567	1.616	1.570	1.588	1.219	1.278	1.287	1.434	1.260	1.235	1.334	1.494	1.554
F	0.420	0.384	0.426	0.409	0.773	0.715	0.711	0.548	0.738	0.763	0.665	0.478	0.440
Cl	0.013	0.000	0.004	0.003	0.008	0.006	0.001	0.018	0.002	0.002	0.001	0.028	0.006
Fe#	0.967	0.966	0.965	0.960	0.957	0.956	0.955	0.963	0.954	0.950	0.955	0.965	0.966

Point_ID: spot identification; c: core; r: rim; i: intermediate zone; - : below detection limit

Table 33: Chlorite in metaluminous syenogranites from the Mandira 1 unit

Sample	**MAN-14**												
Crystal	c1				c2	c3			c4				c5
Point_ID	1-c	1-r1	1-r2	1-r3	2-c	3-r1	3-c	3-r2	4-r1	4-c	4-i	4-r2	5-c
SiO_2 (wt%)	22.11	22.24	22.47	21.82	22.75	22.71	22.46	22.46	22.58	22.28	22.49	23.00	22.48
TiO_2	0.01	0.11	0.06	0.05	0.01	0.04	0.10	0.04	0.05	0.07	0.07	0.02	0.04
Al_2O_3	19.99	20.20	19.73	19.34	19.96	18.92	18.86	19.54	19.19	19.36	19.47	19.79	19.13
FeO	42.53	42.51	42.17	41.63	41.53	42.92	42.67	42.87	42.82	42.94	42.63	42.79	41.82
MnO	0.85	0.74	0.66	0.72	0.73	0.73	0.74	0.68	0.75	0.80	0.70	0.75	0.73
MgO	3.31	3.36	3.84	3.88	3.88	3.91	3.65	3.43	4.06	3.78	3.82	3.81	3.99
CaO	0.03	0.03	0.08	0.06	0.05	0.05	0.07	0.04	0.03	0.05	0.05	0.05	0.02
ZnO	0.09	0.07	0.07	0.05	0.04	0.05	0.07	0.09	0.12	0.07	0.07	0.08	0.08
BaO	0.00	0.00	0.00	0.00	0.00	0.00	0.00	0.02	0.00	0.00	0.00	0.00	0.00
Na_2O	0.03	0.00	0.03	0.05	0.03	0.01	0.00	0.00	0.04	0.02	0.00	0.01	0.01
K_2O	0.01	0.02	0.03	0.02	0.04	0.00	0.03	0.03	0.00	0.03	0.02	0.01	0.04
F	0.00	0.00	0.00	0.00	0.05	0.01	0.00	0.00	0.00	0.03	0.02	0.01	0.00
Cl	0.02	0.01	0.00	0.01	0.01	0.02	0.00	0.00	0.00	0.01	0.02	0.00	0.02
O=F	0.00	0.00	0.00	0.00	0.02	0.00	0.00	0.00	0.00	0.01	0.01	0.01	0.00
O=Cl	0.00	0.00	0.00	0.00	0.00	0.00	0.00	0.00	0.00	0.00	0.00	0.00	0.00
Total	99.47	99.79	99.64	98.13	99.54	99.86	99.14	99.71	100.15	99.93	99.84	100.82	98.86
Structural formulae based on 11 oxygens													
Si (apfu)	2.542	2.546	2.572	2.540	2.602	2.598	2.595	2.578	2.571	2.548	2.571	2.599	2.594
Al^{IV}	1.458	1.454	1.428	1.460	1.398	1.402	1.405	1.422	1.429	1.452	1.429	1.401	1.406
T-site	**4.000**	**4.000**	**4.000**	**4.000**	**4.000**	**4.000**	**4.000**	**4.000**	**4.000**	**4.000**	**4.000**	**4.000**	**4.000**
Al^{VI}	1.252	1.271	1.233	1.194	1.292	1.148	1.162	1.221	1.146	1.158	1.194	1.235	1.196
Ti	0.001	0.009	0.005	0.004	0.000	0.003	0.008	0.004	0.004	0.006	0.006	0.002	0.004
Mn^{3+}	0.000	0.000	0.000	0.000	0.000	0.000	0.000	0.000	0.000	0.000	0.000	0.000	0.000
Fe^{3+}	0.189	0.154	0.154	0.226	0.081	0.234	0.205	0.178	0.257	0.259	0.207	0.147	0.190
Fe^{2+}	3.901	3.915	3.882	3.827	3.891	3.872	3.917	3.937	3.821	3.848	3.869	3.897	3.846
Mn	0.083	0.072	0.064	0.071	0.070	0.071	0.073	0.066	0.073	0.078	0.068	0.072	0.071
Zn	0.007	0.006	0.006	0.004	0.003	0.005	0.006	0.008	0.010	0.006	0.006	0.007	0.007
Mg	0.567	0.573	0.655	0.673	0.662	0.667	0.629	0.587	0.689	0.645	0.651	0.642	0.686
M-site	**6.000**	**6.000**	**6.000**	**6.000**	**6.000**	**6.000**	**6.000**	**6.000**	**6.000**	**6.000**	**6.000**	**6.000**	**6.000**
Ca	0.004	0.004	0.010	0.008	0.006	0.006	0.008	0.005	0.004	0.007	0.006	0.007	0.002
Ba	0.000	0.000	0.000	0.000	0.000	0.000	0.000	0.001	0.000	0.000	0.000	0.000	0.000
Na	0.006	0.001	0.006	0.012	0.007	0.002	0.000	0.001	0.010	0.005	0.000	0.002	0.003
K	0.001	0.003	0.005	0.003	0.006	0.000	0.004	0.004	0.000	0.004	0.004	0.002	0.006
A-site	**0.011**	**0.008**	**0.020**	**0.023**	**0.018**	**0.008**	**0.013**	**0.011**	**0.013**	**0.015**	**0.010**	**0.010**	**0.011**
OH*	7.996	7.999	8.000	7.998	7.981	7.993	8.000	8.000	7.999	7.987	7.991	7.996	7.995
F	0.000	0.000	0.000	0.000	0.018	0.004	0.000	0.000	0.000	0.011	0.006	0.005	0.001
Cl	0.004	0.001	0.000	0.002	0.001	0.003	0.000	0.000	0.001	0.002	0.003	0.000	0.004
Fe#	0.878	0.877	0.860	0.858	0.857	0.860	0.868	0.875	0.855	0.864	0.862	0.863	0.855

Point_ID: spot identification; c: core; r: rim; i: intermediate zone; - : below detection limit

Table 34: Chlorite in greisens from the Mandira 1 unit

Sample	**MAN-6769**												
Crystal	c1				c2			c3			c4		
Point_ID	1-r1	1-c	1-r2	1-r4	2-r1	2-c	2-r2	3-r1	3-r2	3-r3	4-r1	4-c	4b-c
SiO_2 (wt%)	21.31	21.06	21.36	21.75	21.71	21.37	21.88	21.69	21.49	21.80	21.68	21.23	21.35
TiO_2	0.01	0.09	0.01	0.07	0.12	0.08	0.03	0.06	0.01	0.10	0.06	0.01	0.03
Al_2O_3	20.71	20.70	20.66	20.92	21.05	20.72	20.68	20.49	20.33	19.92	20.79	21.65	20.68
FeO	44.71	44.71	45.31	44.59	44.86	44.66	44.57	44.48	44.51	44.99	45.20	44.40	44.75
MnO	1.38	1.42	1.46	1.48	1.39	1.48	1.39	1.51	1.47	1.36	1.52	1.47	1.50
MgO	0.56	0.57	0.52	0.59	0.59	0.52	0.58	0.58	0.57	0.54	0.54	0.46	0.55
CaO	0.02	0.04	0.01	0.02	0.05	0.00	0.00	0.00	0.02	0.02	0.00	0.05	0.02
ZnO	0.03	0.05	0.14	0.14	0.06	0.13	0.04	0.11	0.12	0.11	0.14	0.18	0.05
BaO	0.00	0.00	0.00	0.00	0.00	0.02	0.00	0.02	0.00	0.00	0.00	0.03	0.00
Na_2O	0.02	0.02	0.00	0.00	0.00	0.00	0.00	0.00	0.00	0.02	0.00	0.03	0.00
K_2O	0.00	0.00	0.00	0.01	0.03	0.00	0.18	0.04	0.00	0.07	0.00	0.00	0.02
F	0.00	0.00	0.02	0.00	0.00	0.04	0.01	0.02	0.01	0.01	0.00	0.00	0.01
Cl	0.00	0.00	0.00	0.00	0.01	0.00	0.00	0.00	0.02	0.03	0.00	0.00	0.00
O=F	0.00	0.00	0.01	0.00	0.00	0.02	0.00	0.01	0.00	0.00	0.00	0.00	0.00
O=Cl	0.00	0.00	0.00	0.00	0.00	0.00	0.00	0.00	0.01	0.01	0.00	0.00	0.00
Total	99.26	99.16	99.98	100.06	100.37	99.51	99.86	99.49	99.04	99.44	100.44	100.01	99.46
Structural formulae based on 11 oxygens													
Si (apfu)	2.503	2.478	2.492	2.530	2.518	2.505	2.555	2.543	2.532	2.565	2.514	2.470	2.503
Al^{IV}	1.497	1.523	1.508	1.470	1.482	1.496	1.445	1.457	1.468	1.436	1.486	1.530	1.497
T-site	**4.000**	**4.000**	**4.000**	**4.000**	**4.000**	**4.000**	**4.000**	**4.000**	**4.000**	**4.000**	**4.000**	**4.000**	**4.000**
Al^{VI}	1.370	1.347	1.332	1.397	1.395	1.367	1.402	1.373	1.356	1.326	1.356	1.439	1.361
Ti	0.001	0.008	0.001	0.006	0.010	0.007	0.003	0.005	0.001	0.009	0.005	0.001	0.003
Mn^{3+}	0.000	0.000	0.000	0.000	0.000	0.000	0.000	0.000	0.000	0.000	0.000	0.000	0.000
Fe^{3+}	0.115	0.146	0.171	0.056	0.049	0.113	0.010	0.066	0.105	0.074	0.119	0.067	0.122
Fe^{2+}	4.277	4.253	4.249	4.281	4.302	4.264	4.343	4.295	4.282	4.353	4.264	4.254	4.266
Mn	0.137	0.142	0.144	0.146	0.137	0.147	0.138	0.150	0.147	0.136	0.149	0.145	0.149
Zn	0.003	0.004	0.013	0.012	0.005	0.012	0.003	0.009	0.011	0.010	0.012	0.015	0.004
Mg	0.098	0.101	0.090	0.102	0.103	0.091	0.102	0.102	0.099	0.094	0.094	0.080	0.096
M-site	**6.000**	**6.000**	**6.000**	**6.000**	**6.000**	**6.000**	**6.000**	**6.000**	**6.000**	**6.000**	**6.000**	**6.000**	**6.000**
Ca	0.003	0.005	0.001	0.002	0.006	0.000	0.000	0.000	0.002	0.002	0.000	0.006	0.003
Ba	0.000	0.000	0.000	0.000	0.000	0.001	0.000	0.001	0.000	0.000	0.000	0.002	0.000
Na	0.006	0.003	0.000	0.000	0.001	0.001	0.000	0.000	0.000	0.004	0.000	0.007	0.000
K	0.000	0.000	0.001	0.001	0.004	0.000	0.026	0.005	0.000	0.010	0.001	0.000	0.003
A-site	**0.009**	**0.009**	**0.002**	**0.004**	**0.011**	**0.002**	**0.027**	**0.007**	**0.003**	**0.017**	**0.001**	**0.015**	**0.006**
OH*	7.999	8.000	7.993	8.000	7.997	7.985	7.997	7.993	7.991	7.991	8.000	8.000	7.995
F	0.001	0.000	0.007	0.000	0.002	0.015	0.002	0.008	0.004	0.004	0.000	0.000	0.004
Cl	0.000	0.000	0.000	0.000	0.002	0.000	0.001	0.000	0.005	0.005	0.000	0.000	0.001
Fe#	0.978	0.978	0.980	0.977	0.977	0.980	0.977	0.977	0.978	0.979	0.979	0.982	0.979

Point_ID: spot identification; c: core; r: rim; i: intermediate zone; - : below detection limit

Table 35: Stilpnomelane in metaluminous syenogranites from the Mandira 1 unit

Sample	**MAN-4**												
Crystal	c1	c3			c9			c11			c11b		
Point_ID	1-c	3-c	3b-c	3b-r1	9-c	9-c2	9-c3	11-c	11-c2	11-c3	11b-c	11b-c2	11b-r1
SiO_2 (wt%)	44.23	43.03	42.89	43.13	45.40	43.68	44.75	43.81	43.79	43.50	43.50	43.86	43.79
TiO_2	0.29	0.02	0.03	0.00	0.00	0.01	0.00	0.02	0.00	0.06	0.05	0.00	0.00
Al_2O_3	7.40	6.85	6.66	7.00	6.26	6.86	6.46	6.76	6.85	6.94	6.66	6.63	6.81
FeO	31.35	32.79	32.57	32.12	31.70	32.66	32.05	32.51	32.21	31.27	32.57	31.98	32.07
MnO	1.28	1.55	1.52	1.56	1.40	1.67	1.55	2.07	2.03	1.91	2.04	1.98	1.90
MgO	2.04	1.93	1.95	1.80	1.92	1.87	1.92	2.30	2.30	2.17	2.31	2.33	2.42
ZnO	0.12	0.17	0.08	0.08	0.15	0.15	0.14	0.24	0.22	0.24	0.11	0.28	0.21
CaO	0.10	0.17	0.12	0.16	0.11	0.13	0.08	0.12	0.16	0.11	0.11	0.46	0.12
BaO	0.11	0.13	0.14	0.17	0.13	0.14	0.06	0.08	0.05	0.10	0.13	0.11	0.10
Na_2O	0.16	0.27	0.10	0.38	0.09	0.18	0.24	0.21	0.30	0.35	0.07	0.08	0.11
K_2O	2.91	2.46	3.25	2.68	2.81	2.70	2.50	2.00	2.19	2.54	1.71	2.52	1.90
F	0.00	0.00	0.04	0.00	0.05	0.00	0.05	0.00	0.00	0.00	0.04	0.01	0.05
Cl	0.00	0.00	0.04	0.01	0.01	0.01	0.02	0.00	0.00	0.00	0.00	0.02	0.02
H2O (calc)	7.73	7.83	7.63	7.65	7.57	7.83	7.70	8.11	8.00	7.75	8.15	7.82	8.07
O=F=Cl	0.00	0.00	-0.03	0.00	-0.02	0.00	-0.02	0.00	0.00	0.00	-0.02	-0.01	-0.02
Total	99.70	99.29	99.06	98.77	99.58	99.96	99.52	100.30	100.15	98.92	99.50	100.09	99.59
Structural formulae based on 15 octahedral and tetrahedral cations, and 27 (O,OH,F,Cl)*													
Si (apfu)	7.936	7.790	7.821	7.860	8.161	7.856	8.044	7.791	7.809	7.870	7.779	7.853	7.819
Al^{IV}	1.064	1.210	1.179	1.140	0.839	1.144	0.956	1.209	1.191	1.130	1.221	1.147	1.181
T-site	**9.000**	**9.000**	**9.000**	**9.000**	**9.000**	**9.000**	**9.000**	**9.000**	**9.000**	**9.000**	**9.000**	**9.000**	**9.000**
Al^{VI}	0.501	0.251	0.253	0.363	0.487	0.310	0.413	0.208	0.249	0.350	0.183	0.252	0.252
Ti	0.039	0.003	0.004	0.000	0.000	0.002	0.000	0.003	0.000	0.008	0.007	0.000	0.000
Fe^{2+}	2.023	2.135	2.136	2.105	2.049	2.112	2.072	2.079	2.066	2.035	2.095	2.059	2.059
Fe^{3+}	2.681	2.830	2.831	2.790	2.716	2.800	2.746	2.756	2.738	2.697	2.777	2.730	2.730
Mn	0.194	0.238	0.235	0.241	0.213	0.254	0.236	0.312	0.307	0.293	0.309	0.300	0.287
Zn	0.016	0.023	0.011	0.011	0.020	0.021	0.019	0.032	0.029	0.032	0.015	0.037	0.028
MgO	0.546	0.521	0.530	0.489	0.515	0.501	0.515	0.610	0.611	0.585	0.616	0.622	0.644
Ca	0.019	0.033	0.024	0.030	0.021	0.024	0.016	0.023	0.031	0.021	0.022	0.088	0.024
Ba	0.008	0.009	0.010	0.012	0.009	0.010	0.004	0.005	0.004	0.007	0.009	0.008	0.007
Na	0.056	0.095	0.035	0.134	0.032	0.062	0.082	0.073	0.102	0.122	0.026	0.027	0.038
K	0.666	0.568	0.756	0.623	0.644	0.619	0.573	0.454	0.498	0.586	0.390	0.576	0.433
O-site	**6.749**	**6.706**	**6.825**	**6.799**	**6.706**	**6.715**	**6.676**	**6.555**	**6.635**	**6.737**	**6.447**	**6.698**	**6.501**
Cations	15.75	15.71	15.82	15.80	15.71	15.72	15.68	15.55	15.63	15.74	15.45	15.70	15.50
Anions	27.00	27.00	27.00	27.00	27.00	27.00	27.00	27.00	27.00	27.00	27.00	27.00	27.00
OH*	3.028	3.375	3.192	3.142	2.871	3.279	3.068	3.656	3.533	3.301	3.750	3.362	3.636
F	0.000	0.000	0.023	0.000	0.026	0.000	0.027	0.000	0.000	0.000	0.020	0.005	0.025
Cl	0.000	0.000	0.012	0.002	0.004	0.003	0.005	0.000	0.001	0.000	0.000	0.005	0.007
Fe#	0.864	0.867	0.867	0.870	0.868	0.867	0.865	0.840	0.840	0.843	0.840	0.839	0.837

Point_ID: spot identification; c: core; r: rim; i: intermediate zone; - : below detection limit; Fe#: $Fe_T/(Fe_T+Mn+Mg)$

Table 36: Stilpnomelane in peralkaline granites from the Acaraú unit

Sample	**MAN-5579**						**MAN-6662**						
Crystal	c3			c8			c6			c6b		c10	c10b
Point_ID	3-r1	3-r2	3-c	8-r1	8-r2	8-r3	6-r1	6-c	6-r2	6b-r1	6b-c	10-c	10b-c
SiO_2 (wt%)	43.41	43.58	42.94	43.18	43.45	43.73	43.31	43.47	43.30	43.94	43.92	43.54	43.45
TiO_2	0.00	0.00	0.13	0.14	0.04	0.02	0.01	0.06	0.03	0.04	0.05	0.00	0.02
Al_2O_3	4.98	4.97	4.91	4.96	4.95	5.00	5.43	5.87	5.55	5.67	5.89	5.49	5.48
FeO	37.01	37.02	36.03	36.64	36.79	36.79	36.53	35.78	36.79	35.42	35.07	35.71	35.90
MnO	1.49	1.36	1.39	1.30	1.36	1.34	1.11	1.15	1.19	1.04	0.99	1.26	1.15
MgO	0.36	0.34	0.37	0.35	0.35	0.36	0.26	0.35	0.29	0.30	0.34	0.33	0.35
ZnO	0.81	0.97	0.91	0.83	0.87	0.82	0.49	0.59	0.51	0.40	0.60	0.57	0.63
CaO	0.04	0.05	0.15	0.09	0.00	0.03	0.03	0.05	0.03	0.07	0.13	0.06	0.00
BaO	0.05	0.14	0.18	0.03	0.09	0.08	0.03	0.01	0.05	0.00	0.07	0.04	0.01
Na_2O	0.14	0.17	0.13	0.18	0.12	0.16	0.15	0.17	0.13	0.25	0.23	0.21	0.18
K_2O	1.44	1.44	1.62	1.64	1.55	1.64	1.85	1.94	1.73	2.01	2.01	2.01	1.98
F	0.00	0.02	0.00	0.00	0.04	0.05	0.03	0.00	0.02	0.06	0.00	0.00	0.00
Cl	0.00	0.00	0.00	0.00	0.00	0.01	0.00	0.02	0.01	0.00	0.01	0.01	0.00
H2O (calc)	8.07	8.02	7.77	7.88	7.96	7.91	7.83	7.84	7.94	7.64	7.66	7.73	7.79
O=F=Cl	0.00	-0.01	0.00	0.00	-0.02	-0.02	-0.01	0.00	-0.01	-0.03	0.00	0.00	0.00
Total	100.15	100.43	98.81	99.53	99.90	100.25	99.37	99.56	99.90	99.05	99.20	99.22	99.21
Structural formulae based on 15 octahedral and tetrahedral cations, and 27 (O,OH,F,Cl)*													
Si (apfu)	7.880	7.898	7.917	7.898	7.909	7.934	7.926	7.924	7.878	8.048	8.032	7.978	7.957
Al^{IV}	1.065	1.062	1.067	1.069	1.062	1.066	1.074	1.076	1.122	0.952	0.968	1.022	1.043
T-site	**8.945**	**8.959**	**8.984**	**8.967**	**8.971**	**9.000**	**9.000**	**9.000**	**9.000**	**9.000**	**9.000**	**9.000**	**9.000**
Al^{VI}	0.000	0.000	0.000	0.000	0.000	0.003	0.097	0.185	0.068	0.272	0.301	0.164	0.140
Ti	0.000	0.000	0.018	0.019	0.006	0.002	0.001	0.008	0.005	0.005	0.007	0.000	0.003
Fe^{2+}	2.416	2.413	2.389	2.410	2.408	2.400	2.404	2.346	2.407	2.333	2.306	2.353	2.364
Fe^{3+}	3.203	3.198	3.167	3.195	3.193	3.182	3.187	3.109	3.191	3.093	3.057	3.119	3.134
Mn	0.229	0.209	0.217	0.201	0.210	0.206	0.173	0.177	0.183	0.162	0.154	0.195	0.178
Zn	0.109	0.129	0.124	0.112	0.117	0.110	0.067	0.079	0.069	0.054	0.082	0.077	0.085
MgO	0.098	0.092	0.101	0.096	0.095	0.096	0.072	0.096	0.078	0.082	0.093	0.091	0.095
Ca	0.008	0.009	0.029	0.017	0.001	0.006	0.005	0.010	0.006	0.013	0.025	0.011	0.000
Ba	0.003	0.010	0.013	0.002	0.006	0.006	0.002	0.001	0.004	0.000	0.005	0.003	0.001
Na	0.049	0.061	0.046	0.064	0.044	0.057	0.053	0.060	0.047	0.088	0.081	0.073	0.065
K	0.333	0.333	0.381	0.383	0.360	0.380	0.432	0.451	0.402	0.470	0.469	0.470	0.463
O-site	**6.448**	**6.454**	**6.485**	**6.499**	**6.439**	**6.449**	**6.492**	**6.522**	**6.458**	**6.571**	**6.579**	**6.558**	**6.528**
Cations	15.39	15.41	15.47	15.47	15.41	15.45	15.49	15.52	15.46	15.57	15.58	15.56	15.53
Anions	23.43	23.49	23.61	23.58	23.50	23.58	23.71	23.77	23.61	24.01	24.01	23.83	23.77
OH*	3.566	3.501	3.383	3.415	3.476	3.385	3.271	3.228	3.372	2.959	2.983	3.160	3.233
F	0.000	0.011	0.002	0.002	0.021	0.027	0.019	0.000	0.013	0.035	0.000	0.003	0.000
Cl	0.000	0.000	0.000	0.000	0.000	0.003	0.000	0.005	0.002	0.000	0.003	0.003	0.000
Fe#	0.945	0.949	0.946	0.950	0.948	0.949	0.958	0.952	0.955	0.957	0.956	0.950	0.953

Point_ID: spot identification; c: core; r: rim; i: intermediate zone; - : below detection limit; Fe#: $Fe_T/(Fe_T+Mn+Mg)$

Table 37: Columbite in greisens from the Desemborque Pluton

Sample	GUA-08																				
Crystal	c1					c3					c4			c5			c6	c7			
Point_ID	1-c	1-r1	2-i	2-c	2-r2	3-c	3-c	3-i	3-r2	3-r1	4-c	4c-2	4-r1	5-c	5-r1	5-r2	6-c	7-c	7-c2	7-r1	7-r2
SiO_2 (wt%)	0.31	0.26	0.17	0.16	0.17	0.18	0.18	0.19	0.16	0.21	0.14	0.14	0.21	0.13	0.11	0.18	0.08	0.07	0.12	0.07	0.06
TiO_2	1.57	1.79	0.95	0.96	1.16	1.09	1.15	0.61	1.90	1.04	1.44	1.46	1.48	0.99	0.72	1.35	0.55	0.94	0.98	0.82	0.84
$Al2O_3$	0.89	0.07	0.02	-	0.02	-	-	0.02	0.02	0.02	-	-	0.02	-	0.02	-	0.03	0.02	0.03	0.03	0.03
FeO	14.01	16.07	17.04	17.02	16.18	17.22	17.10	16.32	16.92	15.97	17.26	17.26	16.05	17.29	17.10	17.06	17.04	17.00	16.69	16.59	17.11
MnO	6.82	2.97	4.14	4.09	3.08	4.12	3.96	3.20	4.34	2.99	4.00	3.96	2.82	4.08	3.36	3.94	3.59	3.88	4.17	2.99	3.52
MgO	-	0.02	-	-	-	-	-	-	-	-	-	0.02	-	-	0.02	-	-	-	0.03	-	-
CaO	-	-	-	-	-	0.02	0.02	-	-	-	-	-	0.02	0.02	-	-	-	-	0.06	-	-
SrO	-	0.02	-	-	-	-	0.03	-	0.02	-	-	-	0.02	-	-	-	-	0.04	0.02	-	-
Na_2O	-	0.05	-	-	0.02	-	-	0.04	-	-	-	0.04	0.02	0.03	-	-	0.02	0.05	0.03	0.02	-
Sb_2O_5	-	-	-	-	0.02	-	-	0.06	0.03	-	-	0.04	-	0.05	-	-	0.02	-	-	-	-
V_2O_3	-	0.07	-	0.03	0.04	-	-	-	-	-	-	-	0.04	-	0.03	0.07	-	0.05	0.06	-	-
WO_3	4.36	2.94	1.72	1.52	1.73	1.95	1.85	1.35	6.15	1.84	2.88	3.00	3.35	1.85	1.46	3.24	1.50	1.41	1.76	1.41	1.80
ThO_2	0.05	0.05	-	0.02	-	-	0.05	-	-	0.02	-	-	0.05	-	-	0.04	0.04	0.02	-	0.02	0.03
UO_2	-	0.07	0.04	-	0.15	0.04	-	-	-	0.18	-	0.05	0.13	-	-	-	-	-	0.05	-	-
PbO	-	-	0.02	-	0.07	0.04	0.05	-	0.02	0.03	-	0.02	-	0.05	0.03	0.02	0.04	0.03	0.04	0.08	0.09
Gd_2O_3	-	-	-	0.04	-	-	-	-	-	-	0.06	0.04	-	-	-	-	-	-	-	-	-
Yb_2O_3	0.04	0.09	0.09	0.09	0.07	0.13	0.09	0.03	0.03	0.03	0.09	0.12	0.06	0.11	-	0.06	-	0.05	0.03	0.04	0.03
Y_2O_3	0.02	0.04	-	0.02	-	0.02	-	-	-	0.05	-	0.03	-	0.02	-	-	-	-	-	-	-
ZrO_2	0.06	0.67	0.13	0.12	0.44	0.13	0.16	0.05	0.09	0.54	0.26	0.25	0.59	0.17	0.06	0.09	0.04	0.08	0.16	0.11	0.05
Nb_2O_5	68.32	50.76	66.86	69.07	52.40	68.96	68.54	53.91	65.93	50.44	68.95	69.43	49.65	71.00	61.13	65.02	62.24	61.33	63.55	52.21	62.85
Ta_2O_5	4.47	21.80	5.40	4.36	24.72	4.34	4.23	22.62	4.74	25.98	4.08	3.96	25.74	3.72	15.93	8.21	13.49	9.14	8.85	24.61	14.41
F	-	-	-	-	-	-	-	0.30	-	-	-	-	-	-	-	-	0.32	0.11	-	-	-
Total	101	97.77	96.70	97.54	100	98.27	97.54	98.72	100	99.41	99.17	99.81	100	99.58	100	99.29	99.03	94.21	96.64	99.04	101

Point_ID: spot identification; c: core; r: rim; i: intermediate zone; - : below detection limit

Table 37: (*cont.*) Columbite in greisens from the Desemborque Pluton

Sample	GUA-08																				
Crystal	c1					c3					c4			c5			c6	c7			
Point_ID	1-c	1-r1	2-i	2-c	2-r2	3-c	3-c	3-i	3-r2	3-r1	4-c	4c-2	4-r1	5-c	5-r1	5-r2	6-c	7-c	7-c2	7-r1	7-r2
Structural formulae based on 3 cations and 6 oxygens																					
W (apfu)	0.06	0.05	0.03	0.02	0.03	0.03	0.03	0.02	0.09	0.03	0.04	0.04	0.05	0.03	0.02	0.05	0.02	0.02	0.03	0.02	0.03
Nb	1.78	1.47	1.82	1.84	1.47	1.83	1.83	1.53	1.73	1.46	1.81	1.81	1.42	1.85	1.67	1.74	1.71	1.76	1.76	1.50	1.69
Ta	0.07	0.37	0.09	0.07	0.41	0.07	0.07	0.39	0.07	0.44	0.06	0.06	0.42	0.06	0.26	0.13	0.22	0.15	0.15	0.42	0.23
Ti	0.07	0.08	0.04	0.04	0.05	0.05	0.05	0.03	0.08	0.05	0.06	0.06	0.07	0.04	0.03	0.06	0.03	0.04	0.04	0.04	0.04
Zr	0.00	0.02	0.00	0.00	0.01	0.00	0.00	0.00	0.00	0.02	0.01	0.01	0.02	0.00	0.00	0.00	0.00	0.00	0.00	0.00	0.00
Sb	0.00	0.00	0.00	0.00	0.00	0.00	0.00	0.00	0.00	0.00	0.00	0.00	0.00	0.00	0.00	0.00	0.00	0.00	0.00	0.00	0.00
V	0.00	0.00	0.00	0.00	0.00	0.00	0.00	0.00	0.00	0.00	0.00	0.00	0.00	0.00	0.00	0.00	0.00	0.00	0.00	0.00	0.00
Y	0.00	0.00	0.00	0.00	0.00	0.00	0.00	0.00	0.00	0.00	0.00	0.00	0.00	0.00	0.00	0.00	0.00	0.00	0.00	0.00	0.00
Gd	0.00	0.00	0.00	0.00	0.00	0.00	0.00	0.00	0.00	0.00	0.00	0.00	0.00	0.00	0.00	0.00	0.00	0.00	0.00	0.00	0.00
Yb	0.00	0.00	0.00	0.00	0.00	0.00	0.00	0.00	0.00	0.00	0.00	0.00	0.00	0.00	0.00	0.00	0.00	0.00	0.00	0.00	0.00
Th	0.00	0.00	0.00	0.00	0.00	0.00	0.00	0.00	0.00	0.00	0.00	0.00	0.00	0.00	0.00	0.00	0.00	0.00	0.00	0.00	0.00
U	0.00	0.00	0.00	0.00	0.00	0.00	0.00	0.00	0.00	0.00	0.00	0.00	0.00	0.00	0.00	0.00	0.00	0.00	0.00	0.00	0.00
Pb	0.00	0.00	0.00	0.00	0.00	0.00	0.00	0.00	0.00	0.00	0.00	0.00	0.00	0.00	0.00	0.00	0.00	0.00	0.00	0.00	0.00
Si	0.02	0.02	0.01	0.01	0.01	0.01	0.01	0.01	0.01	0.01	0.01	0.01	0.01	0.01	0.01	0.01	0.00	0.00	0.01	0.00	0.00
Al	0.01	0.00	0.00	0.00	0.00	0.00	0.00	0.00	0.00	0.00	0.00	0.00	0.00	0.00	0.00	0.00	0.00	0.00	0.00	0.00	0.00
B-site	**2.01**	**2.02**	**1.99**	**1.99**	**2.00**	**1.99**	**1.99**	**1.99**	**1.99**	**2.01**	**2.00**	**2.00**	**2.01**	**2.00**	**2.00**	**2.00**	**1.99**	**1.99**	**1.99**	**1.99**	**1.99**
Fe	0.67	0.83	0.83	0.83	0.87	0.84	0.84	0.86	0.82	0.84	0.83	0.83	0.85	0.82	0.85	0.84	0.86	0.83	0.82	0.87	0.85
Mn	0.33	0.16	0.20	0.20	0.16	0.20	0.20	0.17	0.21	0.16	0.20	0.19	0.15	0.20	0.17	0.19	0.17	0.20	0.21	0.16	0.18
Mg	0.00	0.00	0.00	0.00	0.00	0.00	0.00	0.00	0.00	0.00	0.00	0.00	0.00	0.00	0.00	0.00	0.00	0.00	0.00	0.00	0.00
A-site	**1.00**	**0.98**	**1.04**	**1.03**	**1.04**	**1.04**	**1.04**	**1.03**	**1.03**	**0.99**	**1.03**	**1.02**	**1.00**	**1.02**	**1.02**	**1.02**	**1.03**	**1.04**	**1.03**	**1.03**	**1.03**
#Ta	0.04	0.20	0.05	0.04	0.22	0.04	0.04	0.20	0.04	0.23	0.03	0.03	0.23	0.03	0.14	0.07	0.11	0.08	0.08	0.22	0.12
#Mn	0.33	0.16	0.20	0.20	0.16	0.20	0.19	0.17	0.21	0.16	0.19	0.19	0.15	0.19	0.17	0.18	0.16	0.20	0.20	0.15	0.17

#Ta: Ta/(Ta+Nb) and #Mn: Mn/(Mn + Fe)

Table 38: Columbite in greisens and in metaluminous to slightly peraluminous syenogranites from the Desemborque Pluton

	GUA-08							GUA-50C1			GUA-53(1)						
Crystal	c8		c9		c10			c1			3c	3c		c4	c4b		c1
Point_ID	8-c	8-r1	9-c	9-r1	10-c	10-r1	10-r2	1-c	1-r1	1-r2	3-r1	3-c	3-r2	4-r	4b-r2	4b-c	1-c
SiO_2 (wt%)	0.08	0.07	0.08	0.31	0.07	0.08	0.10	0.06	0.06	0.09	0.08	0.14	0.16	0.10	0.09	0.06	0.18
TiO_2	1.03	2.31	0.88	0.57	1.12	1.78	0.37	2.15	2.19	2.30	1.47	2.01	1.97	1.96	1.42	1.48	1.93
$Al2O_3$	-	0.04	0.03	0.06	-	0.04	0.03	0.17	0.02	0.04	0.02	0.19	0.04	0.03	-	-	-
FeO	17.34	16.37	17.17	16.36	17.34	16.70	16.08	17.83	16.97	16.88	16.98	13.13	13.68	14.46	16.82	16.66	16.99
MnO	4.12	2.71	4.17	3.49	4.17	2.80	3.31	3.56	3.48	3.50	4.31	7.97	7.78	6.52	4.40	4.90	3.94
MgO	-	0.03	-	-	-	-	-	-	-	0.04	0.02	-	-	0.02	-	-	-
CaO	-	-	-	-	-	-	-	-	-	-	0.19	-	0.03	0.06	0.04	0.16	-
SrO	0.02	-	0.03	0.02	-	0.02	-	-	-	-	-	-	-	-	-	0.04	-
Na_2O	0.02	-	-	-	-	-	-	0.02	-	0.04	-	-	0.03	-	-	-	0.05
Sb_2O_5	0.02	-	0.04	-	-	-	-	0.04	-	-	-	0.04	-	-	-	-	-
V_2O_3	-	-	0.06	0.05	-	0.06	0.04	0.03	-	-	-	-	0.03	-	-	-	0.03
WO_3	1.38	2.85	1.25	1.54	2.40	5.08	1.08	4.11	3.90	4.18	1.70	1.98	2.67	2.27	1.51	0.92	2.88
ThO_2	-	0.03	-	-	-	-	-	-	0.02	0.04	-	0.08	-	0.02	-	0.02	0.05
UO_2	-	0.31	-	-	-	-	-	-	0.06	0.06	-	0.06	0.08	0.06	-	0.04	-
PbO	0.04	0.09	0.03	0.05	-	0.05	0.06	0.05	0.06	0.07	0.02	-	0.07	0.05	0.04	0.05	0.04
Gd_2O_3	-	0.06	-	-	-	-	0.04	-	-	0.04	0.09	-	-	0.05	-	-	0.10
Yb_2O_3	0.09	0.11	0.11	0.03	0.07	0.04	-	0.06	-	0.05	0.20	0.06	0.08	0.08	0.31	0.14	0.27
Y_2O_3	-	0.05	-	-	-	-	-	0.01	-	0.01	0.15	0.04	0.03	0.09	0.10	0.08	0.08
ZrO_2	0.12	1.27	0.13	0.13	0.14	0.65	0.09	0.27	0.21	0.30	0.21	0.16	0.13	0.12	0.16	0.09	0.31
Nb_2O_5	69.48	45.85	69.31	52.96	69.10	47.37	52.08	65.96	53.61	53.01	70.57	67.01	67.68	66.61	69.98	70.93	68.41
Ta_2O_5	4.06	27.96	4.29	24.44	4.34	26.03	25.10	4.96	18.36	19.15	1.90	4.34	3.96	3.53	2.21	0.98	3.03
F	-	-	0.15	-	-	0.15	0.17	-	-	-	0.34	-	-	-	-	-	0.20
Total	97.86	100	97.73	100	98.81	101	98.55	99.38	99.02	99.80	98.24	97.26	98.46	96.03	97.13	96.58	98.49

Point_ID: spot identification; c: core; r: rim; i: intermediate zone; - : below detection limit

Table 38: (*cont.*) Columbite in greisens and in metaluminous to slightly peraluminous syenogranites from the Desemborque Pluton

Sample	**GUA-08**							**GUA-50C1**			**GUA-53(1)**						
Crystal	c8		c9		c10			c1			3c	3c		c4	c4b		c1
Point_ID	8-c	8-r1	9-c	9-r1	10-c	10-r1	10-r2	1-c	1-r1	1-r2	3-r1	3-c	3-r2	4-r	4b-r2	4b-c	1-c
Structural formulae based on 3 cations and 6 oxygens																	
W (apfu)	0.02	0.05	0.02	0.03	0.04	0.08	0.02	0.06	0.06	0.07	0.03	0.03	0.04	0.03	0.02	0.01	0.04
Nb	1.86	1.32	1.85	1.49	1.84	1.35	1.51	1.75	1.50	1.48	1.86	1.79	1.79	1.81	1.87	1.90	1.81
Ta	0.06	0.48	0.08	0.42	0.07	0.45	0.43	0.08	0.31	0.32	0.03	0.07	0.06	0.06	0.03	0.02	0.05
Ti	0.04	0.11	0.04	0.03	0.05	0.08	0.02	0.09	0.10	0.11	0.06	0.09	0.09	0.09	0.06	0.06	0.08
Zr	0.00	0.04	0.00	0.00	0.00	0.02	0.00	0.01	0.01	0.01	0.01	0.00	0.00	0.00	0.00	0.00	0.01
Sb	0.00	0.00	0.00	0.00	0.00	0.00	0.00	0.00	0.00	0.00	0.00	0.00	0.00	0.00	0.00	0.00	0.00
V	0.00	0.00	0.00	0.00	0.00	0.00	0.00	0.00	0.00	0.00	0.00	0.00	0.00	0.00	0.00	0.00	0.00
Y	0.00	0.00	0.00	0.00	0.00	0.00	0.00	0.00	0.00	0.00	0.00	0.00	0.00	0.00	0.00	0.00	0.00
Gd	0.00	0.00	0.00	0.00	0.00	0.00	0.00	0.00	0.00	0.00	0.00	0.00	0.00	0.00	0.00	0.00	0.00
Yb	0.00	0.00	0.00	0.00	0.00	0.00	0.00	0.00	0.00	0.00	0.00	0.00	0.00	0.00	0.01	0.00	0.00
Th	0.00	0.00	0.00	0.00	0.00	0.00	0.00	0.00	0.00	0.00	0.00	0.00	0.00	0.00	0.00	0.00	0.00
U	0.00	0.00	0.00	0.00	0.00	0.00	0.00	0.00	0.00	0.00	0.00	0.00	0.00	0.00	0.00	0.00	0.00
Pb	0.00	0.00	0.00	0.00	0.00	0.00	0.00	0.00	0.00	0.00	0.00	0.00	0.00	0.00	0.00	0.00	0.00
Si	0.00	0.00	0.00	0.02	0.00	0.00	0.01	0.00	0.00	0.01	0.00	0.01	0.01	0.01	0.01	0.00	0.01
Al	0.00	0.00	0.00	0.00	0.00	0.00	0.00	0.01	0.00	0.00	0.00	0.01	0.00	0.00	0.00	0.00	0.00
B-site	**2.00**	**2.02**	**2.00**	**1.99**	**2.00**	**2.00**	**1.99**	**2.01**	**1.99**	**1.99**	**2.00**	**2.01**	**2.00**	**2.00**	**2.01**	**2.00**	**2.01**
Fe	0.82	0.87	0.81	0.86	0.83	0.87	0.85	0.84	0.87	0.86	0.82	0.64	0.66	0.71	0.81	0.79	0.82
Mn	0.20	0.15	0.21	0.18	0.19	0.15	0.18	0.17	0.18	0.18	0.21	0.40	0.37	0.32	0.21	0.23	0.19
Mg	0.00	0.00	0.00	0.00	0.00	0.00	0.00	0.00	0.00	0.00	0.00	0.00	0.00	0.00	0.00	0.00	0.00
A-site	**1.02**	**1.02**	**1.02**	**1.04**	**1.01**	**1.02**	**1.03**	**1.01**	**1.05**	**1.05**	**1.03**	**1.04**	**1.03**	**1.03**	**1.02**	**1.02**	**1.01**
#Ta	0.03	0.27	0.04	0.22	0.04	0.25	0.22	0.04	0.17	0.18	0.02	0.04	0.03	0.03	0.02	0.01	0.03
#Mn	0.20	0.14	0.20	0.17	0.19	0.15	0.17	0.17	0.17	0.17	0.21	0.38	0.36	0.31	0.21	0.23	0.19

#Ta: Ta/(Ta+Nb) and #Mn: Mn/(Mn + Fe)

Table 39: Fluorite metaluminous to slightly peraluminous syenogranites and greisens from the Desemborque Pluton

Sample	GUA-50C1								GUA-08							
Crystal	c3					c3a			c2				c3			
Point_ID	3-r1(d)	3-c(d)	3-c(b)	3-r1(b)	3-r2(d)	3a-i	3a-r1(b)	3a-r2(b)	2a-(d)	2a-(b)	2a-(b)	2a-(b2)	3-i	3-(b)	3-(b2)	3-i
Na (wt%)	0.20	0.16	0.20	0.09	0.04	0.16	0.15	0.19	0.00	0.17	0.18	0.35	0.40	0.18	0.25	0.13
Y	1.98	1.98	2.90	2.66	0.19	2.10	2.82	2.85	0.84	3.97	3.75	3.07	2.64	3.21	2.98	2.46
Si	0.05	0.05	0.02	0.03	0.05	0.00	0.03	0.00	0.06	0.05	0.05	0.06	0.01	0.03	0.06	0.06
Ce	0.98	1.42	1.58	0.99	0.02	1.22	1.42	1.43	0.13	1.04	1.16	0.62	0.47	0.90	0.87	0.13
Nd	0.74	0.68	0.79	0.73	0.08	0.66	0.64	0.69	0.06	0.64	0.65	0.54	0.43	0.55	0.61	0.09
Pr	0.21	0.19	0.32	0.16	0.08	0.22	0.34	0.09	0.05	0.24	0.27	0.12	0.04	0.13	0.18	0.01
Sm	0.14	0.23	0.26	0.30	0.00	0.29	0.26	0.17	0.02	0.13	0.14	0.34	0.18	0.22	0.27	0.08
Gd	0.17	0.45	0.52	0.39	0.02	0.27	0.72	0.42	0.02	0.34	0.53	0.02	0.26	0.21	0.47	0.20
Ca	44.43	45.35	42.29	44.74	48.01	44.43	43.13	45.16	47.64	44.51	44.44	44.03	44.10	45.45	44.80	47.05
Th	0.18	0.10	0.17	0.00	0.00	0.00	0.14	0.20	0.00	0.01	0.10	0.11	0.07	0.04	0.02	0.05
Tb	0.14	0.11	0.10	0.04	0.00	0.13	0.07	0.01	0.00	0.08	0.00	0.01	0.05	0.07	0.11	0.12
Dy	0.56	0.33	0.48	0.50	0.06	0.43	0.54	0.54	0.15	0.19	0.30	0.53	0.45	0.28	0.51	0.30
Er	0.24	0.34	0.30	0.13	0.02	0.33	0.22	0.27	0.01	0.27	0.21	0.34	0.37	0.37	0.40	0.22
Yb	0.05	0.11	0.42	0.22	0.00	0.37	0.28	0.29	0.11	0.29	0.37	0.42	0.51	0.19	0.42	0.35
Ho	0.08	0.04	0.27	0.38	0.07	0.04	0.25	0.23	0.03	0.56	0.00	0.21	0.05	0.26	0.00	0.00
Lu	0.82	0.00	0.00	0.09	0.14	0.02	0.00	0.00	0.00	0.00	0.20	0.00	0.20	0.00	0.00	0.16
F	44.41	43.19	43.00	43.21	43.79	43.38	42.89	42.67	44.48	42.00	43.64	42.47	43.04	43.08	44.24	41.64
Al	0.01	0.00	0.01	0.01	0.03	0.01	0.01	0.00	0.03	0.02	0.01	0.01	0.00	0.01	0.00	0.02
Total	95.40	94.72	93.61	94.67	92.61	94.05	93.90	95.22	93.64	94.52	96.01	93.25	93.27	95.17	96.19	93.08

Point_ID: spot identification; c: core; r: rim; i: intermediate; b: bright; d: dark zone; - : below detection limit

Table 40: Fluorite in peralkaline alkali feldspar granites from the Mandira granites

Sample	MAN-2A										MAN-13A						
Crystal	c3		c3b			c3c			c12		c1						
Point_ID	3-i	3-i	3b-(b)	3b-(b)	3b-(b2)	3c-(b)	3c-(b2)	3c-(b3)	12-i	12-(b)	1-(d)	1-(d2)	1-(b)	1-(d)	1-i	1-(b)	1-i2
Na (wt%)	0.57	1.99	1.64	1.59	1.56	1.60	1.70	1.27	0.48	1.64	0.02	0.09	1.69	0.13	0.82	0.76	0.71
Y	5.03	5.47	5.05	5.17	4.89	4.99	5.07	7.75	4.71	5.57	0.15	0.15	4.33	0.30	3.28	4.61	2.93
Si	0.00	0.02	0.00	0.02	0.03	0.00	0.02	0.03	0.02	0.03	0.02	0.04	0.03	0.02	0.04	0.00	0.01
Ce	0.55	1.48	0.92	1.62	1.39	1.29	1.57	1.04	0.53	3.33	0.04	0.04	1.59	0.00	0.44	0.42	0.34
Nd	0.22	1.03	0.58	0.85	0.94	0.85	0.86	0.86	0.20	1.72	0.01	0.01	1.10	0.00	0.17	0.27	0.11
Pr	0.21	0.31	0.15	0.20	0.20	0.22	0.19	0.15	0.07	0.41	0.00	0.09	0.35	0.00	0.06	0.04	0.00
Sm	0.11	0.36	0.23	0.33	0.43	0.36	0.27	0.47	0.10	0.42	0.05	0.00	0.37	0.01	0.14	0.13	0.02
Gd	0.00	0.70	0.36	0.47	0.63	0.58	0.54	0.79	0.03	0.87	0.13	0.08	0.65	0.00	0.19	0.24	0.00
Ca	43.02	38.41	41.14	40.86	40.38	41.62	39.99	37.74	42.33	37.01	51.25	50.74	40.25	50.51	45.95	43.28	46.51
Th	0.00	0.00	0.04	0.00	0.03	0.00	0.08	0.00	0.02	0.00	0.00	0.03	0.00	0.00	0.00	0.03	0.10
Tb	0.13	0.08	0.05	0.17	0.02	0.03	0.11	0.17	0.00	0.19	0.00	0.08	0.09	0.00	0.00	0.03	0.11
Dy	0.29	0.93	0.62	0.56	0.60	0.51	0.74	1.15	0.20	0.70	0.00	0.02	0.61	0.00	0.19	0.41	0.16
Er	0.25	0.56	0.44	0.59	0.27	0.49	0.47	0.69	0.28	0.35	0.00	0.00	0.32	0.07	0.26	0.32	0.22
Yb	0.05	0.56	0.50	0.60	0.39	0.20	0.33	0.55	0.19	0.21	0.12	0.00	0.34	0.05	0.26	0.36	0.36
Ho	0.00	0.15	0.40	0.35	0.27	0.00	0.17	0.16	0.11	0.11	0.00	0.00	0.00	0.11	0.00	0.10	0.02
Lu	0.18	0.00	0.30	0.20	0.04	0.00	0.00	0.44	0.47	0.26	0.02	0.07	0.00	0.00	0.00	0.11	0.02
F	45.09	42.16	45.17	42.34	43.00	43.93	43.50	41.94	44.98	43.17	46.70	44.52	42.95	45.17	45.05	44.41	43.53
Al	0.04	0.00	0.01	0.00	0.00	0.00	0.01	0.00	0.00	0.11	0.00	0.00	0.00	0.00	0.00	0.00	0.01
Total	95.75	94.22	97.58	95.93	95.08	96.67	95.62	95.20	94.74	96.10	98.50	95.97	94.66	96.36	96.86	95.52	95.16

Point_ID: spot identification; c: core; r: rim; i: intermediate; b: bright; d: dark zone; - : below detection limit

Table 41: Fluorite in peralkaline alkali feldspar granites from the Mandira granites

Sample	**MAN-13A**		**MAN-20S**													
Crystal	c11c		c1													
Point_ID	11c-(d)	11c-i	1-(d)	1-i	1b-(d)	1c-(d)	1c-(b)	1c-i	4-i	4-i2	5-(b)	5-(d)	5b-(d)	5b-(d)	5b-(d2)	9-(d)
Na	0.13	0.97	0.00	1.31	0.08	0.15	1.25	0.54	0.60	0.69	1.67	0.72	1.75	1.40	1.09	1.08
Y	0.35	3.67	0.15	3.10	0.18	0.32	3.00	2.65	1.24	2.85	4.91	3.77	4.65	4.91	4.79	4.23
Si	0.04	0.05	0.02	0.01	0.04	0.03	0.02	0.02	0.07	0.17	0.03	0.06	0.01	0.01	0.02	0.03
Ce	0.03	0.68	0.03	1.14	0.05	0.25	1.43	0.21	0.85	0.44	1.49	0.47	1.97	1.19	1.37	0.58
Nd	0.03	0.17	0.00	0.67	0.09	0.13	0.72	0.29	0.39	0.43	1.13	0.44	1.35	1.02	0.93	0.70
Pr	0.15	0.01	0.12	0.19	0.00	0.03	0.13	0.00	0.14	0.00	0.21	0.05	0.25	0.11	0.20	0.07
Sm	0.00	0.07	0.04	0.25	0.00	0.11	0.34	0.13	0.17	0.18	0.50	0.22	0.41	0.31	0.43	0.37
Gd	0.00	0.09	0.07	0.55	0.04	0.07	0.38	0.24	0.16	0.26	0.58	0.33	0.80	0.66	0.51	0.45
Ca	50.05	44.81	50.23	43.61	50.25	49.64	43.43	45.11	45.81	45.31	39.94	44.75	38.10	41.13	39.90	42.22
Th	0.00	0.00	0.00	0.05	0.07	0.02	0.00	0.00	0.01	0.01	0.00	0.00	0.08	0.06	0.08	0.00
Tb	0.00	0.09	0.00	0.12	0.00	0.03	0.13	0.03	0.02	0.03	0.00	0.08	0.00	0.08	0.14	0.09
Dy	0.07	0.46	0.00	0.40	0.16	0.13	0.43	0.32	0.06	0.49	0.74	0.50	0.64	0.63	0.65	0.76
Er	0.09	0.38	0.00	0.17	0.06	0.12	0.29	0.41	0.03	0.08	0.43	0.37	0.50	0.64	0.39	0.45
Yb	0.00	0.42	0.08	0.24	0.00	0.00	0.15	0.30	0.12	0.15	0.42	0.34	0.47	0.31	0.77	0.28
Ho	0.14	0.22	0.00	0.03	0.00	0.00	0.29	0.08	0.19	0.14	0.45	0.00	0.33	0.42	0.00	0.22
Lu	0.00	0.29	0.00	0.00	0.54	0.00	0.07	0.01	0.13	0.51	0.07	0.09	0.00	0.00	0.00	0.66
F	46.97	45.75	45.88	44.60	45.53	45.74	44.07	43.70	46.00	45.77	44.20	44.24	44.33	43.23	44.97	43.17
Al	0.01	0.00	0.02	0.01	0.03	0.01	0.01	0.01	0.12	0.05	0.02	0.01	0.00	0.04	0.05	0.01
Total	98.05	98.14	96.64	96.45	97.12	96.78	96.16	94.05	96.11	97.56	96.79	96.45	95.64	96.16	96.29	95.38

Point_ID: spot identification; c: core; r: rim; i: intermediate; b: bright; d: dark zone; - : below detection limit

Table 42: Fluocerite in peralkaline alkali feldspar granites from the Mandira granites (compositions in wt %)

Sample	MAN-13B												
Crystal	c1b		c1c	c1d		c2		c3		c3b	c8	c8b	c5c
Point_ID	1b	1b-2	1c	1d	1d-r	2	2b	3	3-b	3b-2	8	8b	8c
Na (wt%)	0.085	0.159	0.036	0.106	0.000	0.068	0.094	0.107	0.063	0.032	0.078	0.000	0.065
Y	0.015	0.069	0.179	0.031	0.045	0.167	0.146	0.053	0.104	0.040	0.092	0.068	0.098
Si	0.056	0.076	0.000	0.072	0.063	0.051	0.059	0.073	0.028	0.069	0.034	0.043	0.056
La	15.070	17.360	14.640	15.550	15.300	13.900	15.150	13.970	13.890	16.450	13.030	11.990	15.640
Ce	36.740	37.530	39.200	36.080	36.660	32.410	33.610	33.020	36.310	38.220	34.780	35.600	37.450
Nd	3.850	3.760	4.470	13.540	14.870	3.950	4.020	4.510	14.880	12.450	17.380	18.150	13.860
Pr	15.370	12.250	12.640	4.290	4.550	18.280	16.580	17.170	4.460	4.000	4.530	4.710	4.420
Ca	0.098	0.051	0.042	0.066	0.000	0.189	0.270	0.195	0.151	0.102	0.049	0.000	0.173
Th	0.430	0.224	0.679	0.595	0.420	1.210	1.010	0.625	0.302	0.402	0.126	0.000	0.818
Sr	0.000	0.000	0.000	0.055	0.000	0.000	0.006	0.051	0.071	0.064	0.000	0.014	0.013
Sm	1.710	1.480	0.870	1.320	1.630	2.460	1.920	1.920	1.200	1.390	2.180	1.990	1.150
Gd	0.480	0.467	0.094	0.053	0.551	0.285	0.332	0.372	0.528	0.327	0.661	0.506	0.560
Dy	0.090	0.200	0.181	0.135	0.111	0.204	0.098	0.009	0.130	0.283	0.000	0.112	0.011
Yb	0.159	0.217	0.112	0.196	0.000	0.309	0.137	0.125	0.254	0.221	0.088	0.289	0.132
F	29.460	28.580	29.370	29.120	28.230	28.190	28.270	27.310	29.600	29.260	26.790	29.770	28.870
Al	0.002	0.000	0.029	0.002	0.022	0.034	0.022	0.053	0.000	0.015	0.006	0.000	0.078
Total	103.61	102.42	102.54	101.21	102.45	101.71	101.72	99.56	101.97	103.33	99.82	103.24	103.39
REE	73.47	73.26	72.21	71.16	73.67	71.80	71.85	71.09	71.65	73.34	72.65	73.35	73.22
LREE	72.74	72.38	71.82	70.78	73.01	71.00	71.28	70.59	70.74	72.51	71.90	72.44	72.52
HREE	0.73	0.88	0.39	0.38	0.66	0.80	0.57	0.50	0.91	0.83	0.75	0.91	0.70

Point_ID: spot identification; c: core; r: rim; i: intermediate; b: bright; d: dark zone; - : below detection limit

Table 43: Gagarinite in peralkaline alkali feldspar granites from the Mandira granites

Sample	MAN-13A								MAN-13B								
Crystal	c1	c1b	c1c						c1			c2					
Point_ID	1	1b	1c-i	1c-i	1c-i	3	11	11c	1	1b	1c	2	2-r	2b	2c	2c-r1	2c-r2
Na	4.74	4.39	6.90	6.79	6.33	3.69	4.11	3.88	5.06	5.19	5.80	4.43	4.37	4.55	4.53	4.55	4.68
Y	17.88	16.98	21.30	21.36	20.81	16.21	16.63	16.72	20.30	20.04	19.72	21.17	21.11	21.56	22.86	22.81	22.61
Si	0.12	0.20	0.00	0.00	0.00	0.08	0.04	0.06	0.16	0.30	0.19	0.07	0.08	0.22	0.07	0.07	0.14
Ce	3.89	4.06	2.91	3.45	2.82	4.95	4.29	4.09	2.05	1.94	1.92	1.36	1.32	1.34	0.84	0.69	0.72
Nd	6.18	6.09	3.37	3.17	3.19	7.47	8.16	8.01	6.65	6.45	7.03	5.80	5.90	5.66	4.16	4.30	4.25
Pr	1.15	1.16	0.53	0.51	0.56	1.21	1.24	1.30	0.80	0.90	1.01	0.51	0.71	0.76	0.47	0.42	0.63
Sm	2.73	2.53	1.75	1.60	1.60	3.17	3.31	3.35	2.95	2.70	2.95	3.05	3.40	3.23	2.79	3.14	3.23
Gd	3.59	3.69	3.36	2.61	2.66	4.02	4.32	4.29	3.68	3.54	3.78	4.06	4.51	4.17	4.42	4.65	4.48
Ca	12.32	12.16	12.50	12.67	12.41	12.30	12.19	12.20	12.18	11.85	12.15	12.30	12.30	12.03	12.43	12.37	12.53
Th	0.01	0.25	0.02	0.03	0.00	0.06	0.00	0.04	0.03	0.00	0.00	0.00	0.00	0.09	0.09	0.03	0.09
Tb	0.57	0.43	0.38	0.37	0.62	0.53	0.61	0.58	0.55	0.63	0.63	0.63	0.65	0.54	0.60	0.65	0.52
Dy	3.68	3.79	3.62	3.37	3.37	3.63	3.85	3.65	3.89	3.76	3.98	4.14	3.92	4.27	4.67	5.08	5.02
Er	1.73	1.83	1.65	1.68	1.67	1.73	1.91	1.73	1.76	1.68	1.60	2.15	1.94	2.00	2.01	2.23	2.08
Yb	1.03	1.02	0.46	0.84	0.70	0.97	0.77	0.82	0.76	0.90	0.87	0.93	0.84	0.81	0.87	0.80	0.75
Ho	0.57	1.14	0.99	0.77	0.63	0.45	0.55	0.83	0.66	1.01	0.62	1.25	0.70	0.88	0.55	0.67	0.52
Lu	0.51	0.39	0.00	0.32	0.01	0.29	0.53	0.24	0.22	0.00	0.52	0.14	0.00	0.00	0.49	0.22	0.00
F	37.95	34.01	34.72	34.82	34.73	34.07	33.13	34.63	34.76	35.18	35.93	34.28	34.24	33.22	36.01	35.39	34.59
Al	0.00	0.00	0.00	0.00	0.00	0.02	0.01	0.00	0.00	0.00	0.00	0.00	0.00	0.00	0.00	0.00	0.00
Total	98.65	94.11	94.45	94.36	92.11	94.84	95.65	96.42	96.46	96.08	98.71	96.27	96.00	95.33	97.87	98.06	96.84
REE	25.63	26.13	19.01	18.69	17.83	28.42	29.54	28.89	23.97	23.51	24.91	24.01	23.90	23.66	21.87	22.84	22.21
LREE	13.95	13.84	8.56	8.73	8.17	16.80	17.00	16.75	12.45	11.99	12.91	10.72	11.33	10.99	8.26	8.54	8.84
HREE	11.68	12.29	10.45	9.96	9.66	11.62	12.54	12.14	11.52	11.52	12.00	13.29	12.56	12.67	13.61	14.30	13.37

Point_ID: spot identification; c: core; r: rim; i: intermediate; b: bright; d: dark zone; - : below detection limit

Table 44: Monazite in metaluminous to slightly peraluminous syenogranites from the Desemborque Pluton

Sample	GUA-50C												50C1
Crystal	c1a	c1b	c1c				c1e				c1f		c1b
Point_ID	1a-c	1b-c	1c-r1	1c-c	1c-r2	1c-c	1e-r1	1e-c	1e-r2	1e-r4	1f-c2	1f-c3	1b-i
SiO_2 (wt%)	0.60	0.75	0.53	0.58	0.58	0.41	0.14	0.93	0.75	0.12	0.24	0.15	0.75
$Al2O_3$	0.02	0.02	0.02	0.02	0.02	0.01	0.00	0.01	0.00	0.01	0.00	0.01	0.01
CaO	0.06	0.07	0.14	0.25	0.14	0.09	0.22	0.08	0.06	0.42	0.40	0.46	0.19
FeO	0.22	0.47	0.34	0.28	0.35	0.25	0.46	0.21	0.28	0.42	0.16	0.43	0.26
La_2O_3	14.48	17.04	15.45	14.96	12.42	16.09	13.36	13.47	13.14	13.77	16.47	16.39	11.38
Ce_2O_3	33.38	34.88	34.24	33.31	28.81	34.88	33.09	32.51	32.42	31.99	32.60	32.38	30.43
Pr_2O_3	3.69	3.40	3.60	3.55	3.56	3.58	3.66	3.63	3.77	3.49	3.38	3.32	3.74
Nd_2O_3	12.14	9.82	11.36	11.77	14.77	10.91	11.65	12.19	12.29	11.75	11.24	10.48	14.19
Sm_2O_3	1.91	1.23	1.55	2.03	3.42	1.65	2.42	2.09	1.92	2.15	1.93	1.39	2.73
Gd_2O_3	0.85	0.52	0.82	0.85	2.39	0.64	1.47	1.14	1.09	1.35	0.99	1.10	1.67
Dy_2O_3	0.21	0.33	-	0.27	0.56	-	0.52	0.46	0.63	0.64	0.34	0.38	0.71
Yb_2O_3	0.73	-	0.69	-	-	0.72	-	-	-	-	-	-	-
P_2O_5	28.89	28.97	29.50	28.64	28.64	29.47	29.81	28.44	28.32	29.44	29.72	30.28	29.19
ThO_2	2.29	2.85	2.41	2.76	2.29	1.95	1.29	3.16	2.92	2.06	1.84	2.03	2.31
UO_2	0.08	0.10	0.09	0.10	0.04	0.08	0.08	0.11	0.09	0.14	0.08	0.07	0.15
Y_2O_3	0.40	0.15	0.20	0.22	0.34	0.21	1.19	0.84	0.80	1.12	0.77	1.22	1.64
PbO	0.06	0.08	0.06	0.07	0.06	0.05	0.05	0.10	0.09	0.07	0.06	0.07	0.08
Total	99.99	100.9	101.2	99.85	98.38	101.2	99.38	99.35	98.54	98.90	100.8	100.1	99.39
Structural formulae based on 16 oxygens													
Si (apfu)	0.095	0.119	0.083	0.092	0.094	0.065	0.021	0.148	0.120	0.018	0.038	0.023	0.119
P	3.896	3.880	3.903	3.898	3.900	3.931	3.969	3.848	3.878	3.971	3.960	3.980	3.897
P-site	**3.991**	**3.999**	**3.985**	**3.990**	**3.994**	**3.996**	**3.990**	**3.996**	**3.998**	**3.989**	**3.998**	**4.003**	**4.015**
Th	0.083	0.103	0.086	0.100	0.084	0.070	0.046	0.115	0.106	0.074	0.065	0.072	0.083
U	0.002	0.002	0.002	0.003	0.001	0.002	0.002	0.003	0.002	0.004	0.002	0.002	0.004
Al	0.004	0.004	0.004	0.004	0.005	0.002	0.001	0.002	0.000	0.001	0.000	0.002	0.002
Fe^{3+}	0.026	0.032	0.041	0.034	0.042	0.030	0.055	0.026	0.033	0.015	0.019	0.051	0.031
Y	0.034	0.013	0.017	0.018	0.029	0.018	0.100	0.071	0.067	0.094	0.064	0.101	0.138
La	0.830	0.977	0.891	0.864	0.737	0.918	0.775	0.791	0.782	0.804	0.909	0.939	0.662
Ce	1.939	1.991	1.961	1.921	1.696	1.966	1.905	1.895	1.898	1.859	1.866	1.840	1.757
Pr	0.213	0.196	0.206	0.205	0.209	0.206	0.210	0.211	0.218	0.201	0.193	0.188	0.215
Nd	0.688	0.555	0.627	0.655	0.848	0.614	0.654	0.693	0.697	0.675	0.628	0.581	0.799
Sm	0.104	0.067	0.084	0.111	0.190	0.090	0.131	0.115	0.105	0.117	0.104	0.074	0.148
Gd	0.045	0.027	0.043	0.045	0.127	0.033	0.077	0.060	0.057	0.071	0.051	0.057	0.087
Dy	0.011	0.017	0.009	0.014	0.029	0.009	0.026	0.023	0.032	0.033	0.017	0.019	0.036
Yb	0.030	0.013	0.033	0.009	0.000	0.035	0.000	0.000	0.000	0.000	0.029	0.000	0.000
Ca	0.011	0.012	0.024	0.042	0.024	0.016	0.037	0.014	0.010	0.071	0.066	0.077	0.031
Pb	0.003	0.003	0.002	0.003	0.003	0.002	0.002	0.004	0.003	0.003	0.002	0.002	0.003
Ce-site	**4.023**	**4.011**	**4.031**	**4.028**	**4.023**	**4.010**	**4.021**	**4.023**	**4.012**	**4.023**	**4.017**	**4.004**	**3.996**
Cations	**8.014**	**8.010**	**8.016**	**8.018**	**8.016**	**8.006**	**8.011**	**8.019**	**8.010**	**8.012**	**8.014**	**8.007**	**8.012**

Point_ID: spot identification; c: core; r: rim; i: intermediate zone; - : below detection limit

Table 45: Monazite in metaluminous to slightly peraluminous syenogranites from the Desemborque Pluton

Sample	GUA-50C1			GUA-50C2					GUA-50C4				
Crystal	c2	c5		c1		c1b	c1d	c11	c5	c5b	c5c	c5d	c5f
Point_ID	2-c	5-c	5b-i	1-c	1-r1	1b-c	1d-c	11-c	5-c	5b-c	5c-c	5d-c	5f-c
SiO_2 (wt%)	0.48	0.48	0.24	0.60	0.73	0.50	0.24	1.14	0.34	0.16	0.25	0.36	0.51
$Al2O_3$	0.04	0.24	0.04	0.01	0.02	0.29	0.05	0.02	0.01	0.02	0.03	0.02	0.03
CaO	0.33	0.23	0.18	0.15	0.16	0.18	0.37	0.25	0.22	0.42	0.29	0.14	0.13
FeO	0.35	0.89	0.41	0.11	0.12	0.57	0.32	0.49	0.24	0.23	0.31	0.35	0.54
La_2O_3	10.91	12.05	10.73	10.08	11.79	14.61	14.49	13.18	16.79	12.81	11.30	15.84	16.72
Ce_2O_3	30.25	31.58	30.16	28.92	30.52	33.50	33.76	34.46	32.50	31.61	30.71	34.88	34.94
Pr_2O_3	3.90	3.69	3.75	3.89	3.71	3.59	3.66	3.66	3.22	3.62	3.68	3.44	3.30
Nd_2O_3	14.31	12.07	13.36	14.37	13.46	11.81	11.65	10.89	10.39	12.20	12.95	10.10	9.62
Sm_2O_3	2.90	2.67	3.02	3.04	2.82	1.95	1.74	1.72	1.84	2.44	3.29	1.66	1.27
Gd_2O_3	1.67	1.70	2.05	2.34	1.50	1.11	1.25	0.56	1.05	1.58	2.11	0.67	0.59
Dy_2O_3	0.55	0.54	1.03	0.95	0.57	0.56	0.58	-	0.32	0.68	0.89	0.40	0.30
Yb_2O_3	-	-	-	-	-	-	-	1.01	-	-	-	-	-
P_2O_5	29.16	29.03	29.01	28.95	28.53	29.27	29.27	27.81	29.59	29.81	29.33	29.10	29.63
ThO_2	1.74	1.78	1.15	2.21	3.08	1.38	0.82	5.31	1.92	2.06	1.44	1.84	2.03
UO_2	0.12	0.10	0.08	0.11	0.12	0.04	0.05	0.15	0.09	0.14	0.10	0.07	0.06
Y_2O_3	1.39	1.22	1.83	2.40	1.12	0.58	1.19	0.18	0.65	1.02	1.67	0.34	0.35
PbO	0.07	0.06	0.05	0.08	0.11	0.05	0.03	0.15	0.06	0.07	0.06	0.06	0.05
Total	98.13	98.29	97.05	98.14	98.31	100.3	99.43	101.2	99.26	98.83	98.35	99.50	100.4
Structural formulae based on 16 oxygens													
Si (apfu)	0.076	0.076	0.053	0.095	0.115	0.079	0.038	0.150	0.053	0.025	0.039	0.056	0.079
P	3.916	3.933	3.937	3.898	3.877	3.920	3.917	3.834	3.954	3.975	3.951	3.943	3.919
P-site	**3.992**	**4.009**	**3.990**	**3.993**	**3.992**	**3.999**	**3.955**	**3.984**	**4.007**	**4.000**	**3.990**	**4.000**	**3.998**
Th	0.063	0.064	0.041	0.079	0.111	0.049	0.030	0.193	0.069	0.074	0.052	0.066	0.072
U	0.004	0.003	0.002	0.003	0.003	0.001	0.001	0.003	0.002	0.004	0.003	0.002	0.001
Al	0.007	0.044	0.007	0.001	0.004	0.054	0.009	0.003	0.002	0.005	0.005	0.004	0.006
Fe^{3+}	0.042	0.036	0.049	0.013	0.014	0.032	0.038	0.060	0.029	0.028	0.038	0.042	0.064
Y	0.117	0.102	0.153	0.202	0.094	0.049	0.100	0.016	0.054	0.085	0.141	0.029	0.029
La	0.654	0.712	0.650	0.599	0.708	0.829	0.845	0.763	0.977	0.750	0.663	0.914	0.963
Ce	1.785	1.835	1.812	1.730	1.833	1.904	1.954	1.947	1.878	1.840	1.789	1.994	1.998
Pr	0.225	0.212	0.214	0.224	0.215	0.205	0.211	0.207	0.185	0.208	0.213	0.199	0.188
Nd	0.808	0.691	0.748	0.811	0.747	0.663	0.658	0.614	0.586	0.692	0.736	0.571	0.537
Sm	0.158	0.146	0.163	0.165	0.154	0.106	0.095	0.095	0.100	0.132	0.180	0.091	0.068
Gd	0.088	0.089	0.107	0.123	0.079	0.058	0.066	0.030	0.055	0.082	0.111	0.035	0.030
Dy	0.028	0.027	0.052	0.048	0.029	0.028	0.030	0.009	0.016	0.034	0.046	0.021	0.015
Yb	0.000	0.000	0.000	0.000	0.000	0.013	0.000	0.039	0.003	0.000	0.000	0.012	0.017
Ca	0.056	0.039	0.031	0.025	0.028	0.030	0.062	0.043	0.037	0.070	0.049	0.023	0.022
Pb	0.002	0.002	0.001	0.003	0.004	0.002	0.001	0.006	0.002	0.003	0.002	0.002	0.002
Ce-site	**4.036**	**4.002**	**4.031**	**4.026**	**4.024**	**4.023**	**4.098**	**4.028**	**3.996**	**4.007**	**4.029**	**4.005**	**4.013**
Cations	**8.028**	**8.011**	**8.021**	**8.018**	**8.016**	**8.021**	**8.053**	**8.012**	**8.002**	**8.007**	**8.018**	**8.005**	**8.011**

Point_ID: spot identification; c: core; r: rim; i: intermediate zone; - : below detection limit

Table 46: Monazite in greisens from the Desemborque Pluton

Sample	GUA-08												
Crystal	c1								c1d	c5			c5b
Point_ID	1-c	1-r1	1-r2	1-r2b	1-r3	1-r4	1-r5	1-r6	1d-c	5-r1	5-r3	5-r4	5b-r1
SiO_2 (wt%)	0.94	0.58	0.86	1.55	1.01	0.94	0.97	2.03	0.85	0.44	0.87	1.13	0.87
$Al2O_3$	0.03	0.06	0.08	0.52	0.07	0.12	0.05	0.79	0.09	0.06	0.03	0.09	0.05
CaO	0.42	0.56	0.67	0.28	0.55	0.36	0.58	0.31	0.85	0.11	0.07	0.20	0.04
FeO	0.19	0.28	0.14	0.42	1.01	0.63	0.29	1.59	0.77	0.24	0.18	0.26	0.39
La_2O_3	11.44	17.51	10.53	11.73	10.61	12.64	10.77	12.60	11.19	10.76	11.35	11.58	11.43
Ce_2O_3	32.58	34.86	32.20	32.80	32.12	32.79	32.34	31.75	30.70	31.16	31.64	29.83	34.44
Pr_2O_3	3.79	3.14	3.95	3.78	3.84	3.69	3.89	3.50	3.53	3.86	3.78	3.52	4.15
Nd_2O_3	11.81	8.84	12.15	11.86	11.95	11.18	12.01	10.69	11.32	14.35	13.62	12.40	13.62
Sm_2O_3	2.31	1.08	2.31	2.02	1.98	1.68	2.33	1.25	2.02	4.19	3.88	3.67	2.04
Gd_2O_3	0.84	0.42	0.87	1.17	0.26	0.56	0.77	0.78	0.80	1.73	1.33	1.79	0.89
Dy_2O_3	-	-	-	-	-	-	-	-	0.51	0.32	-	0.63	0.50
Yb_2O_3	-	1.35	-	0.81	-	-	-	0.87	0.90	-	-	-	0.79
P_2O_5	27.89	28.59	28.29	28.14	27.58	28.16	27.98	26.91	27.64	29.17	28.59	28.45	29.09
ThO_2	5.47	2.52	6.74	4.07	6.32	4.83	6.40	4.32	6.98	1.97	3.75	3.92	1.86
UO_2	0.15	0.04	0.12	0.13	0.20	0.10	0.22	0.17	0.14	0.02	0.06	0.14	0.02
Y_2O_3	0.16	0.11	0.09	0.21	0.14	0.11	0.14	0.10	0.15	0.24	0.11	1.25	0.67
PbO	0.16	0.07	0.18	0.12	0.18	0.13	0.18	0.12	0.19	0.05	0.10	0.11	0.05
Total	98.18	100.8	99.68	99.62	98.31	98.45	99.48	97.78	98.62	99.21	99.49	98.93	100.9
Structural formulae based on 16 oxygens													
Si (apfu)	0.150	0.108	0.137	0.159	0.111	0.150	0.157	0.160	0.136	0.070	0.139	0.178	0.138
P	3.844	3.907	3.845	3.838	3.875	3.862	3.839	3.872	3.868	3.931	3.866	3.827	3.876
P-site	**3.994**	**4.015**	**3.982**	**3.997**	**3.986**	**4.012**	**3.996**	**4.031**	**4.005**	**4.001**	**4.005**	**4.005**	**4.013**
Th	0.199	0.091	0.245	0.148	0.228	0.175	0.233	0.156	0.253	0.071	0.136	0.141	0.067
U	0.004	0.000	0.002	0.003	0.005	0.002	0.006	0.005	0.003	0.000	0.001	0.004	0.000
Al	0.007	0.009	0.015	0.019	0.013	0.022	0.009	0.019	0.016	0.012	0.005	0.016	0.009
Fe^{3+}	0.023	0.012	0.017	0.024	0.048	0.028	0.035	0.191	0.042	0.029	0.022	0.031	0.047
Y	0.014	0.009	0.008	0.018	0.012	0.010	0.012	0.008	0.013	0.020	0.010	0.105	0.056
La	0.687	0.977	0.621	0.697	0.663	0.741	0.636	0.735	0.661	0.632	0.669	0.674	0.668
Ce	1.919	2.012	1.886	1.931	1.904	1.926	1.884	1.839	1.805	1.816	1.850	1.781	1.915
Pr	0.221	0.182	0.230	0.220	0.222	0.214	0.227	0.202	0.205	0.224	0.220	0.202	0.240
Nd	0.680	0.512	0.694	0.681	0.688	0.657	0.681	0.604	0.651	0.816	0.777	0.699	0.771
Sm	0.127	0.059	0.127	0.111	0.108	0.098	0.118	0.068	0.117	0.230	0.214	0.200	0.111
Gd	0.044	0.022	0.046	0.062	0.014	0.029	0.041	0.041	0.042	0.091	0.070	0.094	0.047
Dy	0.015	0.010	0.018	0.021	0.000	0.012	0.008	0.000	0.026	0.017	0.007	0.032	0.026
Yb	0.000	0.048	0.025	0.039	0.024	0.026	0.020	0.042	0.044	0.026	0.000	0.000	0.038
Ca	0.072	0.051	0.081	0.048	0.073	0.044	0.099	0.053	0.104	0.019	0.013	0.034	0.006
Pb	0.006	0.003	0.007	0.005	0.007	0.005	0.007	0.005	0.008	0.002	0.004	0.005	0.002
Ce-site	**4.018**	**3.998**	**4.022**	**4.025**	**4.009**	**3.988**	**4.015**	**3.967**	**3.990**	**4.005**	**3.997**	**4.016**	**4.004**
Cations	**8.013**	**8.013**	**8.005**	**8.022**	**7.995**	**8.000**	**8.011**	**7.998**	**7.994**	**8.006**	**8.003**	**8.021**	**8.017**

Point_ID: spot identification; c: core; r: rim; i: intermediate zone; - : below detection limit

Table 47: Monazite in greisens from the Desemborque Pluton

Sample	GUA-08												
Crystal	c5b				c7						c11		
Point_ID	5b-r2	5b-c	5b-i	5b-r3	7-r1	7-r2	7-c	7-r3	7-r4	7a-c	11-r1	11-r2	11-r3
SiO_2 (wt%)	0.78	0.81	0.75	0.75	0.94	0.97	0.78	1.03	0.67	0.65	0.64	0.84	1.10
$Al2O_3$	0.03	0.01	0.02	0.04	0.04	0.03	0.02	0.06	0.01	0.03	0.02	0.02	0.01
CaO	1.05	1.11	1.04	0.94	0.34	0.31	0.25	0.53	0.54	0.14	0.06	0.19	0.11
FeO	0.64	0.42	0.35	0.68	0.06	0.04	0.02	0.02	0.04	0.33	0.18	0.14	0.14
La_2O_3	9.66	9.64	8.78	9.42	11.35	11.84	11.63	10.58	12.35	14.03	16.18	13.20	10.16
Ce_2O_3	31.26	30.94	31.35	31.52	33.89	33.90	34.61	33.10	34.02	33.65	35.03	34.43	29.54
Pr_2O_3	3.93	3.87	4.02	3.99	3.99	3.93	4.09	4.02	3.88	3.72	3.43	3.83	3.87
Nd_2O_3	12.28	12.03	12.74	12.49	12.24	12.09	12.63	12.39	11.93	10.87	9.80	10.76	14.48
Sm_2O_3	1.87	2.12	2.00	2.11	1.69	1.81	2.16	1.88	1.94	1.72	1.60	1.39	4.00
Gd_2O_3	0.71	0.68	0.75	0.82	0.75	0.64	0.52	0.64	0.68	1.07	0.48	0.38	1.78
Dy_2O_3	-	0.31	0.50	0.43	-	-	0.23	-	0.33	0.38	-	-	0.64
Yb_2O_3	-	-	0.92	-	-	-	-	0.90	-	0.45	-	1.30	-
P_2O_5	29.24	28.68	28.56	28.33	28.40	28.64	28.75	27.99	28.57	28.89	28.65	28.53	28.01
ThO_2	8.19	8.66	7.88	7.43	5.27	5.27	4.14	6.47	3.66	3.20	3.12	4.93	4.89
UO_2	0.18	0.18	0.17	0.17	0.08	0.09	0.05	0.10	0.04	0.018	0.04	0.07	0.08
Y_2O_3	0.17	0.13	0.13	0.14	0.16	0.11	0.04	0.07	0.16	0.14	0.11	0.07	0.33
PbO	0.22	0.24	0.22	0.21	0.13	0.13	0.11	0.18	0.10	0.078	0.08	0.13	0.13
Total	100.8	100.2	100.2	99.45	99.64	100.4	100.4	99.99	98.96	99.36	99.82	100.2	99.26
Structural formulae based on 16 oxygens													
Si (apfu)	0.123	0.128	0.120	0.119	0.150	0.154	0.124	0.165	0.107	0.104	0.101	0.134	0.177
P	3.877	3.865	3.874	3.863	3.843	3.847	3.863	3.829	3.903	3.893	3.892	3.850	3.821
P-site	**4.000**	**3.993**	**3.994**	**3.983**	**3.993**	**4.000**	**3.987**	**3.994**	**4.010**	**3.997**	**3.994**	**3.984**	**3.998**
Th	0.292	0.312	0.285	0.270	0.192	0.190	0.150	0.235	0.132	0.116	0.113	0.179	0.179
U	0.004	0.004	0.003	0.003	0.001	0.001	0.000	0.001	0.000	0.001	0.000	0.001	0.001
Al	0.005	0.001	0.004	0.007	0.008	0.005	0.004	0.011	0.003	0.005	0.003	0.004	0.003
Fe^{3+}	0.077	0.051	0.042	0.047	0.007	0.005	0.002	0.003	0.005	0.040	0.021	0.017	0.017
Y	0.014	0.011	0.011	0.012	0.014	0.009	0.003	0.006	0.014	0.012	0.009	0.006	0.028
La	0.558	0.562	0.515	0.555	0.669	0.693	0.681	0.624	0.722	0.824	0.933	0.776	0.604
Ce	1.792	1.791	1.809	1.844	1.983	1.969	2.011	1.926	1.975	1.961	2.026	2.009	1.743
Pr	0.224	0.223	0.227	0.232	0.232	0.227	0.237	0.234	0.224	0.216	0.199	0.222	0.227
Nd	0.687	0.679	0.713	0.713	0.699	0.685	0.716	0.707	0.676	0.618	0.558	0.613	0.833
Sm	0.101	0.116	0.110	0.116	0.093	0.099	0.118	0.104	0.106	0.094	0.088	0.076	0.222
Gd	0.037	0.036	0.040	0.043	0.040	0.034	0.027	0.034	0.036	0.056	0.025	0.020	0.095
Dy	0.009	0.016	0.025	0.022	0.006	0.006	0.012	0.001	0.017	0.020	0.000	0.000	0.033
Yb	0.020	0.017	0.045	0.000	0.009	0.025	0.020	0.044	0.001	0.022	0.020	0.063	0.000
Ca	0.177	0.188	0.176	0.161	0.058	0.053	0.042	0.075	0.092	0.024	0.011	0.032	0.019
Pb	0.009	0.009	0.009	0.008	0.006	0.005	0.005	0.007	0.004	0.003	0.003	0.005	0.005
Ce-site	**4.005**	**4.015**	**4.015**	**4.034**	**4.018**	**4.006**	**4.028**	**4.014**	**4.007**	**4.010**	**4.011**	**4.024**	**4.010**
Cations	**8.005**	**8.008**	**8.009**	**8.016**	**8.012**	**8.007**	**8.015**	**8.008**	**8.017**	**8.007**	**8.005**	**8.008**	**8.008**

Point_ID: spot identification; c: core; r: rim; i: intermediate zone; - : below detection limit

Table 48: Monazite in greisens from the Desemborque Pluton

Sample	GUA-08			GUA-08B									
Crystal				c2f						c10a			c1a
Point_ID	11-c	11-r4	11-r5	2f-c	2f-r2	10-i	10-c	10-r2	10-r3	10a-r1	10a-c	10a-r3	1a-c
SiO_2 (wt%)	0.59	1.48	0.70	1.19	1.16	1.18	1.28	0.81	0.75	1.52	0.80	0.61	0.60
$Al2O_3$	0.06	0.02	0.02	0.87	0.25	0.00	0.01	0.06	0.05	0.48	0.01	0.05	0.02
CaO	1.21	0.09	0.21	0.25	0.11	0.48	0.33	0.50	0.49	0.28	0.27	0.11	0.06
FeO	0.05	0.16	0.06	0.15	0.28	0.05	0.07	0.16	0.63	0.66	0.16	0.18	0.22
La_2O_3	9.47	10.21	12.48	10.85	10.12	11.54	11.95	12.95	12.94	12.73	12.52	15.37	14.18
Ce_2O_3	30.86	29.39	33.84	29.55	29.13	32.57	32.93	32.05	32.06	32.99	33.23	34.57	33.38
Pr_2O_3	3.85	3.84	3.84	3.68	3.87	3.70	3.73	3.43	3.53	3.63	3.75	3.59	3.69
Nd_2O_3	12.49	14.14	11.52	13.84	15.08	11.35	11.14	10.46	10.24	11.22	11.66	10.35	12.14
Sm_2O_3	2.33	3.46	1.94	3.71	3.81	1.78	1.83	1.89	1.35	2.06	2.02	1.82	1.91
Gd_2O_3	0.61	1.51	0.91	1.98	1.87	0.59	0.82	0.79	0.69	0.78	1.13	1.03	0.85
Dy_2O_3	-	0.61	0.35	-	-	-	-	-	-	-	-	-	0.21
Yb_2O_3	-	-	-	-	-	-	0.62	-	1.07	0.73	-	-	0.63
P_2O_5	28.60	27.39	28.57	28.18	27.31	27.59	27.48	28.80	28.64	28.41	28.75	29.27	29.00
ThO_2	8.04	6.26	4.47	3.90	3.33	7.07	6.83	6.61	6.57	4.74	4.56	2.81	2.29
UO_2	0.16	0.10	0.05	0.07	0.06	0.10	0.10	0.11	0.09	0.09	0.06	0.04	0.055
Y_2O_3	0.17	0.45	0.13	0.44	0.59	0.13	0.11	0.15	0.13	0.15	0.17	0.13	0.40
PbO	0.22	0.16	0.12	0.10	0.09	0.18	0.18	0.18	0.18	0.13	0.12	0.07	0.060
Total	99.27	99.25	99.44	98.75	97.04	98.89	99.41	99.26	99.42	100.6	99.21	100.3	99.70
Structural formulae based on 16 oxygens													
Si (apfu)	0.110	0.239	0.112	0.186	0.184	0.190	0.204	0.129	0.120	0.238	0.127	0.096	0.095
P	3.878	3.767	3.876	3.844	3.825	3.801	3.790	3.881	3.867	3.755	3.875	3.912	3.896
P-site	**3.988**	**4.005**	**3.988**	**4.030**	**4.009**	**3.992**	**3.994**	**4.011**	**3.987**	**3.992**	**4.002**	**4.008**	**3.991**
Th	0.292	0.230	0.163	0.139	0.120	0.259	0.249	0.239	0.238	0.168	0.165	0.101	0.083
U	0.003	0.002	0.000	0.001	0.001	0.001	0.001	0.002	0.001	0.002	0.001	0.000	0.002
Al	0.012	0.004	0.003	0.160	0.047	0.001	0.002	0.012	0.010	0.088	0.003	0.009	0.004
Fe^{3+}	0.007	0.019	0.008	0.018	0.034	0.006	0.009	0.019	0.076	0.079	0.019	0.022	0.026
Y	0.015	0.038	0.011	0.037	0.049	0.011	0.010	0.013	0.011	0.012	0.014	0.011	0.034
La	0.599	0.607	0.738	0.608	0.602	0.685	0.705	0.760	0.759	0.733	0.735	0.873	0.830
Ce	1.832	1.735	1.985	1.688	1.753	1.920	1.928	1.868	1.866	1.885	1.937	1.969	1.939
Pr	0.224	0.226	0.224	0.210	0.224	0.217	0.217	0.199	0.204	0.206	0.218	0.206	0.213
Nd	0.723	0.814	0.659	0.773	0.854	0.653	0.636	0.595	0.581	0.626	0.663	0.584	0.688
Sm	0.128	0.192	0.107	0.200	0.208	0.099	0.101	0.104	0.074	0.111	0.111	0.099	0.104
Gd	0.032	0.081	0.048	0.103	0.098	0.032	0.043	0.042	0.036	0.040	0.060	0.054	0.045
Dy	0.008	0.031	0.018	0.000	0.000	0.019	0.021	0.015	0.014	0.016	0.025	0.025	0.011
Yb	0.019	0.000	0.012	0.000	0.000	0.028	0.030	0.015	0.052	0.035	0.000	0.017	0.030
Ca	0.087	0.015	0.036	0.041	0.018	0.083	0.057	0.086	0.084	0.046	0.046	0.019	0.011
Pb	0.009	0.007	0.005	0.004	0.004	0.008	0.008	0.007	0.007	0.005	0.005	0.003	0.003
Ce-site	**3.991**	**4.001**	**4.017**	**3.981**	**4.013**	**4.021**	**4.016**	**3.976**	**4.013**	**4.053**	**4.001**	**3.993**	**4.023**
Cations	**7.978**	**8.006**	**8.005**	**8.010**	**8.022**	**8.013**	**8.010**	**7.987**	**8.000**	**8.045**	**8.003**	**8.000**	**8.014**

Point_ID: spot identification; c: core; r: rim; i: intermediate zone; - : below detection limit

Table 49: Monazite in greisens from the Desemborque Pluton

Sample	GUA-08B												
Crystal	c1b	c1c				c1e							
Point_ID	1b-c	1c-r1	1c-c	1c-r2	1c-c	1e-r1	1e-c	1e-r2	1e-r4	1f-c2	1f-c3	1b-i	1b-r1
SiO_2 (wt%)	0.75	0.53	0.58	0.58	0.41	0.14	0.93	0.75	0.12	0.24	0.15	0.75	10.85
$Al2O_3$	0.02	0.02	0.02	0.02	0.01	0.00	0.01	0.00	0.01	0.00	0.01	0.01	0.02
CaO	0.07	0.14	0.25	0.14	0.09	0.22	0.08	0.06	0.42	0.40	0.46	0.19	0.22
FeO	0.27	0.35	0.29	0.35	0.26	0.47	0.22	0.28	0.13	0.17	0.44	0.26	0.26
La_2O_3	16.74	15.35	14.76	12.42	15.79	13.36	13.47	13.34	13.77	15.77	16.39	11.38	10.05
Ce_2O_3	34.38	34.04	33.05	28.81	34.08	33.09	32.51	32.62	32.09	32.60	32.38	30.43	27.19
Pr_2O_3	3.40	3.60	3.55	3.56	3.58	3.66	3.63	3.77	3.49	3.38	3.32	3.74	3.40
Nd_2O_3	9.82	11.16	11.55	14.77	10.91	11.65	12.19	12.29	11.95	11.24	10.48	14.19	12.94
Sm_2O_3	1.23	1.55	2.03	3.42	1.65	2.42	2.09	1.92	2.15	1.93	1.39	2.73	2.81
Gd_2O_3	0.52	0.82	0.85	2.39	0.64	1.47	1.14	1.09	1.35	0.99	1.10	1.67	1.58
Dy_2O_3	0.33	-	0.28	0.56	-	0.52	0.46	0.63	0.64	0.34	0.39	0.71	0.83
Yb_2O_3	-	0.69	-	-	0.72	-	-	-	-	0.60	-	-	-
P_2O_5	28.97	29.30	29.01	28.64	29.47	29.81	28.54	28.83	29.64	29.92	30.28	29.19	26.61
ThO_2	2.85	2.41	2.76	2.29	1.95	1.29	3.16	2.92	2.06	1.84	2.03	2.31	1.76
UO_2	0.071	0.070	0.075	0.015	0.063	0.068	0.078	0.063	0.122	0.059	0.054	0.127	0.119
Y_2O_3	0.15	0.20	0.22	0.34	0.21	1.19	0.84	0.80	1.12	0.77	1.22	1.64	1.48
PbO	0.076	0.062	0.072	0.058	0.052	0.037	0.085	0.079	0.061	0.050	0.054	0.067	0.053
Total	99.91	100.47	99.53	98.36	100.06	99.39	99.43	99.44	99.11	100.30	100.14	99.40	100.17
Structural formulae based on 16 oxygens													
Si (apfu)	0.119	0.083	0.092	0.094	0.065	0.021	0.148	0.120	0.018	0.038	0.023	0.119	1.542
P	3.880	3.903	3.898	3.900	3.931	3.969	3.848	3.878	3.971	3.960	3.980	3.897	3.203
P-site	**3.999**	**3.985**	**3.990**	**3.994**	**3.996**	**3.990**	**3.996**	**3.998**	**3.989**	**3.998**	**4.003**	**4.015**	**4.745**
Th	0.103	0.086	0.100	0.084	0.070	0.046	0.115	0.106	0.074	0.065	0.072	0.083	0.057
U	0.002	0.002	0.003	0.001	0.002	0.002	0.003	0.002	0.004	0.002	0.002	0.004	0.004
Al	0.004	0.004	0.004	0.005	0.002	0.001	0.002	0.000	0.001	0.000	0.002	0.002	0.003
Fe^{3+}	0.032	0.041	0.034	0.042	0.030	0.055	0.026	0.033	0.015	0.019	0.051	0.031	0.028
Y	0.013	0.017	0.018	0.029	0.018	0.100	0.071	0.067	0.094	0.064	0.101	0.138	0.112
La	0.977	0.891	0.864	0.737	0.918	0.775	0.791	0.782	0.804	0.909	0.939	0.662	0.527
Ce	1.991	1.961	1.921	1.696	1.966	1.905	1.895	1.898	1.859	1.866	1.840	1.757	1.415
Pr	0.196	0.206	0.205	0.209	0.206	0.210	0.211	0.218	0.201	0.193	0.188	0.215	0.176
Nd	0.555	0.627	0.655	0.848	0.614	0.654	0.693	0.697	0.675	0.628	0.581	0.799	0.657
Sm	0.067	0.084	0.111	0.190	0.090	0.131	0.115	0.105	0.117	0.104	0.074	0.148	0.138
Gd	0.027	0.043	0.045	0.127	0.033	0.077	0.060	0.057	0.071	0.051	0.057	0.087	0.074
Dy	0.017	0.009	0.014	0.029	0.009	0.026	0.023	0.032	0.033	0.017	0.019	0.036	0.038
Yb	0.013	0.033	0.009	0.000	0.035	0.000	0.000	0.000	0.000	0.029	0.000	0.000	0.000
Ca	0.012	0.024	0.042	0.024	0.016	0.037	0.014	0.010	0.071	0.066	0.077	0.031	0.033
Pb	0.003	0.002	0.003	0.003	0.002	0.002	0.004	0.003	0.003	0.002	0.002	0.003	0.002
Ce-site	**4.011**	**4.031**	**4.028**	**4.023**	**4.010**	**4.021**	**4.023**	**4.012**	**4.023**	**4.017**	**4.004**	**3.996**	**3.264**
Cations	**8.010**	**8.016**	**8.018**	**8.016**	**8.006**	**8.011**	**8.019**	**8.010**	**8.012**	**8.014**	**8.007**	**8.012**	**8.009**

Point_ID: spot identification; c: core; r: rim; i: intermediate zone; - : below detection limit

Table 50: Xenotime greisen from the Desemborque Pluton

Sample	GUA-08									GUA-08B			
Crystal	c10				c10b	c15				c2		C6a	
Point_ID	10-r1	10-r2	10-i	10-c	10b-c2	15-r1	15-c	15-r2	15-r3	2-c	2-r4	6-i2	6-r1
SiO_2 (wt%)	0.10	0.62	0.05	0.03	0.64	0.14	0.32	0.82	0.19	0.84	1.32	0.12	0.17
$Al2O_3$	-	-	-	-	-	-	-	-	-	-	0.18	-	-
CaO	0.16	0.17	0.13	0.12	0.06	0.01	0.00	-	-	0.01	0.01	-	0.02
FeO	0.01	0.02	0.00	0.00	0.03	0.12	0.14	0.10	0.32	0.20	0.33	0.12	0.26
Ce_2O_3	0.06	-	0.02	-	-	0.07	0.08	-	0.04	0.06	0.04	0.06	0.08
Pr_2O_3	0.03	0.03	0.03	-	-	0.04	0.00	0.03	-	0.06	-	-	0.05
Nd_2O_3	0.41	0.15	0.14	0.08	0.08	0.34	0.46	0.11	0.38	0.38	0.33	0.35	0.38
Sm_2O_3	0.66	0.41	0.58	0.47	0.47	0.50	0.73	0.38	0.60	0.68	0.63	0.64	0.59
Gd_2O_3	1.99	1.73	3.54	4.28	2.11	1.56	2.11	1.67	1.74	2.26	2.00	1.92	1.80
Tb_2O_3	0.58	0.70	1.78	1.99	0.80	0.51	0.70	0.73	0.57	0.74	0.62	0.63	0.54
Dy_2O_3	4.11	5.33	13.90	14.16	5.95	3.58	4.61	5.26	3.73	4.67	3.99	4.23	3.77
Ho_2O_3	0.96	1.40	3.27	3.00	1.43	0.86	1.00	1.42	0.94	1.15	0.95	0.96	0.95
Er_2O_3	3.53	5.26	10.62	9.55	5.34	3.42	3.85	5.32	3.34	3.91	3.44	3.52	3.41
Yb_2O_3	4.28	6.36	8.13	6.95	5.91	4.76	4.75	6.75	4.25	4.15	3.93	4.62	4.36
Lu_2O_3	0.96	1.34	1.79	1.61	1.23	0.92	1.16	1.41	0.92	0.99	0.89	1.08	0.95
P_2O_5	35.13	33.64	31.22	31.70	33.60	35.26	34.49	33.17	34.86	33.65	36.19	35.31	35.82
Y_2O_3	43.73	39.52	23.10	25.06	38.75	44.91	42.84	39.35	45.04	41.55	44.35	43.71	45.21
ThO_2	0.19	0.85	0.03	0.01	0.75	0.10	0.26	0.58	0.16	0.32	0.20	0.16	0.16
UO_2	-	0.10	0.04	0.01	0.07	-	-	0.04	0.01	0.02	0.01	-	0.01
PbO	0.01	0.03	0.01	-	0.03	-	-	0.02	-	0.01	-	-	-
Total	96.91	97.65	98.39	99.03	97.23	97.10	97.51	97.17	97.09	95.65	99.46	97.47	98.52
Structural formulae based on 16 oxygens													
Si (apfu)	0.014	0.084	0.008	0.005	0.087	0.018	0.043	0.114	0.025	0.079	0.078	0.017	0.022
P	3.993	3.923	3.983	3.986	3.937	3.981	3.969	3.906	3.978	3.927	3.957	3.990	4.002
P-site	**4.006**	**4.007**	**3.992**	**3.991**	**4.024**	**3.999**	**4.012**	**4.021**	**4.004**	**4.006**	**4.035**	**4.006**	**4.024**
Th	0.006	0.027	0.001	0.000	0.023	0.003	0.008	0.018	0.005	0.010	0.006	0.005	0.005
U	0.000	0.003	0.001	0.000	0.002	0.000	0.000	0.002	0.000	0.000	0.000	0.000	0.000
Al	0.000	0.000	0.000	0.000	0.000	0.000	0.000	0.000	0.000	0.000	0.029	0.000	0.000
Fe^{3+}	0.001	0.002	0.000	0.000	0.003	0.013	0.014	0.011	0.032	0.021	0.022	0.012	0.026
Y	3.183	2.938	1.841	1.967	2.898	3.253	3.099	2.913	3.231	3.111	3.158	3.168	3.189
Ce	0.003	0.000	0.001	0.000	0.000	0.004	0.004	0.000	0.002	0.003	0.002	0.003	0.004
Pr	0.001	0.001	0.002	0.000	0.000	0.002	0.000	0.002	0.001	0.003	0.001	0.001	0.002
Nd	0.019	0.007	0.007	0.004	0.004	0.017	0.022	0.005	0.018	0.019	0.015	0.017	0.018
Sm	0.031	0.020	0.030	0.024	0.022	0.023	0.034	0.018	0.028	0.033	0.029	0.030	0.027
Gd	0.088	0.079	0.176	0.210	0.096	0.070	0.095	0.077	0.078	0.104	0.092	0.089	0.081
Tb	0.025	0.031	0.088	0.097	0.036	0.023	0.031	0.033	0.025	0.034	0.027	0.028	0.023
Dy	0.185	0.235	0.676	0.671	0.263	0.156	0.202	0.236	0.162	0.209	0.174	0.186	0.165
Ho	0.041	0.061	0.156	0.141	0.062	0.037	0.043	0.063	0.040	0.051	0.040	0.041	0.040
Er	0.148	0.226	0.504	0.445	0.230	0.145	0.164	0.232	0.141	0.170	0.147	0.152	0.146
Tm	0.025	0.038	0.067	0.058	0.037	0.026	0.028	0.040	0.024	0.027	0.023	0.026	0.025
Yb	0.181	0.266	0.371	0.314	0.247	0.196	0.197	0.286	0.175	0.175	0.162	0.192	0.175
Lu	0.039	0.055	0.081	0.072	0.051	0.037	0.048	0.059	0.037	0.042	0.036	0.043	0.038
Ca	0.024	0.024	0.021	0.019	0.008	0.001	0.001	0.000	0.000	0.002	0.002	0.001	0.003
Pb	0.000	0.001	0.000	0.000	0.001	0.000	0.000	0.001	0.000	0.000	0.000	0.000	0.000
Y-site	**4.000**	**4.015**	**4.023**	**4.023**	**3.983**	**4.006**	**3.991**	**3.997**	**4.001**	**4.013**	**3.966**	**3.994**	**3.966**
Cations	**8.006**	**8.022**	**8.015**	**8.014**	**8.008**	**8.006**	**8.004**	**8.018**	**8.004**	**8.020**	**8.001**	**8.000**	**7.990**

Point_ID: spot identification; c: core; r: rim; i: intermediate zone; - : below detection limit

Table 51: Xenotime greisen from the Desemborque Pluton

Sample	GUA-08B												
Crystal							c6b						
Point_ID	6-i	6-i3	6-c	6-i4	6-i5	6-r4	6-i6	6-r5	6-i8	6-r6	6-i9	6-r9	6-r10
SiO_2 (wt%)	0.98	0.40	0.40	0.54	0.57	0.28	0.91	3.41	0.18	0.15	0.44	0.14	0.20
$Al2O_3$	-	-	-	-	-	-	-	1.69	-	-	-	-	-
CaO	0.01	0.37	0.02	0.01	0.01	0.01	0.01	0.02	0.01	0.01	0.01	0.03	0.02
FeO	0.12	0.18	0.14	0.13	0.13	0.23	0.12	0.99	0.11	0.19	0.15	0.19	0.26
Ce_2O_3	0.02	0.07	0.05	0.10	0.08	0.08	0.02	0.05	0.07	0.06	0.07	0.07	0.07
Pr_2O_3	-	0.04	-	0.08	0.04	-	-	0.05	-	-	-	-	-
Nd_2O_3	0.20	0.38	0.35	0.62	0.48	0.50	0.22	0.34	0.48	0.41	0.43	0.36	0.44
Sm_2O_3	0.63	0.86	0.91	1.15	1.01	0.85	0.57	0.69	0.78	0.79	0.83	0.63	0.76
Gd_2O_3	2.30	2.40	2.61	3.07	2.99	2.42	2.30	2.18	2.25	2.36	2.33	2.11	2.22
Tb_2O_3	0.84	0.79	0.83	0.92	0.91	0.70	0.88	0.71	0.67	0.71	0.72	0.71	0.66
Dy_2O_3	5.78	4.82	5.20	5.64	5.73	4.52	6.31	4.61	4.41	4.50	4.46	4.91	4.05
Ho_2O_3	1.34	0.92	1.06	1.13	1.29	0.99	1.44	1.23	1.03	1.12	1.01	1.09	1.00
Er_2O_3	4.81	3.56	3.84	3.74	4.03	3.40	5.44	3.96	3.47	3.49	3.46	3.94	3.34
Yb_2O_3	5.70	4.26	4.59	3.91	4.26	3.85	6.07	4.28	3.97	4.08	3.99	4.29	4.01
Lu_2O_3	1.13	0.85	1.05	0.96	1.02	0.90	1.30	0.90	0.94	1.08	0.93	1.05	0.77
P_2O_5	33.41	34.21	34.48	34.03	33.56	34.69	33.04	31.62	35.19	35.23	34.93	34.94	35.45
Y_2O_3	39.00	42.68	42.35	41.67	41.13	44.21	38.64	41.68	43.79	43.36	43.52	42.89	44.09
ThO_2	1.21	0.41	0.46	0.45	0.49	0.27	0.69	0.35	0.24	0.26	0.32	0.18	0.27
UO_2	0.10	0.19	0.03	0.01	0.03	0.01	0.09	0.08	0.01	0.01	0.02	0.02	0.01
PbO	0.04	0.02	0.02	0.01	0.01	0.01	0.01	0.01	-	-	0.01	0.01	0.01
Total	97.65	97.42	98.39	98.17	97.77	97.94	98.08	98.86	97.59	97.83	97.63	97.57	97.64
Structural formulae based on 16 oxygens													
Si (apfu)	0.066	0.054	0.054	0.074	0.078	0.038	0.126	0.452	0.024	0.019	0.058	0.019	0.027
P	3.930	3.940	3.957	3.929	3.917	3.960	3.885	3.548	3.991	3.992	3.949	4.002	3.993
P-site	**3.996**	**3.994**	**4.011**	**4.003**	**3.996**	**3.997**	**4.012**	**4.000**	**4.016**	**4.011**	**4.007**	**4.021**	**4.019**
Th	0.038	0.013	0.014	0.014	0.015	0.008	0.022	0.011	0.007	0.008	0.010	0.006	0.008
U	0.003	0.006	0.001	0.000	0.001	0.000	0.003	0.002	0.000	0.000	0.001	0.000	0.000
Al	0.000	0.000	0.000	0.000	0.000	0.000	0.000	0.264	0.000	0.000	0.000	0.000	0.000
Fe^{3+}	0.012	0.019	0.014	0.013	0.014	0.023	0.013	0.100	0.012	0.019	0.015	0.020	0.027
Y	2.931	3.084	3.053	3.035	3.010	3.172	2.856	2.940	3.156	3.138	3.164	3.088	3.173
Ce	0.001	0.003	0.003	0.005	0.004	0.004	0.001	0.002	0.003	0.003	0.004	0.004	0.003
Pr	0.001	0.002	0.000	0.004	0.002	0.001	0.000	0.002	0.000	0.001	0.000	0.001	0.000
Nd	0.010	0.018	0.017	0.030	0.023	0.024	0.011	0.016	0.023	0.020	0.021	0.017	0.021
Sm	0.030	0.040	0.042	0.054	0.048	0.039	0.027	0.031	0.036	0.037	0.038	0.029	0.035
Gd	0.105	0.112	0.117	0.138	0.136	0.108	0.106	0.096	0.101	0.105	0.103	0.095	0.098
Tb	0.038	0.035	0.037	0.041	0.041	0.031	0.040	0.031	0.030	0.031	0.032	0.032	0.029
Dy	0.256	0.214	0.226	0.246	0.254	0.196	0.282	0.197	0.192	0.194	0.196	0.214	0.175
Ho	0.059	0.039	0.046	0.049	0.056	0.043	0.064	0.052	0.044	0.048	0.043	0.047	0.043
Er	0.208	0.155	0.163	0.159	0.174	0.144	0.237	0.165	0.147	0.147	0.149	0.167	0.140
Tm	0.035	0.025	0.027	0.025	0.027	0.024	0.038	0.026	0.024	0.024	0.024	0.027	0.024
Yb	0.239	0.183	0.189	0.162	0.179	0.158	0.257	0.173	0.164	0.167	0.167	0.177	0.164
Lu	0.047	0.037	0.043	0.039	0.042	0.036	0.055	0.036	0.038	0.043	0.038	0.043	0.031
Ca	0.001	0.054	0.002	0.001	0.001	0.001	0.001	0.002	0.002	0.002	0.002	0.004	0.003
Pb	0.001	0.001	0.001	0.000	0.001	0.000	0.001	0.001	0.000	0.000	0.000	0.000	0.000
Y-site	**4.017**	**4.041**	**3.996**	**4.016**	**4.029**	**4.014**	**4.015**	**4.147**	**3.980**	**3.986**	**4.005**	**3.970**	**3.975**
Cations	**8.012**	**8.034**	**8.007**	**8.019**	**8.024**	**8.012**	**8.027**	**8.147**	**7.996**	**7.997**	**8.012**	**7.992**	**7.995**

Point_ID: spot identification; c: core; r: rim; i: intermediate zone; - : below detection limit

Table 52: Zircon in metaluminous to slightly peraluminous syenogranites from the Desemborque Pluton

Sample	GUA-02													
Crystal	c1							c5			c12			
Point_ID	1-c	1-r1	1-r2	1b-c	1c-c	1c-r1	1c-r2	5-c	5-r1	5-r2	12-c	12-i2	12-i3	12-r1
Stage	Late	Post	Post	Post	Post	Post	Post	Late	Post	Post	Late	Late	Post	Post
SiO_2 (wt%)	29.040	29.620	29.150	30.620	30.230	31.050	29.510	32.930	30.230	31.110	32.380	30.890	27.660	32.790
TiO_2	0.187	0.342	0.336	0.318	0.167	0.514	0.435	0.166	0.219	0.190	0.117	0.096	0.115	0.573
Al_2O_3	0.735	0.348	0.709	0.576	0.274	0.034	0.429	1.692	0.459	0.599	-	0.003	0.099	0.027
Fe_2O_3	1.740	1.690	2.210	1.367	0.984	0.832	1.430	1.680	1.007	1.650	0.177	0.208	2.230	0.203
MnO	0.452	0.472	0.445	0.346	0.275	0.211	0.349	0.378	0.401	0.442	-	-	-	-
MgO	0.013	0.017	0.016	0.030	0.015	-	0.020	0.047	0.035	0.020	-	0.015	0.002	0.003
CaO	0.305	0.385	0.298	0.324	0.258	0.461	0.291	0.227	0.340	0.235	0.015	0.017	0.751	-
ThO_2	0.764	0.568	0.726	0.308	0.181	0.090	0.264	0.276	0.365	0.165	0.458	0.488	1.890	0.064
UO_2	1.420	1.019	1.280	0.541	0.848	0.408	0.742	0.634	0.717	0.689	0.581	0.625	1.017	0.538
La_2O_3	0.095	0.050	0.118	0.109	-	-	-	0.076	-	0.094	-	-	-	-
Ce_2O_3	0.431	0.247	0.396	0.192	0.106	-	0.129	0.200	0.105	0.278	-	-	-	-
Nd_2O_3	0.143	-	0.124	-	-	-	-	-	0.074	0.061	0.085	-	-	0.079
Sm_2O_3	-	-	-	-	-	-	-	-	-	-	-	-	-	0.092
Gd_2O_3	0.144	0.096	0.133	0.110	0.098	-	0.116	0.107	0.090	0.121	0.105	0.140	0.145	-
Dy_2O_3	0.145	0.100	0.225	0.083	-	0.060	0.146	0.175	0.132	-	0.112	0.113	0.290	0.120
Er_2O_3	0.380	0.298	0.433	0.265	0.202	0.175	0.369	0.241	0.322	0.198	0.296	0.341	0.525	0.220
Yb_2O_3	1.440	1.460	1.890	1.410	0.846	0.585	1.530	1.180	1.660	0.725	1.031	1.340	1.670	0.708
Y_2O_3	1.930	1.258	1.800	0.632	0.632	0.131	1.015	1.061	0.865	1.174	1.790	2.020	3.390	0.147
ZrO_2	54.490	54.420	53.650	57.990	59.570	56.670	55.190	57.950	58.230	60.590	62.910	61.000	55.080	56.910
HfO_2	2.420	4.560	3.470	4.460	2.580	7.580	6.100	1.840	3.190	2.480	1.640	1.590	1.890	8.560
Nb_2O_5	0.111	0.088	0.210	0.077	0.018	0.003	0.149	0.067	-	0.033	0.033	0.052	0.208	-
Ta_2O_5	0.067	0.106	0.126	0.080	0.076	0.099	0.070	0.031	0.002	0.045	0.035	0.029	0.044	0.092
P_2O_5	0.256	0.147	0.207	0.141	0.069	0.011	0.077	0.138	0.170	0.116	0.296	0.386	1.003	0.029
Total	96.73	97.31	98.01	100.00	97.49	98.99	98.48	101.16	98.71	101.06	102.09	99.36	98.15	101.19

Point_ID: spot identification; c: core; r: rim; i: intermediate zone; - : below detection limit; Eu not analysed

Table 52: (*cont.*) Zircon in metaluminous to slightly syenogranites from the Desemborque Pluton

Sample	GUA-02													
Crystal	c1							c5			c12			
Point_ID	1-c	1-r1	1-r2	1b-c	1c-c	1c-r1	1c-r2	5-c	5-r1	5-r2	12-c	12-i2	12-i3	12-r1
Stage	Late	Post	Post	Post	Post	Post	Post	Late	Post	Post	Late	Late	Post	Post
Structural formulae based on 16 oxygens														
Si (apfu)	3.893	3.949	3.814	3.875	3.894	3.975	3.816	3.972	3.875	3.889	4.027	3.907	3.643	4.080
Al	0.112	0.053	0.109	0.086	0.042	0.005	0.065	0.245	0.069	0.088	0.000	0.000	0.015	0.004
P	0.028	0.016	0.023	0.015	0.007	0.001	0.008	0.014	0.018	0.012	0.031	0.041	0.112	0.003
Sum T	**4.033**	**4.018**	**3.946**	**3.976**	**3.943**	**3.981**	**3.889**	**4.231**	**3.962**	**3.989**	**4.058**	**3.948**	**3.770**	**4.087**
Zr	3.443	3.422	3.423	3.578	3.742	3.538	3.543	3.448	3.640	3.633	3.682	3.762	3.537	3.469
Hf	0.090	0.168	0.130	0.161	0.095	0.277	0.225	0.065	0.117	0.088	0.058	0.057	0.071	0.309
Th	0.023	0.017	0.022	0.009	0.005	0.003	0.008	0.008	0.011	0.005	0.013	0.014	0.057	0.002
U	0.041	0.029	0.037	0.015	0.024	0.012	0.021	0.017	0.020	0.019	0.016	0.018	0.030	0.015
Y	0.133	0.086	0.125	0.043	0.043	0.009	0.070	0.069	0.059	0.078	0.118	0.136	0.238	0.010
La	0.005	0.002	0.006	0.005	0.000	0.000	0.002	0.003	0.002	0.004	0.001	0.000	0.002	0.001
Ce	0.020	0.012	0.019	0.009	0.005	0.000	0.006	0.009	0.005	0.013	0.000	0.000	0.002	0.001
Nd	0.007	0.000	0.006	0.001	0.000	0.001	0.003	0.002	0.003	0.003	0.004	0.000	0.002	0.004
Sm	0.001	0.001	0.003	0.000	0.000	0.000	0.001	0.001	0.002	0.000	0.000	0.000	0.000	0.004
Gd	0.006	0.004	0.006	0.005	0.004	0.002	0.005	0.004	0.004	0.005	0.004	0.006	0.006	0.000
Dy	0.006	0.004	0.009	0.003	0.002	0.002	0.006	0.007	0.005	0.002	0.004	0.005	0.012	0.005
Er	0.015	0.012	0.018	0.011	0.008	0.007	0.015	0.009	0.013	0.008	0.012	0.014	0.022	0.009
Yb	0.057	0.057	0.075	0.054	0.033	0.023	0.060	0.044	0.065	0.028	0.039	0.052	0.067	0.027
Ti	0.018	0.033	0.033	0.030	0.016	0.050	0.042	0.015	0.021	0.018	0.011	0.009	0.011	0.054
Fe^{3+}	0.170	0.164	0.218	0.130	0.095	0.080	0.139	0.155	0.097	0.155	0.017	0.020	0.221	0.019
Mn	0.050	0.052	0.049	0.037	0.030	0.023	0.038	0.039	0.044	0.047	0.000	0.000	0.002	0.001
Mg	0.003	0.003	0.003	0.006	0.003	0.000	0.004	0.009	0.007	0.004	0.000	0.003	0.000	0.000
Ca	0.042	0.053	0.042	0.044	0.036	0.063	0.040	0.030	0.047	0.031	0.002	0.002	0.106	0.000
Nb	0.007	0.005	0.012	0.004	0.001	0.000	0.009	0.004	0.000	0.002	0.002	0.003	0.012	0.000
Ta	0.002	0.004	0.004	0.003	0.003	0.003	0.002	0.001	0.000	0.002	0.001	0.001	0.002	0.003
Sum A	**4.139**	**4.128**	**4.240**	**4.148**	**4.145**	**4.093**	**4.239**	**3.939**	**4.162**	**4.145**	**3.984**	**4.102**	**4.400**	**3.933**
Zr/Hf_{atomic}	38.26	20.37	26.33	22.22	39.39	12.77	15.75	53.05	31.11	41.28	63.48	66.00	49.82	11.23
100*Hf/(Hf+Zr)	2.530	4.680	3.650	4.310	2.470	7.260	5.980	1.840	3.110	2.380	1.560	1.500	1.970	8.170
Th/U_{atomic}	0.561	0.586	0.595	0.600	0.208	0.250	0.381	0.471	0.550	0.263	0.813	0.778	1.900	0.133
$(REE+Y)^{3+}$	0.250	0.179	0.267	0.131	0.096	0.045	0.168	0.149	0.159	0.140	0.183	0.212	0.351	0.060
$U+Th+(REE+Y)^{3+}$	0.314	0.225	0.326	0.155	0.125	0.060	0.197	0.174	0.190	0.164	0.212	0.244	0.438	0.077
Si/(Zr+Hf)	1.102	1.100	1.073	1.036	1.015	1.042	1.013	1.131	1.031	1.045	1.077	1.023	1.010	1.080

Table 53: Zircon in metaluminous to slightly peraluminous syenogranites from the Desemborque Pluton

Sample	GUA-50C1													
Crystal	c4			c8				c11						c12
Point_ID	4-c	4-i	4-r1	8-c	8-i	8-i2	8-r1	11-c	11-i	11-i2	11-r1	11-r2	11-r3	12-c
Stage	Late	Late	Late	Early	Early	Early	Late	Early	Early	Early	Late	Post	Late	Late
SiO_2 (wt%)	29.980	32.200	31.480	32.510	32.130	32.100	27.880	32.570	32.650	32.250	30.070	32.080	29.800	29.540
TiO_2	0.172	0.166	0.115	0.076	0.105	0.122	0.170	0.096	0.080	0.082	0.126	0.341	0.161	0.098
Al_2O_3	0.460	0.007	0.056	0.013	0.025	0.000	0.229	0.013	0.011	0.026	0.504	0.078	0.480	0.518
Fe_2O_3	0.719	0.029	0.562	0.128	0.207	0.297	1.790	0.146	0.149	0.434	1.470	0.716	1.770	1.265
MnO	0.503	0.014	0.269	-	0.071	0.099	0.285	-	-	0.097	0.608	0.052	0.655	0.705
MgO	0.019	0.017	-	-	-	-	-	-	-	-	0.019	-	0.023	0.017
CaO	0.259	0.002	0.032	-	0.021	0.027	0.524	0.051	0.038	0.083	0.269	0.431	0.313	0.283
ThO_2	0.413	-	0.159	0.031	0.166	0.109	0.911	0.049	0.065	0.211	0.454	0.087	1.106	0.721
UO_2	0.509	0.103	0.305	0.095	0.302	0.250	1.590	0.011	0.068	0.197	0.644	0.176	1.029	0.745
La_2O_3	-	-	-	-	-	-	-	-	-	-	-	0.070	-	-
Ce_2O_3	-	-	-	-	-	-	-	-	-	-	0.082	-	0.242	-
Nd_2O_3	-	-	-	-	-	-	0.061	-	-	-	0.109	-	0.143	0.102
Sm_2O_3	-	-	-	-	-	-	-	-	-	-	0.069	0.120	0.116	0.075
Gd_2O_3	0.064	-	-	-	-	0.060	0.156	-	-	-	0.139	-	0.137	0.157
Dy_2O_3	0.123	-	0.067	0.066	-	0.077	0.225	-	-	0.074	0.200	-	0.175	0.101
Er_2O_3	0.197	0.058	0.143	0.077	0.117	0.077	0.581	0.049	0.052	0.207	0.219	0.150	0.401	0.238
Yb_2O_3	1.134	0.245	0.494	0.180	0.532	0.319	2.200	0.130	0.248	0.560	0.967	0.260	1.390	0.590
Y_2O_3	1.310	0.156	0.598	0.274	0.539	0.379	2.700	0.072	0.335	0.890	1.580	0.230	2.460	1.710
ZrO_2	59.470	65.380	62.660	65.750	64.870	65.970	54.950	67.030	67.200	65.230	59.410	62.300	58.070	58.320
HfO_2	2.070	2.300	2.030	1.770	1.570	1.690	2.130	1.310	1.280	1.330	1.790	4.560	1.950	1.450
Nb_2O_5	0.041	-	0.051	-	-	0.025	-	-	-	0.021	0.045	0.022	-	0.095
Ta_2O_5	0.053	0.031	-	0.029	0.028	-	0.066	-	0.005	0.059	-	-	0.061	0.068
P_2O_5	0.313	0.059	0.137	0.061	0.288	0.251	1.984	0.041	0.083	0.243	0.704	0.068	0.747	0.241
Total	97.96	100.80	99.25	101.15	101.07	101.86	98.48	101.63	102.42	102.13	99.48	101.89	101.27	97.09

Point_ID: spot identification; c: core; r: rim; i: intermediate zone; - : below detection limit; Eu not analysed

Table 53: (*cont.*) Zircon in metaluminous to slightly peraluminous syenogranites from the Desemborque Pluton

Sample	GUA-50C1													
Crystal	c4			c8				c11						c12
Point_ID	4-c	4-i	4-r1	8-c	8-i	8-i2	8-r1	11-c	11-i	11-i2	11-r1	11-r2	11-r3	12-c
Stage	Late	Late	Late	Early	Early	Early	Late	Early	Early	Early	Late	Post	Late	Late
Structural formulae based on 16 oxygens														
Si (apfu)	3.863	3.984	3.941	3.980	3.967	3.934	3.694	3.966	3.979	3.899	3.794	3.938	3.778	3.838
Al	0.069	0.001	0.008	0.002	0.004	0.000	0.035	0.002	0.002	0.004	0.075	0.011	0.072	0.078
P	0.034	0.006	0.015	0.006	0.030	0.026	0.215	0.004	0.009	0.025	0.075	0.007	0.080	0.026
Sum T	**3.966**	**3.991**	**3.964**	**3.988**	**4.001**	**3.960**	**3.944**	**3.972**	**3.990**	**3.928**	**3.944**	**3.956**	**3.930**	**3.942**
Zr	3.707	3.884	3.825	3.901	3.845	3.889	3.427	3.946	3.910	3.883	3.655	3.730	3.528	3.677
Hf	0.075	0.081	0.073	0.062	0.055	0.060	0.078	0.046	0.045	0.047	0.064	0.160	0.071	0.053
Th	0.012	0.000	0.005	0.001	0.005	0.003	0.027	0.001	0.002	0.006	0.013	0.002	0.032	0.021
U	0.014	0.003	0.008	0.003	0.008	0.007	0.045	0.000	0.002	0.005	0.018	0.005	0.029	0.021
Y	0.088	0.010	0.040	0.018	0.035	0.025	0.184	0.005	0.022	0.059	0.106	0.015	0.166	0.117
La	0.002	0.002	0.000	0.000	0.002	0.000	0.000	0.001	0.000	0.002	0.000	0.003	0.002	0.000
Ce	0.002	0.000	0.000	0.001	0.000	0.000	0.002	0.001	0.000	0.002	0.004	0.001	0.011	0.002
Nd	0.001	0.000	0.000	0.001	0.000	0.000	0.003	0.001	0.002	0.001	0.005	0.002	0.006	0.005
Sm	0.001	0.000	0.001	0.001	0.000	0.000	0.000	0.000	0.002	0.000	0.003	0.005	0.005	0.003
Gd	0.003	0.000	0.002	0.000	0.000	0.002	0.007	0.000	0.001	0.001	0.006	0.001	0.006	0.007
Dy	0.005	0.000	0.003	0.003	0.001	0.003	0.009	0.000	0.001	0.003	0.008	0.002	0.007	0.004
Er	0.008	0.002	0.006	0.003	0.005	0.003	0.023	0.002	0.002	0.008	0.009	0.006	0.016	0.010
Yb	0.044	0.009	0.019	0.007	0.020	0.012	0.086	0.005	0.009	0.021	0.037	0.010	0.054	0.023
Ti	0.016	0.015	0.011	0.007	0.010	0.011	0.016	0.009	0.007	0.008	0.012	0.032	0.015	0.009
Fe^{3+}	0.069	0.003	0.053	0.012	0.019	0.028	0.172	0.014	0.014	0.040	0.140	0.066	0.169	0.122
Mn	0.054	0.001	0.029	0.001	0.007	0.010	0.031	0.000	0.000	0.010	0.065	0.005	0.070	0.077
Mg	0.004	0.003	0.002	0.002	0.002	0.000	0.001	0.000	0.001	0.000	0.004	0.001	0.004	0.003
Ca	0.035	0.000	0.004	0.000	0.003	0.004	0.072	0.007	0.005	0.011	0.036	0.057	0.042	0.039
Nb	0.002	0.000	0.003	0.000	0.001	0.001	0.000	0.000	0.000	0.001	0.003	0.001	0.000	0.006
Ta	0.002	0.001	0.000	0.001	0.001	0.000	0.002	0.000	0.000	0.002	0.000	0.000	0.002	0.002
Sum A	**4.144**	**4.014**	**4.084**	**4.024**	**4.019**	**4.058**	**4.185**	**4.038**	**4.025**	**4.110**	**4.188**	**4.104**	**4.235**	**4.201**
Zr/Hf_{atomic}	49.43	47.95	52.40	62.92	69.91	64.82	43.94	85.78	86.89	82.62	57.11	23.31	49.69	69.38
100*Hf/(Hf+Zr)	1.980	2.050	1.860	1.580	1.420	1.510	2.220	1.150	1.130	1.200	1.730	4.110	1.960	1.420
Th/U_{atomic}	0.857	0.000	0.625	0.333	0.625	0.429	0.600		1.000	1.200	0.722	0.400	1.103	1.000
$(REE+Y)^{3+}$	0.154	0.023	0.070	0.034	0.063	0.046	0.314	0.015	0.039	0.097	0.178	0.045	0.273	0.171
$U+Th+(REE+Y)^{3+}$	0.180	0.026	0.083	0.038	0.076	0.056	0.386	0.016	0.043	0.108	0.209	0.052	0.334	0.213
Si/(Zr+Hf)	1.021	1.005	1.011	1.004	1.017	0.996	1.054	0.993	1.006	0.992	1.020	1.012	1.050	1.029

Table 54: Zircon in metaluminous to slightly peraluminous syenogranites from the Desemborque Pluton

Sample	GUA-50C1			GUA-50C2										
Crystal	c12			c1b							c2a			
Point_ID	12-i	12-r1	12-r3	1b-c	1b-i	1b-i2	1b-r1	1c-c	1c-r1	1c-r2	2a-c	2a-i	2a-i2	2a-r1
Stage	Late	Late	Late	Early	Early	Early	Early	Early	Late	Late	Late	Late	Late	Late
SiO_2 (wt%)	32.570	31.500	29.140	32.350	32.260	32.310	32.740	31.920	33.110	31.430	29.610	32.220	30.400	30.270
TiO_2	0.140	0.070	0.132	0.090	0.074	0.096	0.108	0.099	0.112	0.092	0.144	0.152	0.123	0.141
Al_2O_3	0.040	0.087	0.415	0.007	0.012	0.014	0.018	0.012	0.029	0.025	0.683	0.097	0.550	0.484
Fe_2O_3	0.097	0.516	0.836	0.151	0.234	0.461	0.680	0.280	0.458	0.564	1.690	0.737	1.650	1.620
MnO	0.030	0.209	0.365	-	0.014	0.013	-	0.005	-	0.012	0.754	0.037	0.615	0.538
MgO	-	-	0.033	-	-	-	-	0.029	-	-	-	-	-	-
CaO	-	0.070	0.528	-	-	-	0.021	-	-	0.035	0.372	0.135	0.278	0.268
ThO_2	0.029	0.173	0.822	-	-	0.025	0.085	0.015	0.095	-	0.368	0.118	0.463	0.440
UO_2	0.022	0.330	0.041	0.059	-	-	-	-	0.006	-	0.563	0.176	0.439	0.374
La_2O_3	-	-	-	-	-	-	-	-	-	-	-	-	-	-
Ce_2O_3	-	0.059	0.216	-	-	-	-	-	-	-	0.084	-	-	-
Nd_2O_3	-	-	-	-	-	0.075	-	-	-	-	-	-	-	-
Sm_2O_3	-	-	0.128	-	-	-	-	-	-	-	-	-	-	-
Gd_2O_3	-	-	0.350	-	-	-	-	-	-	-	0.129	-	-	0.063
Dy_2O_3	-	-	0.494	-	-	-	0.074	-	-	-	0.075	0.069	0.112	-
Er_2O_3	0.069	0.148	0.420	0.058	0.055	-	0.053	0.072	0.089	0.096	0.192	0.113	0.175	0.169
Yb_2O_3	0.288	0.720	1.136	0.203	0.110	0.081	0.213	0.077	0.344	0.151	0.764	0.247	0.557	0.719
Y_2O_3	0.229	0.849	2.380	0.290	0.133	0.172	0.245	0.242	0.537	0.346	1.176	0.456	1.007	0.980
ZrO_2	66.120	63.280	57.920	65.860	66.800	66.460	67.080	66.010	66.750	64.390	60.650	65.590	59.920	60.240
HfO_2	1.830	1.540	1.470	1.430	1.260	1.270	1.330	1.059	1.420	1.410	1.310	1.620	1.520	1.510
Nb_2O_5	-	0.034	0.233	-	-	-	-	-	0.025	-	0.070	0.040	0.075	0.081
Ta_2O_5	0.055	0.070	-	-	-	-	-	-	-	-	-	0.050	-	-
P_2O_5	0.040	0.131	0.296	0.053	0.069	0.052	0.081	0.058	0.118	0.074	0.361	0.085	0.148	0.160
Total	101.71	99.88	97.48	100.68	101.05	101.18	102.89	100.03	103.30	98.77	99.03	102.12	98.06	98.24

Point_ID: spot identification; c: core; r: rim; i: intermediate zone; - : below detection limit; Eu not analysed

Table 54: (*cont.*) Zircon in metaluminous to slightly peraluminous syenogranites from the Desemborque Pluton

Sample	GUA-50C1			GUA-50C2										
Crystal	c12			c1b							c2a			
Point_ID	12-i	12-r1	12-r3	1b-c	1b-i	1b-i2	1b-r1	1c-c	1c-r1	1c-r2	2a-c	2a-i	2a-i2	2a-r1
Stage	Late	Late	Late	Early	Early	Early	Early	Early	Late	Late	Late	Late	Late	Late
Structural formulae based on 16 oxygens														
Si (apfu)	3.972	3.924	3.791	3.974	3.965	3.940	3.963	3.934	3.890	3.930	3.751	3.909	3.861	3.846
Al	0.006	0.013	0.064	0.001	0.002	0.002	0.003	0.002	0.004	0.004	0.102	0.014	0.082	0.072
P	0.004	0.014	0.033	0.006	0.007	0.005	0.008	0.006	0.012	0.008	0.039	0.009	0.016	0.017
Sum T	**3.982**	**3.951**	**3.888**	**3.981**	**3.974**	**3.947**	**3.974**	**3.942**	**3.906**	**3.942**	**3.892**	**3.932**	**3.959**	**3.935**
Zr	3.902	3.844	3.675	3.921	3.944	3.947	3.889	3.967	3.948	3.926	3.746	3.882	3.711	3.732
Hf	0.064	0.055	0.055	0.050	0.044	0.045	0.047	0.037	0.050	0.050	0.047	0.057	0.055	0.055
Th	0.001	0.005	0.024	0.000	0.000	0.001	0.002	0.000	0.003	0.000	0.011	0.003	0.013	0.013
U	0.001	0.009	0.001	0.002	0.000	0.000	0.000	0.000	0.000	0.000	0.016	0.005	0.012	0.011
Y	0.015	0.056	0.165	0.019	0.009	0.011	0.016	0.016	0.035	0.023	0.079	0.030	0.068	0.066
La	0.000	0.001	0.000	0.000	0.000	0.000	0.001	0.001	0.000	0.000	0.000	0.000	0.000	0.001
Ce	0.002	0.003	0.010	0.000	0.000	0.000	0.001	0.001	0.000	0.001	0.004	0.002	0.000	0.002
Nd	0.002	0.000	0.005	0.001	0.001	0.003	0.002	0.000	0.001	0.002	0.000	0.001	0.000	0.002
Sm	0.000	0.000	0.006	0.000	0.000	0.002	0.001	0.000	0.001	0.000	0.000	0.003	0.000	0.001
Gd	0.001	0.000	0.015	0.001	0.000	0.000	0.001	0.001	0.002	0.000	0.005	0.001	0.000	0.003
Dy	0.000	0.002	0.021	0.001	0.000	0.002	0.003	0.002	0.002	0.002	0.003	0.003	0.005	0.002
Er	0.003	0.006	0.017	0.002	0.002	0.001	0.002	0.003	0.003	0.004	0.008	0.004	0.007	0.007
Yb	0.011	0.027	0.045	0.008	0.004	0.003	0.008	0.003	0.013	0.006	0.030	0.009	0.022	0.028
Ti	0.013	0.007	0.013	0.008	0.007	0.009	0.010	0.009	0.010	0.009	0.014	0.014	0.012	0.013
Fe^{3+}	0.009	0.048	0.082	0.014	0.022	0.043	0.063	0.026	0.043	0.053	0.161	0.068	0.158	0.155
Mn	0.003	0.022	0.040	0.001	0.001	0.001	0.001	0.001	0.001	0.001	0.081	0.004	0.066	0.058
Mg	0.001	0.003	0.006	0.003	0.000	0.001	0.002	0.005	0.001	0.001	0.003	0.002	0.003	0.003
Ca	0.002	0.009	0.074	0.001	0.001	0.000	0.003	0.002	0.001	0.005	0.051	0.018	0.038	0.036
Nb	0.000	0.002	0.014	0.000	0.000	0.000	0.000	0.000	0.001	0.000	0.004	0.002	0.004	0.005
Ta	0.002	0.002	0.001	0.001	0.000	0.001	0.000	0.000	0.001	0.001	0.001	0.002	0.000	0.000
Sum A	**4.032**	**4.101**	**4.269**	**4.033**	**4.035**	**4.070**	**4.052**	**4.074**	**4.116**	**4.084**	**4.264**	**4.110**	**4.174**	**4.193**
Zr/Hf_{atomic}	60.97	69.89	66.82	78.42	89.64	87.71	82.74	107.22	78.96	78.52	79.70	68.11	67.47	67.85
100*Hf/(Hf+Zr)	1.620	1.400	1.460	1.260	1.110	1.120	1.180	0.930	1.260	1.270	1.250	1.450	1.460	1.450
Th/U_{atomic}	1.000	0.556	24.000	0.000	-	-	-	-	-	-	0.688	0.600	1.083	1.182
$(REE+Y)^{3+}$	0.034	0.095	0.283	0.032	0.016	0.023	0.035	0.027	0.059	0.038	0.129	0.054	0.101	0.111
$U+Th+(REE+Y)^{3+}$	0.036	0.109	0.308	0.034	0.016	0.024	0.037	0.027	0.062	0.038	0.156	0.062	0.126	0.135
Si/(Zr+Hf)	1.002	1.006	1.016	1.001	0.994	0.987	1.007	0.983	0.973	0.988	0.989	0.992	1.025	1.016

Table 55: Zircon in metaluminous to slightly peraluminous syenogranites from the Desemborque Pluton

Sample	GUA-50C2							GUA-53					
Crystal	c2					c3		c2			c10		
Point_ID	2a-r2	2b-c	2b-i	2b-r1	2b-r2	3-c	3-i	2-c	2-i	2-r1	10-c	10-r2	10b-c
Stage	Post	Late	Late	Late	Late	Post	Post	Late	Late	Late	Late	Late	Late
SiO_2 (wt%)	30.790	30.440	31.260	30.910	30.450	27.360	27.710	31.850	32.390	31.530	30.800	31.430	27.880
TiO_2	0.359	0.125	0.134	0.145	0.399	0.311	0.740	0.162	0.124	0.126	0.107	0.101	0.073
Al_2O_3	0.511	0.599	0.255	0.400	0.163	1.009	0.649	0.016	0.056	0.048	0.641	0.079	0.941
Fe_2O_3	1.960	1.650	1.470	1.670	1.281	1.950	2.170	1.105	0.945	1.241	0.712	0.582	1.530
MnO	0.544	0.835	0.411	0.456	0.358	0.686	0.605	0.116	-	0.206	0.221	0.194	0.452
MgO	-	-	-	-	-	-	0.031	-	0.021	0.025	0.049	-	0.060
CaO	0.190	0.263	0.148	0.225	0.068	0.253	0.223	-	-	0.046	0.162	0.363	0.282
ThO_2	0.170	0.350	0.256	0.384	0.138	0.556	0.390	0.126	0.068	0.143	0.356	0.206	1.330
UO_2	0.367	0.810	0.397	0.283	0.248	1.010	0.961	0.251	0.151	0.295	0.508	0.393	0.912
La_2O_3	-	-	-	-	-	0.050	-	-	0.067	-	-	0.053	-
Ce_2O_3	-	0.081	-	0.053	-	0.308	0.149	-	-	-	0.065	0.064	0.155
Nd_2O_3	-	0.093	-	-	-	0.157	0.105	-	-	-	-	-	0.174
Sm_2O_3	-	-	0.060	-	-	0.062	-	-	-	-	-	0.066	0.123
Gd_2O_3	-	-	0.129	-	-	0.325	0.321	-	-	0.073	0.101	-	0.183
Dy_2O_3	-	-	-	-	-	0.421	0.352	-	-	-	0.073	-	0.279
Er_2O_3	0.127	0.139	0.128	0.146	0.103	0.740	0.710	0.128	0.097	0.145	0.258	0.148	0.283
Yb_2O_3	0.480	0.718	0.535	0.609	0.367	2.380	2.050	0.374	0.164	0.427	0.912	0.440	0.811
Y_2O_3	0.428	0.460	0.718	1.032	0.538	4.530	3.010	0.674	0.625	0.628	1.490	0.621	2.200
ZrO_2	58.430	60.370	62.960	62.650	61.560	49.570	44.420	64.650	65.500	65.130	61.260	63.050	56.800
HfO_2	4.020	1.480	1.530	1.460	1.720	3.390	8.940	1.670	1.510	1.420	1.580	1.910	1.360
Nb_2O_5	-	-	-	0.021	-	0.471	0.705	-	-	-	-	0.032	0.132
Ta_2O_5	0.066	0.020	0.043	0.030	-	0.093	0.140	-	0.041	0.020	-	0.058	0.060
P_2O_5	0.083	0.228	0.122	0.213	0.111	0.355	0.253	0.191	0.086	0.339	0.196	0.311	0.305
Total	98.70	98.75	100.67	100.74	97.67	96.00	94.70	101.50	102.01	101.99	99.53	100.17	96.35

Point_ID: spot identification; c: core; r: rim; i: intermediate zone; - : below detection limit; Eu not analysed

Table 55: (*cont.*) Zircon in metaluminous to slightly peraluminous syenogranites from the Desemborque Pluton

Sample	GUA-50C2							GUA-53					
Crystal	c2					c3		c2			c10		
Point_ID	2a-r2	2b-c	2b-i	2b-r1	2b-r2	3-c	3-i	2-c	2-i	2-r1	10-c	10-r2	10b-c
Stage	Post	Late	Late	Late	Late	Post	Post	Late	Late	Late	Late	Late	Late
Structural formulae based on 16 oxygens													
Si (apfu)	3.899	3.846	3.876	3.826	3.873	3.704	3.836	3.889	3.986	3.857	3.867	3.903	3.693
Al	0.076	0.089	0.037	0.059	0.024	0.158	0.106	0.002	0.008	0.007	0.095	0.012	0.147
P	0.009	0.024	0.013	0.022	0.012	0.040	0.030	0.020	0.009	0.035	0.021	0.033	0.034
Sum T	**3.984**	**3.959**	**3.926**	**3.907**	**3.909**	**3.902**	**3.972**	**3.911**	**4.003**	**3.899**	**3.983**	**3.948**	**3.874**
Zr	3.608	3.720	3.794	3.782	3.818	3.299	2.999	3.862	3.811	3.862	3.750	3.818	3.669
Hf	0.145	0.053	0.054	0.052	0.062	0.128	0.353	0.059	0.053	0.050	0.057	0.068	0.051
Th	0.005	0.010	0.007	0.011	0.004	0.017	0.012	0.004	0.002	0.004	0.010	0.006	0.040
U	0.010	0.023	0.011	0.008	0.007	0.030	0.030	0.007	0.004	0.008	0.014	0.011	0.027
Y	0.029	0.031	0.047	0.068	0.036	0.319	0.222	0.044	0.041	0.041	0.100	0.041	0.155
La	0.002	0.001	0.002	0.000	0.001	0.002	0.001	0.001	0.003	0.000	0.001	0.002	0.001
Ce	0.001	0.004	0.002	0.002	0.000	0.015	0.008	0.002	0.000	0.001	0.003	0.003	0.007
Nd	0.001	0.004	0.001	0.001	0.001	0.007	0.005	0.000	0.001	0.003	0.000	0.001	0.008
Sm	0.001	0.000	0.003	0.000	0.000	0.003	0.002	0.000	0.001	0.000	0.000	0.003	0.006
Gd	0.002	0.002	0.005	0.001	0.002	0.014	0.015	0.001	0.002	0.003	0.004	0.000	0.008
Dy	0.001	0.001	0.001	0.000	0.001	0.018	0.016	0.002	0.002	0.002	0.003	0.002	0.012
Er	0.005	0.006	0.005	0.006	0.004	0.031	0.031	0.005	0.004	0.006	0.010	0.006	0.012
Yb	0.019	0.028	0.020	0.023	0.014	0.096	0.087	0.014	0.006	0.016	0.035	0.017	0.033
Ti	0.034	0.012	0.012	0.014	0.038	0.031	0.077	0.015	0.011	0.012	0.010	0.009	0.007
Fe^{3+}	0.187	0.157	0.137	0.157	0.123	0.194	0.226	0.103	0.087	0.115	0.067	0.054	0.153
Mn	0.058	0.089	0.043	0.048	0.039	0.077	0.071	0.012	0.000	0.022	0.024	0.020	0.051
Mg	0.001	0.002	0.001	0.001	0.002	0.004	0.006	0.001	0.004	0.005	0.009	0.001	0.012
Ca	0.026	0.036	0.020	0.030	0.009	0.036	0.033	0.002	0.001	0.006	0.022	0.048	0.040
Nb	0.000	0.000	0.001	0.001	0.001	0.028	0.044	0.000	0.000	0.001	0.000	0.002	0.008
Ta	0.002	0.001	0.001	0.001	0.000	0.003	0.005	0.001	0.001	0.001	0.000	0.002	0.002
Sum A	**4.137**	**4.180**	**4.167**	**4.206**	**4.162**	**4.352**	**4.243**	**4.135**	**4.034**	**4.158**	**4.119**	**4.114**	**4.302**
Zr/Hf_{atomic}	24.88	70.19	70.26	72.73	61.58	25.77	8.50	65.46	71.91	77.24	65.79	56.15	71.94
100*Hf/(Hf+Zr)	3.870	1.410	1.410	1.350	1.610	3.740	10.540	1.500	1.370	1.280	1.490	1.740	1.380
Th/U_{atomic}	0.500	0.435	0.636	1.375	0.571	0.567	0.400	0.571	0.500	0.500	0.714	0.545	1.481
$(REE+Y)^{3+}$	0.060	0.076	0.085	0.102	0.060	0.506	0.386	0.070	0.060	0.072	0.156	0.074	0.242
$U+Th+(REE+Y)^{3+}$	0.075	0.109	0.103	0.121	0.071	0.553	0.428	0.081	0.066	0.084	0.180	0.091	0.309
Si/(Zr+Hf)	1.039	1.019	1.007	0.998	0.998	1.081	1.144	0.992	1.032	0.986	1.016	1.004	0.993

Table 56: Zircon in greisens from the Desemborque Pluton

Sample	GUA-08A												
Crystal	c1				c2a			c2b		c3a			c4
Point_ID	1-r1	1-r2	1-r3	1-c	2a-i	2a-r2	2a-r3	2b-r4	2b-r5	3a-r	3a-r2	3a-r2	4-c
Stage	Post	Post	Post	Post	Post	Post	Post	Post	Post	Post	Post	Post	Post
SiO_2 (wt%)	30.120	29.460	28.990	28.930	30.390	31.030	30.700	29.670	30.130	28.910	29.020	29.230	29.640
TiO_2	0.254	0.164	0.134	0.132	0.161	0.152	0.151	0.148	0.129	0.165	0.130	0.140	0.183
Al_2O_3	0.334	0.712	0.665	0.514	0.421	0.194	0.339	0.668	0.692	0.384	0.341	0.363	0.699
Fe_2O_3	0.973	1.780	1.590	1.265	0.893	0.637	0.784	1.196	1.308	0.870	0.826	0.827	1.227
MnO	0.373	1.021	0.962	0.973	0.784	0.410	0.629	0.863	0.890	0.537	0.507	0.504	0.795
MgO	0.025	-	-	-	-	-	-	-	-	-	-	-	-
CaO	0.166	0.134	0.928	0.136	0.269	1.187	0.908	1.023	0.520	0.192	0.172	0.166	0.135
ThO_2	0.578	0.317	1.230	3.650	0.726	0.235	0.072	0.158	0.142	0.106	0.180	0.123	0.361
UO_2	0.580	1.260	1.230	1.560	1.350	0.487	0.909	0.778	0.863	0.825	0.922	0.832	1.094
La_2O_3	-	-	-	-	-	-	-	-	-	-	-	-	-
Ce_2O_3	-	-	-	-	-	0.043	0.044	-	0.061	0.050	-	-	-
Nd_2O_3	-	-	-	-	-	-	-	0.088	-	-	-	-	-
Sm_2O_3	-	-	-	-	-	-	-	-	-	-	-	-	-
Gd_2O_3	0.146	-	0.093	0.140	-	0.139	-	-	0.079	0.137	0.268	0.172	-
Dy_2O_3	0.165	0.138	0.158	0.122	0.019	0.194	0.102	0.087	0.053	0.190	0.280	0.215	0.081
Er_2O_3	0.415	0.350	0.288	0.431	0.180	0.260	0.135	0.153	0.178	0.303	0.364	0.264	0.165
Yb_2O_3	1.430	1.480	1.400	1.690	0.775	0.766	0.449	0.697	0.624	0.689	0.940	0.751	0.624
Y_2O_3	0.901	0.626	0.878	1.350	0.275	0.704	0.196	0.591	0.480	1.103	1.550	1.073	0.229
ZrO_2	58.500	56.470	56.650	54.110	59.090	61.010	61.710	59.260	60.020	58.510	58.400	58.360	57.920
HfO_2	2.980	2.190	1.760	1.800	2.730	2.870	2.740	2.700	2.670	2.600	2.680	2.750	2.580
Nb_2O_5	0.026	-	0.028	0.085	-	0.053	-	-	-	0.022	-	-	-
Ta_2O_5	0.074	-	0.022	0.047	-	0.009	0.043	0.012	0.055	0.027	0.049	0.038	-
P_2O_5	0.264	0.783	0.665	1.151	0.202	0.230	0.192	0.228	0.201	1.261	1.269	1.150	0.179
Total	98.33	97.05	97.72	98.10	98.35	100.63	100.20	98.44	99.14	96.93	97.94	97.03	95.97

Point_ID: spot identification; c: core; r: rim; i: intermediate zone; - : below detection limit; Eu not analysed

Table 56: (*cont.*) Zircon in greisens from the Desemborque Pluton

Sample	GUA-08A												
Crystal	c1				c2a			c2b		c3a			c4
Point_ID	1-r1	1-r2	1-r3	1-c	2a-i	2a-r2	2a-r3	2b-r4	2b-r5	3a-r	3a-r2	3a-r2	4-c
Stage	Post	Post	Post	Post	Post	Post	Post	Post	Post	Post	Post	Post	Post
Structural formulae based on 16 oxygens													
Si (apfu)	3.871	3.812	3.759	3.785	3.890	3.872	3.843	3.792	3.817	3.742	3.738	3.778	3.868
Al	0.051	0.109	0.102	0.079	0.064	0.029	0.050	0.101	0.103	0.058	0.052	0.055	0.107
P	0.029	0.086	0.073	0.127	0.022	0.024	0.020	0.025	0.022	0.138	0.138	0.126	0.020
Sum T	**3.951**	**4.007**	**3.934**	**3.991**	**3.976**	**3.925**	**3.913**	**3.918**	**3.942**	**3.938**	**3.928**	**3.959**	**3.995**
Zr	3.666	3.563	3.582	3.453	3.688	3.712	3.767	3.693	3.707	3.693	3.668	3.678	3.686
Hf	0.109	0.081	0.065	0.067	0.100	0.102	0.098	0.099	0.097	0.096	0.099	0.101	0.096
Th	0.017	0.009	0.036	0.109	0.021	0.007	0.002	0.005	0.004	0.003	0.005	0.004	0.011
U	0.017	0.036	0.035	0.045	0.038	0.014	0.025	0.022	0.024	0.024	0.026	0.024	0.032
Y	0.062	0.043	0.061	0.094	0.019	0.047	0.013	0.040	0.032	0.076	0.106	0.074	0.016
La	0.000	0.002	0.000	0.000	0.000	0.000	0.000	0.001	0.001	0.000	0.000	0.001	0.002
Ce	0.000	0.000	0.001	0.000	0.000	0.002	0.002	0.001	0.003	0.002	0.001	0.000	0.000
Nd	0.000	0.001	0.001	0.001	0.000	0.000	0.002	0.004	0.001	0.000	0.000	0.001	0.000
Sm	0.001	0.001	0.000	0.000	0.002	0.000	0.000	0.002	0.000	0.001	0.000	0.001	0.001
Gd	0.006	0.001	0.004	0.006	0.001	0.006	0.001	0.002	0.003	0.006	0.011	0.007	0.000
Dy	0.007	0.006	0.007	0.005	0.001	0.008	0.004	0.004	0.002	0.008	0.012	0.009	0.003
Er	0.017	0.014	0.012	0.018	0.007	0.010	0.005	0.006	0.007	0.012	0.015	0.011	0.007
Yb	0.056	0.058	0.055	0.067	0.030	0.029	0.017	0.027	0.024	0.027	0.037	0.030	0.025
Ti	0.025	0.016	0.013	0.013	0.016	0.014	0.014	0.014	0.012	0.016	0.013	0.014	0.018
Fe^{3+}	0.094	0.173	0.155	0.125	0.086	0.060	0.074	0.115	0.125	0.085	0.080	0.080	0.121
Mn	0.041	0.112	0.106	0.108	0.085	0.043	0.067	0.093	0.095	0.059	0.055	0.055	0.088
Mg	0.005	0.003	0.000	0.001	0.001	0.001	0.003	0.000	0.000	0.002	0.002	0.001	0.000
Ca	0.023	0.019	0.129	0.019	0.037	0.159	0.122	0.140	0.071	0.027	0.024	0.023	0.019
Nb	0.002	0.001	0.002	0.005	0.000	0.003	0.000	0.000	0.000	0.001	0.001	0.001	0.000
Ta	0.003	0.000	0.001	0.002	0.000	0.000	0.001	0.000	0.002	0.001	0.002	0.001	0.000
Sum A	**4.151**	**4.139**	**4.265**	**4.138**	**4.132**	**4.217**	**4.217**	**4.268**	**4.210**	**4.139**	**4.157**	**4.116**	**4.125**
Zr/Hf_{atomic}	33.63	43.99	55.11	51.54	36.88	36.39	38.44	37.30	38.22	38.47	37.05	36.42	38.40
100*Hf/(Hf+Zr)	2.900	2.220	1.790	1.910	2.630	2.680	2.530	2.600	2.540	2.540	2.620	2.680	2.540
Th/U_{atomic}	1.000	0.250	1.029	2.422	0.553	0.500	0.080	0.227	0.167	0.125	0.192	0.167	0.344
$(REE+Y)^{3+}$	0.149	0.127	0.141	0.191	0.060	0.102	0.045	0.086	0.074	0.133	0.182	0.133	0.053
$U+Th+(REE+Y)^{3+}$	0.183	0.172	0.212	0.345	0.119	0.123	0.072	0.113	0.102	0.160	0.213	0.161	0.096
Si/(Zr+Hf)	1.025	1.046	1.031	1.075	1.027	1.015	0.994	1.000	1.003	0.988	0.992	1.000	1.023

Table 57: Zircon in greisens from the Desemborque Pluton

Sample	GUA-08A									
Crystal	c4				c5	c9			c9b	
Point_ID	4-i	4-r1	4-r2	4-r3	5-c	9-c	9-i	9-r1	9b-c	9b-r1
Stage	Post	Post	Post	Post	Post	Post	Post	Post	Post	Post
SiO_2 (wt%)	29.910	30.810	31.240	30.530	30.160	32.540	31.360	31.030	32.700	30.150
TiO_2	0.559	0.196	0.387	0.406	0.128	0.270	0.266	0.254	0.366	0.196
Al_2O_3	0.412	0.387	0.409	0.723	0.332	-	-	0.369	-	0.657
Fe_2O_3	0.786	0.721	0.711	1.424	1.292	0.084	0.674	0.793	0.143	1.193
MnO	0.444	0.398	0.374	0.689	0.749	-	0.332	0.344	-	0.578
MgO	-	-	-	-	-	-	-	-	-	-
CaO	0.110	0.131	0.135	0.155	0.093	-	0.037	0.145	-	0.154
ThO_2	0.284	0.113	0.156	0.200	1.820	0.127	0.133	0.130	0.099	0.209
UO_2	1.240	0.728	0.540	0.649	1.026	0.238	0.410	0.518	0.144	0.935
La_2O_3	-	-	-	-	-	-	-	-	-	-
Ce_2O_3	-	-	-	-	-	-	0.046	-	-	-
Nd_2O_3	-	-	-	-	-	-	-	-	-	-
Sm_2O_3	-	-	-	-	-	-	0.055	0.052	-	-
Gd_2O_3	-	-	-	-	-	-	-	0.104	-	-
Dy_2O_3	0.089	-	0.086	-	0.097	0.083	-	0.107	-	-
Er_2O_3	0.239	0.165	0.243	0.190	0.295	0.131	0.142	0.177	0.111	0.155
Yb_2O_3	0.872	0.626	1.250	0.583	1.380	0.415	0.934	0.881	0.528	0.689
Y_2O_3	0.158	0.256	0.210	0.165	0.584	0.173	0.215	0.261	0.066	0.223
ZrO_2	53.310	59.600	57.430	56.490	57.840	61.890	59.710	59.550	61.990	58.490
HfO_2	7.610	2.840	5.790	5.930	2.130	4.140	4.230	3.510	5.210	2.600
Nb_2O_5	0.038	-	-	0.044	-	-	-	-	-	-
Ta_2O_5	0.097	0.057	0.039	0.131	0.038	0.063	0.062	0.023	0.043	-
P_2O_5	0.040	0.090	0.068	0.069	0.741	0.065	0.079	0.171	0.022	0.173
Total	96.28	97.26	99.13	98.41	98.76	100.38	98.71	98.48	101.48	96.51

Point_ID: spot identification; c: core; r: rim; i: intermediate zone; - : below detection limit; Eu not analysed

Table 57: (*cont.*) Zircon in greisens from the Desemborque Pluton

Sample	GUA-08A									
Crystal	c4				c5	c9			c9b	
Point_ID	4-i	4-r1	4-r2	4-r3	5-c	9-c	9-i	9-r1	9b-c	9b-r1
Stage	Post	Post	Post	Post	Post	Post	Post	Post	Post	Post
Structural formulae based on 16 oxygens										
Si (apfu)	3.965	3.947	3.974	3.909	3.857	4.030	3.981	3.938	4.021	3.897
Al	0.064	0.058	0.061	0.109	0.050	0.002	0.001	0.055	0.002	0.100
P	0.005	0.010	0.007	0.007	0.080	0.007	0.008	0.018	0.002	0.019
Sum T	**4.034**	**4.015**	**4.042**	**4.025**	**3.987**	**4.039**	**3.990**	**4.011**	**4.025**	**4.016**
Zr	3.446	3.723	3.562	3.527	3.607	3.737	3.696	3.686	3.717	3.686
Hf	0.288	0.104	0.210	0.217	0.078	0.146	0.153	0.127	0.183	0.096
Th	0.009	0.003	0.005	0.006	0.053	0.004	0.004	0.004	0.003	0.006
U	0.037	0.021	0.015	0.018	0.029	0.007	0.012	0.015	0.004	0.027
Y	0.011	0.017	0.014	0.011	0.040	0.011	0.015	0.018	0.004	0.015
La	0.000	0.000	0.000	0.001	0.000	0.001	0.000	0.000	0.000	0.000
Ce	0.000	0.001	0.000	0.000	0.000	0.000	0.002	0.000	0.001	0.000
Nd	0.000	0.001	0.001	0.000	0.000	0.002	0.000	0.002	0.000	0.000
Sm	0.001	0.000	0.000	0.000	0.000	0.000	0.002	0.002	0.000	0.001
Gd	0.002	0.002	0.001	0.001	0.002	0.001	0.001	0.004	0.000	0.000
Dy	0.004	0.001	0.004	0.000	0.004	0.003	0.000	0.004	0.000	0.002
Er	0.010	0.007	0.010	0.008	0.012	0.005	0.006	0.007	0.004	0.006
Yb	0.035	0.024	0.048	0.023	0.054	0.016	0.036	0.034	0.020	0.027
Ti	0.056	0.019	0.037	0.039	0.012	0.025	0.025	0.024	0.034	0.019
Fe^{3+}	0.078	0.069	0.068	0.137	0.124	0.008	0.064	0.076	0.013	0.116
Mn	0.050	0.043	0.040	0.075	0.081	0.001	0.036	0.037	0.001	0.063
Mg	0.001	0.002	0.000	0.000	0.001	0.000	0.000	0.003	0.000	0.001
Ca	0.016	0.018	0.018	0.021	0.013	0.002	0.005	0.020	0.000	0.021
Nb	0.002	0.001	0.000	0.003	0.000	0.001	0.000	0.000	0.000	0.000
Ta	0.004	0.002	0.001	0.005	0.001	0.002	0.002	0.001	0.001	0.000
Sum A	**4.050**	**4.058**	**4.034**	**4.092**	**4.111**	**3.972**	**4.059**	**4.064**	**3.985**	**4.086**
Zr/Hf_{atomic}	11.97	35.80	16.96	16.25	46.24	25.60	24.16	29.02	20.31	38.40
100*Hf/(Hf+Zr)	7.710	2.710	5.570	5.790	2.110	3.770	3.980	3.340	4.690	2.540
Th/U_{atomic}	0.243	0.143	0.333	0.333	1.828	0.571	0.333	0.267	0.750	0.222
$(REE+Y)^{3+}$	0.064	0.054	0.078	0.043	0.112	0.040	0.062	0.072	0.030	0.052
$U+Th+(REE+Y)^{3}$	0.110	0.078	0.098	0.067	0.194	0.051	0.078	0.091	0.037	0.085
Si/(Zr+Hf)	1.062	1.031	1.054	1.044	1.047	1.038	1.034	1.033	1.031	1.030

Table 58: Zircon in peralkaline alkali feldspar granites from the Mandira unit

Sample	MAN-13B												
Crystal	c1			c1b			c1b-3			c1b-8			c1b-9
Point_ID	1-c	1-r1	1-r3	1b-c	1b-r1	1b-r2	1b-3-c	1b-3-r1	1b-3-r2	1b-8-c	1b-8-r1	1b-8-r2	1b-9-c
Stage	Early	Early	Post	Early	Early	Early	Early	Early	Early	Early	Post	Post	Early
SiO_2 (wt%)	32.580	32.870	30.680	32.440	32.950	30.590	32.330	32.530	32.950	32.590	30.390	31.270	33.070
TiO_2	0.079	0.074	0.236	0.060	0.064	0.087	0.058	0.065	0.113	0.066	0.135	0.154	0.092
Al_2O_3	-	-	-	-	-	-	-	-	-	-	0.147	-	-
Fe_2O_3	0.089	0.139	0.914	0.073	0.213	0.947	0.219	0.279	0.324	0.337	1.362	1.500	0.287
MnO	-	-	0.061	-	-	0.086	-	-	0.020	-	0.140	0.025	-
MgO	-	-	-	-	-	-	-	-	-	-	-	-	-
CaO	-	-	0.043	-	-	0.072	-	-	0.029	-	0.557	0.052	-
ThO_2	-	0.043	1.840	-	-	0.477	0.090	0.115	0.057	0.106	1.008	0.448	0.075
UO_2	0.065	0.031	0.186	0.063	0.048	0.223	0.000	0.062	0.081	0.073	0.216	-	0.026
La_2O_3	-	-	-	-	-	-	-	-	-	-	-	-	-
Ce_2O_3	-	-	-	-	-	-	-	-	-	-	-	-	-
Nd_2O_3	-	-	-	-	-	-	-	-	-	-	0.079	-	-
Sm_2O_3	-	-	0.126	-	-	-	-	-	-	0.131	0.072	-	-
Gd_2O_3	0.065	-	0.227	-	-	0.404	-	0.071	-	-	0.243	0.196	0.070
Dy_2O_3	0.070	0.101	0.313	0.090	-	0.563	-	0.013	-	0.060	0.345	0.361	0.085
Er_2O_3	0.099	0.127	0.681	0.129	0.088	0.507	0.099	0.104	0.138	0.094	0.744	0.688	0.101
Yb_2O_3	0.296	0.315	1.980	0.220	0.343	0.942	0.293	0.207	0.332	0.249	2.380	1.670	0.309
Y_2O_3	0.527	0.753	0.861	0.573	0.516	1.930	0.549	0.565	0.709	0.583	1.500	2.080	0.723
ZrO_2	66.630	66.460	58.660	66.280	66.730	62.200	66.460	67.190	66.130	66.410	59.190	60.560	66.150
HfO_2	0.954	0.829	2.250	0.955	0.983	0.802	0.927	0.969	0.945	0.941	1.880	2.320	0.897
Nb_2O_5	-	-	0.048	0.019	0.020	0.048	0.007	0.000	0.000	0.009	0.057	0.051	0.000
Ta_2O_5	0.030	0.009	0.028	0.021	0.035	0.000	0.000	0.038	0.016	0.013	0.033	0.026	0.000
P_2O_5	0.049	0.031	1.002	0.028	0.035	0.543	0.076	0.067	0.034	0.063	0.803	0.683	0.048
Total	101.57	101.93	100.21	101.08	102.18	100.62	101.20	102.43	102.00	101.79	101.32	102.19	102.05

Point_ID: spot identification; c: core; r: rim; i: intermediate zone; - : below detection limit; Eu not analysed

Table 58: (*cont.*) Zircon in peralkaline alkali feldspar granites from the Mandira unit

Sample	MAN-13B												
Crystal	c1			c1b			c1b-3			c1b-8			c1b-9
Point_ID	1-c	1-r1	1-r3	1b-c	1b-r1	1b-r2	1b-3-c	1b-3-r1	1b-3-r2	1b-8-c	1b-8-r1	1b-8-r2	1b-9-c
Stage	Early	Early	Post	Early	Early	Early	Early	Early	Early	Early	Post	Post	Early
Structural formulae based on 16 oxygens													
Si (apfu)	3.979	3.980	3.879	4.003	4.001	3.820	3.980	3.976	4.001	3.992	3.830	3.914	4.011
Al	0.000	0.002	0.001	0.001	0.000	0.021	0.000	0.001	0.001	0.000	0.022	0.006	0.000
P	0.005	0.003	0.107	0.003	0.004	0.057	0.008	0.007	0.004	0.007	0.086	0.072	0.005
Sum T	**3.984**	**3.985**	**3.987**	**4.007**	**4.005**	**3.898**	**3.988**	**3.984**	**4.006**	**3.999**	**3.938**	**3.992**	**4.016**
Zr	3.921	3.913	3.604	3.898	3.892	3.787	3.912	3.903	3.867	3.883	3.594	3.574	3.864
Hf	0.033	0.029	0.081	0.034	0.035	0.029	0.033	0.034	0.033	0.033	0.068	0.083	0.032
Th	0.000	0.001	0.053	0.001	0.001	0.014	0.003	0.003	0.002	0.003	0.029	0.013	0.002
U	0.002	0.001	0.005	0.002	0.001	0.006	0.000	0.002	0.002	0.002	0.006	0.000	0.001
Y	0.034	0.042	0.058	0.038	0.034	0.128	0.036	0.037	0.047	0.038	0.101	0.139	0.048
La	0.000	0.000	0.000	0.001	0.000	0.000	0.000	0.001	0.000	0.000	0.000	0.001	0.001
Ce	0.000	0.002	0.000	0.001	0.000	0.001	0.002	0.002	0.002	0.002	0.001	0.000	0.000
Nd	0.000	0.001	0.003	0.000	0.001	0.000	0.000	0.000	0.002	0.000	0.004	0.000	0.001
Sm	0.000	0.000	0.006	0.001	0.002	0.001	0.001	0.002	0.000	0.006	0.003	0.001	0.002
Gd	0.003	0.001	0.009	0.000	0.001	0.017	0.000	0.003	0.000	0.000	0.010	0.008	0.003
Dy	0.003	0.004	0.013	0.004	0.001	0.023	0.000	0.001	0.000	0.002	0.014	0.015	0.003
Er	0.004	0.005	0.027	0.005	0.003	0.020	0.004	0.004	0.005	0.004	0.030	0.027	0.004
Yb	0.011	0.012	0.076	0.008	0.013	0.036	0.011	0.008	0.013	0.009	0.084	0.064	0.012
Ti	0.007	0.007	0.022	0.006	0.006	0.008	0.005	0.006	0.011	0.006	0.013	0.014	0.009
Fe^{3+}	0.008	0.013	0.087	0.007	0.020	0.089	0.020	0.026	0.030	0.031	0.130	0.141	0.027
Mn	0.000	0.001	0.007	0.000	0.001	0.009	0.000	0.002	0.002	0.000	0.015	0.003	0.000
Mg	0.001	0.003	0.001	0.000	0.000	0.000	0.003	0.003	0.003	0.000	0.003	0.001	0.001
Ca	0.002	0.001	0.006	0.002	0.001	0.010	0.001	0.000	0.004	0.002	0.076	0.007	0.001
Nb	0.000	0.000	0.003	0.001	0.001	0.003	0.000	0.000	0.000	0.000	0.003	0.003	0.000
Ta	0.001	0.000	0.001	0.001	0.001	0.000	0.000	0.001	0.001	0.000	0.001	0.001	0.000
Sum A	**4.030**	**4.036**	**4.062**	**4.010**	**4.014**	**4.181**	**4.031**	**4.038**	**4.024**	**4.021**	**4.185**	**4.095**	**4.011**
Zr/Hf_{atomic}	118.818	134.931	44.494	114.647	111.200	130.586	118.545	114.794	117.182	117.667	52.853	43.060	120.750
100*Hf/(Hf+Zr)	0.850	0.740	2.200	0.860	0.880	0.750	0.830	0.860	0.860	0.850	1.860	2.270	0.810
Th/U_{atomic}	0.000	1.000	10.600	0.500	1.000	2.333		1.500	1.000	1.500	4.833		2.000
$(REE+Y)^{3+}$	0.055	0.068	0.192	0.058	0.055	0.226	0.054	0.057	0.069	0.062	0.248	0.254	0.074
$U+Th+(REE+Y)^{3+}$	0.057	0.070	0.250	0.061	0.057	0.246	0.057	0.062	0.073	0.067	0.283	0.267	0.077
Si/(Zr+Hf)	1.006	1.010	1.053	1.018	1.019	1.001	1.009	1.010	1.026	1.019	1.046	1.070	1.030

Table 59: Zircon in peralkaline alkali feldspar granites from the Mandira unit

Sample	MAN-13B													
Crystal	c1b-9		c1b-11				c2		c5		c7			
Point_ID	1b-9-r1	1b-9-r2	1b-11-c	1b-11-r1	1b-11-r2	1b-11-r3	2-c	2-r1	5-c	5-r1	7-r1	7-r2	7-r3	7-c
Stage	Early	Late	Early	Late	Early	Early	Late	Late	Late	Late	Post	Post	Late	Early
SiO_2 (wt%)	32.800	32.550	32.590	30.670	30.760	30.380	31.630	32.000	31.260	29.800	30.600	32.600	31.410	31.150
TiO_2	0.109	0.093	0.081	0.040	0.062	0.050	0.121	0.068	0.086	0.122	0.131	0.374	0.097	0.083
Al_2O_3	-	-	-	0.049	0.045	0.183	0.042	0.068	0.132	0.606	0.080	-	0.084	0.106
Fe_2O_3	0.569	0.743	0.041	0.606	0.557	0.858	0.586	0.742	0.740	1.189	1.018	0.091	0.416	0.895
MnO	-	0.041	-	0.149	0.177	0.196	0.094	0.140	0.151	0.261	0.164	0.002	0.067	0.156
MgO	-	-	-	-	-	0.040	-	-	-	0.044	-	-	0.023	0.026
CaO	-	0.004	0.004	0.103	0.077	0.122	0.023	0.053	0.110	0.164	0.087	-	0.076	0.064
ThO_2	0.065	0.113	0.008	0.178	0.105	0.327	0.071	0.132	0.569	0.939	0.742	0.374	0.041	0.135
UO_2	0.049	0.172	0.051	0.495	0.521	0.379	0.272	0.281	0.367	0.431	0.393	0.089	0.340	0.413
La_2O_3	-	-	-	-	-	-	-	-	-	-	-	-	-	-
Ce_2O_3	-	-	-	-	-	0.072	-	-	0.065	-	-	-	-	0.051
Nd_2O_3	-	-	-	0.060	-	-	-	-	-	-	-	-	-	-
Sm_2O_3	0.079	-	0.018	-	-	0.052	-	-	-	0.073	-	-	-	-
Gd_2O_3	-	0.066	-	-	-	0.144	-	-	0.126	0.340	0.137	-	0.065	0.115
Dy_2O_3	-	0.108	-	-	-	0.079	0.063	-	0.135	-	0.182	0.152	0.068	-
Er_2O_3	0.133	0.348	0.099	0.355	0.246	0.316	0.137	0.148	0.307	0.618	0.265	0.229	0.163	0.270
Yb_2O_3	0.347	2.260	0.409	1.380	1.220	1.330	0.769	0.682	0.938	1.270	0.762	0.361	0.711	1.240
Y_2O_3	0.720	0.542	0.483	0.523	0.406	0.606	0.377	0.358	1.121	2.290	0.959	0.921	0.451	0.577
ZrO_2	66.210	64.040	66.340	63.730	63.840	62.050	65.010	64.580	61.980	57.790	61.010	60.780	64.440	63.070
HfO_2	0.935	1.164	0.964	1.009	0.876	0.925	1.510	1.470	1.480	1.260	1.780	5.030	1.320	1.026
Nb_2O_5	-	0.025	-	0.024	-	0.021	-	0.030	-	-	0.028	-	-	-
Ta_2O_5	-	-	-	0.037	-	-	0.030	-	0.039	0.020	-	0.076	0.039	0.043
P_2O_5	0.054	0.172	0.059	0.357	0.502	0.354	0.168	0.155	0.266	0.757	0.265	0.256	0.216	0.385
Total	102.17	102.51	101.24	99.89	99.53	98.51	100.95	101.02	99.92	98.52	98.78	101.38	100.09	99.89

Point_ID: spot identification; c: core; r: rim; i: intermediate zone; - : below detection limit; Eu not analysed

Table 59: (cont.) Zircon in peralkaline alkali feldspar granites from the Mandira unit

Sample	MAN-13B													
Crystal	c1b-9		c1b-11				c2		c5		c7			
Point_ID	1b-9-r1	1b-9-r2	1b-11-c	1b-11-r1	1b-11-r2	1b-11-r3	2-c	2-r1	5-c	5-r1	7-r1	7-r2	7-r3	7-c
Stage	Early	Late	Early	Late	Early	Early	Late	Late	Late	Late	Post	Post	Late	Early
Structural formulae based on 16 oxygens														
Si (apfu)	3.992	3.994	3.993	3.847	3.853	3.856	3.902	3.942	3.909	3.810	3.884	4.033	3.900	3.884
Al	0.002	0.003	0.002	0.007	0.007	0.027	0.006	0.010	0.019	0.091	0.012	0.000	0.012	0.016
P	0.006	0.018	0.006	0.038	0.053	0.038	0.018	0.016	0.028	0.082	0.029	0.027	0.023	0.041
Sum T	**4.000**	**4.015**	**4.001**	**3.892**	**3.913**	**3.921**	**3.926**	**3.968**	**3.956**	**3.983**	**3.925**	**4.060**	**3.935**	**3.941**
Zr	3.858	3.758	3.910	3.898	3.899	3.841	3.899	3.849	3.780	3.603	3.776	3.627	3.901	3.834
Hf	0.033	0.041	0.034	0.036	0.031	0.034	0.054	0.052	0.053	0.046	0.064	0.179	0.047	0.037
Th	0.002	0.003	0.000	0.005	0.003	0.009	0.002	0.004	0.016	0.027	0.021	0.011	0.001	0.004
U	0.001	0.005	0.001	0.014	0.015	0.011	0.008	0.008	0.010	0.012	0.011	0.002	0.009	0.011
Y	0.047	0.036	0.032	0.035	0.027	0.041	0.025	0.024	0.075	0.156	0.065	0.061	0.030	0.038
La	0.000	0.001	0.001	0.001	0.000	0.001	0.000	0.001	0.000	0.000	0.001	0.000	0.000	0.001
Ce	0.000	0.000	0.000	0.000	0.001	0.003	0.001	0.000	0.003	0.002	0.002	0.000	0.001	0.002
Nd	0.001	0.001	0.000	0.003	0.002	0.000	0.001	0.000	0.000	0.002	0.002	0.000	0.000	0.000
Sm	0.003	0.000	0.001	0.000	0.000	0.002	0.000	0.002	0.002	0.003	0.002	0.000	0.002	0.000
Gd	0.000	0.003	0.001	0.002	0.000	0.006	0.000	0.001	0.005	0.014	0.006	0.002	0.003	0.005
Dy	0.001	0.004	0.000	0.002	0.002	0.003	0.003	0.000	0.005	0.019	0.007	0.006	0.003	0.002
Er	0.005	0.014	0.004	0.014	0.010	0.013	0.005	0.006	0.012	0.025	0.011	0.009	0.006	0.011
Yb	0.013	0.086	0.015	0.053	0.047	0.051	0.029	0.026	0.036	0.050	0.030	0.014	0.027	0.047
Ti	0.010	0.009	0.008	0.004	0.006	0.005	0.011	0.006	0.008	0.012	0.012	0.035	0.009	0.008
Fe^{3+}	0.053	0.069	0.004	0.057	0.053	0.082	0.055	0.070	0.070	0.114	0.097	0.009	0.039	0.084
Mn	0.000	0.004	0.001	0.016	0.019	0.021	0.010	0.015	0.016	0.028	0.018	0.000	0.007	0.016
Mg	0.001	0.001	0.000	0.000	0.002	0.008	0.002	0.000	0.003	0.008	0.003	0.000	0.004	0.005
Ca	0.000	0.000	0.000	0.014	0.010	0.017	0.003	0.007	0.015	0.023	0.012	0.000	0.010	0.009
Nb	0.001	0.001	0.000	0.001	0.000	0.001	0.000	0.002	0.000	0.000	0.002	0.000	0.000	0.000
Ta	0.000	0.000	0.001	0.001	0.000	0.000	0.001	0.001	0.001	0.001	0.000	0.003	0.001	0.001
Sum A	**4.029**	**4.036**	**4.013**	**4.156**	**4.127**	**4.149**	**4.109**	**4.074**	**4.110**	**4.145**	**4.142**	**3.958**	**4.100**	**4.115**
Zr/Hf_{atomic}	116.909	91.659	115.000	108.278	125.774	112.971	72.204	74.019	71.321	78.326	59.000	20.263	83.000	103.622
100*Hf/(Hf+Zr)	0.850	1.090	0.860	0.920	0.800	0.870	1.350	1.340	1.380	1.260	1.680	4.710	1.180	0.940
Th/U_{atomic}	2.000	0.600	0.000	0.357	0.200	0.818	0.250	0.500	1.600	2.250	1.909	5.500	0.111	0.364
$(REE+Y)^{3+}$	0.071	0.144	0.054	0.110	0.089	0.121	0.063	0.059	0.138	0.271	0.124	0.092	0.071	0.107
$U+Th+(REE+Y)^{3+}$	0.074	0.152	0.055	0.129	0.107	0.141	0.073	0.071	0.164	0.310	0.156	0.105	0.081	0.122
Si/(Zr+Hf)	1.026	1.051	1.012	0.978	0.980	0.995	0.987	1.011	1.020	1.044	1.011	1.060	0.988	1.003

APPENDIX B: LASER ABLATION INDUCTIVELY COUPLED PLASMA MASS SPECTROMETRY ANALYSIS IN SITU OF MINERALS

Table 60: Amphiboles in peralkaline alkali feldspar granites from the Mandira unit

Sample	**MAN-13A**						**MAN-4777**					
Mineral	Riebeckite						Arfvedsonite					
Point_ID	12	2σ error	17	2σ error	16	2σ error	4	2σ error	5	2σ error	6	2σ error
Li	1939	190	1999	213	2146	240	2429	152	2135	135	2533	161
Be	14.1	1.3	16.8	1.6	27.8	2.6	15.4	1.2	21.1	1.6	27.8	2.1
P	3.0	1.3	4.7	1.3	4.1	1.7	5.9	2.2	5.2	2.8	4.7	2.2
Sc	1.7	0.1	1.1	0.1	2.1	0.2	1.3	0.1	1.1	0.1	1.6	0.1
Ti	3119	234	3686	290	4678	380	5144	335	4365	288	5351	358
V	0.2	<2σ	0.3	0.0	0.4	0.1	0.3	0.0	0.1	0.1	0.4	0.1
Cr	0.1	<2σ	0.2	0.1	0.1	0.1	0.1	0.1	0.1	0.1	0.3	0.1
Co	0.2	<2σ	0.4	0.0	0.3	<2σ	0.2	<2σ	0.4	<2σ	0.4	<2σ
Ni	0.0	<2σ	0.2	0.0	0.1	<2σ	0.2	<2σ	0.1	<2σ	0.0	<2σ
Cu	0.5	0.1	0.8	0.1	0.4	0.1	1.2	0.1	1.3	0.2	0.3	0.1
Zn	2298	173	3013	237	3860	312	3571	272	3034	238	3341	271
Ga	9.1	0.8	11.2	1.0	14.9	1.4	12.5	1.0	12.6	1.1	12.7	1.1
Rb	10.6	0.7	15.0	1.0	22.8	1.5	26.9	2.4	10.9	1.0	35.0	3.4
Sr	3.4	0.2	0.7	0.1	3.2	0.2	0.1	<2σ	0.3	<2σ	0.1	<2σ
Y	100	7.8	41.2	3.4	73	6.2	19.6	1.7	101	9.1	17.4	1.6
Zr	430	34.9	667	57	924	81.9	702	62	483	44	780	75.0
Nb	34.4	2.3	39.1	2.7	47.7	3.3	31.4	2.4	38.7	3.1	38.7	3.2
Mo	0.1	<2σ	0.1	0.0	0.1	0.0	0.1	0.0	0.3	0.1	0.1	<2σ
Sn	27.9	1.9	37.6	2.6	58.5	4.2	62.2	4.8	23.5	1.9	68.7	5.7
Sb	0.0	<2σ	0.0	<2σ	b.d.l	<2σ	b.d.l	<2σ	b.d.l	<2σ	b.d.l	0.1
Cs	0.2	<2σ	0.1	<2σ	0.0	<2σ	0.3	<2σ	0.0	<2σ	0.3	<2σ
Ba	1.3	0.2	3.7	0.3	1.2	0.1	0.9	0.1	0.8	0.1	0.4	0.1
La	15.4	1.0	6.4	0.4	8.4	0.6	2.1	0.1	11.7	0.8	3.7	0.3
Ce	53.5	3.4	29.0	1.9	35.3	2.3	9.2	0.6	47.5	3.3	15.1	1.1
Pr	9.5	0.7	5.2	0.4	6.7	0.5	1.6	0.1	8.4	0.6	2.7	0.2
Nd	48.1	3.4	25.4	1.9	33.8	2.5	8.0	0.6	45.2	3.5	19.0	1.5
Sm	17.1	1.2	10.0	0.7	12.9	0.9	2.9	0.3	17.2	1.5	4.3	0.4
Eu	0.2	<2σ	0.1	0.0	0.2	0.0	0.1	<2σ	0.3	<2σ	0.1	<2σ
Gd	16.6	1.3	8.5	0.7	11.3	1.0	2.5	0.2	16.2	1.5	3.5	0.4
Tb	3.1	0.2	1.6	0.1	2.1	0.2	0.5	<2σ	3.0	0.2	0.6	0.1
Dy	21.0	1.8	10.5	1.0	14.4	1.4	4.0	0.3	19.9	1.4	3.6	0.3
Ho	4.8	0.4	2.6	0.2	3.8	0.4	1.2	0.1	4.9	0.4	0.9	0.1
Er	18.5	1.5	13.4	1.2	18.4	1.6	6.6	0.5	19.6	1.5	4.4	0.4
Tm	4.5	0.4	4.2	0.4	5.5	0.6	2.3	0.2	4.8	0.4	1.5	0.1
Yb	60.7	6.3	55.3	6.2	68.8	8.0	31.9	2.3	55.9	4.0	24.3	1.8
Lu	14.0	1.5	12.7	1.5	15.6	1.9	7.8	0.5	11.7	0.8	6.7	0.5
Hf	24.1	2.3	26.8	2.7	45.6	4.7	31.5	2.2	19.4	1.4	38.6	2.9
Ta	0.5	0.1	0.5	0.1	0.6	0.1	0.4	<2σ	0.4	<2σ	0.4	<2σ
^{206}Pb	15.6	2.2	11.9	1.8	15.8	2.6	17.4	1.3	20.1	1.6	10.3	0.8
^{208}Pb	16.3	1.1	12.4	0.9	16.7	1.2	18.1	2.0	21.3	2.5	10.6	1.3
Th	1.0	0.1	0.1	<2σ	0.3	<2σ	1.6	0.1	1.0	0.1	0.6	0.1
U	0.2	<2σ	<2σ	<2σ	0.1	<2σ	0.6	<2σ	0.4	<2σ	0.2	<2σ
REE	287		185		237		81		266		90	
LREE	144		76		97		23.856		130.28		45	
HREE	143		109		140		56.763		135.84		45	

Trace element LA-ICP-MS compositions (ppm); b.d.l.: below detection limit; <2σ: : below 2σ error

Table 61: Amphiboles in metaluminous syenogranites from the Mandira 1 unit

Sample	**MAN-5**						**MAN-6764**					
Mineral	Ferro-ferri-hornblende						Hastingsite					
Point_ID	1	2σ error	2	2σ error	6b	2σ error	2	2σ error	3	2σ error	4	2σ error
Li	26.49	3.6	30.5	4.3	24.0	4.5	35.3	4.1	33.9	4.1	25.4	3.3
Be	11.99	3.9	9.0	3.0	6.2	2.7	20.0	3.1	12.8	2.1	17.6	2.6
P	18.99	23.0	13.5	16.9	9.3	15.3	16.1	9	b.d.l	7.6	11.0	5.4
Sc	91.96	6.1	65.9	4.4	49.8	3.6	55.6	5	49.5	4.4	52.9	4.9
Ti	9963.9	632	8849	561	8366	539	10270	784	9748	771	10027	827
V	59.14	3.9	89.0	5.9	91.9	6.5	15.5	1.5	7.5	0.8	9.0	0.9
Cr	5.75	0.5	70.7	4.6	28.4	2.2	3.2	0.5	0.4	0.3	0.6	0.2
Co	24.4	1.9	23.0	1.8	23.7	2.3	9.1	0.9	9.0	0.9	9.2	1.0
Ni	18.65	1.6	14.8	1.3	16.1	2.1	3.9	0.7	3.9	0.6	3.8	0.5
Cu	1.26	0.3	1.4	0.3	2.2	0.7	0.8	0.4	1.1	0.4	0.8	0.2
Zn	709.97	77.1	774	84.6	762	91.7	1543	207	1610	231	1502	233
Ga	37.33	3.6	34.7	3.4	33.1	4.2	51.8	6.0	51.5	6.3	47.5	6.2
Rb	12.66	1.5	5.2	0.6	5.6	1.0	9.6	1.2	11.7	1.5	8.5	1.2
Sr	9.3	0.8	9.5	0.9	9.5	1.1	2.4	0.3	2.5	0.3	2.0	0.3
Y	663.03	63.1	473	46.1	395	47.1	672	76	688	82.5	602	77.5
Zr	94.68	9.3	88	8.8	85	10.5	107	13	107	13.3	92	12.3
Nb	148.97	11.6	124	9.8	97	8.9	364	43	336	42.3	326	44.1
Mo	1.2	0.2	1.5	0.3	1.3	0.5	1.5	0.4	1.2	0.3	1.0	0.2
Sn	4.35	0.5	5.6	0.6	6.8	1.1	17.6	2.2	12.0	1.5	13.0	1.7
Sb	b.d.l	0.1	b.d.l	0.1	0.1	0.1	b.d.l	0.1	b.d.l	0.1	0.1	0.1
Cs	0.25	<2σ	0.0	<2σ	0.0	<2σ	0.0	<2σ	0.4	0.1	b.d.l	<2σ
Ba	19.72	2.4	14.0	1.8	16.2	3.0	11.8	1.8	11.7	1.8	5.1	0.9
La	179.72	16.8	180	17.3	172	20.2	171	22	170	23.6	137	20.6
Ce	631	57.2	587	54.4	541	61.3	544	74	538	78.7	538	85.4
Pr	104.6	8.6	87	7.3	78	7.8	106	15	103	15.6	96	15.8
Nd	523	42.9	392	32.7	334	33.2	541	81	528	85.6	502	88.3
Sm	151	12.8	99	8.5	81	8.7	159	20	162	21.5	152	21.7
Eu	1.8	0.2	1.8	0.2	1.8	0.3	1.5	0.3	1.4	0.3	1.1	0.2
Gd	137	8.8	86	5.6	69	5.3	139	15	151	16.6	134	15.7
Tb	24.44	1.6	15	1.0	13	1.0	25.1	3.2	26.2	3.6	24.2	3.6
Dy	146	9.8	95	6.4	84	6.5	148	18	157	20.5	143	20.1
Ho	28.12	1.9	19	1.3	16	1.3	27.7	3.1	29.0	3.4	26.4	3.3
Er	66.83	5.2	49	3.9	43	4.2	68.5	7.5	68.7	7.9	62.8	7.7
Tm	8.58	0.7	7.0	0.5	6.3	0.6	9.2	1.0	8.9	1.0	8.0	1.0
Yb	54.3	3.6	46.0	3.1	40.2	3.3	62.3	7.3	57.8	7.2	52.8	7.0
Lu	6.77	0.5	6.2	0.4	5.3	0.5	9.4	1.2	8.9	1.2	7.4	1.0
Hf	6.17	0.6	5.9	0.5	6.4	1.0	9.4	1.7	8.9	1.6	7.8	1.5
Ta	2.43	0.2	2.6	0.2	2.4	0.3	4.9	0.7	4.6	0.7	4.3	0.7
^{206}Pb	4.31	0.5	3.8	0.4	4.3	0.8	15.9	2.5	6.8	1.2	5.0	0.9
^{208}Pb	4.37	0.5	3.8	0.4	4.4	0.7	16.7	2.0	6.8	0.9	5.5	0.8
Th	0.53	0.1	0.3	0.1	0.3	0.1	0.4	0.1	0.4	0.1	0.3	0.1
U	0.14	<2σ	0.1	<2σ	0.1	<2σ	2.1	0.3	0.1	<2σ	0.1	<2σ
REE	2065		1670		1484		2012		2009		1886	
LREE	1592		1346		1208		1522.8		1502		1427	
HREE	472.9		324		277		489.34		506.99		459	

Trace element LA-ICP-MS compositions (ppm); b.d.l.: below detection limit; <2σ: : below 2σ error

Table 62: Amphiboles in peralkaline alkali feldspar granites from the Acaraú unit

Sample	**MAN-6728**						**MAN-579**					
Mineral	Ferro-edenite						Ferro-ferri-winchite					
Point_ID	1a	2σ error	1b	2σ error	1c	2σ error	1	2σ error	4b	2σ error	5	2σ error
Li (ppm)	183	14.9	141	11.7	138	12.7	187	17.2	100	10.3	170	18.5
Be	621	66.5	474	52.5	527	65.5	42.7	1.2	29	1.0	51	1.1
P	24.1	13.4	10.2	8.4	12.0	17.5	b.d.l	4.9	b.d.l	5.4	10	5.9
Sc	23.7	2.0	25.3	2.0	50.6	4.5	26.0	2.4	5.5	0.6	125	13.2
Ti	7854	636	6927	584	6890	621	899	68.8	848	70.0	6080	517
V	3.6	0.6	3.3	0.4	4.0	0.8	2.0	0.2	1.0	0.2	22	2.1
Cr	b.d.l	0.5	0.3	0.3	b.d.l	0.7	b.d.l	0.2	0.4	0.2	8.9	1.0
Co	3.4	0.5	4.0	0.4	3.4	0.6	4.0	0.4	3.3	0.3	3.8	0.4
Ni	2.2	0.8	3.8	0.7	3.1	1.2	1.4	0.3	1.3	0.2	4.1	0.6
Cu	4.0	1.0	5.9	0.9	12.7	2.5	0.5	0.2	b.d.l	0.2	0.4	0.2
Zn	3055	256	2923	254	3322	311	2521	203	2557	224.1	2484	227
Ga	50.2	4.8	53.3	5.0	59.0	6.4	18.5	1.9	13.6	1.6	34	4.1
Rb	84.6	9.4	36.2	4.3	32.3	4.4	17.3	1.7	4.6	0.5	20	2.3
Sr	10.7	1.1	15.1	1.4	13.0	1.5	11.9	1.4	4.3	0.6	3.1	0.4
Y	1096	93.1	1745	154.9	1123	106	125	12.0	139	14.9	230	25.9
Zr	192	16.7	191	17.2	306	29.6	59.7	6.0	22	2.5	104	12.3
Nb	991	73.4	722	55.1	1059	84.8	57.8	5.1	31	3.1	276	28.1
Mo	1.8	0.6	0.6	0.3	0.9	0.6	b.d.l	0.1	b.d.l	<2σ	0.5	0.1
Sn	270	17.6	221	14.1	188	13.5	448	42.2	253	26.4	27	3.0
Sb	b.d.l	0.1	0.1	0.1	b.d.l	0.2	b.d.l	0.1	b.d.l	0.1	b.d.l	<2σ
Cs	1.4	0.3	0.3	0.1	0.5	0.2	1.3	0.1	0.1	<2σ	0.4	0.1
Ba	39.8	4.6	82.1	7.7	38.3	5.5	13.8	1.1	1.0	0.2	3.5	0.4
La	853	64.1	1603	124	1052	85.7	12.7	0.8	3.2	0.2	55	3.4
Ce	1814	134	2784	211	2235	178	38.4	2.4	18.2	1.2	164.04	10.3
Pr	224	17.2	346	27.3	206	17.4	8.0	0.6	4.59	0.4	25.55	2.0
Nd	1037	71.9	1481	103	814	60.9	47.4	3.3	31.59	2.3	119.95	8.2
Sm	269	22.0	354	29.0	197	18.6	22.1	1.8	18.53	1.6	35.58	3.0
Eu	7.8	0.9	13.4	1.2	6.8	1.0	0.4	0.1	0.329	0.1	0.40	0.1
Gd	271	24.8	365	34.3	182	19.5	24.2	1.7	22.67	1.7	33.32	2.4
Tb	38.4	3.7	60.5	5.9	29.3	3.3	4.8	0.4	4.87	0.4	7.17	0.6
Dy	221	22.3	315	33.0	175	20.8	28.6	2.2	30.48	2.5	51.25	4.3
Ho	40.8	4.8	53.4	6.7	34.9	4.9	5.0	0.4	5.55	0.4	10.67	0.9
Er	91.2	8.3	126	11.6	88.1	9.2	11.5	1.0	13.48	1.2	31.35	2.8
Tm	12.0	1.0	16.3	1.3	15.2	1.5	1.5	0.2	2.02	0.2	5.25	0.6
Yb	88.6	7.5	123	10.1	112	10.6	13.9	1.3	19.84	2.0	47.83	4.9
Lu	14.1	1.3	19.4	1.8	19.4	2.1	3.5	0.3	5.11	0.5	9.66	1.1
Hf	29.7	3.9	30.6	3.8	81.8	11.3	7.5	0.8	2.13	0.3	9.44	1.0
Ta	37.6	4.0	30.0	3.3	106	12.8	3.4	0.3	1.91	0.2	3.09	0.3
^{206}Pb	71.5	7.7	58.6	6.4	55.3	7.4	7.4	0.9	4.55	0.7	10.66	1.5
^{208}Pb	71.8	5.5	61.6	4.6	55.2	4.9	7.6	0.6	4.47	0.4	10.64	1.0
Th	1.8	0.3	1.9	0.2	2.8	0.5	0.7	0.1	0.05	<2σ	3.12	0.2
U	0.9	0.2	1.5	0.2	0.7	0.2	0.6	0.1	0.04	<2σ	0.35	<2σ
REE	4982		7661		5167		222		180		597	
LREE	4205		6582		4511		128.96		76.479		401	
HREE	777		1079		656		92.9		104.02		197	

Trace element LA-ICP-MS compositions (ppm); b.d.l.: below detection limit; <2σ: : below 2σ error

Table 63: Astrophyllite in peralkaline alkali feldspar granites from the Mandira unit

Sample	**MAN-13A**						**MAN-4776**						**MAN-13A**			
Mineral	Astrophyllite 1						Astrophyllite 2a						Astrophyllite 2b			
Point_ID	10	2σ error	14c	2σ error	21	2σ error	1	2σ error	2	2σ error	3	2σ error	1	2σ error	22	2σ error
Li (ppm)	131	12.2	147	14.3	328	33.9	245.4	24.1	199	20.7	254	27.9	136	11.3	261	27.5
Sc	10.43	1.4	8.1	1.0	4.1	0.7	3.5	0.52	3.75	0.44	3.82	0.48	7.24	0.8	1.4	0.3
Ti	49129	3771	47460	3860	40303	3415	63668	6858	57281	6688	59836	7376	47031	3403	58952	5081
Zn	3198	229	2731	199	2983	226	3439	401	3496	442	3343	449	2989	202.5	2981	227
Ga	19.18	2.40	16.49	1.90	8.79	1.32	18.29	2.88	16	2.5	13.57	2.3	12.2	1.2	16.4	2.1
Rb	5531.80	510	4975	504	4761	510	5536	644	4736	601	4278	575	4945	417	4457	490
Sr	5.66	0.72	1.76	0.20	3.10	0.44	12.9	2.20	15.4	2.8	19.7	3.8	3.6	0.3	5.0	0.6
Y	205	20.3	28.3	3.1	158	18.1	132	19.8	35.6	5.9	33.4	5.9	22.7	2.1	93.2	10.9
Zr	31073	2884	25640	2607	12769	1371	11122	1923	11363	2183	11392	2340	21538	1832	3570	393
Nb	4051	386	10738	1123	23040	2544	7361	1391	5889	1239	6459	1455	10153	886	2019	229
Cs	779	97.1	656.0	92.6	1613	244	826	167	639	144	406	97.8	855.5	94	814.6	128
Ba	66.65	9.98	28.0	4.40	4.87	1.32	60.2	10.5	54.3	9.9	64.3	12.6	26.9	3.4	70.4	12.2
La	410	47.8	231	30	162	22.7	422	69.6	320	58.7	394	77.2	160.2	16.6	544.5	78.4
Ce	1301	210	1000	186	324	64.9	1444	219	1192	201	1544	278	639.7	89.6	1982	412
Pr	142.42	23.4	150.2	28.2	49.9	10.1	216	25.3	161	20.6	206	28.1	88.6	12.7	278.6	58.3
Nd	561	99.1	635	128	220	48	920	128	629	97	809	133	359	55.1	1186	266
Sm	145	25.9	131	26.3	60	13.3	159	23.1	105	16.6	147	24.8	68.3	10.6	252	56.1
Eu	0.92	0.30	0.34	0.09	0.64	0.22	0.78	0.24	0.5	0.1	0.7	0.2	0.1	0.1	1.3	0.3
Gd	103.22	17.3	51.4	9.6	50.4	10.4	76.2	12.8	42.6	7.8	64.5	12.6	28.6	4.2	138.1	28.8
Tb	16.24	2.3	4.7	0.7	8.7	1.4	8.4	1.3	5.0	0.8	8.1	1.4	2.9	0.4	16.6	2.7
Dy	69.35	9.9	14.3	2.2	45.0	7.5	30.8	5.3	20.3	3.7	29.6	5.8	10.4	1.4	60.5	10.1
Ho	12.82	1.8	1.9	0.3	7.8	1.3	4.2	0.6	2.8	0.4	3.6	0.5	1.5	0.2	7.6	1.3
Er	25.14	2.9	4.2	0.5	18.9	2.4	8.5	1.3	6.6	0.9	6.1	1.0	4.2	0.5	12.0	1.6
Tm	1.98	0.3	0.6	0.1	1.8	0.3	0.7	0.2	0.9	0.1	0.6	0.1	0.5	0.1	1.0	0.2
Yb	10.32	1.8	4.3	0.7	8.6	1.7	4.8	0.9	6.4	0.7	2.7	0.4	3.3	0.5	6.67	1.2
Lu	1.28	0.3	0.6	0.1	0.9	0.2	0.5	0.1	0.8	0.1	0.3	0.1	0.5	0.1	0.65	0.1
Hf	1349	150	1124	140	3407	454	700	76.0	796	94.2	755	94.8	1066	106	86.82	12.1
Ta	30.97	3.1	846.55	88.3	74.39	8.3	432.97	43.9	257.49	28.3	239.36	27.8	124.57	10.7	27.16	3.1
Pb	2821	324	1787	231	500	69.6	3110	310	3137	338	3079	350	1284	131	4007.2	573
Th	25.09	2.1	2.8	0.2	25.3	2.2	194	20.2	275	31.1	25.1	3.0	1.5	0.2	4.61	0.5
U	9.58	0.9	8.2	0.6	2.1	0.3	23.2	2.7	28.2	3.48	6.2	0.86	5.1	0.38	4.71	0.4
LREE	2560		2147		816		3162		2408		3100		1316		4244.4	
HREE	240		82		142		134		85		116		52		243	

Trace element LA-ICP-MS compositons (ppm); b.d.l.: below detection limit; <2σ: : below 2σ error

Table 64: Astrophyllite in peralkaline alkali feldspar granites from the Papanduva Pluton

Sample	**MR-01A**										**MR-21**					
Mineral	Astrophyllite 1										Astrophyllite 2b					
Point_ID	1b	2σ error	2a	2σ error	3	2σ error	4	2σ error	5a	2σ error	1a	2σ error	1b	2σ error	1c	2σ error
Li (ppm)	371.8	36.94	206.2	20.78	190.1	19.90	359.56	19.86	383.3	22.4	84.06	3	70.48	2.96	119.15	5
Sc	5.23	3773	8.90	3378	8.10	0.76	3.45	0.23	4.45	0.29	0.52	0.05	0.57	0.08	0.32	0.1
Ti	52746	0.34	46964	0.28	45444	3328	51315	1931	54195	2102	57616	3185	62155	3634	58773	3678
Zn	2116	209.0	2031	203.0	2145	222.5	2230	122.3	2386	138	1434	103	1436.7	109.59	1444.22	118
Ga	7.39	0.82	6.98	0.72	7.78	0.80	10.95	0.68	8.54	0.6	3	0.2	2.76	0.27	3.64	0.3
Rb	2382	204.7	2751	238.9	2491	222.9	2522	117.7	2502	122	2724	129	2628.4	129.93	2481.32	130
Sr	34.57	3.24	30.94	2.92	115.69	11.16	29.43	1.54	79.80	4.3	16.73	0.8	13.13	0.71	16.9	0.9
Y	55.92	4.44	21.86	1.76	18.85	1.56	81.44	3.48	142.96	6.3	16.42	0.8	16.44	0.86	14.42	0.8
Zr	16027	1383.16	27942	2436	25462	2288	10530	492.99	13920	683	322.3	14	369.01	16.79	215.44	10
Nb	9137	725.8	8091	648.3	13148	1081	11225	478.43	12452	553	1777.04	100	1344	79.89	427.85	27
Cs	328.3	27.64	193.2	12.34	135.5	11.86	137.6	6.32	195.1	9	729.7	40.6	599	35.1	570.54	35.6
Ba	449.4	37.44	102.1	16.30	466.5	39.96	316.0	14.43	447.4	21.1	67.48	3.9	58.78	3.8	53.6	3.7
La	115.9	9.18	437.03	8.14	91.21	7.44	147.49	6.26	126.18	5.6	125.6	5.9	129.46	6.4	139.65	7.3
Ce	543.7	43.1	78.33	34.90	415.9	34.02	633.02	26.83	591.04	26	434.6	22.3	435.16	23	458.29	26
Pr	96.57	7.22	403.7	5.88	77.63	5.94	113.86	4.53	107.25	4.4	58.96	3.5	53.95	3.4	60.36	4.0
Nd	542.8	39.6	109.4	29.52	418.8	31.08	631.1	24.35	578.0	23	238.0	13	203.1	12	240.15	15
Sm	170.8	14.52	0.79	9.36	108.1	9.46	163.3	7.63	187.8	9.1	38.64	1.7	32.5	1.7	37.06	2.0
Eu	4.17	0.44	48.95	0.11	2.03	0.22	1.17	0.12	3.13	0.2	0.452	0.0	0.513	0.1	0.357	0.1
Gd	99.26	8.82	5.92	4.42	44.18	4.10	73.85	3.72	95.99	5.0	12.17	0.6	11.67	0.7	12.84	0.8
Tb	13.66	1.26	20.23	0.56	5.12	0.50	8.05	0.44	13.25	0.7	1.30	0.1	1.23	0.1	1.13	0.1
Dy	51.26	5.10	2.02	2.08	17.34	1.84	27.07	1.63	52.40	3.1	6.59	0.3	4.75	0.4	4.49	0.4
Ho	5.89	0.62	2.72	0.22	1.82	0.20	3.36	0.22	6.61	0.4	1.15	0.1	0.89	0.1	0.84	0.1
Er	7.53	0.82	0.16	0.32	2.58	0.32	7.21	0.48	10.73	0.7	3.33	0.2	2.48	0.2	1.97	0.2
Tm	0.30	0.06	0.85	0.03	0.20	0.04	0.78	0.08	0.73	0.1	0.52	0.0	0.53	0.1	0.20	0.0
Yb	0.98	0.24	0.11	0.17	1.02	0.19	2.79	0.30	3.12	0.3	3.7	0.2	2.9	0.29	2.21	0.25
Lu	0.11	0.034	1002	0.03	0.14	0.03	0.23	0.04	0.30	0.0	0.50	0.0	0.52	0.06	0.42	0.05
Hf	506.2	61.74	193.0	123.9	1357	175.1	283.8	19.46	309.3	22.6	5.58	0	10.89	0.74	4.05	0.35
Ta	854.8	103.8	176.3	23.80	1562	200.8	432.2	29.37	160.7	11.6	28.96	1.38	15.44	0.81	2.53	0.17
Pb	223.6	27.16	0.22	21.70	199.5	25.62	224.5	15.40	238.7	17	354.6	18	376.1	19.75	408.79	22.72
Th	0.49	0.088	9.65	0.04	0.14	0.03	3.03	0.23	1.10	0.1	12.07	0.6	3.99	0.26	4.19	0.28
U	8.18	0.92		1.06	4.35	0.52	8.15	0.53	8.95	0.61	5.02	0.2	3.18	0.2	2.96	0.19
LREE	1470		1029		1112		1689		1590		896		854		936	
HREE	179		1034		72		123		183		29		25		24	

Trace element LA-ICP-MS compositons (ppm); b.d.l.: below detection limit; <2σ: : below 2σ error

Table 65: Columbite in greisens and syenogranites from the Desemborque Pluton

Sample	**GUA-08**												**GUA-53**				
Facies	Greisen												Syenogranite				
Mineral	Columbite 1												Columbite 2				
Point_ID	2	2σ error	2b	2σ error	2c	2σ error	3b	2σ error	3c	2σ error	3d	2σ error	4	2σ error	15	2σ error	1
Li (ppm)	38.93	18.3	73.26	14.76	2.01	1.56	b.d.l	1.48	b.d.l	1.72	b.d.l	1.24	3.14	2.3	364.7	5.6	28.14
Mg	31.05	40.04	224.8	31.66	73.13	93.76	38.65	7.84	35.29	7.76	28.14	7.66	58.56	42.32	476.6	100.1	71.4
Al	5417	1465	8941	1109	44.06	46.76	48.91	16.36	140.9	28.6	30.64	14.18	153.8	131.58	14522	914.4	1149.3
Sc	349.05	32.5	304.08	26.52	253.57	24.68	335.02	35.1	306.57	29.78	273.8	28.12	274.1	90.48	687.06	232.2	440.83
Ti	3714	332.7	3695	301.9	2845	251	2734	284.28	3435	329.42	3112	318.68	3892	855.1	6948	1474.5	5870
Zn	129.4	28.6	191.2	32.56	179.6	29.9	310.4	40.5	233.0	38.44	214.8	37.08	261.6	162.72	542.6	167.2	198.8
Ga	5.72	2.54	12.0	2.62	0.7	0.8	1.12	0.8	1.18	0.94	1.24	0.76	5.09	2.34	28.87	1.6	4.08
Sr	4.52	1.44	0.93	0.54	0.54	1.1	0.75	0.34	0.46	0.36	0.33	0.34	122.29	40.88	7.07	1.2	0.68
Y	216.4	16.1	173.2	14.14	163.5	12.28	115.5	12.1	169.7	13.88	158.5	13.34	2701	1183.9	551.2	206.6	595.1
Zr	2123	303.6	925.5	146.9	694.7	110.94	676.0	163.18	825.6	154.32	706.6	140	776.3	274.52	343.8	146.3	797.2
Nb	419426	26536	419426	26536	419426	26532.5	419426	26532.4	419426	26533	419426	26533	419426	26531	419426	26538.7	419426
Sn	658.4	61.82	735.3	63.22	370.2	36.3	298.1	30.32	389.3	38.52	473.6	48.42	307.8	58.58	2422	694.0	1259
Cs	8.46	2.64	15.55	2.92	0.59	0.38	0.42	0.34	0.54	0.44	0.44	0.38	0.66	0.56	11.74	0.8	0.92
Ba	2.83	5.58	5.0	4.54	4.09	5.26	b.d.l	2.8	b.d.l	2.86	2.63	3.36	225.15	106.96	14.03	5.9	b.d.l
La	b.d.l	0.56	1.92	0.78	0.34	0.54	0.59	0.48	0.82	0.62	b.d.l	0.32	108.75	37.52	13.65	4.1	10.33
Ce	3.55	1.22	4.33	1.26	2.38	0.78	2.09	0.68	3.78	1.06	0.6	0.48	240.03	67.96	36.31	8.2	33.88
Pr	0.89	0.58	1.06	0.58	0.91	0.52	1.07	0.56	1.02	0.48	0.61	0.42	40.15	13.8	6.74	2.2	7.16
Nd	12.06	8.14	13.83	9.64	b.d.l	5.6	b.d.l	5.6	8.38	7.5	4.17	5.08	188.61	27.4	46.34	13.5	36.29
Sm	9.0	4.62	10.09	5.76	5.72	3.36	5.48	4.14	11.55	5.4	2.94	3.6	93.21	13.08	28.32	7.9	26.88
Eu	b.d.l	0.62	b.d.l	0.72	b.d.l	0.74	b.d.l	0.88	b.d.l	0.84	b.d.l	0.46	1.47	1.18	b.d.l	1.2	b.d.l
Gd	27.16	8.02	21.43	7.12	16.57	5.14	b.d.l	3.9	16.51	5.48	10.38	4.26	182.25	66.6	65.84	28.4	71.27
Tb	9.54	2.24	7.88	2.04	5.87	1.46	3.97	1.66	6.6	1.76	7.79	1.98	53.93	20.12	19.77	9.0	25.1
Dy	123.4	23.46	101.25	22.06	98.04	19.1	65.18	18.1	82.25	20.56	87.43	21.46	483.82	244.2	206.95	141.8	238.21
Ho	45.81	5.4	33.95	5	31.98	3.7	21.57	3.68	28.95	4.06	28.14	3.92	137.57	56.78	54.89	26.4	75.88
Er	200.2	26.78	161.1	26.62	167.1	21.82	97.1	21.22	151.2	25.7	136.7	23.9	596.7	331.44	223.1	152.6	316.4
Tm	54.59	8.7	51.54	9.84	51.08	8.06	27.18	7.18	41.72	8.24	40.43	8.22	137.2	33.38	42.83	13.1	64.79
Yb	938	171.7	663.7	152.4	725.8	138.94	438.9	125.94	531.0	131.3	560.5	143.52	1508	406.38	450.6	141.6	577.5
Lu	123.0	12.06	102.6	12.34	101.2	9.8	64.22	9.6	84.3	10.34	85.15	10.3	225.07	62.7	50.94	20.3	89.38
Hf	673.3	70.76	180.0	30.68	125.6	18.96	178.4	34.8	158.8	24.98	156.3	24.24	117.0	47.6	19.81	13.0	62.23
Ta	69171	10473	29209	5464	43920	8473.06	119874	20516.1	70776	14795.6	35968	7600.7	16639	8178.1	21129	10536.1	24670
W	19430	2567	14614	2218	9260	1314	9310	1794.38	10411	1844.22	9508	1764.8	6878	2888.4	10985	4912.8	10114
Pb	15.58	4.9	38.15	7.04	5.92	2.42	15.86	2.74	111.0	17.1	5.3	2.06	73.77	34.34	503.5	137.0	256.0
Th	33.17	4.56	14.27	3.12	10.9	1.78	11.12	2.1	18.6	3.22	5.89	1.44	104.2	35.18	156.1	62.1	193.2
U	457.48	59.92	139.63	25.94	103.63	15.22	99.98	20.94	157.06	30.04	89.13	16.94	178.28	88.82	511.81	266.0	585.62

Trace element LA-ICP-MS compositons (ppm); b.d.l.: below detection limit

Table 66: Monazite in greisens and syenogranites from the Desemborque Pluton

Sample	**GUA-08**															
Facies	Greisen															
Point_ID	1	2σ error	5	2σ error	7	2σ error	7a	2σ error	11a	2σ error	11b	2σ error	10	2σ error	10b	2σ error
Li (ppm)	94.37	18.8	43.33	41.6	236.6	60.36	16.01	5.84	8.82	2.78	7.00	2.36	9.94	1.48	36.25	14.98
Sc	b.d.l	0.3	68.34	12.6	12.93	5.46	b.d.l	0.5	b.d.l	0.13	b.d.l	0.11	b.d.l	0.14	b.d.l	0.62
Ti	51.79	8.5	28.17	0.4	266.3	53.48	12.76	3.98	2.56	0.64	2.81	0.72	3.82	0.6	10.74	4.52
Zn	48.05	10.4	26.94	3.04	123.7	40.88	3.92	2.88	0.48	0.5	b.d.l	0.46	1.13	0.56	15.26	7.56
Ga	16.18	2.5	6.75	1867.4	173.44	32.4	10.89	3.36	4.38	0.98	3.93	0.9	3.72	0.66	13.17	5.66
Rb	157.2	31.6	80.62	37.6	118.1	30.72	0.89	0.54	b.d.l	0.102	0.13	0.088	b.d.l	0.11	42.12	17.68
Sr	483	62.2	57.44	24.8	8506	1230	453	118	590	97.04	253	39.9	681	112	479	201
Y	1364	278	3606	47893	33547.43	8637.4	1736	618	515.4	165.56	411.6	143	462.8	60.6	1423	575
Zr	30.26	3.9	b.d.l	31.54	3319	458	257.0	65.64	0.18	0.078	0.29	0.08	5.08	0.76	1.61	0.80
Nb	22.97	3.9	70.49	2	865.6	176	53.22	16.42	0.08	0.042	0.07	0.04	2.72	0.42	3.39	1.46
Cs	8.19	1.3	4.41	13.64	22	5.04	b.d.l	0.102	b.d.l	0.04	b.d.l	0.03	b.d.l	0.04	2.09	0.94
Ba	32.67	11.0	23.62	12398	410.1	176.82	18.14	10.96	b.d.l	0.46	b.d.l	0.42	1.51	0.8	3.76	3.02
La	78716.2	17722.0	25814.1	27620	1303615	374470	81043.3	31179	35633.3	12898.3	30487.1	12036.5	35114.7	6351	103429	44262
Ce	212484	32928.0	62613.2	3354	3464761	640507	236187	68651	92312.8	20495.8	82107	18869.8	87599.2	12906	236167	97045
Pr	24704.3	4469	7380	13353	409453	91787	27984.8	9094.6	11276.4	3116.26	9821	2892.46	9862.99	1304.4	26871.7	10872
Nd	82035.4	20507.0	26907.7	3460.8	1343606	431096	94383	39415	37034.8	15018.6	33122.1	14717.9	31466.4	5039.6	84362.9	35176
Sm	14117.7	3421	7042.76	5.02	223091.6	69429	14948.2	6105.2	6641	2615.36	5747	2479.68	5085	662	16210.8	6544.7
Eu	17.46	3.1	10.91	2066	287.5	62.46	18.09	6.02	7.27	1.94	5.39	1.52	6.23	1.06	24.06	10.22
Gd	6953	1866	4058	217	96515	33385.1	6047	2672.6	2851	1241.36	2365	1125.92	2436	446	8801	3777
Tb	742.53	116.2	490.6	822	9597	1802.82	579.1	170	296.6	66.96	232.8	54.42	263.9	37	989.5	404
Dy	2212	370.5	1837	131	31251	6388.38	1901	585	879.6	219.98	695.1	184	840.9	137	2977.96	1246.6
Ho	216.7	48.3	274.61	354	3726	1053.26	206.4	78.38	87.43	30.84	65.72	25.08	85.73	11.84	276.3	113
Er	336.5	74.2	b.d.l	61.9	7728	2160.66	412.9	156	128.3	44.94	101.3	38.48	120.7	19.04	359.6	150
Tm	26.52	5.4	b.d.l	501	854.8	218.18	44.53	15.9	7.51	2.42	5.81	2.02	7.76	1.14	20.41	8.44
Yb	137.17	19.0	b.d.l	94.34	5526	853	262.9	71.1	23.76	4.44	19.37	3.54	29.51	4.68	72.16	30.46
Lu	14.78	2.6	b.d.l	2996	668.6	140	27.23	8.62	2.11	0.56	1.86	0.52	2.45	0.38	5.89	2.5
Hf	11.26	4.0	b.d.l	12.58	250.7	106.68	14.68	8.26	3.41	1.86	3.26	1.88	4.22	0.96	12.58	6.18
Ta	0.97	0.3	27.29	316	28.62	7.56	3.77	1.42	0.252	0.1	0.18	0.07	0.23	0.08	0.57	0.38
Pb	1572	272.3	701.5	7503.2	24106	5089.36	1909	597	772.1	198	821.4	223	860.1	135	1339.96	557
Th	39345.2	6032	17036.7	1121.6	566039.9	103379	44403.3	12821	19768.8	4319.14	20879.4	4698.92	22630.7	2994.1	33804.7	13675
U	301.1	35.5	2636	0.0	12211	1558.32	672.7	167	64.28	9.08	81.52	10.3	45.97	8.68	49.34	21.42

Trace element LA-ICP-MS compositions (ppm); b.d.l.: below detection limit

Table 67: Monazite in greisens and syenogranites from the Desemborque Pluton

Sample	**GUA-08**															
Facies	Greisen															
Point_ID	3b	2σ error	4-r1	2σ error	4-i	2σ error	4-r2	2σ error	10b	2σ error	10a	2σ error	15	2σ error	6	2σ error
Li (ppm)	94.47	19.8	196	39.84	177	37.7	345	76.78	104	24.68	135	33.72	140	36.74	141	11.32
Sc	b.d.l	1.74	2.77	1.16	2.61	1.12	1.81	1.14	1.86	1.4	b.d.l	1.04	1.85	1.32	8.8	1.22
Ti	15.64	7.18	26.11	11.98	7.51	3.64	55.96	27.86	b.d.l	0.82	b.d.l	0.68	9.74	5.7	14.75	1.46
Zn	b.d.l	7.76	31.32	12.68	b.d.l	3.86	107	43.86	b.d.l	4.16	b.d.l	3.86	8.7	7.16	8.83	3.7
Ga	b.d.l	0.72	1.95	0.86	0.8	0.5	7.47	2.86	b.d.l	0.56	b.d.l	0.4	0.7	0.62	b.d.l	0.42
Rb	19.54	9.28	143	66.4	48.05	23.34	362	183	34.93	18.6	29.87	16.68	21.89	12.86	19.67	1.94
Sr	18.15	5.12	20.97	5.6	10.49	2.98	10.94	3.3	15.7	4.9	15.68	5.18	12.96	4.54	105.1	11.58
Y	338598	21423.2	322850	20420.9	251980	15938.6	330724	20920.1	251980	15940.5	299227	18929.5	338598	21420.2	267729	16934.4
Zr	537	160	1644	508	2843	916	1368	462	2424	859	1304	486	799	313	7172	515
Nb	27.85	9.36	27.31	9.24	41.68	14.68	71.45	26.4	b.d.l	0.36	b.d.l	0.26	885	380	57.8	5
Cs	b.d.l	0.44	8.08	1.84	2.42	0.68	36.26	8.56	b.d.l	0.24	b.d.l	0.28	0.19	0.24	b.d.l	0.26
Ba	5.09	6.64	b.d.l	3.34	2.72	2.82	5.28	4.74	b.d.l	4.28	b.d.l	2.98	4.26	5.08	9.76	2.96
La	117	28.58	30.95	7.76	16.95	4.54	41.16	11.26	1.16	0.8	11.75	4	38.82	12.4	168	14.1
Ce	752	242	340	113	218	75.62	457	166	26.83	10.56	176	70.1	472	197	696	74.8
Pr	281	114	169	71.28	121	53.54	245.3	114	27.15	13.4	108	55.9	241	131	234	16.88
Nd	3134.19	1924	2695	1718	1978	1318	3553	2482	718	528	1796	1386	3049	2473	2773.03	249
Sm	5482.01	2344	6455	2866.98	4711	2186	7416	3607	2955.01	1510	4241.97	2278	4700	2654	4693	652
Eu	14.26	5.94	21.66	7.88	13.46	5.16	21.95	8.8	11.61	5.12	13.21	6.06	8.78	4.4	13.93	1.74
Gd	15412.1	2813	22251.2	4228	14205.9	2828	19100.3	3999	16483.6	3638	17251.4	4019	13874.3	3414	12592.3	1424
Tb	3856	1130	7174	2180	3902	1236	5063	1678	5903	2051	5423	1977	3655.99	1398	3462	256
Dy	30011	10659	60662.8	22474	30815.9	11969.8	38523.7	15742.1	54880.7	23640.3	49559.8	22526.8	30223.1	14498.8	27728.1	2182
Ho	7653	1965	14888.2	3970	6886	1917	8710	2541	13716.5	4200	12569	4044	7337	2481	6686	435
Er	27119.2	7853	49441.9	14849.8	23649.9	7406	29935.5	9806	47536.3	16321.4	43538	15683.2	26507.6	10019.3	21951.1	2260
Tm	4063	825	7042	1480	3652.97	799	4249	971	6334.97	1516	6172	1548	4400	1157	3700	251
Yb	33808.5	17948.8	55381.3	30440.6	30765.7	17599.7	33224.7	19847.6	45833.3	28646.5	51249.3	33541.8	39684	27197.9	29011.1	1972
Lu	4666.96	1520	6312	2134	3604.95	1272	4066	1501	5881	2278	5837	2373	5274	2252	3957	289
Hf	151	99.18	358	240	277	194	204	150	380	294	310	252	171	146.6	452	37.5
Ta	17.61	2.9	31.59	3.26	17.29	1.98	19.17	2.42	31.46	3.8	27.95	3.62	27.39	3.74	14.31	1.52
Pb	96.11	35.24	279	103	114	44.02	149	60.34	191	80.74	176	78.28	185	86	129	14.7
Th	2490	641	6721	1796	2620	731.82	3659	1071	4331	1332	4143	1341	2418	823	2690	170
U	243	112.5	2642	1256	1415	697	4394	2253	346	185	332.46	185	2919	1697	1030	87.88

Trace element LA-ICP-MS compositions (ppm); b.d.l.: below detection limit

Table 68: Zircon in syenogranites from the Desemborque Pluton

Facies	**Biotite Granite (Desemborque Pluton)**															
Sample	**GUA-50C1**								**GUA-50C2**							
Point_ID	12a	2σ error	12	2σ error	2	2σ error	8	2σ error	1c	2σ error	2	2σ error	3	2σ error	9	2σ error
P (ppm)	1297	1759.7	1845.7	2487.2	452	612.96	614	837	358	327.98	1217.7	1067.8	1182.7	999	1353.5	1115
Sc	219	19.6	213	19.58	229	22.2	217	22.14	232	60.8	353	102	365	115	254	88
Ti	26.31	6.4	45.66	5.24	62.81	7.2	6.36	2.52	5.55	3.94	166	67.82	851	370	55.98	27.12
Mn	2983	262	3833	350	171	16.64	920	92.94	5.7	1.94	5070	1284	3981	1105	4004	1215
Rb	14.43	1.7	9.93	0.9	34.01	2.7	72.29	5.2	0.91	0.5	52.18	13.7	54.38	15.3	7.86	2.5
Sr	42.9	3.4	82.61	5.6	5.76	0.7	13.34	1.1	1.14	0.4	62.95	20.9	65.12	23.6	82.55	32.9
Y	11650	982	16077	1409	4554	418	4808	465	2797	697	10145	2765	26297	7878	16308	5364
Zr	454550	28773	454550	28756	481201	30446	485125	30688	486383	30777	458103	29025	347871	22015	492676	31167
Nb	680	43	842	52.0	320	20	211.78	13	74.55	15.5	881	198	2426	595	463	124
Mo	4.24	1.8	2.7	0.9	3.77	1.1	3.82	0.8	7.33	2.6	41272	12814	5.13	2.2	8.08	3.2
Sn	36.17	6.4	41.16	6.5	7.94	2.1	3.54	1.2	1.9	1.3	203	53.6	394	111	145	44.8
Ba	77.79	12.0	120	15.2	6.39	2.1	18.59	3.3	1.6	1.3	172	61.8	239	91.4	102	42.8
La	118	14	310	38.2	8.01	1.3	9.83	1.5	4.7	1.3	125	34.3	235	70.3	127	41.9
Ce	1033	101	1684	173	52.03	5.9	69.51	8.1	29.77	8.6	651	204.1	1335	461	642	244
Pr	75.03	6	195.82	14.9	3.62	0.5	6.18	0.6	2.06	0.7	103	30.7	189	61.26	89.32	31.88
Nd	425	41	1104	101	21.66	3.8	35.03	4.5	16.27	5.0	419	118.5	882	269	378	126
Sm	390	37	850	76.9	20.79	3.5	19.46	2.8	18.17	6.1	234	78.5	493	178	200	79.4
Eu	0.72	0.5	1.2	0.4	b.d.l	0.3	0.181	0.2	b.d.l	0.2	2.96	1.4	8.33	2.5	3.07	1.04
Gd	728	79	1384	154	77.05	10.4	59.73	8.1	70.71	20.4	361	112.5	835	282	328	122
Tb	214	17.1	386	30.6	33.92	3.1	29.24	2.7	23.9	6.1	123	34.1	295	89.12	112	37.38
Dy	1866	167	2882	263	431	43	386	40	277	81.5	1275	410	3263	1150	1363	528
Ho	507	36.2	743	53.2	163	12.3	164	12.5	104	27.7	410	120	1009	323	502	176
Er	2030	130	2694	170	744	48	781	50.3	432	104	1856	489	4487	1296	2384	757
Tm	403	29.4	521	38.1	175	13.4	182	14.2	85.53	21.8	394	110.0	938	287	537	181
Yb	3456	405	4322	535	1604	213	1735	247	767	235	3906	1309	8509	3133	4948	2003
Lu	577	43.2	695	52.6	295	23.3	297	24.0	142	37.2	645	184	1329	418	820	284
Hf	16257	1653	15143	1622	12688	1447	20047	2442	9521	2720	13842	4324	66564	22817	16476	6193
Ta	57.71	5.5	45.51	4.2	7.81	1.0	78.37	7.7	5.05	1.3	35.59	9.7	189	54.60	46.87	14.92
^{206}Pb	813	57.4	823	55.3	175	13.7	702	48.0	62.76	16.0	3340	896	760	224	633	204
^{207}Pb	183	17.4	174	14.3	23.67	3.5	90.87	8.3	7.05	2.7	2088	683	263	94.72	114.89	45.54
^{208}Pb	251	28.5	255	29.5	31.78	4.4	132	17.4	11.39	3.2	2598	739	306	95.74	173	59.34
Th	4257	284	5361	359	859	58.8	1746	120	250	60.8	7651	2030	10810	3151	4934	1579
U	4034	302	4892	375	595	47.6	3112	256	176	40.7	5377	1353	7278	2011	4448	1348

Trace element LA-ICP-MS compositions (ppm); b.d.l.: below detection limit; <2σ: : below 2σ error

Table 69: Zircon in syenogranites from the Desemborque Pluton

Facies	**Biotite Granite (Desemborque Pluton)**																
Sample	**GUA-53**																
Point_ID	2a	2σ error	2c	2σ error	3	2σ error	3-r	2σ error	12	2σ error	13	2σ error	13c	2σ error	15	2σ error	15b
P (ppm)	835	1154	702	966	2693	3595	3049	4063	1833	2441	1094	1462	1989	2669	1065	1436	1488
Sc	220	28.06	214	28.34	387	52.78	430	59.98	276	39.28	211	31.66	275	43.4	316	51.18	375
Ti	b.d.l	161.1	b.d.l	1505	469	33.28	404	32.48	110	10.02	12.32	4.46	89.9	8.86	109	9.28	221
Mn	969	70.38	1368	101	3879	289	3261	246	2499	190	3017	235	2346	187	2337	189	2812
Rb	11.16	1.4	1.46	1.08	25.03	3.2	28.91	4	30.45	4	4.79	0.96	8.88	1.42	17.44	2.6	9
Sr	6.25	0.7	6.43	1.3	93.53	8.56	74.74	7.26	99.82	9.4	51.16	5.2	77.66	7.92	41.22	4.3	61.02
Y	5595	461	5172	432	25231	2166	22793	1983	28757	2537	12130	1106	28227	2667	10085	972	15256
Zr	481889	30486	485050	30733	481201	30443	481201	30458	481201	30444	438485	27749	488604	30914	481201	30441	481201
Nb	209	21	751.75	77.04	1433	151	541	58.46	1361	149	467	53.6	1075	129	338.4	41.62	905
Mo	4.06	1.1	4.61	2.94	5.19	1.24	4.06	1.7	3.69	1.26	3.72	1.46	6.11	1.52	4.21	1.06	5.01
Cs	7.78	1.6	92.87	12.08	80.2	7.9	88.95	9.84	23.37	3.02	8.96	2.2	44.27	5.26	158	16.36	350
Ba	14.11	2.8	9.29	5.6	152	18.56	255	32.68	369	44.94	44.86	7.54	328	43.98	105	14.84	169
La	11.02	1.0	9.03	1.6	116	7.9	119	8.56	152	10.36	68.02	5.04	183	12.68	92.35	6.48	122.2
Ce	82.17	6.42	78.44	7.34	1047	81.1	943.3	74.2	1143	90.32	1501	121.62	1589	132	775	65.46	1371
Pr	9.56	1	8.81	1.56	170	15.74	168	16.06	197	18.84	130.1	13.06	260	26.82	138	14.5	242
Nd	64.45	7.06	39.57	9.54	1071	97.64	1036	98.34	1150	108	786	78.02	1544	156	761	78.52	1387
Sm	54.77	6.2	45.26	9.58	1195	117	1256	127	999	101	500	54.22	1347	148	600	67.86	1099
Eu	b.d.l	0.26	b.d.l	0.78	3.4	0.68	3.92	1.06	3.04	0.68	1.21	0.54	2.89	0.7	1.49	0.42	2.69
Gd	142	13.7	124	17.36	2102	194	2229	211	1888	180	706	71.3	2380	243.8	913	95.8	1610
Tb	52.1	4.48	48.94	5.28	615	52.8	678	59.3	538	47.56	178	16.52	630	59.7	258	24.98	455
Dy	567	44.42	522	47.42	4847	384	5327	428	4401	357	1506	127	4798	413	2049	180	3392
Ho	214	17.2	192	16.86	1231	102	1356	114	1210	103	459.2	40.42	1210	109.2	527	48.5	807
Er	923	83.28	841	80.14	4203	397	4705	452	4293	419	1746.15	177.7	4065	430	1882	204	2793
Tm	206	18.02	180	17.04	783	71.2	929	86.04	836	78.38	362	35.42	759	76.86	405	41.96	551
Yb	1903	253	1516	211	6614	944	8002	1168	6891	1029	3309	521	6482	1078	3887	665	5010
Lu	318	26.6	266	23.84	1048	90.92	1325	116.86	1049	93.64	478.5	44.46	992	95.08	642.02	62.72	821
Hf	16078	1364	14859	1286	18736	1662	23260	2094	19085	1743	13861	1311	19919	1955	29734	2977	32227
Ta	32	3.08	49.75	5.66	132	12.66	99.84	10.08	120	11.94	59.01	6.32	104	11.18	79.88	8.76	179
^{206}Pb	875	78.64	881	86.12	3012	283	3673	352	4983	483	1168	119.3	4347	457	1727	186	2541
^{207}Pb	453	60.16	548	78.54	2020	288	2725	398	3994	596	623	99.42	3472	580	1073	185	1756
^{208}Pb	515	57.18	618	71.98	2327.2	275	3050	369	4500	555	741	96.56	4034	551	1193	168	1994
Th	1507	160	1511	165	10262	1159	8027	924	11107	1304	4593	564	9636	1244	5419	718	6373
U	2088	187	1727	158	8143	764	7137	680	6265	607	4381	441	6441	675	4479	479	5418

Trace element LA-ICP-MS compositions (ppm); b.d.l.: below detection limit; <2σ: : below 2σ error

Table 70: Zircon in greisen from the Desemborque Pluton

Facies	**Biotite-quartz-sericite Greisen (Desemborque Pluton)**																
Sample	**GUA-08**																
Point_ID	1b	2σ error	1d	2σ error	3	2σ error	4-r	2σ error	5	2σ error	7a	2σ error	7b	2σ error	9c	2σ error	9d
P (ppm)	1353	1291	517	493	1031	978	585	558	1081	1049	4102	3932	5103	4895	2264	2201	1066
Sc	302	23.5	362	27.4	544	41.92	375	29.48	244	21.52	296	25.54	245	20.82	332	30.06	300
Ti	19.13	9.48	21.81	4.72	16.76	3.78	8.92	3.02	97.54	21.96	90.49	18.18	64.47	9.14	20.19	4.88	45.48
Mn	5552	672.6	3613	455	5918	786	4092	561	4624	679	7878	1198	8329	1312	6423	1128	3701
Rb	21.31	3.22	8.06	1.1	12.38	1.36	6.64	0.88	556	57.94	53.62	6.82	18.77	2.22	15.29	2.08	10.94
Sr	92.72	9.7	82.01	8.06	86.1	8.64	93.49	9.64	58.05	7.72	86.11	10.48	68.07	7.88	92.7	11.76	191
Y	3806	260	2311	159	3406	238	2000	141	3928	287	10482	769	12897	958	5247	409	4452
Zr	417756	26484	417756	26437	432489	27361	421606	26675	428195	27179	446554	28305	446554	28253	446554	28258	446554
Nb	139	10.8	150.57	10.46	50.35	3.6	151	10.5	210	16.9	216	16.58	268	19.14	169	12.72	167
Mo	7.09	3.46	3.69	1.26	4.75	1.18	4.17	1.22	5.64	3.62	3.87	2.74	3.78	1.08	4.52	1.38	51.12
Cs	34.69	7.16	37.95	4.88	31.52	3.84	27.56	3.68	68.75	12.88	26.1	6.2	15.62	2.6	21.59	3.74	36.58
Ba	55.77	12.06	25.52	4.52	56.8	7.08	23.54	3.76	24.19	9.42	59.36	13.16	37.62	5.86	44.37	7.72	69.78
La	39.21	4.16	27	2.26	49.97	3.64	16.13	1.38	20.52	3.26	74.58	6.88	48.95	3.78	34.67	2.98	101
Ce	111	15.1	141	19	143	20.24	69.03	10.16	83.88	14.34	339	55.7	152	25.7	120	22.7	277
Pr	15.89	2.3	26.04	2.44	24.69	2.24	10.68	1.1	10.04	2.1	45.6	5.28	22.4	2.3	17.12	2	43.19
Nd	89.51	15.46	144	14.46	145	13.42	64.18	7.1	58.18	14.7	240	30.86	119	12.58	97.04	11.88	218
Sm	68.93	12.96	117	13.68	127	14.26	70.07	8.72	57.19	14.06	164	25.44	133	17.24	83.24	12.62	132
Eu	0.88	0.86	b.d.l	0.34	b.d.l	0.3	b.d.l	0.26	1.97	1.38	0.79	0.7	b.d.l	0.26	b.d.l	0.32	3.1
Gd	155	20.6	187.1	19.08	263	25.98	131.71	14.02	128	22.06	363	45.1	371	41.62	192	24.52	233
Tb	70.96	7.24	77.79	6.92	89.14	7.92	49.71	4.64	49.65	6.46	144	15.06	163.24	16.14	84.75	9.28	88.82
Dy	793	74.04	791	69.88	837	75.56	595	55.42	667	74.64	1735	178	2099	214	1045	117	1087
Ho	275	25.66	264	24.22	251	23.78	214	20.8	236	26.02	632	67.26	769	82.92	401	47.64	330
Er	1426	126	1326	117.5	1093	100	1169	110	1265	131	3379	345	3792	395	2214	253	1526
Tm	374	28.56	348	25.82	263	19.78	342	26.06	314	27.02	833	67.62	906	73.36	587	50.66	369
Yb	4081	324	3749	295	2763	223	3974	326	3491	312	8411	737	8878	786	6298	598	3766
Lu	710.95	71.26	630	64.52	471	50.54	666	73.44	666	80	1549	189	1560	196	1152	161	703
Hf	25686	1896	36883	2753	26767	2048	48698	3783	20622	1679	23326	1925	19553	1638	22855	2047	28169
Ta	145	11.1	240	15.98	16.28	1.28	297	19.68	99.74	9.14	107	8.82	132.87	9.2	200	14.16	88.65
^{206}Pb	2172	202	1803	168	4904	470	3620	355	1007	115	2351	256	2672	293	2792	336	2846
^{207}Pb	238	28.84	133	14.24	418	40.84	266	27.22	116	21	180	25.68	192	22.16	172	22.22	612
^{208}Pb	701	79.08	453	51.68	1985	235	1354	165	233	34.06	823	113	1142	159	1054	163	1434
Th	5386	712	2021	279	22069	3230	1907	289	2917	477	32417	5485	52112	9164	24165	4780	19651
U	8646	585	7926	538	13028	895	8361	579	5503	391.3	11713	835	16841	1209	13184	980	9613

Trace element LA-ICP-MS compositions (ppm); b.d.l.: below detection limit; <2σ: : below 2σ error

Table 71: Zircon in peralkaline granites from the Mandira granites

Facies	**Riebeckite akali feldspar granite (Mandira Pluton)**																
Sample	**MAN-13A**										**MAN-13B**						
Point_ID	15-r1	2σ error	15-r2	2σ error	10	2σ error	10a	2σ error	10b	2σ error	1a-r	2σ error	1a-c	2σ error	1b-c	2σ error	1b-c2
P (ppm)	450	342	529	401	445	341	291	223	389	302	170	153	193	173	1105	143	175
Sc	194	17.58	199	18.7	196	19.34	200	20.46	194	21.08	223	62.52	228	64.56	2032	64.88	214
Ti	24.14	4.3	9.36	2.9	19.64	4.5	26.82	3.7	62.78	8.62	4.16	2.86	2.86	2.52	3.946	2.56	3.47
Mn	481	51.76	865	97.28	1370	162	891	112	1330	177	b.d.l	0.64	b.d.l	0.64	b.d.l	0.68	b.d.l
Rb	3.91	0.64	2.9	0.52	3.12	0.64	26.26	2.74	90.14	9.76	2.41	0.8	0.99	0.44	1	0.5	0.46
Sr	10.41	0.92	15.44	1.18	31.5	2.36	16.73	1.2	31.06	2.44	0.94	0.32	0.66	0.24	0.68	0.26	0.52
Y	2061	132	2810	181	2774	181	2005	132	3426	228	3989	1050	5102	1359	5645	1528	4262
Zr	469504	29697	469504	29696	469504	29698	469504	29696	469504	29699	492454	31154	492454	31153	492306	31145	481201
Nb	24.93	1.86	33.79	2.34	19.95	1.66	11.37	0.9	11.69	1.2	37.03	9.7	15.99	4.26	16.55	4.48	40.67
Mo	b.d.l	0	b.d.l	0	b.d.l	0	b.d.l	0	b.d.l	0	4.2	1.56	4.86	1.7	5.21	1.9	4.25
Cs	b.d.l	0	b.d.l	0	b.d.l	0	b.d.l	0	b.d.l	0	b.d.l	1.02	b.d.l	0.94	1.28	1.1	b.d.l
Ba	35.69	5.34	59.93	7.86	78.94	11.26	46.56	6.6	77.6	12.44	b.d.l	0.82	b.d.l	0.72	b.d.l	0.92	b.d.l
La	11.41	1.14	16.7	1.48	66.72	5.58	21.47	1.88	49.38	4.58	1.08	0.36	0.65	0.22	2.43	0.13	0.14
Ce	74.23	5.44	160	11.4	323	23.4	105	7.8	178	13.8	64.98	18.54	33.5	9.7	34.61	10.2	63.43
Pr	18.08	1.48	28.58	2.14	54.69	4.16	20.92	1.62	26.3	2.34	0.499	0.19	0.47	0.19	0.31	0.16	0.29
Nd	134	12.72	179	16.04	309	28.7	148	14.06	124	14.48	5.12	2.16	6.3	2.46	6.94	2.84	2.98
Sm	104	9.32	115	9.74	161	14.5	74.9	6.8	74.87	8.8	11.53	3.8	17.04	5.38	19.94	6.44	12.81
Eu	0.82	0.36	1	0.34	3.57	0.8	1.63	0.38	1.56	0.6	0.46	0.28	0.63	0.32	0.54	0.32	0.34
Gd	136	11.42	154	12.42	210.73	17.86	93.06	8.02	107	11.08	83.87	24.96	106	31.74	111	33.78	82.8
Tb	44.4	3.48	55.71	4.28	59.76	4.86	34.27	2.78	52.16	4.62	34.04	9.16	44.27	12	48.51	13.38	34.94
Dy	495	57.22	647	77.66	602	77.02	438	58.92	698	101	409	109	525	142	575	158	430
Ho	177	16.14	250	23.42	215	21.24	175	18.04	277	30.2	150	37.5	198	50.2	211	54.3	157
Er	930	62.82	1205	81.6	1031	71.62	900	62.88	1362	97.82	635	183	836	243	894	264	669
Tm	234	17.88	284.95	22.08	270.2	21.74	242	19.9	333	28.7	118	33.3	152	43.3	160	46.42	120
Yb	2293	172	2671	204	2567	203	2483	201	3131	264	970	302	1215	382	1264	404	985
Lu	327	21.86	377	25.26	361	24.74	370	25.34	441	31.12	139	37.0	184	49.6	193	53	148
Hf	12238	902	13680	1029	12598	975	12214	973	13288	1097	8263	2590	8256	2615	8314	2673	8211
Ta	1.26	0.28	1.48	0.28	1.24	0.32	0.97	0.2	0.94	0.32	6.68	1.84	3.57	1.02	3.21	0.94	6.69
^{206}Pb	b.d.l	0	b.d.l	0	b.d.l	0	b.d.l	0	b.d.l	0	127	35.9	97.41	27.96	102	29.94	127
^{207}Pb	b.d.l	0	b.d.l	0	b.d.l	0	b.d.l	0	b.d.l	0	8.96	3.16	6.25	2.28	7.06	2.68	7.92
^{208}Pb	197	16.7	179	15.44	269	24.16	167	15.26	277	26.88	14.21	4.46	11.15	3.56	10.17	3.34	14.71
Th	12298	1021	2604	223	3793	337	1593	148	2563	249	309	83.36	216	58.8	221	61.34	314
U	2873	289	2357	247	3182	351	2035	237	2375	293	371	115	297	93.36	293	93.84	382

Trace element LA-ICP-MS compositions (ppm); b.d.l.: below detection limit; <2σ: : below 2σ error

Table 72: Zircon in peralkaline granites from the Mandira granites

Facies	**Riebeckite akali feldspar granite (Mandira Unit)**																
Sample	**MAN-13B**																
Point_ID	1b-r1	2σ error	1b-r2	2σ error	1b-9-c	2σ error	1a-11-c	2σ error	7-r1	2σ error	7-r2	2σ error	8-r1	2σ error	8-r2	2σ error	8-r3
P (ppm)	493	456	271	255	710	676	1398	1346	788	788	1078	1103	652	675	662	699	677
Sc	216	66.58	218	69.4	209	68.58	207	70.1	208	75.18	186	69.92	207	80.1	208	83.42	208
Ti	289.9	103.52	59.87	22.5	25.37	11.34	51.53	21.32	13.22	7.42	119	54.84	55.53	25.32	168	78.62	998
Mn	433	145	90.94	31.44	84.77	30.32	1133	417	189	74.56	548	224	741	313	1134	496.44	1549
Rb	9.94	3.16	1.38	0.6	3.25	1.34	4.6	1.76	1.92	0.98	2.39	1.48	13.15	5.1	6.71	2.72	15.85
Sr	29.21	9.14	6.3	2.08	15.56	5.28	47.83	16.34	6.48	2.48	17.97	7.12	27.06	10.52	52.03	20.86	42.19
Y	7788	2258	4413	1317	7087	2180	7865	2498	5795	1968	5737	2017	2728	993	5060	1907	5115
Zr	481201	30448	481201	30445	484606	30681	473724	29986	462619	29286	462619	29341	469504	29704	469504	29703	469504
Nb	82.47	23.6	35.68	10.52	113	34.22	141	43.94	113	37.48	168	58.08	88.23	31.32	193	70.9	310
Mo	3.51	1.66	4.05	1.72	4.61	2.42	5.33	2.58	3.38	2.02	5.25	3.82	4.49	2.08	3.97	1.92	4.7
Cs	44.36	13.66	7.02	2.62	56.74	18.76	9.57	3.86	14.73	5.9	27.23	11.6	15.93	6.2	55.18	21.6	77.89
Ba	8.65	3.5	5.26	2.38	6.1	3.44	117	43.1	20.35	8.9	57.68	25.98	54.16	22.58	61	26.26	79.39
La	14.49	4.16	8.67	2.58	6.04	2.0	33.42	10.4	4.66	1.7	13.09	4.9	25.54	8.98	24.11	8.76	20.28
Ce	106	33.46	47.45	15.4	53.26	17.96	240	82.92	51.57	19.16	98.81	38.16	134	53.2	267	110	192
Pr	6.92	2.06	3.39	1.06	5.83	1.94	43.14	13.58	6.1	2.16	15.28	5.66	24.47	8.74	50.84	18.7	27.79
Nd	43.9	16.02	21.57	8.3	41.09	16.6	251.3	97.42	41.74	18.18	78.82	36.46	124	54.64	352	160.36	163.85
Sm	56.94	18.88	22.74	7.98	54.27	19.68	190.44	67.74	48.23	19	65.45	28.02	55.2	22.38	205	84.98	122.4
Eu	1.95	0.8	0.32	0.3	1.79	0.94	3.15	1.32	1.05	0.68	0.89	0.96	0.87	0.44	2.67	1.12	2.35
Gd	209	68.4	104	34.98	198	69.38	335	120	154	59.42	153.5	62.94	76.81	31.62	256	108	208
Tb	90.17	26.56	47.14	14.3	87.56	27.44	135	43.42	84.14	29.02	91.96	33.1	39.24	14.46	92.29	35.12	87.4
Dy	1104	324	580	176	1162	363	1685	542	1108	382	1140	408	633	233	1086	414	1140
Ho	396	110	214	61.1	469	138	616	187	406	132	457	155	288	101	384	139	417
Er	1603	508	907	296	2212	744	3228	1121	1745	649	2108	812	1606	639	1879	775	2064
Tm	318	99.16	166	53.42	488	162	760	260	351	128	462	175	420	165	434	177	473
Yb	2524	863	1320	464	4227	1533	6913	2586	2746	1098	4020	1666	3799	1627	3596	1594	4004
Lu	376	111	200	60.54	596	186	901	291	370	127.7	530	190	521	193	488	187	532
Hf	8824	3030	8428	2974	11111	4038	8533	3198	36013	14399	32805	13563	16056	6863.3	16738	7398.8	15368
Ta	21.26	6.34	8.72	2.7	18.32	5.9	6.6	2.28	9.45	3.4	10.02	4	9.8	3.66	9.51	3.68	11.41
^{206}Pb	202	63.18	174	56.04	205	68.56	485	166	339	124	637	243	634	248	678	275	927
^{207}Pb	33.37	12.08	21.11	7.96	25.14	10.32	148	57.42	69.3	29.3	252	110	179	79.48	206	94.96	298
^{208}Pb	43.05	14.76	25.15	8.92	48.18	17.78	168	63.04	106	42.6	281	118	250	107	312	139	480
Th	833	247	449	137	1190	374	1870	606	1213	420	2100	752	3958	1466	2711	1039	8475
U	661	227	523	185	686	251	3479	1313	1095	443	2168	908	2506	1088	3134	1410	5000

Trace element LA-ICP-MS compositions (ppm); b.d.l.: below detection limit; <2σ: : below 2σ error